Artificial Radionuclides in the Environment
2018

環境における人工放射能の研究（2018 年版）

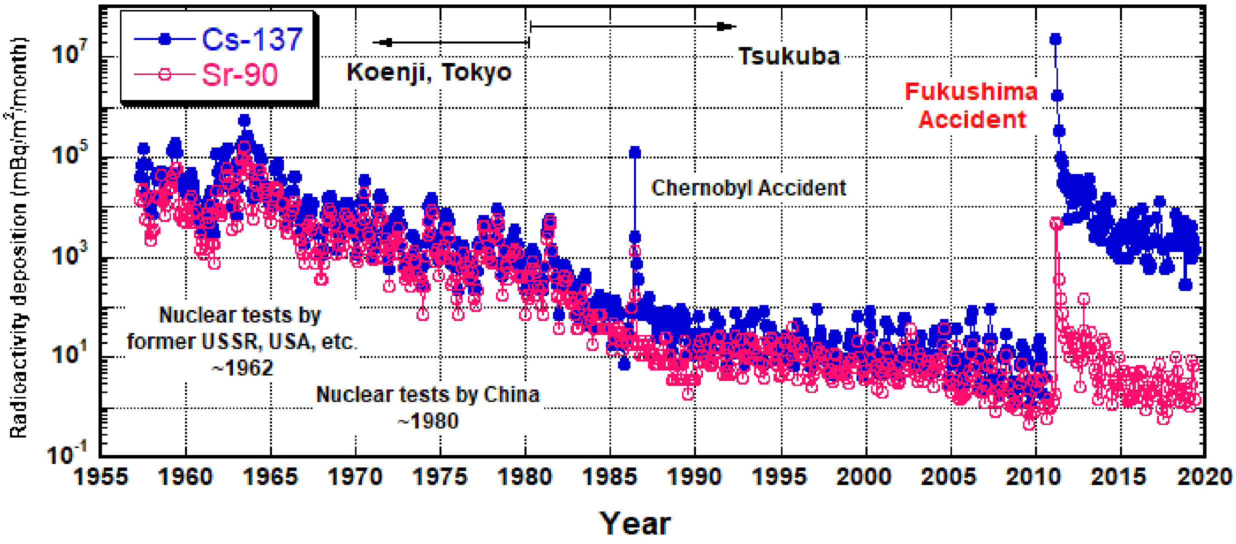

Sr–90 および Cs–137 月間降下量

Meteorological Research Institute

JMA

March 2020

気象庁　気象研究所

最終ページに図の詳しい説明があります。

See figure caption at the end page of this publication.

「環境における人工放射能の研究（2018 年版）」について

気象研究所では、1954 年以来、主に現在の原子力規制庁放射能調査研究費により大気及び海洋の環境放射能の研究を実施してきました。特に人工放射性核種の降下量を 60 年余りの長期にわたり、東京・つくばで精密測定してきました。この観測は、世界でも最長の定点観測です。このモニタリング観測の期間では、1950 年代から 1960 年代にかけては、旧ソ連や米国等による核実験が行われ、また、その後も 1986 年には旧ソ連のチェルノブイリ原子力発電所の事故が発生するなどがありましたが、この観測によって、それらの影響を含めたバックグラウンドの人工放射性核種の長期的変動を明らかにし、国民の安全・安心に寄与してきました。2011 年には不幸にして東日本大震災に伴う福島第一原子力発電所事故が発生し、それによって放出された放射性核種の推移を調査するという課題も担うこととなりました。今後も長期的視点で、人工放射性核種の変動を監視する必要があります。

放射性物質の再飛散・輸送・沈着による変動のメカニズムを正しく理解し、将来の変動を予測するためには、長期観測や再飛散観測、サンプルの分析等に加えて、数値計算モデルを用いた解析が必要です。気象研究所では、気候変動や降水予測の研究のため、大気中の微粒子の動きを表現する数値モデルを開発してきましたが、そのような数値モデルを利用した、バックグラウンド放射能の変動メカニズムを解析する研究も行ってきました。

この研究によるこれまでの観測や解析から、長期的変動に対しては、一旦地面などに沈着した人工放射性核種が、土壌粒子・生物由来の粒子等を通じて空気中へ再飛散する過程が重要である可能性がわかりました。

本論文集「環境における人工放射能の研究（2018 年版）」 は、その研究成果を、関係省庁の担当者の方々及び大学や試験研究機関の研究者の方々に広く周知するために、2016 年から 2018 年までの期間に出版された論文（主に英語論文）を、過去から現在までの成果と最近のトピックスに関するテーマ毎に分類し、各テーマの冒頭に簡単な日本語の解説を加えて、一冊にまとめたものです。

令和 2 年 3 月

気象研究所 研究総務官　高薮　出

Contents

0. Preface

1. Temporal trends of radioactivity concentrations in the atmosphere and observational approaches for their resuspension mechanisms

2. Physical and chemical characteristics of the radioactive materials in the atmosphere

3. Evaluations of resuspension , transportation and deposition processes of radioactive materials using numerical models

4. Publications 2016-2018

5. Publication list 1954-2018

6. Publication list (in Japanese) 1954-2018

7. History of the studies at the Meteorological Research Institute

8. A caption of cover art

目次

0. はじめに

1. 大気中の放射性物質の濃度変動、再浮遊観測

2. 大気中の放射性物質の物理・化学性状

3. 放射性物質の再浮遊、輸送、沈着過程のモデルによる評価

4. 出版論文　2016-2018

5. 論文リスト（英文誌）1954-2018

6. 論文リスト（和文誌）1954-2018

7. 表：研究の歴史

8. 表紙説明

0. はじめに

気象研究所（2019 年 3 月現在は環境・応用気象研究部および予報研究部）では、1954 年以来、環境放射能の観測・測定法の開発、放射能汚染の実態の把握、大気や海洋における物質輸送解明のトレーサーとしての利用を目的として、60 年余にわたって環境放射能の研究を実施してきた。1957 年以降、各省庁がそれぞれの所掌で実施してきた環境放射能調査研究関連業務は、まず旧科学技術庁、その後文部科学省が所管してきた。さらに原子力規制委員会と原子力規制庁の発足に伴って 2013 年からは、原子力規制庁が所管することとなった。このような長期にわたり多数の研究者が係わり、観測・研究を継続してきた結果、環境放射能について世界的にも他に類を見ない貴重な時系列データが内外に提供され、また様々な気象学・海洋学的発見をもたらしてきた。この間の研究成果は 200 編以上の原著論文や解説資料として内外の雑誌や成書で公表されている。

1954 年 3 月 1 日に米国によりビキニ環礁で行われた水爆実験により、危険水域外で操業していた第五福竜丸乗組員が放射性物質を含む降灰（いわゆる死の灰）による被ばくを受けた事件を契機にして、日本における環境放射能研究が本格的に始まった。当時の気象研究所地球化学研究室は環境の放射能の分析・研究において日本で有数の研究室であり、海洋及び大気中の放射能汚染の調査・研究に精力的に取り組んだ。その結果、当時予想されていなかった海洋の放射能汚染、さらに大気を経由した日本への影響など放射能汚染の拡大の実態を明らかにすることができた。1958 年には、放射能調査研究費による特定研究課題の一つである「放射化学分析（落下塵・降水・海水中の放射性物質の研究）」を開始し、以降、地点の変動はあるが、札幌、仙台、東京、大阪、福岡の五つの管区気象台、秋田、稚内、釧路、石垣島の 4 地方気象台、輪島、米子の 2 測候所の全国 11 気象官署及び観測船で採取した海水中の人工放射性核種（^{90}Sr、^{137}Cs、^{3}H 及びプルトニウム）の分析を実施してきた。

東京・つくばにおける大気中の人工放射性核種の降下量は 1961 年から 1962 年に行われた大規模な大気圏核実験の翌年である 1963 年に最大値を観測した。その後、「部分的核実験禁止条約」の締結により米ソの大気圏核実験が中止された結果、降下量はおよそ 1 年の半減時間で減少した。この放射性核種の降下量の減少率は成層圏にまきあげられた物質の滞留時間を反映している。その後も、中国及びフランスにより大気圏核実験は続けられ、人工放射性核種の降下量は増減を繰り返した。1980 年の中国による最後の大気圏核実験の後、フォールアウトは再度 1 年の半減期間で減少し、1985 年には 1957 年の観測開始以降最も低いレベルになった。しかし、1986 年の旧ソ連のチェルノブイリ原子力発電所事故により、大気中の人工放射性核種濃度（特に揮発性の高い ^{131}I、^{134}Cs、^{137}Cs など）は日本でも 1963 年に近いレベルに達するほど著しく増加した。大部分の放射性核種は対流圏の滞留時間（25 日）で減少したが一部 ^{137}Cs は成層圏にも輸送されていることが分かった。1988 年以降は低いレベルで推移しているが、明瞭な減少の傾向は見られなかった。この原因は一度地上に降下した放射性核種の再飛散に由来すると考えている。さらに、再飛散がどこで起るかについて研究を進め、東アジアの砂漠域で発生する黄砂が有力な候補であることを明らかにした。黄砂の発生は大陸域の環境変化と関連しており、降下物中の人工放射性核種は、砂漠化や関連する植生変化など大陸域の環境変化の指標となりうることが分かった。

大気フォールアウトの研究とともに、海洋における放射性核種の挙動も長期的に調査研究を実施してきた。日本周辺海域ばかりでなく、太平洋の広域に亘って海水試料の採取を実施し、

放射能汚染の実態を明らかにした。1960年代後半から1970年代の調査で、海洋表面水中の放射能が北半球の中緯度で高いことを明らかにし、フォールアウトの緯度分布を反映していることが分かった。その後、海洋表面水中の放射性核種は海洋の物質循環に支配されていることを明らかにした。さらに、海水中の人工放射性核種の分析法の高度化を実現し少量の試料で分析可能にし、海洋の ^{137}Cs 濃度の精密鉛直断面を描き、核実験由来の ^{137}Cs の主な部分は北太平洋の亜熱帯中層に存在していることを明らかにした。フォールアウトによる人工放射性核種の海洋への主な降下以来、数10年以上経過し、その広がりは北太平洋から、インド洋など他の海盆に及んでいる。これに関連して 2003－4 年に実施された BEAGLE2003 の航海で採取された海水について人工放射性核種の分析を行って、その広がりについて知見が得られた。1993年旧ソ連/ロシアによる放射性廃棄物の日本海等への海洋投棄の実態が明らかにされ、それに伴う日本海の放射能調査の実施に参加した。放射性廃棄物による影響は検出されなかったが、調査の結果を踏まえ、日本海における固有水の生成過程及び生成場所（ウラジオストック沖）についての知見を得ることができた。これらは、海洋放射能のデータベースとして公開されている。

1990年以降の環境放射能汚染として、1997年の旧動力炉核燃料開発事業団「アスファルト固化処理施設」の火災爆発事故や1999年のJCOウラン燃料工場の臨界事故があるが、いずれも環境中に放出された放射能は極めて低いレベルで、その影響は殆どなかった。しかしながら、2011年3月に起きた東日本大震災にともなう東京電力福島第一原子力発電所事故により、^{137}Cs の総量だけで 10 PBq（ペタベクレル）以上という過去日本では経験したことのない大量の人工放射性核種が環境中に放出され、その 2 割程度が日本の国土に降下し、残りの 8 割は北太平洋に降下したと考えられている。これらの影響評価やその後の環境中での拡散状況の把握のためにも、環境放射能調査・研究は今後とも重要である。

2006年4月より2011年3月まで、気象研究所では放射能調査研究費による特定研究課題として「放射性降下物の長期変動と再浮遊に関する研究」及び「海洋環境における放射性核種の長期挙動に関する研究」の二課題で環境放射能研究に取り組んできた。また、2011年8月からは、「大気を通じた人工放射性核種の陸圏・水圏への沈着およびその後の移行過程の解明研究」の課題のもと、過去の知見を十分に活用しながら、同年3月11日に発生した東日本大震災にともなう福島第一原子力発電所の事故以降の新たな事態に対応し、放出された大量の人工放射性核種の挙動を解明する研究を行った。目の前の大気に加えて、北太平洋におけるこれらの核種による汚染実態の把握やその動態の解明に取り組んだ。

過去60年余にわたり実施されてきたこうした研究成果を踏まえ、2015年4月からは「人工放射性核種のバックグラウンド大気監視と数値解析に関する研究」を新たに開始した。本報告書では、この研究課題で得られた成果を含め、最新の成果やトピックスをテーマ毎に記述した。関係各位の今後の研究や業務に役立つ資料とすべく、編集作業を行った。我が国における環境放射能研究や大気科学研究に多少なりとも寄与できたとすれば、著者一同の望外の喜びである。

1. 大気中の放射能物質の濃度変動、再浮遊観測

1）はじめに

気象研究所では、大気圏内核実験が盛んに実施された1950年代後期から現在までの期間にわたり、大気圏での人工放射性核種の濃度水準の実態とその変動要因を明らかにすべく、環境影響の大きい重要な核種について観測を継続してきた。^{90}Sr（半減期 28.8 年）および^{137}Cs（半減期 30.2年）の月間降下量（大気降下物）の長期観測結果は満60年を超え、世界でも稀にみる長期変動に関して重要な知見をもたらしている。また、2003年3月からは大気中浮遊粒子の採取、及び放射能分析も開始し、2011年3月の東京電力福島第一原子力発電所事故（福島第一原発事故）に関する環境影響に関して重要な知見を取得し、また大気モデル改善に貢献し、その結果をいち早く学会で報告するとともに、気象研究所のホームページにも掲載し一般に公開してきた。複数台有するGe半導体分析装置は他研究機関の持つ環境試料の測定にも貢献し、福島第一原発事故の影響解明にも大きく貢献してきた。前報のIgarashi et al., (2015) では福島第一原発事故以降の三年間に着目した大気降下物および大気中放射能について報告をしてきたが、事故後七年が経過し、その濃度は徐々に下がってきたため、より高精度な測定技術が求められてきた。本報ではより高精度に^{134}Csを測定するための定量方法の開発結果について報告し、事故後数年経過した現在における放射性物質の再飛散（二次飛散）や環境中での動態プロセスに関する考察について解説する。

2）研究方法

月間大気降下物の捕集は、茨城県つくば市長峰にある気象研究所の露場観測実験棟屋上に設置した大気降下物捕集用のプラスチック製水盤（面積4m^2）で1980年代以降実施してきた。福島第一原発事故以降（2011年4月以降）は放射能水準の上昇を考慮し、気象研究所屋上にて1 m^{2}水盤２基での捕集を実施した。2015年8月以降は放射能水準の低下を考慮して1m^{2}水盤４基での大気降下物採取を開始した。大気中浮遊粒子は、上記露場観測実験棟前に設置したハイボリューム・エアサンプラー(HV-1000R、柴田科学)に石英繊維フィルター(QR-100、柴田科学)を装着して、空気流量700LPMで一週間単位でのサンプリングを行った。

得られた大気降下物試料はポリ製保管容器で保存しつつ、ロータリーエバポレーターや蒸発皿等を使用して全量を蒸発濃縮・固化し、Ge半導体検出器によりγ線放出核種（放射性Cs等）を測定した。次いで試料の一部を分取して発煙硝酸処理・放射化学分離により^{90}Srを精製し、最終的に炭酸Srとして固定、低バックグラウンド2πガスフロー検出器でβ放射能を測定した。福島第一原発事故後の試料については、事故により放出された^{89}Srの影響があるため、生成固定した炭酸Sr線源のβ放射能を繰り返し測定することで、^{90}Yの放射平衡達成と^{89}Sr放射能の減衰の様子とを確認しつつ評価し、必要な場合は計算で^{89}Srの影響を除去した。フィルターサンプルの場合には8等分の短冊にし、金型と油圧プレスで成型することで試料形状を一定形状にし、Ge半導体検出器によりγ線放出核種（放射性Cs等）を測定した。

^{134}Cs/^{137}Cs放射能比は発生源の特定につながる重要なパラメーターであるが、前述の通り^{134}Cs（半減期 2.06 年）の濃度は事故直後から見て大きく低下し、より高精度での測定が必要となってきたため、その解析手法について開発検討を行った。着目した開発点は^{134}Csの補正方法である。^{134}Csはカスケードピークを持つことからサム効果による測定影響が生じる。同標準線源でピーク効率を求める際に、一般にはサム補正は不必要とされているが、本研究のフィルター試料成型では試料内での放射能分布に偏りがあることが考えられ、その際に誤差を生じると考えられる。そこで、サム効果補正が可能であるソフトウェア(P-SCAN、スカラベ・コーポレーション)を使用してサム補正を行い、補正の有無でどの程度定量に差が出るかを比較検討した。

3）結果・議論

3.1) ^{134}Cs/^{137}Cs 放射能比の分析結果

P-SCAN ではγ線スペクトルの光電ピーク面積と、それらの計数効率・全効率の間に成り立つ高次・多元連立方程式を直接解くという方法を採用し、壊変後にカスケードγ線を放出する核種については観測されるピーク数をパターン化して数式化している。ピークの測定には気象研究所の 4 台(#6、#7、#8、#10)のゲルマニウム半導体検出器を使用した。標準試料の測定は通常通り行い、次に福島第一原発事故時の放射能強度が高い環境試料を測定、サム効果補正計算を行い、そうでない場合と比較した。

大気中浮遊粒子試料の測定結果を Table1 に示す。^{137}Cs ではサム効果は見られないため、P-SCAN の使用有無による有意な違いは生じなかった。一方で ^{134}Cs では P-SCAN で得られた結果の方が数%低い結果となった。^{134}Cs/^{137}Cs 比については PSCAN を使用した場合の方がばらつきは非常に小さかった。このことから、^{134}Cs/^{137}Cs 比を測定する場合には P-SCAN を使用した方がよいと考えられるが、絶対値の正しさについては今後の検討が必要である。

Table1. Comparison when using P-SCAN and normal calculation in 4 detectors (result of measuring the same sample).

			Cs-134				Cs-137					
Detector	Sampling period	134+137 (Bq)	Normal calculation		Using P-SCAN		Normal calculation		Using P-SCAN		Normal calculation	Using P-SCAN
			mBq/m3	Err	mBq/m3	Err	mBq/m3	Err	mBq/m3	Err	134/137 ratio	134/137 ratio
#6	2011/04/11 ～04/19	898	60.1	0.4	59.0	0.4	55.2	0.1	55.3	0.1	1.09	1.07
#7			62.0	0.3	57.8	0.3	55.3	0.1	54.5	0.1	1.12	1.06
#8			61.7	0.3	58.6	0.3	55.3	0.1	54.6	0.1	1.12	1.07
#10			60.6	0.4	57.6	0.4	55.4	0.1	54.3	0.1	1.09	1.06
										σ	0.014	0.006

二種類のγ線エネルギーの 605keV/662keV 比はサムピークの比を表す。サムピークの発生確率は検出器と試料の距離に関係し、距離が離れるほどサムピークは生じにくくなる。相対距離 0cm から 5cm ごとに距離を離してサム効果の比率を求めた結果を Fig. 1 に示す。また、サムピークの代表値として 1400keV/605keV 比を求めた結果を Fig. 2 に示す。

605keV/662keV 比より、15cm 以上、検出器と試料の距離を保てば光電ピーク比が安定することが分かった。また、1400keV/605keV 比から 15cm 以上離せばサムピークの影響が無視できることが分かった。

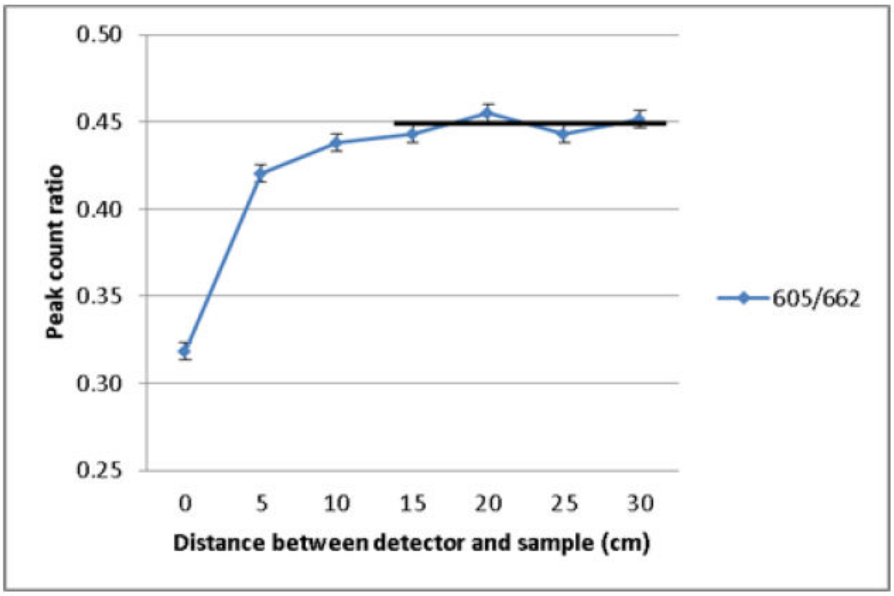

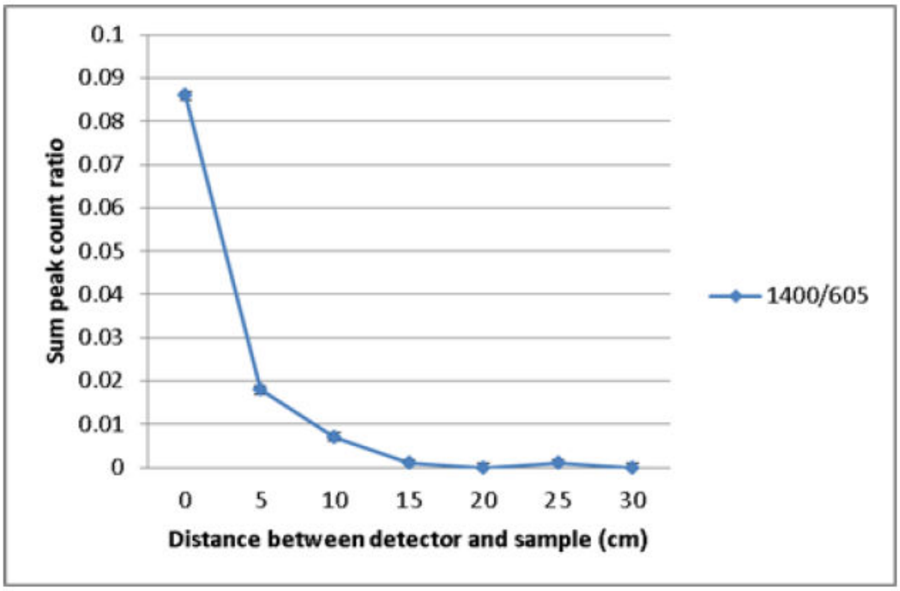

3.2) モンゴル土壌中の ^{137}Cs、およびプルトニウム、ウラン同位体の測定

モンゴル土壌中には過去に行われた核実験などにより放出された人工放射性同位体が含まれており、アジアダストのトレーサーとしてしばしば使われている。Hirose et al. (2017)の結果、モンゴル土壌中のプルトニウム同位体・ウラン同位体比を始めて明らかにした。ここで得られたプルトニウム同位体比は、大気降下物として測定される核実験により放出された放射性核種（グローバル・フォールアウト）の同位体比と一致しており、モンゴル土壌中の人工放射性核種がグローバル・フォールアウトに起因するものだということが分かった。^{137}Cs とも関係性が見られ、つくば土壌でも同じように関係性が見られることが分かったが、その傾きは大きく異なった。その原因は放射性核種それぞれの物理的・化学的な移動過程の違いによるものと考えられる。

3.3) 福島第一原発事故に起因する放射性セシウムとバイオエアロゾル

Igarashi et al. (2019) および Kinase et al. (2018) では 2011 年 7 月～2015 年 3 月までに福島県の浪江町・川俣町にて採取した大気中粒子試料の ^{134}Cs,^{137}Cs を測定し、その季節変化を明らかにした(Fig. 3)。その結果、つくばで観測される大気中放射性セシウムの季節変化とは明らかに異なることが分かり、5–6 月、および 8–9 月に極大となる二山ピークを持つことが分かった。これは、過去における研究で明らかにされてきた再飛散プロセスと、福島高濃度汚染地域における主要な再飛散プロセスが異なっていることを示唆する結果である。

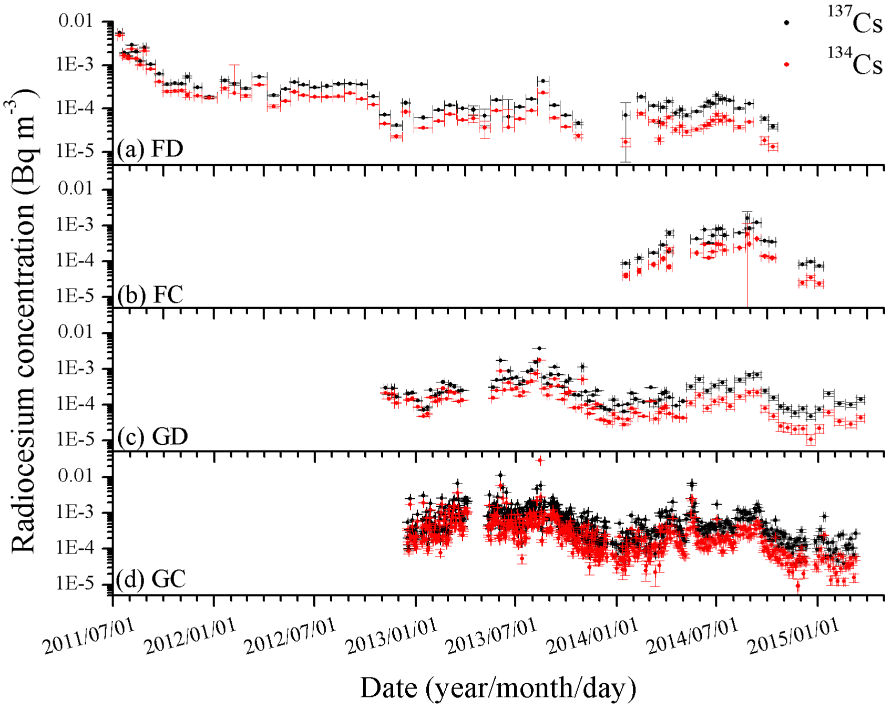

Fig. 3. Activity concentrations of ^{134,137}Cs (Bq m^{-3}) measured at the FD, FC, GD, and GC sites in the Fukushima prefecture in July 2011 to March 2015. These results show high concentrations in late spring, summer, and early autumn and low concentrations in winter and early spring at all of the presented observation locations.

気象研究所内の走査型電子顕微鏡(SEM)及び EDX によるフィルター試料の観察結果より、大気中放射性セシウム濃度の上昇がみられる試料には、胞子や菌類などのバイオエアロゾルが多く見つかることが分かった（Fig.　4）。

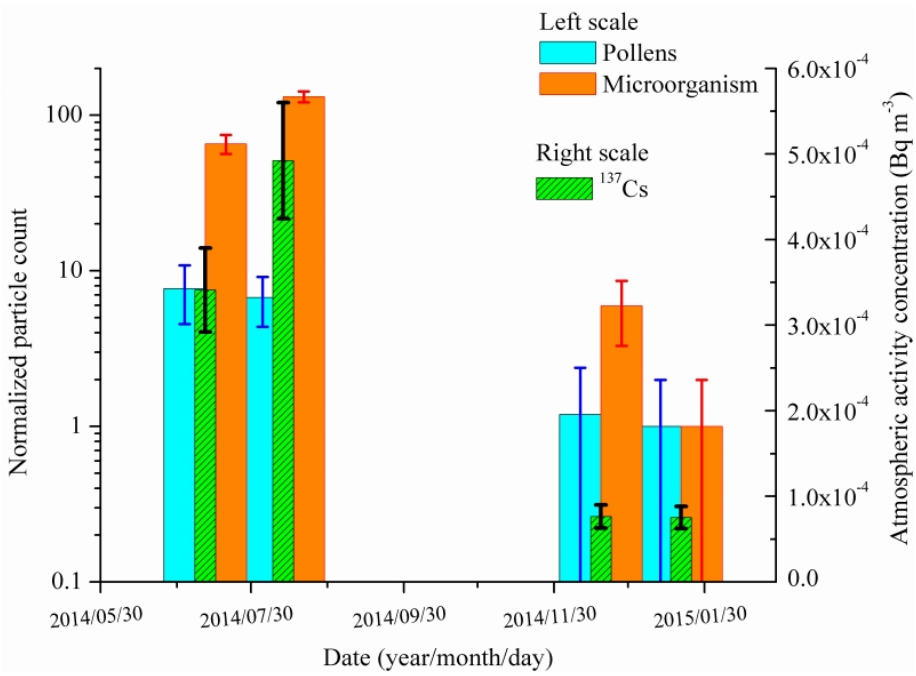

The normalized particle counts of the bioaerosols using SEM (in relative values, the error bar shows the Poisson standard deviation) and atmospheric concentrations of ^{137}Cs activity sampled at the GD site during summer (July and August 2014) and winter (December 2014 and January 2015). The counts of microorganisms include those of spores (see the text).

上記結果を踏まえ、Igarashi et al. (2019)では SEM-EDX 分析に加え、DAPI 染色による蛍光顕微鏡による観察(Fig.　5)、メタゲノム解析によるバイオエアロゾル種の解析を行った(Fig. 6)。その結果、大気中放射性セシウム濃度とバイオエアゾルの大気中濃度には相関がみられ(Fig.　7)、バイオエアロゾルの 1/3～半数が担子菌及び子嚢菌だということが分かった。

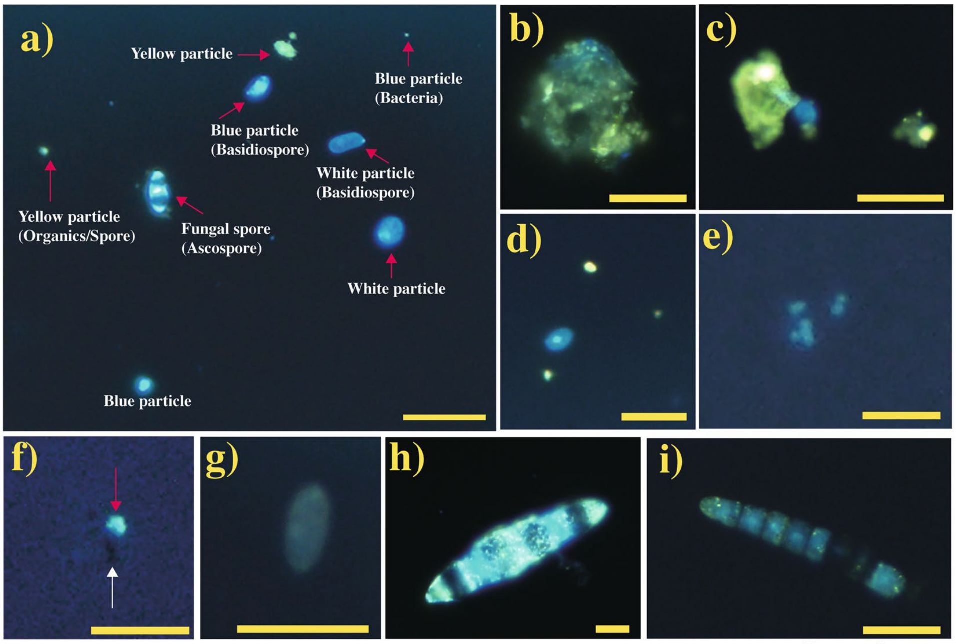

Bar = 5 μm

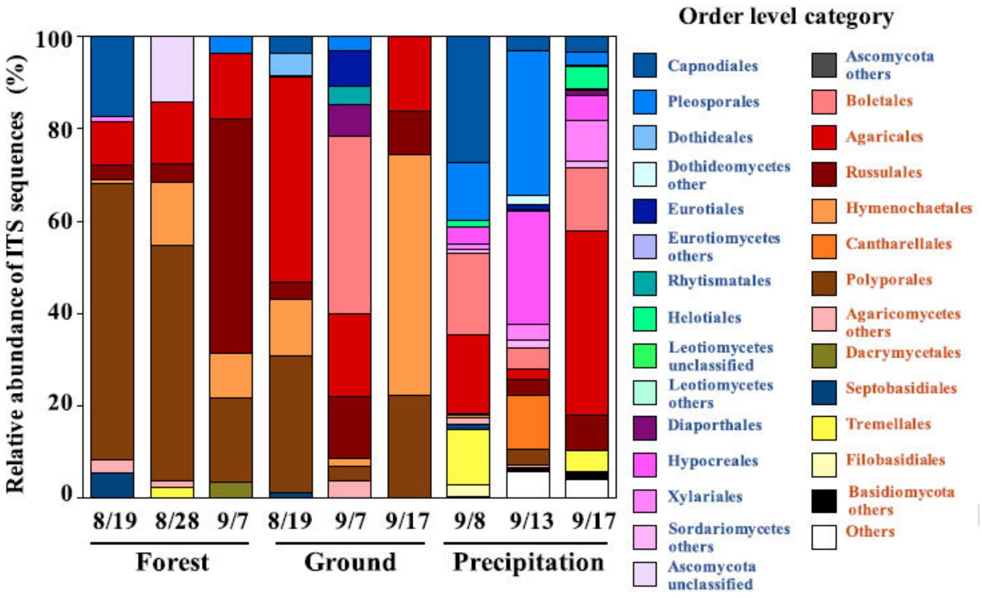

Fig. 6. Results of the metagenomic analysis showing the relative abundance of identified fungal taxa in the samples collected at the forested and bare soil sites in Namie and contained in rain water collected at the site during summer 2015. Sampling dates are expressed as mm/dd. The compositional differences among sampling dates may reflect seasonal and weather differences.

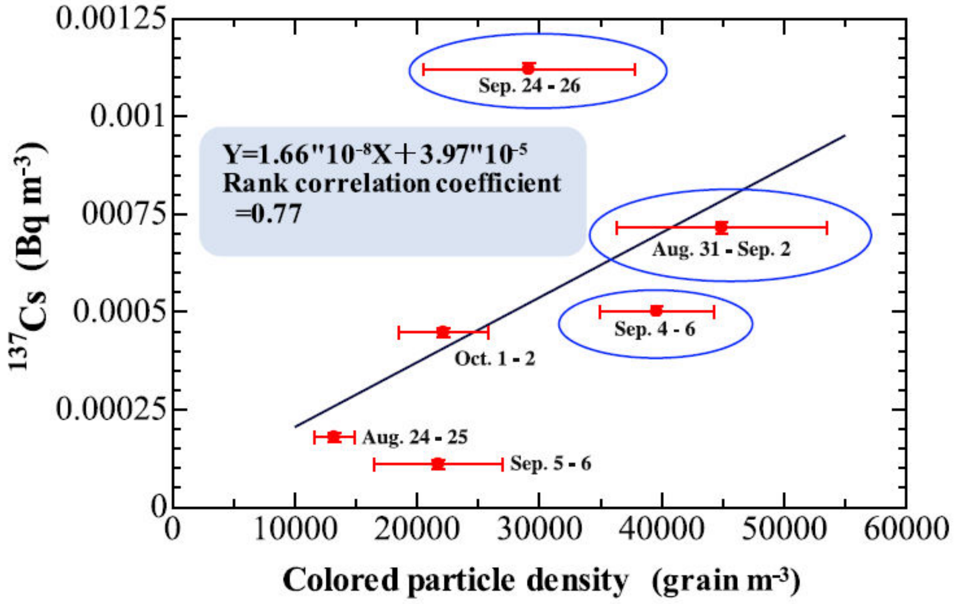

3.4)　福島第一原発事故に起因する河川及び地下水中の水溶性放射性セシウム

Iwagami et al. (2017)では、福島県山木屋地区で河川水および地下水中の水溶性放射性セシウムの長期的観測を実施した。その結果、チェルノブイリ事故と比較して河川・地下水の汚染は低く、その汚染低下のプロセスには二つあることが分かった。まず一つ目のプロセスは、大量の雨による表層土ごと洗い流す過程であり、事故後初期の段階で周辺の水中放射性セシウムを急激に低下させた。もう一つのプロセスは、土壌中への放射性セシウムの浸透と固定化による、水中放射性セシウム濃度低下の鈍化であり、事故後しばらくたってからの影響として現在も観測されている。この研究により、河川水及び二地点での地下水について環境中での半減期が明らかとなり、それぞれ 0.69–1.5 y、0.46–0.58y、0.50–3.3y となった（Fig.　8）。河川水中の ^{137}Cs の減少傾向はキャノピーに見られる放射性セシウムの脱離傾向と似ていることが分かった。

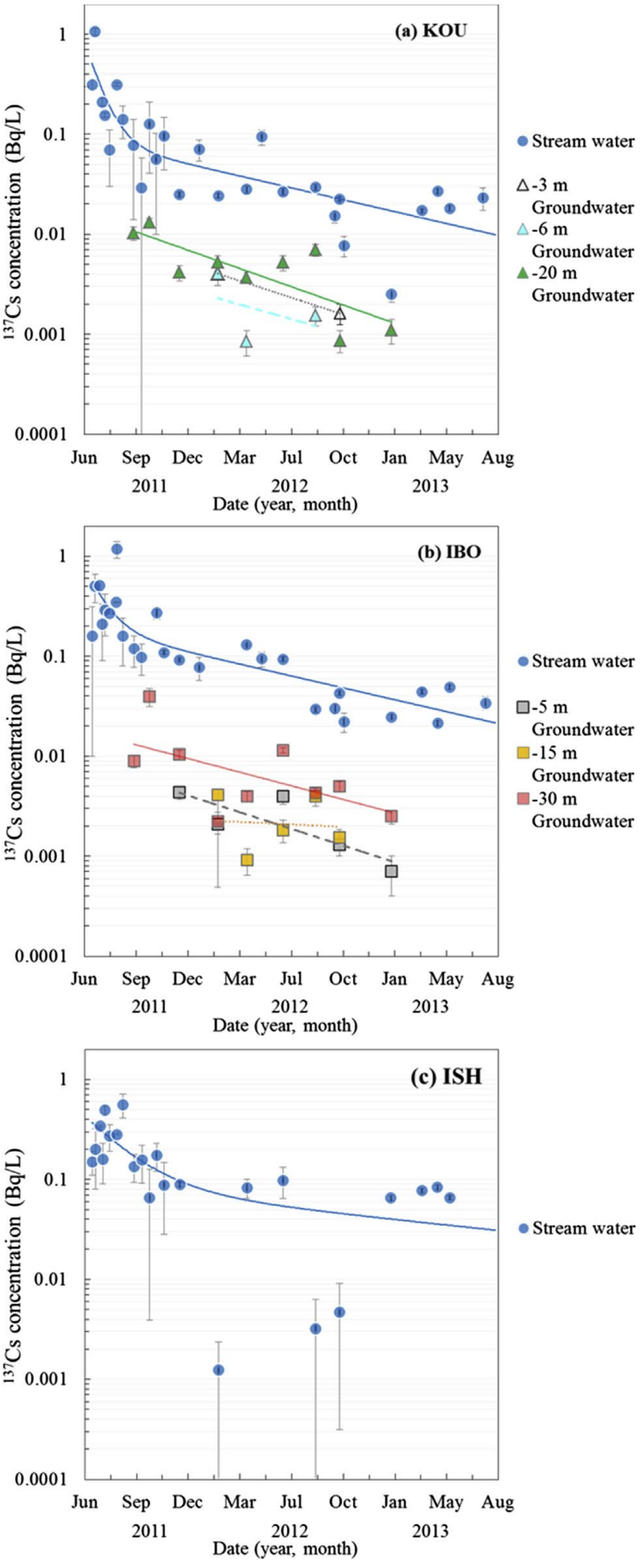
(a) KOU
(b) IBO
(c) ISH
^{137}Cs concentration (Bq/L)
1
0.1
0.01
0.001
0.0001
Jun
Sep
Dec
Mar
Jul
Oct
Jan
May
Aug
2011
2012
2013
Date (year, month)
Stream water
-3 m Groundwater
-6 m Groundwater
-20 m Groundwater
-5 m Groundwater
-15 m Groundwater
-30 m Groundwater

4）まとめと今後に向けて

本研究所における、より高精度な測定に向けた ^{134}Cs 測定方法開発、モンゴル土壌における人工放射能の観測、福島第一原発事故後の大気中人工放射能観測の結果と他地域には見られない新しい再飛散プロセスの提案、水中に溶存する放射性セシウムの環境中における動態の傾向について報告した。前報にあるように、事故後 7 年が経過した現時点では、福島第一原発事故直後と比較すると、つくばでの降下量は数桁も低下し、甚大な汚染というべき水準ではない。^{90}Sr については、事故以前の降下量とほぼ同じ水準に戻りつつある。しかし、本報で報告した ^{134}Cs 測定技術の改善により、今後も高精度での人工放射能観測が期待できる。また、^{137}Cs については依然として 3～4 桁より大きな値となっている。水準低下にはまだ時間がかかると考えられ、継続した観測と動態傾向の分析が肝要である。

事故直後に見られた一次放出に替わり、大気へのこれらの核種の供給を続けている過程は、いわゆる再飛散（二次放出）であり、現在はこの再飛散プロセスにより大気中・降下物中の人工放射能濃度が支配されていると考える。再飛散は周辺の環境に由来し、周辺の汚染度がつくばに比し数桁高い地域においては、大気中濃度・降下量もそれに比例し数桁高い。従って、再飛散プロセスの解明は必須な科学的課題である。

従来、汚染した地表面からの表土ダスト、汚染植生からの再浮遊、または汚染したゴミの燃焼、野焼き等による放射性物質の大気への揮散などが想定されてきた。しかし、本報で報告したように、福島原発事故により高濃度に汚染された地域では、通常の汚染地域とは異なり森林生態系からの放出、すなわちバイオエアロゾルの寄与がとても大きいと分かってきた。特にキノコに由来する胞子や担子菌・子嚢菌が放射性セシウムの担体として重要と考えられるが、まだ定量的には解明できていない。今後は、バイオエアロゾル観測の定量化と、継続的な連続観測を実施することで定量的な理解を得ていくことが肝要である。そのためには、森林内での各高度や樹間密度ごとのバイオエアロゾル放出量（フラックス）を定量的に観測する必要があり、顕微鏡と目視による粒子同定だけでなく、リアルタイムで測定可能な手法の開発が望まれる。

上記に加えて、こうした長期の観測においては分析やデータの品質管理が必ず問題となる。このような点についても常に留意しながら、観測の継続を図っていくことが肝要である。

参考文献

Hirose, K., Kikawada, Y., Igarashi, Y., Fujiwara, H., Jugder, D., Matsumoto, Y., Oi, T., and Nomura, M. Plutonium, ^{137}Cs and uranium isotopes in Mongolian surface soils, Journal of Environmental Radioactivity, 166, 97-103, 2017. http://dx.doi.org/10.1016/j.jenvrad.2016.01.007

Igarashi, Y., Kita., K., Maki, T., Kinase, T., Hyashi, N., Hotaka, K., Adachi, K., Kajino, M., Ishizuka, M., Sekiyama, T., T., Zaizen, Y., Takenaka, C., Ninomiya, K., Okochi, H., and Sorimachi, A. Fungal spore involvement in the resuspension of radiocaesium in summer, Scientific Reports, 9:1-10, 2019. 2019. DOI:10.1038/s41598-018-37698-x

Iwagami, S., Tsujimura, M., Onda, Y., Nishino, M., Konuma, R., Abe, Y., Hada, M., Pun, I., Sakaguchi, , A., Kondo, H., Yamamoto, M., Miyata, Y., and Igarashi, Y. Temporal changes in dissolved ^{137}Cs concentrations in groundwater and stream water in Fukushima after the Fukushima Dai-ichi Nuclear Power Plant accident. Journal of Environmental Radioactivity, 166, 458-465, 2017. http://dx.doi.org/10.1016/j.jenvrad.2015.03.025

木村徹,五十嵐康人,財前裕二,「ガンマ線スペクトル解析ソフト P-SCAN を用いた高精度な 134Cs/137Cs 放射能比の導出」Proceedings of the 18th Workshop Environmental Radioactivity. KEK Proceedings 2017

Kinase, T., K, Kita, Igarashi, Y., Adachi, K., Ninomiya, K., Shinohara, A., Okochi, H., Ogata, H., Ishizuka, M., Toyoda, S., YamadaN, K., Yoshida, N., Zaizen, Y., Mikami, M., Demizu, H., and Onda, Y. The seasonal variations of atmospheric ^{134,137}Cs activity and possible host particles for their resuspension in the contaminated areas of Tsushima and Yamakiya, Fukushima, Japan, Progress in Earth and Planetary Science 5:12, 2018. https://doi.org/10.1186/s40645-018-0171-z

2. 大気中の放射性物質の物理・化学性状

1）はじめに

大気中で観測される放射性物質は、ガスや粒子（エアロゾル）として大気中に漂い、やがて雨による除去や重力沈降によって地上や海水面に降下する。このような大気中での放射性物質の振る舞いはその放射能や核種に依存せず、物理的な粒径や密度、形態、また水溶性などの化学性質に依存する。そのため、放射性物質の大気拡散や環境動態、また発生メカニズムを理解するには、放射性物質がどのような物理化学性状を持ち、またどのようなエアロゾルを担体としているかを解明する必要がある。本章では、その放射性物質の物理化学性状の理解を目指した例として、東日本大震災で発生した福島第一原子力発電所事故によって直接放出された放射性物質に関する研究成果を報告する。

2011 年 3 月に発生した事故によって様々な放射性物質が大気・海洋に放出されたが、放出された放射性物質の重量は非常に微量であり、放射能測定以外の分析手法で環境試料から検出することは一般には困難とされてきた。しかしながら、電子顕微鏡や放射光分析などの微小領域化学分析を用いることで、放射性物質の物理化学特性を明らかにすることが可能であることが気象研究所の研究によって明らかになってきた。本研究においては、それらの手法を用いて 2011 年 3 月 14-15 日につくば市で採取されたフィルター試料中の放射性粒子の特定を行った先駆的な研究（Adachi et al., 2013）を発端として、多くの研究事例が報告されている。ここでは、それらの研究例のうち、前回の報告書から後に発表された小野ら（2017）や Satou (2016,2018)の論文、またこれらの研究例をまとめた総説論文（足立、2017）を紹介する。

2）主な研究成果

東日本大震災で発生した福島第一原子力発電所事故によって直接放出された放射性物質は、本放射能調査研究費研究でモニタリングを継続していた気象研究所におけるフィルター試料から発見された（Adachi et al., 2013）。この研究では、走査型電子顕微鏡（SEM-EDS）を用いて 2011 年 3 月 14－15 日にかけてつくばに飛来した放射性粒子を分析し、その物理化学性状を初めて明らかにした。その結果、セシウム、鉄、亜鉛や多くの核燃料由来と考えられる元素を含み、水に溶けにくい２マイクロメートル前後の球状ガラス様粒子であることが明らかとなった。これらの詳細な物理特性は、事故時における粒子の拡散モデルの精度向上に重要であることを、モデル比較実験で明らかにした。その後、Abe et al. (2014）や Yamaguchi et al. (2016)によって、粒子のさらに詳細な微量成分や内部構造が明らかとなった。これらの先駆的な研究を受けて、本研究期間ではエアロゾル試料やその大気中微粒子が沈着した結果生じた表層土壌汚染地域からの試料を採取して、そこにふくまれる放射性粒子を単離して、電子顕微鏡や放射光分析を用いてその個別粒子の物理化学性状を明らかにし、また少なくとも 2 種類の異なった物理化学性質を持つ放射性粒子が存在することを明らかにした。

Satou et al (2016)では、事故があった原子力発電所から20ｋｍほど離れた地点の土壌から、６㎛ほどの放射性粒子を新たに開発し手法で単離し、それらがエアロゾル試料で見つかった粒子と似た、ケイ素、鉄、亜鉛、セシウムなどを含む化学組成をしていることが分かった。これらの粒子は大気中のエアロゾル試料に見つかった粒子よりも大きく、また放射能強度も強い特徴を持ち、近隣地域にはより大きな粒子が重力沈降で沈着した可能性を示唆した。

小野ら（2017）の論文では、さらに土壌試料中に比放射能（単位質量あたりの放射能）はエアロゾルから分離された粒子より低いものの、大きさが 100µm ほどの放射性粒子を発見し、放射光分析でその詳細な化学成分を明らかにした。これらの大きな粒子は、球状粒子が複数溶融したような形態をしており、ケイ素を主成分とする特徴を示し、また 20 元素以上の様々な微量成分が検出された。これらの粒子は、Adachi et al (2013)で見つかった粒子と異なる物理化学性質を持っており、異なった放出プロセスがあったことを示唆する。Satou et al (2018)では、それらの粒子のセシウム 134、137 の比が異なることを見つけて、その同位体比の違った粒子のうち比放射能が高く、数 μ 程度で比較的球状に近い粒子を A タイプとし、比放射能は低いものの大きな粒子を B タイプとして分類した。

足立（2017）の論文ではこれらの成果をまとめて、今後の研究の発展に資するデータのまとめを行った。その一例の表を下記に示す。

Table 1 Summary of insoluble radioactive particles from nine studies

References	Sampling place	Sample type	Diameter (μm) of spherical particles	Diameter (μm) of non-spherical particles	Radioactivity (Bq) of ^{137}Cs	Particle number
Adachi et al (2013)	Ibaraki	Aerosol filter	2.0-2.6		3.3-0.7	3
Abe et al (2014)	Ibaraki	Aerosol filter	1.4-2.8		1.1-1.5	3
Yamaguchi et al. (2016)	Fukushima	Non-woven fabric cloth & Cedar	2.2-2.5		3.1-5.0	2
Satou et al., (2016)	Fukushima	Soil	3.0-4.0	4.5-6.4	5-67	4
Kogure et al. (2016)	Fukushima	Non-woven fabric cloth & Wheat	0.8-2.7		1.9-3.3	3
Furuki et al (2017)	Fukushima	Soil & Gravel	2.0-3.3	3.4	0.9-11.3	3
Yamaguchi et al. (2017)	Fukushima	Aerosol filter & Plant tissue		1.4-3.6	0.5-1.9	4
Ono et al. (2017)	Fukushima	Soil	2.6-3.6	50-250	33-109	7
Higaki et al. (2017)	Fukushima	Mask	2.1	6.6-12	1-70	4

足立（2017）エアロゾル研究 32 巻 4 号より。

3）まとめ

本放射能調査費によって行われた研究成果により、福島第一原子力発電所事故において放出された放射性物質の大気中の物理化学特性の一部が明らかとなった。これらの研究をもとに、今後事故から放出された放射性物質の発生源メカニズムの解明や環境動態の予測への貢献が期待される。

参考文献

Y. Satou, K. Sueki, K. Sasa, H. Yoshikawa, S. Nakama, H. Minowa, Y. Abe, I. Nakai, T. Ono, K. Adachi and Y. Igarashi, Analysis of two forms of radioactive particles emitted during the early stages of the Fukushima Dai-ichi Nuclear Power Station accident, Geochemical Journal, Vol. 52, 2018、

足立光司、原子力発電所事故で放出された不溶性放射性粒子の形態と組成、エアロゾル研究 32-4, 255-260, 2017

小野貴大, 飯澤勇信, 阿部善也, 中井 泉, 寺田靖子, 佐藤志彦, 末木啓介, 足立光司, 五十嵐康人、福島第一原子力発電所事故により 1 号機から放出された放射性粒子の 放射光マイクロビーム X 線分析を用いる化学性状の解明、分析化学 66（4） 2017

Y. Satou, K. Sueki, K. Sasa, K. Adachi, Y. Igarashi, First successful isolation of radioactive particles from soil near the Fukushima Daiichi Nuclear Power Plant, Anthropocene, Volume 14, Pages 71-76, 2016 Abe, Y., Iizawa, Y., Terada, Y., Adachi, K., Igarashi, Y., and Nakai, I., Detection of uranium and chemical state analysis of individual radioactive microparticles emitted from the Fukushima nuclear accident using multiple synchrotron radiation X-ray analyses, Analytical Chemistry, 86, 8521-8525, 2014.

Adachi, K., Kajino, M., Zaizen, Y., and Igarashi, Y., Emission of spherical cesium-bearing particles from an early stage of the Fukushima nuclear accident, Scientific Reports, 3, 2554, 2013.

Yamaguchi, N., Mitome, M., Kotone, A. H., Asano, M., Adachi, K., and Kogure, T., Internal structure of cesium-bearing radioactive microparticles released from Fukushima nuclear power plant. Scientific Reports, 6, 20548, 2016.

3. 放射性物質の再浮遊、輸送、沈着モデルによる評価

1） 福島原子力事故後の放射性セシウム大気濃度の長期評価：裸地と森林生態系からの再飛散

福島原子力事故による汚染土壌や森林からの ^{137}Cs 再飛散の長期的影響を、汚染地域（福島県浪江町）の土壌からの再飛散実験結果，および汚染地域内（浪江）・外（茨城県つくば市）の大気濃度測定，および数値シミュレーションを併用して実施した（Kajino et al., 2016）。評価期間は 2013 年の 1 年間である。推定された再飛散率は約 10^{-6}/day であり、福島県におけるガンマ線線量率の減少率（10^{-4}-10^{-3}/day）よりも明らかに低かった．すなわち，再飛散は陸上の放射能の減少にはほとんど寄与していなかったことが分かる。再飛散メカニズムは、特に森林生態系に関しては，未知のままである。今後は，メカニズム解明の実験研究に基づいた影響評価を行っていく必要がある。

Fig. 1 に計算された 2013 年の 1 年間の再飛散量と、再沈着量を示す。領域・時間積算再飛散量は、初期の沈着量 2.68 PBq（NRA, 2012）の 0.048%に相当した。

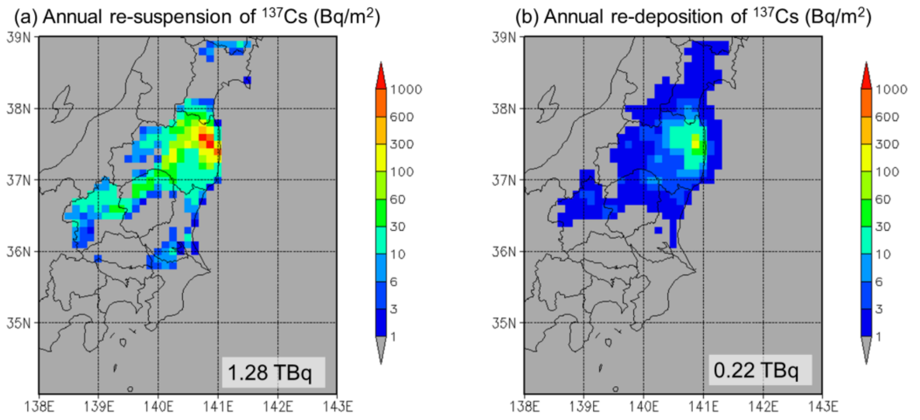

Fig. 1. Annual total amounts of (a) the re-suspension and (b) the re-deposition of ^{137}Cs. The total activities are presented as numbers.

2） 福島原発事故時の地上プリューム移流予測に及ぼす地上風データ同化の影響

2011 年 3 月の福島原発事故で排出された放射性セシウムを大気トレーサーとして用い、対流圏下層のプルーム移流の予測可能性と AMeDAS 地上風データ同化の影響を調べた（Sekiyama et al., 2017）。気象庁非静力学モデルと局所アンサンブルカルマンフィルタ（JMANHM-LETKF）データ同化システムを用いて、実験を行った。40 の観測地点における、放射性セシウムのプルーム到着時間について調べたところ、標準実験（標準的な観測データのみ同化）のプルーム到着時間の平均誤差は 82.0 分であった。それに対して、AMeDAS 実験（標準的な観測データと AMeDAS 地上風観測の両方を同化する）の平均誤差は 72.8 分であり、これは標準実験に比べて 9.2 分（11%）高精度であった。本研究は、プルーム予測モデルが緊急時対応のために十分な精度を有し、予測結果が地上風データ同化によって著しく改善され得ることを示すものである。

Fig. 2 に、埼玉県久喜市において観測された大気濃度（SPM テープ：浮遊粒子状物質観測用フィルタ上の ^{137}Cs 濃度、Tsuruta et al., 2014; Oura et al., 2015）と、データ同化前後の計算結果の比較を示す。データ同化を行っていないものを STD Exp.（実線）、地上風データ同化を行ったものを AMeDAS Exp.（破線）としている。プリュームの到達時間に明らかな改善が見られている。

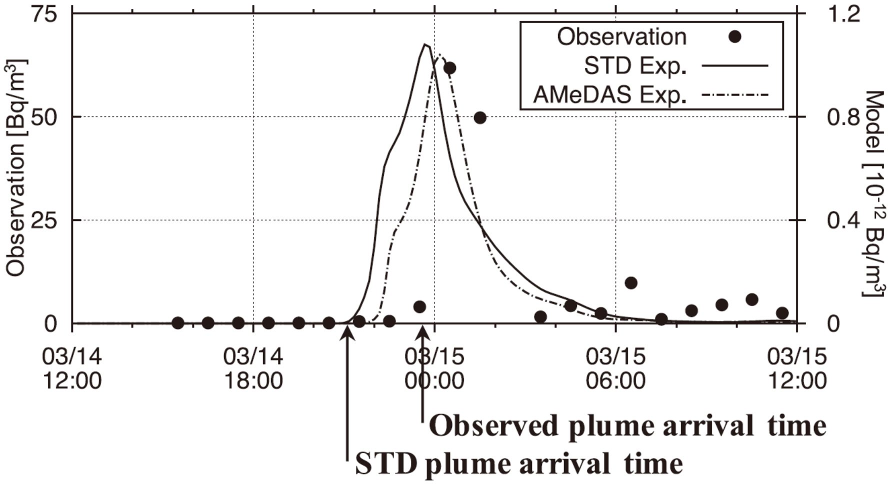

Fig. 2 An example of time series of the radioactive cesium (^{137}Cs) concentrations derived from the SPM-tape sampling observations and two model experiments (STD and AMeDAS) from 12:00 UTC on March 14 to 12:00 UTC on March 15, 2011. The advection of the plumes was examined using the data from Kuki City, Saitama Prefecture.

3） 福島原子力事故後の大気モデリング研究から学んだ教訓：アンサンブルシミュレーション、データ同化、素過程モデリング、逆解析

福島第一原子力発電所事故に伴う放射性セシウムの大気拡散と沈着に関するモデリング研究について、フランス放射線防護・原子力安全研究所と気象庁気象研究所の共同研究に着目しながら、レビューを行った（Kajino et al., 2018）。これまでのモデル研究により、湿性沈着過程が重要なプロセスであることが判明しているが、その影響の大きさは不明のままである。また、モデルによって計算結果が大きく異なることが判明しているが、その原因は定かではない。本共同研究では、大気素過程、特に湿性沈着過程の理解のために、アンサンブルシミュレーション、データ同化、素過程モデリング、逆解析などのさまざまな数値技術を使用して、シミュレーションの各要素の不確実性を定量化することを目指した。本論文では、これらの共同研究の成果を紹介するとともに、今後の大気モデル研究の将来の方向性についても議論した。

4） 福島第一原子力発電所から放出された ^{137}Cs プルームの質量フラックス解析

Sekiyama and Iwasaki (2018) では、^{137}Cs プルームの質量フラックス解析を行い、2011 年 3 月に福島第一原子力発電所から放出された ^{137}Cs のプルームについて質量フラックスの流れを定量的に示すことができた。この ^{137}Cs のプルームは 3km の水平分解能を持つオイラー型の大気移流拡散モデルによって計算した。鉛直積分した質量フラックスは ^{137}Cs 濃度の地上観測値に基づく移流経路推定とほぼ一致していたが、地上とプルーム層との間に風速シアーがある場合には不一致が生じた。この不一致は、地表面の水平質量フラックスと鉛直積分した質量フラックスの二つを組み合わせることによって理解できる（Fig. 3 参照）。質量密度と風速の積である質量フラックスの概念は気象力学においては一般的であるが、大気汚染の研究においてはほとんど使用されてこなかった。しかし質量フラックス解析は、数値モデルが計算する 4 次元（x,y,z,t）の出力値を 2 次元（x,y）プロットに縮小することによって、大気微量成分の主要な流れの位置、方向、および沈着の振る舞いを明瞭にすることができるため定量的な可視化ツールとして最適である。本研究では、大気中の放射性物質（この場合は ^{137}Cs）の移流拡散を調べることによって、大気汚染の研究においても質量フラックス解析が非常に有用な手法であることを示すことができた。

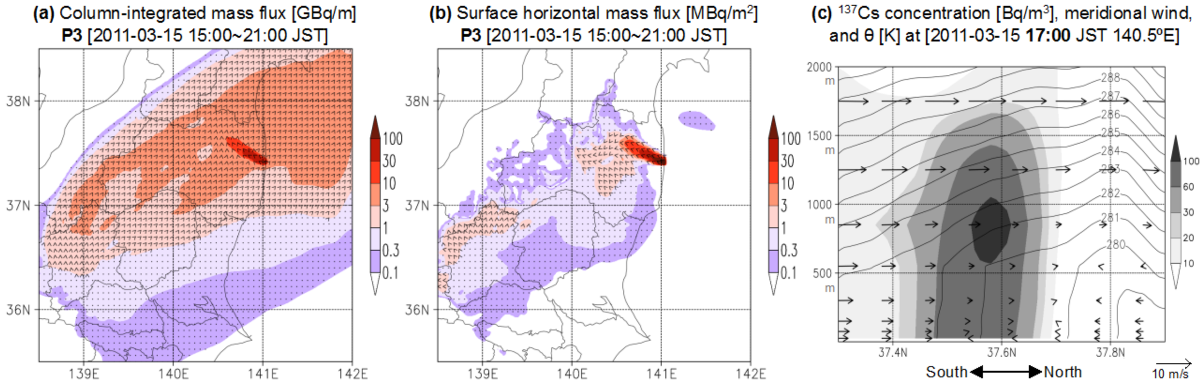

Fig. 3 Time-integrals from 15:00 to 21:00 JST on 15 March 2011 of (a) the column-integrated mass flux of plume P3 and (b) the horizontal mass flux of plume P3 at the ground surface. Color shading indicates the magnitude of the mass flux. Small arrowheads indicate the direction of the mass flux. A large gray arrow illustrates the depiction in Nakajima et al. (2017) for plume P3 at 18:00 JST on March 15, shown in Fig. 2. (c) Latitude-altitude cross-sections at 140.5E for 137Cs concentrations (gray shading), meridional winds (arrows), and potential temperature (h; contours) at 17:00 JST on 15 March 2011. The cross-section is located at the green line in panel (b).

参考文献

Kajino, M., M. Ishizuka, Y. Igarashi, K. Kita, C. Yoshikawa, M. Inatsu. Long-term assessment of airborne radiocesium after the Fukushima nuclear accident: Re-suspension from bare soil and forest ecosystems, *Atmos. Chem. Phys.*, 16, 13149-13172, doi:10.5194/acp-16-13149-2016, 2016.

Kajino, M., T. T. Sekiyama, A. Mathieu, I. Korsakissok, R. Périllat, D. Quélo, A. Quérel, O. Saunier, K. Adachi, S. Girard, T. Maki, K. Yumimoto, D. Didier, O. Masson, Y. Igarashi, Lessons learned from atmospheric modeling studies after the Fukushima nuclear accident: Ensemble simulations, data assimilation, elemental process modeling, and inverse modeling, *Geochemical Journal* 52(2), 85-101, doi:10.2343/geochemj.2.0503, 2018.

Nakajima. T., S. Misawa, Y. Morino, H. Tsuruta, D. Goto, and co-authors. Model depiction of the atmospheric flows of radioactive cesium emitted from the Fukushima Daiichi Nuclear Power Station accident. *Prog. Earth Planet. Sci.* 4:2, DOI:10.1186/s40645-017-0117-x, 2017.

NRA (Nuclear Regulation Authority), Airborne Monitoring Results in each prefecture, available at http://radioactivity.nsr.go.jp/en/list/203/list-1.html, 2012. (last access: 21 January 2019)

Oura, Y., M. Ebihara, H. Tsuruta, T. Nakajima, T. Ohara, M. Ishimoto, H. Sawahata, Y. Katsumura, W. Nitta. A database of hourly atmospheric concentration of radiocesium (134Cs and 137Cs) in suspended particulate matter collected in March 2011 at 99 air pollution monitoring stations in Eastern Japan. *J. Nucl. Radiochem. Sci.*, 15(2), 15-26, 2015.

Sekiyama, T. T., M. Kajino, M. Kunii. The impact of surface wind data assimilation on the predictability of near-surface plume advection in the case of the Fukushima Nuclear Accident, *J. Meteor. Soc. Japan*, 95(6), 447-454, doi:10.2151/jmsj.2017-025, 2017.

Sekiyama, T. T. and T. Iwasaki: Mass flux analysis of ^{137}Cs plumes emitted from the Fukushima Daiichi Nuclear Power Plant, *Tellus B*, 70(1), 1–11, doi:10.1080/16000889.2018.1507390, 2018.

Tsuruta, H., Y. Oura, M. Ebihara, T. Ohara, T. Nakajima. First retrieval of hourly atmospheric radionuclides just after the Fukushima accident by analyzing filter-tapes of operational air pollution monitoring stations. *Sci. Rep.*, 4, 6717, doi:10.1038/srep06717, 2014.

4. Publications 2016-2018

出版論文 2016-2018

5. Publication list 1954-2018

論文リスト（英文誌）1954-2018

2018

1. Hirose, K., Kikawada, Y., Igarashi, Y., Fujiwara, H., Jugder, D., Matsumoto, Y., Oi, T., and Nomura, M. Plutonium, ^{137}Cs and uranium isotopes in Mongolian surface soils, Journal of Environmental Radioactivity, 166, 97-103, 2017. http://dx.doi.org/10.1016/j.jenvrad.2016.01.007
2. Igarashi, Y., Kita., K., Maki, T., Kinase, T., Hyashi, N., Hotaka, K., Adachi, K., Kajino, M., Ishizuka, M., Sekiyama, T., T., Zaizen, Y., Takenaka, C., Ninomiya, K., Okochi, H., and Sorimachi, A. Fungal spore involvement in the resuspension of radiocaesium in summer, Scientific Reports, 9:1-10, 2019. 2019. DOI:10.1038/s41598-018-37698-x
3. Iwagami, S., Tsujimura, M., Onda, Y., Nishino, M., Konuma, R., Abe, Y., Hada, M., Pun, I., Sakaguchi, , A., Kondo, H., Yamamoto, M., Miyata, Y., and Igarashi, Y. Temporal changes in dissolved ^{137}Cs concentrations in groundwater and stream water in Fukushima after the Fukushima Dai-ichi Nuclear Power Plant accident. Journal of Environmental Radioactivity, 166, 458-465, 2017. http://dx.doi.org/10.1016/j.jenvrad.2015.03.025
4. Kajino, M.., Sekiyama, T. T., Mathieu, A,. Korsakissok, I., Périllat, R., Quélo, D., Quérel, A., Saunier, O., Adachi, K., Girard, S., Maki, T., Yumimoto, K., Didier, D., Masson, O., and Igarashi, Y., Lessons learned from atmospheric modeling studies after the Fukushima nuclear accident: Ensemble simulations, data assimilation, elemental process modeling, and inverse modeling, Geochemical Journal, Vol. 52, 2018.
5. Kinase, T., Kita, K., Igarashi, I., Adachi, K., Ninomiya, K., Shinohara, A., Okochi, H., Ogata, H., Ishizuka, M., Toyoda, S., Yamada, K., Yoshida, N., Zaizen, Y., Mikami, M,. Demizu, H., and Onda, Y., The seasonal variations of atmospheric 134,137Cs activity and possible host particles for their resuspension in the contaminated areas of Tsushima and Yamakiya, Fukushima, Japan, Progress in Earth and Planetary Science, 5:12, 2018.
6. Satou, Y., Sueki, K., Sasa, K., Yoshikawa, H., Nakama, S., Minowa, H., Abe, Y., Nakai, I., Ono, T., Adachi, K., and Igarashi, Y., Analysis of two forms of radioactive particles emitted during the early stages of the Fukushima Dai-ichi Nuclear Power Station accident, Geochemical Journal, Vol. 52, 137-143, 2018. doi:10.2343/geochemj.2.0514.
7. Sekiyama, T. T. and T. Iwasaki, Mass flux analysis of ^{137}Cs plumes emitted from the Fukushima Daiichi Nuclear Power Plant, Tellus B, 70(1), 1–11, doi:10.1080/16000889.2018.1507390, 2018.

2017

1. Iwagami, S., Tsujimura, M., Onda, Y., Nishino, M., Konuma, R., Abe, Y., Hada, M., Pun, I., Sakaguchi, A., Kondo, H., Yamamoto, M., Miyata, Y., and Igarashi, Y., Temporal changes in dissolved ^{137}Cs concentrations in groundwater and stream water in Fukushima after the Fukushima Dai-ichi Nuclear Power Plant accident, Journal of Environmental Radioactivity,166, 458-465, 2017.
2. Hirose, K., Kikawada, Y., Igarashi, Y., Fujiwara, H., Jugder, D., Matsumoto, Y., Oi, T., Nomura, M., Plutonium, ^{137}Cs and uranium isotopes in Mongolian surface soils, Journal of Environmental Radioactivity, 166, 97-103, 2017.
3. Sekiyama, T. T., Kajino, M., and Kunii, K., The Impact of Surface Wind Data Assimilation on the Predictability of Near-Surface Plume Advection in the Case of the Fukushima Nuclear Accident, Journal of the Meteorological Society of Japan, Vol. 95, 447-454, 2017. doi: 10.2151/jmsj.2017-025.

2016

1. Kajino, M., Ishizuka, M., Igarashi, Y., Kita, K., Yoshikawa, C., and Inatsu, M., Long-term assessment of airborne radiocerium after the Fukushima nuclear accident: re-suspension from bare soil and forest ecosystems, Atmos. Chem. Phys, 16, 13149-13172, 2016.
2. Satou,Y., Sueki, K., Sasa, K., Adachi, K., and Igarashi, Y., First successful isolation of radioactive particles from soil near the Fukushima Daiichi Nuclear Power Plant, Anthropocene, 14, 71-76, 2016.
3. Yamaguchi, N., Mitome, M., Kotone, A-H., Asano, M., Adachi, K., and Kogure, T., Internal structure of cesium-bearing radioactive microparticles released from Fukushima nuclear power plant. Scientific Reports. 6, 20548, 2016.

2015

1. Igarashi, Y., Kajino, M., Zaizen, Y., Adachi, K., and Mikami, M., Atmospheric radioactivity over Tsukuba, Japan: a summary of three years of observations after the FDNPP accident, Progress in Earth and Planetary Science 2:44, 2015. doi: 10.1186/s40645-015-0066-1.
2. Kajino, M., G-3. NHM-Chem: Sensitivity of Cs deposition to the size and hygroscopicity of Cs-bearing aerosols, Technical Reports of the Meteorological Research Institute, 76, 132–142, 2015.
3. Sekiyama, T. T., Kunii, M., Kajino, M., and Shinbori, T., Horizontal Resolution Dependence of Atmospheric Simulations of the Fukushima Nuclear Accident Using 15-km, 3-km, and 500-m Grid Models, J. Meteorol. Soc. Jpn., 93B, 49–64, 2015.

2014

1. Abe, Y., Iizawa, Y., Terada, Y., Adachi, K., Igarashi, Y., and Nakai, I., Detection of uranium and chemical state analysis of individual radioactive microparticles emitted from the Fukushima nuclear accident using multiple synchrotron radiation X-ray analyses, Analytical Chemistry, 86, 8521-8525, 2014.

2013

1. Aoyama, M., Uematsu, M., Tsumune, D., and Hamajima, Y., Surface pathway of radioactive plume of TEPCO Fukushima NPP1 released ^{134}Cs and ^{137}Cs, Biogeosciences, 10, 3067-3078, 2013. doi: 10.5194/bg-10-3067-2013.
2. Tsumune, D., Tsubono, T., Aoyama, M., Uematsu, M., Misumi, K., Maeda, Y., Yoshida, Y., and Hayami, H., One-year, regional-scale simulation of ^{137}Cs radioactivity in the ocean following the Fukushima Daiichi Nuclear Power Plant accident, Biogeosciences, 10, 5601-5617, 2013.
3. Povinec, P.P., Aoyama, M., Biddulph, D., Breier, R., Buesseler, K., Chang, C., Golser, R., Hou, X., Ješkovský, M., and Jull, A., Cesium, iodine and tritium in NW Pacific waters-a comparison of the Fukushima impact with global fallout. Biogeosciences, 10, 5481-5496. 2013.
4. Kumamoto, Y., Murata, A., Kawano, T., and Aoyama, M., Fukushima-derived radiocesium in the northwestern Pacific Ocean in February 2012, Applied Radiation and Isotopes, 81, 335-339, 2013. doi: 10.1016/j.apradiso.2013.03.085.
5. Toyama, C., Muramatsu, Y., Igarashi, Y., and Aoyama, M., Atmospheric fallout of ^{129}I in Japan before the Fukushima accident: Regional and global contributions, 1963-2005, Environmental Science & Technology, 47(15), 8383-8390, 2013. doi: 10.1021/es401596z.
6. Adachi, K., Kajino, M., Zaizen, Y., and Igarashi, Y., Emission of spherical cesium-bearing particles from an early stage of the Fukushima nuclear accident. Scientific Reports, 3, Article number 2554, 2013. doi:10.1038/srep02554.

2012

1. Toyama, C., Muramatsu, Y., Uchida, Y., Igarashi, Y., Aoyama, M., and Matsuzaki, H., Variations of ^{129}I in the atmospheric fallout of Tokyo, Japan 1963-2003, Journal of Environmental Radioactivity, 113, 116-122, 2012. doi: 10.1016/j.jenvrad.2012.04.014.
2. Inomata, Y., Aoyama, M., Tsumune, D., Motoi, T., and Nakano, H., Optimum interpolation analysis of basin-scale ^{137}Cs transport in surface seawater in the North Pacific Ocean, Journal of Environmental Monitoring, 14, 3146-3155, 2012. doi: 10.1039/C2EM30707C.
3. Aoyama, M., Tsumune, D., Uematsu, M., Kondo, F., and Hamajima, Y., Temporal variation of ^{134}Cs and ^{137}Cs activities in surface water at stations along the coastline near the Fukushima Dai-ichi Nuclear Power Plant accident site, Japan. Geochem. J, 46, 321-325, 2012.
4. Aoyama, M., Tsumune, D., and Hamajima, Y., Distribution of ^{137}Cs and ^{134}Cs in the North Pacific Ocean: impacts of the TEPCO Fukushima-Daiichi NPP accident, Journal of Radioanalytical and Nuclear Chemistry, 1-5, 2012. doi: 10.1007/s10967-012-2033-2.
5. Honda, M. C., Aono, T., Aoyama, M., Hamajima, Y., Kawakami, H., Kitamura, M., Masumoto, Y., Miyazawa, Y., Takigawa, M., and Saino, T., Dispersion of artificial caesium-134 and-137 in the western North Pacific one month after the Fukushima accident, Geochem. J, 46, e1-e9, 2012.
6. Povinec, P. P., Hirose, K., and Aoyama, M., Radiostrontium in the Western North Pacific: characteristics, behavior, and the Fukushima impact, Environmental Science & Technology, 46, 10356-10363, 2012. doi: 10.1021/es301997c.
7. Tsumune, D., Tsubono, T., Aoyama, M., and Hirose, K., Distribution of oceanic ^{137}Cs from the Fukushima Dai-ichi Nuclear Power Plant simulated numerically by a regional ocean model, Journal of Environmental Radioactivity, 111, 100-108, 2012.

2011

1. Aoyama, M., Fukasawa, M., Hirose, K., Hamajima, Y., Kawano, T., Povinec, P.P., and Sanchez-Cabeza, J. A., Cross Equator transport of ^{137}Cs from North Pacific Ocean to South Pacific Ocean, BEAGLE2003 cruises, Progress in Oceanography, 89, 7-16, 2011. doi:10.1016/j.pocean.2010.12.003.
2. Buesseler, K., Aoyama, M., and Fukasawa, M., Impacts of the Fukushima nuclear power plants on marine radioactivity. Environmental Science & Technology, 45(23), 9931-9935, 2011. doi: 10.1021/es202816c.
3. Povinec, P. P., Aoyama, M., Fukasawa, M., Hirose, K., Komura, K., Sanchez-Cabeza, J.A., Gastaud, J., Jeskovsky, M., Levy, I., and Sykora, I., ^{137}Cs water profiles in the South Indian Ocean - an evidence for accumulation of pollutants in the subtropical gyre. Progress in Oceanography, 89 , 17-30, 2011. doi:10.1016/j.pocean.2010.12.004.
4. Gastaud, J., Povinec, P.P., Aoyama, M., Hirose, K., Sanchez-Cabeza, J.A., Levy, I., Roos, P., Eriksson, M., Bosc, E. and Rezzoug, S., Transport and scavenging of Pu in surface waters of the Southern Hemisphere Oceans, Progress in Oceanography, 89, 92-100, 2011. doi:10.1016/j.pocean.2010.12.009.
5. Hirose, K., Kim, C.S., Yim, S.A., Aoyama, M., Fukasawa, M., Komura, K., Povinec, P.P., and Sanchez-Cabeza, J.A., Vertical profiles of plutonium in the central South Pacific, Progress in Oceanography, 89, 101-107, 2011. doi:10.1016/j.pocean.2010.12.010.
6. Tsumune, D., Aoyama, M., Hirose, K., Bryan, F., Lindsay, K. and Danabasoglu, G., Transport of ^{137}Cs to the Southern Hemisphere in an Ocean General Circulation Model, Progress in Oceanography, 89, 38-48, 2011. doi:10.1016/j.pocean.2010.12.006.
7. Sanchez-Cabeza, J.A., Levy, I., Gastaud, J., Eriksson, M., Osvath, I., Aoyama, M., Povinec, P.P. and Komura, K., Transport of North Pacific ^{137}Cs labeled waters to the south-eastern Atlantic Ocean. Progress in Oceanography, 89, 31-37, 2011. doi:10.1016/j.pocean.2010.12.005.
8. Levy, I., Povinec, P.P., Aoyama, M., Hirose, K., Sanchez-Cabeza, J.A., Comanducci, J-F., Gastaud, J., Eriksson, M., Hamajima, Y., Kim, C.S., Komura, K., Osvath, I., Roos, P. and Yim, S.A., Marine anthropogenic radiotracers in the Southern Hemisphere: new sampling and analytical strategies, Progress in Oceanography, 89, 120-133, 2011. doi:10.1016/j.pocean.2010.12.012.

2010

1. Inomata,Y., Igarashi, Y., Yoshioka, K., Tanaka, T. Y., and M, Chiba., Temporal variation of ^{222}Rn at the summit of Mt. Fuji associated with the Asian continental outflow, Atmospheric Environment, 44,3856-3865, 2010.
2. Nakano, H., Motoi, T., Hirose, K., and Aoyama, M., Analysis of ^{137}Cs concentration in the Pacific using a Lagrangian approach. Journal of Geophysical Research, 115, C06015, 2010. doi:10.1029/2009JC005640.
3. Hirose, K., Igarashi, Y., Aoyama, M., and Inomata, Y., Depositional behaviors of plutonium and thorium isotopes at Tsukuba and Mt. Haruna in Japan indicate the sources of atmospheric dust. Journal of Environmental Radioactivity, 101,106-112, 2010.
4. Zhang, Y., Zeng, J., Yamada, M., Wu, F., Igarashi, Y., and Hirose, K., Characterization of Pu concentration and its isotopic composition in a reference fallout material. Science of the Total Environment, 408(5), 1139-1144, 2010.

2009

1. Aoyama, M., Hamajima, Y., Fukasawa, M., Kawano, T., and Watanabe, S., Ultra low level deep water ^{137}Cs activity in the South Pacific Ocean, Journal of Radioanalytical and Nuclear Chemistry, 2009. doi:10.1007/s10967-009-0253-x.
2. Hirose, K., Aoyama, M., and Povinec, P.P., ^{239,240}Pu /^{137}Cs ratios in the water column of the North Pacific: a proxy of biogeochemical processes, Journal of Environmental Radioactivity, 100, 258-262, 2009.
3. Igarashi, Y., Inomata, Y., Aoyama, M., Hirose, K., Takahashi, H., Shinoda, Y., Sugimoto, N., Shimizu, A., and Chiba, M., Possible change in Asian dust source suggested by atmospheric anthropogenic radionuclides during the 2000s, Atmospheric Environment, 43, 2971-2980, 2009.

4. Inomata, Y., Aoyama, M., and Hirose, K., Analysis of 50-y record of surface ^{137}Cs concentrations in the global ocean using the HAM-global database, Journal of Environmental Monitoring, 11(1), 116-125, 2009. doi: 10.1039/b811421h.
5. Hirose, K., Igarashi, Y., Aoyama, M., and Inomata, Y., Depositional behaviors of plutonium and thorium isotopes at Tsukuba and Mt.Haruna in Japan indicate the sources of atmospheric dust, Journal of Environmental Radioactivity, 101(2), 106-112, 2009. doi:10.1016/j.jenvrad.2009.09.003.
6. Igarashi Y., Kikawada, Y., Oda, K., Yamauchi, R., Nomura, M., Honda, T., Oi, T., and Hirose, K., Anomalous Uranium Isotope Ratio in Atmospheric Deposits in Japan, Journal of Nuclear Science and Technology, 46(12), 1094-1098. 2009.

2008

1. Aoyama, M., Hirose, K., Nemoto, K., Takatsuki, Y., and Tsumune, D., Water masses labeled with global fallout ^{137}Cs formed by subduction in the North Pacific, Geophysical Research Letters, 35, L01604, 2008. doi:10.1029/2007GL031964.
2. Hirose, K., Igarashi, Y., and Aoyama, M., Analysis of the 50-year records of the atmospheric deposition of long-loved radionuclides in Japan, Applied Radiation and Isotopes, 66, 1675-1678, 2008.
3. Hirose, K., Aoyama, M., Igarashi, Y., and Komura, K., Improvement of ^{137}Cs analysis in small volume seawater samples using the Ogoya underground facility, Journal of Radioanalytical and Nuclear Chemistry, 276,3,795-798, 2008.
4. Aoyama, M., Hirose, K., Nemoto, K., Takatsuki, Y., and Tsumune, D., Water masses labeled with global fallout ^{137}Cs formed by subduction in the North Pacific, Geophysical Research Letters, 35, L01604, 2008. doi:10.1029/2007GL031964.

2007

1. Hirose, K., Aoyama, M., and Kim, C.S., Plutonium in Seawater of the Pacific Ocean, Journal of Radioanalytical and Nuclear Chemistry, 274 No. 3, 635-638, 2007.
2. Hirose, K., Igarashi, Y., and Aoyama, M., 50 years records of atmospheric deposition of long-lived anthropogenic radionuclides in Japan, International Conference on Environmental Radioactivity: From Measurements and Assessments to Regulation, IAEA-CN-145, 95-96, 2007.
3. Hirose, K., Igarashi, Y., and Aoyama, M., Recent trends of plutonium fallout observed in Japan: Comparison with natural lithogenic radionuclides, thorium isotopes, Journal of Radioanalytical and Nuclear Chemistry, 273 No.1, 115-118, 2007.
4. Hirose, K., Aoyama, M., Fukasawa, M., Kim, C. S., Komura, K., Povinec, P. P., and Sanchez-Cabeza, J. A., Plutonium and ^{137}Cs in surface water of the South Pacific Ocean, Science of the Total Environment, 381, 243-255, 2007.

2006

1. Yamamoto, M., Sakaguchi, A., Sasaki, K., Hirose, K., Igarashi, Y., and Kim, C.K., Seasonal and spatial variation of atmospheric ^{210}Pb and ^{7}Be deposition: features of the Japan Sea side of Japan, Journal of Environmental Radioactivity, 86, 110-131, 2006.
2. Hirose, K., Aoyama, M., Kim, C.S., Kim, C.K., and Povinec, P.P., Plutonium isotopes in seawater of the North Pacific: effects of close-in fallout, INTERNATIONAL CONFERENCE ON ISOTOPES AND ENVIRONMENTAL STUDIES. Eds. P. Povinec, J.A. Sanchez-Cabeza. Vol. 8 of Radioactivity in the Environment, Elsevier, London, 2006.
3. Aoyama, M., Hirose, K., and Igarashi, Y., Re-construction and updating our understanding on the global weapons tests ^{137}Cs fallout, Journal of Environmental Monitoring, 8, 431-438, 2006.
4. Aoyama, M., Fukasawa, M., Hirose, K., Mantoura, R.F.C., Povinec, P.P., Kim, C.S., and Komura, K., Southern Hemisphere Ocean Tracer Study (SHOTS): An overview and preliminary results, INTERNATIONAL CONFERENCE ON ISOTOPES AND ENVIRONMENTAL STUDIES. Eds. P. Povinec, J.A. Sanchez-Cabeza, Vol. 8 of Radioactivity in the Environment, Elsevier, London, 2006.

5. Inoue, H.Y., Matsueda, H., Igarashi, Y., Sawa, Y., Wada, A., Nemoto, K., Sartorius, H., and Schlosser, C., Seasonal and long-term variations in atmospheric CO_2 and ^{85}Kr in Tsukuba, Central Japan, Journal of the Meteorological Society of Japan, 84/6, 959-968, 2006.

2005

1. Hirose, K., Aoyama, M., Igarashi, Y., and Komura, K., Extremely low background measurements of ^{137}Cs in seawater samples using an underground facility (Ogoya), Journal of Radioanalytical and Nuclear Chemistry, 263, 349-353, 2005.
2. Povinec, P.P., Aarkrog, A., Buesseler, K.O., Delfanti, R., Hirose, K., Hong, G.H., Ito, T., Livingston, H.D., Nies, H., Noshkin, V.E., Shima, S., and Togawa, O., ^{90}Sr, ^{137}Cs and ^{239,240}Pu concentration surface water time series in the Pacific and Indian Oceans- WOMARS results, Journal of Environmental Radioactivity, 81, 63-87, 2005.
3. Igarashi, Y., Aoyama, M., Hirose, K., Povinec, P.P., and Yabuki, S., What anthropogenic radionuclides (^{90}Sr and ^{137}Cs) in atmospheric deposition, surface soils and Aeoliandusts suggest for dust transport over JAPAN, Water, Air, and Soil Pollution: Focus, 5, 51-69, 2005.

2004

1. Hirose, K., Kim, C.K., Kim, C.S., Chang, B.W., Igarashi, Y., and Aoyama, M., Wet and dry depositions of plutonium in Daejeon, Korea, The Science of the Total Environment, 332, 243-252, 2004.
2. Povinec, P.P., Hirose, K., Honda, T., Ito, T., MarianScott, E., and Togawa, O., Spatial distribution of ^{3}H, ^{90}Sr, ^{137}Cs and ^{239,240}Pu in surface waters of the Pacific and Indian Oceans - GLOMARD database, Journal of Environmental Radioactivity, 76, 113-137, 2004.
3. Aoyama, M., and Hirose, K., Artificial Radionuclides database in the Pacific Ocean: Ham database, TheScientificWorldJOURNAL, 4, 200-215, 2004.
4. Hirota, M., Nemoto, K., Wada, A., Igarashi, Y., Aoyama, M., Matsueda, H., Hirose, K., Sartorius, H., Schlosser, C., Schmid, S., Weiss, W., and Fujii, K., Spatial and Temporal Variations of Atmospheric ^{85}Kr Observed During 1995-2001 in Japan: Estimation of Atmospheric ^{85}Kr inventory in the Northern Hemisphere, Journal of Radiation Research, 45, 405-413, 2004.
5. Hirose, K., Chemical Speciation of Thorium in Marine Biogenic Particulate matter, The Scientific World JOURNAL 4, 67-76, 2004.

2003

1. Hirose, K., and Aoyama, M., Analysis of ^{137}Cs and ^{239,240}Pu concentrations in surface waters of the Pacific Ocean, Deep-Sea Research II, 50, 2675-2700, 2003.
2. Hirose, K., Aoyama, and Povinec, P.P., Concentration of particulate plutonium in surface and deep-water, samples collected during the IAEA'97 expedition, Deep-Sea Research II, 50, 2639-2647, 2003.
3. Povinec, P.P., Livingston, H.D., Shima, S., Aoyama, M., Gastaud, J., Goroncy, I., Hirose, K., Huynh-Ngoc, L., Ikeuchi, Y., Ito, T., Rosa, J.L., Kwong, L.L.W., Lee, S.H., Moriya, H., Mulsow, S., Oregioni, B., Pettersson, H., and Togawa, O., IAEA'97 expedition to the NW Pacific Ocean-Results of oceanographic and radionuclide investigations of the water column, Deep-Sea Research II, 50,2607-2637, 2003.
4. Ito, T., Povinec, P.P., Togawa, O., and Hirose, K., Temporal and Spatial variation of anthropogenic radionuclides in seawater of the Japan Sea, Deep-Sea Research II, 50, 2701-2711, 2003.
5. Tsumune, D., Aoyama, M., and Hirose, K., Behavior of ^{137}Cs and concentrations in the North Pacific in an ocean general circulation model, Journal of Geophysical Research, 108, C8, 3262, 2003.
6. Hirose, K., and Aoyama, M., Present Background Levels of Surface ^{137}Cs and ^{239,240}Pu Concentrations in the Pacific, Journal of Environmental Radioactivity, 69(1-2), 53-60, 2003.
7. Tsumune, D., M. Aoyama, and K. Hirose, Numerical simulation of ^{137}Cs and ^{239,240}Pu concentrations by an ocean general circulation model, Journal of Environmental Radioactivity, 69(1-2), 61-84, 2003.

8. Aoyama, M., and Hirose, K., Temporal variation of ^{137}Cs water column inventory in the North Pacific since the 1960s, Journal of Environmental Radioactivity, 69(1-2),107-117, 2003.
9. Hirose, K., Igarashi, Y., Aoyama, M., Kim, C.K., Kim, C.S., Chang, B.W., Recent trends of plutonium fallout observed in Japan: plutonium as a proxy for desertification, J. Environ. Monit, 5, 302-307, 2003.
10. Igarashi, Y., Aoyama, M., Hirose, K., Miyao, T., Nemoto, K., Tomita, M., and Fujikawa, T., Resuspension: Decadal Monitoring Time Series of the Anthropogenic Radioactivity Deposition in Japan, Journal of Radiation Research, 44, 319-328, 2003.
11. Kim, C.K., Kim, C.S., Chang, B.U., Choi, S.W., Chung, C.S., Hong, G.H., Hirose, K., and Igarashi, Y., Plutonium isotopes in seas around the Korean Peninsula, The Science of the Total Environment, 318, 197-209, 2003.
12. Kim, C.K., Kim, C.S., Chang, B.U., Choi, S.W., Chung, C.S., Hong, G.H., Hirose, K., and Pettersson, H.B.L., ^{240}Pu /^{239}Pu atom ratios in the bottom sediments of the NW Pacific Ocean, Journal of Radioanalytical and Nuclear Chemistry, 258(2), 265-268, 2003.
13. Lee, H.N., Tanaka, T., Chiba, M., and Igarashi, Y., Long range transport of Asian dust from dust storms and its impact on Japan, Water, Air, and Soil Pollution, 3, 231-243, 2003
14. Hirose, K., Implication of POC/^{234}Th ratios in oceanic particulate matter: an approach to particle aggregation, Papers of Meteorology and Geophysics, 53, 4, 109-118, 2003.

2002

1. Hirose, K., Miyao, T., Aoyama, M., and Igarashi, Y., Plutonium isotopes in the Sea of Japan, Journal of Radioanalytical and Nuclear Chemistry, 252, 293-299, 2002.
2. Hirose, K., and Aoyama, M., Chemical speciation of plutonium in seawater, Analytical and Bioanalytical Chemistry, 372, 418-420, 2002.
3. Hong, G.H., Kim, Y.I., Lee, S.H., Cooper, L.W., Choe, S.M., Tkalin, A.V., Lee, T., Kim, S.H., Chung, C.S., and Hirose, K., $^{239+240}$Pu and ^{137}Cs concentrations for zooplankton and nekton in the Northwest Pacific and Antarctic Oceans 1993-1996, Marine Pollution Bulletin, 44, 660-665, 2002.

2001

1. Igarashi, Y., Aoyama, M., Nemoto, K., Hirose, K., Miyao, T., Fushimi, K., Suzuki, M., Yasui, S., Asai, Y., Aoki, I., Fujii, K., Yamamoto, S., Sartorius, H., and Weiss, W., ^{85}Kr measurement system for continuous monitoring at Meteorological Research Institute, Japan, Journal of Environmental Monitoring, 3, 688-696, 2001.
2. Igarashi, Y., Aoyama, M., Hirose, K., Miyao, T., and Yabuki, S., Is it Possible to use ^{90}Sr and ^{137}Cs as tracers for the aeolian transport?, Water. Air. And Soil Pollution, 130, 349-354, 2001
3. Hirose, K., Igarashi, Y., Aoyama, M., and Miyao, T., Long-term trends of plutonium fallout observed in Japan, In Plutonium in the Environment, 251-266, 2001.
4. Aoyama, M., Hirose, K., Miyao, T., Igarashi, Y., and Povinec, P.P., ^{137}Cs activity in surface water in the western North Pacific, J. Radioanal. Nucl. Chem., 248, 3, 789-793, 2001.
5. Aoyama, M., Hirose, K., Miyao, T., Igarashi, Y., and Povinec, P.P., Temporal variation of ^{137}Cs inventory in the western North Pacific, J Radioanal Nucl Chem, 248, 3, 785-787, 2001
6. Hirose, K., Aoyama, M., Miyao, T., and Igarashi, Y., Plutonium in seawaters on the western North Pacific, J Radioanal Nucl Chem, 248, 3, 771-776, 2001.
7. Tsumune. D., Aoyama, M., Hirose, K., Maruyama, K., and Nakashiki, N., Caluculation of Artificial Radionuclides in the Ocean by an Ocean General Circulation Model, J Radioanal Nucl Chem, 248, 3, 777-783, 2001.

2000

1. Shiraishi, K., Kimura, S., Yonehara, H., Takada, J., Ishikawa, M., Igarashi, Y., Aoyama, M., Komura, K., and Nakazima, T., Survey of external dose around the JCO facility using sugar samples and ESR method, Adv. ESR Appl, 16, 9-14, 2000.

2. Komura, K, Yamamoto, M., Muroyama, T., Murata, Y., Nakanishi, T., Hoshi, M., Takada, J., Ishikawa, M., Kitagawa, K., Suga, S., Endo, A., Tozaki, N., Mitsugashira, T., Hara, M., Hashimoto, T., Takano, M., Yanagawa, Y., Tsuboi, T., Ichimasa, M., Ichimasa, Y., Imura, H., Sasajima, E., Seki, R., Saito, Y., Kondo, M., Kojima, S., Muramatsu, Y., Yoshida, S., Shibata, S., Yonehara, H., Watanabe, Y., Kimura, S., Shiraishi, K., Bannai, T., Sahoo, S.K., Igarashi, Y., Aoyama, M., Hirose, K., Uehiro, M., Doi, T., and Matsuzawa, T., The JCO criticality accident at Tokai-mura, Japan: an overview of the sampling campaign and preliminary results, J. Environ. Radioactivity, 50, 3-14, 2000.
3. Igarashi, Y., Miyao, T., Aoyama, M., Hirose, K., Sartorius, H., and Weiss, W., Radioactive noble gases in the surface air monitored at MRI, Tsukuba, before and after the JCO accident, J. Environ. Radioactivity, 50, 107-118, 2000.
4. Miyao, T., Hirose, K., Aoyama, M., and Igarashi, Y., Trace of the recent deep water formation in the Japan Sea deduced from historical ^{137}Cs data, Geophys. Res. Lett., 27, 22, 3731-3734, 2000.
5. Aoyama, M., Hirose, K., Miyao, T., and Igarashi, Y., Low level ^{137}Cs measurements in deep seawater samples, Appl. Radiat. Isot, 53, 159-162, 2000.
6. Igarashi, Y., Sarutorius, H., Miyao, T., Weiss, W., Fushimi, K., Aoyama, M., Hirose, K., and Inoue, H.Y., ^{85}Kr and ^{133}Xe monitoring at MRI, Tsukuba and its importance, J. Environ. Radioactivity, 48, 191-202, 2000.

1999

1. Hirose, K., Amano, H., Baxter, M.S., Chaykovskaya, E., Chumichev, V.B., Hong, G.H., Isogai, K., Kim, C.K., Kim, S.H., Miyao, T., Morimoto. T, Nikitin, A., Oda, K., Pettersson, H.B.L., Povinec, P.P., Seto, Y., Tkalin, A., Togawa, O., and Veletova, N.K., Anthropogenic radionuclides in seawater in the East Sea/Japan Sea: Results of the first-stage Japanese-Korean-Russian expedition, J. Environ. Radioactivity, 43, 1-13, 1999.
2. Igarashi, Y., Aoyama, M., Miyao, T., Hirose, K., Komura, K., and Yamamoto, M., Air concentration of radiocaesium in Tsukuba, Japan following the release from the Tokai waste treatment plant: comparisons of observations with predictions, Applied Radiation and Isotopes, 50, 1063-1073, 1999.
3. Igarashi, Y., Aoyama, M., Miyao, T., Hirose, K., and Tomita, M., Anomalous ^{90}Sr deposition during the fall, 1995 at MRI, Tsukuba, Japan, J. Radioanal. Nucl. Chem, 239(3), 539-542, 1999.
4. Ikeuchi, Y., Amano, H., Aoyama, M., Berezhnov, V.I., Chaykovskaya, E., Chumichev, V.B., Chung, C.S., Gastaud, J., Hirose, K., Hong, G.H., Kim, C.K., Kim, S.H., Miyao, T., Morimoto, T., Nikitin, A., Oda, K., Pettersson, H.B.L., Povinec, P.P., Tkalin, A., Togawa, O., and Veletova, N.K., Anthropogenic radionuclides in seawater of the Far Eastern Seas, Sci. Total Environ., 237/238, 203-212, 1999.
5. Pettersson, H.B.L., Amano, H., Berezhnov, V.I., Chaykovskaya, E., Chumichev, V.B., Chung, C.S., Gastaud, J., Hirose, K., Hong, G.H., Kim, C. K., Lee, S.H., Morimoto, T., Nikitin, A., Oda, K., Povinec, P.P., Suzuki, E., Tkalin, A., Togawa, O., Veletova, N.K., Volkov, Y., and Yoshida, K., Anthropogenic radionuclides in sediments in the NW Pacific Ocean and its marginal seas:results of the 1994-1995 Japanese-Korean-Russian expeditions, Sci. Total Environ, 237/238, 213-224, 1999.

1998

1. Igarashi, Y., Hirose, K., and Otsuji-Hatori, M., Beryllium-7 Deposition and Its Relation to Sulfate Deposition, J. Atmos. Chem, 29, 217-231, 1998.
2. Miyao, T., Hirose, K., Aoyama, M., and Igarashi, Y., Temporal variation of ^{137}Cs and $^{239, 240}$Pu in the sea of Japan, J. Environ. Radioactivity, 40, 239-250, 1998.

1997

1. Hirose, K., Complexation-scavenging of plutonium in the ocean, Radioprotection - Colloq, 32, C2-225 - C2-230, 1997.

1996

1. Igarashi, Y., Otsuji-Hattori, M., and Hirose, K., Recent deposition of ^{90}Sr and ^{137}Cs observed in Tsukuba, J. Environ. Radioactivity, 31, 157-169, 1996.
2. Otsuji-Hatori. M., Igarashi, Y., and Hirose, K., Preparation of a Reference Fall out Material for Activity Measurements, J. Environ Radioactivity, 31, 2, 143-155, 1966.

1995

1. Aoyama, M., and Hirose, K., The temporal and spatial variation of ^{137}Cs concentration in the western North Pacific and its marginal seas during the period from 1979 to 1988, J. Environ. Radioactivity, 29, 57-74, 1995.
2. Hirose, K., Geochemical studies on the Chernobyl radioactivity in environmental samples, J. Radioanal. Nucl. Chem., Articles, 197, 315-335, 1995.

1994

1. Hirose, K., Takatani, S., and Aoyama, M., Deposition of ^{90}Sr and plutonium isotopes derived from the Chernobyl accident in Japan, J. Radioanal. Nucl. Chem., Articles, 182, 349-358, 1994.

1993

1. Hirose, K., and Sugimura, Y., Chemical speciation of particulate ^{238}U, $^{239,\,240}$Pu and Th isotopes in seawater, Sci. Total Environ., 130/131, 517-524, 1993.
2. Hirose, K., Takatani, S., and Aoyama, M., Wet deposition of radionuclides derived from the Chernobyl accident, J. Atmos. Chem., 17, 61-71, 1993.
3. Shiraishi, K., Igarashi, Y., Yamamoto, M., and Nakajima, T., Concentrations of thorium and uranium in freshwater samples collected in the former USSR, J. Radioanal. Nucl. Chem., 185,157-165, 1993.

1992

1. Aoyama, M., Hirose, K., and Takatani, S., Particle size dependent dry deposition velocity of the Chernobyl radioactivity, In Precipitation Scavenging and Atmosphere - Surface Exchange.volume 3, The 22e Summers Volume: Application and Appraisals. Coordinated by S.E. Schwartz and W.G.N. Slinn. Hemisphere Publishing Corporation, Washington, 1581-1593, 1992.
2. Hirose, K., Sugimura, Y., and Aoyama, M., Plutonium and ^{137}Cs in the western North Pacific: estimation of residence time of plutonium in surface water, Appl. Radiat. Isot, 43, 349-359, 1992.

1991

1. Aoyama, M., Hirose, K., and Sugimura, Y., The temporal variation of stratospheric fallout derived from the Chernobyl accident, J. Environ. Radioactivity, 13, 103-115, 1991.
2. Hirose, K., and Sugimura, Y., Chemical speciation of particulate uranium in seawater, J. Radioanal. Nucl. Chem., Articles, 149, 83-96, 1991.

1990

1. Hirose, K., and Sugimura, Y., Plutonium isotopes in the surface air in Japan: effect of Chernobyl accident, J. Radioanal. Nucl. Chem., Articles, 138, 127-138, 1990.
2. Hirose, K., Aoyama, M., and Sugimura, Y., Plutonium and cesium isotopes in river waters in Japan, J. Radioanal. Nucl. Chem., Articles, 141, 191-202, 1990.
3. Hirose, K., Aoyama, M., and Sugimura, Y., Short and long term effects of Chernobyl radioactivity on deposition and air concentrations in Japan, IAEA-SM 306/129, 141-149, 1990.

1988

1. Aoyama, M., Evidence of stratospheric fallout of caesium isotopes from Chernobyl accident, Geophys. Res. Lett., 15, 327-330, 1988.
2. Miyake, Y., Saruhashi, K., Sugimura, Y., Kanazawa, T., and Hirose, K., Contents of ^{137}Cs, plutonium and americium isotopes in the southern ocean waters, Pap. Met. Geophys, 39, 95-113, 1988.

1987

1. Aoyama, M., Hirose, K., and Sugimura, Y., Deposition of gamma-emitting nuclides in Japan after the reactor-IV accident at Chernobyl, J. Radioanal. Nucl. Chem., Articles, 116, 291-306, 1987.
2. Hirose, K., Aoyama, M., Katsuragi, Y., and Sugimura, Y., Annual deposition of Sr-90, Cs-137 and Pu-239, 240 from the 1961-1980 nuclear explosions: a simple model, J. Meteor. Soc. Japan, 65, 259-277, 1987.

1986

1. Aoyama, M., Hirose, K., Suzuki, Y., and Sugimura, Y., High level radioactive nuclides in Japan in May, Nature, 321, 819-820, 1986.
2. Hirose, K., Sugimura, Y., and Katsuragi, Y., ^{90}Sr and $^{239+240}$Pu in the surface air in Japan: their concentrations and size distributions, Pap. Met. Geophys, 37, 255-269, 1986.
3. Katsuragi, Y., and Aoyama, M., Seasonal variation of Sr-90 fallout in Japan through the end of 1983, Pap. Met. Geophys., 37, 15-36, 1986.
4. Suzuki, Y., Inoue, H., Katsuragi, Y., and Sugimura, Y., The distribution of 85Krin the air over the North and South Pacific Ocean Mem., Natl. Inst. Polar Res., Spec. Issue, 40, 462-466, 1986.

1985

1. Hirose, K., and Sugimura, Y., A new method of plutonium speciation in seawater, J. Radioanal. Nucl. Chem, Articles, 92, 363-369, 1985.

1984

1. Hirose, K., and Sugimura, Y., Plutonium in the surface air in Japan, Health Phys., 46, 1281-1285, 1984.
2. Inoue, H., Katsuragi, Y., and Shigehara, K., Tritiated water vapor in the surface air at Tokyo, Pap. Met. Geophys, 35, 11-20, 1984.

1983

1. Katsuragi, Y., A study of ^{90}Sr fallout in Japan, Pap. Met. Geophys., 33, 277-291, 1983.
2. Katsuragi, Y., Kawamura, K., and Inoue, H., Tritium fallout in Tokyo, Pap. Met. Geophys, 34, 21-30, 1983.

1982

1. Inoue, H., and Katsuragi, Y., A study of tritium fallout in Japan, Pap. Met. Geophys, 32, 21-28, 1982.
2. Katsuragi, Y., Hirose, K., and Sugimura, Y., A study of plutonium fallout in Japan, Pap. Met. Geophys, 33, 85-93, 1982.

1981

1. Hirose, K., and Sugimura, Y., Concentration of Uranium and the activity ratio of ^{234}U /^{238}U in surface air-effect of atmospheric burn-up of cosmos-954, Pap. Met. Geophys., 32, 317-322, 1981.
2. Hirose, K., and Sugimura, Y., Plutonium content of river water in Japan, Pap. Met. Geophys, 32, 301-305, 1981.
3. Sugimura, Y., and M. Mayeda, An improved method of analysis of uranium in sea water using chelating resin, Pap. Met. Geophys, 32, 167-171, 1981.

1980

1. Sugimura, Y., The uranium content and the activity ratio ^{234}U /^{238}U in sea water in the Pacific ocean, Isotope Marine Chemistry, 211-246, 1980.

1979

1. Sugiura, Y., Saruhashi, K., and Miyake, Y., Evaluation on the disposal of radioactive wastes into the North Pacific. - the effect of steady flow and up - welling, Proc. The 3rd NEA Seminar on Marine Radioecology, 1979.

1978

1. Miyake, Y., Nuclear weapons and radioactive pollution of the earth's environment, In, Proc. Internal Symp. On the damage and after-effects of the atomic bombing of Hiroshima and Nagasaki July 21-Aug., 9, 1977, Tokyo, 164-188, 1978.

1976

1. Miyake, Y., and Saruhashi, K., A critical study on the IAEA definition of high level radioactive waste unsuitable for dumping at sea, Pap. Met. Geophys. 27, 75-80, 1976.
2. Miyake, Y., and Saruhashi, K., Disposal of radioactive waste into deep seas, J. Radiat. Res., 17, 42-43, 1976.
3. Miyake, Y., and Sugimura, Y., The plutonium content in the Pacific Ocean waters, Proc. of Symp. on Transuranium Nuclides in the Environment, San Francisco, 17-21 Nov. 1975, USERDA and IAEA, IAEA-SM-199/22, 91-105,1976.
4. Sugimura, Y., Symposium II plutonium in environment, II-1.Distribution and behavior of plutonium in the global environments, J. Radiat. Res., 17, 4-5, 1976.
5. Sugiura, Y., Saruhashi, K., and Miyake, Y., Evaluation on the disposal of radioactive wastes into the North Pacific, Pap. Met. Geophys, 27, 81-87, 1976.

1975

1. Miyake, Y., Shimada, T., Kawamura, K., Sugimura, Y., Shigehara, K., and Saruhashi, K., Distribution of tritium in the Pacific ocean, Rec. Oceanogr. Works Japan, 13, 17, 1975.
2. Miyake, Y., Katsuragi, Y., and Sugimura, Y., Plutonium fallout in Tokyo, Pap. Met. Geophys, 26, 1-8, 1975.
3. Miyake, Y., Sugimura, Y., and Hirao, Y., Uranium, thorium and potassium contents in granitic and basaltic rocks in Japan, In, The Natural Radiation Environment II, II, Proc. 2nd Intnl. Symp. On Natural Radiation Environment, Aug. 7-11, 1972, Houston, Texas, USA, ed. J. A. S. Adams, W. M. Lowder, T. F. Gesell, 535-558,1975.
4. Saruhashi, K., I-1 The global radioactive contamination due to nuclear weapon testings, J. Radiat. Res., 16, 47, 1975.
5. Saruhashi, K., Katsuragi, Y., Kanazawa, T., Sugimura, Y., and Miyake, Y., ^{90}Sr and ^{137}Cs in the Pacific waters, Rec. Oceanogr. Works Japan, 13, 1-15, 1975.

1973

1. Miyake, Y., and Saruhashi, K., The radio-carbon model of the ocean, Pap. Met. Geophys, 24, 263-271, 1973.
2. Miyake, Y., Saruhashi, K., and Sugimura, Y., The isotopic ratio ^{234}U /^{238}U in sea water and its bearings on the isotopic ratio in river waters, Oceanogr. Works Japan, 12, 23-25, 1973.
3. Miyake, Y., Sugimura, Y., and Saruhashi, K., Content of plutonium in river water in Japan, Pap. Met. Geophys, 24, 75-78, 1973.
4. Miyake, Y., Sugimura, Y., and Yasujima, T., Thorium isotope content in river water in Japan, Pap. Met. Geophys, 24, 67-73, 1973.

1972

1. Miyake, Y., Sugimura, Y., and Uchida, T., A new method of spectrophotometric determination of uranium in sea water and uranium content with ^{234}U /^{238}U ratio in the Pacific water, Rec. Oceanogr. Works Japan, 11, 53-63, 1972.

1970

1. Miyake, Y., Katsuragi, Y., and Sugimura, Y., A study on plutonium fallout, J. Geophys. Res., 75, 2329-2330, 1970.
2. Miyake, Y., Sugimura, Y., and Mayeda, M., The uranium content and the activity ratio ^{234}U /^{238}U in marine organisms and sea water in the western North Pacific, J. Oceanogr. Soc. Japan, 26, 123-129, 1970.

1969

1. Miyake, Y., Radioactive contamination of the ocean, Bull. Jpn. Soc. Fisheries Oceanogr., Nov., 1969, 1969.

1968

1. Miyake, Y., and Sugimura, Y., Plutonium content in the western North Pacific waters, Pap. Met. Geophys, 19, 481-485, 1968.
2. Miyake, Y., Katsuragi, Y., and Sugimura, Y., Deposition of plutonium in Tokyo through the end of 1966, Pap. Met. Geophys, 19, 267-276, 1968.

1967

1. Miyake, Y., and Kanazawa, T., Atmospheric ozone and radioactive fallout, Pap. Met. Geophys., 18, 311-326, 1967.
2. Miyake, Y., Radioactive contamination of the ocean, J. Radiat. Res., 8, 1, 1967.
3. Miyake, Y., Sea, radioactivity in, International Dictionary of Geophysics, 1-7, 1967.

1966

1. Miyake, Y., and Saruhashi, K., On the radio-carbon age of the ocean waters, Pap. Met. Geophys., 17, 218-223, 1966.
2. Miyake, Y., and Sugimura, Y., Ratio $^{234}U/^{238}U$ and the uranium concentration in seawater in the western North Pacific, J. Geophys. Res., 71, 3083-3087, 1966.

1965

1. Kuroda, P. K., Miyake, Y., and Nemoto, J., Strontium isotopes Global circulation after the Chinese nuclear explosion of 14 May 1965, Science, 150, 1289-1290, 1965.
2. Miyake, Y., Saruhashi, K., Katsuragi K., and Kanazawa, T., Radioactivity of dust and rain - the ratio of Cs-137 and Sr-90 in the radioactive fallout, Proc. Internl. Conf. On Cloud Physics,Tokyo, IAMAP, 395-399, 1965.
3. Park, K., George, M.J., Miyake, Y., Saruhashi, K., Katsuragi, Y., and Kanazawa, T., Strontium-90 and caesium-137 in Columbia river plume, July 1964, Nature, 208, 1084-1085, 1965.

1964

1. Miyake, Y., and Sugimura, Y., Uranium and radium in the western North Pacific waters, Studies on Oceanography, Prof. K. Hidaka Sixtieth Birthday Commemorative Volume, Univ. of Tokyo Press, Tokyo, 274-278, 1964.
2. Miyake, Y., and Ohtsuka, Y., Beryllium-7 in rain water, Pap. Met. Geophys, 15, 89-92, 1964.
3. Miyake, Y., A sequential procedure for the radiochemical analysis of marine material, Annex to safety series 11."Method of surveying and monitoring marine radioactivity, IAEA, Vienna, 26, 1964.
4. Miyake, Y., Atomic weapons and the pollution of the sea, The East, 3, 64-68, 1964.
5. Miyake, Y., Saruhashi, K., Katsuragi, Y., Kanazawa, T., and Sugimura, Y., Uranium, radium, thorium, Ionium, strontium 90 and cesium 137 in coastal waters of Japan, In, Recent Researches in the Fields of Hydrosphere, Atmosphere and Nuclear Geochemistry, published by Editorial Committee of Sugawara Festival Volume, Maruzen Co. Ltd., 127-141, 1964.
6. Miyake, Y., Sugimura, Y., and Tsubota, H., Content of uranium, radium, and thorium in river waters in Japan, In, The Natural Radiation Environment, ed. By J. A. S. Adams and W. M. Lowder, Univ. of Chicago Press, Chicago, Rice Univ. Semicentennial Series, 219-225, 1964.
7. Sugimura, Y., Torii, T., and Murata, S., Uranium distribution in drake passage waters, Nature, 204, 464-465, 1964.

1963

1. Folsom, T.R., and Saruhashi, K., A comparison of analytical techniques used for determination of fallout cesium in sea water for oceanographic purpose, J. Radiat. Res., 4, 39-53, 1963.
2. Miyake, Y., and Tsubota, H., Estimation of the direct contribution of meteoric water to river waters by means of fall-out radio-cesium and radiostrontium, "Radioisotopes in Hydrology" Proc. IAEA Symp., Tokyo. IAEA, Vienna, 425-431, 1963.

3. Miyake, Y., Artificial radioactivity in the Pacific ocean, IUGG Monograph, 20 Radioactive traces in oceanography, 1963.
4. Miyake, Y., Saruhashi, K., Katsuragi, K., and Kanazawa, T., Deposition of Cs-137 and Sr-90 in Tokyo through the end of July 1963, Pap. Met. Geophys, 13, 180-181, 1963.
5. Miyake, Y., Saruhashi, K., Katsuragi, Y., Kanazawa, T., and Tsunogai, S., Deposition of ^{90}Sr and ^{137}Cs in Tokyo through the end of July 1963, Pap. Met. Geophys, 14, 58-65, 1963.
6. Miyake, Y., Sugiura, Y., and Tsubota, H., II. Contents of uranium, radium, and thorium in river waters in Japan, The Natural Radiation Environment, RICE Univ. semicentennial Pub, 1963.

1962

1. Miyake, Y., Saruhashi, K., Katsuragi, Y., and Kanazawa, T., Seasonal variation of radioactive fallout, J. Geophys. Res., 67, 189-193, 1962.
2. Miyake, Y., Saruhashi, K., Katsuragi, Y., and Kanazawa, T., Penetration of ^{90}Sr and ^{137}Cs in deep layers of the Pacific and vertical diffusion rate of deep water, J. Radiat. Res., 3, 141-147, 1962.
3. Miyake, Y., Saruhashi, K., Katsuragi, Y., and Kanazawa, T., The peak in radioactive fallout in the temperate zone of the northern hemisphere, J. Radiat. Res., 3,148-152, 1962.
4. Sugimura, Y., and Sugimura, T., Uranium in recent Japanese sediments, Nature, 194, 568-569, 1962.

1961

1. Miyake, Y., Saruhashi, K., Katsuragi, Y., and Kanazawa, T., Cesium 137 and strontium 90 in sea water, J. Radiat. Res., 2 25-28, 1961.
2. Miyake, Y., Saruhashi, K., Katsuragi, Y., and Kanazawa, T., Cesium 137 and strontium 90 in sea water, Pap. Met. Geophys., 12, 85-88, 1961.

1960

1. Miyake, Y., and Saruhashi, K., Vertical and horizontal mixing rates of radioactive material in the ocean, Disposal of Radioactive wastes IAEA Vienna, 167-173, 1960.
2. Miyake, Y., and Katsuragi, Y., Strontium 90 in western North Pacific surface waters, Pap. Met. Geophys., 11, 188-190, 1960.
3. Miyake, Y., Saruhashi, K., Katsuragi, Y., and Kanazawa, T., Radioactive fallout in Japan and its bearings on meteorological conditions, Pap. Met. Geophys., 11, 151-158, 1960.

1959

1. Miyake, Y., Saruhashi, K., and Katsuragi, Y., The Sr-90 fallout and the air motion, Pap. Met. Geophys., 9, 172-176, 1959.
2. Miyake, Y., Special committee on oceanic research, Working Group on Radioactivity in the Ocean, 1959.

1958

1. Miyake, Y., and Saruhashi, K., Distribution of man-made radio-activity in the North Pacific through summer 1955, J. Mar. Res., 17, 383-389, 1958.
2. Miyake, Y., and Sugiura, Y., The method of measurement of radioactivity in sea water, Pap. Met. Geophys., 9, 48-50, 1958.
3. Miyake, Y., Hazards to human health of radioactive dust, Radio Japan, 2, 3-5, 1958.
4. Miyake, Y., The distribution of artificial radioactivity in the equatorial region in the Pacific in the summer of 1956, The Proc. 9th Pacific Science Congress, 16, 227, 1958.

1957

1. Miyake, Y., and Saruhashi, K., The world-wide strontium 90 deposition during the period from 1951 to the fall of 1955, Pap. Met. Geophys., 8, 241-243, 1957.
2. Miyake, Y., The biological effects of nuclear tests - warning by Japanese scientists, Radio Japan, 1, 3-5, 1957.

3. Miyake, Y., XI. Methods for the measurement of radioactivity in sea water, Annuals of International Geophysical Year, 5, 1957.
4. Miyake, Y., XII. Radioactivity as a tracer of air motions in the atmosphere, Symp. On radioactivity, IGY, Utrecht, 360, 1957.
5. Miyake, Y., Sugiura, Y., Saruhashi, K., and Kanazawa, T., The estimation of the amount of Sr-90 deposition and the external infinite gamma does in Japan due to man-made radioactivity, Pap. Met. Geophys., 8, 222-231, 1957.

1956

1. Miyake, Y., On the distribution of radioactivity in the North Pacific ocean in 1954-1955, Internl. Conf. For Peaceful Uses of Atomic Energy in Geneva, August 1955, 13, pp.381-384, 1956.
2. Miyake, Y., Radioactivity in rain water and air, Proc. Internl. Conf. For Peaceful Uses of Atomic Energy in Geneva, August 1955, 13, 345-349, 1956.
3. Sugiura, Y., and Kanazawa, T., On the radioactive fallout collected in Tokyo on 26th November, 1955, Pap. Met. Geophys., 7, 128-135, 1956.

1955

1. Miyake, Y., and Sugiura, Y., Radiochemical analysis of radio-nuclides in sea water collected near BIKINI atoll, Pap. Met. Geophys., 6, 90-92, 1955.
2. Miyake, Y., Effects of atomic explosions on the atmosphere and sea, The research in the effects and influences of the nuclear bomb text explosions, 1-6, 1955.
3. Miyake, Y., Kigoshi, K., and Saruhashi, K., Radiochemical analysis of fission products contained in the soil collected at Tokyo, May, 1954, Pap. Met. Geophys., 6, 1, 93-94, 1955.
4. Miyake, Y., The artificial radioactivity in rain water observed in Japan, 1954-1955, Research in the Effects and Influences of the Nuclear Bomb Test Explosions Science, 151-159, 1955.
5. Miyake, Y., The artificial radioactivity in rain water observed in Japan, from autumn 1954 to spring 1955, Pap. Met. Geophys., 6, 26-32, 1955.
6. Miyake, Y., Sugiura, Y., and Kameda, K., On the artificial radioactivity in the sea near Japan, Pap. Met. Geophys., 6, 90-92, 1955.
7. Miyake, Y., Sugiura, Y., and Kameda, K., On the distribution of radioactivity in the sea around Bikini atoll in June, 1954, Pap. Met. Geophys., 5, 253-262, 1955.
8. Miyake, Y., Sugiura, Y., and Kameda, K., Research in the effects and influence of the nuclear bomb test explosions, Soc. For Promotion of Science, 415-417, 1955.

1954

1. Miyake, Y., Kigoshi, K., Sugiura, Y., and Saruhashi, K., A study on the productivity in coastal waters by means of the radio-carbon, Pap. Met. Geophys., 5, 89-94, 1954.
2. Miyake, Y., The artificial radioactivity in rain water observed in Japan from May to August, 1954, Pap. Met. Geophys, 5, 173-177, 1954.

6. Publication list (in Japanese) 1954-2018

論文リスト（和文誌）1954-2018

2017

1. 足立光司, 福島原子力発電所事故で放出された不溶性放射性粒子の形態と組成, エアロゾル研究, 32-4,255–260, 2017.
2. 五十嵐康人, 放射性物質の大気沈着・拡散および陸域からの再浮遊について, Proceedings of the 17th Workshop Environmental Radioactivity. KEK Proceedings, 2017-6, 50-55, 2017.
3. 小野貴大, 飯澤勇信, 阿部善也, 中井 泉, 寺田康子, 佐藤志彦, 末木啓介, 足立光司, 五十嵐康人, 福島第一原子力発電所事故により 1 号機から放出された放射性粒子の放射光マイクロビーム X 線分析を用いる化学性状の解明, 分析化学 66（4）, 2017.
4. 梶野瑞王, 大気エアロゾルの環境動態シミュレーション,安全工学, 57-6, 433-441, 2018
5. 木村徹, 五十嵐康人, 財前祐二, ガンマ線スペクトル解析ソフト P-SCAN を用いた高精度な Cs^{134}/Cs^{137} 放射能比の導出, Proceedings of the 17th Workshop Environmental Radioactivity. KEK Proceedings, 2017-6, 262-266, 2017.

2016

1. 木村徹, 五十嵐康人, 財前祐二, 2016: IAEA-TEL-2015-03 Proficiency Test 試料の測定, Proceedings of the 17th Workshop Environmental Radioactivity. KEK Proceedings, 2016-8, 228-231.

2015

1. 足立光司, 電子顕微鏡がとらえた放射性粒子, 地球化学, 49,185–193, 2015.
2. 木村徹, 五十嵐康人,「大気降下物試料の放射能分析の品質管理」, Proceedings of the 16th Workshop Environmental Radioactivity. KEK Proceedings 2015-4 , 23-27, 2015.

2014

1. 青山道夫, 東電福島原発事故後の海洋での放射能汚染の推移 （With English Abstract）. YAKUGAKU ZASSHI, Journal of the Pharmaceutical Society of Japan. 2014.

2013

1. 青山道夫, 極低レベル放射能測定：少量表層海水および極深層海水試料への応用.放射線, 39(1), 17-20, 2013.

2012

1. 青山道夫, 福島第一原子力発電所から放出された放射性セシウム同位体の北太平洋における総量と分布, 日本原子力学会誌, 54, 780-783, 2012.
2. 青山道夫, 五十嵐康人, 1957 年から始まる気象研究所における環境放射能研究の歴史, 放射線, 38(3), 123-128, 2012.
3. 青山道夫, 海洋に放出された放射性物質の長期地球規模での挙動, 検証！福島第一原発事故 -放射性物質の実際と科学者たちの活動の記録（化学 4 月号別冊）. 4, 33-38, 2012.
4. 青山道夫, 五十嵐康人, 広瀬勝己, 月間降下物測定 660 ヶ月が教えること-^{90}Sr, ^{137}Cs および Pu 降下量 1957 年 4 月～2012 年 3 月-. 科学, 82(4), 0442-0457, 2012.

2011

1. 青山道夫, 福島原子力発電所事故による海洋汚染. 理大科学フォーラム, 11(通 巻 329 号), 42-45, 2011.
2. 津旨大輔, 坪野考樹, 青山道夫, 廣瀬勝巳, 福島第一原子力発電所から漏洩した ^{137}Cs の海洋拡散シミュレーション(With English Abstract). 電力中央研究所報告書, V11002, PP.18, 2011.

2009

1. 五十嵐康人, 放射性同位体分析, In 岩坂泰信, 西川雅高, 山田丸, 洪天祥（編）, 黄砂, 古今書院, pp81-87, 東京, 2009.
2. Igarashi, Y., Anthropogenic Radioactivity in Aerosol -A Review Focusing on Studies during the 2000s-, 保健物理, 44(3), 2009.

3. 猪股弥生, 五十嵐康人, 千葉長, 青山道夫, 廣瀬勝己, 再現期間を用いた降水時における高ガンマ線線量率の異常値判定. Radioisotopes, 58, 37-42, 2009.

2007

1. 三浦誓也, 貝森優希, 工藤英嗣, 野呂幸男, 時枝隆之, 廣瀬勝己, 青森県における大気中クリプトン-85　濃度調査,　青森県原子力センター所報, 1, 43-44, 2007.
2. 廣瀬勝己, 青山道夫, Kim、S.A. Kim, 太平洋の海水中のプルトニウムの挙動について,　日本放射化学会誌 別冊, 8 supplement, 103, 2007.

2006

1. 青山道夫, 大気と海洋深層における核実験起源放射性降下物の超低レベル放射能測定, ADIOISOTOPES, 55, 429-438, 2006.
2. 小村和久, 青山道夫, 秋山正和, 氏平祐輔, 大田裕二, 大塚良仁, 大西勝基, 櫻井敬久, 篠原伸夫, Ge 検出器の使用状況に関するアンケート報告, RADIOISOTOPES, 55, 699-707,2006.

2004

1. 廣瀬勝己, 化学トレーサーを利用した海洋変動の研究, 測候時報第 71 巻特別号, 71,　S81-S86, 2004.
2. 五十嵐康人, 廣瀬勝己, 放射性降下物標準試料の調製を通じた ^{90}Sr, ^{137}Cs,プルトニウムなどの人工放射性核種分析の相互比較と参照値の決定,　放射化分析, No. 17, 39-42, 2004.

2002

1. 五十嵐康人, ^{90}Sr と ^{137}Cs を用いたダスト輸送過程と再飛散, エアロゾル研究, 12, 17(4), 252, 2002.

1986

1. 鈴木款, 井上久幸, 杉村行勇, 大気中の放射性クリプトンの分布, 地球化学, 20, 106-108, 1986.

1978

1. 葛城幸雄, 人工放射性物質, 天気, 25, 第 11 号, 20-23, 1978.
2. 猿橋勝子, 海洋中の放射性物質を指標とした物質の移動・拡散, 水汚染の機構と解析－環境科学持論－, 日本地球化学編, 東京, 産業図書, 271-287, 1978.
3. 三宅泰雄, 猿橋勝子, 杉村行勇, 葛城幸雄, 金沢照子, 核兵器と地球環境の放射能汚染, 被爆の実相と被爆者の実情 －1977 年 NGO 被爆問題シンポジウム報告書, ISDA－ JNPC 編集, 朝日イブニングニュース社発行, 182-212, 1978.

1976

1. 葛城幸雄, 日本における放射性降下物, 天気, 23, No. 7, 333-345, 1976.
2. 杉村行雄, 環境のなかのプルトニウム, 自然, 3 月号, 1976.

1975

1. 三宅泰雄, 島田利夫, 川村清, 重原好次, 地上大気のトリチウム含量と気象との関係, 日本地球化学会 “環境問題特別号”, 131-135, 1975.

1974

1. 三宅泰雄, 葛城幸雄, 最近の ^{90}Sr 降下物の起源, 天気, 21, 639-644, 1974.

1971

1. 葛城幸雄, 人工放射能による大気汚染, 気象研究ノート, 107, 258-282, 1971

1970

1. 三宅泰雄, 葛城幸雄, 最近の日本における放射性塵の降下, 天気, 17, 593-598, 1970.

1965

1. 葛城幸雄, 日本における Cs-137 および Sr-90 降下について(I), 天気, 12, 323-328, 1965.
2. 葛城幸雄, 日本における Cs-137 および Sr-90 降下について(II) "成層圏における人工放射性物質の滞留時間の推定", 天気, 12, 377-384, 1965.

1964

1. 三宅泰雄, 葛城幸雄, 金沢照子, 放射性降下物の現状と将来, 科学, 34, 142-148, 1964.

1963

1. 三宅泰雄, 放射性降下物の気象学の側面, 天気, 9, No. 1, 1962.

1962

1. 三宅泰雄, 放射性降下物の気象学的側面, 天気, 9, 1-6, 1962.
2. 三宅泰雄, 猿橋勝子, 放射能による水の汚染, 水利科学, 23, 1-14, 1962.

1958

1. 三宅泰雄, 猿橋勝子, 放射化学と海洋, 科学, 28, 510-513, 1958.

1956

1. 三宅泰雄, 杉浦吉雄, 葛城幸雄, 1955 年 4 月旭川地方に降った放射性の落下塵,気象集誌, 第 2 号, 34, 226-230, 1956.

1955

1. 三宅泰雄, 放射能雨の性格, 測候時報, 22, 196-202, 1955.
2. 三宅泰雄, 日本に降った人工放射性雨・雪[II]9 月～12 月, 天文と気象, 21, 1-8, 1955.
3. 三宅泰雄, 杉浦吉雄, 亀田和久, 日本近海の海水放射能について, 昭和 29 年度海洋資源開発調査報告（黒潮班）, 81-82, 1955.
4. 三宅泰雄, 放射能雨の性格, 測候時報, 22, No. 7, 196-202, 1955.

1954

1. 三宅泰雄, 日本に降った人工放射性雨(1954 年 5-7 月), 天文と気象, 20, 1-8, 1954.
2. 三宅泰雄, 杉浦吉雄,亀田和久, ビキニ海域における人工放射能の分布とその海洋学的考察" ビキニ灰とそれによる傷害 第三", 科学, 24, 601-605, 1954.
3. 三宅泰雄, 有住直介, 磯野謙治, 田島英三, ビキニの灰とそれによる傷害（つづき）日本に降った放射能雨, 科学, 24, No. 8, 405-409, 1954.

年代・雑誌名不明

1. 三宅泰雄, 放射能とその作用, 遺伝,（1975？）
2. 三宅泰雄, 第 II 編 環境の放射能汚染と化学分析,（1970？）
3. 三宅泰雄, 猿橋勝子, 杉村行勇, 海洋における放射性核種, 海洋化学講座, 第 6 巻, 海洋無機化学, 第 4 章, 109-170,（1969？）
4. 三宅泰雄, 田島英三, 日米放射能会議, 8-18,（1954？）

7. History of the studies at the Meteorological Research Institute

表：研究の歴史

表紙の図説明

2018年 3月までの ^{90}Sr および ^{137}Cs 月間降下量

福島第一原発事故後の大気の放射能汚染の実態把握を継続しています。2011年3月の事故以降に確定できた^{90}Srおよび^{137}Cs月間降下量を対数軸で誤差と併せてプロットしています。^{134}Csは事故直後には^{137}Csとほぼ等量降下していますから、放射性セシウム全体ではこのプロットのほぼ倍量となります。ただし、^{90}Sr、^{137}Csはどちらもおよそ30年の半減期で減衰しますが、^{134}Csはおよそ2年で半減します。図示した誤差は計測の統計誤差で、1シグマです。測定誤差は本来全ての測定値につき表示すべきですが、グラフが見づらくなるため、従来はあえて表示してきませんでした。また、数十年前のデータについては誤差データが伝えられていません。

福島第一原発事故以前に採取され、分析や前処理途上だった試料については、事故の汚染によって実験室環境および測定室環境、測定機器のバックグラウンドなどが大幅に上昇したため、蒸発濃縮工程においても試料の汚染（コンタミネーションと言います）の問題が発生します。そのため、観測値を求めること自体が困難になっていましたが、試料を汚染の水準の低い関西にて分析しこの問題の回避に努めました。しかし、細心の注意と努力にもかかわらず、2010年の後半および2011年初のデータは欠測となってしまいました。

徐々に実験環境の除染や測定機器の入れ替えなどを実施して事故以前のきれいな実験環境を追求し、データを求めるように努めています。また、IAEAが実施した分析相互比較に参画するなどし、その精度の維持管理に努めていますので、現状のデータの信頼性は担保できていると考えています。

8. A caption of the cover art

Monthly depositions of ^{90}Sr and ^{137}Cs before March 2018.

We have been monitoring the deposition amounts for the purpose of understanding the actual condition of radioactive pollution after the accident of Fukushima Daiichi Nuclear Power Plant (FDNPP). The monthly deposition amounts of both ^{90}Sr and ^{137}Cs, which were successfully fixed values after the accident in March 2011, are shown in logarithmic axis with error widths. Since the deposition amounts of ^{134}Cs were nearly equal to those of ^{137}Cs, the total amounts of radioactive cesium were approximately two times of the values in this figure. We would like to note that the half-lives of ^{90}Sr and ^{137}Cs are approximately 30 years, however, ^{134}Cs decays to half in about 2 years. The error widths are one sigma in statistical error of measurements. Although the error widths of all measurement values were better to be shown, error values used to be not shown on purpose to avoid busy figure in the former versions. In addition, error data before several decades are not handed down.

For the analysis of samples collected before the accident of FDNPP and not measured then, significant increase of background values were severe problem, because environments including laboratories and instruments were polluted, and it was also problem that samples could have been polluted in the operations of concentration or other preprocesses (contamination problem). We overcame the difficulty by carrying the analysis out in western Japan (Kansai area) where the pollution level was low, however, the data during the latter part of 2010 and the former part of 2011 were lacked in spite of our efforts.

We are making efforts to recover clean working environment as before the accident, by cleaning of the environments, exchanging instruments, etc. for the purpose of acquire the correct data. In addition, we maintain the precision of the data, for example, by participating inter-comparison programs performed by IAEA, so that, the credibility of the data are assured (please refer to the section: quality control of radioactive analysis of atmospheric deposition samples).

最終ページに図の詳しい説明があります。

See figure caption at the end page of this publication.

「環境における人工放射能の研究（2018年版）」について

気象研究所では、1954年以来、主に現在の原子力規制庁放射能調査研究費により大気及び海洋の環境放射能の研究を実施してきました。特に人工放射性核種の降下量を60年余りの長期にわたり、東京・つくばで精密測定してきました。この観測は、世界でも最長の定点観測です。このモニタリング観測の期間では、1950年代から1960年代にかけては、旧ソ連や米国等による核実験が行われ、また、その後も1986年には旧ソ連のチェルノブイリ原子力発電所の事故が発生するなどがありましたが、この観測によって、それらの影響を含めたバックグラウンドの人工放射性核種の長期的変動を明らかにし、国民の安全・安心に寄与してきました。2011年には不幸にして東日本大震災に伴う福島第一原子力発電所事故が発生し、それによって放出された放射性核種の推移を調査するという課題も担うこととなりました。今後も長期的視点で、人工放射性核種の変動を監視する必要があります。

放射性物質の再飛散・輸送・沈着による変動のメカニズムを正しく理解し、将来の変動を予測するためには、長期観測や再飛散観測、サンプルの分析等に加えて、数値計算モデルを用いた解析が必要です。気象研究所では、気候変動や降水予測の研究のため、大気中の微粒子の動きを表現する数値モデルを開発してきましたが、そのような数値モデルを利用した、バックグラウンド放射能の変動メカニズムを解析する研究も行ってきました。

この研究によるこれまでの観測や解析から、長期的変動に対しては、一旦地面などに沈着した人工放射性核種が、土壌粒子・生物由来の粒子等を通じて空気中へ再飛散する過程が重要である可能性がわかりました。

本論文集「環境における人工放射能の研究（2018年版）」は、その研究成果を、関係省庁の担当者の方々及び大学や試験研究機関の研究者の方々に広く周知するために、2016年から2018年までの期間に出版された論文（主に英語論文）を、過去から現在までの成果と最近のトピックスに関するテーマ毎に分類し、各テーマの冒頭に簡単な日本語の解説を加えて、一冊にまとめたものです。

令和2年 3月

気象研究所 研究総務官　高薮　出

Contents

0. Preface

1. Temporal trends of radioactivity concentrations in the atmosphere and observational approaches for their resuspension mechanisms

2. Physical and chemical characteristics of the radioactive materials in the atmosphere

3. Evaluations of resuspension , transportation and deposition processes of radioactive materials using numerical models

4. Publications 2016-2018

5. Publication list 1954-2018

6. Publication list (in Japanese) 1954-2018

7. History of the studies at the Meteorological Research Institute

8. A caption of cover art

目次

0. はじめに

1. 大気中の放射性物質の濃度変動、再浮遊観測

2. 大気中の放射性物質の物理・化学性状

3. 放射性物質の再浮遊、輸送、沈着過程のモデルによる評価

4. 出版論文　2016-2018

5. 論文リスト（英文誌）1954-2018

6. 論文リスト（和文誌）1954-2018

7. 表：研究の歴史

8. 表紙説明

0. はじめに

気象研究所（2019 年 3 月現在は環境・応用気象研究部および予報研究部）では、1954 年以来、環境放射能の観測・測定法の開発、放射能汚染の実態の把握、大気や海洋における物質輸送解明のトレーサーとしての利用を目的として、60 年余にわたって環境放射能の研究を実施してきた。1957 年以降、各省庁がそれぞれの所掌で実施してきた環境放射能調査研究関連業務は、まず旧科学技術庁、その後文部科学省が所管してきた。さらに原子力規制委員会と原子力規制庁の発足に伴って 2013 年からは、原子力規制庁が所管することとなった。このような長期にわたり多数の研究者が係わり、観測・研究を継続してきた結果、環境放射能について世界的にも他に類を見ない貴重な時系列データが内外に提供され、また様々な気象学・海洋学的発見をもたらしてきた。この間の研究成果は 200 編以上の原著論文や解説資料として内外の雑誌や成書で公表されている。

1954 年 3 月 1 日に米国によりビキニ環礁で行われた水爆実験により、危険水域外で操業していた第五福竜丸乗組員が放射性物質を含む降灰（いわゆる死の灰）による被ばくを受けた事件を契機にして、日本における環境放射能研究が本格的に始まった。当時の気象研究所地球化学研究室は環境の放射能の分析・研究において日本で有数の研究室であり、海洋及び大気中の放射能汚染の調査・研究に精力的に取り組んだ。その結果、当時予想されていなかった海洋の放射能汚染、さらに大気を経由した日本への影響など放射能汚染の拡大の実態を明らかにすることができた。1958 年には、放射能調査研究費による特定研究課題の一つである「放射化学分析（落下塵・降水・海水中の放射性物質の研究）」を開始し、以降、地点の変動はあるが、札幌、仙台、東京、大阪、福岡の五つの管区気象台、秋田、稚内、釧路、石垣島の 4 地方気象台、輪島、米子の 2 測候所の全国 11 気象官署及び観測船で採取した海水中の人工放射性核種（^{90}Sr、^{137}Cs、^{3}H 及びプルトニウム）の分析を実施してきた。

東京・つくばにおける大気中の人工放射性核種の降下量は 1961 年から 1962 年に行われた大規模な大気圏核実験の翌年である 1963 年に最大値を観測した。その後、「部分的核実験禁止条約」の締結により米ソの大気圏核実験が中止された結果、降下量はおよそ 1 年の半減時間で減少した。この放射性核種の降下量の減少率は成層圏にまきあげられた物質の滞留時間を反映している。その後も、中国及びフランスにより大気圏核実験は続けられ、人工放射性核種の降下量は増減を繰り返した。1980 年の中国による最後の大気圏核実験の後、フォールアウトは再度 1 年の半減期間で減少し、1985 年には 1957 年の観測開始以降最も低いレベルになった。しかし、1986 年の旧ソ連のチェルノブイリ原子力発電所事故により、大気中の人工放射性核種濃度（特に揮発性の高い ^{131}I、^{134}Cs、^{137}Cs など）は日本でも 1963 年に近いレベルに達するほど著しく増加した。大部分の放射性核種は対流圏の滞留時間（25 日）で減少したが一部 ^{137}Cs は成層圏にも輸送されていることが分かった。1988 年以降は低いレベルで推移しているが、明瞭な減少の傾向は見られなかった。この原因は一度地上に降下した放射性核種の再飛散に由来すると考えている。さらに、再飛散がどこで起るかについて研究を進め、東アジアの砂漠域で発生する黄砂が有力な候補であることを明らかにした。黄砂の発生は大陸域の環境変化と関連しており、降下物中の人工放射性核種は、砂漠化や関連する植生変化など大陸域の環境変化の指標となりうることが分かった。

大気フォールアウトの研究とともに、海洋における放射性核種の挙動も長期的に調査研究を実施してきた。日本周辺海域ばかりでなく、太平洋の広域に亘って海水試料の採取を実施し、

放射能汚染の実態を明らかにした。1960年代後半から1970年代の調査で、海洋表面水中の放射能が北半球の中緯度で高いことを明らかにし、フォールアウトの緯度分布を反映していることが分かった。その後、海洋表面水中の放射性核種は海洋の物質循環に支配されていることを明らかにした。さらに、海水中の人工放射性核種の分析法の高度化を実現し少量の試料で分析可能にし、海洋の ^{137}Cs 濃度の精密鉛直断面を描き、核実験由来の ^{137}Cs の主な部分は北太平洋の亜熱帯中層に存在していることを明らかにした。フォールアウトによる人工放射性核種の海洋への主な降下以来、数10年以上経過し、その広がりは北太平洋から、インド洋など他の海盆に及んでいる。これに関連して 2003－4 年に実施された BEAGLE2003 の航海で採取された海水について人工放射性核種の分析を行って、その広がりについて知見が得られた。1993年旧ソ連/ロシアによる放射性廃棄物の日本海等への海洋投棄の実態が明らかにされ、それに伴う日本海の放射能調査の実施に参加した。放射性廃棄物による影響は検出されなかったが、調査の結果を踏まえ、日本海における固有水の生成過程及び生成場所（ウラジオストック沖）についての知見を得ることができた。これらは、海洋放射能のデータベースとして公開されている。

1990年以降の環境放射能汚染として、1997年の旧動力炉核燃料開発事業団「アスファルト固化処理施設」の火災爆発事故や1999年のJCOウラン燃料工場の臨界事故があるが、いずれも環境中に放出された放射能は極めて低いレベルで、その影響は殆どなかった。しかしながら、2011年3月に起きた東日本大震災にともなう東京電力福島第一原子力発電所事故により、^{137}Cs の総量だけで 10 PBq（ペタベクレル）以上という過去日本では経験したことのない大量の人工放射性核種が環境中に放出され、その 2 割程度が日本の国土に降下し、残りの 8 割は北太平洋に降下したと考えられている。これらの影響評価やその後の環境中での拡散状況の把握のためにも、環境放射能調査・研究は今後とも重要である。

2006年4月より2011年3月まで、気象研究所では放射能調査研究費による特定研究課題として「放射性降下物の長期変動と再浮遊に関する研究」及び「海洋環境における放射性核種の長期挙動に関する研究」の二課題で環境放射能研究に取り組んできた。また、2011年8月からは、「大気を通じた人工放射性核種の陸圏・水圏への沈着およびその後の移行過程の解明研究」の課題のもと、過去の知見を十分に活用しながら、同年3月11日に発生した東日本大震災にともなう福島第一原子力発電所の事故以降の新たな事態に対応し、放出された大量の人工放射性核種の挙動を解明する研究を行った。目の前の大気に加えて、北太平洋におけるこれらの核種による汚染実態の把握やその動態の解明に取り組んだ。

過去60年余にわたり実施されてきたこうした研究成果を踏まえ、2015年4月からは「人工放射性核種のバックグラウンド大気監視と数値解析に関する研究」を新たに開始した。本報告書では、この研究課題で得られた成果を含め、最新の成果やトピックスをテーマ毎に記述した。関係各位の今後の研究や業務に役立つ資料とすべく、編集作業を行った。我が国における環境放射能研究や大気科学研究に多少なりとも寄与できたとすれば、著者一同の望外の喜びである。

1. 大気中の放射能物質の濃度変動、再浮遊観測

1）はじめに

気象研究所では、大気圏内核実験が盛んに実施された1950年代後期から現在までの期間にわたり、大気圏での人工放射性核種の濃度水準の実態とその変動要因を明らかにすべく、環境影響の大きい重要な核種について観測を継続してきた。^{90}Sr（半減期 28.8 年）および ^{137}Cs（半減期 30.2 年）の月間降下量（大気降下物）の長期観測結果は満60年を超え、世界でも稀にみる長期変動に関して重要な知見をもたらしている。また、2003 年 3 月からは大気中浮遊粒子の採取、及び放射能分析も開始し、2011 年 3 月の東京電力福島第一原子力発電所事故（福島第一原発事故）に関する環境影響に関して重要な知見を取得し、また大気モデル改善に貢献し、その結果をいち早く学会で報告するとともに、気象研究所のホームページにも掲載し一般に公開してきた。複数台有するGe半導体分析装置は他研究機関の持つ環境試料の測定にも貢献し、福島第一原発事故の影響解明にも大きく貢献してきた。前報のIgarashi et al., (2015) では福島第一原発事故以降の三年間に着目した大気降下物および大気中放射能について報告をしてきたが、事故後七年が経過し、その濃度は徐々に下がってきたため、より高精度な測定技術が求められてきた。本報ではより高精度に ^{134}Cs を測定するための定量方法の開発結果について報告し、事故後数年経過した現在における放射性物質の再飛散（二次飛散）や環境中での動態プロセスに関する考察について解説する。

2）研究方法

月間大気降下物の捕集は、茨城県つくば市長峰にある気象研究所の露場観測実験棟屋上に設置した大気降下物捕集用のプラスチック製水盤（面積 4m^2）で 1980 年代以降実施してきた。福島第一原発事故以降（2011 年 4 月以降）は放射能水準の上昇を考慮し、気象研究所屋上にて 1 m^2 水盤２基での捕集を実施した。2015年8月以降は放射能水準の低下を考慮して 1m^2 水盤４基での大気降下物採取を開始した。大気中浮遊粒子は、上記露場観測実験棟前に設置したハイボリューム・エアサンプラー(HV-1000R、柴田科学)に石英繊維フィルター(QR-100、柴田科学)を装着して、空気流量700LPMで一週間単位でのサンプリングを行った。

得られた大気降下物試料はポリ製保管容器で保存しつつ、ロータリーエバポレーターや蒸発皿等を使用して全量を蒸発濃縮・固化し、Ge 半導体検出器によりγ線放出核種（放射性Cs等）を測定した。次いで試料の一部を分取して発煙硝酸処理・放射化学分離により ^{90}Sr を精製し、最終的に炭酸 Sr として固定、低バックグラウンド 2πガスフロー検出器でβ放射能を測定した。福島第一原発事故後の試料については、事故により放出された ^{89}Sr の影響があるため、生成固定した炭酸 Sr 線源のβ放射能を繰り返し測定することで、^{90}Y の放射平衡達成と ^{89}Sr 放射能の減衰の様子とを確認しつつ評価し、必要な場合は計算で ^{89}Sr の影響を除去した。フィルターサンプルの場合には8等分の短冊にし、金型と油圧プレスで成型することで試料形状を一定形状にし、Ge半導体検出器によりγ線放出核種（放射性Cs等）を測定した。

^{134}Cs/^{137}Cs 放射能比は発生源の特定につながる重要なパラメーターであるが、前述の通り ^{134}Cs（半減期 2.06 年）の濃度は事故直後から見て大きく低下し、より高精度での測定が必要となってきたため、その解析手法について開発検討を行った。着目した開発点は ^{134}Cs の補正方法である。^{134}Cs はカスケードピークを持つことからサム効果による測定影響が生じる。同標準線源でピーク効率を求める際に、一般にはサム補正は不必要とされているが、本研究のフィルター試料成型では試料内での放射能分布に偏りがあることが考えられ、その際に誤差を生じると考えられる。そこで、サム効果補正が可能であるソフトウェア(P-SCAN、スカラベ・コーポレーション)を使用してサム補正を行い、補正の有無でどの程度定量に差が出るかを比較検討した。

3）結果・議論

3.1) ^{134}Cs/^{137}Cs 放射能比の分析結果

P-SCAN ではγ線スペクトルの光電ピーク面積と、それらの計数効率・全効率の間に成り立つ高次・多元連立方程式を直接解くという方法を採用し、壊変後にカスケードγ線を放出する核種については観測されるピーク数をパターン化して数式化している。ピークの測定には気象研究所の 4 台(#6、#7、#8、#10)のゲルマニウム半導体検出器を使用した。標準試料の測定は通常通り行い、次に福島第一原発事故時の放射能強度が高い環境試料を測定、サム効果補正計算を行い、そうでない場合と比較した。

大気中浮遊粒子試料の測定結果を Table1 に示す。^{137}Cs ではサム効果は見られないため、P-SCAN の使用有無による有意な違いは生じなかった。一方で ^{134}Cs では P-SCAN で得られた結果の方が数%低い結果となった。^{134}Cs/^{137}Cs 比については PSCAN を使用した場合の方がばらつきは非常に小さかった。このことから、^{134}Cs/^{137}Cs 比を測定する場合には P-SCAN を使用した方がよいと考えられるが、絶対値の正しさについては今後の検討が必要である。

Table1. Comparison when using P-SCAN and normal calculation in 4 detectors (result of measuring the same sample).

			Cs-134				Cs-137					
Detector	Sampling period	134+137 (Bq)	Normal calculation		Using P-SCAN		Normal calculation		Using P-SCAN		Normal calculation	Using P-SCAN
			mBq/m3	Err	mBq/m3	Err	mBq/m3	Err	mBq/m3	Err	134/137 ratio	134/137 ratio
#6	2011/04/11 ～04/19	898	60.1	0.4	59.0	0.4	55.2	0.1	55.3	0.1	1.09	1.07
#7			62.0	0.3	57.8	0.3	55.3	0.1	54.5	0.1	1.12	1.06
#8			61.7	0.3	58.6	0.3	55.3	0.1	54.6	0.1	1.12	1.07
#10			60.6	0.4	57.6	0.4	55.4	0.1	54.3	0.1	1.09	1.06
										σ	0.014	0.006

二種類のγ線エネルギーの 605keV/662keV 比はサムピークの比を表す。サムピークの発生確率は検出器と試料の距離に関係し、距離が離れるほどサムピークは生じにくくなる。相対距離 0cm から 5cm ごとに距離を離してサム効果の比率を求めた結果を Fig. 1 に示す。また、サムピークの代表値として 1400keV/605keV 比を求めた結果を Fig. 2 に示す。

605keV/662keV 比より、15cm 以上、検出器と試料の距離を保てば光電ピーク比が安定することが分かった。また、1400keV/605keV 比から 15cm 以上離せばサムピークの影響が無視できることが分かった。

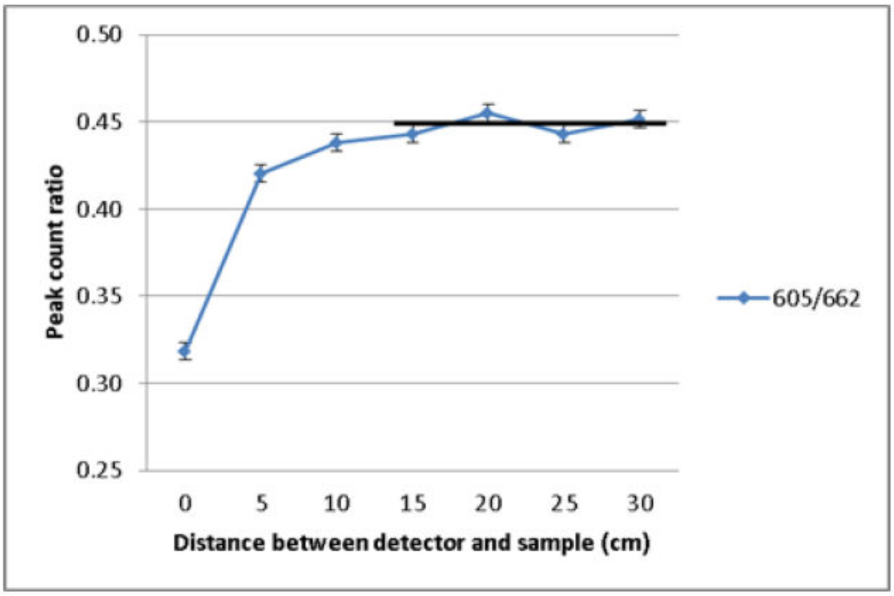

Fig.　1. Relationship between distance to sample and 605/662keV photo-peak count ratio.

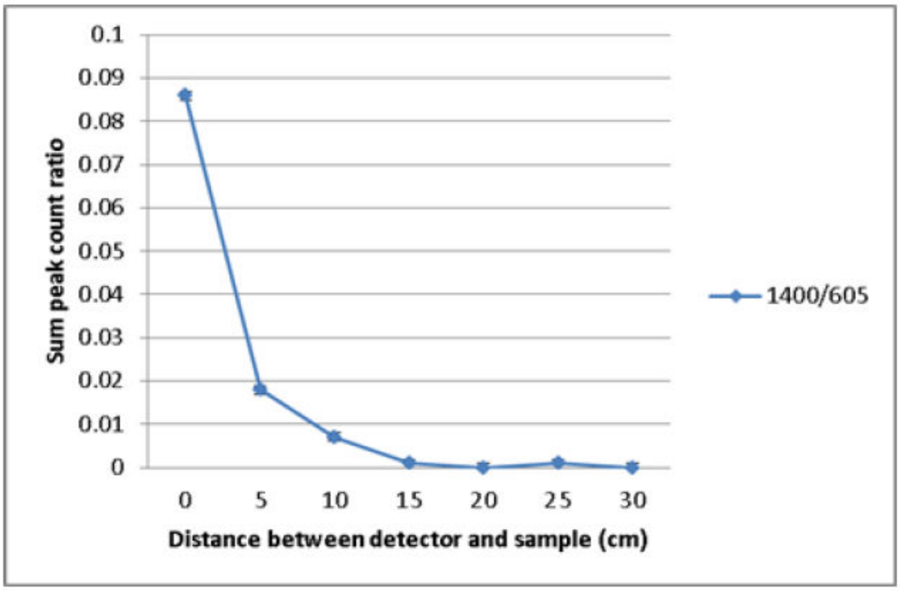

Fig.　2. Relationship between distance to sample and 1400/605 keV photo-peak count ratio.

3.2)　モンゴル土壌中の ^{137}Cs、およびプルトニウム、ウラン同位体の測定

モンゴル土壌中には過去に行われた核実験などにより放出された人工放射性同位体が含まれており、アジアダストのトレーサーとしてしばしば使われている。Hirose et al. (2017)の結果、モンゴル土壌中のプルトニウム同位体・ウラン同位体比を始めて明らかにした。ここで得られたプルトニウム同位体比は、大気降下物として測定される核実験により放出された放射性核種（グローバル・フォールアウト）の同位体比と一致しており、モンゴル土壌中の人工放射性核種がグローバル・フォールアウトに起因するものだということが分かった。^{137}Cs とも関係性が見られ、つくば土壌でも同じように関係性が見られることが分かったが、その傾きは大きく異なった。その原因は放射性核種それぞれの物理的・化学的な移動過程の違いによるものと考えられる。

3.3)　福島第一原発事故に起因する放射性セシウムとバイオエアロゾル

Igarashi et al. (2019) および Kinase et al. (2018) では2011年7月～2015年3月までに福島県の浪江町・川俣町にて採取した大気中粒子試料の ^{134}Cs,^{137}Cs を測定し、その季節変化を明らかにした(Fig. 3)。その結果、つくばで観測される大気中放射性セシウムの季節変化とは明らかに異なることが分かり、5–6月、および8–9月に極大となる二山ピークを持つことが分かった。これは、過去における研究で明らかにされてきた再飛散プロセスと、福島高濃度汚染地域における主要な再飛散プロセスが異なっていることを示唆する結果である。

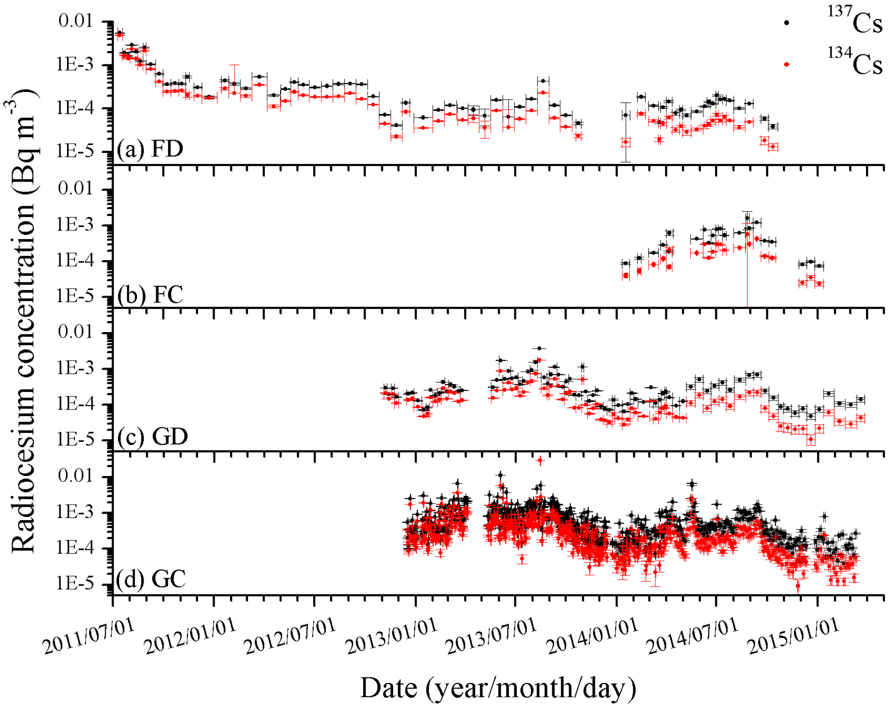

Fig. 3. Activity concentrations of ^{134,137}Cs (Bq m^{-3}) measured at the FD, FC, GD, and GC sites in the Fukushima prefecture in July 2011 to March 2015. These results show high concentrations in late spring, summer, and early autumn and low concentrations in winter and early spring at all of the presented observation locations.

気象研究所内の走査型電子顕微鏡(SEM)及び EDX によるフィルター試料の観察結果より、大気中放射性セシウム濃度の上昇がみられる試料には、胞子や菌類などのバイオエアロゾルが多く見つかることが分かった（Fig.　4）。

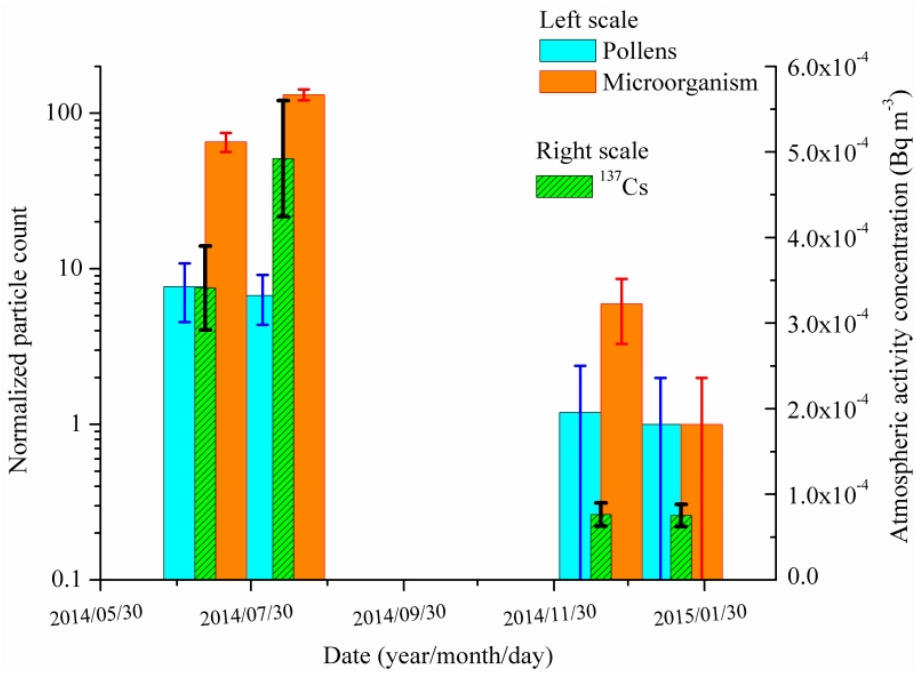

Fig.　4.　The normalized particle counts of the bioaerosols using SEM (in relative values, the error bar shows the Poisson standard deviation) and atmospheric concentrations of ^{137}Cs activity sampled at the GD site during summer (July and August 2014) and winter (December 2014 and January 2015). The counts of microorganisms include those of spores (see the text).

上記結果を踏まえ、Igarashi et al. (2019)では SEM-EDX 分析に加え、DAPI 染色による蛍光顕微鏡による観察(Fig.　5)、メタゲノム解析によるバイオエアロゾル種の解析を行った(Fig. 6)。その結果、大気中放射性セシウム濃度とバイオエアゾルの大気中濃度には相関がみられ(Fig.　7)、バイオエアロゾルの 1/3～半数が担子菌及び子嚢菌だということが分かった。

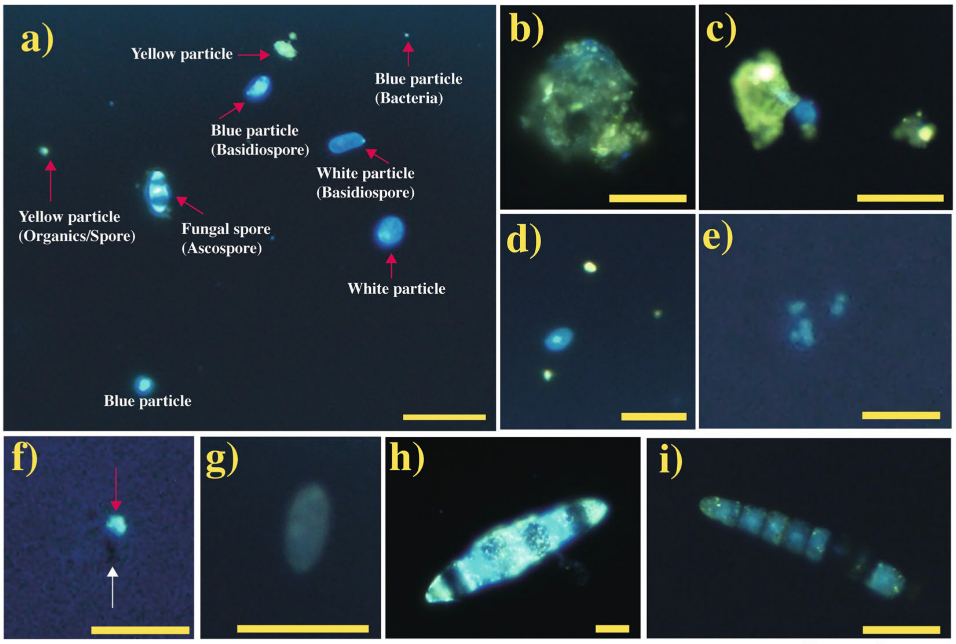

Bar = 5 µm

Fig. 5. Fluorescent micrographs of DAPI-stained particles (indicated by red arrows) in the bioaerosol samples collected at Namie site in August and September 2015 (a). The aggregated particles observed as yellow particles (b,c), yellow and blue particles (d), blue particles (e), black (indicated by the white arrow) and white (indicated by the red arrow) particles (f), white particles (g) and spores form particles that are likely ascospores (h,i). The bars indicate a length of 10 µm. In the photo, white and yellow particles may not exhibit the colours seen by the naked eye on the microscopic screen.

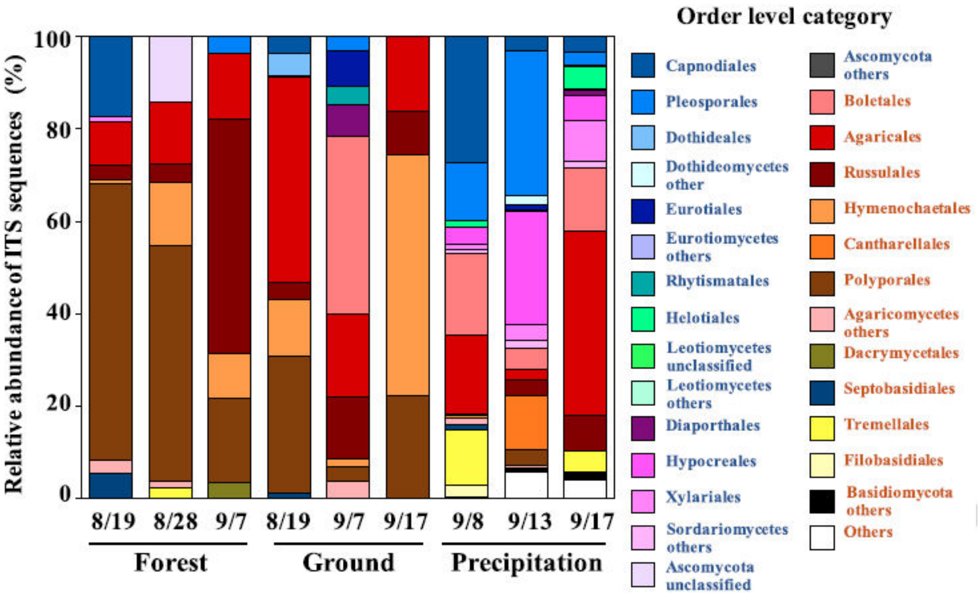

Fig. 6. Results of the metagenomic analysis showing the relative abundance of identified fungal taxa in the samples collected at the forested and bare soil sites in Namie and contained in rain water collected at the site during summer 2015. Sampling dates are expressed as mm/dd. The compositional differences among sampling dates may reflect seasonal and weather differences.

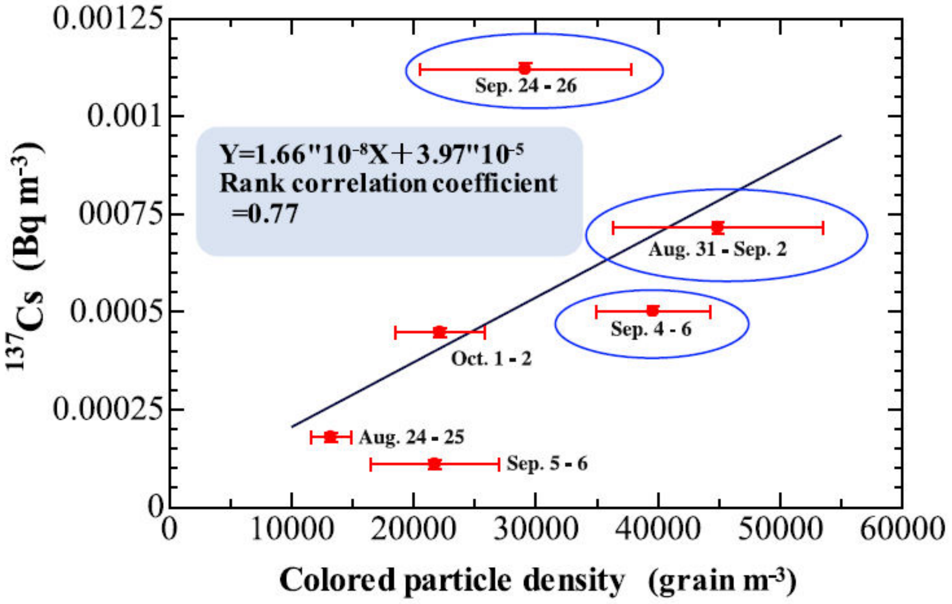

Fig. 7. The relationship between the concentration of coloured fungal spores (countable without DAPI staining by optical microscopy) and the ^{137}Cs activity in air at the Namie site in summer 2016. The sampling duration was 24 hours of daytime or nighttime (circled data; e.g., daytime data from Aug. 24–25 indicates that sampling was performed from 6:00 to 18:00 on August 24 and 25, a total of 24 hours). Despite the large scatter, the spore number and ^{137}Cs concentration exhibited a positive correlation (rank correlation; significant at 8% based on a t-test). The slope of the fitted curve (1.66 × 10−8 Bq/grain) corresponds to the lower range of estimated values (see Supplementary Tables S3–S5).

3.4) 福島第一原発事故に起因する河川及び地下水中の水溶性放射性セシウム

Iwagami et al. (2017)では、福島県山木屋地区で河川水および地下水中の水溶性放射性セシウムの長期的観測を実施した。その結果、チェルノブイリ事故と比較して河川・地下水の汚染は低く、その汚染低下のプロセスには二つあることが分かった。まず一つ目のプロセスは、大量の雨による表層土ごと洗い流す過程であり、事故後初期の段階で周辺の水中放射性セシウムを急激に低下させた。もう一つのプロセスは、土壌中への放射性セシウムの浸透と固定化による、水中放射性セシウム濃度低下の鈍化であり、事故後しばらくたってからの影響として現在も観測されている。この研究により、河川水及び二地点での地下水について環境中での半減期が明らかとなり、それぞれ 0.69–1.5 y、0.46–0.58y、0.50–3.3y となった（Fig. 8）。河川水中の ^{137}Cs の減少傾向はキャノピーに見られる放射性セシウムの脱離傾向と似ていることが分かった。

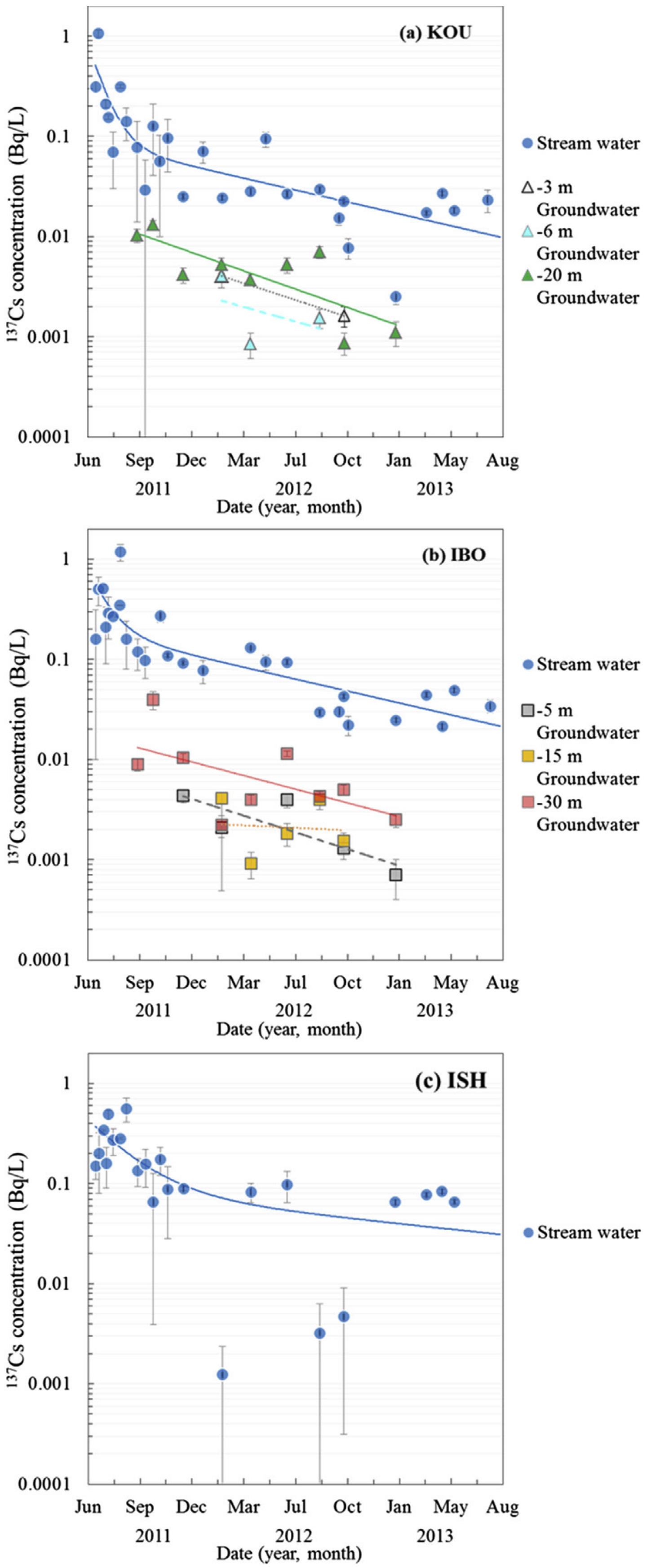

Fig. 8. Time series of dissolved ^{137}Cs concentrations in stream water in normal flow condition and groundwater at (a) Koutaishi-yama, (b) Iboishi-yama, and only stream water at (c) Ishidaira-yama with exponential regression lines. Error bar shows a standard deviation from counting statistics.

4）まとめと今後に向けて

本研究所における、より高精度な測定に向けた ^{134}Cs 測定方法開発、モンゴル土壌における人工放射能の観測、福島第一原発事故後の大気中人工放射能観測の結果と他地域には見られない新しい再飛散プロセスの提案、水中に溶存する放射性セシウムの環境中における動態の傾向について報告した。前報にあるように、事故後 7 年が経過した現時点では、福島第一原発事故直後と比較すると、つくばでの降下量は数桁も低下し、甚大な汚染というべき水準ではない。^{90}Sr については、事故以前の降下量とほぼ同じ水準に戻りつつある。しかし、本報で報告した ^{134}Cs 測定技術の改善により、今後も高精度での人工放射能観測が期待できる。また、^{137}Cs については依然として 3〜4 桁より大きな値となっている。水準低下にはまだ時間がかかると考えられ、継続した観測と動態傾向の分析が肝要である。

事故直後に見られた一次放出に替わり、大気へのこれらの核種の供給を続けている過程は、いわゆる再飛散（二次放出）であり、現在はこの再飛散プロセスにより大気中・降下物中の人工放射能濃度が支配されていると考える。再飛散は周辺の環境に由来し、周辺の汚染度がつくばに比し数桁高い地域においては、大気中濃度・降下量もそれに比例し数桁高い。従って、再飛散プロセスの解明は必須な科学的課題である。

従来、汚染した地表面からの表土ダスト、汚染植生からの再浮遊、または汚染したゴミの燃焼、野焼き等による放射性物質の大気への揮散などが想定されてきた。しかし、本報で報告したように、福島原発事故により高濃度に汚染された地域では、通常の汚染地域とは異なり森林生態系からの放出、すなわちバイオエアロゾルの寄与がとても大きいと分かってきた。特にキノコに由来する胞子や担子菌・子嚢菌が放射性セシウムの担体として重要と考えられるが、まだ定量的には解明できていない。今後は、バイオエアロゾル観測の定量化と、継続的な連続観測を実施することで定量的な理解を得ていくことが肝要である。そのためには、森林内での各高度や樹間密度ごとのバイオエアロゾル放出量（フラックス）を定量的に観測する必要があり、顕微鏡と目視による粒子同定だけでなく、リアルタイムで測定可能な手法の開発が望まれる。

上記に加えて、こうした長期の観測においては分析やデータの品質管理が必ず問題となる。このような点についても常に留意しながら、観測の継続を図っていくことが肝要である。

参考文献

Hirose, K., Kikawada, Y., Igarashi, Y., Fujiwara, H., Jugder, D., Matsumoto, Y., Oi, T., and Nomura, M. Plutonium, ^{137}Cs and uranium isotopes in Mongolian surface soils, Journal of Environmental Radioactivity, 166, 97-103, 2017. http://dx.doi.org/10.1016/j.jenvrad.2016.01.007

Igarashi, Y., Kita., K., Maki, T., Kinase, T., Hyashi, N., Hotaka, K., Adachi, K., Kajino, M., Ishizuka, M., Sekiyama, T., T., Zaizen, Y., Takenaka, C., Ninomiya, K., Okochi, H., and Sorimachi, A. Fungal spore involvement in the resuspension of radiocaesium in summer, Scientific Reports, 9:1-10, 2019. 2019. DOI:10.1038/s41598-018-37698-x

Iwagami, S., Tsujimura, M., Onda, Y., Nishino, M., Konuma, R., Abe, Y., Hada, M., Pun, I., Sakaguchi, , A., Kondo, H., Yamamoto, M., Miyata, Y., and Igarashi, Y. Temporal changes in dissolved ^{137}Cs concentrations in groundwater and stream water in Fukushima after the Fukushima Dai-ichi Nuclear Power Plant accident. Journal of Environmental Radioactivity, 166, 458-465, 2017. http://dx.doi.org/10.1016/j.jenvrad.2015.03.025

木村徹,五十嵐康人,財前裕二,「ガンマ線スペクトル解析ソフト P-SCAN を用いた高精度な 134Cs/137Cs 放射能比の導出」Proceedings of the 18th Workshop Environmental Radioactivity. KEK Proceedings 2017

Kinase, T., K, Kita, Igarashi, Y., Adachi, K., Ninomiya, K., Shinohara, A., Okochi, H., Ogata, H., Ishizuka, M., Toyoda, S., YamadaN, K., Yoshida, N., Zaizen, Y., Mikami, M., Demizu, H., and Onda, Y. The seasonal variations of atmospheric ^{134,137}Cs activity and possible host particles for their resuspension in the contaminated areas of Tsushima and Yamakiya, Fukushima, Japan, Progress in Earth and Planetary Science 5:12, 2018. https://doi.org/10.1186/s40645-018-0171-z

2. 大気中の放射性物質の物理・化学性状

1）はじめに

大気中で観測される放射性物質は、ガスや粒子（エアロゾル）として大気中に漂い、やがて雨による除去や重力沈降によって地上や海水面に降下する。このような大気中での放射性物質の振る舞いはその放射能や核種に依存せず、物理的な粒径や密度、形態、また水溶性などの化学性質に依存する。そのため、放射性物質の大気拡散や環境動態、また発生メカニズムを理解するには、放射性物質がどのような物理化学性状を持ち、またどのようなエアロゾルを担体としているかを解明する必要がある。本章では、その放射性物質の物理化学性状の理解を目指した例として、東日本大震災で発生した福島第一原子力発電所事故によって直接放出された放射性物質に関する研究成果を報告する。

2011 年 3 月に発生した事故によって様々な放射性物質が大気・海洋に放出されたが、放出された放射性物質の重量は非常に微量であり、放射能測定以外の分析手法で環境試料から検出することは一般には困難とされてきた。しかしながら、電子顕微鏡や放射光分析などの微小領域化学分析を用いることで、放射性物質の物理化学特性を明らかにすることが可能であることが気象研究所の研究によって明らかになってきた。本研究においては、それらの手法を用いて 2011 年 3 月 14-15 日につくば市で採取されたフィルター試料中の放射性粒子の特定を行った先駆的な研究（Adachi et al., 2013）を発端として、多くの研究事例が報告されている。ここでは、それらの研究例のうち、前回の報告書から後に発表された小野ら（2017）や Satou (2016,2018)の論文、またこれらの研究例をまとめた総説論文（足立、2017）を紹介する。

2）主な研究成果

東日本大震災で発生した福島第一原子力発電所事故によって直接放出された放射性物質は、本放射能調査研究費研究でモニタリングを継続していた気象研究所におけるフィルター試料から発見された（Adachi et al., 2013）。この研究では、走査型電子顕微鏡（SEM-EDS）を用いて 2011 年 3 月 14－15 日にかけてつくばに飛来した放射性粒子を分析し、その物理化学性状を初めて明らかにした。その結果、セシウム、鉄、亜鉛や多くの核燃料由来と考えられる元素を含み、水に溶けにくい２マイクロメートル前後の球状ガラス様粒子であることが明らかとなった。これらの詳細な物理特性は、事故時における粒子の拡散モデルの精度向上に重要であることを、モデル比較実験で明らかにした。その後、Abe et al. (2014）や Yamaguchi et al. (2016)によって、粒子のさらに詳細な微量成分や内部構造が明らかとなった。これらの先駆的な研究を受けて、本研究期間ではエアロゾル試料やその大気中微粒子が沈着した結果生じた表層土壌汚染地域からの試料を採取して、そこにふくまれる放射性粒子を単離して、電子顕微鏡や放射光分析を用いてその個別粒子の物理化学性状を明らかにし、また少なくとも 2 種類の異なった物理化学性質を持つ放射性粒子が存在することを明らかにした。

Satou et al (2016)では、事故があった原子力発電所から20ｋｍほど離れた地点の土壌から、６㎛ほどの放射性粒子を新たに開発し手法で単離し、それらがエアロゾル試料で見つかった粒子と似た、ケイ素、鉄、亜鉛、セシウムなどを含む化学組成をしていることが分かった。これらの粒子は大気中のエアロゾル試料に見つかった粒子よりも大きく、また放射能強度も強い特徴を持ち、近隣地域にはより大きな粒子が重力沈降で沈着した可能性を示唆した。

小野ら（2017）の論文では、さらに土壌試料中に比放射能（単位質量あたりの放射能）はエアロゾルから分離された粒子より低いものの、大きさが 100µm ほどの放射性粒子を発見し、放射光分析でその詳細な化学成分を明らかにした。これらの大きな粒子は、球状粒子が複数溶融したような形態をしており、ケイ素を主成分とする特徴を示し、また 20 元素以上の様々な微量成分が検出された。これらの粒子は、Adachi et al (2013)で見つかった粒子と異なる物理化学性質を持っており、異なった放出プロセスがあったことを示唆する。Satou et al (2018)では、それらの粒子のセシウム 134、137 の比が異なることを見つけて、その同位体比の違った粒子のうち比放射能が高く、数 μ 程度で比較的球状に近い粒子を A タイプとし、比放射能は低いものの大きな粒子を B タイプとして分類した。

足立（2017）の論文ではこれらの成果をまとめて、今後の研究の発展に資するデータのまとめを行った。その一例の表を下記に示す。

Table 1 Summary of insoluble radioactive particles from nine studies

References	Sampling place	Sample type	Diameter (µm) of spherical particles	Diameter (µm) of non-spherical particles	Radioactivity (Bq) of ^{137}Cs	Particle number
Adachi et al (2013)	Ibaraki	Aerosol filter	2.0-2.6		3.3-0.7	3
Abe et al (2014)	Ibaraki	Aerosol filter	1.4-2.8		1.1-1.5	3
Yamaguchi et al. (2016)	Fukushima	Non-woven fabric cloth & Cedar	2.2-2.5		3.1-5.0	2
Satou et al., (2016)	Fukushima	Soil	3.0-4.0	4.5-6.4	5-67	4
Kogure et al. (2016)	Fukushima	Non-woven fabric cloth & Wheat	0.8-2.7		1.9-3.3	3
Furuki et al (2017)	Fukushima	Soil & Gravel	2.0-3.3	3.4	0.9-11.3	3
Yamaguchi et al. (2017)	Fukushima	Aerosol filter & Plant tissue		1.4-3.6	0.5-1.9	4
Ono et al. (2017)	Fukushima	Soil	2.6-3.6	50-250	33-109	7
Higaki et al. (2017)	Fukushima	Mask	2.1	6.6-12	1-70	4

足立（2017）エアロゾル研究 32 巻 4 号より。

3）まとめ

本放射能調査費によって行われた研究成果により、福島第一原子力発電所事故において放出された放射性物質の大気中の物理化学特性の一部が明らかとなった。これらの研究をもとに、今後事故から放出された放射性物質の発生源メカニズムの解明や環境動態の予測への貢献が期待される。

参考文献

Y. Satou, K. Sueki, K. Sasa, H. Yoshikawa, S. Nakama, H. Minowa, Y. Abe, I. Nakai, T. Ono, K. Adachi and Y. Igarashi, Analysis of two forms of radioactive particles emitted during the early stages of the Fukushima Dai-ichi Nuclear Power Station accident, Geochemical Journal, Vol. 52, 2018、

足立光司、原子力発電所事故で放出された不溶性放射性粒子の形態と組成、エアロゾル研究 32-4, 255-260, 2017

小野貴大, 飯澤勇信, 阿部善也, 中井 泉, 寺田靖子, 佐藤志彦, 末木啓介, 足立光司, 五十嵐康人、福島第一原子力発電所事故により 1 号機から放出された放射性粒子の 放射光マイクロビーム X 線分析を用いる化学性状の解明、分析化学 66（4） 2017

Y. Satou, K. Sueki, K. Sasa, K. Adachi, Y. Igarashi, First successful isolation of radioactive particles from soil near the Fukushima Daiichi Nuclear Power Plant, Anthropocene, Volume 14, Pages 71-76, 2016 Abe, Y., Iizawa, Y., Terada, Y., Adachi, K., Igarashi, Y., and Nakai, I., Detection of uranium and chemical state analysis of individual radioactive microparticles emitted from the Fukushima nuclear accident using multiple synchrotron radiation X-ray analyses, Analytical Chemistry, 86, 8521-8525, 2014.

Adachi, K., Kajino, M., Zaizen, Y., and Igarashi, Y., Emission of spherical cesium-bearing particles from an early stage of the Fukushima nuclear accident, Scientific Reports, 3, 2554, 2013.

Yamaguchi, N., Mitome, M., Kotone, A. H., Asano, M., Adachi, K., and Kogure, T., Internal structure of cesium-bearing radioactive microparticles released from Fukushima nuclear power plant. Scientific Reports, 6, 20548, 2016.

3. 放射性物質の再浮遊、輸送、沈着モデルによる評価

1） 福島原子力事故後の放射性セシウム大気濃度の長期評価：裸地と森林生態系からの再飛散

福島原子力事故による汚染土壌や森林からの ^{137}Cs 再飛散の長期的影響を、汚染地域（福島県浪江町）の土壌からの再飛散実験結果，および汚染地域内（浪江）・外（茨城県つくば市）の大気濃度測定, および数値シミュレーションを併用して実施した（Kajino et al., 2016）。評価期間は 2013 年の 1 年間である。推定された再飛散率は約 10^{-6}/day であり、福島県におけるガンマ線線量率の減少率（10^{-4}-10^{-3}/day）よりも明らかに低かった．すなわち，再飛散は陸上の放射能の減少にはほとんど寄与していなかったことが分かる。再飛散メカニズムは、特に森林生態系に関しては，未知のままである。今後は，メカニズム解明の実験研究に基づいた影響評価を行っていく必要がある。

Fig. 1 に計算された 2013 年の 1 年間の再飛散量と、再沈着量を示す。領域・時間積算再飛散量は、初期の沈着量 2.68 PBq（NRA, 2012）の 0.048%に相当した。

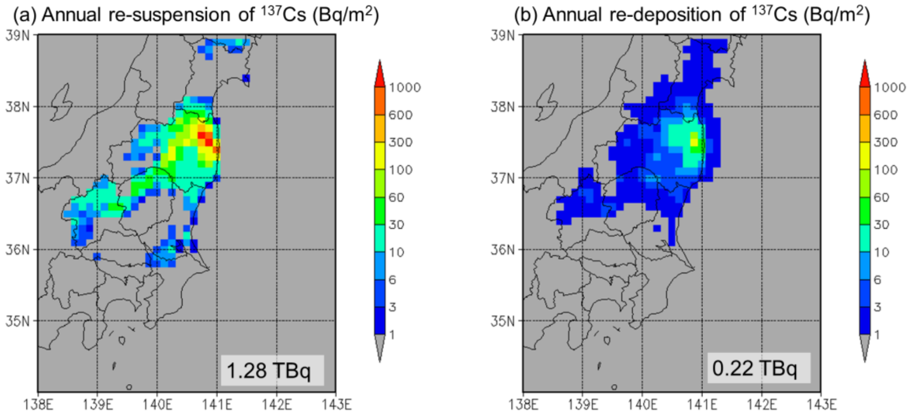

Fig. 1. Annual total amounts of (a) the re-suspension and (b) the re-deposition of ^{137}Cs. The total activities are presented as numbers.

2） 福島原発事故時の地上プリューム移流予測に及ぼす地上風データ同化の影響

2011 年 3 月の福島原発事故で排出された放射性セシウムを大気トレーサーとして用い、対流圏下層のプルーム移流の予測可能性と AMeDAS 地上風データ同化の影響を調べた（Sekiyama et al., 2017）。気象庁非静力学モデルと局所アンサンブルカルマンフィルタ（JMANHM-LETKF）データ同化システムを用いて、実験を行った。40 の観測地点における、放射性セシウムのプルーム到着時間について調べたところ、標準実験（標準的な観測データのみ同化）のプルーム到着時間の平均誤差は 82.0 分であった。それに対して、AMeDAS 実験（標準的な観測データと AMeDAS 地上風観測の両方を同化する）の平均誤差は 72.8 分であり、これは標準実験に比べて 9.2 分（11%）高精度であった。本研究は、プルーム予測モデルが緊急時対応のために十分な精度を有し、予測結果が地上風データ同化によって著しく改善され得ることを示すものである。

Fig. 2 に、埼玉県久喜市において観測された大気濃度（SPM テープ：浮遊粒子状物質観測用フィルタ上の ^{137}Cs 濃度、Tsuruta et al., 2014; Oura et al., 2015）と、データ同化前後の計算結果の比較を示す。データ同化を行っていないものを STD Exp.（実線）、地上風データ同化を行ったものを AMeDAS Exp.（破線）としている。プリュームの到達時間に明らかな改善が見られている。

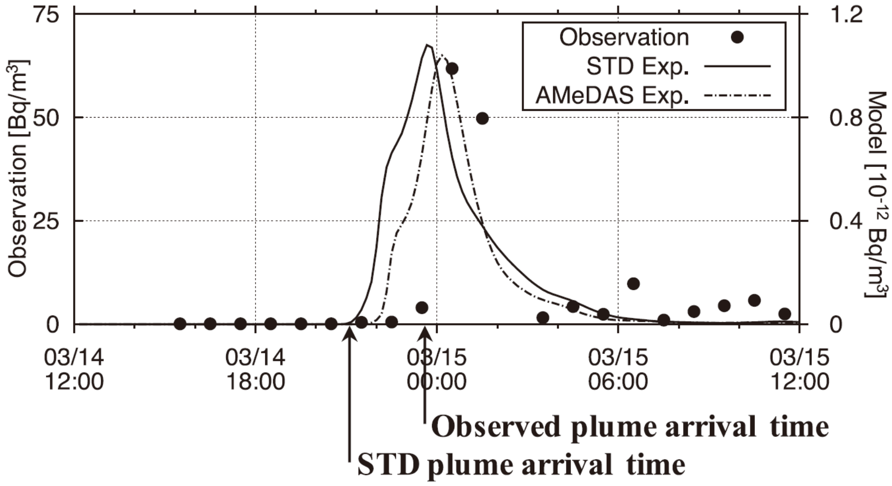

Fig. 2 An example of time series of the radioactive cesium (^{137}Cs) concentrations derived from the SPM-tape sampling observations and two model experiments (STD and AMeDAS) from 12:00 UTC on March 14 to 12:00 UTC on March 15, 2011. The advection of the plumes was examined using the data from Kuki City, Saitama Prefecture.

3）福島原子力事故後の大気モデリング研究から学んだ教訓：アンサンブルシミュレーション、データ同化、素過程モデリング、逆解析

福島第一原子力発電所事故に伴う放射性セシウムの大気拡散と沈着に関するモデリング研究について、フランス放射線防護・原子力安全研究所と気象庁気象研究所の共同研究に着目しながら、レビューを行った（Kajino et al., 2018）。これまでのモデル研究により、湿性沈着過程が重要なプロセスであることが判明しているが、その影響の大きさは不明のままである。また、モデルによって計算結果が大きく異なることが判明しているが、その原因は定かではない。本共同研究では、大気素過程、特に湿性沈着過程の理解のために、アンサンブルシミュレーション、データ同化、素過程モデリング、逆解析などのさまざまな数値技術を使用して、シミュレーションの各要素の不確実性を定量化することを目指した。本論文では、これらの共同研究の成果を紹介するとともに、今後の大気モデル研究の将来の方向性についても議論した。

4）福島第一原子力発電所から放出された ^{137}Cs プルームの質量フラックス解析

Sekiyama and Iwasaki (2018) では、^{137}Cs プルームの質量フラックス解析を行い、2011 年 3 月に福島第一原子力発電所から放出された ^{137}Cs のプルームについて質量フラックスの流れを定量的に示すことができた。この ^{137}Cs のプルームは 3km の水平分解能を持つオイラー型の大気移流拡散モデルによって計算した。鉛直積分した質量フラックスは ^{137}Cs 濃度の地上観測値に基づく移流経路推定とほぼ一致していたが、地上とプルーム層との間に風速シアーがある場合には不一致が生じた。この不一致は、地表面の水平質量フラックスと鉛直積分した質量フラックスの二つを組み合わせることによって理解できる（Fig. 3 参照）。質量密度と風速の積である質量フラックスの概念は気象力学においては一般的であるが、大気汚染の研究においてはほとんど使用されてこなかった。しかし質量フラックス解析は、数値モデルが計算する４次元（x,y,z,t）の出力値を２次元（x,y）プロットに縮小することによって、大気微量成分の主要な流れの位置、方向、および沈着の振る舞いを明瞭にすることができるため定量的な可視化ツールとして最適である。本研究では、大気中の放射性物質（この場合は ^{137}Cs）の移流拡散を調べることによって、大気汚染の研究においても質量フラックス解析が非常に有用な手法であることを示すことができた。

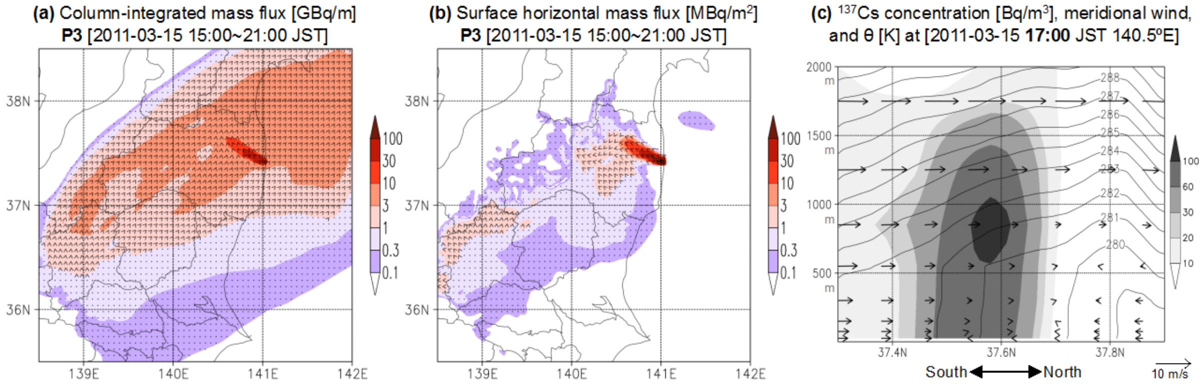

Fig. 3 Time-integrals from 15:00 to 21:00 JST on 15 March 2011 of (a) the column-integrated mass flux of plume P3 and (b) the horizontal mass flux of plume P3 at the ground surface. Color shading indicates the magnitude of the mass flux. Small arrowheads indicate the direction of the mass flux. A large gray arrow illustrates the depiction in Nakajima et al. (2017) for plume P3 at 18:00 JST on March 15, shown in Fig. 2. (c) Latitude-altitude cross-sections at 140.5E for 137Cs concentrations (gray shading), meridional winds (arrows), and potential temperature (h; contours) at 17:00 JST on 15 March 2011. The cross-section is located at the green line in panel (b).

参考文献

Kajino, M., M. Ishizuka, Y. Igarashi, K. Kita, C. Yoshikawa, M. Inatsu. Long-term assessment of airborne radiocesium after the Fukushima nuclear accident: Re-suspension from bare soil and forest ecosystems, *Atmos. Chem. Phys.*, 16, 13149-13172, doi:10.5194/acp-16-13149-2016, 2016.

Kajino, M., T. T. Sekiyama, A. Mathieu, I. Korsakissok, R. Périllat, D. Quélo, A. Quérel, O. Saunier, K. Adachi, S. Girard, T. Maki, K. Yumimoto, D. Didier, O. Masson, Y. Igarashi, Lessons learned from atmospheric modeling studies after the Fukushima nuclear accident: Ensemble simulations, data assimilation, elemental process modeling, and inverse modeling, *Geochemical Journal* 52(2), 85-101, doi:10.2343/geochemj.2.0503, 2018.

Nakajima. T., S. Misawa, Y. Morino, H. Tsuruta, D. Goto, and co-authors. Model depiction of the atmospheric flows of radioactive cesium emitted from the Fukushima Daiichi Nuclear Power Station accident. *Prog. Earth Planet. Sci.* 4:2, DOI:10.1186/s40645-017-0117-x, 2017.

NRA (Nuclear Regulation Authority), Airborne Monitoring Results in each prefecture, available at http://radioactivity.nsr.go.jp/en/list/203/list-1.html, 2012. (last access: 21 January 2019)

Oura, Y., M. Ebihara, H. Tsuruta, T. Nakajima, T. Ohara, M. Ishimoto, H. Sawahata, Y. Katsumura, W. Nitta. A database of hourly atmospheric concentration of radiocesium (134Cs and 137Cs) in suspended particulate matter collected in March 2011 at 99 air pollution monitoring stations in Eastern Japan. *J. Nucl. Radiochem. Sci.*, 15(2), 15-26, 2015.

Sekiyama, T. T., M. Kajino, M. Kunii. The impact of surface wind data assimilation on the predictability of near-surface plume advection in the case of the Fukushima Nuclear Accident, *J. Meteor. Soc. Japan*, 95(6), 447-454, doi:10.2151/jmsj.2017-025, 2017.

Sekiyama, T. T. and T. Iwasaki: Mass flux analysis of ^{137}Cs plumes emitted from the Fukushima Daiichi Nuclear Power Plant, *Tellus B*, 70(1), 1–11, doi:10.1080/16000889.2018.1507390, 2018.

Tsuruta, H., Y. Oura, M. Ebihara, T. Ohara, T. Nakajima. First retrieval of hourly atmospheric radionuclides just after the Fukushima accident by analyzing filter-tapes of operational air pollution monitoring stations. *Sci. Rep.*, 4, 6717, doi:10.1038/srep06717, 2014.

4. Publications 2016-2018

出版論文 2016-2018

Journal of Environmental Radioactivity 166 (2017) 97–103

Contents lists available at ScienceDirect

Journal of Environmental Radioactivity

journal homepage: www.elsevier.com/locate/jenvrad

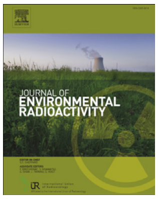

Plutonium, ^{137}Cs and uranium isotopes in Mongolian surface soils

K. Hirose [a, *], Y. Kikawada [a], Y. Igarashi [b], H. Fujiwara [c], D. Jugder [d], Y. Matsumoto [a], T. Oi [a], M. Nomura [e]

[a] Department of Material and Life Sciences, Faculty of Science and Technology, Sophia University, 7-1 Kioi-cho, Ciyoda-Ku, Tokyo 102-8554, Japan
[b] Atmospheric Environment and Applied Meteorology Research Department, Meteorological Research Institute, Tsukuba, Ibaraki 305-0052 Japan
[c] Soil Environment Division, National Institute for Agro-Environmental Sciences, Tsukuba, Ibaraki 305-8601, Japan
[d] Institute of Meteorology and Hydrology, Ulaanbaatar 46, Mongolia
[e] Research Laboratory for Nuclear Reactors, Tokyo Institute of Technology, Ookayama 2-12-1, Meguro-Ku, Tokyo 152-8550, Japan

ARTICLE INFO

Article history:
Received 29 October 2015
Received in revised form
12 January 2016
Accepted 14 January 2016
Available online 30 January 2016

Keywords:
^{239,240}Pu
^{238}Pu/^{239,240}Pu activity ratio
^{137}Cs/^{239,240}Pu activity ratio
^{235}U/^{238}U isotope ratio
Mongolian surface soil
Migration

ABSTRACT

Plutonium (^{238}Pu and ^{239,240}Pu), ^{137}Cs and plutonium activity ratios (^{238}Pu/^{239,240}Pu) as did uranium isotope ratio (^{235}U/^{238}U) were measured in surface soil samples collected in southeast Mongolia. The ^{239,240}Pu and ^{137}Cs concentrations in Mongolian surface soils (<53 μm of particle size) ranged from 0.42 ± 0.03 to 3.53 ± 0.09 mBq g^{-1} and from 11.6 ± 0.7 to 102 ± 1 mBq g^{-1}, respectively. The ^{238}Pu/^{239,240}Pu activity ratios in the surface soils (0.013–0.06) coincided with that of global fallout. The ^{235}U/^{238}U atom ratios in the surface soil show the natural one. There was a good correlation between the ^{239,240}Pu and ^{137}Cs concentrations in the surface soils. We introduce the migration depth to have better understanding of migration behaviors of anthropogenic radionuclides in surface soil. We found a difference of the migration behavior between ^{239,240}Pu and ^{137}Cs from ^{137}Cs/^{239,240}Pu – ^{137}Cs plots for the Mongolian and Tsukuba surface soils; plutonium in surface soil is migrated easier than ^{137}Cs.

1. Introduction

Increasing human activities and resulting environmental effects such as climate change alter global environment, ex, desertification. In order to assess environmental effects of human activities, therefore, it is necessary to better understand what kinds of environmental change occur globally. Radionuclides and their isotope ratios have been used as indicators of the environmental change such as desertification and erosion (Hirose, 2011). Anthropogenic radionuclides, especially plutonium and fission products, in environmental samples, which were dominantly derived from global fallout due to the atmospheric nuclear tests during the period of the 1950s to the early 1960s (UNSCEAR, 2000), are a useful tool to solve long-term environmental changes. After 1990, plutonium and fission products (^{137}Cs, ^{90}Sr and others) in aerosol and deposition samples before the Fukushima Daiichi Nuclear Power Plant accident in 2011 (Povinec et al., 2013; Hirose and Povinec, 2015), whose major sources are dust blown by severe storms in the deserts and arid regions, are recognized as a proxy of environmental change due to human activities/climate change and others (Fujiwara et al., 2007; Hirose, 2011; Hirose et al., 2003, 2004; Igarashi et al., 2005, 2009, 2011).

Plutonium has been released into the environment due to the atmospheric nuclear-weapons tests, burn-up of nuclear-battery satellite, nuclear reactor accidents, and others (Harley, 1980). Plutonium, which is one of chemically reactive elements, is cycled in the globe according to physical and biogeochemical processes. Effectively to use radionuclides as a tracer, it is important to elucidate geographical distributions of radionuclides in continental land surface. In the past 50 years, the Pu distribution in land surface across many countries has been determined and published (Hardy et al., 1973). However, data on the geographical distribution of Pu in soil of East Asian continental regions including China and Mongolia is scarce. Zhu et al. (2002) reported the ^{239,240}Pu concentrations in Chinese soils estimated from the ^{137}Cs concentrations and the global fallout ^{239,240}Pu/^{137}Cs ratio (0.02). Zheng et al. (2009) studied concentrations and characterization of Pu isotopes in loess collected from Gansu Province, Northwest China, which corresponds to the downwind regions of Lop Nor Chinese nuclear test site. Dong et al. (2010) determined ^{239,240}Pu concentrations and ^{240}Pu/^{239}Pu atom ratios in soil

---

* Corresponding author.
E-mail address: hirose45037@mail2.accsnet.ne.jp (K. Hirose).

http://dx.doi.org/10.1016/j.jenvrad.2016.01.007
0265-931X/

columns in central China. Recently Bu et al. (2015) reported comprehensive research of Pu isotopes in loess collected from Gansu Province to elucidate effects of local fallout due to the Chinese nuclear testing. Within our knowledge, however, no systematic study has been published in the literature on the distribution of ^{239,240}Pu in Mongolian surface soil. It is important to have better understanding of plutonium isotopes and uranium isotopes in Mongolian surface soil because Mongolia is a potential source region of the Asian dust (Igarashi et al., 2011).

The atomic abundance ratio between the two primordial isotopes of uranium, ^{235}U and ^{238}U, shows no significant variation in nature except in fossil natural reactors (Cowan, 1976). However, uranium isotope ratios in environmental samples have altered as a result of anthropogenic activities such as burn up of nuclear satellites (Krey et al., 1979) and use of depleted uranium (Carvalho and Oliveira, 2010). As did plutonium isotopes, uranium isotopes (^{234}U/^{238}U activity ratios and ^{235}U/^{238}U isotope ratios) are a tracer of anthropogenic activities and natural processes. In fact, anomalous uranium isotope ratios (^{235}U/^{238}U) have been recognized in fallout samples (Kikawada et al., 2009, 2012, 2015) and archived samples (Warneke et al., 2002). In the East Asian Continent, including atmospheric nuclear test sites, it may be likely that surface soils have been contaminated by fissile materials. It is, therefore, is important to have information on uranium isotope ratios (^{235}U/^{238}U) in surface soils in Mongolia, where is downstream of the Chinese nuclear test site and also source region of the Asian dust.

In this report, we describe the first sight of plutonium concentrations and uranium isotopes in surface fine soils of the southeast Mongolia, where the desertification is a significant recent problem, which suggests that the Asian dust source region may have been expanding after the 2000s (e.g. Igarashi et al., 2011; Kido et al., 2012). We also discuss about mobility of plutonium in surface soils.

2. Sampling and measurements

Undisturbed surface soil sampling campaign was conducted in southeastern Mongolia in fall 2007 (Igarashi et al., 2011), in which most of the sampling sites are located in the desert-steppe zone; annual precipitation amounts at the sampling sites of Mongolia ranges from about 100 to 300 mm yr^{-1} (Igarashi et al., 2011). Annual precipitation amounts at Tsukuba, Japan as a reference station were in the range from 1069 to 1607 mm yr^{-1} in the 2000s. Sampling locations are shown in Fig. 1 and Table S1. At each site, at spots as far from vehicular traffic and ruts as possible, an approximate 1-kg of undisturbed surface soil was collected to a depth of 5 cm by using a core sampler. After sample preparation treatments including an autoclave treatment, removal of stones, pebbles, grasses and roots by hand and homogenization, a fraction that passed through a 53-μm mesh (nominal), which almost corresponds to silts and/or clay, was subjected to analysis of ^{137}Cs and plutonium because this fraction was considered as a candidate for dust suspended and transported by strong wind (Igarashi et al., 2011). After being packed into a uniform plastic container, each sample was subjected to gamma-ray spectrometry using a Ge semiconductor detector for ^{137}Cs measurements. After the ^{137}Cs measurements, 24 soil samples were used for plutonium analysis. The soil samples were decomposed and dissolved by strong acids. After the radiochemical separation and purification (Otsuji-Hatori et al., 1996), plutonium isotopes were measured by α-spectrometry.

Ten Mongolian soil samples were also subjected to the uranium isotope measurement. For three soil samples, we divided into three particle size fractions (100–500 μm, 45–100 μm and <45 μm) by using sieve. For the measurement, the samples were first subjected to the acid (4 M HNO_3) leaching treatments (acid soluble fraction). Residue (acid insoluble fraction) was decomposed by HF, $HClO_4$ and conc. HNO_3 and finally dissolved in 4 M HNO_3 solution. After chemical isolation by Eichrom UTEVA resin, the uranium concentrations and the ^{235}U/^{238}U ratios in the acid soluble and acid insoluble fractions were measured by ICP-QMS separately. The obtained ^{235}U/^{238}U ratios in the samples were corrected by that in seawater as a conventional standard, whose isotope ratio is regarded as the natural ratio. The details of these analytical procedures are described in Kikawada et al. (2009).

3. Results and discussion

3.1. Levels of plutonium and ^{137}Cs in soil

Concentrations of ^{239,240}Pu and ^{137}Cs in Mongolian surface soils (24 samples) are summarized in Table 1. The ^{239,240}Pu concentrations in surface soil in the southeast Mongolia ranged from 0.42 ± 0.03 to 3.53 ± 0.09 mBq g^{-1} with an average of 1.59 mBq g^{-1}, and from 11.6 ± 0.7 to 102 ± 1 mBq g^{-1} with an average of 46.9 mBq g^{-1}, respectively. The results reveal that there are large spatial variations of the ^{239,240}Pu and ^{137}Cs concentrations in the Mongolian surface soils. It is likely that precipitation amounts are closely related to the ^{239,240}Pu and ^{137}Cs concentrations in surface soil because plutonium and ^{137}Cs in surface soil were deposited by wet and dry depositions and they tightly adsorb on soil surface (Pálsson et al., 2013). Igarashi et al. (2011) examined the relationship between the ^{137}Cs concentrations in the Mongolian surface soils and annual precipitation amounts, in which they found a correlation between the ^{137}Cs concentrations in the surface soil and annual precipitation amounts, suggesting that the level of the ^{137}Cs concentrations in surface soil is mainly controlled by wet deposition. These findings suggest that the spatial distribution of the Mongolian surface ^{239,240}Pu is governed by wet deposition, as did ^{137}Cs.

We compared with the ^{239,240}Pu concentrations in Japanese and Chinese surface soils. Although direct comparison between Mongolian and Chinese surface soil ^{239,240}Pu is difficult because of different sample preparations, the ^{239,240}Pu concentrations in the Mongolian surface soils seems to be generally higher than reported ones for the Chinese soils; their values for Gansu (Zheng et al., 2009) and central China (Hubei) (Dong et al., 2010) were 0.02–0.16 and 0.3–0.5 mBq g^{-1}, respectively. On the other hand, the ^{239,240}Pu concentrations between the Mongolian and Tsukuba surface soils can be compared each other because soil fractions for Tsukuba was passed through a 53-μm mesh, as did the Mongolian soils. The level of ^{239,240}Pu in the Mongolian surface soils was about one order of magnitude greater than that in Tsukuba, Japan, ranging from 0.019 ± 0.005 to 0.41 ± 0.03 mBq g^{-1} as an average of 0.18 mBq g^{-1}. It is noteworthy that the soil samples collected at Tsukuba contained ones in cultivated areas. The ^{239,240}Pu concentrations in surface soil collected in central-eastern Japan around the 1970s were determined, where includes the Kanto area locating at Tsukuba (Yang et al., 2015). We examine frequency distributions of the ^{239,240}Pu concentrations in surface soils of Mongolia and central-eastern Japan. The frequency distributions of the soil ^{239,240}Pu (Fig. 2) reveal that the ^{239,240}Pu concentrations in surface soils of Mongolia are systematically greater than that in central-eastern Japan. Especially, Yang et al. (2015) reported that the low ^{239,240}Pu concentrations in surface soils occurred in the Kanto area. The similar results were observed for ^{137}Cs and ^{90}Sr in Mongolian surface soils; median levels of activity concentrations of ^{137}Cs and ^{90}Sr in the Mongolian surface soil were 2 and 8 times higher than those in Tsukuba, respectively (Igarashi et al., 2011).

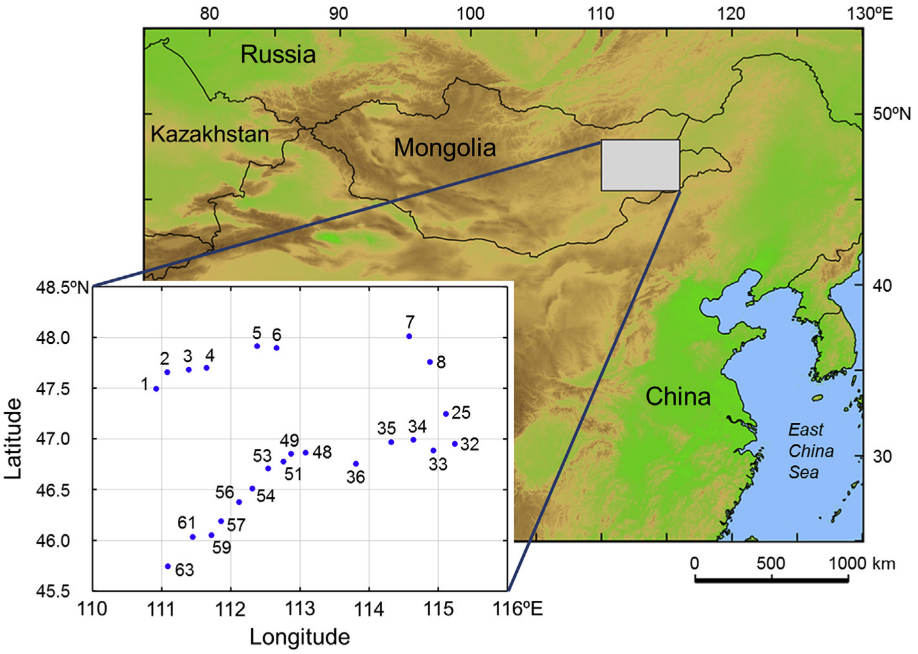

Fig. 1. Sampling location of surface soil in Mongolia. Numerals correspond to sampling sites shown in Table 1.

Table 1
Concentrations of ^{239,240}Pu, ^{238}Pu and ^{137}Cs in surface soil in Mongolia.

	Latitude	Longitude	^{239,240}Pu mBq g^{-1}	^{238}Pu mBq g^{-1}	^{238}Pu/^{239,240}Pu mBq g^{-1}	^{137}Cs mBq g^{-1}	^{137}Cs/^{239,240}Pu mBq g^{-1}
1[a]	47.495	110.92	0.71 ± 0.04			20.1 ± 0.5	28.3
2	47.658	111.08	3.53 ± 0.09	0.078 ± 0.013	0.022	102 ± 1	28.9
3	47.683	111.39	2.43 ± 0.06	0.107 ± 0.014	0.044	74.3 ± 0.9	30.6
4	47.702	111.65	1.81 ± 0.07	0.043 ± 0.01	0.024	62.4 ± 0.8	34.5
5	47.916	112.38	2.48 ± 0.07	0.114 ± 0.015	0.046	75.2 ± 0.9	30.3
6	47.898	112.66	2.42 ± 0.07	0.031 ± 0.008	0.013	78.0 ± 0.8	32.2
7	48.012	114.58	1.85 ± 0.06	0.111 ± 0.014	0.06	63.3 ± 1.1	34.2
8	47.76	114.88	1.33 ± 0.05	0.022 ± 0.007	0.017	42.4 ± 1	31.9
25	47.248	115.11	0.74 ± 0.04			22.3 ± 0.4	30.1
32	46.953	115.24	1.71 ± 0.06			57.5 ± 1	33.7
33	46.888	114.93	2.05 ± 0.06	0.062 ± 0.01	0.03	65.9 ± 1.1	32.1
34	46.993	114.64	2.54 ± 0.07	0.076 ± 0.011	0.03	74.3 ± 1.2	29.3
35	46.969	114.32	2.74 ± 0.07	0.085 ± 0.013	0.031	77.2 ± 1.2	28.2
36	46.757	113.81	0.99 ± 0.05	0.021 ± 0.008	0.021	26.2 ± 0.8	26.5
48	46.866	113.08	1.21 ± 0.05	0.03 ± 0.008	0.025	26.8 ± 0.8	22.1
49	46.855	112.87	1.56 ± 0.06			42.3 ± 0.5	27.1
51	46.778	112.76	1.44 ± 0.06	0.035 ± 0.008	0.024	37.5 ± 0.9	26
53	46.711	112.54	0.80 ± 0.04	0.024 ± 0.007	0.03	25.9 ± 0.8	32.2
54	46.513	112.31	0.46 ± 0.03			11.6 ± 0.7	25.4
56	46.38	112.12	0.60 ± 0.04			14.7 ± 0.8	24.6
57	46.19	111.86	1.92 ± 0.07	0.038 ± 0.01	0.02	49.7 ± 1	25.9
59	46.053	111.72	0.42 ± 0.03			13.1 ± 0.4	31.1
61	46.034	111.45	1.24 ± 0.07			32.3 ± 0.8	26.1
63	45.746	111.09	1.07 ± 0.06			30.1 ± 0.9	28.1

Radioactive decay of ^{137}Cs and ^{238}Pu were corrected at sampling time (Oct. 2007).
[a] Number of sampling location as shown in Fig. 1.

3.2. ^{238}Pu and ^{238}Pu/^{239,240}Pu activity ratio in Mongolian soils

The ^{238}Pu/^{239,240}Pu activity ratio is a kind of fingerprint to identify sources of plutonium in the environmental samples. The ^{238}Pu concentrations and ^{238}Pu/^{239,240}Pu activity ratio in the Mongolian soils are shown in Table 1. The ^{238}Pu/^{239,240}Pu activity ratios in the Mongolian surface soil were in the range of 0.013–0.06 with an average of 0.029. The similar ^{238}Pu/^{239,240}Pu activity ratios were observed in the Sahara dust (Pham et al., 2005; Mason et al., 2010). The ^{238}Pu/^{239,240}Pu activity ratios coincide with that in global fallout (0.03–0.05) from the 1961–62 large-scale atmospheric nuclear tests (UNSCEAR, 1982). These finding suggests that plutonium in the Mongolian surface soils is primarily derived from global fallout.

3.3. Uranium isotopes in Mongolian soil

Uranium concentrations in Mongolian soil samples, summarized in Table S2, are in the range of 0.8–2.5 μg g^{-1}. The uranium concentrations in Mongolian soils are the same order of magnitude as that in igneous and sedimentary rocks (0.45–3.7 μg g^{-1}) (Faure, 1991) and Chinese loess (2.72–4.08 μg g^{-1}) (Ding et al., 2001; Tayler

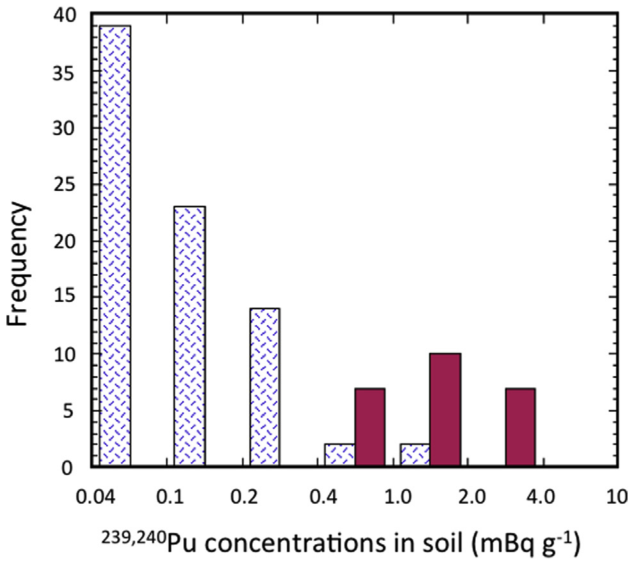

Fig. 2. Frequency distributions of ^{239,240}Pu concentrations in surface soils of Mongolia and central-eastern Japan. Red colored column: Mongolian soils, blue dot column: central-eastern Japan soils (cited from Yang et al., 2015) (For interpretation of the references to color in this figure legend, the reader is referred to the web version of this article).

et al., 1983). The percentages of acid soluble uranium to total uranium (Table S3) ranged from 8.3 to 50%. We examined ^{235}U/^{238}U isotope ratios in both acid soluble and acid insoluble fractions of the Mongolian soil samples. The ^{235}U/^{238}U isotope ratios in both the acid soluble and acid insoluble fractions of the Mongolian soil samples were in ranges of 0.996 ± 0.003–1.004 ± 0.003 and 0.997 ± 0.006–1.002 ± 0.005 as seawater base, respectively, which coincide with the natural ratio within analytical uncertainty, although the leaching proportion of uranium varied sample by sample widely. We examined ^{235}U/^{238}U isotope ratios in three soil particle size fractions (100–500 μm, 45–100 μm and <45 μm) of the Mongolian soil samples. The ^{235}U/^{238}U isotope ratios in three particle fractions of the Mongolian soils (Table S3) were 0.998 ± 0.006–1.005 ± 0.012, 0.999 ± 0.015–1.005 ± 0.008, and 0.997 ± 0.011–1.001 ± 0.005 for particle ranges of 100–500 μm, 45–100 μm and <45 μm, respectively. These findings suggest that irrespective of chemical forms and particle size, there is no fractionation of the uranium isotope ratio in the Mongolian soils.

3.4. *Plutonium as an indicator of Asian dust*

Atmospheric Pu deposition observed in Japan changed from the 1990s to the 2000s; typically, higher ^{239,240}Pu deposition occurred in spring of the 2000s with higher massic concentrations of ^{239,240}Pu than those in the 1990s (Hirose et al., 2008). As its causes, dust events in the East Asian continent desert and arid regions increased in the 2000s; especially, the dust storm activities increased in the Mongolian Plateau and adjacent source regions (Kurosaki and Mikami, 2003; Lim and Chun, 2006; Kim, 2008). The high ^{239,240}Pu concentrations in the Mongolian soils, which can support the high ^{239,240}Pu massic concentrations in deposition at the Meteorological Research Institute (MRI), Tsukuba, suggest that the source region of Asian dust changed not only from the Tarim Basin but also from the Mongolian Plateau and adjacent regions. These findings suggest that long-term change of the deposition of anthropogenic radionuclides reflects environmental changes in the East Asian continent, corresponding to desertification due to human activities such as over-clopping and over-grazing and/or climate change (Igarashi et al., 2011).

3.5. *Anthropogenic radionuclides as an indicator of erosion processes*

In order to have better understanding of behavior of plutonium in the Mongolian surface soil, it is valuable to compare between fission products and plutonium in the surface soils because both sources are derived from the nuclear weapons tests. The difference of migration behaviors between ^{90}Sr and ^{137}Cs in the terrestrial environment has been recognized (Forsberg and Strandmark, 2001; Igarashi et al., 2011). We examined the relationship between plutonium and ^{137}Cs in the Mongolian surface soils, in which plutonium exists as insoluble oxides and/or organic complexes (Druteikienè et al., 2002) whereas ^{137}Cs is tightly incorporated into clay minerals (Cremers et al., 1988; Fukushi et al., 2014; Hirose et al., 2015; Kogure et al., 2012). The plot of plutonium to ^{137}Cs in the Mongolian soils as did Tsukuba (Japan) soils is shown in Fig. 3, in which radioactive decay of ^{137}Cs was corrected at each soil sampling time. The ^{239,240}Pu concentrations in the Mongolian and Tsukuba surface soils well correlated with that of ^{137}Cs in the corresponding soils, in which correlation factors for Mongolia and Tsukuba are 0.982 and 0.968, respectively. Correlation slopes for the Mongolian and Tsukuba surface soils were 0.032 and 0.022, respectively, in which ^{239,240}Pu/^{137}Cs ratios of global fallout at the soil sampling times of Mongolia (Oct. 2007) and Tsukuba (Jan. 2000) were 0.034 ± 0.003 and 0.029 ± 0.003, respectively. The correlation slope for the Tsukuba surface soil is smaller than that of the Mongolian surface soil, which suggests that migration behaviors of anthropogenic radionuclides in surface soil differ between Mongolia and Tsukuba.

To elucidate the migration behaviors of plutonium in surface soil, we introduce a simple model, in which migration depth of anthropogenic radionuclide in surface soil as a new concept is deduced. The concentrations of anthropogenic radionuclides in surface soil ($C_{rad,\ soil}$) is calculated from cumulative deposition of anthropogenic radionuclides ($D_{rad,\ soil}$), where subscript rad denotes individual anthropogenic radionuclide, and corresponding migration depth (d_m) as following equation.

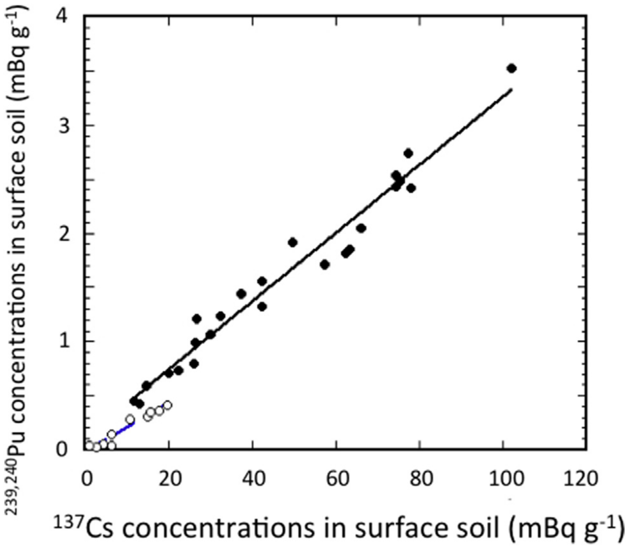

Fig. 3. Relationships between ^{239,240}Pu and ^{137}Cs concentrations in surface soils. Closed circle: Mongolia, open circle: Tsukuba.

$$C_{rad,soil} = D_{rad,soil}/(d_m \times \rho) \tag{1}$$

where ρ denotes density of soil. Now we assume that the migration depth of anthropogenic radionuclide in soil column is expressed as a sum of radionuclide-dependent and radionuclide-independent terms, which correspond to chemical processes such as sorption-desorption with soil particles and physical processes such as mixing and bio-perturbation; $d_m = d_{m,c,rad} + d_{m,p}$. The latter term ($d_{m,p}$) is common for both radionuclides. When this relationship applies to ^{137}Cs and ^{239,240}Pu in surface soil, we have a following equation.

$$C_{Cs-137,soil}/C_{Pu,soil} = D_{Cs-137,soil}/D_{Pu,soil} + \{(d_{m,c,Pu} - d_{m,c,Cs-137})\rho/D_{Pu,soil}\}C_{Cs-137,soil} \tag{2}$$

This equation means that the ^{137}Cs/^{239,240}Pu activity ratios in surface soil are linearly related to the ^{137}Cs concentrations in surface soil. We examined the relationship between the ^{137}Cs/^{239,240}Pu activity ratios and ^{137}Cs concentrations in the surface soils in Mongolia and Tsukuba, in which radioactive decay of ^{137}Cs was corrected at each soil sampling time. The result is shown in Fig. 4. We have linear relationships between the ^{137}Cs/^{239,240}Pu ratios and the ^{137}Cs concentrations in the Mongolian and Tsukuba surface soils, whose correlation factors are 0.428 and 0.878, respectively. The correlation intercepts, which correspond to the ratio of the depositions of ^{137}Cs and ^{239,240}Pu; $D_{Cs\text{-}137,soil}/D_{Pu,soil}$, are 26.6 ± 1.3 and 29.5 ± 3.6 for the Mongolian and Tsukuba surface soils, respectively, which are in good agreement with ^{137}Cs/^{239,240}Pu ratios of global fallout at soil sampling times (29 ± 3 in 2007 and 34 ± 3 in 2000) (Hodge et al., 1996). The positive correlations suggest that the migration depths of plutonium in land surface in Mongolia and Tsukuba are deeper than those of ^{137}Cs, which suggests that the plutonium in soil column is easier migrated than ^{137}Cs due to the chemical erosion processes. The correlation slopes for the Mongolian and Tsukuba surface soils are 0.055 ± 0.025 and 0.108 ± 0.026, respectively. Taken into account cumulative ^{239,240}Pu deposition at the MRI, Tsukuba (44 Bq m^{-2}) (Hirose et al., 2001), the relative migration depth of ^{239,240}Pu ($=(d_{m,c,Pu} - d_{m,c,Cs\text{-}137})$) in Tsukuba soils is calculated to be 0.30 cm, assuming the soil density of 1.6 g cm^{-3} (Feng et al., 2004). The relative migration depth of plutonium in the Mongolian surface soil is smaller than that at Tsukuba, if the ^{239,240}Pu inventory in Mongolia is similar to that at Tsukuba. In this case, the result may mean that plutonium in the Tsukuba surface soil is easier migrated than that in the Mongolian surface soil. The ^{239,240}Pu inventories in the southeast Mongolia are calculated from the ^{137}Cs inventories (Fujiwara: personal information) and ^{137}Cs/^{239,240}Pu ratio in the Mongolian surface soil. The calculated ^{239,240}Pu inventories in the southeast Mongolia, ranging from 7.6 to 75 Bq m^{-2}, are the same order of magnitude as that in China (10–546 Bq m^{-2}) (Bu et al., 2014, 2015; Dong et al., 2010; Xu et al., 2015; Zheng et al., 2009). The large spatial variability of the ^{239,240}Pu inventories in the southeast Mongolia causes that of the annual precipitation amount; the ^{137}Cs concentrations in the Mongolian surface soils correlated with the annual precipitation amount in the corresponding location (Igarashi et al., 2011). Although there is a large variability of the ^{239,240}Pu inventories in the southeast Mongolia, we found the linear relationship between the ^{137}Cs/^{239,240}Pu activity ratios and the ^{137}Cs concentrations in the Mongolia surface soils, suggesting that the relative migration depth of ^{239,240}Pu in surface soil may be linearly related with the ^{239,240}Pu inventories. Assuming that the slope of the ^{137}Cs/^{239,240}Pu – ^{137}Cs plot for the Mongolian soils is constant, the relative migration depth of ^{239,240}Pu in the Mongolian soils is calculated to be in a range of 0.032–0.32 cm, which is shorter than that at Tsukuba. This finding suggests that plutonium in soil column of deserts is migrated chemically less than in higher precipitation area such as Tsukuba, because chemical movement of plutonium in soil columns occurs via pore water between soil particles. Concept of the relative migration depth is an important tool to understand the migration behavior of radionuclides in surface soil because it is related to difference of biogeochemical conditions and soil chemistry (inorganic complexation including hydrolysis and organic complexation) in addition to difference of precipitation amounts between the Mongolian and Tsukuba surface soils; higher precipitation amounts in Tsukuba may lead to increase of chemical and biogeochemical activities. These findings reveal that the ^{137}Cs/^{239,240}Pu – ^{137}Cs plots are effective to characterize the migration properties of radionuclides including chemical erosion processes and related soil chemical properties.

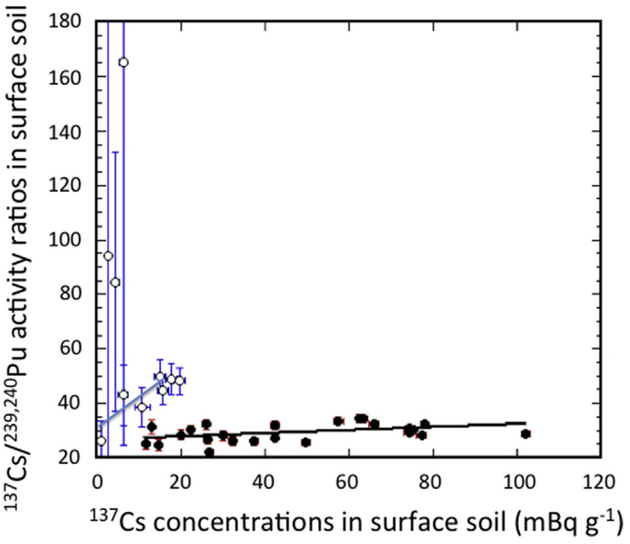

Fig. 4. Relationships between ^{137}Cs/^{239,240}Pu activity ratios and ^{137}Cs concentrations in surface soils. Closed circle: Mongolia, open circle: Tsukuba.

Igarashi et al. (2011) revealed that there is a good positive correlation between ^{137}Cs/^{90}Sr activity ratios and ^{137}Cs concentrations in the Mongolian and Tsukuba surface soils, which indicates that ^{90}Sr in the both surface soils is easily migrated comparing with ^{137}Cs. Taken into account cumulative ^{90}Sr deposition at Tsukuba (1000 Bq m^{-2} in 2000) (Hirose et al., 2001) and the correlation slope of the ^{137}Cs/^{90}Sr – ^{137}Cs plot for Tsukuba (Igarashi et al., 2011), the relative migration depth of ^{90}Sr ($=(d_{m,c,Sr\text{-}90} - d_{m,c,Cs137})$) in Tsukuba soils is calculated to be 34 cm. The correlation slope for ^{90}Sr in the Tsukuba surface soils is about 10-times deeper than that in the Mongolian soils, whereas the correlation slope for plutonium in the Tsukuba surface soils is about twice deeper than that in the Mongolian soils. These findings suggest that ^{90}Sr in the surface soils is easier migrated than plutonium in surface soil.

4. Conclusion

This is the first report that provides information on plutonium isotopes and uranium isotope ratio (^{235}U/^{238}U) in surface soils of Mongolia. The ^{239,240}Pu concentrations in surface fine soil (<53 μm of particle size) of Mongolia are generally higher than that in Tsukuba. The ^{238}Pu/^{239,240}Pu activity ratios in Mongolian surface soil coincide with that of global fallout, which means that most of the plutonium in the Mongolian soils originated from global fallout.

The ^{239,240}Pu concentrations in the Mongolian soils well correlate with the ^{137}Cs concentrations in the corresponding soils as do soil samples at Tsukuba. The correlation slope of the ^{239,240}Pu –

^{137}Cs plots for the Mongolian soils differs from that for the Tsukuba soils. We introduce migration depth of anthropogenic radionuclides in surface soil, consisting of radionuclide-independent and radionuclide-dependent terms, which correspond to physical and chemical processes, respectively. In this case, a linear relationship between ^{137}Cs/^{239,240}Pu activity ratios and the ^{137}Cs concentrations in surface soil is expected. This relationship is confirmed for the ^{239,240}Pu, ^{137}Cs and ^{90}Sr concentrations in the Mongolian and Tsukuba soils (Igarashi et al., 2011). The analysis reveals that the migration tendency of three radionuclides in surface soil is a following order: ^{90}Sr>>^{239,240}Pu > ^{137}Cs.

The ^{235}U/^{238}U ratios in the Mongolian soil samples, irrespective of chemical forms and particle size of soils, coincide with the natural ratio within analytical uncertainty.

Acknowledgments

The authors thank the Mongolian Institute of Meteorology and Hydrology for supporting our survey. All samples were exported and imported following all regulations and with the approval of both Mongolian and Japanese authorities. Sample preparation and radiochemical analyses were carried out by K. Inukai, Y. Togashi, M. Tomita, and T. Mizo, KANSO Co. Ltd. Part of the expense for conducting the Mongolian survey and the sample analysis was covered by the fund for Radioactivity Survey in Japan from the Ministry of Education, Culture, Sports, Science and Technology.

Appendix A. Supplementary data

Supplementary data related to this article can be found at http://dx.doi.org/10.1016/j.jenvrad.2016.01.007.

References

Bu, W., Ni, Y., Guo, Q., Zheng, J., Uchida, S., 2015. Pu isotopes in soils collected downwind from Lop Nor: regional fallout vs. global fallout. Sci. Rep. 5, 12262. http://dx.doi.org/10.103/srep12262.

Bu, W., Zheng, J., Guo, Q., Uchida, S., 2014. Vertical distribution and migration of global fallout Pu in the forest soils of southwestern China. J. Environ. Radioact. 136, 174–180.

Carvalho, F.P., Oliveira, J.M., 2010. Uranium isotopes in the Balkan's environment and foods following the use of depleted uranium in the war. Environ. Intern. 36, 352–360.

Cowan, G.A., 1976. A natural fission reactor. Sci. Am. 36, 235–245.

Cremers, A., Elsen, A., De Preter, P., Maes, A., 1988. Qunatitative analysis of radiocaesium retention in soils. Nature 335, 247–249.

Ding, Z.L., Sun, J.M., Yong, S.L., Liu, T.S., 2001. Geochemistry of the Pliocene red clay formation in the Chinese Loess Plateau and implications for its origin, source provenance and paleoclimate change. Geochim. Cosmochim. Acta 65, 901–913.

Dong, W., Tims, S.G., Fifield, L.K., Guo, Q., 2010. Concentration and characterization of plutonium in soils of Hubei in central China. J. Environ. Radioact. 101, 29–32.

Druteikienè, R., Luksienè, B., Gvozdaitè, R., 2002. Influence of soil factors on the vertical profile of plutonium physicochemical forms. Ekol. (Vilnius) 2, 42–46.

Faure, G., 1991. Principles and Application of Inorganic Geochemistry. Prentice Hall, Inc., USA.

Feng, Q., Liu, Y., Mikami, M., 2004. Geostatistical analysis of soil moisture variability in grassland. J. Arid. Environ. 58, 357–372.

Forsberg, S., Setrandmark, M., 2001. Migration and chemical availability of ^{137}Cs and ^{90}Sr in Swedish long-term experimental pastures. Water, Air Soil Poll. 127, 157–171.

Fukushi, K., Sakai, H., Itono, T., Tamura, A., Arai, S., 2014. Desorption of intrinsic caesium from Semectite: Inhibitive effects of clay particle organization on cesium desorption. Environ. Sci. Technol. 48, 10743–10749.

Fujiwara, H., Fukuyama, T., Shirato, Y., Ohkuro, T., Taniyama, I., Zhang, T.-H., 2007. Deposition of atmospheric ^{137}Cs in Japan associated with the Asian dust event of March 2002. Sci. Total Environ. 384, 306–315.

Harley, J.H., 1980. Plutonium in the environment - a review. J. Radiat. Res. 21, 83–104.

Hardy, E.P., Krey, P.W., Volchok, H.L., 1973. Global inventory and distribution of fallout plutonium. Nature 241, 444–445.

Hirose, K., 2011. Uranium, thorium and anthropogenic radionuclide as atmospheric tracers. In: Baskaran, M. (Ed.), Handbook of Environmental Isotope Geochemistry, Advanced in Isotope Geochemistry. Springer-Verlag, Berlin Heidelberg, pp. 591–612. Chap. 29.

Hirose, K., Igarashi, Y., Aoyama, M.T., Miyao, T., 2001. Long-term trends of plutonium fallout observed in Japan. In: Kudo, A. (Ed.), Plutonium in the Environment. Elsevier Science, pp. 251–266.

Hirose, K., Igarashi, Y., Aoyama, M., 2008. Analysis of 50 years records of atmospheric deposition of long-lived radionuclides in Japan. Appl. Radiat. Isot. 66, 1675–1678.

Hirose, K., Igarashi, Y., Aoyama, M., Kim, C.K., Kim, C.S.B.W., Chang, B.W., 2003. Recent trends of plutonium fallout observed in Japan: plutonium as a proxy for desertification. J. Environ. Monit. 5, 302–307.

Hirose, K., Kim, C.K., Kim, C.S., Chang, B.W., Igarashi, Y., Aoyama, M., 2004. Plutonium deposition observed in Daejeon, Korea: wet and dry depositions of plutonium. Sci. Total Environ. 332, 243–252.

Hirose, K., Povinec, P.P., 2015. Sources of plutonium in the atmosphere and stratosphere-troposphere mixing. Sci. Rep. 5, 15703. http://dx.doi.org/10.1038/strep15707.

Hirose, M., Kikawada, Y., Tsukamoto, A., Oi, T., Honda, T., Hirose, K., Takahashi, H., 2015. Chemical forms of radioactive Cs in soils originated from Fukushima Daiichi nuclear Power Plant accident studied by sequential extraction experiments. J. Radioanal. Nucl. Chem. 303, 1357–1359.

Hodge, V., Smith, C., Whiting, J., 1996. Radiocesium and plutonium: still together in "background" soils after more than thirty years. *Chemosphere* 32, 2067–2075.

Igarashi, Y., Aoyama, M., Hirose, K., Povinec, P.P., Yabuki, S., 2005. What anthropogenic radionuclides (^{90}Sr and ^{137}Cs) in atmospheric deposition, surface soils and Aeolian dusts suggest for dust transport over Japan. Water, Air Soil Poll. Focus 5, 51–69.

Igarashi, Y., Fujiwara, H., Jugder, D., 2011. Change of the Asian dust source region deduced from the composition of anthropogenic radionuclides in surface soil in Mongolia. Atmos. Chem. Phys. 11, 7069–7080.

Igarashi, Y., Inomata, Y., Aoyama, M., Hirose, K., Takahashi, H., Shinoda, Y., Sugimoto, N., Shimizu, A., Chiba, M., 2009. Possible change in Asian dust source suggested by atmospheric anthropogenic radionuclides during the 2000s. Atmos. Environ. 43, 2971–2980.

Kido, H., Fujiwara, H., Jamsran, U., Endo, A., 2012. The simulation of long-range transport of ^{137}Cs from East Asia to Japan in 2002 and 2006. J. Environ. Radioact. 103, 7–14.

Kikawada, Y., Oda, K., Yamauchi, R., Nomura, M., Honda, T., Oi, T., Hirose, K., Igarashi, Y., 2009. 2009. Anomalous uranium isotope ratio in atmospheric deposits in Japan. J. Nucl. Sci. Tech. 46, 1094–1098.

Kikawada, Y., Oda, K., Nomura, M., Honda, T., Oi, T., Hirose, K., Igarashi, Y., 2012. Origin of enriched uranium contained in Japanese atmospheric deposits. Nat. Sci. 4, 936–942 special issue.

Kikawada, Y., Suzuki, H., Yamauchi, R., Oi, T., Hirose, K., 2015. ^{235}U/^{238}Uisotope ratios in monthly atmospheric deposits collected at Akita, Japan in 1977 and 1978. Procedia Earth Planet. Sci. 15, 675–679.

Kim, J., 2008. Transport routes and source regions of Asian dust observed in Korea during the past 40 years (1965–2004). Atmos. Environ. 42, 4778–4789.

Kogure, T., Morimoto, K., Tamura, K., Sato, H., Yamagishi, A., 2012. XRD and HRTEM evidence for fixation of cesium ions in vermiculite clay. Chem. Lett. 41, 380–382.

Krey, P.W., Leifer, R., Benson, W.K., Dietz, L.A., Hendrikson, H.C., Coluzza, L., 1979. Atmospheric burn up of the Cosmos-954 reactor. Science 205, 583–585.

Kurosaki, Y., Mikami, M., 2003. Recent frequent dust events and their relation to surface wind in. East asia. geophys. Res. Lett. 30, 1736. http://dx.doi.org/10.1029/2003GL017261.

Lim, J.-Y., Chun, Y., 2006. The characteristics of Asian dust events in Northeast Asia during the springtime from 1993 to 2004. Glob. Planet. Change 52, 231–247.

Masson, O., Piga, D., Gurriaran, R., D'Amico, D., 2010. Impact of an exceptional Saharan dust outbreak in France: PM10 and artificial radionuclides concentrations in air and in dust deposit. Atmos. Environ. 44, 2478–2486.

Otsuji-Hatori, M., Igarashi, Y., Hirose, K., 1996. Preparation of a reference fallout material for activity measurements. J. Environ. Radioact. 31, 143–156.

Pálsson, S.E., Howard, B.J., Bergan, T.D., Paatero, J., Isaksson, M., Nielsen, S.P., 2013. A simple model to estimate deposition based on a statistical reassessment of global fallout data. J. Environ. Radioact. 121, 75–86.

Pham, M.K., La Rosa, J.J., Lee, S.H., Oregioni, B., Povinec, P.P., 2005. Deposition of Saharan dust in Monaco rain 2001-2002: radionuclides and elemental compositions. Phys. Scr. T118, 14–17.

Povinec, P.P., Hirose, K., Aoyama, M., 2013. Fukushima Accident: Radioactivity Impact on the Environment. Elsevier, Amsterdam.

Taylor, S.R., McLennan, S.M., McCulloch, M.T., 1983. Geo-chemistry of loess, continental crustal composition and crust model ages. Geochim. Cosmochim. Acta 47, 1897–1905.

UNSCEAR, 1982. Ionising Radiation: Sources and Biological Effects. Report to the General Assembly, with Annexes. United Nations Scientific Committee on the Effects of Atomic Radiation, p. 773.

UNSCEAR, 2000. Report to the General Assembly. Sources and Effects of Ionising Radiation, 1. United Nations Scientific Committee on the Effects of Atomic Radiation. Annex C.

Warneke, T., Croudace, I.W., Warwick, P.E., Taylor, R.N., 2002. A new ground-level record of uranium and plutonium isotopes for northern temperate latitudes. Earth Planet. Sci. Lett. 203, 1047–1057.

Xu, Y., Qiao, J., Pan, S., Hou, X., Roos, P., Cao, L., 2015. Plutonium as a tracer for soil erosion assessment in northeast. China. Sci. Total Environ. 511, 176–185.

Yang, G., Zheng, J., Tagami, K., Uchida, S., 2015. Plutonium concentration and isotopic ratio in soil samples from central-eastern Japan collected around the 1970s. Sci. Rep. 5, 9636. http://dx.doi.org/10.1038/srep09636.

Zheng, J., Yamada, M., Wu, F., Liao, H., 2009. Characterization of Pu concentration and its isotopic composition in soils of Gansu in northwestern China. J. Environ. Radioact. 100, 71–75.

Zhu, Y.G., Yang, J.G., Zhu, Y.I., 2002. Radiological research in China: current status and perspectives. In: Borretzen, P., Jolle, T., Strand, P. (Eds.), Proceedings from the International Conference on Radioactivity in the Environment, Monaco, pp. 595–599.

Journal of Environmental Radioactivity 166 (2017) 458–465

Contents lists available at ScienceDirect

Journal of Environmental Radioactivity

journal homepage: www.elsevier.com/locate/jenvrad

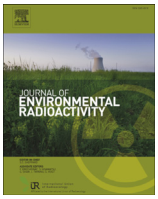

Temporal changes in dissolved ^{137}Cs concentrations in groundwater and stream water in Fukushima after the Fukushima Dai-ichi Nuclear Power Plant accident

Sho Iwagami [a, *], Maki Tsujimura [b], Yuichi Onda [a], Masataka Nishino [c], Ryohei Konuma [d], Yutaka Abe [b], Manami Hada [b], Ishwar Pun [b], Aya Sakaguchi [e], Hiroaki Kondo [e], Masayoshi Yamamoto [f], Yoshiki Miyata [f], Yasuhito Igarashi [g]

[a] *Center for Research in Isotopes and Environmental Dynamics, University of Tsukuba, Tsukuba 305-8577, Japan*
[b] *Department of Sustainable Environmental Studies, Graduate School of Life and Environmental Sciences, University of Tsukuba, Tsukuba 305-8572, Japan*
[c] *Department of Geoenvironmental Sciences, Graduate School of Life and Environmental Sciences, University of Tsukuba, 305-8572, Japan*
[d] *College of Geoscience, School of Life and Environmental Sciences, University of Tsukuba, 305-8572, Japan*
[e] *Department of Earth and Planetary Systems Science, Graduate School of Science, Hiroshima University, 739-8526, Japan*
[f] *Low Level Radioactivity Laboratory, Institute of Nature and Environmental Technology, Kanazawa University, 923-1224, Japan*
[g] *Atmospheric Environment and Applied Meteorology Research Department, Meteorological Research Institute, 305-0052, Japan*

ARTICLE INFO

Article history:
Received 16 May 2014
Received in revised form
11 February 2015
Accepted 8 March 2015
Available online 11 May 2015

Keywords:
Dissolved ^{137}Cs
Fukushima Dai-ichi Nuclear Power Plant
Stream water
Groundwater
Rainstorm event

ABSTRACT

The concentration of dissolved ^{137}Cs in groundwater and stream water in the headwater catchments in Yamakiya district, located ~35 km north west of Fukushima Dai-ichi Nuclear Power Plant (FDNPP), was monitored from June 2011 to July 2013, after the earthquake and tsunami disaster. Groundwater and stream water were sampled at intervals of approximately 2 months at each site. Intensive sampling was also conducted during rainstorm events. Compared with previous data from the Chernobyl NPP accident, the concentration of dissolved ^{137}Cs in stream water was low. In the Iboishi-yama catchment, a trend was observed for the concentration of dissolved ^{137}Cs in stream water to decline, which could be divided into two phases by October 2011 (a fast flush of activity as a result of rapid washoff and a slow decline as a result of soil fixation and redistribution processes). The highest ^{137}Cs concentration recorded at Iboishi-yama was 1.2 Bq/L on August 6, 2011, which then declined to 0.021–0.049 Bq/L during 2013 (in stream water under normal water-flow conditions). During the rainfall events, the concentration of dissolved ^{137}Cs in stream water increased temporarily. The concentration of dissolved ^{137}Cs in groundwater at a depth of 30 m at Iboishi-yama displayed a decreasing trend from 2011 to 2013, with a range from 0.039 Bq/L to 0.0025 Bq/L. The effective half-lives of stream water in the initial fast flush and secondary phases were 0.10–0.21 and 0.69–1.5 y, respectively in the three catchments. The effective half-life of groundwater was 0.46–0.58 y at Koutaishi-yama and 0.50–3.3 y at Iboishi-yama. The trend for the concentration of dissolved ^{137}Cs to decline in groundwater and stream water was similar throughout 2012–2013, and the concentrations recorded in deeper groundwater were closer to those in stream water. The declining trend of dissolved ^{137}Cs concentrations in stream water was similar to that of the loss of canopy ^{137}Cs by throughfall, as shown in other reports of forest sites in the Yamakiya district.

1. Introduction

The Fukushima Dai-ichi Nuclear Power Plant (FDNPP) accident, following the earthquake and tsunami disaster on March 11, 2011, resulted in a substantial release of radionuclides to the environment. The ^{137}Cs atmospheric deposition rate observed at the Meteorological Research Institute, Tsukuba, Japan, showed that the atmospheric deposition rate of ^{137}Cs was less than 0.1 Bq/m^2/month during the 2000s, whereas it increased to approximately 130 Bq/m^2/month after the Chernobyl reactor accident in April 1986 (Aoyama et al., 1991; Igarashi, 2009). In contrast, the present research areas have received far heavier local fallout of

---

* Corresponding author.
E-mail address: sho.iwagami@gmail.com (S. Iwagami).

http://dx.doi.org/10.1016/j.jenvrad.2015.03.025
0265-931X/© 2016 Published by Elsevier Ltd.

0.3–1.0 MBq/m^2 of radiocesium (^{134}Cs and ^{137}Cs) from the FDNPP accident (MEXT, 2011). Most of the area in which the radionuclides were deposited was forested (Hashimoto et al., 2012). Studies of forested areas in Fukushima have shown that radionuclides are remaining in the forest. For example, Kato et al. (in this issue) showed the transfer of canopy-intercepted radiocesium to the forest floor by measuring throughfall, stemflow, and litterfall. A radionuclide profile of the soil has been reported in Kato et al. (2012) and Takahashi et al. (2014). Takahashi et al. (2014) showed a vertical distribution of ^{137}Cs in soil profiles under eight different land uses including forests.

Generally, radiocesium that reaches the ground surface will be rapidly absorbed into the surface soil (Walling, 1998). It has been reported that ^{137}Cs will readily absorb into “frayed edge sites” on clay minerals (Cremers et al., 1988). Tanaka et al. (2014) studied the particle-size-dependent distribution of radiocesium in fluvial suspended sediments in Fukushima after the FDNPP accident. They reported that smaller particles had higher radiocesium concentrations, reflecting their larger specific surface areas. The contribution of clay-size fractions, which had the highest ^{137}Cs concentration, was small because of their low frequency. The downward migration of ^{137}Cs in the soil is reported to be slow. The ^{137}Cs derived from the Chernobyl accident is reported to migrate downward by less than 1 cm/y, and therefore more than 80% of ^{137}Cs remains in the upper 10 cm of the soil (Arapis et al., 1997; Rosén et al., 1999). Plant roots also extract dissolved ^{137}Cs from the soil (Bunzl et al., 1999; Prorok et al., 2006). Kliashtorin et al. (1994) reported that the washout of radiocesium with soil water infiltration from the forest litter accounted for only a small portion of the total radiocesium in the area within 30 km of the Chernobyl NPP. The rate of transport of radiocesium from the soil to groundwater and stream water may depend on site-specific conditions as well as the physical and chemical properties of the deposited radiocesium.

We are focusing on the process whereby the radionuclides deposited to the forested headwater catchment migrate to the groundwater and stream water, from infiltration to discharge. Cesium-137 contamination of groundwater intended for domestic use and that of river water intended for agricultural use is of great concern for the public. A trend for the concentration of dissolved ^{137}Cs to decline in river water after the Chernobyl accident was shown in a two-component exponential model (Nylén and Grip, 1997; Smith et al., 2000, 2002) and a three-component exponential model (Monte, 1997; Smith et al., 2004, 2005). Nylén and Grip (1997) reported that the concentration of ^{137}Cs in stream water in northern Sweden declined from approximately 20–0.1 Bq/L within 8 y after the Chernobyl NPP accident. The IAEA (2006) reported that the observed ^{137}Cs concentration in shallow groundwater declined from approximately 8 Bq/L to less than 0.1 Bq/L from 1989 to 1999 in the Red Forest area near the Chernobyl accident site.

Several studies have reported on the transport of dissolved radiocesium in river water in Fukushima (Sakaguchi et al., 2012; Yasutaka et al., 2012; Ikeuchi, 2013). Yasutaka et al. (2012) focused on Abukuma River, the riverine system of which broadly covers a large part of the northwest of the contaminated FDNPP area. Sakaguchi et al. (2012) reported that Kuchibuto River, which is one of the branches of the Abukuma River and is located in the headwater area, showed higher ^{137}Cs values (0.46 Bq/kg) than the Abukuma River (0.25 Bq/kg). However, there is little information about the headwater catchment. Because a large part of the area affected by FDNPP fallout is forested, the forested area could be the source of dissolved ^{137}Cs in the local river systems. Therefore, detailed studies of the forested headwater catchment are required. Additionally, there is no report on the dissolved ^{137}Cs in the groundwater at the headwaters of the forested catchment. As the transport of radionuclides through subsurface flow is of great concern around the Chernobyl NPP (Levchuk et al., 2012), it is also important to evaluate the transport of radiocesium through groundwater in the Fukushima area.

There are reports of fluctuations in radiocesium concentrations in the river water during rainfall events. For example, Nagao et al. (2013) measured the concentration of total (dissolved and suspended) radioactivity of ^{137}Cs in river water during heavy rainfall associated with a typhoon. The total ^{137}Cs radioactivity in the river water increased during the high-water-level period as a result of increased suspended contributions. In addition, Nylén and Grip (1997) suggested that the ^{137}Cs discharge increase was caused by the occurrence of surface runoff. These reports assessed both dissolved and suspended radiocesium, and highlighted that radiocesium migration mainly occurs by suspended sediments (Ueda et al., 2013).

The objective of this study was to investigate the trend and distribution of dissolved ^{137}Cs concentrations in groundwater and stream water in the headwater region of the Yamakiya district in Fukushima, to clarify the process of dissolved ^{137}Cs transport through the water flow path from a hydrological perspective. The concentrations of dissolved ^{137}Cs are also important data that can be used in simulation models for the prediction of future radiocesium distributions.

2. Study area and methods

2.1. Study area

Hydrometric observations and dissolved radiocesium concentrations were recorded in three small catchments in Yamakiya District, Nihonmatsu City, Fukushima Prefecture, Japan: Koutaishi-yama (KOU, 0.54 km^2, 94% forested: 72% conifer, 22% broad-leaf), Iboishi-yama (IBO, 0.17 km^2, 71% forested: 44% conifer, 27% broad-leaf) and Ishidaira-yama (ISH, 0.075 km^2, 92% forested: 13% conifer, 79% broad-leaf). The catchments are located ~35 km northwest of FDNPP and received heavy local fallout (0.30–1.0 MBq/m^2 of ^{137}Cs) after the FDNPP accident (MEXT, 2011). The average ^{137}Cs deposition density in the KOU, IBO and ISH catchment areas was 916, 544, and 298 kBq/m^2 respectively (MEXT, 2011). The catchments are located at the headwater of the Abukuma River, which is the major river in Fukushima Prefecture and is an important industrial and domestic water resource. The study area and the location of the three observation sites are shown in Fig. 1. Contour lines of ^{137}Cs deposition are also shown, which were obtained by aircraft monitoring by the Ministry of Education, Culture, Sports, Science and Technology (MEXT, 2011).

2.2. Stream water sampling and observation

Sampling of stream water was conducted from June 6, 2011 to July 21, 2013. Stream water was sampled directly at gauging stations during each field survey. The water level in the streams was recorded using a water level recorder (TruTrack WT-HR500, Intech Instruments Ltd., Christchurch, New Zealand) installed on a Parshall flume (Takeuchi Ironworks, Japan). Stream water discharge was calculated based on the relationship between water level and manually measured discharge. Rainfall was measured in 0.2-mm increments by a tipping-bucket rain gauge (Davis #7852M, CA, USA) close to the stream water observation point at IBO. During a rainfall event, stream water was sampled using an automated water sampler (Sigma SD900, HACH, Loveland, CO, USA) at intervals of a few hours.

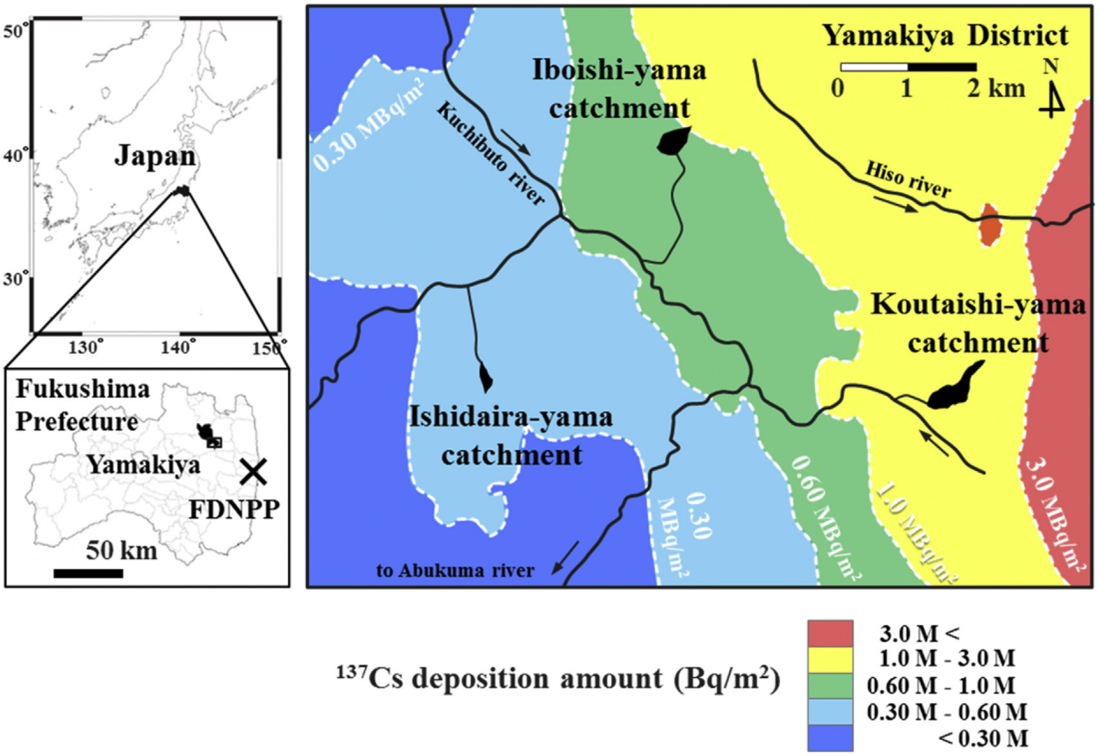

Fig. 1. Study area and locations of three observation sites with the contour line of ^{137}Cs deposition obtained by aircraft monitoring (Ministry of Education, Culture, Sports, Science and Technology http://ramap.jmc.or.jp/map/).

2.3. Groundwater sampling and observation

Groundwater was sampled from boreholes, which were instrumented on August 31, 2011 at IBO and KOU. The boreholes at IBO were 170 m upslope from the stream water sampling point, while those at KOU were 55 m upslope from the stream water sampling point. The structure (depth and range of the screen for water intake) of the borehole and the average water level at IBO and KOU during the observation period are shown in Fig. 2. The diameter of the borehole was 0.065 m. The upper part of the borehole was sealed with cement and the final part of the screen was made from silica sand. The depths of the boreholes at IBO were 5, 15, and 30 m (the screen depth of each borehole was 2–5, 5–15, and 20–30 m, respectively). The depths of the boreholes in KOU were 3, 6, and 20 m (the screen depth of each borehole was 2–3, 3–6, and 12–20 m, respectively).

The groundwater was sampled using a portable water pump (DIK-665A, Daiki Rika Kogyo Co., Ltd., Japan). During groundwater sampling, care was taken not to contaminate the groundwater in the borehole with material from the surrounding environment. Fresh groundwater samples were collected after pumping out the pooled water in the borehole. Fresh groundwater was distinguished based on the change of water temperature and the amount of the pumped out ponded water. The groundwater level was monitored continuously using a water level recorder (HOBO CO-U20-001-01, Tempcon instrumentation Ltd., UK), which was suspended by a wire rope inside each borehole.

2.4. Analysis of dissolved ^{137}Cs

All water samples were filtered through a 0.45-μm pore-size membrane (HA type, Millipore, Billerica, MA, USA). The ^{137}Cs concentration was determined using γ-ray spectrometry with a germanium semiconductor detector at the Meteorological Research Institute (GEM-90205-P, Seiko EG&G Co., LTD, Japan), University of Tsukuba (a 40% coaxial type Ge detector, GC4019, Canberra Industries Inc., Meriden, CT, U.S.A.) and Kanazawa University (a 40% closed-end coaxial type Ge detector, GC4019, Canberra Industries, Inc., Meriden, CT, U.S.A). The spectrometers were calibrated with (i) a standard prepared by the Low Level Radioactivity Laboratory of Kanazawa University using NBL (New Brunswick Laboratory) Reference Material No.42-1 (4.04% U), (ii) a γ-ray certified reference material (JSAC 0471) including ^{134}Cs and ^{137}Cs, from the JSAC (the Japan Society for Analytical Chemistry), and (iii) analytical grade (KCl). Early phase samples taken just after the FDNPP accident were analyzed at the MRI. Most of the samples were analyzed at Kanazawa University to detect low-level dissolved ^{137}Cs at low-background facility (Low Level Radioactivity Laboratory, Kanazawa University: Komura and Hamajima, 2004).

Samples with low-concentrations of ^{137}Cs were concentrated using the ammonium molybdophosphate (AMP)/Cs compound method (Tanaka et al., 2006) at Hiroshima University. A portion of the AMP powder was dissolved with 1.25% tetramethylammonium hydroxide (TAMAPURE-AA) to determine the concentration of ^{133}Cs as a yield tracer. To measure ^{133}Cs in the solubilized AMP samples, an ICP mass spectrometer (Agilent 7700: Agilent Technologies, Santa Clara, CA, USA) was used. In this case, rhenium (10 ng/ml) was employed as an on-line internal standard. The chemical yields for all of the processes were in the range 95–98%, and the concentration of ^{137}Cs was recalculated with chemical yield. The physical decay of ^{137}Cs was corrected to the sampling date.

3. Results and discussion

3.1. The concentration of dissolved ^{137}Cs in stream water

A time series of the concentration of dissolved ^{137}Cs in stream water at the three sites (KOU, IBO, and ISH) is shown in Fig. 3. The dissolved ^{137}Cs concentration of stream water in normal flow condition is shown in Table S1 in supplementary materials. The concentration of dissolved ^{137}Cs in stream water was high in mid-2011 (the highest concentration at each observation site was 1.1 Bq/L at KOU on June 25, 2011, 1.2 Bq/L at IBO on August 6, 2011, and 0.56 Bq/L at ISH on August 17, 2011) and a rapidly declining trend continued until the end of 2011. During 2012–2013, the concentration of dissolved ^{137}Cs in stream water decreased slightly at each site. During normal water-flow conditions, the majority of dissolved ^{137}Cs concentrations in the stream water ranged from 0.02 to 0.08 Bq/L after 2012, whereas some measurements from KOU and ISH showed concentrations of less than 0.01 Bq/L. On the other hand, the concentration of dissolved ^{137}Cs in stream water was comparatively high (up to one order of magnitude higher) during rainfall events. The concentration of dissolved ^{137}Cs in stream water at KOU was lower than that at the other two catchments despite the higher initial ^{137}Cs deposition density.

Kato et al. (in this issue) and Loffredo et al. (2014) reported that the ^{137}Cs flux from canopy to forest floor by throughfall, stemflow and litterfall is higher in coniferous forests compared to broad-leaf forests. However, in this study, the forest composition may not have had an effect on the dissolved ^{137}Cs concentrations in the stream water. At the KOU site, 6% of the catchment is grassland that was used as pasture before the NPP accident, but the stream water

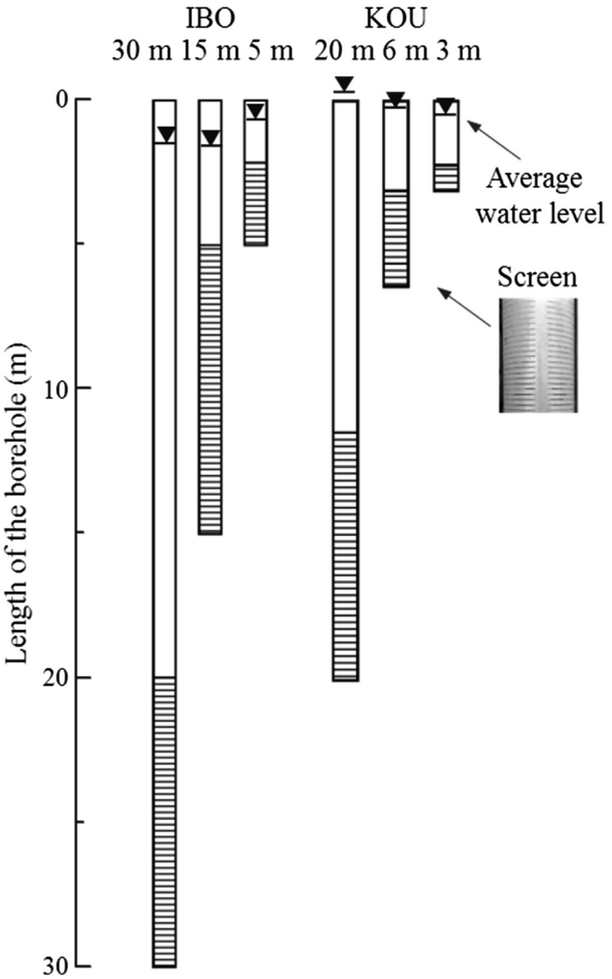

Fig. 2. The structure and average water level at each borehole at Iboishi-yama and Koutaishi-yama.

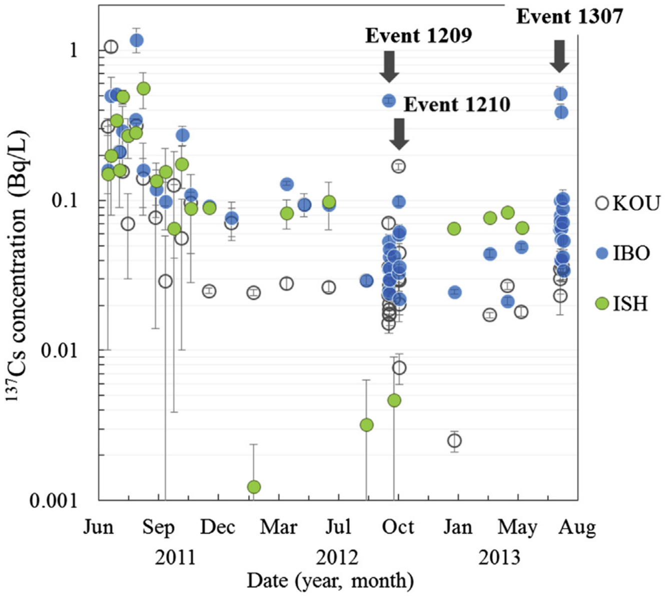

Fig. 3. Time series of dissolved ^{137}Cs concentrations in stream water at three sites (Koutaishi-yama, Iboishi-yama, and Ishidaira-yama). Error bar shows a standard deviation from counting statistics. Three arrows show rainfall events.

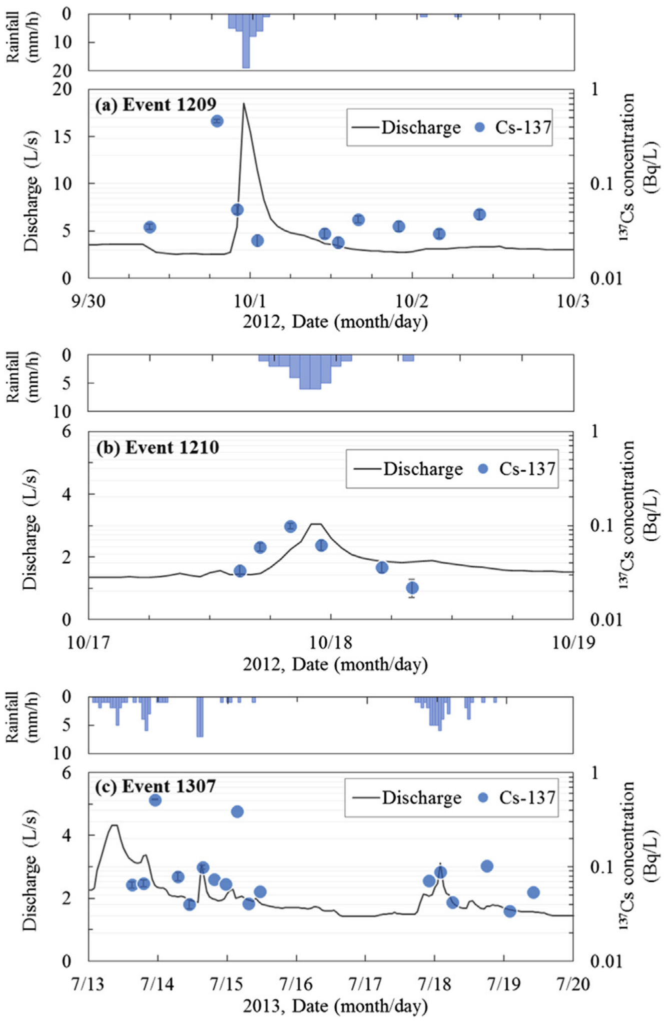

Fig. 4. Time series of dissolved ^{137}Cs concentrations in stream water at Iboishi-yama during (a) Event 1209, (b) Event 1210 and (c) Event 1307 with the hydrograph. Error bar shows a standard deviation from counting statistics.

passes through the forested area. In addition, at the IBO site, 21% of the catchment is grassland that exists close to the spring point, while at 8% of the catchment is grassland at ISH. Surface runoff will rarely occur in a forested area except in an untreated artificial forest with a hard bare soil surface and low infiltration capacity (Gomi et al., 2008). The USLE plot was constructed in Yamakiya town (also at the KOU, IBO, and ISH sites) for monitoring soil erosion and ^{137}Cs discharge from various land uses related to soil erosion (Yoshimura et al., 2014). The water discharge from the USLE plot has been monitored and only occurred during rainfall events. Based on the amount of discharge from the USLE plot, 3% of the surface runoff from the grassland area in the catchment is assumed to be stream water discharge from the IBO site, which includes the largest area of grassland. Usually the discharge from an USLE plot will not occur or negligibly small. Therefore, almost all of the stream water was assumed to originate from the spring, and the land use in this case is not considered to be a determining factor of the dissolved ^{137}Cs concentration in stream water.

3.2. *The concentration of dissolved ^{137}Cs in stream water during rainfall events*

A time series of the concentration of dissolved ^{137}Cs in stream water at IBO during rainfall events in the periods (a) September 30 - October 1, 2012 (Event 1209, total precipitation 47 mm), (b) October 17–19, 2012 (Event 1210, total precipitation 30 mm), and (c) July 13–19, 2013 (Event 1307, total precipitation 234 mm) is shown with a hydrograph in Fig. 4. The dissolved ^{137}Cs concentration of stream water in IBO during rainfall event is shown in Table S2 in supplementary materials. The fluctuation of dissolved ^{137}Cs concentration in stream water was 0.02–0.5 Bq/L during Event 1209, 0.02–0.1 Bq/L during Event 1210, and 0.03–0.5 Bq/L during Event 1307 respectively. During Event 1209, the highest concentration of dissolved ^{137}Cs in stream water was observed before the start of rainfall, whereas during Event 1210 and Event 1307 an increase in the concentration of dissolved ^{137}Cs in stream water corresponded with the rise in discharge. During Event 1210, the peak value of the concentration of dissolved ^{137}Cs in stream water almost corresponded to the discharge peak.

During Event 1209, an increase in the concentration of dissolved ^{137}Cs in stream water occurred before the rise in the water level. The increase in the concentration of dissolved ^{137}Cs could be elution from organic matter or suspended sediment. To understand the timing of elution, intense sampling of organic matter or suspended sediment over a short time period is required. It is important to characterize where, when, and how dissolved ^{137}Cs will enter the water flow throughout the rainfall-runoff process. Event 1209 was a typhoon event, which was characterized by strong winds and a spike of very intense rainfall, whereas Event 1307 was a seasonal rainfall event, which was characterized by a weaker rainfall intensity and a lack of strong wind. It is possible that this difference in the characteristics of the rainfall events affected the timing of the high concentration of dissolved ^{137}Cs in stream water. Since groundwater and soil water could contribute to stream water by piston flow, to investigate where, when, and how dissolved ^{137}Cs will be attached to the stream water flow, it would be desirable to combine inorganic ion concentrations and stable isotope ratio data.

3.3. *Concentrations of dissolved ^{137}Cs in groundwater*

In Fig. 2, it can be seen that the groundwater level observed in the deeper borehole was higher than the groundwater level in the shallower borehole throughout the observation period from mid-July to mid-August at KOU. Therefore, an upward hydraulic gradient was dominant around the borehole at KOU, suggesting that the site is a discharge area of the groundwater flow system. In contrast, the hydraulic gradient in the borehole at IBO was downward, which suggests that IBO is a recharge area for the groundwater flow system.

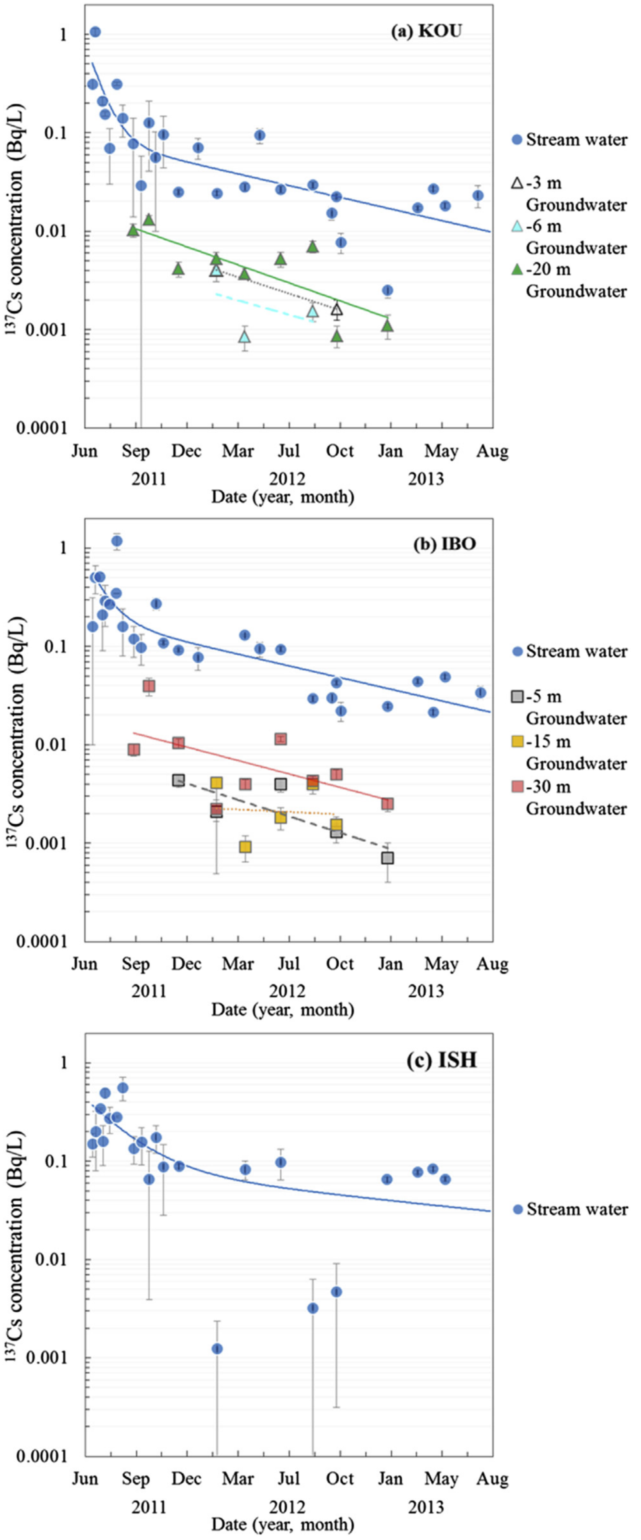

Fig. 5. Time series of dissolved ^{137}Cs concentrations in stream water in normal flow condition and groundwater at (a) Koutaishi-yama, (b) Iboishi-yama, and only stream water at (c) Ishidaira-yama with exponential regression lines. Error bar shows a standard deviation from counting statistics.

Time series of the concentrations of dissolved ^{137}Cs in stream water in normal water flow at all sites and those in groundwater at three different depths at KOU and IBO, are shown with an exponential regression line in Fig. 5. The dissolved ^{137}Cs concentration of groundwater in KOU is shown in Table S3 and dissolved ^{137}Cs concentration of groundwater in IBO is shown in Table S4 in supplementary materials. The declining trend of groundwater was less clear compared to stream water, but exponential regression lines are shown to assess the effective half-live value. At both KOU and IBO, the concentration of dissolved ^{137}Cs in groundwater decreased throughout the observation period. The concentration of dissolved ^{137}Cs in groundwater at KOU (depth of 20 m) was 0.013 Bq/L on October 8, 2011, but decreased to 0.0011 Bq/L by January 18, 2013. The concentration of dissolved ^{137}Cs in groundwater at IBO (depth of 30 m) was 0.039 Bq/L on October 8, 2011, but decreased to 0.0025 Bq/L by January 18, 2013. The concentration of dissolved ^{137}Cs in groundwater was one order of magnitude lower than in the stream water. At both sites, the concentration of dissolved ^{137}Cs in deeper groundwater was closer to that of stream water; the concentrations of dissolved ^{137}Cs in groundwater at IBO, for example, on June 22, 2012 at depths of 5, 15, and 30 m were 0.0039, 0.0018, and 0.011 Bq/L, respectively. The deeper groundwater could potentially contribute to the stream water, because upward or horizontal groundwater flow was dominant, as indicated by the higher average groundwater level in the deeper boreholes (Fig. 2).

Contamination during sampling (from something on the ground that entered the borehole) is a major concern for measurements of dissolved ^{137}Cs in groundwater. However, even if contamination is present, Cs can easily be adsorbed to the soil surrounding the inside wall of the borehole. The groundwater was fluctuating dynamically and the concentration of dissolved ^{137}Cs displayed a similar declining trend to that of stream water. Therefore, in this study, contamination was considered unlikely to be a serious problem when measuring the concentration of dissolved ^{137}Cs in groundwater.

3.4. *The trend for the concentration of dissolved ^{137}Cs to decline in groundwater and stream water*

A trend for the concentration of dissolved ^{137}Cs to decline in river water after the Chernobyl accident was shown in a two-component exponential model (Nylén and Grip, 1997; Smith et al., 2000, 2002) and in a three-component exponential model (Monte, 1997; Smith et al., 2004).

$$C(t) = \alpha e^{-k1t} + \beta e^{-k2t} + \gamma e^{-k3t} \tag{1}$$

where C (Bq/L) is the ^{137}Cs concentration, α, β, γ (Bq/L) and k_1, k_2, k_3 (y^{-1}) are empirically determined (radionuclide-specific) constants, and t is time after the deposition. The k values may be expressed as effective half-lives (T_{eff}). The three exponential terms represent: (1) the fast flush of activity as a result of rapid washoff (~1 y after deposition), (2) a slow decline as a result of soil fixation and redistribution processes (1–8 y), and (3) the very long-term equilibrium situation, respectively (Smith et al., 2005). Kato et al. (in this issue) mentioned that the two-component exponential model could well estimate ^{137}Cs loss from the canopies by throughfall, stemflow, and litterfall compared to the single exponential or offset exponential model, though all models could not follow seasonal changes in the ^{137}Cs loss. Loffredo et al. (2014) showed the declining trend of fallout densities of ^{137}Cs in throughfall and stemflow, which indicated the inflection point of the double exponential fitting line to be around October 2011. The samples for those measurements (Kato et al., in this issue; Loffredo et al., 2014) were taken in forest sites within the study area of this report. In Fig. 5, the trend for the concentration of dissolved ^{137}Cs to decline in stream water was divided into two phases from October 2011 (two-component exponential model), which is because of the clear change in the declining trend and because it coincided with the end of the typhoon season in 2011. The concentration of dissolved ^{137}Cs in groundwater is shown by a single exponential line due to the lack of data for the fast flush in 2011. Also there might be no fast flush phase in the trend for the concentration of dissolved ^{137}Cs in groundwater, however it cannot be confirmed. The trend for the concentration of dissolved ^{137}Cs to decline in stream water during the second phase was similar to that observed for groundwater. The T_{eff} values for stream water in the initial fast flush and secondary phase were 0.10–0.21 and 0.69–1.5 y, respectively in the three catchments. The T_{eff} values for groundwater was 0.46–0.58 y at KOU and 0.50–3.3 y at IBO. Parameters describing the dissolved ^{137}Cs concentration in stream water and groundwater in two-component exponential model and T_{eff} value obtained from the parameters for three catchments are shown in Table 1. In contrast, the T_{eff} values for stream water in the initial and secondary phases in Europe after the Chernobyl accident were approximately 1–3 and 7–8 y, respectively (Smith et al., 2005).

Smith et al. (2004) reported that the concentrations of radionuclides in water sources were strongly correlated with the area covered by inland water. For Chernobyl, they showed that inland water covered up to 20% of the land area studied, whereas in the area considered in this study, the land covered by inland water was extremely small, because the study area is at a headwater region. This might be a reason for the short T_{eff} of the stream water in this study. The declining trend of dissolved ^{137}Cs concentrations in

Table 1
Parameters describing the dissolved ^{137}Cs concentration in stream water and groundwater in two-component exponential model and T_{eff} value obtained from the parameters for three catchments.

Catchment sample	Fast flush			Secondary phase		
	α (Bq/L)	k_1 (y^{-1})	T_{eff} (y)	β (Bq/L)	k_2 (y^{-1})	T_{eff} (y)
KOU						
Stream water	20	−14	0.10	0.11	−1.0	0.69
Groundwater at 3 m depth borehole	–	–	–	0.015	−1.4	0.50
Groundwater at 6 m depth borehole	–	–	–	0.0073	−1.2	0.58
Groundwater at 20 m depth borehole	–	–	–	0.023	−1.5	0.46
IBO						
Stream water	7.8	−11	0.15	0.24	−1.0	0.69
Groundwater at 5 m depth borehole	–	–	–	0.012	−1.4	0.50
Groundwater at 15 m depth borehole	–	–	–	0.0027	−0.21	3.3
Groundwater at 30 m depth borehole	–	–	–	0.023	−1.1	0.63
ISH						
Stream water	1.1	−4.9	0.21	0.094	−0.46	1.5

stream water is similar to that of the loss of canopy ^{137}Cs by throughfall, as shown by Kato et al. (in this issue) at a forest site in the Yamakiya district. Therefore, there may be a relationship between dissolved ^{137}Cs concentration in stream water and ^{137}Cs activity in throughfall at the forest site. The concentrations of dissolved ^{137}Cs in this study were low compared to those recorded in Europe after the Chernobyl accident. Monitoring of radionuclides in the aqueous phase has been performed for approximately 20 y after the Chernobyl NPP accident (IAEA, 2006). It will also be necessary to continuously monitor radionuclide concentrations in the subsurface and surface water in the area affected by the FDNPP accident.

4. Conclusions

The concentration of dissolved ^{137}Cs in groundwater and stream water in Yamakiya district, approximately 35 km North West of Fukushima Dai-ichi Nuclear Power Plant, was monitored from June 2011 (August 2011 for groundwater) to July 2013. A trend for the concentration of dissolved ^{137}Cs to decline in stream water was observed and could be divided into two phases, consisting of a fast flush and a slow decline. The highest concentration of dissolved ^{137}Cs in stream water was 1.2 Bq/L at Iboishi-yama on August 6, 2011, which then declined to 0.021–0.049 Bq/L during 2013 (in stream water under normal flow conditions). The effective half-lives of stream water in the initial fast flush and secondary phases were 0.10–0.21 and 0.69–1.5 y, respectively in the three catchments. The effective half-life of groundwater was 0.46–0.58 y at Koutaishi-yama and 0.50–3.3 y at Iboishi-yama. During rainfall events, the concentration of dissolved ^{137}Cs in stream water temporarily increased. The concentration of dissolved ^{137}Cs in groundwater displayed a decreasing trend throughout 2011–2013, decreasing from 0.039 Bq/L to 0.0025 Bq/L at a depth of 30 m at Iboishi-yama. The trend for the concentration of dissolved ^{137}Cs in groundwater and stream water to decline was similar during 2012–2013. To gain a better understanding of the behavior and potential impacts of dissolved ^{137}Cs, it is necessary to combine these results with other water quality data, such as the concentration of inorganic ions or stable isotopes, and to undertake further analyses, such as hydrograph separation.

Acknowledgments

This work was conducted as a commissioned study from the JAEA, as a part of the MEXT-funded FY2012 project entitled, ‘The establishment of the grasp method to determine long-term effects caused by radioactive materials from the Fukushima Dai-ichi Nuclear Power Plant accident’.

Appendix A. Supplementary data

Supplementary data related to this article can be found at http://dx.doi.org/10.1016/j.jenvrad.2015.03.025.

References

Aoyama, M., Hirose, K., Sugimura, Y., 1991. The temporal variation of stratospheric fallout derived from the Chernobyl accident. J. Environ. Radioact. 13, 103–115.

Arapis, G., Petrayev, E., Shagalova, E., Zhukova, O., Sokolik, G., Ivanova, T., 1997. Effective migration of ^{137}Cs and ^{90}Sr as a function of the type of soils in Belarus. J. Environ. Radioact. 34, 171–185.

Bunzl, K., Albers, B.P., Shimmack, W., Rissanen, K., Suomela, M., Puhakainen, M., Rahola, T., Steinnes, E., 1999. Soil to plant uptake of fallout ^{137}Cs by plants from boreal areas polluted by industrial emissions from smelters. Sci. Total Environ. 234, 213–221.

Cremers, A., Elsen, A., De Preter, P., Maes, A., 1988. Quantitative analysis of radiocaesium retention in soils. Nature 335, 247–249.

Gomi, T., Sidle, R.C., Ueno, M., Miyata, S., Kosugi, K., 2008. Characteristics of overland flow generation on steep forested hillslopes of central Japan. J. Hydrol. 361, 275–290.

Hashimoto, S., Ugawa, S., Nanko, K., Shichi, K., 2012. The total amounts of radioactively contaminated materials in forests in Fukushima, Japan. Sci. Rep. 2 (416), 1–5.

IAEA (International Atomic Energy Agency), 2006. Environmental Consequences of the Chernobyl Accident and Their Remediation: Twenty Years of Experience/ Report of the Chernobyl Forum Expert Group ‘Environment’. IAEA, Vienna, 166pp.

Igarashi, Y., 2009. Anthropogenic radioactivity in aerosol – a review focusing on studies during the 2000s. Jpn. Health Phys. 44 (3), 313–323.

Ikeuchi, Y., 2013. Study on distribution and migration of radioactive substances around Fukushima Daiichi Nuclear Power Plant by Japan Chemical Analysis Center (JCAC). Radioisotopes 62, 799–809 (in Japanese).

Kato, H., Onda, Y., Teramage, M., 2012. Depth distribution of ^{137}Cs, ^{134}Cs, and ^{131}I in soil profile after Fukushima Daiichi Nuclear Power Plant accident. J. Environ. Radioact. 111, 59–64.

Kato, H., Onda, Y., Hisadome, K., Loffredo, N., Kawamori, A., 2015. Temporal changes of radiocesium deposition in various forest stands after the Fukushima Daiichi nuclear power plant accident (in this issue).

Kliashtorin, A.L., Tikhomirov, F.A., Scheglov, A.I., 1994. Vertical radionuclide transfer by infiltration water in forest soils in the 30-km Chernobyl accident zone. Sci. Total Environ. 157, 285–288.

Komura, K., Hamajima, Y., 2004. Ogoya underground laboratory for the measurement of extremely low levels of environmental radioactivity: review of recent projects carried out at OUL. Appl. Radiat. Isotopes 61, 185–189.

Levchuk, S., Kashparov, V., Maloshtan, I., Yoschenko, Y., Van Meir, N., 2012. Migration of transuranic elements in groundwater from the near-surface radioactive waste site. Appl. Geochem. 27, 1339–1347.

Loffredo, N., Onda, Y., Kawamori, A., Kato, H., 2014. Modeling of leachable 137Cs in throughfall and stemflow for Japanese forest canopies after Fukushima Daiichi Nuclear Power Plant accident. Sci. Total Environ. 493, 701–707. http://dx.doi.org/10.1016/j.scitotenv.2014.06.059.

MEXT, 2011. Ministry of education, culture, sports, science and technology. Housha-senryo tou Bumpu mappu. http://ramap.jaea.go.jp/map/map.html (in Japanese).

Monte, L., 1997. A collective model for predicting the long-term behavior of radionuclides in rivers. Sci. Total Environ. 201, 17–29.

Nagao, S., Kanamori, M., Ochiai, S., Tomihara, S., Fukushi, K., Yamamoto, M., 2013. Export of ^{134}Cs and ^{137}Cs in the Fukushima river systems at heavy rains by Typhoon Roke in September 2011. Biogeosci. Discuss. 10, 2767–2790.

Nylén, T., Grip, H., 1997. The origin and dynamics of ^{137}Cs discharge from a coniferous forest catchment. J. Hydrol. 192, 338–354.

Prorok, V.V., Melnichenko, L.Yu, Mason, C.F.V., Ageyev, V.A., Ostashko, V.V., 2006. The transfer of dissolved CS-137 from soil to plants. Waste Management 2006 Symposium, 40(32).

Rosén, K., Oborn, I., Lonsjo, H., 1999. Migration of radiocaesium in Swedish soil profiles after the Chernobyl accident, 1987-1995. J. Environ. Radioact. 46, 45–66.

Sakaguchi, A., Kadokura, A., Steier, P., Tanaka, K., Takahashi, Y., Chiga, H., Matsushima, A., Nakashima, S., Onda, Y., 2012. Isotopic determination of U, Pu and Cs in environmental waters following the Fukushima Daiichi Nuclear Power Plant accident. Geochem. J. 46, 355–360.

Smith, J.T., Comans, R.N.J., Beresford, N.A., Wright, S.M., Howard, B.J., Camplin, W.C., 2000. Chernobyl's legacy in food and water. Nature 405, 141.

Smith, J.T., Cross, M.A., Wright, S.M., 2002. Predicting transfers of ^{137}Cs in terrestrial and aquatic environments: a whole-ecosystem approach. Radioprot. - Coll. 37, 37–42.

Smith, J.T., Wright, S.M., Cross, M.A., Monte, L., Kudelsky, A.V., Saxén, R., Vakulovsky, S.M., Timms, D.N., 2004. Global analysis of the riverine transport of ^{90}Sr and ^{137}Cs. Environ. Sci. Technol. 38, 850–857.

Smith, J.T., Belova, N.V., Bulgakov, A.A., Comans, R.N., Konoplev, A.V., Kudelsky, A.V., Madruga, M.J., Voitsekhovitch, O.V., Zibold, G., 2005. The “AQUASCOPE” simplified model for predicting 89,90Sr, 131I, and 134,137Cs in surface waters after a large-scale radioactive fallout. Health Phys. 89, 628–644.

Takahashi, J., Tamura, K., Suda, T., Matsumura, R., Onda, Y., 2014. Vertical distribution and temporal changes of 137Cs in soil profiles under various land uses after Fukushima Dai-ichi Nuclear Power Plant Accident. J. Environ. Radioact. http://dx.doi.org/10.1016/j.jenvrad.2014.07.004.

Tanaka, K., Iwatani, H., Sakaguchi, A., Takahashi, Y., Onda, Y., 2014. Relationship between particle size and radiocesium in fluvial suspended sediment related to the Fukushima Daiichi Nuclear Power Plant accident. J. Radioanal. Nucl. Chem. 301 (2), 607–613. http://dx.doi.org/10.1007/s10967-014-3159-1.

Tanaka, K., Inoue, M., Misono, J., Komura, K., 2006. Vertical profiles of ^{226}Ra, ^{228}Ra and ^{137}Cs activities in seawater around the Yamamoto Ridge and coastal areas of the Sea of 15 Japan. Chikyu Kagaku (Geochemistry) 40, 167–176 (in Japanese).

Ueda, S., Hasegawa, H., Kakiuchi, Hideki, Akata, Naofumi, Ohtsuka, Y., Hisamatsu, S., 2013. Fluvial discharges of radiocaesium from watersheds contaminated by the Fukushima Dai-ichi Nuclear Power Plant accident, Japan. J. Environ. Radioact. 118, 96–104.

Walling, D.E., 1998. Use of ^{137}Cs and other fallout radionuclides in soil erosion investigation: progress, problems and prospects. In: IAEA (Ed.), Use of ^{137}Cs in the Study of Soil Erosion and Sedimentation: Proceedings of a

Consultants Meeting Organized by the Joint FAO/IAEA Division of Nuclear Technologies in Food and Agriculture and held in Vienna, 13-16 November 1995, pp. 39–62.

Yasutaka, T., Kawabe, Y., Kurosawa, A., Komai, T., 2012. Monitoring dissolved radioactive cesium in Abukuma River in Fukushima Prefecture. In: Proceedings of International Symposium on Environmental monitoring and dose estimation of residents after accident of TEPCO's Fukushima Daiichi Nuclear Power Station.

Yoshimura, K., Onda, Y., Kato, H., 2014. Evaluation of radiocaesium wash-off by soil erosion from various land uses using USLE plots. J. Environ. Radioact. 139, 362–369. http://dx.doi.org/10.1016/j.jenvrad.2014.07.019.

放射性物質の大気沈着・拡散および陸域からの再浮遊について

五十嵐康人　気象研究所・環境・応用気象研究部

はじめに：　本稿では平成 24 年から開始した新学術領域研究「福島原発事故により放出された放射性核種の環境挙動に関する学際的研究（ISET-R；領域代表：恩田裕一筑波大教授）」の A01-2 計画研究班「放射性物質の大気沈着・拡散過程および陸面相互作用の理解」（A01-2 班）における研究の全体概略を紹介する. 同班では, 1）福島事故により大気中に放出された放射性核種がどのような物理・化学性状で大気中を浮遊したか, およびその成因を理解すること（一次放出）, 2）広域的な放射性物質濃度の時間・空間的変動調査や沈着物の測定を通じ, 大気輸送・拡散モデルの精度向上と, それを用いた事故放出量の推定に寄与すること, 3）陸域（土壌・生態系を含む）への沈着と大気中への放射性核種の再飛散量, その物理・化学形状および放出源（二次放出）を理解し, 大気―陸面相互作用を定量化することを目的とした. これらを通じて, 領域研究全体が目標とする放射性物質の大気―陸域―水圏の移行モデルの確立や, 各地での呼吸による内部被ばく量の推定の基礎データにも寄与することを目指すとともに, 人体の内部被ばくに係わる大気放射能の情報を社会に提供し, 国民の安全・安心の確保に貢献することを目指した.

研究の背景：　原子力発電所の事故による環境や健康影響を考えるうえで大気科学の観点から重要なことは，放出，輸送・拡散，沈着の量的な関係の正確な把握である．この目的達成のためには，観測とモデルそれぞれ一辺倒ではなく, 両者を有機的に連携させ互いの短所を補い, 長所を強化することが大切になる．観測で得られるのは，時系列か２次元（場合によっては３次元）の分布であって，それ以上は極度に困難となる．他方，モデルでは動画を容易に得られるが，未知のプロセスがあった場合，考慮不能である．従って，放出，輸送・拡散，沈着において主要なプロセスを解明し，新規にスキーム導入する等してモデルの精度向上も図りつつ，再現計算を進めることが肝要である．これらは他の人為起源汚染問題全般についても成り立つが，放射性物質による環境汚染でも共通する[1] [2] [3]．さらに，放射能量で表すと福島第一原発事故による放射性物質の放出量は PBq と極めて大だが，物質重量に換算するとわずか数 kg にしかならず，最大放出量となる ^{137}Cs にしても，せいぜい 5 kg（評価により放出量は異なるが，最大評価値でも 10 数 kg）である．他方，代表的な大気エアロゾル構成物質である硫酸の前駆体 SO_2 の我が国での日排出量は, 2 kt 程度で[4], 重量で６桁以上の差がある．このように物質量としてはわずかな放射性核種は，希ガス，ヨウ素を除き単体で浮遊するものは少なく，放出および輸送過程においてさまざまな担体（キャリアとなるエアロゾル）と内部混合した放射性エアロゾルを構成したと考える方が合理的であろう[5]．このため，環境や人体影響に関わる大気中の輸送・除去（地表への沈着）過程は，放射性エアロゾルがもつ粒径（物理特性）と湿度特性（化学性状）によって左右されたであろう（Fig.1 参照）．従って，量的な評価に加えて，放射性エアロゾルの物理・化学性状の解明が求められ，これらの点を意識しつつ研究がすすめられた．

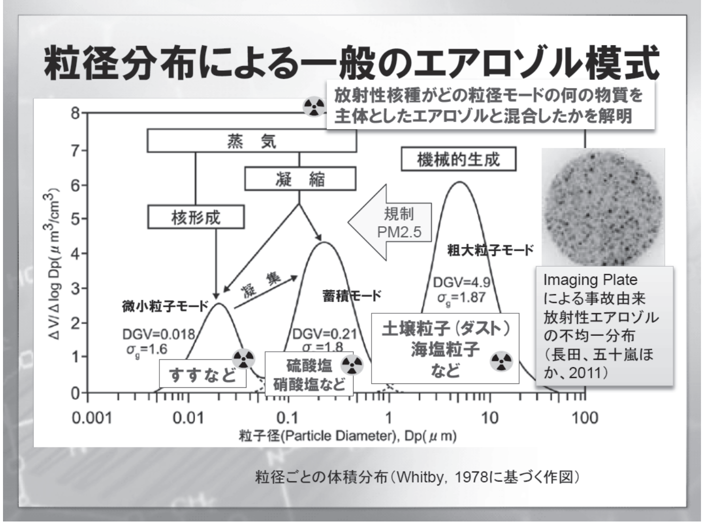

粒径分布による一般のエアロゾル模式

放射性核種がどの粒径モードの何の物質を主体としたエアロゾルと混合したかを解明

Imaging Plate による事故由来放射性エアロゾルの不均一分布（長田、五十嵐ほか、2011）

粒径ごとの体積分布（Whitby, 1978に基づく作図）

Fig.1　Schematics of internal mixing of radionuclides with the typical atmospheric aerosols having size distribution[6] with some modifications by the author

結果：　研究遂行の結果，従来知見の範囲にない新規の知見の取得を含め，下記に述べるような顕著な成果が得られた．

1）初期の Cs 放出には従来想定されていた水溶性サブミクロン・サルフェート粒子に加え，不溶性粗大球状 Cs 粒子が存在することを世界で初めて明らかにし，放射性物質の湿性沈着の妥当性を検証するため，このような Cs 粒子の特性を組み込んだ高解像度モデルによる沈着量計算を実施した[7]．球状 Cs 粒子は，直径数 μm 前後で，主要な構成元素として Fe, Zn, Cs, O 等を含み，その後の SPring-8 での分析で，Ba, Te, Sn, Mo, Rb 等の重元素をも含むこと[8]や SiO_2 主体であること等[9]が判明した．現在も多くの研究者が本課題に取り組みつつあり，さらに新規の知見が得られつつある．

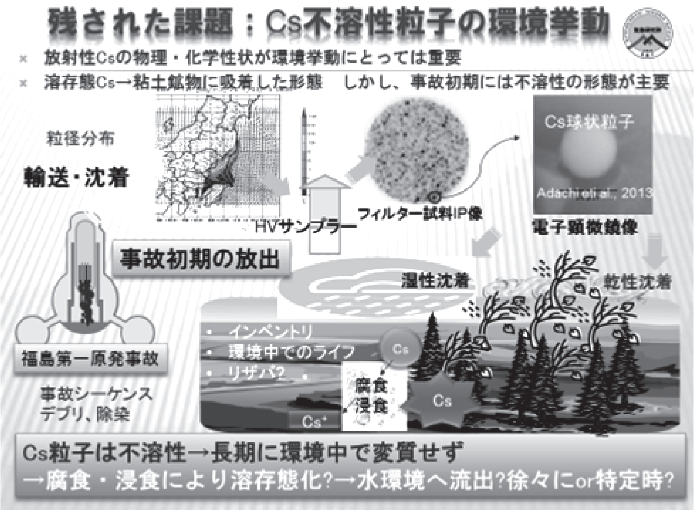
残された課題：Cs不溶性粒子の環境挙動

- 放射性Csの物理・化学性状が環境挙動にとっては重要
- 溶存態Cs→粘土鉱物に吸着した形態　しかし、事故初期には不溶性の形態が主要

Cs粒子は不溶性→長期に環境中で変質せず
→腐食・浸食により溶存態化?→水環境へ流出?徐々にor特定時?

Fig.2　Summary of problems remaining related to environmental behavior of insoluble Cs particles

しかしながら多くの進展があったにも関わらず，この不溶性 Cs 粒子の環境挙動に関しては，未解決のまま残っている点が多々ある（Fig.2）．事故初期に放出が生じたことは理解されているが，その生成メカニズムと事故事象との関連，放出起源（号炉），放出インベントリ（量的評価），Cs の水溶性―非水溶性の割合等に関し解明が求められる．さらに，環境中での寿命（いつ腐食・浸食により Cs が溶存態化するのか），腐食・浸食は徐々に進むのか，それともある時期に一気に生ずるのか，結果放出されるだろう水溶性 Cs の影響評価など，今後の一層の研究展開が望まれる．事故の際に炉内で発生した事象の解明，より効率的な廃炉作業・除染作業，除染廃棄物の減容・圧縮をはじめとして，帰還地域住民の安全・安心の一層の担保などの達成のため，継続的な研究取り組みが必要である．

2）事故により放出された放射性核種は，裸地面や農地，森林などの様々な地表に沈着し，地表面土壌に吸着したものが二次放出として強風により再飛散することが危惧された．そこで，ほぼ裸地の福島県浪江町の学校グラウンドにおいて，放射性物質の再飛散の観測を行った．グラウンドに HV サンプラーを設置し，また，カスケードインパクタを接続して，粒径別のサンプリングを行い，それぞれ捕捉された土粒子の放射能濃度を分析した．このエアロゾル粒径別個数濃度と Cs 濃度の集中観測，摩擦速度（風応力）等気象観測のデータ比較により，放射性物質の再飛散簡略化スキーム（1D 放射能飛散モデル）を開発し，土粒子による再飛散モデルを構築した[10]．本モデルでは，土壌の汚染量から土粒子 1 個あたりの放射能を計算し，ダストフラックスを乗じることで，飛散した土粒子による大気放射能フラックスを算定する．その際，飛散した土粒子の粒径分布は，Sand，Loamy soil，Silty clay loam，Clay などの地表面土壌の粒径タイプに依存するモデルとした．そして，飛散したダスト粒子の混合層高さ，ダストの発生面積，ダストイベントの継続時間を仮定し，粒径別の大気放射能濃度を推定した．その結果，簡易的なモデルだが，2012 年冬季と 2013 年春季につき，粒径別の大気放射能濃度を

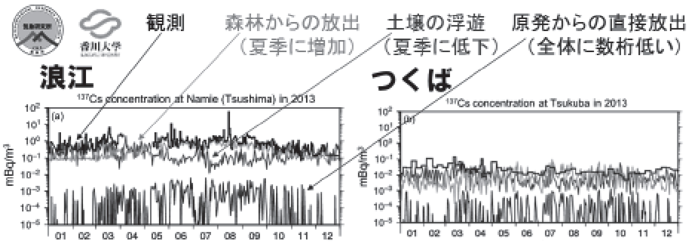

大気中Cs-137濃度の観測値と複数の放出源を想定した
濃度再現計算結果

森林からの放出フラックス算定式:

$$F_{forest} = f_{forest}\, f_{green}\, r_{const}\, B_{obs}\, R_{decay}\,(t)\,,$$

ここで f_{forest}, f_{green} および r_{const} は、森林被覆領域の割合，月別の緑領域の割合、および 森林域での再浮遊定数(/s)を表し，また r_{const} は^{137}Cs濃度を観測値に整合させるための定数; ここでは10^{-7} /hに設定した．

Kajino et al., ACP, 2016

Fig.3　Simulation of resuspension by aerosol transport model and comparison with the observation

推定することができた.

しかし，様々な仮定があり不確実性を有するため，土壌再飛散モデルを領域エアロゾル輸送モデルへ組み込み，その検証を進めると同時に再現計算を行った[11]. 用いたモデルは，ラグランジュ型移流拡散モデルであり，気象庁メソ解析データ（約 11 km 格子，3 時間間隔）を用いて，移流・乱流拡散，乾性・湿性沈着（rainout/washout），放射性壊変を計算する. 2013 年 1 年間の再飛散について，数値モデルと避難区域内（浪江町）および区域外（つくば市）での大気観測を用いてその領域収支の定量的評価を行った. その結果，東日本の計算領域からは年間再浮遊量は 1.01 TBq で，そのうちの 0.22 TBq が同領域に再沈着すると計算された. これは，それぞれ，同領域の地表面汚染に対して，0.3%以下および 0.03%以下と考えられ，再浮遊は地表面汚染の減少に寄与しないことがわかった. なお，本計算では，土壌，陸上生態系からの二つの Cs 再飛散と福島第一原発からの低レベルで継続する一次放出を考慮している. 結果として，浪江町に比べつくば市では，大気中の Cs 濃度が 1-2 桁低い値となった. これは観測結果のオーダーを再現し，広域的な Cs の移流拡散を良好に表現できた（Fig.3 参照）. また，季節的な変化では，浪江町では夏季に高く，冬季に低く，つくば市では冬季に高い特徴が得られており，上記に示した土壌からの再飛散量を 5 倍することで冬季の Cs 濃度を再現できた. しかし，浪江町の夏季の Cs 濃度上昇は再現できず，再飛散係数 10^{-7} 毎時の森林生態系からの Cs 放出を仮定することによってはじめて，浪江町での夏季の Cs 上昇をほぼ定量的に説明することができた. 後者は，森林生態系からの再浮遊の正体解明が極めて重要なことを示唆する.

このほか，全球エアロゾル輸送モデルによる再現計算とその評価[12]，全球エアロゾル輸送モデルと逆解析による ^{137}Cs 総放出量推定[13]，領域輸送モデルの高空間分解能化への応答研究[14]など放射性物質を含む化学輸送モデルの高精度化につながる斬新な研究を進めた.

3）茨城県つくば市での降下量や大気濃度の変動から，福島第一原発事故由来の放射性物質の再浮遊について定量的な議論を行った[15]. 次いで，福島県内の汚染地域で放射性セシウムの大気への再飛散を長期観測した結果，ｉ）都市部での観測結果と異なり，典型的な里山である観測点では夏季に放射性 Cs の大気中濃度が上昇し，ⅱ）これを担う粒子は，見た目や光学顕微鏡像からダストと思われたが，意外にもその大部分が生物由来であることを見出した[16]（Fig.4 参照；. 電子顕微鏡でバイオエアロゾル等を計数し，Cs 濃度と比較した例を Fig.5 に示す[17]. バイオエアロゾルの個数濃度は Cs 同様に夏季に高く冬季に低い. また花粉の個数濃度よりもバクテリアや胞子[17]では両者の区別が達成できていない）の個数濃度の変動の方が変動幅が大きかった. さらに電子顕微鏡での炭素 X 線の強度変動は Cs 濃度変動とよく相関し，バイオエアロゾルが担体となって Cs の再浮遊が生じていると推測された. 従来知見からすると，真菌類が Cs を濃縮するため，胞子へも Cs が移行して，その胞子が放出されることで，Cs の大気への再浮遊を担うと考えられ，関連する知見が集められつつある[16]. 再浮遊プロセスの不明点が解消されることは，住民の安全・安心の確保に関わりたいへん重要であろう.

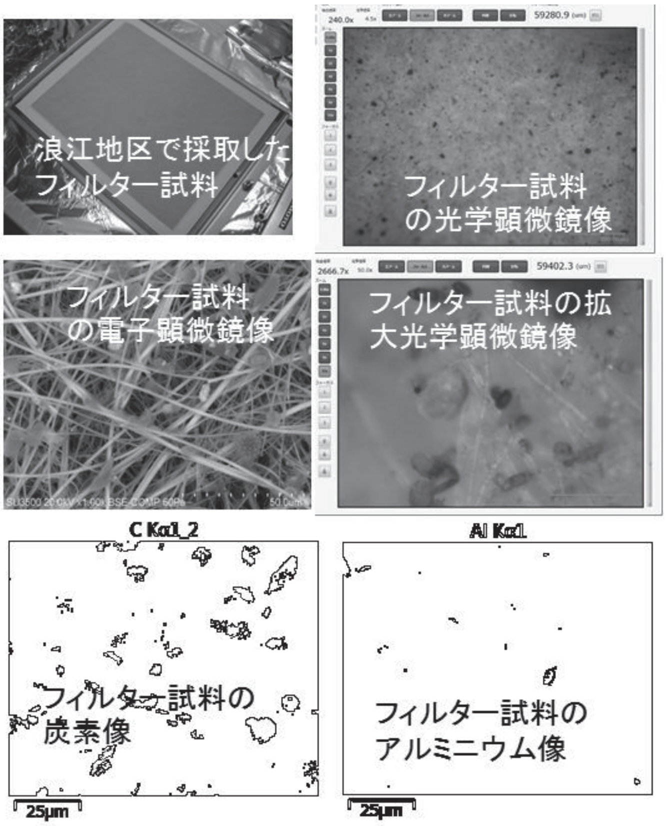

Fig.4 Optical and electron microscopic images of HV filter sample collected in the contaminated area (Igarashi et al. in preparation)

4)これらのほか, 一次放出に関するCsの担体, 硫酸エアロゾルの大気中の挙動に関して知見を与える中性子放射化で炉内で生成した^{35}Sの大気中での挙動を追跡した研究[18], 大気中Cs濃度変動の数理科学的考察[19], 海洋への放射性物質の輸送・沈着の量的評価研究[20]をはじめおよそ50報の原著論文の発表に寄与した.

まとめ

福島第一原発事故で大気環境中に放出された放射性核種(一次放出)に関し, 量的な評価のみならず, その物理・化学性状の解明を行った. その結果, はじめて1)不溶性で球状のCsを見出し, その性状の解明を行った. 2)エアロゾルモデルを利用・改良し, 土壌粒子, 森林生態系からの再浮遊(二次放出)を評価, 再現計算し, 福島第一原発事故からの直接放出についても評価を行った. その結果, 森林生態系からの放出により特に夏季に大気中濃度が支えられていることが分かった. 3) 森林生態系からの再浮遊を含む, 再浮遊過程につき観測をすすめ, 森林生態系からのバイオエアロゾル等が担体となったCs再浮遊が夏季に発生していることを初めて解明した. 4) これらに加えて中性子放射化反応で生じた^{35}Sの研究などをはじめ, 関連するさまざまな課題についても研究を進め, 着実な成果を得た.

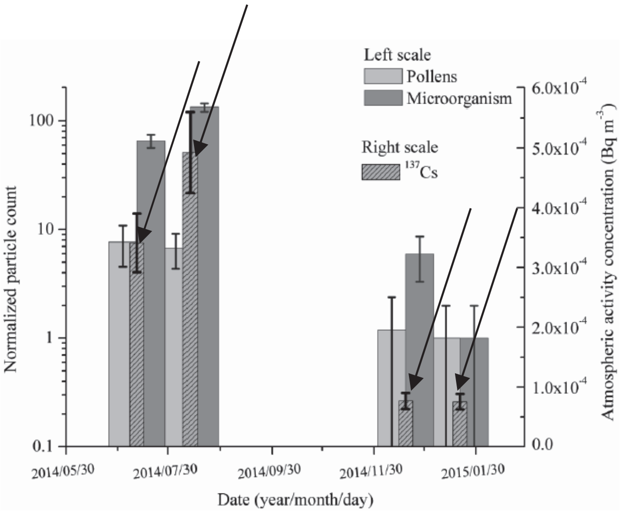

Fig.5 Comparison of bioaerosol number concentration (pollen and microorganism including fungal spore) by electron microscopy with ^{137}Cs concentration (arrow) based on HV filter sample collected in the contaminated area

謝辞：本研究の遂行には多数の方々の分担, 連携, 協力を得た. 以下に記して感謝する(敬称略). 1)分担: 北和之(茨城大), 吉田尚弘(東工大), 石塚正秀(香川大), 故里村雄彦(京大), 大河内博(早大), 2)連携: 山田桂太(東工大), 田中泰宙, 関山剛, 眞木貴史, 財前祐二, 足立光司(気象研), 川島洋人(秋田県立大), 3)協力: 中井泉, 阿部善也(東理大), 西口講平, 故宇谷啓介(ジェイ・サイエンス), 梶野瑞王(気象研), 豊田栄, 服部祥平(東工大), 羽田野祐子(筑波大), 青山智夫(現江戸川大), 吉川知里(JAMSTEC), 緒方裕子(早稲田大), 三上正男(現JMBSC), 谷田貝亜紀代(弘前大), 山田豊(理研), 村上茂樹(森林総研), 新村信雄(茨城大), 渡邊明(福島大), 長田直之(岡山大), 牧輝弥(金沢大), 佐藤志彦(現JAEA).

参考文献

[1]. 近藤裕昭, 里村雄彦, 竹村俊彦, 山澤弘実, 渡邉明編集 (2012) 2011年度秋季大会スペシャルセッション「放射性物質輸送モデルの現状と課題」報告, 天気, 59(4), 41-52. 節2.2 北和之, 笠原理絵, 渡邊明, 鶴田治雄, 植松光夫, 桧垣正吾, 吉田尚弘, 豊田栄, 山田桂大, 篠原厚, 三上正男, 五十嵐康人, 恩田裕一, 末木啓介, 滝川雅之, 日本地球化学会=日本地球惑星科学連合=日本放射化学会連携緊急放射性物質サンプリングチーム大気班および分析班「大気放射性物質の広域観測と土壌からの再飛散の影響」, 節2.4 眞木貴史, 梶野瑞王, 田中泰宙, 関山剛, 千葉長, 五十嵐康人, 三上正男「逆解析を用いた初期放射線量推定システムの構築」, 節2.9 梶野瑞王, 五十嵐康人, 田中泰宙, 眞木貴史, 関山剛, 千葉長, 青柳曉典, 出牛真, 大島長, 三上正男, 「気象研領域モデルによる福島第一原発事故に伴う放射性物質の輸送・沈着実験」, 節2.11 田中泰宙, 猪股弥生, 五十嵐康人, 梶野瑞王, 眞木貴史, 関山剛, 三上正男, 千葉長, 「気象研究所全球モデルによる放射性物質輸送シミュレーションの現状と課題」, 節2.12 五十嵐康人, 三上正男, 青山道夫「核災害を含む緊急時対応システム－欧州の先行事例から」

[2]. 五十嵐康人 (2013) 日本地球惑星科学連合2013年大会セッション「最新の大気化学:福島原発事故放射能の大気・陸圏輸送, 沈着問題」の報告, 天気, 60(11), 975-976.

[3]. 鶴田 治雄, 五十嵐 康人, 井上 智博, 大河内 博, 大原 利眞, 梶野 瑞王, 兼保 直樹, 北 和之, 反町

篤行，平木 隆年，堀江 洋佑，森口 祐一，森野 悠，渡邊 明（2016）福島第一原子力発電所事故による放射性物質の大気環境影響調査研究の現状と課題，大気環境学会誌，51(2), A11-A19.

[4]. 東アジア大気汚染物質排出量グリッドデータベース(EAGrid2000)，国立環境研究所地球環境研究センター，　http://www.cger.nies.go.jp/db/eagrid/eagrid_index_j.html

[5]. 高橋幹二（1989）原子力とエアロゾル，エアロゾル研究，4, 4–10.

[6]. 環境省委員会資料（MOE2013），http://www.env.go.jp/council/former2013/07air/y078-02/mat02-1.pdf

[7]. Adachi, K., Kajino, M., Zaizen, Y. and Igarashi, Y. (2013) Emission of spherical cesium-bearing particles from an early stage of the Fukushima nuclear accident, Sci. Rep. 3,：2554. doi:10.1038/srep02554

[8]. Abe, Y., Y. Iizawa, Y. Terada, K. Adachi, Y. Igarashi, and I. Nakai (2014) Detection of uranium and chemical state analysis of individual radioactive microparticles emitted from the Fukushima nuclear accident using multiple synchrotron radiation X-ray analyses, Anal. Chem.86 (17)：8521–8525. doi: 10.1021/ac501998d

[9]. Satou, Y., K. Sueki, K. Sasa, K. Adachi and Y. Igarashi (2016) First successful isolation of radioactive particles from soil near the Fukushima Daiichi Nuclear Power Plant, Anthropocene, 14：71-76. doi.org/10.1016/j.ancene.2016.05.001

[10]. Ishizuka M., M. Mikami, T. Y. Tanaka, Y. Igarashi, K. Kita, Y. Yamada, N. Yoshida, S. Toyoda, Y. Satou, T. Kinase, K. Ninomiya, A. Shinohara (2017) Use of a size-resolved 1-D resuspension scheme to evaluate resuspended radioactive material associated with mineral dust particles from the ground surface, J. Environ. Radioact. 166(3)：436-448. doi:10.1016/j.jenvrad.2015.12.023

[11]. Kajino, M., M. Ishizuka, Y. Igarashi, K. Kita, C. Yoshikawa and M. Inatsu (2016) Long-term assessment of airborne radiocesium after the Fukushima nuclear accident: Re-suspension from bare soil and forest ecosystems, Atmos. Chem. Phys. 16：13149-13172. doi:10.5194/acp-16-13149-2016

[12]. 田中泰宙 (2013) 放射性物質の全球シミュレーション，日本風工学会誌，38(4), 388-395. doi:10.5359/jawe.38.388

[13]. Maki, T., T., Y. Tanaka, T. T. Sekiyama, M. Kajino, Y. Igarashi, and M. Mikami, Radioactive Nuclei Emission Analysis from Fukushim Dai-ichi Nuclear Power Plant by Inverse Model, 93rd American Meteorological Society, 6 January 2013, Austin, USA. https://ams.confex.com/ams/93Annual/webprogram/Manuscript/Paper216873/mri_maki_rev.pdf

[14]. Sekiyama T. T., M. Kunii, M. Kajino, and T. Shimbori (2015) Horizontal resolution dependence of atmospheric simulations of the Fukushima nuclear accident using 15-km, 3-km, and 500m grid models. J. Meteor. Soc. Japan, 93(1):49–64, doi:10.2151/jmsj.2015-002

[15]. Igarashi, Y., M. Kajino, Y. Zaizen, K. Adachi, M. Mikami (2015) Atmospheric radioactivity over Tsukuba, Japan: a summary of three years of observations after the FDNPP accident, Progress in Earth and Planetary Science, 2:44, doi:10.1186/s40645-015-0066-1

[16]. Igarashi, Y., K. Kita, T. Kinase, T. Maki, C. Takenaka, M. Kajino, K. Adachi, M. Ishizuka, T. T. Sekiyama, Y. Zaizen, K. Ninomiya, H. Okochi, A. Sorimachi, (2016) Novel hypothesis for Fukushima re-suspension: Biological processes, 2016 European Aerosol Conference, Tours, France.（招待講演）

[17]. Kinase T., K. Kita; Y. Igarashi, K. Adachi; K. Ninomiya, A. Shinohara, H. Okochi, H. Ogata, M. Ishizuka, S. Toyoda, K. Yamada, N. Yoshida, Y. Zaizen, M. Mikami, H. Demizu and Y. Onda (2017) The seasonal variation of atmospheric ^{134,137}Cs and their possible resuspension host particles at Tsushima and Yamakiya, Fukushima, Japan, Progress in Earth and Planetary Science, in review

[18]. Priyadarshi, A., Hatakeyama, S., Noguchi, I., Nojiri, Y., Tanimoto, H., Falkenthal, J. H., Thiemens, M. H., Yoshida, N., Toyoda, S., Yamada, K., Mukotaka, A., Fujii, A., and Uematsu, M. (2013) Detection of Radioactive ^{35}S at Fukushima and other Japanese sites, J. Geophys. Res. Atmos. 118(2), 1020-1027.

[19]. Ichige, H., Fukuchi, S. and Hatano Y. (2015) Stochastic model for the fluctuations of the atmospheric concentration of radionuclides and its application to uncertainty evaluation, Atmos. Environ., 103, 156-162.

[20]. Aoyama, M., Kajino, M., Tanaka, Y. T., Sekiyama, T. T., Tsumune, D., Tsubono, T., Hamajima , Y., Inomata, Y., and Gamo, T. (2016) ^{134}Cs and ^{137}Cs in the North Pacific Ocean derived from the March 2011 TEPCO Fukushima Dai-ichi Nuclear Power Plant accident, Japan. Part two: estimation of ^{134}Cs and ^{137}Cs inventories in the North Pacific Ocean, J. Oceanogr. 72:67–76

Understanding of atmospheric deposition, diffusion processes and land atmosphere interaction of radioactive materials

Yasuhito Igarashi
Atmospheric Environment and Applied Meteorology Research
Department, Meteorological Research Institute

In March 2011, at the Fukushima Dai-ichi nuclear power plant (FDNPP) a severe accident happened and it caused a serious environmental pollution not only in the vicinity but also in a wide range of eastern Japan. Interdisciplinary Study on Environmental Transfer of Radionuclides from the Fukushima Daiichi NPP Accident (ISET-R) project was thus launched in 2012 and has undertaken various features of the radioactive pollution in the environment. Here a brief summary of the research achievements by the team A01-2 of the ISET-R is presented. Not only the quantitative assessment, we clarified but also the physical and chemical properties of radionuclide (primary emission) released into the atmospheric environment due to the FDNPP accident. As a result, for the first time 1) insoluble spherical Cs was found in primary emission and clarified its properties. 2) Resuspension of radionuclide (secondary emission) could be evaluated, reproduced and calculated, which due to soil particle suspension and forest ecosystem by using and improving aerosol model and evaluated delayed direct release from the FDNPP accident, too. It should be noted that atmospheric concentrations of Cs were supported especially in summer by the discharge from the forest ecosystem. 3) We carried out observations on the resuspension process, including that from the forest ecosystem, and for the first time clarified the occurrence of Cs resuspension in summer attributable to bioaerosol (fungal spores, etc.) emission from the forest ecosystem. 4) In addition to these, we conducted research on various related tasks, including behavior of ^{35}S produced by neutron activation reaction and so forth, and finally achieved about 50 original papers' publication.

IAEA-TEL-2015-03 Proficiency Test 試料の測定

〇木村徹＊[1]，五十嵐康人＊[2]，財前祐二＊[2]

＊[1]㈱アトックス　　＊[2]気象研究所

１．はじめに

IAEA Proficiency Test（PT）は、環境試料に含まれる人工・自然放射性核種の測定技能を確認することを目的とした、国際原子力機関（IAEA）の相互比較評価の一つに位置づけられている。ところで、アトックスでは数年前から気象研究所で実施されている大気降下物中の ^{90}Sr と ^{137}Cs の観測の一部を請負い、環境・応用研究部にて放射能分析を実施してきた。この研究グループが参画している新学術領域研究「福島原発事故により放出された放射性核種の環境動態に関する学際的研究」において、分析の品質向上の目的で、代表者の恩田裕一筑波大教授が率先して PT 参加を募った。適正な分析品質を確保する観点から積極的に PT に参加し測定技能を確認することは、重要な事である。今回は PT でどのように試料を分析・測定したか、またその精度について結果をまとめ報告する。

２．分析試料

技術水準の確認に用いた分析試料は IAEA から供された水・玄米・土壌試料(Fig.1)である。IAEA から供された試料のうち水試料の１つは既知量の放射性核種 ^{152}Eu（下限数量以下）が添加されたものであった。このほか、気象研究所から供された標準試料(Fig.2)の分析も併せて行っている。この標準試料は 1963 年～1979 年にかけて日本全国１４地点で採取された降下物試料を、気象研究所において混合・調製したものである。なおこの試料は、調製後に他の分析機関においても分析が行われ、参照値が与えられている[1,2]。

Fig.1 IAEA-PT sample

Fig.2 Reference fallout materials

３．分析・測定方法

γ線放出核種は、水試料については 500ml ポリ瓶に分取、玄米・土壌試料については外径 6cm のプラスチック容器(丸型Ｖ式容器 V-7)に詰め、高さを測定後、Ge 半導体検出器(Fig.3)で測定した。
水試料は、193.1Bq/kg の ^{152}Eu が添加された試料 No.3 約 500g を元にエネルギー効率曲線(Fig.4)を作成し、検出した核種の定量を実施した。また、^{134}Cs については、サム効果補正のために試料と検出器との距離を 0～142mm まで 5 段階で測定を行い、^{137}Cs の計数率を基準とし、距離 0mm での ^{134}Cs の計数率とサム効果が無視できる距離での計数率との差からサム効果の補正値を算出した(Table-1)。玄米・土壌試料は、高さを変えた気象研降下物標準試料から、高さ効率曲線(Fig.5)を作成し、多核種混合線源から得られたエネルギー効率曲線(Fig.6)で補正を行った。

^{90}Sr については水試料は 10g、40g、土壌試料は 10g、15g を分取しテフロン容器内に入れ、濃硝酸と過酸化水素を加えて 200℃に加熱し有機物を分解後、不溶残渣をろ過で除去する。担体として Sr 50mg 相当を加えたろ液に水酸化ナトリウムを加えアルカリにして、炭酸塩沈殿法、つづいてシュウ酸塩沈殿法、発煙硝酸法によるカルシウム除去、クロム酸塩沈殿法によるバリウム・ラジウム除去、水酸化鉄沈殿法によるイットリウム除去により化学分離し、最終的に炭酸ストロンチウムとして回収しろ紙ばさみに固定した。二週間以上放置し、^{90}Sr と ^{90}Y とが放射平衡に達した後に、低バックグラウンドガスレス検出器(CANBERRA 社製 iMatic)(Fig.7)で測定した[2]。

Sr の回収率については、以下の計算式による。

$$Y = \frac{W_2}{W_1} * 100$$

Y : Sr yield(%)、W_1 : The quantity of added strontium as a carrier (mg)、

W_2 : The quantity of recovered strontium (mg)

Fig.3 A Ge semiconductor detector

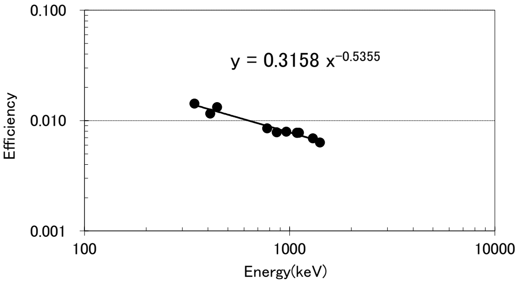

Fig.4 Water sample energy efficiency curve

Table-1 Relative count rate and coincidence summing effect revision

Distance(mm)	Relative count rate(605/662keV)	
0	0.80 ±0.11	・・・a
35.5	0.91 ±0.19	
71	0.98 ±0.17	
106.5	0.89 ±0.12	
142	0.95 ±0.04	
71-142mm average	0.94 ±0.11	・・・b

	(b/a)
Coincidence summing effect revision	1.18 ±0.21

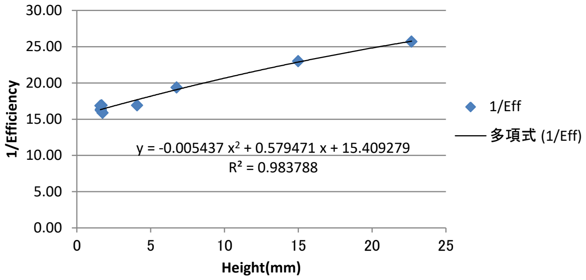

Fig.5 Height efficiency curve

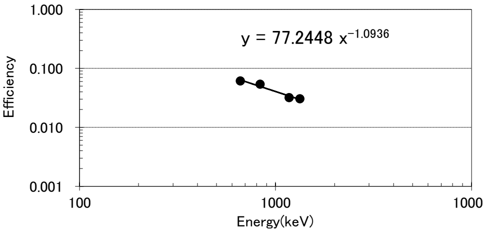

Fig.6 Rice/soil sample energy efficiency curve

Fig.7 A gas-less α/β detector

４．評価方法

分析値はIAEAが示す以下の手順で評価した。

正確度の評価については、以下の式による。

$$Bias_{relative} = \frac{Value_{reported} - Value_{target}}{Value_{target}} \times 100\%$$

$Bias_{relative}$ ：Relative bias、$Value_{reported}$ ：Analysis value、$Value_{target}$ ：Target value

測定工程や分析法を考慮し、測定対象ごとに定められた最高受容相対バイアス（*MARB*:*Maximum Acceptable Relative Bias*）と上式の$Bias_{relative}$を比較し、$Bias_{relative} \leqq MARB$の場合、正確度は”受容可能”となる。

精度の評価については、以下の式による。

$$\mathrm{P} = \sqrt[2]{\left(\frac{u_{target}}{Value_{target}}\right)^2 + \left(\frac{u_{reported}}{Value_{reported}}\right)^2} \times 100$$

P ：Precision、$Value_{target}$ ：Target value、$Value_{reported}$ ：Analysis value、
u_{target} ：Target uncertainty、$u_{reported}$ ：Analisys uncertainty

$P \leqq MARB$及び、$Bias_{relative} \leqq k*P$の場合、精度は“受容可能”となる。

kは包含係数で、95%の信頼度で2.56となる。

最終評価について　A:受容可能　正確度と精度の両方が受容可能であるとき
N:受容不可　正確度が受容不可であるとき
W:警告　正確度は受容可能だが、精度が不可のとき

Table-2 Comparison of target value and analysis value

Sample code	1	1	1	2	2	4	4	4	5	5
Analyte	Sr-90	Cs-134	Cs-137	Na-22	Zn-65	K-40	Cs-134	Cs-137	Sr-90	Cs-137
Target value[Bq/kg]	29.6 ±0.8	30 ±0.9	30.1 ±0.9	65.1 ±1.5	177.3 ±5.7	72.1 ±3.5	12 ±0.4	38.6 ±0.9	36.2 ±2.7	715 ±30
MARB	15%	15%	15%	15%	15%	25%	15%	15%	20%	15%
Analysis value[Bq/kg]	30.2 ±1.3	35 ±6.4	34 ±1.7	55.2 ±1.8	180 ±2.4	83 ±4.0	11 ±2.5	35 ±1.7	37.8 ±1.9	640 ±2.6
Relative bias	2.03%	16.67%	12.96%	-15.51%	1.52%	15.12%	-8.33%	-9.33%	4.42%	-10.49%
Accuracy	A	N	A	N	A	A	A	A	A	A
P	5.08	18.53	5.83	4.00	3.48	6.84	22.97	5.39	8.99	4.22
Precision	A	N	A	A	A	A	N	A	A	A
Final score	A	N	A	N	A	A	W	A	A	A

・Sample code 1・2 is water sample,4 is brown rice sample,5 is soil sample

・IAEA evaluation criteria, A：Accepted, N：Not Accepted, W:Warning

５．結果と考察

測定結果について、各分析値と IAEA 発表の目標値との比較と評価を表－１に示す。測定結果は概ね良好なばらつきの範囲内であったが、^{134}Cs は独自に実施したサム効果補正の誤差影響で不確かさが大きくなった。^{90}Sr については、分析の都合上、報告期限に間に合わなかった為、IAEA には未報告であるが、分析値は目標値とよく一致している。よって、分析・測定が全体として適正に行われていると判断している。結果として、アトックスが分析を請負って以降の気象研究所における環境放射能試料の分析・測定データの信頼性については、良好に保たれていると判断する。今後も適正な分析品質を確保する観点から積極的に PT 等に参加していきたい。

「参考文献」

[1] 五十嵐康人,広瀬勝己,「放射性降下物標準試料の調製を通じた ^{90}Sr、^{137}Cs、プルトニウムなどの人工放射性核種分析の相互比較と参照値の決定」、放射化分析研究会,17,39-42 (2004)

[2] M. Otsuji-Hatori, Y. Igarashi & K. Hirose, Preparation of Reference Fallout Material for Activity Measurements, J. Environ. Radioactivity, 31, 143-155 (1996)

The measurement of the IAEA-TEL-2015-03 Proficiency Test sample

○Toru Kimura *1, Yasuhito Igarashi *2, Yuji Zaizen *2
1 ATOX Co.,Ltd. , 2 Meteorological Research Institute

IAEA Proficiency Test (PT) was intended to confirm the measurement skills of artificial and natural radionuclides contained in the environmental samples, are located in one of the mutual comparative evaluation of the International Atomic Energy Agency (IAEA). By the way, a part of the observation of ^{90}Sr and ^{137}Cs in atmospheric deposition have been carried out in the Meteorological Research Institute, was undertaken by ATOX Co. from a few years ago.How I analyze and measure the sample in the PT, also reported results are summarized for its accuracy. The analysis sample which I used for the confirmation of technical standards is water, unpolished rice, soil sample offered by IAEA. The gamma ray-releasing nuclide analysis was measured with a Ge detector. For ^{90}Sr analysis, after decomposition of organic substances, Sr fraction was radiochemically-separated and finally purified strontium carbonate was measured with a low background gas-less counter. Comparing the targeted value of the IAEA announcement with the analytical ones, analysis results were generally within the favorable range. However, the ^{134}Cs analytical values uncertainty was grows big under error influence of the coincidence summing effect correction value that I carried out originally.

The ^{90}Sr, it is unreported in IAEA, but analytical values were in good agreement with the targeted values. Therefore, it is concluded that the measurement of the environmental radioactivity sample in the Meteorological Research Institute has been done properly.

ガンマ線スペクトル解析ソフトP-SCANを用いた高精度な Cs-134/Cs-137放射能比の導出

○木村徹＊[1]，五十嵐康人＊[2]，財前祐二＊[2]
＊[1]㈱アトックス　　＊[2]気象研究所

１．はじめに

気象研究所では、大気降下物中の^{90}Sr、^{134}Cs及び^{137}Csの長期モニタリングを実施している。このうち^{134}Csは、複数のγ線をカスケードで放出するため、ゲルマニウム半導体検出器での測定においては、サム効果の補正が必要であるが、通常、^{134}Csの標準線源（面線源）でピーク効率を求める場合にはサム効果補正は要しない1)と言われている。大気中のCs測定用の試料は、ハイボリュームサンプラーで大気エアロゾルを石英フィルター上に捕集した後、フィルターを短冊状に8分割し放射能が均等になるように金型に入れて油圧プレスで圧縮固化し、標準面線源と同一形状に加工している。しかし、この過程で、放射能分布は必ずしも完全に均一ではなくなり、標準線源の放射性核種の分布とのずれが僅かだが生じて、試料毎にサム効果が微妙に異なる可能性が考えられる。^{134}Cs/^{137}Cs放射能比（134/137比）の高精度の測定は、発生源の特定に繋がることもあり、重要視している。そこで、試料毎（スペクトル毎）にサム効果補正を行うことが可能なソフトウェアであるP-SCAN（㈱スカラベ・コーポレーション製）の活用を考えた。この研究では、このソフトウェアを用いて、一番端的な事例であるフィルター試料に関し134/137比を高精度で測定することを試み、サム効果補正を行わない定量方法（スペクトル解析ソフトとしてITECH Instruments製InterWinnerを使用）との比較を行った。

２．分析試料

校正用の標準試料として、多核種混合面線源(Eckert＆Ziegler製 ^{134}Cs 118Bq、^{137}Cs 213Bq（2015/12/1における保証値））を用いた。これは、石英繊維フィルター（SIBATA製QR-100）を油圧プレスで圧力を加えて円形（直径約51mm、厚さ約2mm）に圧縮固化し、その表面に均等にRI溶液を添加して容器に封入したものである。

分析試料は東日本大震災直後の2011年4月に気象研究所で採取した大気フィルター試料（^{134}Csはまだ減衰しきっていない）を用いた。この試料はハイボリュームサンプラー（SIBATA製HV-1000F）で大気中浮遊塵を採取した石英繊維フィルターを標準試料と同様に円形に圧縮固化し、標準面線源と同形状の容器に封入したものである。

３．P-SCANによる定量原理

ガンマ線スペクトルの光電ピーク面積と、それらの計数効率・全効率の間に成り立つ高次・多元連立方程式を直接解くという方法を採用している。^{134}Csの様な壊変後にカスケード関係にあるγ線を放出する核種においては、観測されるピークの数をパターン化して数式化する。このようにして得られた複数の連立方程式を解き、最尤適合関数を求めることで、ピーク計数効率関数を決定している2-5)。試料測

定により“InterWinner”から得られたチャンネルごとの計数値をこのソフトウェアに入力すると、ピークを再解析し、選択した核種の効率や放出比も掛け合わされたピーク毎の崩壊数計算値として出力される。サム効果が発生する対象核種については補正計算が実行されて、サム効果補正後の崩壊数計算値が出力される。ここで得られた計算値を測定時間、減衰補正係数、さらに試料量で除算することで放射能濃度を得ることができる。

４．測定方法

気象研究所の4台(#6、#7、#8、#10)のゲルマニウム半導体検出器を使用した(Fig.1)。まず、標準試料で校正し、大気中浮遊塵試料を測定して“InterWinner”で計数値を得た。得られた計数値に対して以下の放射能計算式でデータを算出した。また、“P-SCAN”でピークを再解析しサム効果補正計算処理を行った。

$$\mathrm{n} = \frac{a_S}{t_s} - \frac{a_b}{t_b} \quad , \quad \mathrm{A} = \frac{n \cdot d}{P \cdot \varepsilon \cdot V}$$

n：Net count rate(cps)、a_s：Sample peak area(count)、a_b：Background peak area(count)、t_s：Sample measurement time(s)、t_b：Background measurement time(s)、A：Radioactivity concentration(Bq/m^3)、d：Attenuation correction、P：Gamma ray emission rate、 ε ：Counting efficiency(cps/Bq)、V：Air suction volume(m^3)

サム効果の比率を確認するため、^{134}Cs が放出するγ線のうち放出率が 97.6%と最も高い 605keV の計数値と、相対計数値の基準としてサム効果が発生しない ^{137}Cs の 662keV の計数値の比を、#8 検出器で、標準面線源との距離を 0cm から 30cm まで 5cm 間隔で離して測定した。検出器から距離を離すことにより、同時にγ線が入射する確率が減るためにサム効果は起こりにくくなり、605keV/662keV の光電ピークの比が一定値に近づく。0cm のカウント比を 1 として、一定値に達したときの距離のカウント比からサム効果の比率が分かる。

さらに、^{134}Cs のサムピークの代表値として 605keV と 796keV（放出率 85.4%）が同時に入射した際に検出される 1400keV と 605keV とのカウント比の関係についても算出した。

Fig.1 Ge semiconductor detector

Table-1 Comparison when using P-SCAN and normal calculation in 4 detectors
(results of measuring the same sample)

			Cs-134				Cs-137					
Detector	Sampling period	134+137(Bq)	Normal calculation		Using P-SCAN		Normal calculation		Using P-SCAN		Normal calculation	Using P-SCAN
			mBq/m3	Err	mBq/m3	Err	mBq/m3	Err	mBq/m3	Err	134/137 ratio	134/137 ratio
#6	2011/04/11 ～04/19	898	60.1	0.4	59.0	0.4	55.2	0.1	55.3	0.1	1.09	1.07
#7			62.0	0.3	57.8	0.3	55.3	0.1	54.5	0.1	1.12	1.06
#8			61.7	0.3	58.6	0.3	55.3	0.1	54.6	0.1	1.12	1.07
#10			60.6	0.4	57.6	0.4	55.4	0.1	54.3	0.1	1.09	1.06
										σ	0.014	0.006

Table-2 Detector distance and count ratio

Ge#8	Count ratio		Ratio to 0 cm	
cm	605/662	1400/605	605/662	1400/605
0	0.318	0.086	1.00	1.00
5	0.420	0.018	1.32	0.21
10	0.438	0.007	1.38	0.08
15	0.443	0.001	1.39	0.01
20	0.455	0.000	1.43	0.00
25	0.443	0.001	1.39	0.01
30	0.452	0.000	1.42	-0.01

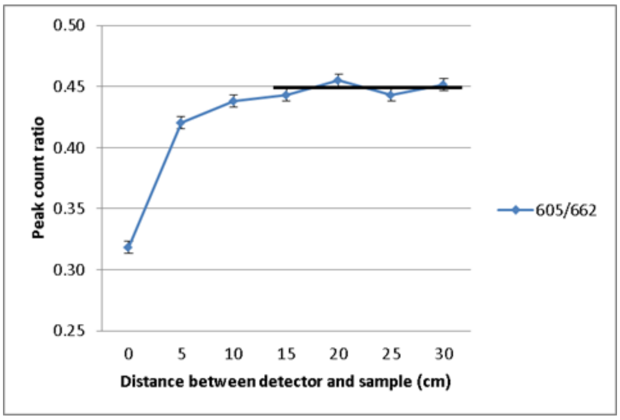

Fig.3 Relationship between distance to sample and 605/662 keV photo-peak count ratio

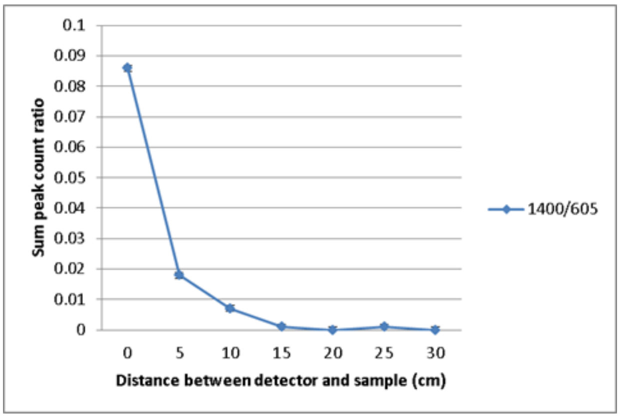

Fig.4 Relationship between distance to sample and 1400/605 keV photo-peak count ratio

５．結果と考察

大気中浮遊塵試料の測定結果を Table-1 に示す。^{137}Cs については、両手法による測定結果はよく一致したが、^{134}Cs については P-SCAN で得たデータの方が数%低めの値であった。また、134/137 比については、P-SCAN データの方が検出器間のばらつきが非常に小さかった。このことから、134/137 比の測定については P-SCAN を用いた方が精度が良いと考えられるが、絶対値としてどちらがより正確な値であるかの判断はできない。今後、濃度の異なる他の面線源の測定を行い再現性の確認等データの検証を行う必要がある。また、通常の計算法と P-SCAN を用いた場合との差は 10%以内であったので、環境放射能試料の測定において測定値の再計算等が必要とされるような重大な影響は無い。

距離と光電ピーク比の関係をTable-2およびFig.3に、また、距離と1400/605光電ピーク比の関係をFig.4に示す。15cm以上離せば605/662光電ピーク比は安定し、1400/605光電ピーク比の関係からもサムピークの影響は無視できるほど小さくなる（サム効果が弱まり0に近づくことが分かる）ことが確認された。体積線源を用いる大気降下物試料については今回の検討には含まれていないため、今後さらに、補正方法の改善やP-SCANの適用を検討していく。

参考文献

1)　日本アイソトープ協会理工学部会、NaI(Tl)シンチレーションスペクトロメータによるγ線スペクトロメトリーガイダンス(2015)

2)　日本アイソトープ協会理工学部会次世代スペクトル解析専門委員会、ガンマ線スペクトル解析におけるピーク探査と面積計算実態と今後のスペクトル解析のあるべき姿、RADIOISOTOPES、65、267-285 (2016)

3)　山田崇裕、石津秀剛、高野直人、加算同時計数効果を用いたGe検出器の計数効率関数決定法、第51回アイソトープ・放射線研究発表会要旨集、50（2014）

4)　仁木工芸株式会社、P-SCANカタログ（2014）

5)　文部科学省、放射能測定シリーズ7　ゲルマニウム半導体検出器によるガンマ線スペクトロメトリー（1992）

Aiming at higher precision measurement of Cs-134 and Cs-137 radioactivity ratios by using P-SCAN gamma ray data analysis software

○ Toru Kimura * 1, Yasuhito Igarashi * 2, Yuji Zaizen * 2
1 ATOX Co.,Ltd. , 2 Meteorological Research Institute

At the Meteorological Research Institute (MRI), long-term monitoring of ^{90}Sr, ^{134}Cs, and ^{137}Cs in atmospheric fallout is carried out. For the sample for measuring Cs in the atmosphere, after collecting atmospheric aerosol on a quartz filter with a high volume sampler, it is compressed and solidified and processed into the same shape as the standard surface source. However, in this process, the radioactivity distributes not necessarily completely uniform, slight deviation from the distribution of the radionuclide of the standard radiation source occurs, and the sum effect potentially varies slightly for each sample. Therefore, we considered utilization of P-SCAN (manufactured by SCARABS CORPORATION), which is software capable of correcting sum effect for each specimen (spectrum). In this research, we tried to measure 134/137 radioactivity ratios for filter samples with high precision using this software and compared with a quantitative method without sum effect correction.

First, we calibrated with the standard source , then we measured airborne dust sample and got the count value by "InterWinner". Data was calculated for the obtained count value by the radioactivity calculation formula. Moreover, the peak was re-analyzed with "P-SCAN" and the sum effect correction calculation process was performed.

For ^{137}Cs, the results were in good agreement, but for ^{134}Cs, P-SCAN led lower values. As for the concentration ratio of ^{134}Cs/^{137}Cs, P-SCAN gave a much smaller variation for all detectors. From this result, it can be considered that the precision of P-SCAN is better, but it cannot be judged which one is the accurate measurement result by this measurement alone. In the future, it is necessary to measure other surface radiation sources with different concentrations and verify data as confirmation of reproducibility. Also, since the difference between the usual calculation method and P-SCAN was within 10%, there is no need to recalculate/correct in the measurement of environmental radioactivity samples.

Kinase *et al. Progress in Earth and Planetary Science* (2018) 5:12
https://doi.org/10.1186/s40645-018-0171-z

Progress in Earth and
Planetary Science

RESEARCH ARTICLE

Open Access

The seasonal variations of atmospheric ^{134,137}Cs activity and possible host particles for their resuspension in the contaminated areas of Tsushima and Yamakiya, Fukushima, Japan

Takeshi Kinase[1,2*], Kazuyuki Kita[3], Yasuhito Igarashi[4], Kouji Adachi[4], Kazuhiko Ninomiya[5], Atsushi Shinohara[5], Hiroshi Okochi[6], Hiroko Ogata[6], Masahide Ishizuka[7], Sakae Toyoda[8], Keita Yamada[8], Naohiro Yoshida[8,9], Yuji Zaizen[10], Masao Mikami[11], Hiroyuki Demizu[12] and Yuichi Onda[13]

Abstract

A large quantity of radionuclides was released by the Fukushima Daiichi Nuclear Power Plant accident in March 2011, and those deposited on ground and vegetation could return to the atmosphere through resuspension processes. Although the resuspension has been proposed to occur with wind blow, biomass burning, ecosystem activities, etc., the dominant process in contaminated areas of Fukushima is not fully understood. We have examined the resuspension process of radiocesium (^{134,137}Cs) based on long-term measurements of the atmospheric concentration of radiocesium activity (the radiocesium concentration) at four sites in the contaminated areas of Fukushima as well as the aerosol characteristic observations by scanning electron microscopy (SEM) and the measurement of the biomass burning tracer, levoglucosan.

The radiocesium concentrations at all sites showed a similar seasonal variation: low from winter to early spring and high from late spring to early autumn. In late spring, they showed positive peaks that coincided with the wind speed peaks. However, in summer and autumn, they were correlated positively with atmospheric temperature but negatively with wind speed. These results differed from previous studies based on data at urban sites. The difference of radiocesium concentrations at two sites, which are located within a 1 km range but have different degrees of surface contamination, was large from winter to late spring and small in summer and autumn, indicating that resuspension occurs locally and/or that atmospheric radiocesium was not well mixed in winter/spring, and it was opposite in summer/autumn. These results suggest that the resuspension processes and the host particles of the radiocesium resuspension changed seasonally. The SEM analyses showed that the dominant coarse particles in summer and autumn were organic ones, such as pollen, spores, and microorganisms. Biological activities in forest ecosystems can contribute considerably to the radiocesium resuspension in these seasons. During winter and spring, soil, mineral, and vegetation debris were predominant coarse particles in the atmosphere, and the radiocesium resuspension in these seasons can be attributed to the wind blow of these particles. Any proofs that biomass

(Continued on next page)

---

* Correspondence: t.kinase.J52@gmail.com
[1]Graduate School of Science and Engineering, Ibaraki University, 2-1-1 Bunkyo, Mito, Ibaraki 310-8512, Japan
[2]Hitachi Power Solutions Co., Ltd, 2-2-3 Saiwaicho, Hitachi, Ibaraki 317-0073, Japan
Full list of author information is available at the end of the article

(Continued from previous page)
burning had a significant impact on atmospheric radiocesium were not found in the present study.

Keywords: Radiocesium, Atmospheric radioactivity, Seasonal variation, Resuspension, Fukushima, Nuclear accident, Bioaerosol, Spore, Mineral dust, Host particle

Introduction

In March 2011, abundant and various radionuclides were released into the atmosphere (e.g., Chino et al. 2011) as a result of the nuclear accident at the Fukushima Daiichi Nuclear Power Plant (FDNPP) caused by the Great East Japan Earthquake (Holt et al. 2012), and their amounts and diffusion have been of public concern because of their health impacts (Report: Working Group on Risk Management of Low-dose Radiation Exposure 2011). Radiocesium isotopes ^{134}Cs and ^{137}Cs were two of the main radionuclides released from the FDNPP accident (Steinhauser et al. 2014). As an example, the total amount of released ^{137}Cs was estimated by Chino et al. (2011) to be 1.3×10^{16} Bq (13 PBq). The ^{134}Cs emission inventory should be almost the same as that of ^{137}Cs, i.e., 1.2×10^{16} Bq (12 PBq; Steinhauser et al. 2014) because the activity ratio of these two isotopes was almost united in the case of the FDNPP accident (e.g., Merz et al. 2013). There have been concerns that the deposited radiocesium will influence the contaminated area for an extended period, in contrast to the effects of radioiodine, because the half-lives of ^{134}Cs and ^{137}Cs are relatively long: 2.06 years and 30.17 years, respectively (Dietz and Pachucki 1973; Unterweger 2002). Figure 1 shows the contaminated deposition density map for $^{134,\ 137}$Cs (the unit of deposition density is Bq m^{-2}) measured from October to November 2011 by the Ministry of Education, Culture, Sports, Science and Technology, Japan (MEXT) (2011). The radionuclides released by the FDNPP were deposited on the ground, vegetation, houses, and other objects, causing serious contamination of widespread areas, especially areas in the northwest of the FDNPP.

Although more than 5 years have passed since the FDNPP accident, significant atmospheric radiocesium activity concentrations (hereafter called the radiocesium concentration), on the order of approximately 10^{-4} Bq m^{-3}, have still been observed in the contaminated area (e.g., Ochiai et al. 2016). These concentrations are at least two orders of magnitude higher than those observed in East Japan before the FDNPP accident (~ 1 μBq/m^3; Igarashi et al. 2015). Several studies showed that this atmospheric radiocesium could not be attributed to the direct emissions/leakage from the FDNPP site (e.g., Igarashi et al. 2015; Kajino et al. 2016) but could be supplied by secondary emissions of the deposited radiocesium, which is called resuspension to the atmosphere (e.g., Igarashi 2009; Igarashi et al. 2015; Kajino et al. 2016). Igarashi et al. (2015) concluded that the delayed primary emissions from the FDNPP could not be a major source of the current (till March 2015) radiocesium in the atmosphere based on the atmospheric observations in Tsukuba and the emission inventory data from Tokyo Electric Power Co., Inc. (TEPCO) (2012). Kajino et al. (2016) also showed that resuspension could predominantly contribute to the atmospheric radiocesium concentrations in the year 2013 using a 3D aerosol model simulation and the emission data from TEPCO.

The soluble form of primary radiocesium is carried by submicron particles (Masson et al. 2013), which would most likely be non-sea salt sulfate (nss-SO_4^{2-}), as suggested by Doi et al. (2013) and Kaneyasu et al. (2012). In general, water-soluble cesium ions from SO_4^{2-} are considered to be adsorbed or attached to mineral particles in a soil environment (Bostic et al. 2002; Dumat and Staunton 1999; Mukai et al. 2014). These mineral particles were shown to act as resuspended host particles in an atmospheric environment by the previous investigations of the global fallout from atmospheric nuclear weapon tests (e.g., Igarashi et al. 2005; Masson et al. 2010). Therefore, a major resuspension source has been thought to be the suspension of contaminated dust particles by wind (Igarashi et al. 2016; Ishizuka et al. 2017; Sýkora et al. 2012), even for the case of the FDNPP accident contamination. In addition, a significant amount of water-soluble cesium ions has been absorbed by living organisms, such as mushrooms (Yoshida et al. 1994) and plants, and has been relocated within vegetation, from bacteria (Tomioka et al. 1992), through plant roots (Ehlken and Kirchner 2002), to pollen and then to honey (Barišić et al. 1992; Kanasashi et al. 2015). Such contaminated forest ecosystems could be another source for radiocesium re-emission into the atmosphere (also we call “resuspension” in this study). The cedar pollen in contaminated forests contains significant amounts of radiocesium. The highest total radiocesium concentration in Fukushima cedar pollen was reported to be 25.4 Bq g^{-1} (dry weight) in 2014 (Forestry Agency, Japan (FAJ) 2015), suggesting that pollen emissions could still be a candidate for the host particles of radiocesium resuspensions, although pollen emissions occur during limited durations of weeks or months each year

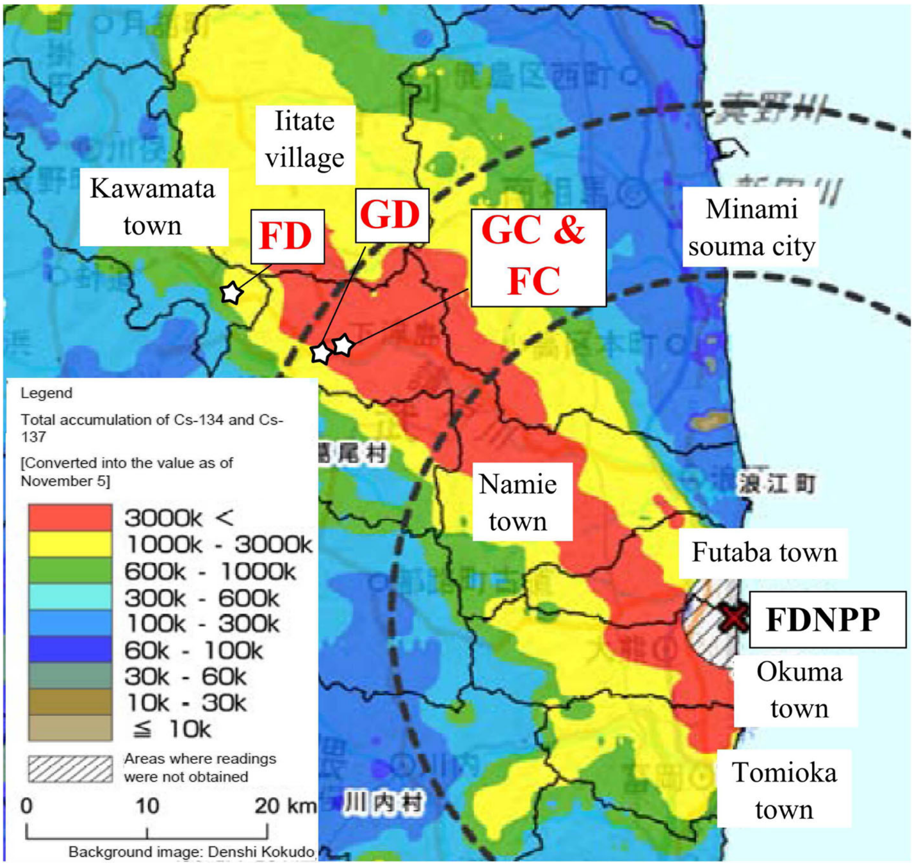

Fig. 1 The four sampling locations in this study plotted over the deposition density map for ^{134,137}Cs obtained by the Japanese government (Ministry of Education, Culture, Sports, Science and Technology, Japan (MEXT) 2011). The radius of dotted outer circle is 30 km

depending on plant species. Furthermore, open biomass burning of contaminated vegetation is also a candidate for the radiocesium resuspension process (Bourcier et al. 2010; Igarashi 2009; Lujanienė et al. 2009; Sýkora et al. 2012; Yoschenko et al. 2006).

Many studies have been carried out to address the environmental radiocesium contamination resulting from the FDNPP accident, but the processes of radiocesium resuspension have not yet been fully identified in this case. Knowledge of the host particles of such secondary radiocesium emissions and their long-term variations is limited (e.g., Igarashi et al. 2015) because of the lack of long-term and intensive studies in Fukushima. Ishizuka et al. (2017) discussed the processes contributing to the radiocesium resuspension with soil dust particles from the surface based on measurements within the contaminated area in Fukushima. Their proposed scheme can be applied to evaluate secondary emissions caused by aeolian resuspension of radioactive materials associated with mineral dust particles from the ground surface. However, their study only focused on the resuspension from winter to spring; the seasonal variations and other processes of resuspension were not discussed. A recent work by Kajino et al. (2016) has revealed that the forest ecosystem could be another source of radiocesium during the warm seasons, in addition to that of dust suspension. These authors applied a novel scheme for radiocesium resuspension from the forest (as the green fraction) that operates according to forest activity as measured by the normalized difference vegetation index (NDVI) satellite data (Gutman and Ignatov 1998). However, Kajino et al. (2016) showed a model simulation application and did not reveal the actual host material of radiocesium. Recently, Ochiai et al. (2016) added new observational results of the monthly radiocesium concentrations (September 2012 to December 2014) at a contaminated area in western Tsushima that is near our present observation site. These authors applied a two-stage size separation (coarse and fine) in their monitoring and demonstrated that ^{137}Cs activity concentration enhancement during the warm season and the coarse fraction (> 1.1 μm) of ^{137}Cs exhibited seasonal changes along with the concentration increases. These authors interpreted this seasonal trend via the relevance of the seasonal changes in the prevailing local winds and locations of the surface contamination. Although their observational results agree well with our present results, their explanation remains incomplete; no explanations of the radiocesium host particles involved are given. It is important to understand the contributions of each resuspension process in all seasons and to break the current limitations of our understandings, especially in the heavily contaminated areas in the Fukushima prefecture, to evaluate the transport/diffusion of radiocesium from the contaminated areas to other areas. The purposes of this research were thus set as follows: (1) to identify the seasonal variations of the concentrations of atmospheric radiocesium via long-term monitoring, (2) to determine the spatial scales of the resuspension and redistribution of atmospheric radiocesium, and (3) to estimate the sources and host particles that contribute to the resuspension.

Methods/Experimental

For the measurements of the radiocesium concentrations, we have carried out aerosol sampling at four sites (labeled herein as the FD, FC, GD, and GC sites), which are located in heavily contaminated areas in the Fukushima prefecture, as shown in Fig. 1. The areas of the sampling sites belong to typical Japanese villages/towns, which are surrounded by forests in a mountainous area as is the traditional farming landscape in this region (e.g., Berglund 2008). The forests around the sampling sites are secondary forests surrounding farm villages (Satoyama) and are not dense, primeval forests. According to Berglund (2008), Satoyama is defined as "forests surrounding farm villages and managed by farmers for different needs—timber for buildings, wood for fuel and charcoal production, and leaf litter and twigs used as fertilizer for crops, particularly in the rice paddy fields situated in the lowlands." Currently, the agricultural lifestyle has been changing greatly; however, major landscape changes have not occurred. Inhabitants were evacuated from these contaminated areas by the time that this manuscript was revised (up to March 2017), so this area has been free from human activity, except for decontamination and monitoring activities.

The sites labeled with the letters F and G are the forest and open ground sites, respectively, and the sites labeled with the letters D and C are sites where decontamination was conducted or not, respectively. The FD site in the Yamakiya area, Kawamata-town, is located in a cedar forest 35 km northwest of the FDNPP, and its contamination was the lowest of the four observation sites even before decontamination because the radioactive plume was blocked by hills.

We could start the monitoring at the FD site soon after the FDNPP accident, i.e., since July 2011. The area around the FD site was decontaminated between August 2013 and October 2014. The dose rate monitoring by the Nuclear Regulation Authority showed that the average dose rate in this area had decreased from 0.90 μSv h^{-1} in 2012 to 0.28 μSv h^{-1} in 2014 mainly because of the decontamination. The FC, GC, and GD sites are located in the Tsushima area in Namie-town, approximately 30 km northwest of the FDNPP. The GC site was in a school playground (area is 10.7×10^3 m^2), and the aerosol sampling and meteorological observations here started in December 2012 (Ishizuka et al. 2017). The GD site was located in another school playground (area is 5.7×10^3 m^2), within a 1 km distance from the FC and GC sites. Both sites are basically flat and originally paved by sand because of their gymnastic uses. An area of approximately 5×10^4 m^2, including the GD site, had been locally decontaminated during the period of December 2011 to February 2012, and the dose rate at the GD site decreased from 9.60 to 2.8 μSv h^{-1} because of the decontamination (Japan Atomic Energy Agency (JAEA) 2012). The aerosol sampling at this site started in November 2012. The FC site is in a broadleaved forest mixed with red pine trees adjacent to the GC site, and the aerosol sampling at this site started in January 2014. The Tsushima area, including the FC and GC sites, was not decontaminated during our observation period, except around the GD area, and their dose rates were higher (by at least three to ten times) than those at the FD and GD sites. Details of the four sites are summarized in Table 1.

High-volume air samplers (120SL, Kimoto, Japan, and HV-1000R/F, Sibata, Japan) were used for aerosol sampling (a flow rate of 0.7 m^3 min^{-1}) with quartz-fiber filters (2500QAT-UP, Pallflex, USA). Six-stage cascade impactors (TE-236, Tisch Environmental, USA) mounted on other high-volume air samplers (a flow rate of 0.556 m^3 min^{-1}) were also used to collect the aerosols separately according to their aerodynamic diameters, with quartz-fiber filters (TE-230QZ, Tisch Environmental, USA and 2500QAT-UP, Pallflex, USA) applied as collection substrates. This impactor classifies particles as larger than 10.3 μm (stage #1), 4.2–10.3 μm (stage #2), 2.1–4.2 μm (stage #3), 1.3–2.1 μm (stage #4), 0.69–1.3 μm (stage #5), 0.39–0.69 μm (stage #6), and smaller than

Table 1 Information about the observation locations and conditions at the four sites

Site-ID	Latitude	Longitude	Land condition	Decontaminated or contaminated
FD	37° 35′ 07″ N	140° 41′ 29″ E	Cedar forest	Decontaminated
FC	37° 33′ 41″ N	140° 46′ 06″ E	Broad leaf forest	Contaminated
GD	37° 33′ 38″ N	140° 45′ 37″ E	School ground	Decontaminated
GC	37° 33′ 44″ N	140° 46′ 07″ E	School ground	Contaminated

0.39 μm (backup filter) in diameter, in which the collection efficiency exceeds 50%.

The aerosol sampling period at the FD, FC, and GD sites was mostly between 1 week and 1 month. At the GC site, short-term sampling (1–3 days) was carried out using seven high-volume air samplers with timer-controls. The radioactivities of ^{134,137}Cs of the aerosols sampled in filters were measured at the Meteorological Research Institute (MRI), Osaka University, Tokyo Institute of Technology, and Ibaraki University using coaxial-type Ge semiconductor detectors coupled with computed spectrometric analyzers. The radioactivities of ^{134}Cs and ^{137}Cs were identified and determined from the gamma-ray peak intensities at 605 and 662 keV, respectively. Details of the detector models and the spectrometric analyzers are summarized in Table 2. The radiocesium concentration was calculated from the measured radioactivity and the total volume of the sampled air.

A scanning electron microscope (SEM; SU3500, Hitachi High-Technologies Co., Tokyo Japan) with an energy-dispersive X-ray spectroscope (EDS; X-max 50 mm, Horiba Ltd., Kyoto, Japan) was used to observe the shapes and chemical compositions of the aerosols collected in the above samplings to identify the major host particles of the resuspended radiocesium.

Results and discussion

Seasonal and long-term variations of the atmospheric concentrations of radiocesium activity

Figure 2 shows the time series of the radiocesium concentrations of ^{134,137}Cs obtained from the aerosol sampling at the four sites. For the case of the samples obtained using the impactor, the radiocesium concentration values were the sum of all stages. The radiocesium concentration at the FD site showed a rapid exponential decrease during the earlier period from July 2011 to October 2011. After that, the decrease became slower. Igarashi et al. (2015) showed that the direct emissions/leaks of radiocesium from the FDNPP site significantly affected the radiocesium concentrations in 2011 and 2012 (in the early period), when spikes occurred in the radiocesium concentrations monitored at the MRI, Tsukuba (approximately 170 km south–southwest from the FDNPP), and that atmospheric radiocesium was mainly supplied by resuspension after this period. It should be noted here that radiocesium of the resuspension origin is also subjected to transportation and diffusion as is the primary emission.

The radiocesium concentrations at all of the four sites showed similar seasonal variations, being low in winter and early spring and high in late spring, summer, and early autumn, after November 2011. The annual mean, maximum, and minimum values of the ^{137}Cs concentrations measured at each site are summarized in Table 3. Similar seasonal variations at all sites indicate that resuspension occurred with identical processes/sources in both open areas and forests. This result is opposite to that of the seasonal variation (high in winter and low in summer) found in urban areas by other studies (e.g., Igarashi et al. 2015; Sýkora et al. 2012; Watanabe 2014), suggesting that the dominant resuspension processes/sources are different because of the locations/surface conditions of the study areas, specifically between the urban sites and the forest sites. The sampling sites in our study are located in low mountainous areas, where the major land uses are agricultural fields (abandoned because of the evacuation) placed along valleys and forests covering mountain slopes. Because it is a typical surface condition in heavily contaminated areas in Fukushima as mentioned previously, the present seasonal trend is probably typical of these areas. Similar seasonal variations of radiocesium concentrations were found in the contaminated area of the western part of Namie (near the GC site) by Ochiai et al. (2016).

Between spring and autumn, two maxima were found in May and from August to September, especially for the 2014 results; Fig. 3 compares the temporal variations of

Table 2 Information about the instruments used in this study

Measured at	Detector model	Production	Spectrometric analyzer	Production
MRI	GEM50	Seiko EG&G	Multiport	Oxford-Tennelec
	IGC60210	Princeton Gamma-Tech		
	EGPC40	Canberra		
	GEM-90205-P	Seiko EG&G	MCA760092x	Seiko EG&G
Osaka University	GC6020	Canberra		
	GEM40	Ortec	MCA7600	Seiko EG&G
	GEM 80	Ortec		
Tokyo Institute of Technology	GC3018	Canberra	DSA1000	Canberra
Ibaraki University	GC4020	Canberra	Linx	Canberra

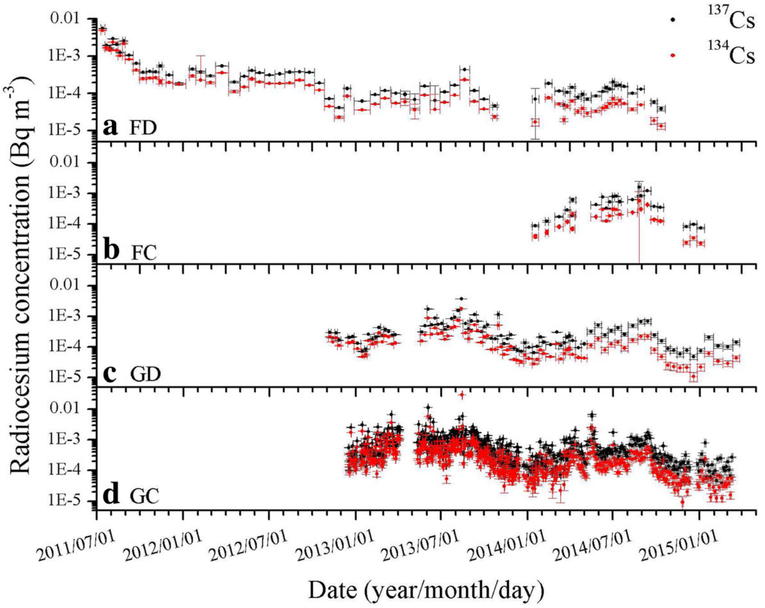

Fig. 2 Activity concentrations of ^{134,137}Cs (Bq m^{-3}) measured at the FD, FC, GD, and GC sites in the Fukushima prefecture in July 2011 to March 2015. These results show high concentrations in late spring, summer, and early autumn and low concentrations in winter and early spring at all of the presented observation locations

(a) the radiocesium concentrations at the GC site with the 30 min averages of various meteorological parameters: (b) wind speed, (c) atmospheric temperature, and (d) precipitation. At the first maximum, occurring around May, the wind speed peaks generally coincided with the radiocesium concentration peaks. During the second maximum, occurring around September, the radiocesium concentration and temperature had similar variations, but the wind speeds were negatively correlated with these variables. These results indicate that the processes or sources of the resuspension are different in these seasons: the physical processes (suspension by wind) are significant in late spring, and another process is dominant in summer/autumn.

Seasonal variations of resuspended host particles found by impactor sampling

To indicate the fractions of ^{137}Cs captured on each stage as well as on the backup filter in the cascade impactor

Table 3 Averages, maximums, and minimums of the ^{137}Cs activity concentration (μBq m^{-3}) at each site

	Average			Maximum				Minimum			
Location (sampling duration)	Year	^{137}Cs	Error	Date (start) m/d h:m	Date (end) m/d h:m	^{137}Cs	Error	Date (start) m/d h:m	Date (end)[a] m/d h:m	^{137}Cs	Error
FD (July 2011–October 2014)	2011	1450	33.7	7/9 16:40	7/18 12:10	5600	66.4	12/9 12:47	2012/1/6 11:16	186	11.0
	2012	287	9.7	3/9 10:43	4/6 11:15	547	7.8	11/16 12:01	12/7 10:18	41.2	2.0
	2013	127	13.6	8/9 14:16	8/30 11:20	432	4.6	10/18 14:48	10/28 10:45	45.9	3.2
	2014	115	8.3	6/29 9:41	7/4 10:30	202	6.4	10/3 10:27	10/20 11:07	38.7	4.6
FC (May 2014–January 2015)	2014	537	78.6	8/22 16:13	8/29 12:52	1620	843	12/26 15:41	2015 1/11 13:24	74.3	5.7
GD (November 2012–June 2015)	2012	213	2.7	11/3 13:40	11/9 12:41	294	2.1	12/28 12:45	2013 1/11 13:46	130	1.4
	2013	521	4.1	8/9 11:55	8/16 11:16	3690	8.0	12/13 12:04	12/23 12:08	72.0	3.0
	2014	243	26.4	9/19 11:16	10/3 10:59	684	94.6	12/26 11:28	2015 1/11 12:07	47.4	8.5
	2015	123	18.7	5/4 11:26	6/4 10:52	225	31.9	4/25 10:41	5/4 11:11	56.8	9.9
GC (December 2012–November 2014)	2012	462	12.2	12/21 13:00	12/22 13:00	2550	28.2	12/19 13:00	12/20 13:00	95.2	4.7
	2013	1170	19.2	8/14 13:00	8/15 13:00	60,400	132	11/12 13:00	11/13 13:00	68.9	11.6
	2014	546	11.6	5/16 13:00	5/18 13:00	6750	31.0	1/15 13:00	1/17 11:38	48.4	7.8

[a] In some cases, the sampling duration crossed over years

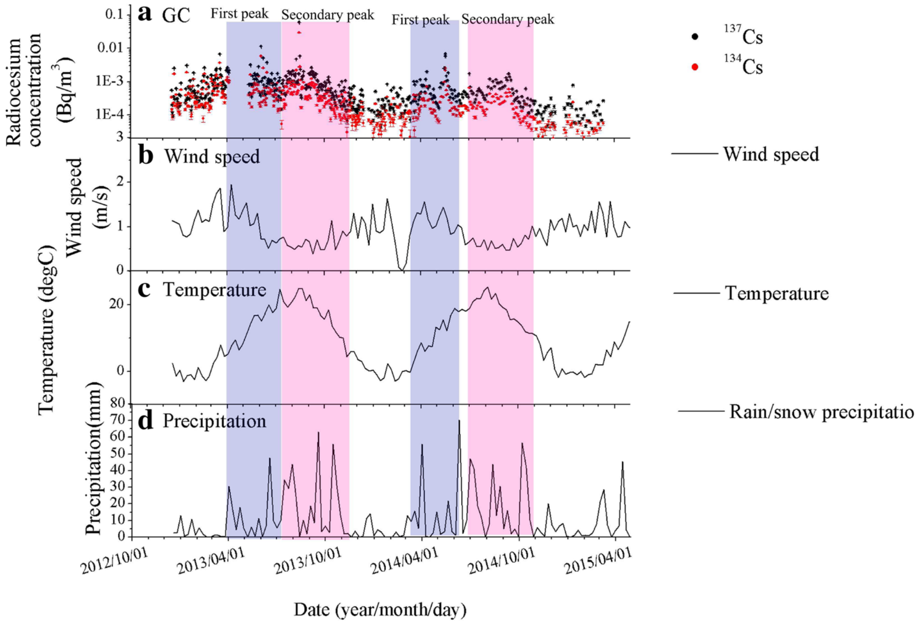

Fig. 3 Time series of (**a**) radiocesium concentrations, (**b**) wind speeds, (**c**) temperatures, and (**d**) rain/snow precipitation. At the GC site, we can see two maxima in the higher concentration seasons: in May and September. The first maxima occurred with wind speed peaks, and the second maxima occurred with atmospheric temperature peaks

sampling, the measured values of the ^{137}Cs radioactivity on the filters $^{137}\mathrm{Cs}_{(i)}$ were normalized as shown in Eq. 1:

$$\text{Normalized } ^{137}\mathrm{Cs}_{(i)} = \frac{^{137}\mathrm{Cs}_{(i)}}{^{137}\mathrm{Cs}_{(\mathrm{Total})}}, \tag{1}$$

where (i) is the stage number, $^{137}\mathrm{Cs}_{(i)}$ is the ^{137}Cs radioactivity of the (i)-th sampling stage collection substrate, and $^{137}\mathrm{Cs}_{(\mathrm{Total})}$ is the total of the ^{137}Cs radioactivity of all of the sampling stage substrates, including the backup filter for each sampling period. The radioactivity of the backup filter was also normalized to the normalized $^{137}\mathrm{Cs}_{(\mathrm{Total})}$ value as $^{137}\mathrm{Cs}_{(7)}$. Figure 4 shows the time series of the ^{137}Cs fraction of stage #2 (nominal aerosol diameter of 4.2–10.3 μm) and the backup filter (< 0.39 μm), where the highest fraction was most often found. In the fraction of stages #1–5, the normalized $^{137}\mathrm{Cs}_{(1-5)}$ showed similar seasonal variations among themselves, i.e., high in summer/autumn (June to November) and low in winter/spring (December to April or May). This result is consistent with that of Ochiai et al. (2016); the coarse fraction (> 1.1 μm) of ^{137}Cs exhibited similar seasonal changes. In contrast, the fraction of the backup filter of normalized $^{137}\mathrm{Cs}_{(7)}$ showed the opposite trend; it was high in winter/spring and low in summer/autumn. In this discussion, we omitted the $^{137}\mathrm{Cs}_{(6)}$ values because they were frequently lower than the detection limit. This seasonal variation of the $^{137}\mathrm{Cs}_{(1-5)}$ and $^{137}\mathrm{Cs}_{(7)}$ fractions could be attributed to a measurement artifact, i.e., the bounce effect, rather than the actual size variations of the host aerosols for the radiocesium resuspension. Bouncing of particles, particularly coarse ones, occurred in stages #1–6, especially during winter/spring, resulting in the considerable amount of coarse particles sampled at the backup filter, although the filter was expected to capture only finer particles. Figure 5 shows a picture of a typical backup filter sample at the GC site in spring, showing many coarse particles, such as pollen and soil/mineral particles. These coarse particles would nominally have been trapped in stages #1 and #2, but they bounced in these earlier stages and accumulated on the backup filter. As indicated by the red rectangles, accumulations of coarse particles were found near the edge of the backup filter, presumably because of the stagnation of air flow or narrower gaps between the filter and the cover plate at the edge. This bounce effect was significant in winter and spring when the normalized $^{137}\mathrm{Cs}_{(7)}$ values were high. This finding enables us to discuss the seasonal differences of the host particles for the radiocesium resuspension, although this finding also makes discussing their size distributions difficult.

Figure 6a, b shows the SEM images of the stage #2 substrate samples obtained (a) on April 10–24, 2014 (NHVB-260424) and (b) on October 17–30, 2014 (NHVB-261030). The $^{137}\mathrm{Cs}_{(2)}$ values were 44.8 ± 7.1 and 28.3 ± 11.3 μBq m^{-3}, respectively, for the NHVB-260424 and NHVB-261030 substrate samples. As shown in Fig. 6b (denoted by the red curve), the adhesion of

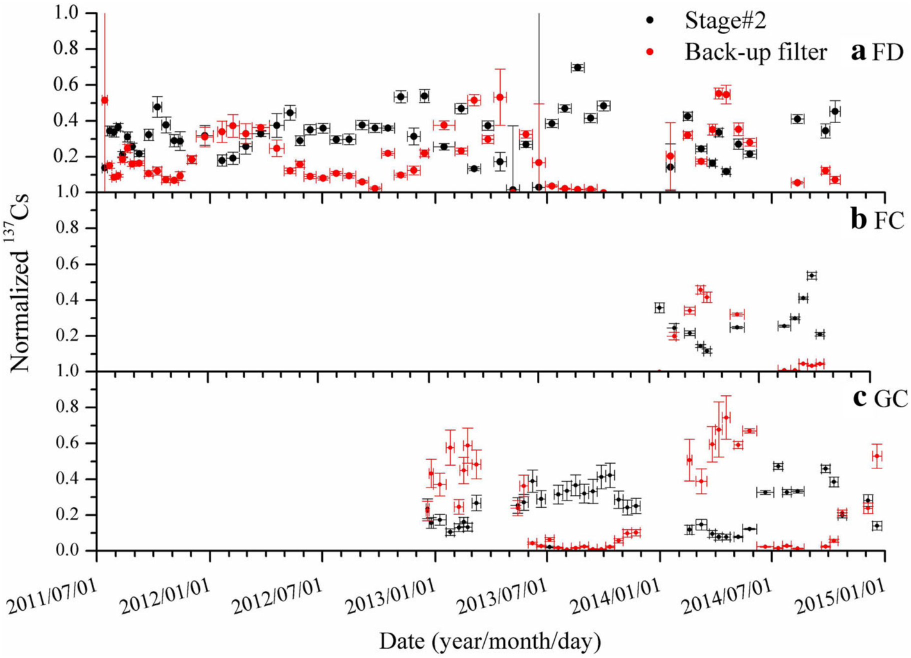

Fig. 4 Time series of the normalized $^{137}Cs_{(2)}$ and $^{137}Cs_{(7)}$ measured at the (**a**) FD, (**b**) FC, and (**c**) GC sites. These results clearly showed the seasonal variation but did not accurately reflect the size distribution of radiocesium in the atmosphere because of the bouncing particles. The amount of bouncing particles significantly changes the collection efficiency of the cascade impactor

organic matter on quartz fibers was frequently found in each stage of substrates in the summer/autumn samples. In contrast, such organic matter adhesion was not found in winter/spring. We also found that most coarse particles could not be removed from the summer/autumn sample substrates via soaking them in water, but that the coarse particles could be easily removed from the winter/spring sample filters. The adhesive organic matter on the quartz fibers probably worked as glue to fix the host particles of radiocesium to the sample substrates and the filter, or the host particles themselves could have firmly attached to the sample filter, reducing bouncing of coarse particles significantly in summer and autumn. In contrast, the host particles did not firmly adhere to the fibers in winter and spring.

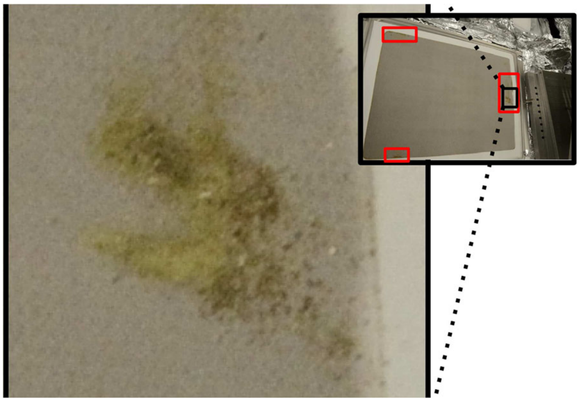

Fig. 5 Picture of a typical backup filter sampled at the GC site in spring (April 2014). We found many coarse particles, which include pollen and coarse soil/mineral dusts, in the areas indicated by the red rectangles

The spatial extent of the resuspension

The atmospheric activity concentrations at the GC and GD sites are compared by adopting their ratio, R_{scale}, as follows:

$$R_{\text{scale}} = \frac{^{137}\text{Cs}_{\text{-GD}}}{^{137}\text{Cs}_{\text{-GC}}}, \tag{2}$$

where $^{137}\text{Cs}_{\text{-GC}}$ and $^{137}\text{Cs}_{\text{-GD}}$ denote the ^{137}Cs concentrations observed at the GC or GD sites, respectively. There are two important points for interpreting the R_{scale} values. Although the GC and GD sites are situated very close together (about 0.75 km), the amount of radiocesium remaining over the ground surface (0–5 cm depth) at the GC site was much higher than that at the GD site because of the local decontamination (approximately 50,000 m^2) around the GD site. By sampling the surface soil (0–5 cm depth) at six points around the high-volume air samplers at each site on June 4, 2015, their radiocesium

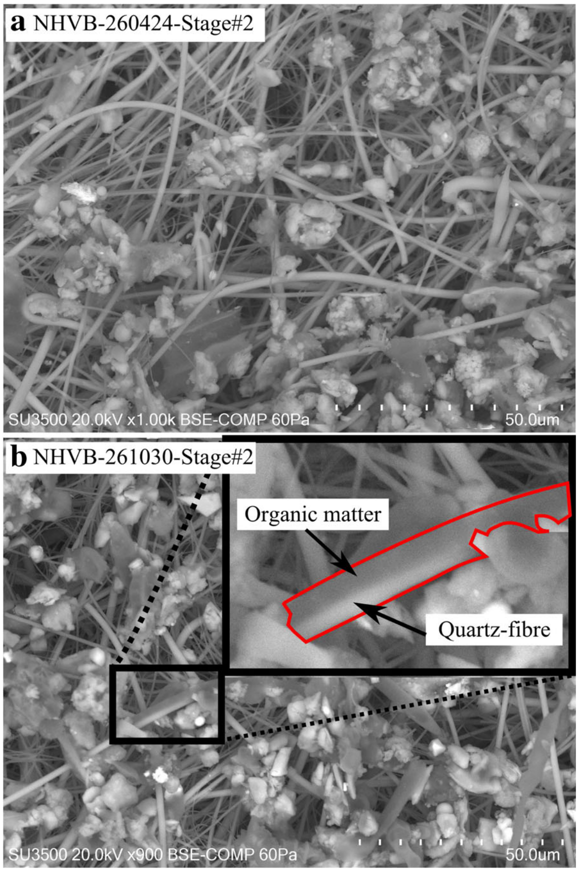

Fig. 6 SEM images of filters for stage #2 sampling at the GC site in **a** spring and **b** autumn. The adhesive organic matter that sticks to the quartz fiber is surrounded by the red line. From the morphology, we suspect that the material was dense liquid when it was suspended in air. This matter probably affects the collection efficiency of the coarse particles on the filter

concentrations were measured. The dried soil samples (approximately 150 g) were put in U-8 plastic containers (AS ONE Corporation, Osaka, Japan), and their ^{137}Cs radioactivities were measured at Ibaraki University. The average soil activity concentrations at the GC and GD sites were 128 ± 3.9 and 2.17 ± 0.07 Bq g^{-1}, respectively. Considering quite similar ground surface conditions, we can assume that the resuspension of ^{137}Cs occurred similarly at both sites. In this case, if the resuspension of ^{137}Cs occurred very locally and/or the host particles were not transported, the R_{scale} values would be approximately 0.017, which is the ratio of the GD surface soil activity to that of GC. In contrast, when the resuspension occurred at larger spatial scales and/or the host particles could be distantly transported and well mixed, R_{scale} could be nearly one. Therefore, R_{scale} is expected to indicate the spatial extent of the resuspension, i.e., R_{scale} is determined by a combination of (1) the extent of those areas wherein similar resuspensions occur and (2) the transport distance of the host particles.

Figure 7a shows that the time series of R_{scale} and its median values varied from 0.24 to 0.82 and were larger than the ratio of the ground surface activities at GD to GC (0.017), indicating that the activity concentration at the GD site was not only governed by local resuspension but also by one in the broader areas around the GD site. These observations also indicate that the host particles in the atmosphere were not completely mixed by their transport/diffusion, especially when R_{scale} was low. Because the absolute value of R_{scale} probably depends on the extent of the decontaminated area around the GD site as well as on the ratio of the surface radioactivity densities at both sites, comparisons of R_{scale} values at various places are meaningless. Therefore, the R_{scale} values indicate the relative variations of the emission scales and the magnitudes of the transport/mixing at a specific pair of sites.

Note that R_{scale} showed clear seasonal variations, such that smaller values occurred in winter/spring and larger values occurred in summer/autumn. In addition, these observed variations were synchronized with those of the fractions of activity of the aerosol particles trapped at the stage #2 substrate and the backup filter in the impactor, as shown in Fig. 4. Figure 7b compares the time series of the normalized $^{137}\mathrm{Cs}_{(7)}$ (the red line) with that of the R_{scale} values, and Fig. 7c shows the correlation between R_{scale} and the normalized $^{137}\mathrm{Cs}_{(7)}$. The green lines in Fig. 7a show the median values (since the data quantities are not sufficient, we used median values instead of average ones) of R_{scale} during summer/autumn, which were $0.60 + 0.07/- 0.05$ (central 50% range) in 2013 and $0.61 + 0.21/- 0.03$ in 2014, and the blue lines show those during winter/spring, which were $0.33 + 0.1/- 0.09$ in 2012–2013 and $0.43 + 0.11/- 0.09$ in 2013–2014. Comparing Fig. 7a, b, the R_{scale} and normalized $^{137}\mathrm{Cs}_{(7)}$ values show nearly synchronized seasonal variations with each other. Fig. 7c shows an evident correlation between them. These results can be interpreted both by the transport of host particles and by the extent of the resuspension area. The transport/mixing of resuspended host particles depends on the wind speed and particle deposition speed. Considering that the average wind speed was lower in summer/autumn than in winter/spring, as shown in Fig. 3b, the R_{scale} decrease in summer/autumn indicates that the deposition speed should decrease considerably as the properties of the particle change (i.e., changes in the size and mass density or both of the host particle). In addition, if the resuspension activity in the areas surrounding the GD sites was similar to that around the GC site in summer/autumn and was lower in winter/spring, the observed seasonal

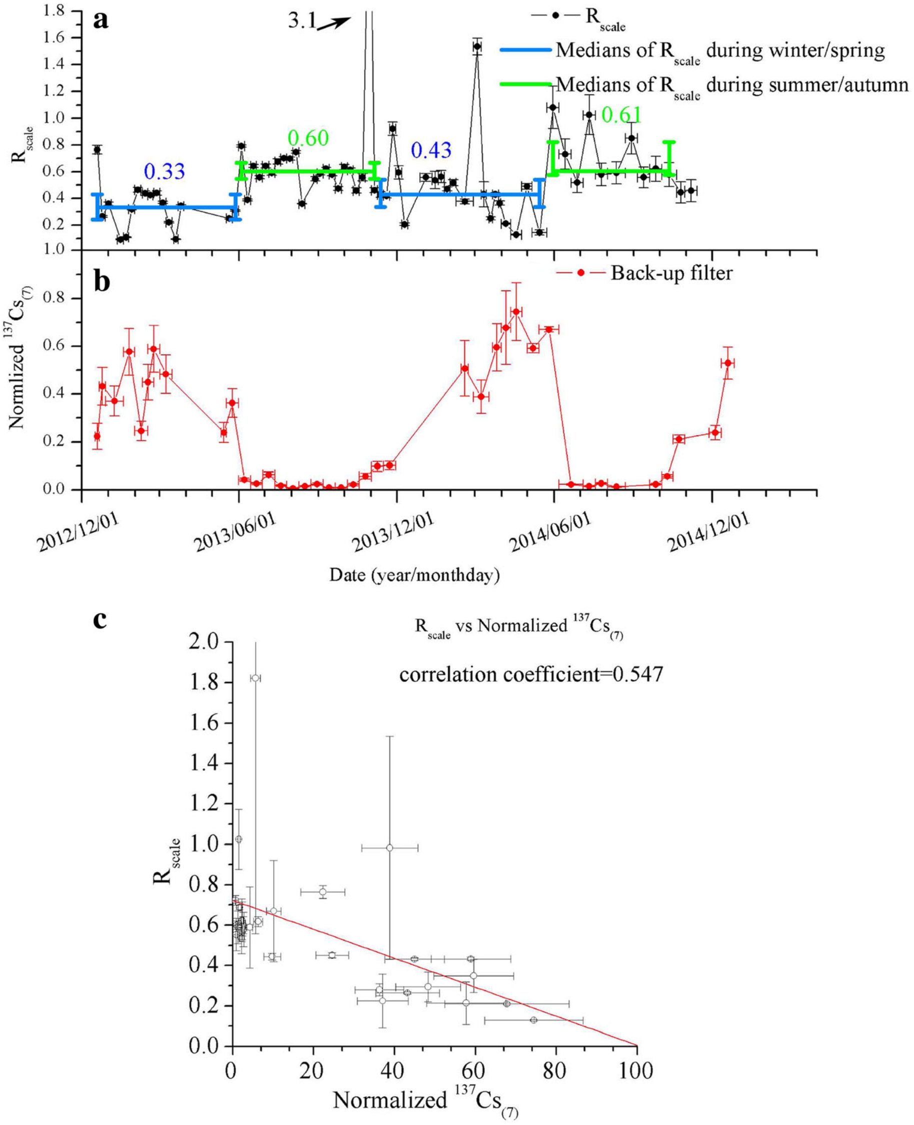

Fig. 7 Time series of **a** R_{scale} and **b** normalized $^{137}\mathrm{Cs}_{(7)}$ at the GC site and **c** the correlation plot of R_{scale} and the normalized $^{137}\mathrm{Cs}_{(7)}$. Green and blue curves in **a** are the medians of R_{scale} in summer/autumn and winter/spring, respectively. The error bars for each curve in **a** and **b** show the range of central 50%

variations could have occurred. However, because the seasonal variations of the R_{scale} values were synchronized with the normalized $^{137}\mathrm{Cs}_{(7)}$, this seasonal variation of the resuspension scale can (at least partly) be attributed to the seasonal changes of the host particle materials.

Possible host particles for radiocesium resuspension

Radiocesium was primarily emitted in the form of submicron water-soluble aerosols during the FDNPP accident (e.g., Kaneyasu et al. 2012). Another type of primary radiocesium emission has been reported to consist of glassy, water-insoluble particles with diameters of approximately 2 μm (Adachi et al. 2013; Abe et al. 2014; Yamaguchi et al. 2016) and with high specific activity (Igarashi et al. 2014). These particles are stable at least for a few years in the environment and have recently been found at the ground surface (Satou et al. 2016). If such particles are scattered by wind, they would contribute to atmospheric radiocesium. However, in the present observations, we could not find serious concentration increases due to such insoluble radiocesium-bearing particles.

Studies performed after the Chernobyl accident showed that biomass burning was a plausible resuspension process of radiocesium in the contaminated area (Bourcier et al. 2010; Igarashi 2009; Lujanienė et al. 2009; Yoschenko et al. 2006). Thus, this study tested the hypothesis of resuspension due to biomass burning. Levoglucosan is known to be an organic tracer of biomass burning (Simoneit et al. 1999), and the positive correlation of radiocesium with levoglucosan indicates the contribution of biomass burning to radiocesium re-emission (Bourcier et al. 2010). In March and May, biomass burning usually increases in the Fukushima prefecture (Local government of Fukushima prefecture 2014). A forest fire occurred on March 17, 2013, at Ootaki, approximately 28 km away from the observation sites (Real time disaster information of Fukushima). We compared the concentration of ^{137}Cs activity with that of levoglucosan in the air. Figure 8 shows the time series of (a) the concentration of the ^{137}Cs activity and (b) that of levoglucosan at GC. In addition, we also compared them with water-soluble organic carbon (WSOC), which is not a tracer of biomass burning but is emitted from various organic aerosol sources. Although the levoglucosan and WSOC showed similar trends (except for short-term spike changes), there was little correlation between the concentrations of ^{137}Cs activity and the levoglucosan and WSOC concentrations in the present work. We focused on the events of the biomass burning on March 17, 2013, and the singular increasing data on March 25. The forest fire on March 17 did not affect the levoglucosan and WSOC concentrations at this observation site. Figure 9a, b illustrates the maps showing the air mass forward and backward trajectories calculated using the NOAA HYSPLIT model (Stein et al. 2015) during the forest fire event periods. Figure 9a shows the forward trajectories from the fire site on March 17 at 16:00 (LT) to March 18 at 13:00. The air mass did not pass over the observational sites; instead, it went north. Therefore, the increased concentration of ^{137}Cs activity on March 17 was not attributable to the biomass burning event. For the event on March 25, with an increased levoglucosan concentration, the backward trajectories from the measurement site GC show two origin areas (Fig. 9b, which is calculated from March 24 at 13:00 (LT) to March 25 at 13:00 (LT)): the Sea of Japan and the mountainous areas to the northwest which is the local contaminated areas. In these areas, there was no official information about the fire disasters at that time, although the possibility of small fires is not fully neglected. Overall, the present results indicate that biomass burning was not a dominant source of the resuspension during our observational period at the sites.

The elements in the aerosol samples taken at the GC and GD sites were analyzed quantitatively using SEM-EDS, showing that the major components were different in winter/spring and summer/autumn. Figure 10a shows a SEM image of the sample filter obtained at the GD site in July 2015 (summer), and Fig. 10b–e are the element map images of C, Fe, Al, and Na, respectively, in the same viewing field with Fig. 10a. Numerous spots of C indicate that carbonaceous aerosols were composed of major coarse particles during summer/autumn, and the Al, Fe, and Na spots probably represent that soil/mineral dust, metal, and (sea) salt particles were rare. We tried to identify these carbonaceous particles as some bioaerosol particles on the basis of their sizes and shapes on the SEM image (Carrera et al. 2007; Chaturvedi et al. 1998; Healy et al. 2012; Laucks et al. 2000). Figure 11a shows an example image of these organic particles in a wide field of view with close-up images of pollen (Fig. 11b), a spore (Fig. 11c), and microorganisms (indicated by the

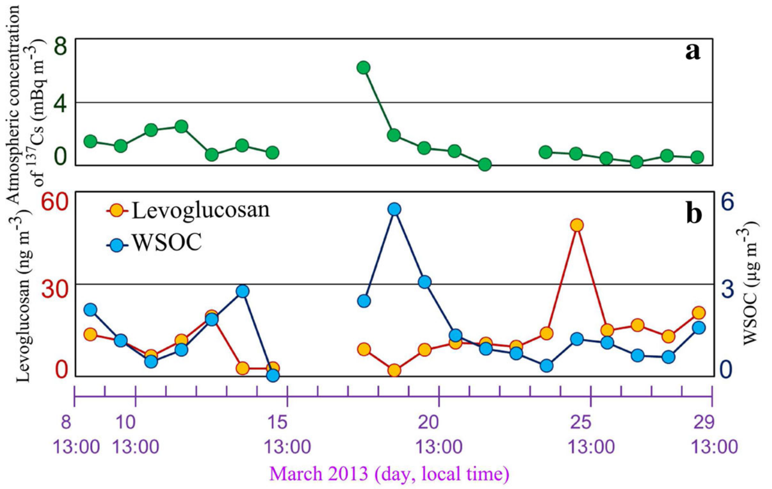

Fig. 8 Time series of **a** the radiocesium concentrations and **b** the concentrations of levoglucosan and WSOC in the atmosphere at GC

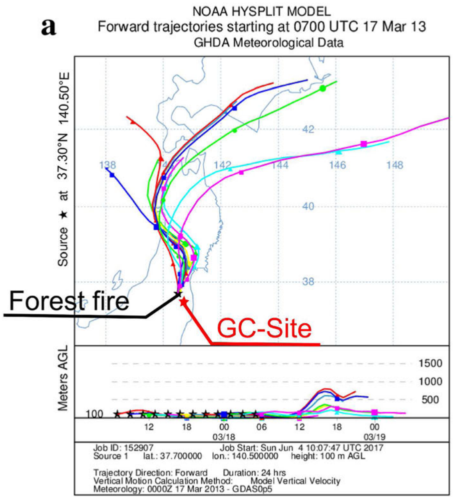

Fig. 9 Maps show the forward and backward trajectories calculated with NOAA HYSPLIT model (Stein et al. 2015) during the forest fire event. **a** The forward trajectories from Ootaki (forest fire area), which are calculated from March 17 at 16:00 (LT) to March 18 at 13:00 (LT). **b** Backward trajectories from the measurement site (GC), which are calculated from March 24 at 13:00 (LT) to March 25 at 13:00 (LT)

red circle in Fig. 11d) at the GD site. However, it was difficult to distinguish spores and microorganism particles only from the SEM images in the present work. We separately counted pollen and microorganism/spores in the SEM images at × 500 and × 1000 magnifications, respectively, of the four sample filters obtained at the GD site in summer (July and August 2014) and winter (December 2014 and January 2015). To compare the magnitudes of these particle counts, the count numbers of the four filter samples were normalized by the sampling air volume and were scaled by the values for the January sample. Figure 12 shows the scaled particle counts of pollen and microorganism/spores with their Poisson standard deviations and compares them with the concentrations of ^{137}Cs activity. Because so many particles had accumulated and overlapped with each other on the sample filters, it was difficult to count these particles precisely. Thus, the absolute values were not highly accurate, and the counts showed only relative amounts. The number of microorganisms/spores as well as that of pollen was much larger in summer than those in winter. This result indicates that these bioaerosol emissions can significantly contribute to the resuspension process. Several studies suggested that ^{137}Cs processed by the ecosystem can be re-emitted into the atmosphere as bioaerosols. For instance, Kuwahara et al. (2005) showed that mushrooms and microorganisms could absorb and accumulate ^{137}Cs from the soil. Furthermore, Kanasashi et al. (2015) showed that the acropetal translocation of ^{137}Cs occurred in Japanese cedars and that their pollen contained ^{137}Cs. Several studies have described the processes of bioaerosol emissions and the seasonal variations in the bioaerosol concentrations and residence time. For instance, Jones and Harrison (2004) showed that bacteria are emitted from nearly all surfaces, such as the ground, vegetation, and so on. Burrows et al. (2009a, 2009b) and Schumacher et al. (2013) described an increase in the bioaerosol concentrations and an extension of the residence time during the warm season because of the greater turbulence and vertical mixing. The results in these studies are consistent with our results in that bioaerosols, such as microorganism, spores, and pollen, which are actively emitted from nearly all surfaces in the contaminated areas in summer/autumn, would increase ^{137}Cs in the atmosphere. The R_{scale} values approached unity, as shown in Fig. 7, in these seasons, which can be attributed to longer bioaerosol residence times, which would result in well-mixed atmospheric ^{137}Cs. In this study, the sampling sites are located in low mountainous areas and are surrounded by forests, and thus, it is natural that the increases of bioaerosols significantly contribute to resuspension, unlike in urban areas. Kajino et al. (2016) simulated resuspension from the soil (Ishizuka et al. 2017) and that from vegetation (details were showed in the "Introduction" section), succeeding in reconstructing the ^{137}Cs activity concentration levels that we observed. In their results, most of atmospheric ^{137}Cs in summer/autumn was supplied by biogenic emissions, which is consistent with our results. These studies show that the enhancement of ecosystem activity in summer/autumn could allow increased emissions of larger amounts of pollen, spores, and microorganisms from contaminated forests than those in winter, resulting in a more active resuspension of ^{137}Cs.

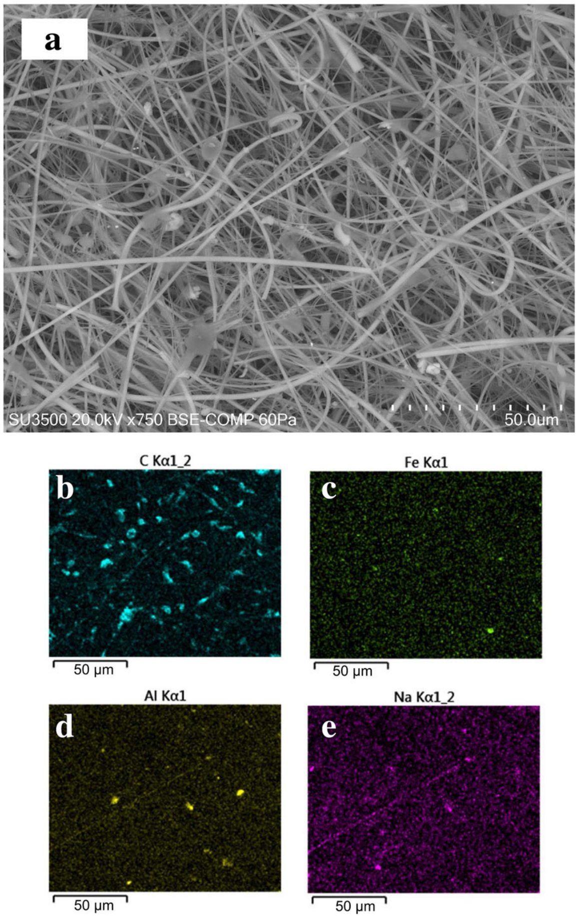

Fig. 10 The SEM image and elemental mapping images of the sample filters obtained at the GD site in July 2015. **a** The SEM image, (**b**) the elemental map of C, (**c**) the elemental map of Fe, (**d**) the elemental map of Al, and (**e**) the elemental map of Na. The characteristic organic particles commonly exist in the filter samples

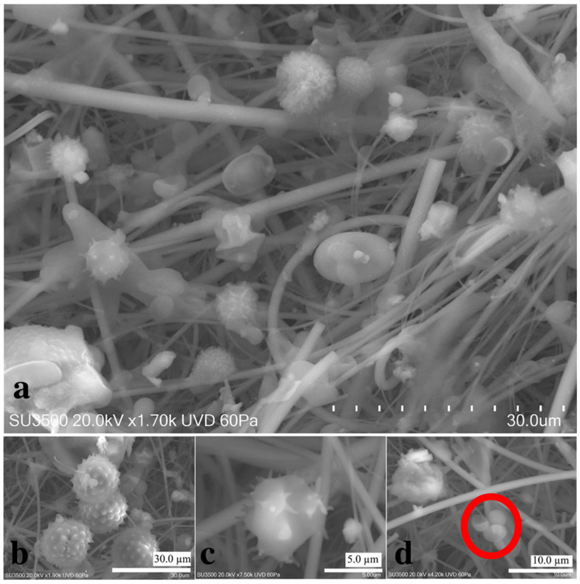

Fig. 11 Examples of organic particles in the samples obtained in September 2014 at the GD site. **a** A SEM image of the wide visible range. **b** Pollen. **c** Spore. **d** Microorganisms (surrounded by red circles)

Figure 13a–e shows the SEM and element map images, which are similar to Fig. 10a–e, of the sample filters obtained at the GD site in January 2015. In contrast to Fig. 10, Fig. 13 shows the soil/mineral dust particles indicated by the numerous Al spots that were the dominant coarse aerosols observed in winter/spring. Although some C spots were detected, they were mostly debris from vegetation rather than from living bioaerosols because these particles have different shapes and sizes than pollen, spores, and microorganisms. The smaller values of R_{scale} in Fig. 7 suggest that resuspension would occur from local surfaces, such as the playground surface, and that the deposition speeds of the host particles were high in winter/spring. Because there were no significant sources of metal and salt particles around the observational sites, these particles were probably emitted by sources far from the observational sites (Igarashi 2009) and were unlikely to be major host particles. On the basis of these results and considerations, the soil and mineral dust particles from nearby ground surfaces as well as the debris from the vegetation were the most likely host particles of the ^{137}Cs resuspension in winter/spring.

Many studies have indicated that ^{137}Cs is firmly adsorbed to clay mineral particles (e.g., Dumat and Staunton 1999; Igarashi et al. 2005; Masson et al. 2010; Mukai et al. 2014; Ishizuka et al. 2017), and the transport of mineral dust particles by wind is considered to be a significant resuspension process. As shown in Fig. 3, we can see a positive correlation between the radiocesium concentrations and wind speeds in spring, indicating that the soil/mineral dust, pollen, forest debris, etc., that were suspended by wind blow were plausible host particles of the resuspension. Ishizuka et al. (2017) used the winter/spring samples obtained with the cascade impactor at the GC site, which was also used in this study, and evaluated the relation between the soil/mineral dust particles and activity concentrations of ^{137}Cs during winter/spring; then, they compared these relationships with those estimated using a size-resolved one-dimensional resuspension scheme, and their conclusion is consistent with our results.

Conclusions

To understand the resuspension process of radiocesium in areas heavily contaminated by the FDNPP accident,

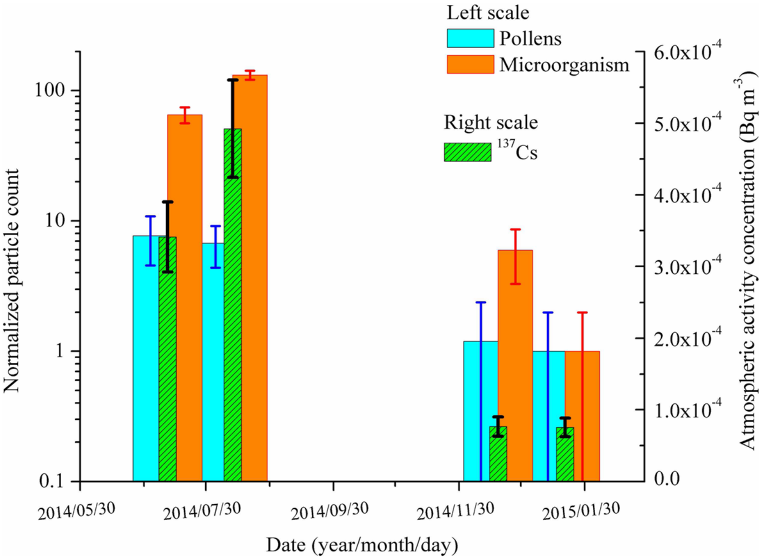

Fig. 12 The normalized particle count of the bioaerosols using SEM (in relative values, the error bar shows the Poisson standard deviation) and atmospheric concentrations of ^{137}Cs activity sampled at the GD site during summer (July and August 2014) and winter (December 2014 and January 2015). The counts of microorganisms include those of spores (see the text)

we conducted long-term measurements of atmospheric radiocesium with high-volume air samplers and impactors in the Tsushima and Yamakiya areas of the Fukushima prefecture. We analyzed the temporal variations of the radiocesium concentrations and examined the particles on the sample substrates of the impactor and its filters using SEM-EDS. We also introduced R_{scale}, which is the ratio of the ^{137}Cs air concentrations from two close sites with similar land uses but different contamination levels, in order to estimate the spatial extent of the resuspension. The main finding in this study is that the seasonal differences of both the radiocesium resuspension processes and the host particle material can be described as shown below:

1. In summer and autumn, the atmospheric radiocesium activity concentration was higher, and both the higher normalized $^{137}\mathrm{Cs}_{(1-5)}$ values and SEM-EDS analysis results indicated that coarse organic particles, such as spores, pollen, and microorganisms, with adhesive organic matter were the dominant host particles of radiocesium resuspension. The larger values of R_{scale} in these seasons are consistent with this result, considering that the deposition velocity of the light biogenic organic particles was probably low and that the resuspended radiocesium on them should be well mixed. These organic particles could be emitted from forest ecosystems.
2. In winter and early spring, the atmospheric radiocesium activity concentrations were lower, and they increased in May. The higher normalized $^{137}\mathrm{Cs}_{(7)}$ values and the SEM-EDS analysis results showed that the dominant coarse particles were dust (soil and mineral) and vegetation debris and that these were the dominant host particles for radiocesium resuspension. The temporal variations of the radiocesium concentrations showed similar variations to those of wind speed, suggesting that wind suspension of contaminated particles from the ground surface is considered as the main resuspension process in these seasons. The smaller R_{scale} values in these seasons are still consistent with this result, considering that the deposition velocity of the dust particles with higher density was probably high and that the resuspended radiocesium on them should be less mixed.
3. No significant correlation between the concentrations of levoglucosan and WSOC and that of radiocesium was found in spring, indicating that biomass burning was not a significant resuspension process of radiocesium.
4. Although many studies have suggested that soil/mineral dusts and bioaerosols could be major host particles of $^{134,\ 137}$Cs, we first identified the seasonal variations of the dominant resuspension processes/host particles. Further research on bioaerosols, such as working to identify specific bioaerosols and evaluating the quantitative relationship between

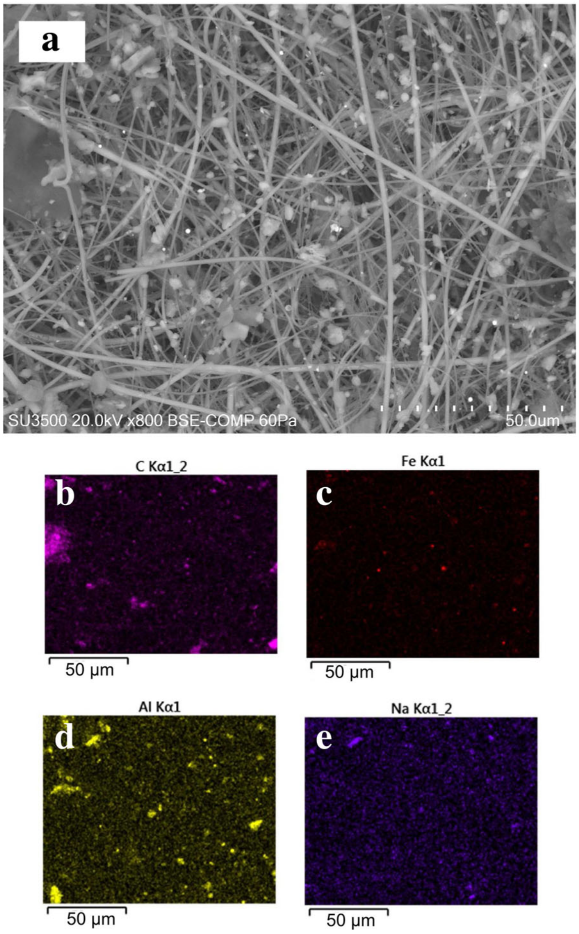

Fig. 13 The SEM and elemental mapping images of the sample filter obtained at the GD site in January 2015. **a** The SEM image, (**b**) the elemental map of C, (**c**) the elemental map of Fe, (**d**) the elemental map of Al, and (**e**) the elemental map of Na. Major coarse particles include Al (clay mineral) and Na (salt or mineral)

bioaerosols and radiocesium, is required. In the near future, we will include more observations of bioaerosols to reveal more detailed radiocesium resuspension processes. A flux measurement of these particles would be necessary to quantitatively evaluate the radiocesium resuspension rate.

Abbreviations

EDS: Energy-dispersive X-ray spectroscopy; FAJ: Forestry Agency Japan; FDNPP: Fukushima Daiichi Nuclear Power Plant; HYSPLIT: The Hybrid Single Particle Lagrangian Integrated Trajectory Model; JAEA: Japan Atomic Energy Agency; MEXT: Ministry of Education, Culture, Sports, Science and Technology, Japan; MRI: Meteorological Research Institute; NDVI: Normalized Difference Vegetation Index; NOAA: National Oceanic and Atmospheric Administration; SEM: Scanning electron microscopy; TEPCO: Tokyo Electric Power Company; WSOC: Water-soluble organic carbon

Acknowledgements

We acknowledge T. Kimura, K. Inukai, K. Kamioka (Atox Co. Ltd.), S. Kakitani (Osaka University), and N. Hayashi (Ibaraki University) for their sample preparation and measurements of radioactivity; T. Kanari (Green Blue Co. Ltd.) for the periodical maintenance of the measurement stations in the field; members of Ibaraki University and the College of Engineering of Ibaraki University for their maintenance of the tools after sampling and work the setting field instruments; Drs. T. Sekiyama (MRI), M. Kajino (MRI), Y. Hatano (University of Tsukuba), and T. Maki (Kanazawa University) for their discussions; and the many people who cooperated this study. We also express our gratitude to the local governments of Kawamata and Namie as well as to Fukushima prefectural government, who kindly offered this monitoring opportunity.

Funding

This work was financially supported by MEXT KAKENHI (a Grant-in-Aid for Scientific Research on Innovative Areas under the A01–1, A01–2 and A04–8 research teams in the "Interdisciplinary Study on Environmental Transfer of Radionuclides from the Fukushima Daiichi NPP Accident"; the grant numbers are 24110002, 24110003, and 24110009, respectively) and the MEXT Japanese Radioactivity Survey at the MRI. Additionally, this study was partly supported by a grant from the Asahi group foundation at Ibaraki University. Thus, this study was discussed and supported by the workshop of ISET-R for writing articles.

Authors' contributions

TK collected and analyzed the samples and summarized these data in this article. KK planned and carried out the measurements as well as the samplings. YI is the leader of our project team, helped in writing the manuscript, and provided important discussions for this article. KA and YZ supported the identification of the aerosols by SEM-EDS. KN, AS, ST, KY, and NY analyzed the radioactivity of filter samples. HOk and HOg analyzed the levoglucosan and WSOC of filter samples. MI and HD supported the maintenance of measurements in the field. MM and YO provided important suggestions for this article. All authors read and approved the final manuscript.

Authors' information

TK studied atmospheric environments, especially focusing on black carbon (BC) aerosols, and received his PhD in atmospheric chemistry from Ibaraki University through the study of Antarctic aerosol science. He has been working at Hitachi Power Solutions Co., Ltd. since 2016 and wrote this article while working. In his studies, he participated in the project of the workshop of Interdisciplinary Study on Environmental Transfer of Radionuclides from the Fukushima Daiichi NPP Accident (ISET-R) to shed light on the environmental transfer of radionuclides and to contribute to the revival of the affected areas in the Fukushima prefecture.

KK received his PhD from Tokyo University in 1990 and worked at Tokyo University until 2002 as a research assistant. He moved to Ibaraki University in 2002. His studies focus on the atmospheric O_3 and NO_2, the effects of BC on global warming, and the resuspension processes of radiocesium.

YI received his PhD from the University of Tsukuba in 1987. From 1987 to 1991, he worked at the former National Institute of Radiological Sciences and moved to the MRI in 1991. His current interests are atmospheric aerosols; their precursors, including Asian dust and $PM_{2.5}$; their possible influences on climate and general environmental changes; and other related phenomena.

KA received his PhD from Kobe University in 2005, worked at Arizona State University between 2005 and 2011 as a postdoctoral/faculty research associate and is currently studying atmospheric aerosols at the MRI.

KN received his PhD from Osaka University in 2007 and worked at Osaka University in 2008. He moved to JAEA and worked as a research scientist between 2009 and 2012; then, he returned to Osaka University. His main research field is nuclear- and radiochemistry.

AS received his PhD from Osaka University in 1985 and then worked at the Japan Society for the Promotion of Science. He moved to Nagoya University, where he worked between 1987 and 1998. Then, he moved to Kyoto University in 1998, before moving to Osaka University in 1999. His main research field is nuclear- and radiochemistry.

HOk worked at Kanagawa University between 1991 and 1999 and received his PhD from Tokyo University in 1997 while he was working. From 1999 to 2003, he worked at the University of East Anglia, UK. He moved to the Tokyo Metropolitan Institute of Technology, where he worked from 2003 to 2005. Then, he moved to Waseda University. His studies are focused on the environmental science topics of the atmosphere, hydrosphere and ecosystems of the forest, and on the development of a technique for environmental remediation via soft-chemical methods.

HOg received her PhD from the Prefectural University of Kumamoto in 2011. She worked at Waseda University between 2011 and 2016, and then, she moved to Sibata Scientific Technology Ltd. Her main research field is atmospheric aerosols.
MI received his PhD from Osaka University in 2000 and then worked at the Faculty of Systems Engineering, Wakayama University from 2000 to 2005. He moved to the Faculty of Engineering, Kagawa University. His studies are centered on the resuspension processes of radionuclides with dust particles as forced by wind, the processes of the suspension of Asian dust, and researching the hydrological environment and its processes.
ST received his PhD from the University of Tokyo in 2007 and started his study on the development of analytical methods for isotopocules, i.e., isotopically substituted molecules, of atmospheric nitrous oxide (N_2O) at Nagoya University as a postdoctoral fellow of the Japan Science and Technology Corporation. After moving to the Tokyo Institute of Technology in 2008, he pursued an investigation of the geochemical cycle of N_2O and is currently expanding his research interests into other trace gasses and aerosols as an associate professor.
KY received his PhD from Tokyo Metropolitan University in 1997. He has worked at the Tokyo Institute of Technology since 2000. He studies the relationship between radionuclides and organics in aerosols.
NY received his PhD from the Tokyo Institute of Technology in 1984. He was with the Mitsubishi-Kagaku Institute of Life Sciences, Toyama Univ., Nagoya Univ., and has been a full professor in charge of two Environmental Departments of the Tokyo Institute of Technology since 1998 and is a Principal Investigator at the Earth-Life Science Institute. He studies “isotopomers: isotopic substituted molecules” as powerful tracers that can help to reduce uncertainties in the biological, chemical, physical, and anthropogenic source and sink processes of environmental molecules, especially for global warming-related species.
YZ graduated the Meteorological College in 1984 and worked at the Nagasaki Marine Observatory, Japan Meteorological Agency from 1984 to 1989. He has been studying atmospheric aerosols at the MRI.
MM received his PhD from Tohoku University in 1996 and has worked at the MRI from 1985 to 2015. He held the position of Senior Researcher for Research Affairs at the Institute. Currently, he is working at the Japan Meteorological Business Support Center.
HD graduated the Faculty of Maritime Sciences of Kobe University in 2005 and worked at a general company of the manufacturing industry. In 2010, he moved to the Technical Services Division of the College of Engineering, Ibaraki University. He works as an engineer providing the technical support at Ibaraki University and helped with our research.
YO graduated and received his PhD from the University of Tsukuba in 1990, working at Nagoya University from 1992 to 1999. Currently, he is working at the University of Tsukuba, where he researches hydrology and the environmental dynamics of radionuclides as well as being the PI of the whole ISET-R project.

Competing interests

The authors declare that they have no competing interests.

Publisher’s Note

Author details

[1]Graduate School of Science and Engineering, Ibaraki University, 2-1-1 Bunkyo, Mito, Ibaraki 310-8512, Japan. [2]Hitachi Power Solutions Co., Ltd, 2-2-3 Saiwaicho, Hitachi, Ibaraki 317-0073, Japan. [3]College of Science, Ibaraki University, 2-1-1 Bunkyo, Mito, Ibaraki 310-8512, Japan. [4]Atmospheric Environment and Applied Meteorology Research Department, Meteorological Research Institute, 1-1 Nagamine, Tsukuba, Ibaraki 305-0052, Japan. [5]Graduate School of Science, Osaka University, 1-1, Machikaneyama, Toyonaka, Osaka 560-0043, Japan. [6]Faculty of Science and Engineering, Waseda University, 3-4-1 Okubo, Shinjuku, Tokyo 169-8555, Japan. [7]Faculty of Engineering, Kagawa University, 2217-20 Hayashi-cho, Takamatsu, Kagawa 761-0396, Japan. [8]Department of Chemical Science and Engineering, School of Materials and Chemical Technology, Tokyo Institute of Technology, 4259 Nagatsuta, Yokohama, Kanagawa 226-8502, Japan. [9]Earth-Life Science Institute, Tokyo Institute of Technology, 2-12-1 Ookayama, Meguro, Tokyo 152-8551, Japan. [10]Forecast Research Department, Meteorological Research Institute, Japan Meteorological Agency, 1-1 Nagamine, Tsukuba, Ibaraki 305-0052, Japan. [11]Japan Meteorological Business Support Center, 3-17 Nishikicho, Kanda, Chiyoda, Tokyo 101-0054, Japan. [12]College of Engineering, Ibaraki University, 4-12-1 Narusawa, Hitachi, Ibaraki 316-8511, Japan. [13]Center for Research in Isotopes and Environmental Dynamics, University of Tsukuba, 1-1-1 Tennodai, Tsukuba, Ibaraki 305-8577, Japan.

Received: 22 August 2016 Accepted: 9 February 2018

References

Abe Y, Iizawa Y, Terada Y, Adachi K, Igarashi Y, Nakai I (2014) Detection of uranium and chemical state analysis of individual radioactive microparticles emitted from the Fukushima nuclear accident using multiple synchrotron radiation X-ray analyses. Anal Chem 86:8521–8525

Adachi K, Kajino M, Zaizen Y, Igarashi Y (2013) Emission of spherical cesium-bearing particles from an early stage of the Fukushima nuclear accident. Nature Sci Rep 3:2554. doi:https://doi.org/10.1038/srep02554.

Barišić D, Lulić S, Kezić N, Vertačnik A (1992) ^{137}Cs in flowers, pollen and honey from the Republic of Croatia four years after the Chernobyl accident. Apidologie 23:71–78

Berglund BE (2008) Satoyama, traditional farming landscape in Japan, compared to Scandinavia. Japan Review 20:53–68

Bostic BC, Vairavamurthy MA, Karthikeyan KG, Chorover J (2002) Cesium adsorption on clay minerals: an EXAFS spectroscopic investigation. Environ Sci Technol 36:2670–2676

Bourcier L, Sellegri K, Masson O, Zangrando R, Barbante C, Gambaro A, Pichon J-M, Boulon J, Laj P (2010) Experimental evidence of biomass burning as a source of atmospheric ^{137}Cs. Atmos Environ 44:2280–2286. https://doi.org/10.1016/j.atmosenv.2010.04.017

Burrows SM, Elbert W, Lawrence MG, Pöschl U (2009a) Bacteria in the global atmosphere–Part 1: review and synthesis of literature data for different ecosystems. Atmos Chem Phys 9:9263–9280

Burrows SM, Butler T, Jöckel P, Tost H, Kerkweg A, Pöschl U, Lawrence MG (2009b) Bacteria in the global atmosphere–Part 2: modeling of emissions and transport between different ecosystems. Atmos Chem Phys 9:9281–9297

Carrera M, Zandomeni RO, Fitzgibbon J, Sagripanti J-L (2007) Difference between the spore sizes of Bacillus anthracis and other Bacillus species. J Appl Microbiol 102:303–312. https://doi.org/10.1111/j.1365-2672.2006.03111.x

Chaturvedi M, Datta K, Nair PKK (1998) Pollen morphology of Oryza (Poaceae). Grana 37:79–86. https://doi.org/10.1080/00173139809362647

Chino M, Nakayama H, Nagai H, Terada H, Katata G, Yamazawa H (2011) Preliminary estimation of release amounts of ^{131}I and ^{137}Cs accidentally discharged from the Fukushima Daiichi Nuclear Power Plant into the atmosphere. J Nucl Sci Technol 48:1129–1134. https://doi.org/10.1080/18811248.2011.9711799

Dietz LA, Pachucki CF (1973) ^{137}Cs and ^{134}Cs half-lives determined by mass spectrometry. J Inor Nucl Chem 35:1769–1776

Doi T, Masumoto K, Toyoda A, Tanaka A, Sibata Y, Hirose K (2013) Anthropogenic radionuclides in the atmosphere observed at Tsukuba: characteristics of the radionuclides derived from Fukushima. J Environ Radioactiv 122:55–62. https://doi.org/10.1016/j.jenvrad.2013.02.001

Dumat C, Staunton S (1999) Reduced adsorption of caesium on clay minerals caused by various humic substances. J Environ Radioactiv 46:187–200

Ehlken S, Kirchner G (2002) Environmental processes affecting plant root uptake of radioactive trace elements and variability of transfer factor data: a review. J Environ Radioactiv 58:97–112

Forestry Agency, Japan (FAJ) (2015) Heisei 26 nendo Sugi obana ni fukumareru houshasei sesiumu noudo no chousa kekka ni tsuite (About FY H26 investigation results on radiocesium concentrations contained in cedar pollen). http://www.rinya.maff.go.jp/j/press/kaihatu/150130.html. in Japanese. Accessed 19 Feb 2018

Gutman G, Ignatov A (1998) The derivation of the green vegetation fraction from NOAA/AVHRR data for use in numerical weather prediction models. Int J Remote Sensing 19:1533–1543

Healy DA, O’Connor DJ, Burke AM, Sodeau JR (2012) A laboratory assessment of the Waveband Integrated Bioaerosol Sensor (WIBS-4) using individual samples of pollen and fungal spore material. Atmos Environ 60:534–543. https://doi.org/10.1016/j.atmosenv.2012.06.052

Holt M, Campbell RJ, Nikitin MB (2012) Fukushima nuclear disaster, congressional research service

Igarashi Y (2009) Anthropogenic radioactivity in aerosol-a review focusing on studies during the 2000s. Jpn J Health Phys 44:313–323

Igarashi Y, Aoyama M, Hirose K, Povinec P, Yabuki S (2005) What anthropogenic radionuclides (^{90}Sr and ^{137}Cs) in atmospheric deposition, surface soils and aeolian dusts suggest for dust transport over Japan. Water Air Soil Poll 5:51–69

Igarashi Y, Adachi K, Kajino M, Zaizen Y (2014) Characteristic of spherical Cs-bearing particles collected during the early stage of FDNPP accident. IAEA meeting https://www-pub.iaea.org/iaeameetings/cn224p/Session3/Igarashi.pdf. Accessed 19 Feb 2018

Igarashi Y, Kajino M, Zaizen Y, Adachi K, Mikami M (2015) Atmospheric radioactivity over Tsukuba, Japan: a summary of three years of observations after the FDNPP accident. Prog Earth Planet Sci 2:44

Ishizuka M, Mikami M, Tanaka T, Igarashi Y, Kita K, Ymada Y, Yoshida N, Toyoda S, Satou Y, Kinase T, Ninomiya K, Shinohara A (2017) Use of a size-resolved 1-D resuspension scheme to evaluate resuspended radioactive material associated with mineral dust particles from the ground surface. J Environ Radioactiv 166:436–448. https://doi.org/10.1016/j.jenvrad.2015.12.023

Japan Atomic Energy Agency (JAEA) (2012) Fukushima daiichi gennshiryokuhatudennsho ni kakawaru hinannkuikutou ni okeru josennjisshougyoumu houkokusho gaiyoubann. Decontamination trial summary report for evacuation areas with the Fukushima daiichi nuclear power plant accident, JAEA https://fukushima.jaea.go.jp/initiatives/cat01/pdf/summary.pdf. Accessed 19 Feb 2018

Jones AM, Harrison M (2004) The effects of meteorological factors on atmospheric bioaerosol concentrations—a review. Sci Total Environ 326:151–180

Kajino M, Ishizuka M, Igarashi Y, Kita K, Yoshikawa C, Inatsu M (2016) Long-term assessment of airborne radiocesium after the Fukushima nuclear accident: re-suspension from bare soil and forest ecosystems. Atmos Chem Phys 16:13149–13172. https://www.atmos-chem-phys.net/16/13149/2016/. https://doi.org/10.5194/acp-16-13149-2016

Kanasashi T, Sugiyama Y, Takenaka C, Hijii N, Umemura M (2015) Radiocesium distribution in sugi (Cryptomeria japonica) in Eastern Japan: translocation from needles to pollen. J Environ Radioactiv 139:398–406

Kaneyasu N, Ohashi H, Suzuki F, Okuda T, Ikemori F (2012) Sulfate aerosol as a potential transport medium of radiocesium from the Fukushima Nuclear Accident. Environ Sci Technol 46:5720–5726. https://doi.org/10.1021/es204667h

Kuwahara C, Fukumoto A, Ohsone A, Furutya N, Sibata H, Sugiyama H, Kato F (2005) Accumulation of radiocesium in wild mushrooms collected from a Japanese forest and cesium uptake by microorganisms isolated from the mushroom-growing soils. Sci Total Environ 345:165–172

Laucks ML, Roll G, Shcweigner G, Davis EJ (2000) Physical and chemical (raman) characterization of bioaerosols–pollens. J Aerosol Sci 31:307–319

Local government of Fukushima prefecture (2014) Shoubou bousai nennpou (H24 nenn ban) (About the monthly number of forest fire at Fukushima prefecture during 2013). https://www.pref.fukushima.lg.jp/uploaded/attachment/37264.pdf in Japanese. Accessed 19 Feb 2018

Lujanienė G, Aninkevičius V, Lujanas V (2009) Artificial radionuclides in the atmosphere over Lithuania. J Environ Radioactiv 100:108–119. https://doi.org/10.1016/j.jenvrad.2007.07.015

Masson O, Piga D, Gurriaran R, D'Amico D (2010) Impact of an exceptional Saharan dust outbreak in France: PM_{10} and artificial radionuclides concentrations in air and in dust deposit. Atmos Environ 44:2478–2486

Masson O, Ringer W, Malá H, Rulik P, Dlugosz-Lisiecka M, Eleftheriadis K, Meisenberg O, Vismes-Ott AD, Gensdarmes F (2013) Size distributions of airborne radionuclides from the Fukushima Nuclear Accident at several places in Europe. Environ Sci Technol 47:10995–11003. https://doi.org/10.1021/es401973c

Merz S, Steinhauser G, Hamada N (2013) Anthropogenic radionuclides in Japanese food: environmental and legal implications. Environ Sci Technol 47:1248–1256

Ministry of Education, Culture, Sports, Science and Technology, Japan (MEXT) (2011) Results of the fourth airborne monitoring survey by MEXT.

Mukai H, Hatta T, Kitazawa H, Yamada H, Yaita T, Kogure T (2014) Speciation of radioactive soil particles in the Fukushima contaminated area by IP autoradiography and microanalyzes. Environ Sci Technol 48:13053–13059. https://doi.org/10.1021/es502849e

Ochiai S, Hasegawa H, Kakiuchi H, Akata N, Ueda S, Tokonami S, Hisamatsu S (2016) Temporal variation of post-accident atmospheric ^{137}Cs in an evacuated area of Fukushima Prefecture: size-dependent behaviors of ^{137}Cs-bearing particle. J Environ Radioactiv:131–139. https://doi.org/10.1016/j.jenvrad.2016.09.014

Satou Y, Sueki K, Sasa K, Adachi K, Igarashi Y (2016) First successful isolation of radioactive particles from soil near the Fukushima Daiichi Nuclear Power Plant. Anthropocene 14:71–76

Schumacher CJ, Pohlker C, Aalto P, Hiltunen V, Petaja T, Kulmala M, Poschl U, Huffman JA (2013) Seasonal cycles of fluorescent biological aerosol particles in boreal and semi-arid forests of Finland and Colorado. Atmos Chem Phys 13:11987–12001

Simoneit BRT, Shcauer JJ, Nolte CG, Ortos DR, Elias VO, Fraser MP, Rogge WF, Cass GR (1999) Levoglucosan, a tracer for cellulose in biomass burning and atmospheric particles. Atmos Environ 33:173–182

Stein AF, Draxler RR, Rolph GD, Stunder BJB, Cohen M (2015) NOAA's HYSPLIT atmospheric transport and dispersion modeling system. Am Meteorol Soc 96:2059–2078

Steinhauser G, Brandl A, Johnson E (2014) Comparison of the Chernobyl and Fukushima nuclear accidents: a review of the environmental impacts. Sci Total Environ 470–471:800–817

Sýkora I, Povince PP, Brest'áková L, Florek M, Holý K, Masarik L (2012) Resuspension processes control variations of ^{137}Cs activity concentrations in the ground-level air. J Radioanal Nucl Chem 293:595–599

Tokyo Electric Power Co., Inc. (TEPCO) (2012): Genshirotateyakarano tuikatekihoushuturyou no hyoukakekka (2012 nenn 10 gatsu 22 nichi) (Estimation of the additional emission from nuclear reactor buildings (22 October 2012)), available at: http://www.meti.go.jp/earthquake/nuclear/pdf/121022/121022_01s.pdf in Japanese

Tomioka N, Uchiyama H, Yagi O (1992) Isolation and characterization of cesium-accumulating bacteria. Appl Environ Microb 58:1019–1023

Unterweger MP (2002) Half-life measurements at the National Institute of Standards and Technology. Appl Radiat Isotopes 56:125–130

Watanabe A (2014) Houshaseibusshitsu no taikichuunoudo / koukaryou nado no choukihenndou. Long time trend of atmospheric concentration/ fallout of radiocesium. J Jpn Soc. Atmos Environ 49:A89–A90. https://www.jstage.jst.go.jp/article/taiki/49/6/49_A89/_pdf

Working Group on Risk Management of Low-dose Radiation Exposure (2011) Report:working group on risk management of low-dose radiation exposure. http://www.cas.go.jp/jp/genpatsujiko/info/twg/Working_Group_Report.pdf

Yoschenko VI, Kashparov VA, Protsak VP, Lundin SM, Levchuk SE, Kadygrib AM, Zvarich SM, Khomutinin YV, Maloshtan IM, Lanshin VP, Kovtun MV, Tschiersch L (2006) Resuspension and redistribution of radionuclides during grassland and forest fires in the Chernobyl exclusion zone: part I. Fire experiments J Environ Radioactiv 86:143–163. https://doi.org/10.1016/k.jenvrad.2005.08.003

Yoshida S, Muramatsu Y, Ogawa M (1994) Radiocesium concentrations in mushrooms collected in Japan. J Environ Radioactiv 22:141–154

Geochemical Journal, Vol. 52, pp. 137 to 143, 2018 doi:10.2343/geochemj.2.0514

Analysis of two forms of radioactive particles emitted during the early stages of the Fukushima Dai-ichi Nuclear Power Station accident

YUKIHIKO SATOU,[1]* KEISUKE SUEKI,[1] KIMIKAZU SASA,[1] HIDEKI YOSHIKAWA,[2] SHIGEO NAKAMA,[2]
HARUKA MINOWA,[3] YOSHINARI ABE,[4] IZUMI NAKAI,[4] TAKAHIRO ONO,[4] KOUJI ADACHI[5] and YASUHITO IGARASHI[5]

[1]Graduate School of Pure and Applied Sciences, University of Tsukuba, 1-1-1 Tennodai, Tsukuba, Ibaraki 305-8577, Japan
[2]Fukushima Environmental Safety Center, Japan Atomic Energy Agency,
10-2 Fukasaku, Miharu, Tamura-gun, Fukushima 963-7700, Japan
[3]Radioisotope Research Facility, Jikei University School of Medicine, 3-25-8, Nishi-shimbashi, Minato, Tokyo 105-8461, Japan
[4]Department of Applied Chemistry, Faculty of Science, Tokyo University of Science,
1-3 Kagurazaka, Shinjuku-ku, Tokyo 162-8601, Japan
[5]Atmospheric Environment and Applied Meteorology Research Department, Meteorological Research Institute,
1-1 Nagamine, Tsukuba, Ibaraki 305-0052, Japan

(*Received August 1, 2017; Accepted December 11, 2017*)

Two types of radioactive particles were isolated from environmental samples collected at various distances from the Fukushima Dai-ichi Nuclear Power Station. “Type A” particles are 2–10 μm in diameter and display characteristic Cs X-ray emissions when analyzed using energy-dispersive X-ray spectrometry (EDS). “Type B” particles are considerably larger, up to 400 μm in diameter, with Cs concentrations too low to be detectable with EDS. These larger particles were isolated from the region north of the nuclear reactor site, which was contaminated on March 12, 2011. The specific activity of Type B particles is much lower than Type A, and the mean ^{134}Cs/^{137}Cs ratios are ~0.93 and 1.04, respectively. The Type B ratio indicates that power station Unit 1 is the source, implying that these larger radioactive particles were discharged on March 12. This study found that different type of radioactive particles were released not only on March 15 but also on March 12.

Keywords: Fukushima Dai-ichi Nuclear Power Station accident, radioactive particles, caesium isotopic ratio, hydrogen explosion, specific radioactivity

INTRODUCTION

Large quantities of radioactive materials were emitted to the environment during the March 2011 Fukushima Dai-ichi Nuclear Power Station (F1NPS) accident (Kinoshita *et al.*, 2011). Radioactive Cs is one of the most prevalent sources of radioactive pollution and is the most widely studied radionuclides dispersed into the environment as a result of the accident. Radioactive particles, which are named Cs-bearing radioactive particles, were discovered in air dust samples collected from 9 pm on March 14 to 9 am on March 15 as far away as Tsukuba, 170 km south of the F1NPS (Adachi *et al.*, 2013). Cs concentrations in the particles were sufficiently high for analysis by energy-dispersive X-ray spectrometry (EDS). The elements Fe, Zn, and Pb were also present. It has since been reported that very similar micron-scale spherical particles have been found 20 km northwest and 3 km south of the F1NPS (Satou *et al.*, 2016; Furuki *et al.*, 2017). Similar particles were isolated from dust on non-woven fabric cloth and needles of Japanese cedar (Yamaguchi *et al.*, 2016; Kogure *et al.*, 2016). This revealed that such Cs-bearing particles were widely dispersed within the Fukushima region. Although their origin could be attributable to any of the various release events that occurred at the F1NPS, the exact source of the radionuclides is unclear. In this study, roadside soil and dust samples from the immediate vicinity of the F1NPS were analyzed using scanning electron microscopy (SEM), EDS, synchrotron radiation micro-beam X-ray fluorescence (SR-μ-XRF) analysis, and gamma spectrometry, with the aim of attributing sources to them.

MATERIALS AND METHODS

Sampling location

Soil and dust samples were collected within the highly

---

*Corresponding author (e-mail: satou.yukihiko@jaea.go.jp)

*Present address: Collaborative Laboratories for Advanced Decommissioning Science (CLADS), Japan Atomic Energy Agency (JAEA), 790-1 Otsuka, Motooka Tomioka, Futaba, Fukushima 979-1151, Japan.

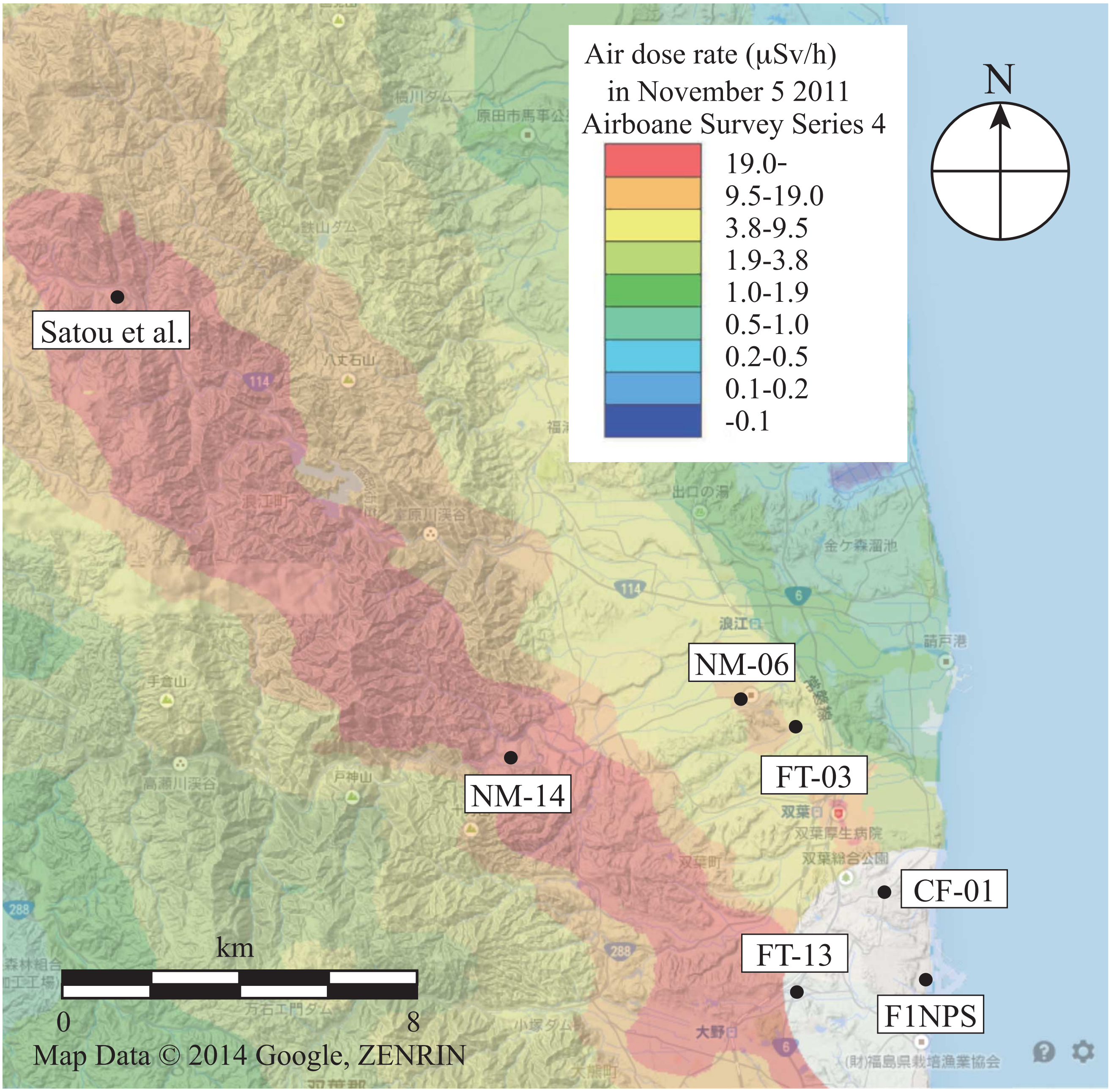

Fig. 1. Sampling locations. "Satou et al." indicates the location of the fragmented and spherical Cs-bearing particles studied of Satou et al. (2016). "F1NPS" indicates the center of the Fukushima Dai-ichi Nuclear Power Station.

contaminated zone around the F1NPS from June 2013 to January 2015, at the locations indicated in Fig. 1 and Table 1. To distinguish between emissions from different sources, samples were collected along two transects extending away from the F1NPS. Contamination on the northern sampling line is understood to have been generated by the hydrogen explosion that occurred within Unit 1 on March 12, 2011 (Satou *et al*., 2015; Chino *et al*., 2016). The method used to sample core soil follows Satou *et al*. (2016). Surface soils were collected by shovel and dust samples were picked up by hand.

Particle extraction

The radioactive particles were extracted from the soil and dust samples using methods reported in previous studies (Adachi *et al*., 2013; Satou *et al*., 2016). Autoradiography, combined with a phosphorus imaging plate and laser readout system, was used to locate radioactive par-

Table 1. Details of the sampling locations

Sample ID	Sampling date	Location	Longitude	Latitude	Sample type
NM-06	13/06/2013	Paddy field	37.4771	140.9857	Core soil
NM-14	01/08/2013	Paddy field	37.4651	140.9272	Core soil
FT-03	12/10/2014	Wasteland	37.4714	140.9998	Bulk soil
FT-13	28/11/2014	Wasteland	37.4178	140.9999	Bulk soil
CF-01	23/01/2015	Pavement	37.4379	141.0223	Dust

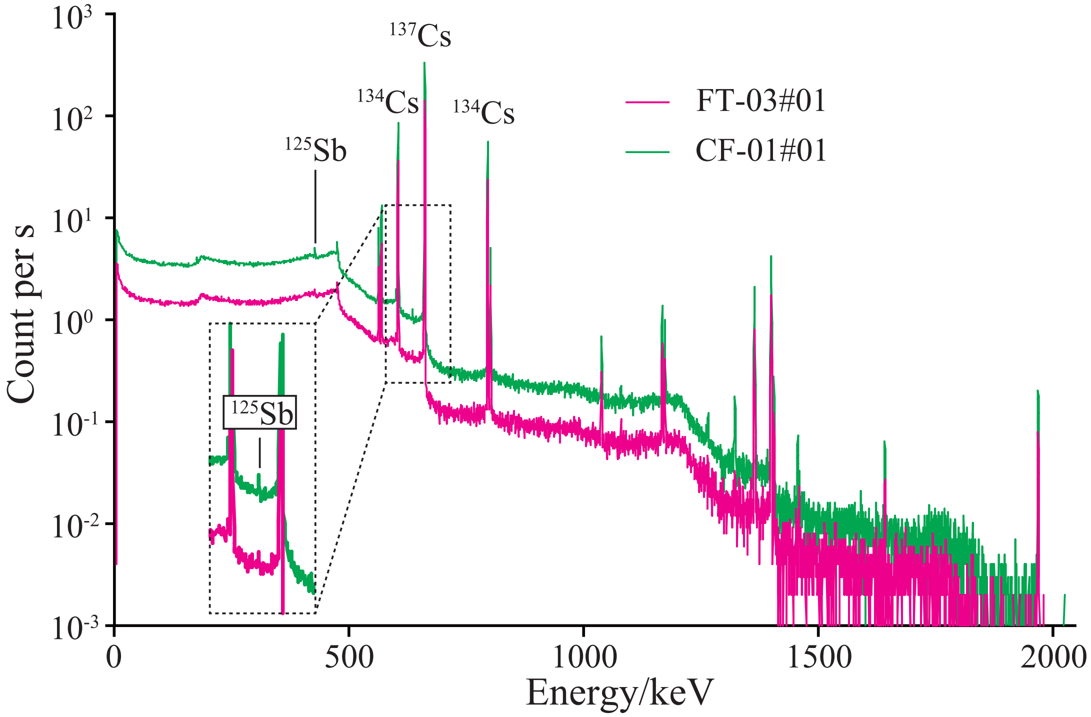

Fig. 2. Gamma-ray spectra of representative particles. Radionuclides are labelled on their main energy peaks.

ticles within the samples, with an exposure time of only five min due to the high specific activity of the former. After the sample contents were sorted, radioactive particles were isolated by hand under an optical microscope using a micro-manipulator system. Radioactivity was confirmed using a Geiger-Müller survey meter and subsequent more accurate gamma radiation measurements.

Analysis of radionuclides

Particles were analyzed for gamma-emitting radionuclides using high-resolution gamma spectrometry with a hyper-pure germanium detector. The detector efficiency was calibrated using standard point ^{134}Cs and ^{137}Cs gamma sources (<1 mm diameter) from the Japan Radioisotope Association.

Particle observation and analysis

Backscattered electron imaging (BEI) with an SEM and associated EDS instruments (SEM: SU 3500, Hitachi High-Technologies Co., Tokyo, Japan; EDS: X-max 50 mm, Horiba Ltd., Kyoto, Japan) were used to study particle surfaces and analyze their compositions. In cases where Cs gamma emissions were detected but the concentration was below EDS detection limits, SR-μ-XRF was performed as a 37.5 keV monochromatic X-ray beam enables detection of Cs K-lines without interference from other elements. The technical procedures followed are as described in Abe *et al.* (2014) and Ono *et al.* (2017).

RESULTS AND DISCUSSION

Radioactivity and morphology

A total of 19 particles were extracted from the soil and dust samples, and all were stable despite exposure to environment for more than four years after the accident. ^{134}Cs and ^{137}Cs were detected in all particles. Particle CF-01#01 contained >20 kBq ^{137}Cs and 300 Bq ^{125}Sb; both of these are volatile elements released from nuclear fuel

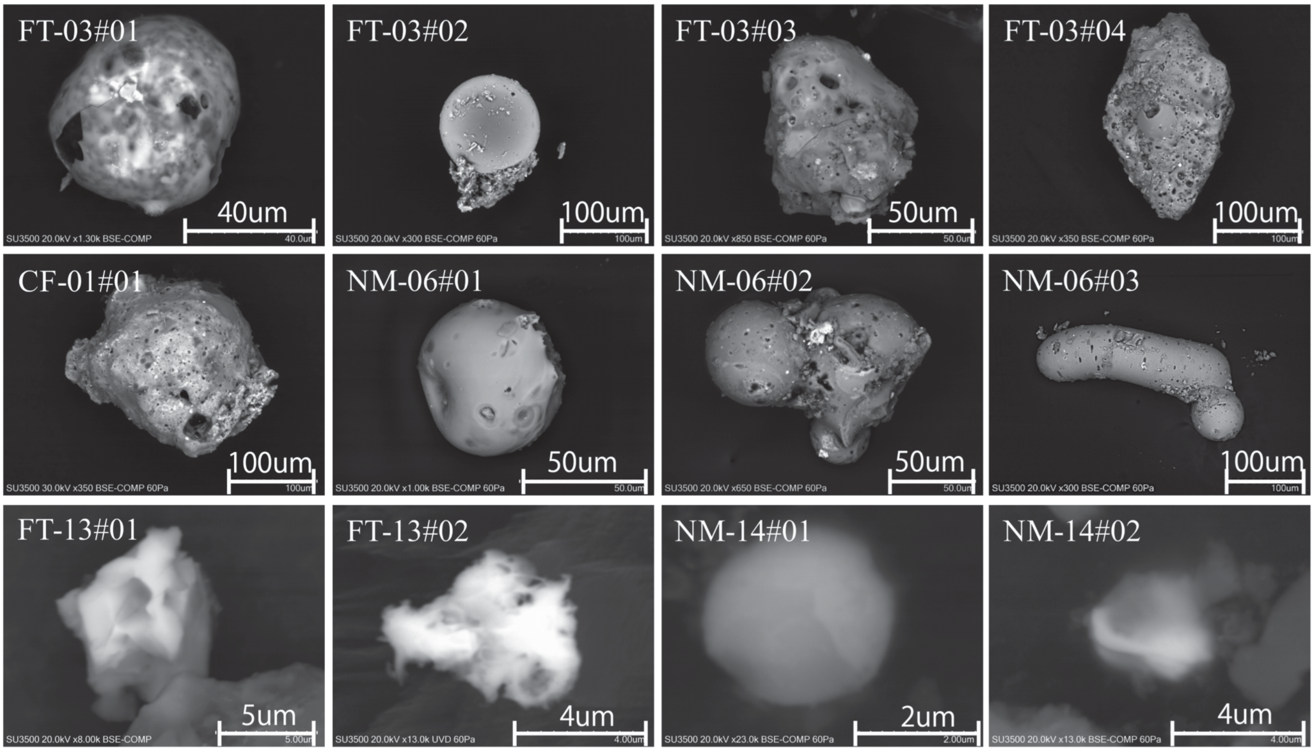

Fig. 3. Backscatter electron images of representative radioactive particles from the environmental samples collected around the Fukushima Dai-ichi Nuclear Power Station.

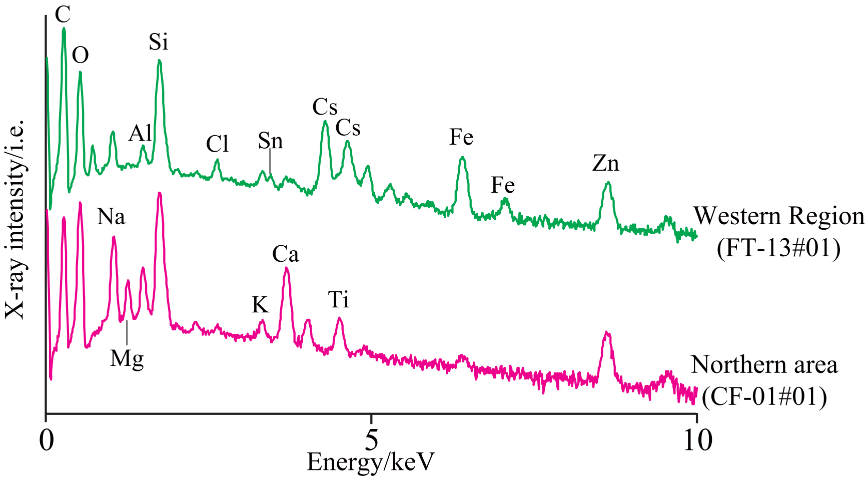

Fig. 4. Elemental dispersive X-ray spectra of representative particles. Note the absence of Cs peaks in the Type B particles.

(Pontillon and Ducros, 2009) (Fig. 2). Other radionuclides such as ^{60}Co and ^{103}Ru, which were found in hot fuel particles around the Chernobyl Nuclear Power Station (ChNPS), were not detected (Devell *et al.*, 1986).

BEI images of several representative particles are shown in Fig. 3. Particles isolated from the northern area (samples CF-01, FT-03, and NM-06) are much larger than those from the western region (FT-13 and NM-14), with maximum dimensions of up to 400 μm. Both spherical and fragmented particles were found at location FT-03, 5 km north of the F1NPS. Similar observations were reported by Satou *et al.* (2016). Particles are evidently not sorted by shape during transport and deposition close to the reactors, with various forms being deposited.

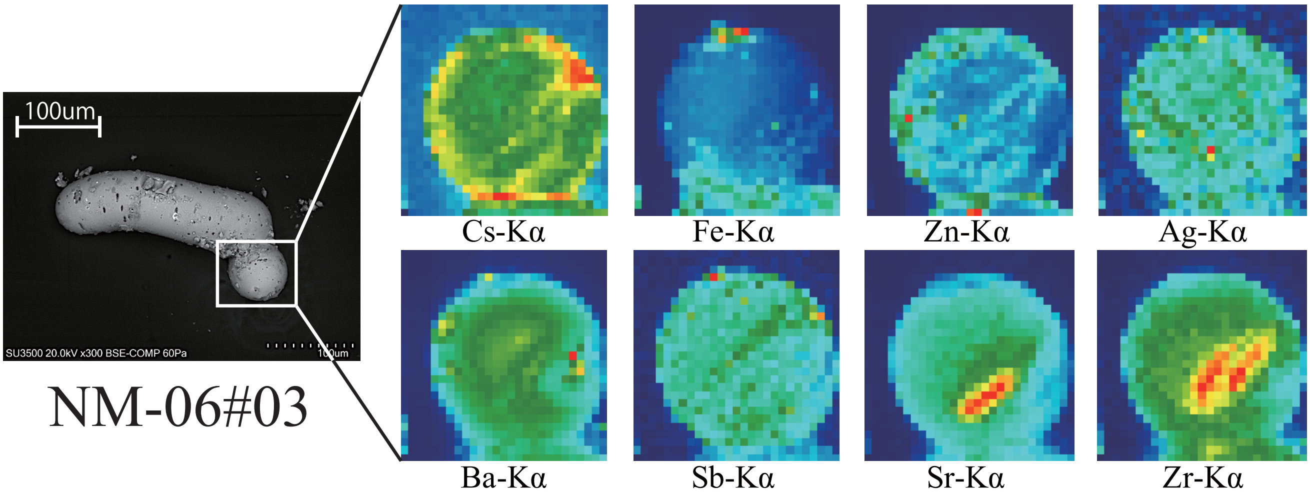

Fig. 5. Micro-beam maps of elemental distributions, showing uneven patterns. Data reconstructed from Ono et al. (2017).

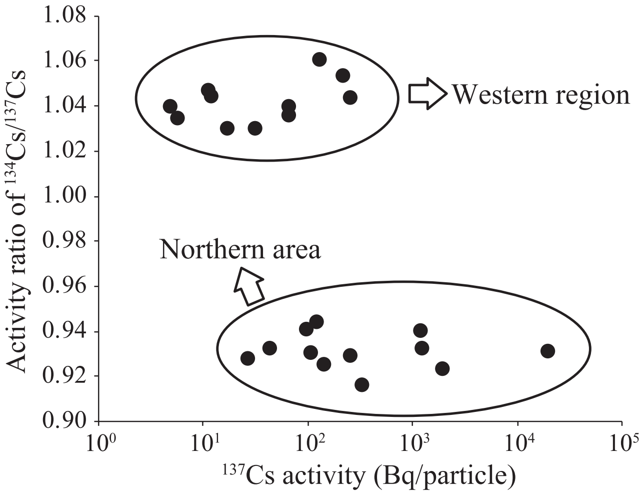

Fig. 6. Scatter-plot of $^{134}Cs/^{137}Cs$ ratio vs ^{137}C content (including data from Satou et al. (2016)), showing the separation of particles into distinct northern and western groups.

Table 2. Characteristics of Type A and Type B particles

	Particle type	
Characteristic	A	B
Size distribution (observed)	1–10 μm	70–400 μm
$^{134}Cs/^{137}Cs$ (mean)	1.04	0.93
Other radionuclides	N/A	Antimony-125 (^{125}Sb)
Distribution	wide	limited (North)
Suspected emission date	March 15, 2011	March 12, 2011
Source reactor(s)	Unit 2 or 3	Unit 1
Specific radioactivity	high	Low
Cs detection method of	SEM-EDS	synchrotron X-ray
Elements contained	Fe, Sn, Cl	Na, Mg, Ca, Ba
Elements in common	Si, O, Zn	

Elemental composition of particles

Figure 4 shows the EDS spectra, obtained by SEM-EDS, of representative particles from the northern area and western region. The compositions of each particle are very similar, primarily silicate, which indicates that unlike in the ChNPS accident, they are not fuel particles (Salbu and Kerkling, 1998). The elemental compositions of particles from the western region are very similar to Cs-bearing particles found 20 km northwest and 170 km south of the F1NPS (Adachi *et al.*, 2013; Satou *et al.*, 2016), with Fe and Zn also being detectable from their characteristic X-rays. Particles from the northern area are slightly different, containing Al, Sn, Cl, Fe, and Mg, with Cs concentrations that were too low for X-ray detection.

SR-μ-XRF mapping was applied to determine the distribution of Cs and other heavy elements in individual particles. A representative result is shown in Fig. 5. Detailed SR-μ-XRF results have been published previously (Ono *et al.*, 2017). Particles from the western region, which are similar to Cs bearing particles, show uniform distribution of Cs and other elements (Satou *et al.*, 2016). In contrast, SR-μ-XRF results of particles from the northern area show an uneven distribution of elements. This result indicates that based on Cs distribution, there are two types of radioactive Cs-bearing particles in the vicinity of the F1NPS site.

Sources of particles

It is possible that the sampling locations were contaminated with radioactive materials from different reactor units. Other studies have shown that the northern and

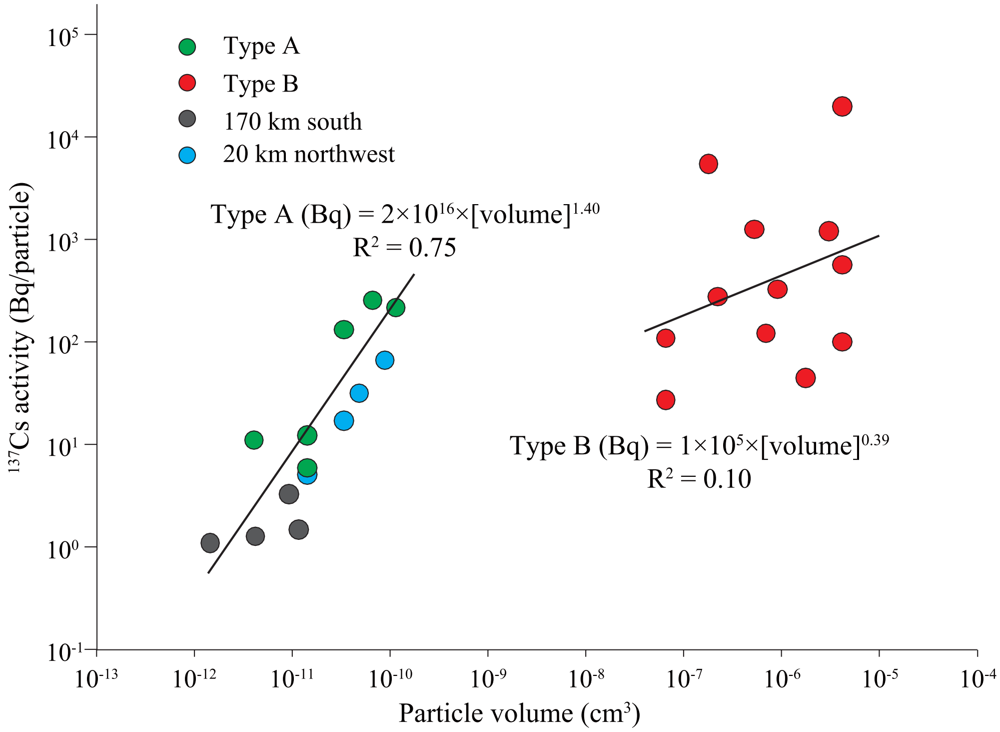

Fig. 7. Scatter-plot of ^{137}Cs content vs particle volume. The "170 km south" and "20 km northwest" labels indicate particles collected by Adachi et al. (2013) and Satou et al. (2016), respectively.

western areas were contaminated by Unit 1 and Units 2 or 3, respectively (Satou *et al*., 2015; Chino *et al*., 2016). The Cs isotopic ratios (^{134}Cs/^{137}Cs), which were decay corrected as of March 11, 2011, form two clearly defined groups of particles, as shown in Fig. 6: particles in the lower group were extracted from the northern area (samples NM-06, FT-03, and CF-01), while those in the upper group were from the western region (including samples from 20 km northwest; Satou *et al*., 2016). The ^{134}Cs/^{137}Cs ratios of 0.93 and 1.04 (the lower and upper groups, respectively, in Fig. 6) that allowed us to distinguish the particles from Unit 1 and Units 2 or 3, respectively, are similar to those obtained using ORIGEN-II performed with JENDL data (Nishihara *et al*., 2012).

A particle isolated from sample CF-01 contained 300 Bq of ^{125}Sb, which indicated that the temperature of nuclear fuel was high enough to produce Sb vapor (Pontillon and Ducros, 2009) and that the surrounding environment was hot enough for the Sb to be transported to the place where the particle was formed. One of the characteristics of Unit 1 was the release of radioactive materials from the reactor at a high temperature. Furthermore, as the dispersion of large particles over significant distances requires considerable energy, meaning that such particles detected in the northern area, within 15 km of the F1NPS, would have been released from the F1NPS during the hydrogen explosion in Unit 1 on March 12.

Particles collected in the northern area are thus considered to have originated from Unit 1.

In contrast, the Cs isotopic ratios in particles from the western region are similar to those present in Units 2 and 3 at the time of the accident, although it is not possible to distinguish between these two units as they were very similar (Unit 2, 1.08; Unit 3, 1.05; Nishihara *et al*., 2012). A more accurate method to measure radioactive Cs in the particles was required to enable a distinction and distinctly identify the source of particles in the western region.

Based on the results of the present study, two types of Cs-bearing particles, Cs isotopic ratio and minor-element content, are defined on the basis of sampling location: Type A, from samples FT-13 and NM-14, and Type B, from samples CF-01, FT-03, and NM-06. The characteristics of the two types are summarized in Table 2. Type A particles are similar to the Cs-bearing particles reported in previous studies (Adachi *et al*., 2013; Satou *et al*., 2016; Yamaguchi *et al*., 2016; Furuki *et al*., 2017).

Particle-specific activity

Specific activity varies between particles, as the scatterplot of particle volume vs ^{137}Cs activity shown in Fig. 7 (the volume of fragmented particles was calculated using the equivalent diameter). There is little variation in specific activity for Type A particles, with significant correlation between activity and volume ($r^2 = 0.75$), similar to the results of a previous study (Satou *et al*., 2016). Type B particles are large in size and have a high Cs activity but at a lower specific activity than Type A particles. Type B particles have significant variability and poor correlation between activity and volume ($r^2 = 0.10$), which explains why the Cs was not detected in EDS X-rays. Particle-specific activity can thus be used to indicate the possibility of different generation and release processes at F1NPS thus providing an additional means of classifying particles.

CONCLUSION

This study identified two types of radioactive particles, Type A and Type B, which are both composed mainly of silicate but with contain different compositions of other elements and have different ^{134}Cs/^{137}Cs ratios and specific activities. Type B particles were isolated from the area north of the F1NPS, which was contaminated on March 12, 2011. Their Cs isotopic ratio is consistent with the theoretical ratio of F1NPS Unit 1, which suggests that the particles were emitted on March 12, 2011. This result indicates that radioactive particles were emitted to the environment not only on March 15, but also on March 12. In addition, radioactive particles emitted during the F1NPS accident are markedly different from those released from the ChNPS, and persist in the environment five years after the event.

Acknowledgments—The authors are indebted to Tsuyoshi Iijima, Kenso Fujiwara, Terumi Dohi, Tetsuya Matsunaka, Tsutomu Takahashi, and Nao Shibayama for their help with sample collection. We also express thanks to Yushin Iizawa at Tokyo University of Science for assistance with the analyses in SPring-8. In addition, the authors are grateful to David A. Richards and Peter G. Martin at the University of Bristol for discussion and English improvements.

This study was supported by MEXT/JSPS KAKENHI grants (numbers 24110003, 24110006, and 15H02340) and by a JAEA-Academia joint study.

The synchrotron radiation experiments were performed at the BL37XU of SPring-8 with the approval of the Japan Synchrotron Radiation Research Institute (JASRI) (proposal numbers 2014B1493, 2015A1895, 2015B1828, and 2016A1705).

REFERENCES

Abe, Y., Iizawa, Y., Terada, Y., Adachi, K., Igarashi, Y. and Nakai, I. (2014) Detection of uranium and chemical state analysis of individual radioactive microparticles emitted from the Fukushima nuclear accident using multiple synchrotron radiation X-ray analyses. *Anal. Chem.* **86**, 8521–8525.

Adachi, K., Kajino, M., Zaizen, Y. and Igarashi, Y. (2013) Emission of spherical caesium-bearing particles from an early stage of the Fukushima nuclear accident. *Sci. Rep.* **3**, 2554.

Chino, M., Terada, H., Nagai, H., Katata, G., Mikami, S., Torii, T., Saito, K. and Nishizawa, Y. (2016) Utilization of ^{134}Cs/^{137}Cs in the environment to identify the reactor units that caused atmospheric releases during the Fukushima Daiichi accident. *Sci. Rep.* **6**, 31376.

Devell, L., Tovedal, H., Bergstrom, U., Appelgren, A., Chyssler, J. and Andersson, L. (1986) Initial observation of fallout from the reactor accident at Chernobyl. *Nature*, **321**, 192–193.

Furuki, G., Imoto, J., Ochiai, A., Yamasaki, S., Nanba, K., Ohnuki, T., Grambow, B., Ewing, R. C. and Utsunomiya, S. (2017) Caesium-rich micro-particles: A window into the meltdown events at the Fukushima Daiichi Nuclear Power Plant. *Sci. Rep.* **7**, 42731.

Kinoshita, N., Sueki, K., Sasa, K., Kitagawa, J., Ikarashi, S., Nishimura, T., Wong, Y. S., Satou, Y., Handa, K., Takahashi, T., Sato, M. and Yamagarata, T. (2011) Assessment of individual radionuclide distributions from the Fukushima nuclear accident covering central-east Japan. *Proc. Natl. Acad. Sci. USA* **108**, 19526–19529.

Kogure, T., Yamaguchi, N., Segawa, H., Mukai, H., Motai, S., Hasegawa, K. A., Mitome, M., Hara, T. and Yaita, T. (2016) Constituent elements and their distribution in the radioactive Cs-bearing silicate glass microparticles released from Fukushima nuclear plant. *Microscopy* **65**, 451–459.

Nishihara, K., Iwamoto, H. and Suyama, K. (2012) Estimation of Fuel Compositions in Fukushima-Daiichi Nuclear Power Plant. *JAEA-Data/Code* **2012-018**.

Ono, T., Iizawa, Y., Abe, Y., Nakai, I., Terada, Y., Satou, Y., Sueki, K., Adachi, K. and Igarashi, Y. (2017) Investigation of the chemical characteristics of individual radioactive microparticles emitted from reactor 1 by the Fukushima Daiichi Nuclear Power Plant accident by using multiple synchrotron radiation X-ray analyse. *Bunseki Kagaku* **66**, 251–261 (in Japanese).

Pontillon, Y. and Ducros, G. (2009) Behaviour of fission products under severe PWR accident conditions: The VERCORS experimental programme—Part 2: Release and transport of fission gases and volatile fission products. *Nucl. Eng. Des.* **240**, 1853–1866.

Salbu, B. and Kerkling, T. (1998) Characterisation of radioactive particles in the environment. *Analyst* **123**, 843–850.

Satou, Y., Sueki, K., Sasa, K., Matsunaka, T., Shibayama, N. and Kinoshita, N. (2015) Classification using ^{110}mAg/^{137}Cs ratio in high dose area at the northwestern from Fukushima Daiichi nuclear plant. *Houshakagaku* **31**, 28–29 (in Japanese).

Satou, Y., Sueki, K., Sasa, K., Adachi, K. and Igarashi, Y. (2016) First successful isolation of radioactive particles from soil near the Fukushima Daiichi Nuclear Power Plant. *Anthropocene* **14**, 71–76.

Yamaguchi, N., Mitome, M., Akiyama, H. K., Asano, M., Adachi, K. and Kogure, T. (2016) Internal structure of caesium-bearing radioactive microparticles released from Fukushima nuclear power plant. *Sci. Rep.* **6**, 20548.

Feature Article

Earozoru Kenkyu, **32** (4), 255–260 (2017) doi: 10.11203/jar.32.255

特集「福島第一原発事故による放射性エアロゾル」

原子力発電所事故で放出された不溶性放射性粒子の形態と組成

足立　光司 [1*]

Shapes and Compositions of Insoluble Radioactive Particles from the Nuclear Accident

Kouji ADACHI [1*]

Received 12 July 2017
Accepted 26 August 2017

Abstract Insoluble radioactive particles emitted from the Fukushima nuclear accident have been found from the samples collected in various environments. This manuscript summarizes the studies that characterized such particles using electron microscopy and synchrotron radiation analyses. The shapes and compositions of 33 radioactive particles from aerosol particles, soil, plant tissues, non-woven fabric cloth, and masks have been identified. These radioactive particles contained radioactive Cs ranging from 0.5 to 109 becquerel per particle. Diameters of spherical particles ranged from 0.8 to 4 μm, and those of non-spherical particles were from 1.4 to 250 μm. They consisted of silicate glass with Cs, Zn, and Fe as well as many minor elements (in total, 33 elements were detected). These particles tended to have more Cs on their surface than the core and contained nano-crystals consisting of, for example, Cu-Zn-Mo, Ag-Te, $CaSO_4$, $FeCr_2O_4$, Sn-Te, Ag-Sb, and iron oxides. Such crystalline structures will be important to understand the formation and degradation processes.

Keywords : Insoluble Radioactive Particles, Electron Microscopy, Synchrotron Radiation, Cs-Bearing Particles, Fukushima Daiichi Nuclear Power Plant Accident, Particle Size, Particle Composition, Particle Shape.

1. はじめに

2011年3月11日に発生した東日本大震災に伴う福島第一原子力発電所事故において，多量の放射性物質が環境中に放出された。これらの放射性物質は，エアロゾルやガスとして大気中に，また水に溶け海洋に拡散した。これらの放射性物質うち，大気を経由して各地に拡散した放射性エアロゾルは，重力や雨などの通常のエアロゾルと同様の沈着プロセスを経て地上に降下した（Adachi *et al.*, 2013）。それらの放射性物質は，森林や土壌などに沈降して植物や土壌に取り込まれ（Sasaki *et al.*, 2016），また一部は湖沼・河川などに流出するなどして環境中を移動していく。放射性エアロゾルは通常のエアロゾルと異なり，土壌などに沈着した後もその放射能を追跡することで，環境動態を追い続けることが可能である。このような放射性物質の環境動態は，その物理化学状態に影響される。たとえば，水溶性の放射性物質は土壌表面に沈着した際粘土鉱物に吸着し，また植物などに取り込まれる。また，水に溶けない不溶性放射性物質は，粒子態として土壌表面や植物の表面などで存在し続ける（Itoh *et al.*, 2014）。加えて，放射性物質の物理化学性状は，事故時の放出プロセスや体内に取り込まれた際の放射線影響の理解，また数値モデルで放射性物質の拡散・挙動予測を行う際にも重要である（Adachi *et al.*, 2013）。本論文は，このような放射性物質のうち，特に地球科学分野などで用いられる機器分析を用いた不溶性放射性粒子の形態や化学組成に関する研究成果をまとめ，環境中における これら粒子の挙動に関する理解を助けることを目的とする。

---

[1] 気象研究所
（〒305-0052　茨城県つくば市長峰1-1）
[1] Meteorological Research Institute
1-1 Nagamine, Tsukuba, Ibaraki 305-0052, Japan
[*] Corresponding Author.
E-mail: adachik@mri-jma.go.jp (K. Adachi)

2. 放射性セシウムを含むエアロゾル粒子

2011年の原発事故で，さまざまな放射性核種が放出された。数時間から数日間で半減期を迎える放射性核種は，事故後比較的短期間で検出レベルを下回る濃度にまで下がった。一方，現在の事故由来の環境放射能の主体は，放射壊変半減期が2年のセシウム134と30年のセシウム137である。この放射性セシウムの大部分は，おもに事故翌日の3月12日から23日にかけて大気中に放出された（Tsuruta *et al.*, 2014）。そのうち，関東地域まで多くの放射性物質が飛来した3月15日と3月20～21日のプルーム（Katata *et al.*, 2015）において，前者が水に溶けない放射性物質を多く含み，後者が水に溶ける放射性物質を多く含んでいることが報告されている（Adachi *et al.*, 2013）。水に溶けない放射性粒子は，フィルタに捕集された放射性物質の放射能強度の二次元分布を測定するイメージングプレート（IP）を用いた分析で，スポット状の強い放射能を有する点として測定される。一方，水に溶ける放射性物質は，IP分析でフィルタ全体にほぼ均一に分布していた。両者は濃硝酸による抽出において，3月20～21日に捕集されたフィルタ上のセシウムがほぼ溶出したのに対し，3月15日に捕集されたフィルタでは30％程度溶け残るなどの違いがみられた（Igarashi *et al.*, 2015）。水に溶けるセシウムの放出時における化学形態はまだ十分には解明されていないが，2011年4月から5月にかけて捕集されたフィルタにおいては，その粒径分布が硫酸塩エアロゾルのものとほぼ一致することから，硫酸塩に取り込まれた化学形態であることが示唆されている（Kaneyasu *et al.*, 2012, 2017）。一方，水に溶けない放射性粒子の形態や化学的な特徴は，これまでに**Table 1**にまとめる9報の論文で電子顕微鏡や放射光分析などを用いて詳しく分析されてきている。本論文では，このような水に溶けない放射性粒子に焦点を絞って報告を行う。なお，本論文で紹介する不溶性放射性粒子の一部は，その形態や組成的な特徴から日本語でセシウムボールなどと呼ばれることがあり，英語でもさまざまな呼称が使われている（第8章参照）。セシウムボールは，おもにセシウムを含んだ球状の不溶性放射性粒子を指すのに対し，本論文では球状を含むさまざまな形態の放射性粒子を紹介する。そのため，ここでは本論文に紹介する全粒子に共通的な特徴として，不溶性放射性粒子，もしくは単に放射性粒子と呼ぶ。また，ここで紹介する放射性粒子は，水溶性を直接実験で確認しなかった粒子も含むが，1）直接風雨に当たる環境から捕集された，2）ガラス状の構造を持つ，3）Adachi *et al.*（2013）によって数時間浸水させて不溶性であることを確認された粒子と同じ特徴を持つ，といった特徴からすべて水に溶けない不溶性放射性粒子であると考える。また，これらの粒子は数時間単位での不溶性を示し，より長い時間では徐々に環境中に溶けだす可能性も示唆されている（Yamaguchi *et al.*, 2016）。

3. 放射性粒子の単離方法

これまでにTable 1でまとめた論文で報告された放射性粒子は33粒子ある。Adachi *et al.*（2013）とAbe *et al.*（2014）が茨城県つくば市の試料で捕集されたエアロゾル試料から放射性粒子を見つけた以外では，いずれも福島県内で得られた試料から見つかっている。これらの粒子は，エアロゾルフィルタ，土壌，植物，農作業で用いられる不織布，帰還困難区域などで作業にあった人が使用していたマスクなどの試料から発見さ

Table 1 Summary of insoluble radioactive particles from nine studies

References	Sampling place	Sample type	Diameter (μm) of spherical particles	Diameter (μm) of non-spherical particles	Radioactivity (Bq) of ^{137}Cs	Particle number
Adachi *et al.* (2013)	Ibaraki	Aerosol filter	2.0–2.6		0.7–3.3	3
Abe *et al.* (2014)	Ibaraki	Aerosol filter	1.4–2.8		1.1–1.5	3
Yamaguchi *et al.* (2016)	Fukushima	Non-woven fabric cloth & Cedar	2.2–2.5		3.1–5.0	2
Satou *et al.* (2016)	Fukushima	Soil	3.0–4.0	4.5–6.4	5–67	4
Kogure *et al.* (2016)	Fukushima	Non-woven fabric cloth & Wheat	0.8–2.7		1.9–3.3	3
Furuki *et al.* (2017)	Fukushima	Soil & Gravel	2.0–3.3	3.4	0.9–11.3	3
Yamaguchi *et al.* (2017)	Fukushima	Aerosol filter & Plant tissue		1.4–3.6	0.5–1.9	4
Ono *et al.* (2017)	Fukushima	Soil	2.6–3.6	50–250	33–109	7
Higaki *et al.* (2017)	Fukushima	Mask	2.1	6.6–12	1–70	4

れている（Table 1）。これらの試料は，次に述べる方法などで放射性粒子以外の粒子を除去して放射性粒子の単離が行われている。なお，放射性粒子はそのほかのエアロゾル粒子や土壌粒子に比べてけた違いに少なく，効率的な単離作業が粒子分析のカギとなる。

1) マイクロマニュピレータを用いた手法（Adachi *et al.*, 2013）：放射性粒子を含むフィルタ試料をカーボンテープに埋め込んで，マイクロマニュピレータを用いてできるだけ小さく分割し，IP やゲルマニウム半導体検出器で放射性粒子が移った試料を特定する。この作業を繰り返すことで，放射性粒子のみを単離させる。
2) 密閉式の袋を用いた方法（Satou *et al.*, 2016）：袋に密閉した土壌試料を IP にかけ，放射性粒子の位置を確認する。その後，袋中の放射性粒子の周囲をほかの土壌粒子から分離し，再び分散させて IP にかける。この作業を繰り返すことで，放射性粒子をほかの土壌粒子から単離させる。
3) テープを用いた方法（Yamaguchi *et al.*, 2016）：カプトンテープなどを使って，試料を挟み込むように 2 枚のテープを張り合わせる。そのテープを引きはがすと，どちらかの面に放射性粒子が残る。その残った面を再び新しいテープと張り合わせ，引き離す。この作業を繰り返すことで，最終的に不純物がほぼなくなった放射性粒子がテープ上に残る。
4) 懸濁液を用いた方法（Furuki *et al.*, 2017）：放射性粒子の入った試料を試験管などに入れて懸濁液とする。その懸濁液を分割し，放射能を測定することで放射性粒子が移った管を特定する。この試料を再び懸濁液として分割を繰り返すことで，不純物を減らして放射性粒子を単離する。

4. 放射性粒子の分析

単離された放射性粒子は，走査型電子顕微鏡（SEM），透過型電子顕微鏡（TEM），放射光分析などの機器分析で物理化学特性が測定できる。

SEM：電子線を試料に照射してその表面形態や組成分析を行う。事故由来の放射性粒子の多くは，セシウムがエネルギー分散型 X 線分析装置（EDS）で検出可能であり，その表面形態や組成を分析するのに有効である（Adachi *et al.*, 2013; Satou *et al.*, 2016; Higaki *et al.*, 2017）。ただし，SEM-EDS では約 0.1 重量パーセント以下の微量成分の分析は困難である。

TEM：電子線を試料に照射し，その透過した電子線を結像し，また EDS 分析をすることで粒子内部の分析を行う。分析試料は，集束イオンビーム（FIB）などを用いて粒子を切断して，粒子断面を露出させる必要がある。TEM を用いた分析では，粒子内部に含まれるナノ粒子や粒子断面の組成分布，また結晶構造などを解析することができる（Yamaguchi *et al.*, 2016, 2017; Kogure *et al.*, 2016; Furuki *et al.*, 2017）。

放射光分析：大型放射光施設 SPring-8 などを用いて，非破壊で放射性粒子の組成，化学状態，また結晶構造を解析することができる。とくに，放射光分析は SEM-EDS に比べ重元素の検出感度が高いため，微量元素の分析に効果的である（Abe *et al.*, 2014; Ono *et al.*, 2017）。

5. 放射性粒子の形態と粒径

これまでに分析されてきた粒子は，その外観から球形と非球形に分けられる。球形粒子は，粒径が 0.8 から 4 マイクロメートルであり，対象としたほとんどの環境試料から見つかっている（**Fig. 1**）。この球形粒子は，いったん溶融した物質が飛散した際に空中などで急速に固化したことを示唆する。一方，非球形粒子は 1.4 から 250 マイクロメートルで，いくつかの球形粒子が寄せ集まった形態（Ono *et al.*, 2017）や角ばった形（Satou *et al.*, 2016），小さな粒子の凝集体（Yamaguchi *et al.*, 2017; Higaki *et al.*, 2017）などがある（**Fig. 2**）。これらの形状の違いは，粒子発生時の物性や発生源・粒子生成メカニズムの違い，また放出後の環境中での崩壊などを示唆する。

6. 放射性粒子のセシウム濃度

放射性粒子の放射能を示す単位ベクレルは，1 秒間に壊変する原子の個数を示し，単離された放射性粒子では一粒子あたりの放射性セシウムの放射能が計測できる。キログラムあたりのベクレル（単位重量あたりの放射能，比放射能と呼ぶ）で表すと，土壌や食料などに比べ，数マイクロメートルの粒子 1 個における比放射能は桁違いに大きくなる。測定された放射性粒子の放射能は，2011 年の事故時の放射能に減衰補正計算したとき，セシウム 137 では一粒子あたり 0.5 から 109 ベクレル程度であった（Table 1）。また，セシウム 137 と 134 の比はおよそ 1：1 と，Kanai（2012）で報告された大気中エアロゾルの比率とほぼ同じであるが，Ono *et al.*（2017）で発見された大型の粒子では ^{134}Cs/^{137}Cs 比が約 0.9, Higaki *et al.*（2017）で見つかった粒子が 1.09 と粒子によって違いがある。このセシウム比率は粒子が発生した炉に依存し，2，3 号炉由来のセシウムは約 1.05～1.08，1 号炉由来の粒子は約 0.94 と推測されており（Higaki *et al.*, 2017），粒子の起源推測に利用できる可能性がある。

球形の放射性粒子の放射能は粒子体積と比例し，放射性セシウムの濃度，つまり比放射能はほぼ一定であることが報告されている（Satou *et al.*, 2016）。それら粒子中のセシウム重量パーセントは，粒子全体として 3～12％程度（Yamaguchi *et al.*, 2016; Kogure *et al.*, 2016; Adachi *et al.*, 2013），また粒子中のセシウム濃度が高い部位で 19％が報告されている（Furuki *et al.*, 2017）。一

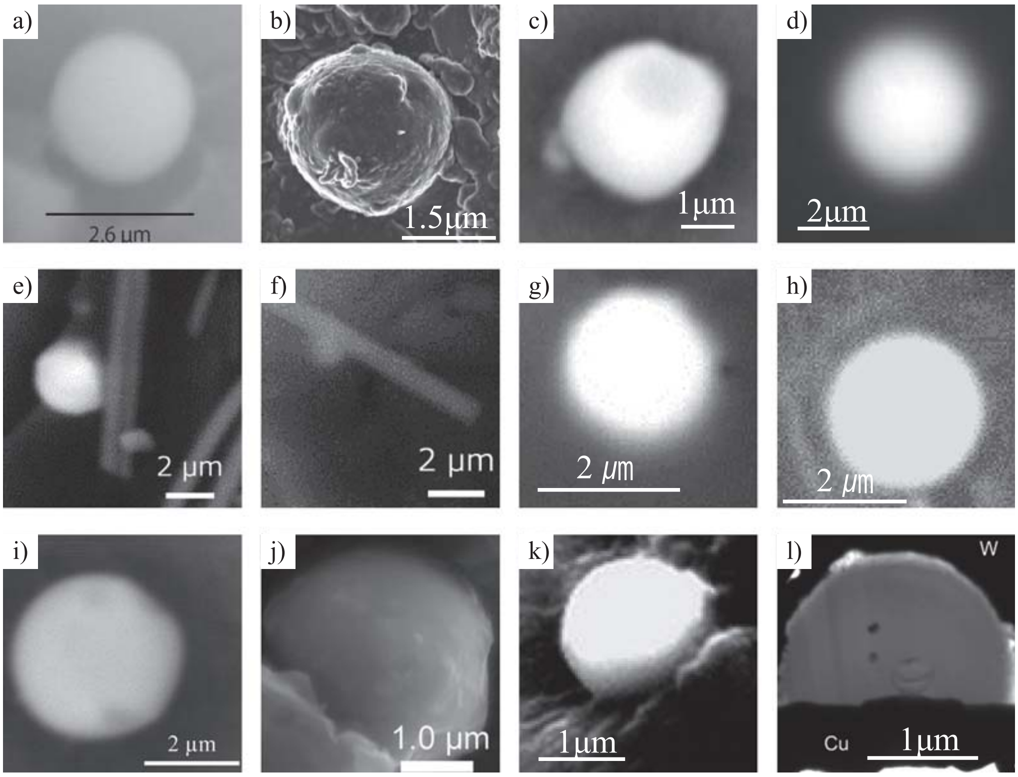

Fig. 1 Scanning and transmission electron microscopy images of spherical radioactive particles. Images are from a) Adachi *et al.* (2013); b) Yamaguchi *et al.* (2016); c) and d) Satou *et al.* (2016); e)–g) Abe *et al.* (2014); reprinted with permission from Abe et al. (2014), copyright 2014, American Chemical Society; h) and i) Ono *et al.* (2017); j) and k) Furuki *et al.* (2017); and l) Yamaguchi *et al.* (2016). Images a)–k) were taken using SEM, and image l) was taken using TEM. Scale bars were either original or replaced to show near the particles with adequate length. Letters in the image l) were shown in the original images and have no meaning in this figure.

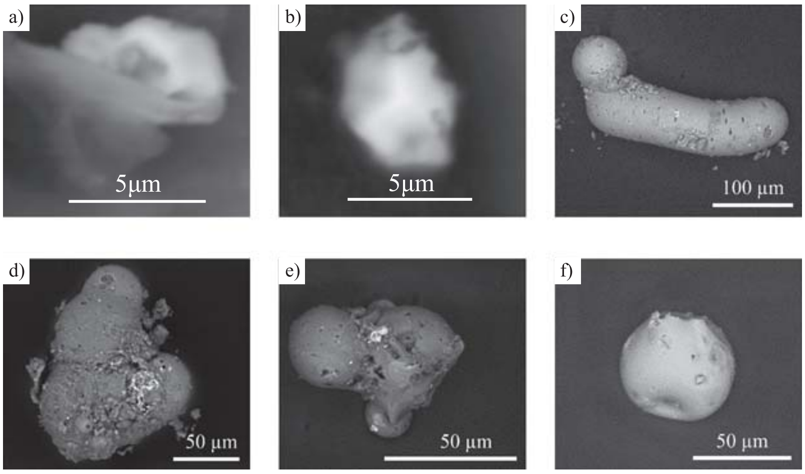

Fig. 2 Scanning electron microscopy images of non-spherical radioactive particles. Images a) and b) are from Satou *et al.* (2016) and those c)–f) are from Ono *et al.* (2017). Scale bars were either original or replaced to show near the particles with adequate length.

方，Ono *et al.*（2017）が土壌中から見つけた比較的大きめの非球形放射性粒子では，粒子あたりの放射能強度は球形粒子よりも100倍近く大きい一方，粒子体積が10^6倍も大きいため，比放射能では球形の放射性粒子に比べ小さい。

7. 放射性粒子の組成とナノ結晶粒子

これまでに放射性粒子から合計で33元素が検出されている（**Table 2**）。すべての報告において，セシウム，鉄，ケイ素，亜鉛，酸素が検出されており，これらの元素が比較的検出感度の低いSEM-EDSでも検出でき

Table 2 Detected elements within insoluble radioactive particles from nine studies

	Elements
Detected from 9 studies	Cs, Fe, O, Si, Zn
Detected from 5–8 studies	Ca, Cl, K, Mn, Rb, Sn, Te
Detected from 2–4 studies	Ag, Al, Ba, Cr, Mo, Ni, Pb, S, Sb, U, Zr
Detected from a study	Cd, Cu, In, Mg, Nb, Pd, Se, Sr, W, Xe

るパーセントオーダーで粒子中に存在することが示唆される。特に多くの放射性粒子の主成分として，ケイ酸塩のガラス態酸化物が報告されている。たとえばKogure *et al.*（2016）では粒子中の SiO_2 重量%を 61〜73%として報告している。Table 2 で示す元素の検出頻度は，それぞれの元素の粒子中での有無に加え，用いた機器の検出感度にも依存する。特に，SEM-EDS のみを使用した分析に比べ，TEM や放射光分析でより多くの元素が検出されている。検出元素の起源は，核燃料由来の核分裂生成物，原子炉や周辺構造物の建材や部材，冷却水中の添加物，海水などが推定されている（Abe *et al.*, 2014; Furuki *et al.*, 2017）。

それぞれの元素の粒子内における分布は，SEM-EDS や放射光分析による表面分析では均一と報告されているが，数十マイクロメートル以上の比較的大きい粒子や TEM を用いた詳細な内部構造解析では分布の偏りが報告されている。特に，いくつかの球形粒子でセシウムが粒子表面に濃集していることが確認されている（Yamaguchi *et al.*, 2016; Kogure *et al.*, 2016）。また，スズ，カドミウム，鉛，塩素が粒子の表面近くで濃集傾向にある粒子も見つかっている（Yamaguchi *et al.*, 2016, 2017; Ono *et al.*, 2017; Kogure *et al.*, 2016）。加えて，TEM 分析で粒子内部に Cu-S，Cu-Zn-Mo，Ag-Te，$CaSO_4$，$FeCr_2O_4$，Sn-Cs，Pb(S, Te)，SnTe，Fe_2O_3，Fe_3O_4，Ag-Sb などのナノ結晶構造が見つかっている（Yamaguchi *et al.*, 2016, 2017; Furuki *et al.*, 2017）。また，Furuki *et al.*（2017）では，ナノスケールの構造として CsCl やウランが Fe-Zn 酸化物の構造に取り込まれていることを報告している。このような結晶構造は，粒子発生時の炉内における温度・圧力や，粒子の元となる物質の成分を推測する手掛かりとなる可能性がある。放射光分析で検出された多くの微量元素も，このような粒子中に取り込まれたナノ粒子を検出した可能性がある。

8. 放射性粒子の名称

今回紹介した不溶性放射性粒子は，論文によってさまざまな名称が用いられている。論文タイトルに使われた名称では，“spherical cesium-bearing particles”，“radioactive microparticles”，“cesium-bearing radioactive microparticles”，“radioactive Cs-bearing silicate glass microparticles”，“caesium-rich micro-particles”，“radioactive Cs-bearing microparticles”，“non-spherical heterogeneous radiocesium-bearing particles” などがあり，また日本語でも（不溶性）放射性粒子や Cs ボール（セシウムボール）といった呼び方が用いられている。粒子の比放射能，形状（球形・非球形），サイズなどによる違いを明らかにした名称が求められるが，いまだに新たな形態の粒子が見つかりつつあり，その呼称の統一は今後の課題となっている。

9. まとめ

2013 年にエアロゾルフィルタから初めて発見されたセシウムを含む放射性粒子は，その後さまざまな環境から発見されている。また，分析手法も放射光分析や透過型電子顕微鏡などを用いた鉱物学的・地球科学的手法が使われるようになり，その詳細な構造が明らかになりつつある。これらの放射性粒子は共通して鉄や亜鉛を含むケイ酸ガラス構造を主体としている。一方で，形態，微量成分，比放射能などに違いがあり，今後，その生成プロセスの解明や統一された呼称の提案が望まれる。また，粒子は内部にナノ結晶を含んでおり，その解析には鉱物学や材料学などの他分野に使われる技術の応用が有効と考えられる。また，このような放射性粒子の物理化学特性に関する知見は，今後の環境中での風化や移送などの環境動態推定，体内にとりこまれた場合の体内動態把握などに有用であり，これらの観点からの解析も必要になると考えられる。

謝辞

本稿は気象研究所，五十嵐康人博士と議論し，貴重な意見をいただいた。本研究の一部は，科研費新学術領域「福島原発事故により放出された放射性核種の環境動態に関する学際的研究」A01–02 班（科研費番号 24110003）の活動および放射能調査研究費課題「人工放射性核種のバックグラウンド大気監視と数値解析に関する研究」の支援を得て行った。ここに記して感謝いたします。

References

Abe, Y., Iizawa, Y., Terada, Y., Adachi, K., Igarashi, Y. and Nakai, I.: Detection of Uranium and Chemical State Analysis of Individual Radioactive Microparticles Emitted from the Fukushima Nuclear Accident Using Multiple Synchrotron Radiation X-ray Analyses, *Anal. Chem.*, **86**, 8521–8525 (2014)

Adachi, K., Kajino, M., Zaizen, Y. and Igarashi, Y.: Emission of Spherical Cesium-Bearing Particles from an Early Stage of the Fukushima Nuclear Accident, *Sci. Rep.*, **3**, 2554 (2013)

Furuki, G., Imoto, J., Ochiai, A., Yamasaki, S., Nanba, K., Ohnuki, T., Grambow, B., Ewing, R. C. and Utsunomiya, S.: Caesium-Rich Micro-Particles: A Window into the Meltdown Events at the Fukushima Daiichi Nuclear Power Plant, *Sci. Rep.*, **7**, 42731 (2017)

Higaki, S., Kurihara, Y., Yoshida, H., Takahashi, Y. and Shinohara, N.: Discovery of Non-Spherical Heterogeneous

Radiocesium-Bearing Particles not Derived from Unit 1 of the Fukushima Dai-ichi Nuclear Power Plant, in Residences Five Years after the Accident, *J. Environ. Radioact.*, **177**, 65–70 (2017)

Igarashi, Y., Kajino, M., Zaizen, Y., Adachi, K. and Mikami, M.: Atmospheric Radioactivity over Tsukuba, Japan: A Summary of Three Years of Observations after the FDNPP Accident, *Progress in Earth and Planetary Science*, **2**, 44 (2015)

Itoh, S., Eguchi, T., Kato, N. and Takahashi, S.: Radioactive Particles in Soil, Plant, and Dust Samples after the Fukushima Nuclear Accident, *Soil Science and Plant Nutrition*, **60**, 540–550 (2014)

Kanai, Y.: Monitoring of Aerosols in Tsukuba after Fukushima Nuclear Power Plant Incident in 2011, *J. Environ. Radioact.*, **111**, 33–37 (2012)

Kaneyasu, N., Ohashi, H., Suzuki, F., Okuda, T. and Ikemori, F.: Sulfate Aerosol as a Potential Transport Medium of Radiocesium from the Fukushima Nuclear Accident, *Environ. Sci. Technol.*, **46**, 5720–5726 (2012)

Kaneyasu, N., Ohashi, H., Suzuki, F., Okuda, T., Ikemori, F., Akata, N. and Kogure, T.: Weak Size Dependence of Resuspended Radiocesium Adsorbed on Soil Particles Collected after the Fukushima Nuclear Accident, *J. Environ. Radioact.*, **172**, 122–129 (2017)

Katata, G., Chino, M., Kobayashi, T., Terada, H., Ota, M., Nagai, H., Kajino, M., Draxler, R., Hort, M. C., Malo, A., Torii, T. and Sanada, Y.: Detailed Source Term Estimation of the Atmospheric Release for the Fukushima Daiichi Nuclear Power Station Accident by Coupling Simulations of an Atmospheric Dispersion Model with an Improved Deposition Scheme and Oceanic Dispersion Model, *Atmos. Chem. Phys.*, **15**, 1029–1070 (2015)

Kogure, T., Yamaguchi, N., Segawa, H., Mukai, H., Motai, S., Akiyama-Hasegawa, K., Mitome, M., Hara, T. and Yaita, T.: Constituent Elements and Their Distribution in the Radioactive Cs-Bearing Silicate Glass Microparticles Released from Fukushima Nuclear Plant, *Microscopy*, **65**, 451–459 (2016)

Ono, T., Iizawa, Y., Abe, Y., Nakai, I. Terada, Y., Satou, Y., Sueki, K., Adachi, K. and Igarashi, Y.: Investigation of the Chemical Characteristics of Individual Radioactive Microparticles Emitted from Reactor 1 by the Fukushima Daiichi Nuclear Power Plant Accident by Using Multiple Synchrotoron Radiation X-Ray Analyses, *BUNSEKI KAGAKU*, **66**, 251–261 (2017) (in Japanese)

Sasaki, Y., Abe, H., Mitachi, K., Watanabe, T., Ishii, Y. and Niizato, T.: The Transfer of Radiocesium from the Bark to the Stemflow of Chestnut Trees (Castanea Crenata) Contaminated by Radionuclides from the Fukushima Dai-ichi Nuclear Power Plant Accident, *J. Environ. Radioact.*, **161**, 58–65 (2016)

Satou, Y., Sueki, K., Sasa, K., Adachi, K. and Igarashi, Y.: First Successful Isolation of Radioactive Particles from Soil near the Fukushima Daiichi Nuclear Power Plant, *Anthropocene*, **14**, 71–76 (2016)

Tsuruta, H., Oura, Y., Ebihara, M., Ohara, T. and Nakajima, T.: First Retrieval of Hourly Atmospheric Radionuclides just after the Fukushima Accident by Analyzing Filter-Tapes of Operational Air Pollution Monitoring Stations, *Sci. Rep.*, **4**, 6717 (2014)

Yamaguchi, N., Mitome, M., Kotone, A. H., Asano, M., Adachi, K. and Kogure, T.: Internal Structure of Cesium-Bearing Radioactive Microparticles Released from Fukushima Nuclear Power Plant, *Sci. Rep.*, **6**, 20548 (2016)

Yamaguchi, N., Kogure, T., Mukai, H., Akiyama-Hasegawa, K., Mitome, M., Hara, T. and Fujiwara, H.: Structures of Radioactive Cs-Bearing Microparticles in Non-Spherical Forms Collected in Fukushima, *Geochemical Journal*, **51** (2017)

BUNSEKI KAGAKU Vol. 66, No. 4, pp. 251–261 (2017)

報　文

福島第一原子力発電所事故により1号機から放出された放射性粒子の放射光マイクロビームX線分析を用いる化学性状の解明

小野　貴大*[1]，飯澤　勇信[1]，阿部　善也*[1]，中井　泉[1]，寺田　靖子[2]，
佐藤　志彦[3]，末木　啓介[4]，足立　光司[5]，五十嵐康人[5]

2011年3月の福島第一原発事故により，1号機由来の放射性物質が飛来したと考えられる原発北西地域の土壌から，強放射性の粒子を7点分離した．分離された粒子は100 μm前後の大きさで歪な形状のものが多く，2号機から放出されたとされる直径数μmの球形粒子（Csボール）とは明らかに異なる物理性状を有していた．これらの粒子に対して，大型放射光施設SPring-8において放射光マイクロビームX線を用いた蛍光X線分析，X線吸収端近傍構造分析，X線回折分析を非破壊で適用し，詳細な化学性状を解明した．1号機由来の粒子はCsボールに比べて含有する重金属の種類に富み，特にSrやBaといった還元雰囲気で揮発性が高くなる元素が特徴的に検出され，粒子内で明確な元素分布の不均一性が見られた．粒子本体はCsボールと同様にケイ酸塩ガラスであったが，Feなど一部の金属元素が濃集した数μm程度の結晶性物質を含有していた．これらの粒子は3月12～13日に大気中に放出されたものであると考えられ，核燃料と格納容器との熔融がかなり早い段階で進行していたことが示唆された．さらに放出源の推定において，放射性物質自体の化学組成情報が放射能比に代わる新たな指標となることが実証された．

1　緒　　言

2011年3月11日の東日本大震災に伴って発生した福島第一原子力発電所（FDNPP）事故により，大量の放射性物質が環境中に放出され，東日本を中心に拡散した1)～3)．事故初期の経緯をまとめると，まず11日の夕方に1号機の核燃料熔融が始まり，燃料被覆管のジルコニウムと冷却水が高温で反応し，発生した水素ガスによって12日の15時36分に最初の水素爆発が起こった2)．翌13日には3号機の核燃料も熔融し，14日11時半頃に水素ガス爆発が起こった．2号機は14日に冷却機能を喪失したが，1，3号機のような水素ガス爆発は起きなかった．しかし，圧力容器や圧力抑制プールが大きく破損したために，結果的に大量の放射性物質を環境に放出したとされる3)．こうして放出された放射性物質は，事故から6年以上が経過した今日においても，廃炉や汚染土壌など事故に関する話題が途切れることがなく，事故により根付いた目に見えない「放射能」に対する懸念は薄れることなく国民の中に残り続けている．そのため事故当時から現在まで，それらが環境中でどのように移行・変化したのかといった理解は，被汚染地域の将来にとってきわめて重要である．

一般的に環境試料中の放射性物質の検出においては，放射性核種そのものを分析するのではなく，壊変により生じるγ線等の放射線を分析する方法が用いられる．特に放射性Csについては，生成過程の異なる2種類の放射性核種（^{134}Csと^{137}Cs）の放射能比が発生源の推定に有効な指標とされる．福島第一原発事故由来の放射性物質においては，2011年3月当時に減衰補正した^{134}Cs/^{137}Cs放射能比の値が約1となることが知られているが，小森ら4)はこの値が1号機由来のものでは約0.9に，2～3号機由来のものでは約1.0となることを明らかとし，詳細な発生源の推定が可能であることを示した．さらに佐藤ら5)は，この値に加えて^{110m}Ag/^{137}Cs放射能比を指標に用いることで，福島第一原発の北西地域で採取された汚染土壌を三つのグループに分類している．しかしながら，こうした放射能分析による評価は，放射線被ばくの危険性の検証や発生源の推定には有効であるものの，物理・化学的性状や環境動態を左右する担体を含めた放射性物質そのものの直接的理解には結び付けづらい．また，一般に環境試料に含まれる放射性物質は非常に微量であるが，事故から6年以上経過したことで現在の^{134}Cs（半減期：2.07年）の放射能濃度は事故当時の

---

* E-mail：B115651@alumni.tus.ac.jp，y.abe@rs.tus.ac.jp
[1] 東京理科大学理学部：162-8601　東京都新宿区神楽坂1-3
[2] JASRI/SPring-8：679-5198　兵庫県佐用郡佐用町光都1-1-1
[3] JAEA廃炉国際共同研究センター：319-1195　茨城県那珂郡東海村白方2-4
[4] 筑波大学アイソトープ環境動態研究センター：305-8577　茨城県つくば市天王台1-1-1
[5] 気象研究所：305-0052　茨城県つくば市長峰1-1

8分の1以下にまで減少し，γ線による検出が困難になりつつある．

一方で，事故由来の放射性物質そのものを分析し，性状を明らかにした研究例も近年増加している．Niimuraら[6]は，放射性物質で汚染された土壌や植物に対してイメージングプレート（IP）を用いたオートラジオグラフィー及び溶出実験を行い，放射性Csの動的挙動を解明した．さらにAdachiら[7]は，より直接的な分析によって，事故当時に放出された放射性物質の1形態を解明した．この研究では，茨城県つくば市で事故直後に採取された大気エアロゾルから放射性Csを含む直径数マイクロメートルの球状粒子（通称Csボール）を分離し，1粒子単位での分析を行った．この研究を皮切りに，Csボールについての多くの研究[8)〜11)]が行われ，核燃料であるUとその核分裂生成物（FPs: Fission Products）及び原子炉の構成材料が混合した高酸化数のケイ酸塩ガラスの粒子であることが明らかとなった．このような放射性粒子の存在及び化学性状は，事故当時の炉内事象を理解する上できわめて重要な情報である．これまでに報告されたCsボールの^{134}Cs/^{137}Cs放射能比はいずれも約1.0であり[7)8)]，また事故当時の状況を踏まえ，現時点でCsボールは福島第一原発の2号機から放出されたものと考えられている．

上述のような1粒子レベルでの詳細な化学性状が報告されているのはCsボールのみであり，津波により最も深刻な影響を受け水素ガス爆発を生じた1号機については，事故によりどのような放射性物質が放出されたのか不明である．そこで本研究では，1号機由来と考えられる放射性粒子を1粒子レベルで分析し，その物理・化学性状を解明することを目的とした．先述の佐藤ら[5]によって原発の北西地域で採取された汚染土壌のうち，^{134}Cs/^{137}Cs放射能比により1号機由来の放射性物質を含むと推定された土壌から強放射性の粒子を分離した．この1号機由来と考えられる粒子と，2号機由来のCsボールとの間に物理・化学性状の差が見いだせれば，1号機と2号機の放射性物質の生成・放出に至る経緯の違いを化学的に考察することが可能となる．さらに^{134}Cs/^{137}Cs放射能比に代わる新たな放出源の推定指標として，放射性物質の化学性状が利用できることも期待される．その一方で，こうした事故由来の放射性物質は事故の初期状況を記録した資料でもあり，また多角的な分析を行う必要性からも，分析に伴う試料の破壊は望ましくない．そこで本研究では，大型放射光施設SPring-8におけるマイクロビームX線を用いた複合X線分析[8]に着目した．放射光マイクロビーム蛍光X線分析（SR-μ-XRF）により粒子の化学組成を，X線吸収端近傍構造分析（SR-μ-XANES）により粒子中の元素の化学状態を，粉末X線回折分析（SR-μ-XRD）により粒子の結晶構造を分析し，非破壊で放射性粒子の化学性状の解明を目指した．

2 実 験

2・1 分析試料及び分離方法

分析試料は，佐藤ら[5]の分類による福島県双葉郡浪江町の「赤グループ」の地域（R-area）で採取された土壌試料から分離した放射性粒子7粒子（Particle 1〜7）である．このグループの土壌試料は佐藤ら[5]によって，^{134}Cs/^{137}Cs放射能比から福島第一原発1号機由来の放射性物質を含むことが指摘されている．また，同様に^{134}Cs/^{137}Cs放射能比から2号機または3号機由来の放射性物質が飛来したと指摘されている同「緑グループ」の地域（G-area）の土壌試料[5]からも，放射性粒子計10粒子を分離し，物理性状及び化学組成の比較に用いた．これら土壌試料より分離された放射性粒子と，先行研究[8]のCsボールの分析結果と比較した．これらのCsボールは，2011年3月14日夜から翌朝にかけて茨城県つくば市の気象研究所にて大気エアロゾルとして採取されたものである．

分離方法は先行研究[7)8)]に準拠し，筑波大学アイソトープ環境動態研究センターにて行った．まずIP上に土壌試料を拡げて密着露光させ，オートラジオグラフィーにより放射性粒子の分布を可視化し，強放射性の粒子が存在する範囲を分離した．この分離操作を数回繰り返し行い，1粒子レベルまで絞り込みを行った．アクリル板にカプトンテープ（寺岡製作所650S #25）を貼り付けたものを用意し，この粘着面に放射性粒子1粒子を貼り付け，測定試料とした．

2・2 分析方法

2・2・1 形態観察及びγ線スペクトル測定 マルチチャネルアナライザと結合したGe半導体検出器（SEIKO EG&G製）を用いて，各試料について1粒子単位でγ線スペクトル測定を行った．得られた^{134}Cs及び^{137}Csの放射能濃度について，2011年3月11日当時として減衰補正を行った．積算時間は^{134}Csのnetカウント（中心エネルギー604 keV）が30000以上積算できるまでとした．さらに気象研究所に設置された低真空走査型電子顕微鏡（SEM: 日立ハイテクノロジーズ製SU 3500）による形態観察と，同装置に接続したエネルギー分散型X線検出器（EDS: 堀場製作所製X-max有効素子面積50 mm^2）による組成分析を行った．SEM-EDS測定に際し，蒸着等の前処理は行わなかった．

2・2・2 放射光X線分析 放射光X線分析は，SPring-8の分光分析ビームラインBL37XU[12]にて行った．このビームラインでは，アンジュレータより発生した硬X線領域の放射光をKirkpatrick-Baez（KB）ミラー集光素子によって縦横約1 μmまで集光することができ，単色X線マイクロビームをプローブとする複数のX線分析を複合的に行うことができる．試料はアクリルホルダごとX-Yステージに固

Table 1　Decay-corrected activity (as of March 2011) of ^{134}Cs and ^{137}Cs in radioactive particles 1-7 separated from soil collected at R-area located at the area northwest of the FDNPP

	Particle 1	Particle 2	Particle 3	Particle 4	Particle 5	Particle 6	Particle 7
^{134}Cs (Bq)	101 ± 0.47	42.0 ± 0.47	35.0 ± 0.2	30.2 ± 0.2	42.8 ± 1.7	66.6 ± 2.7	35.8 ± 1.4
^{137}Cs (Bq)	109 ± 0.03	45.1 ± 0.03	38.7 ± 0.1	33.3 ± 0.1	46.3 ± 1.9	71.3 ± 2.9	38.8 ± 1.6
^{134}Cs/^{137}Cs	0.93	0.93	0.90	0.91	0.92	0.93	0.92

定した．測定条件は先行研究[8)]に準拠した．本研究で用いる入射X線のエネルギーは7.0 keVから37.5 keVまでと幅広いため，測定は高エネルギー用（17.1～37.5 keV）と低エネルギー用（7.0～15.0 keV）の2回のビームタイムに分けて行った．高エネルギー測定においては，入射X線のビームサイズは試料位置で横1.0 μm×縦1.2 μmであり，散乱角90° に設置したCanberra製Si(Li)半導体検出器を用いてSR-μ-XRF及びSR-μ-XANESを行った．低エネルギー測定時のビームサイズは横0.6 μm×縦0.8 μmであり，散乱角90° に設置したシリコンドリフト検出器（Röntec製Xflash 2000）を用いたSR-μ-XRF及びSR-μ-XANESに加え，二次元検出器を用いたSR-μ-XRDを行った．すべての測定は非破壊かつ大気下で行われた．なお，高エネルギー測定と低エネルギー測定で半導体検出器の種類が異なるのは，対象としたエネルギー領域に対する検出感度の違いを考慮し，より適したものを選択したためである．

2･2･3　SR-μ-XRFによる化学組成及び元素分布の分析　37.5 keV，15.0 keV，7.0 keVに単色化された放射光X線を励起光とするSR-μ-XRFにより，各粒子の化学組成を分析した．スペクトルは1試料あたり300秒積算し，トムソン散乱強度により規格化した．またバックグラウンド（BG）として，下地であるカプトンテープ部分でも測定を行った．検出された元素について定量的な考察を行うため，様々な元素を含むガラス製認証標準物質（NIST製SRM 611，SRM 613）を粉砕して同様に分析し，検出された主要な元素について感度係数を算出し，各粒子について含有元素の半定量値を算出した．ここでいう感度係数とは，SRM611及び613の分析で得られた各元素の規格化強度を認証値で割った値のことを指し，本分析法における各元素の励起効率を意味する．さらに，XYステージ上で試料を縦横に走査してXRFイメージングを行い，各元素の分布を可視化した．イメージングにおけるステップ幅は横3.0 μm×縦3.0 μmとし，1点あたりの積算時間は2.0秒とした．イメージングの際の励起X線のエネルギーは基本的には37.5 keVとし，Cs-K$_\alpha$の分布を測定する際にはBa-K$_\alpha$線の影響を除くために36.5 keVに，低エネルギー測定時に粒子の元素分布を把握する際には15.0 keVに，Cr-K$_\alpha$線及びMn-K$_\alpha$線の分布を測定する際にはFe-K$_\alpha$線の影響を除くために7.0 keVに設定した．

2･2･4　SR-μ-XANESによる化学状態の分析　SR-μ-XRFにより検出された元素のうち，Mn，Fe，Zn，Moの4元素について，K吸収端で蛍光法のSR-μ-XANESを行い，粒子内での化学状態を調べた．これらの元素は化学状態を反映した特徴的なXANESを示し，Fe, Zn, Moの3元素については先行研究[8)]においても同様の分析が行われており，またMnについては本研究で対象とする1号機由来と考えられる放射性粒子で特徴的に検出されたため，測定元素として選定した．エネルギーのステップ幅は1 eVとし，吸収端の前後100 eVの範囲を測定した．1点あたりの測定時間は，検出された強度に応じて2～6秒で設定した．参照物質として各元素の金属，酸化物，ガラス等を用意した．ガラスに関しては，試薬のNa_2CO_3，$CaCO_3$，SiO_2を原料とするソーダ石灰ガラスに各金属の酸化物を添加し，電気炉にて酸化雰囲気で焼成して合成した．測定は原則として各粒子の中心付近で行ったが，特徴的な濃集が見られた元素については，その濃集部分についても測定を行った．

2･2･5　SR-μ-XRDによる結晶構造の分析　試料位置から200 mm後方にCMOSフラットパネルセンサーを設置し，透過型デバイ・シェラー法のSR-μ-XRDにより試料の結晶構造を分析した．入射X線のエネルギーは15.0 keVに単色化し，露光時間を440ミリ秒の測定を100回積算した．測定位置はSR-μ-XANESと同様である．なお，参照物質としてSi粉末（NIST SRM 640c）を同条件で測定し，回折パターンから算出された格子面間隔（*d*値）にずれのないことを確かめた．

3　結果と考察

3･1　粒子の放射能及び物理性状

R-areaの土壌試料より分離した放射性粒子7粒子の^{134}Csと^{137}Csの各放射能濃度，及び^{134}Cs/^{137}Cs放射能比をTable 1にまとめた．いずれも^{134}Cs/^{137}Cs放射能比は約0.9となり，この値は先行研究[4)]によれば福島第一原発1号機より放出された放射性物質に該当するものである．よって，土壌の状態で分析した^{134}Cs/^{137}Cs放射能比により1号機由来の放射性物質が含まれることが予想されていたが，実際に分離された放射性粒子を個々に分析しても，1号機由来と判断できる放射能比が示された．

これら7粒子のうち，代表的な4粒子（Particle 1～4）

の SEM 像を Fig. 1a-d に示す．先行研究7)によれば，2 号機由来とされる Cs ボールはいずれも直径数 μm の球形粒子であった．これに対し，1 号機由来の放射性粒子の形状は様々であり，また大きさも 50～250 μm と Cs ボールより明らかに大きかった．この明確な物理性状の差について，試料自体の由来の違い，すなわち土壌から分離されたか大気エアロゾルとして捕集されたかという違いが影響している可能性が考えられる．そこで Fig. 1e 及び f に，G-area の土壌試料から分離された放射性粒子の SEM 像を示す．この土壌は ^{134}Cs/^{137}Cs 放射能比により 2 号機または 3 号機由来の放射性物質を含むと判断されたものであるが，実際にこれらの土壌から分離された粒子（Fig. 1e，f）は，大気エアロゾル中から発見された 2 号機由来の Cs ボールと同様の物理性状を有していた．このことは，1 号機由来の粒子と Cs ボールとの間の物理性状の違いが，土壌か大気エアロゾルかという違いのみに起因するわけではないことを意味している．ただし，R-area と G-area とでは福島第一原発からの距離が異なるため，大きい粒子のみがより原発に近い R-area に飛来した可能性も否定はできない．1 号機由来と判断できる放射性粒子の環境中からの発見例が増えることで，こうした点も明らかになると期待される．

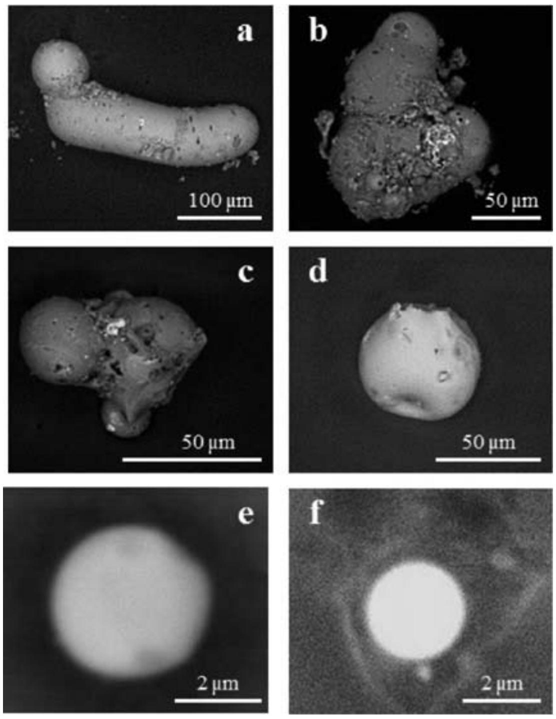

Fig. 1 SEM images of radioactive particles separated from soil samples collected at the area northwest of the FDNPP

(a) Particle 1, (b) Particle 2, (c) Particle 3, (d) Particle 4 separated from soil collected at R-area. (e, f) Radioactive particles separated from soil collected at G-area.

2 号機由来とされる Cs ボールは 1 粒子あたり 1 Bq オーダーの放射性 Cs を含む7)8)．これに対して，今回分析した 1 号機由来の粒子は 1 粒子あたり 10～100 Bq オーダーの放射性 Cs を含み（Table 1 参照），1 粒子単位での放射能として見た場合には，後者の方が明らかに高い．しかしながら粒子の大きさも考慮して比放射能を比較すると，わずか数 μm に 1 Bq レベルの放射性 Cs を含む Cs ボールの方が，比較的粒径の大きい 1 号機由来粒子よりも，比放射能が高いと言える．

1 号機由来とされる 7 粒子のうち，例として Particle 1～4 の SEM-EDS スペクトルを Fig. 2a に示している．EDS スペクトルは縦軸を対数で表記している．ここに示されていない粒子も含め，1 号機由来の粒子はすべて Si と O を主成分とすることが明らかとなった．Particle 1 及び 2 について行った，EDS による Si-K 線のマッピング結果を Fig. 2b，c に示す．いずれの粒子においても，Si の分布は Fig. 1 に示す SEM 像と対応しており，粒子全体に Si が含まれること

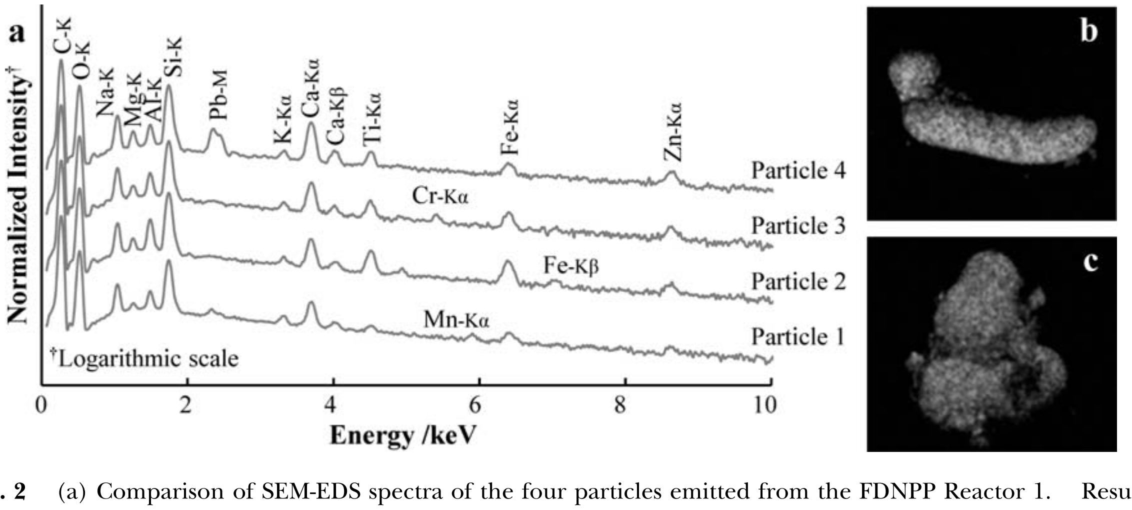

Fig. 2 (a) Comparison of SEM-EDS spectra of the four particles emitted from the FDNPP Reactor 1. Results of SEM-EDS elemental mapping of the Si-K line of (b) Particle 1 and (c) Particle 2

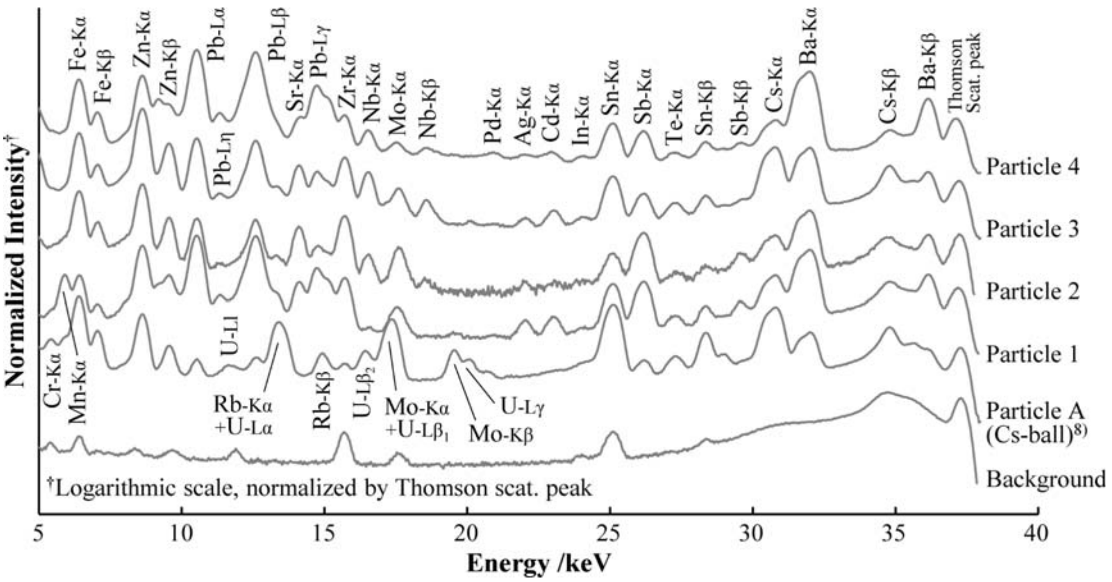

Fig. 3　Comparison of the SR-μ-XRF spectra (excited by 37.5 keV X-rays) of bulk parts of the four radioactive particles emitted from the FDNPP Reactor 1, Particle A (Cs-ball) emitted from the FDNPP reactor 2 8), and the background part of particles

Table 2　Comparison of 21 elements detected by SR-μ-XRF in radioactive particles emitted from the FDNPP reactor 1 and Cs-balls emitted from the FDNPP reactor 2 (○, detected in common; △, detected from some particles; ×, not detected)

	Cr	Mn	Fe	Ni	Zn	Rb	Sr	Zr	Nb	Mo	Pd	Ag	Cd	In	Sn	Sb	Te	Cs	Ba	Pb	U
Particles from reactor 1	△	○	○	△	○	△	○	○	○	○	△	○	○	△	○	○	○	○	○	○	△
Cs-balls	△	○	○	×	○	○	×	○	×	○	×	△	×	△	○	○	○	○	○	△	△

がわかる．これらの結果は，Cs ボール9)〜11)と同様に，1号機由来の粒子も Si と O を主成分とする物質であることを示すものである．また EDS スペクトルでは Fe 及び Zn も検出されているが，これも Cs ボールと類似する特徴7)である．ただし，Cs ボールでは EDS スペクトルにおいても Cs-L 線が検出されたが，1号機由来の粒子においては，EDS による分析では Cs-L 線は検出されなかった．この違いは粒子の Cs の濃度に起因するものであり，先述の比放射能の違いとも対応する．これは1号機と2号機の炉内状況の違い，または粒子の生成・放出過程の違いを反映していると考えられる．

3・2　化学組成と元素分布の解明

1号機由来の7粒子について SR-μ-XRF 分析を行った結果，検出された元素は定性的に類似していた．ここでは検出された元素をすべて網羅できる代表的な4粒子（Particle 1〜4）を例として，37.5 keV 励起で得られた SR-μ-XRF スペクトルを Fig. 3 に示す．これらのスペクトルは縦軸を対数で表記している．なお，後述するようにこれらの粒子には局所的な元素の濃集が存在するが，ここで示したスペクトルはいずれもバルク部分で得られたものである．また比較のために，先行研究8)で分析された3粒子の Cs ボールのうち Particle A のスペクトルと，下地であるカプトン部分のスペクトルについても合わせて示してある．Fig. 3 より，1号機由来の粒子からは，γ線スペクトル測定（Table 1）で検出されていた Cs 以外にも，様々な元素が検出された．15.0 keV 及び 7.0 keV 励起による結果も合わせ，一連の SR-μ-XRF によって1号機由来の粒子及び Cs ボール8)から検出された21元素を Table 2 にまとめ，化学組成を定性的に比較した．Fig. 3 から読み取れるように，1号機由来の粒子は Sr や Ba など還元雰囲気で揮発性が高くなる元素11)を特徴的に含むのに対し，Cs ボールでは酸化雰囲気で揮発性が高くなる Rb が多く検出された．他にも，全体的に1号機由来の粒子の方が含有元素の種類に富み，組成的な違いが見いだされた．

続いて SR-μ-XRF イメージングにより，各元素の粒子内での分布を可視化した．例として Particle 1 の末端部分に対して，元素分布の議論に足る十分な強度が得られ，かつ

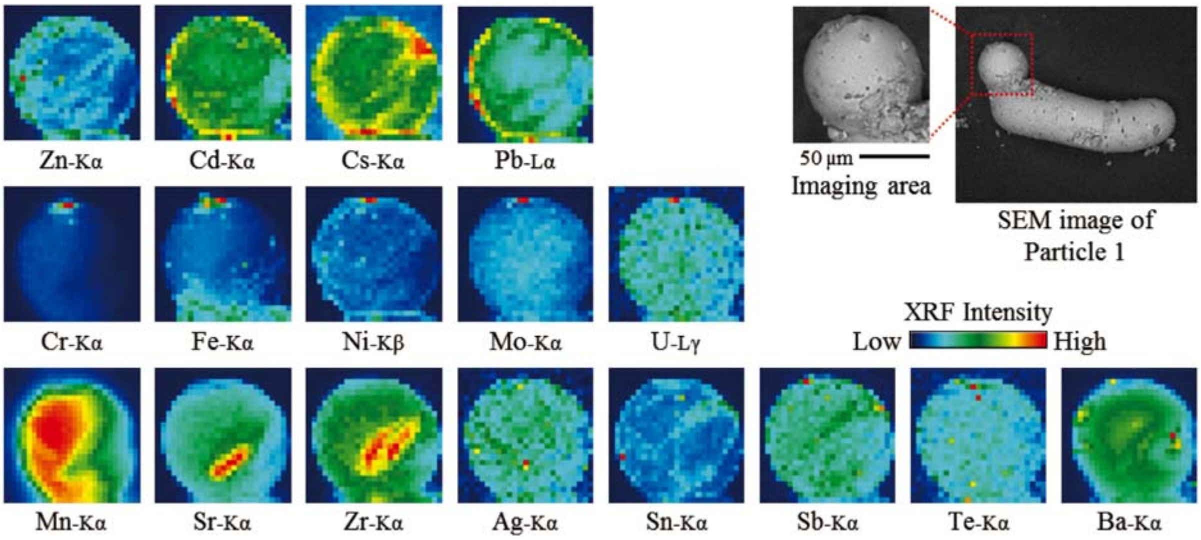

Fig. 4 Distributions of 17 representative elements in Particle 1 obtained by SR-μ-XRF imaging with SEM images corresponding to the imaging area

他の元素との顕著なピークの重複がなかった17元素について，イメージングの結果をFig. 4に示す．Csボールにおける元素分布は，粒子内にnmオーダーで一部元素の濃集が存在することが指摘されているものの[9]，本研究と同じSR-μ-XRFイメージングでは粒子内での顕著な組成的偏在は見られず[8]，比較的均一な組成を有していると考えられる．これに対し1号機由来の粒子においては，粒子内で元素が不均一に分布していることが明らかとなった（Fig. 4参照）．分析した範囲内では，Zn，Cd，Cs，Pbの4元素は比較的類似した分布を示し，粒子の外縁部で強度が高いため，表面に多く存在するものと考えられる．Csボールにおいても，Csが粒子表面に多く存在する可能性が指摘されており[9][10]，関連性に興味が持たれる．さらにCr，Fe，Ni，Moについては粒子末端の数μmの領域に濃集していることが明らかとなり，この点からはUのL線も検出された．Mnは粒子全体に分布していたが，その他の元素はそれぞれ独自の分布を示し，一部元素では数μmの濃集点も見られた．

次にSR-μ-XRFにより1号機由来の放射性粒子から検出された21元素（Table 2）について，Csボールに関する先行研究[8]を基に，その起源を推定した．Uは核燃料に由来すると考えられ，14種類の重元素（Rb，Sr，Zr，Nb，Mo，Pd，Ag，Cd，In，Sn，Sb，Te，Cs，Ba）については核燃料のFPsに含まれる元素である．ただしZrとSnについては，燃料被覆管のZr-Sn合金に由来する可能性も考えられる．なお，ここでSR-μ-XRFにより検出されたAgに関連して，1号機由来の放射性物質を含むR-areaの土壌からは^{110m}Agが検出されている[5]．Pbは格納容器内側のPb板に由来すると考えられ，金属Pbは融点が327.5℃と極めて低いため，容易に熔融したと予想される．Cr，Mn，Fe，Ni，Znについては，原子炉の構成材料に由来するものと考えられる．特にCr，Fe，Niは一般的なステンレス鋼に含まれており，これにMoを加えたSUS316及びSUS316Lは耐腐食性に優れ，福島第一原発1号機炉内でも使用されていた可能性が高い．先述の通り，これらの4元素は同一点に濃集しており，Moを含むステンレス鋼がこの濃集点の生成に深く関係していると推定される．またMn，NiとMoについては，圧力容器のMo-Mn-Ni鋼に由来する可能性もある．Znについては，先行研究[8]では一次冷却水の添加材としているが，上記の構成材料に含まれるか，鍍金として利用されていた可能性も考えられる．これらの元素のほかに，EDSスペクトル（Fig. 2a）では，Siを主成分としてCからCaまでの様々な元素が検出されており，断熱材またはコンクリートに由来するものと推定されるが，具体的な起源を特定するには，実際に炉内で使用されていた物質との直接比較が不可欠である．

3・3 化学状態と結晶構造の解明

Particle 1～3のMn-K吸収端のSR-μ-XANESスペクトルについて，参照物質と合わせてFig. 5aに示す．先述のSR-μ-XRFと同様に，今回分析した7粒子について同様のスペクトルが得られているため，ここでは例として3粒子の結果を示している．3粒子のスペクトルは粒子中央付近で得られたものであり，粒子本体の化学状態を見るために，元素濃集等がないバルク部分を選んでいる．ここに示されていない4粒子も含め，1号機由来の粒子のスペクトルはすべて類似した形状となり，細かな構造を示さない滑らかなスペクトルであったことから，ガラス中にイオンとして存在する状態であると考えられる．また酸化数の異なる参照物質とスペクトルのホワイトラインのエネルギーを比較

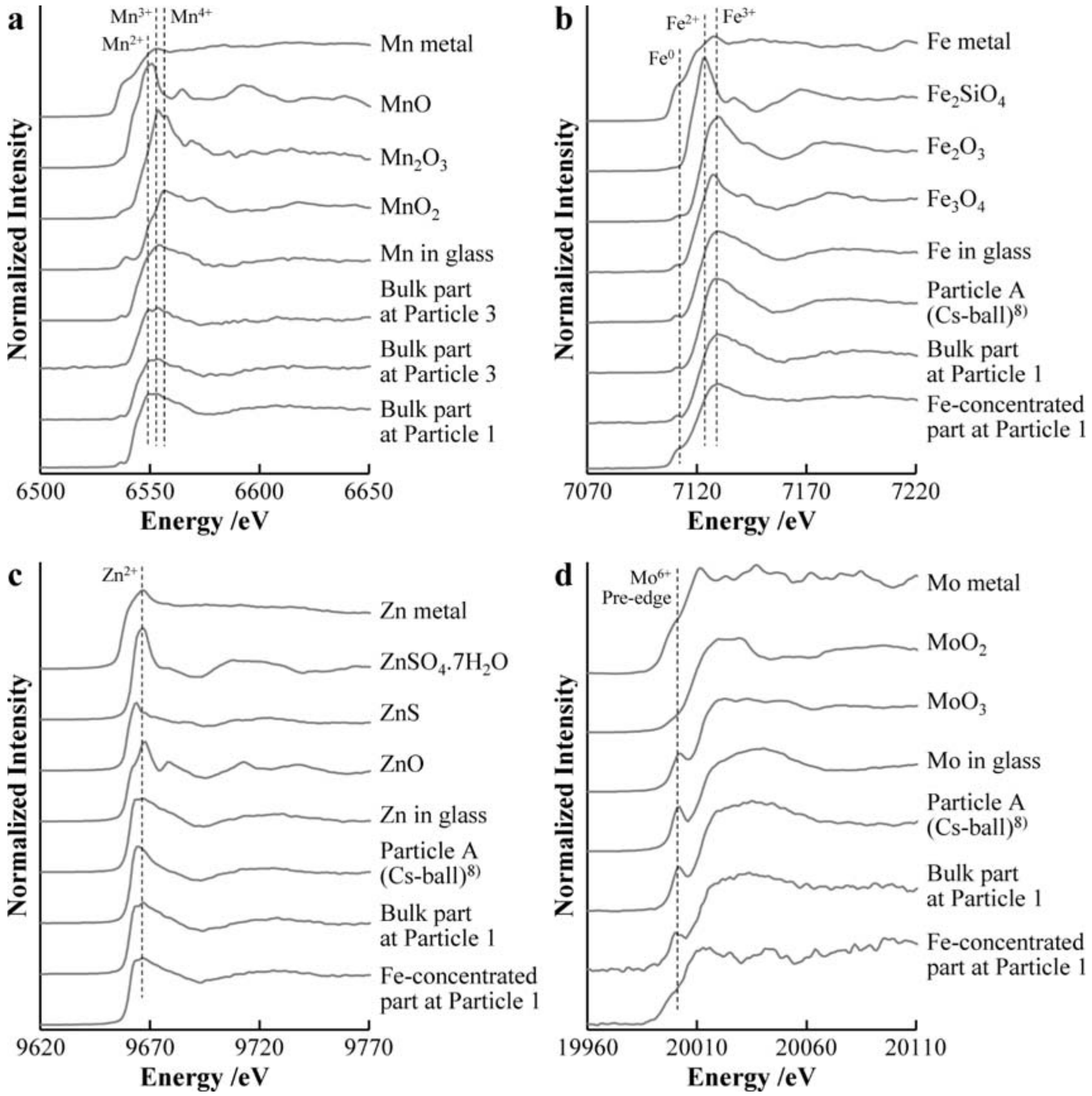

Fig. 5　Results of SR-μ-XANES analyses

Comparison of the (a) Mn-K edge, (b) Fe-K edge, (c) Zn-K edge and (d) Mo-K edge SR-μ-XANES spectra of the radioactive particles and the reference materials.

した結果，Mn^{2+}及びMn^{3+}に対応しており，比較的低い酸化数で存在していることが示された．

続いてParticle 1に着目して，粒子本体部分と，Fig. 4で見られるFe等の濃集点の2か所について，Fe，Zn，MoのK吸収端SR-μ-XANESスペクトルをFig. 5b-dに示す．また比較として，先行研究[8]よりCsボールのParticle Aと，各元素の参照物質のスペクトルも示した．まずParticle 1の粒子本体部分については，Fe，Zn，Moの3元素とも，ガラス中に存在する場合のスペクトルと形状が一致した．特にMo-K吸収端（Fig. 5d）の結果を見ると，Mo^{6+}に特徴的なプリエッジピークが検出されており，高酸化数の状態で存在しているものと考えられる．またFeについても，スペクトルのホワイトラインのエネルギーから，Fe^{3+}が主体であると考えられる．これら3元素のSR-μ-XANESによる高酸化数でガラス状態という結果は，先行研究[8]のCsボールのものとも類似していた．さらに，Particle 1の本体部分についてSR-μ-XRDを行ったが，回折ピークは検出されず，ガラス状態であるとするSR-μ-XANESの結果を支持した．先述のSEM-EDS分析の結果と合わせ，Csボールと同様に，1号機由来の粒子についてもケイ酸塩ガラスが主成分であると考えられる．ケイ酸塩ガラスは環境中で比較的高い安定性を持つため，水溶性の放射性物質とは異なり，この粒子に含まれる放射性核種が環境中に溶脱・拡散していく危険性は低いと考えられる．同時にこの結果は，これらの放射性粒子が環境中で長期的な影響力を持つことを示唆している．

続いて，Particle 1におけるFe等の濃集点（Fig. 4参照）について得られたSR-μ-XANESスペクトルを見てみると，

Table 3　Lattice spacing (*d*-value/Å) of Fe-concentrated part on radioactive particles 1-7 detected by the SR-μ-XRD

Particle No.							α-Fe_2O_3 [14]
1	2	3	4	5	6	7	*d*/hkl
1.81	1.79	1.85	—	—	—	—	1.841/024
1.91	—	—	—	—	—	—	—
2.10	2.11	—	2.03	2.09	2.09	—	—
—	2.22	2.22	—	—	—	—	2.207/113
—	2.32	2.33	—	—	—	2.35	—
—	2.53	2.53	2.60	2.51	2.53	—	2.519/110
2.70	2.71	2.72	—	—	—	—	2.700/104
—	—	—	—	2.95	2.95	—	—
3.20	—	—	—	—	—	—	—
3.34	—	3.35	3.35	—	—	—	—
—	3.70	3.70	—	—	—	—	3.684/012
4.20	—	—	—	—	—	—	—

濃集と無関係なZn（Fig. 5c）では本体部分との明確な差は見いだせなかったが，Fe（Fig. 5b）及びMo（Fig. 5d）については，本体部分と濃集点とで異なるスペクトル形状となった．MoについてはMo^{6+}に特徴的なプリエッジピークが検出されず，Feについても低酸化数の化合物または金属の状態にある可能性が示された．この濃集点についてSR-μ-XRDを行ったところ，本体部分では見られなかった明瞭な回折ピークが多数検出され，結晶性物質の存在が明らかとなった．同様のFeの局所的な濃集は他の6粒子にも存在し，いずれからもSR-μ-XRDにより回折ピークが検出された．7粒子のFe濃集点で得られた回折パターンから算出した*d*値をTable 3にまとめた．異なる粒子間で共通する*d*値の回折線も検出されており，あるいは類似した結晶性物質が複数の粒子に含有されている可能性もある．特に*d*値が3.7，2.7，2.5，2.2，1.8 Åのものについては，それぞれα-Fe_2O_3[14]の012面（d＝3.684 Å，相対強度30），104面（d＝2.700 Å，相対強度100），110面（d＝2.519 Å，相対強度70），113面（d＝2.207 Å，相対強度20），024面（d＝1.841 Å，相対強度40）に対応するものと考えられる．すなわち，1粒子内でガラスの基部と数μmオーダーの結晶性物質が混在しており，化学状態が不均一であるという興味深い結果が示された．

現時点でこれらの結晶性物質について十分な相同定がなされたとは言い難く，またParticle 1のようにMoやU等の特徴的な重元素を含まない場合には，Fe濃集点は土壌からの付着物である可能性も考えられる．顕微ラマン分光分析法等の微小物質の同定に優れた手法の導入，あるいは破壊分析になってしまうものの，結晶部分のみをピックアップしてガンドルフィーカメラを用いたXRDを行うことで，これらの結晶性物質の正体が解明されるものと期待される．

3·4　事故当時の炉内状況の推定

上記の通り，1号機由来と考えられる放射性粒子に関して，2号機由来とされるCsボールとは異なる物理・化学性状を有することが明らかとなった．以下ではその性状の違いに基づき，事故当時の1号機と2号機の炉内状況の違いと，粒子の生成・放出過程を考察する．

化学組成における重要な違いは，先述した通り1号機由来の粒子がSrやBaといった還元雰囲気下で揮発性が高くなる元素を特徴的に含む点である．これは粒子の生成段階で1号機と2号機の炉内雰囲気に差があったことを示唆する重要な知見である．続いてSR-μ-XANESの結果を見ると，低酸化数であるとする結果（Mn及び濃集点でのMo）と，高酸化数であるとする結果（Fe及び本体部分のMo）の双方が示された．粒子の生成後に金属元素の還元反応が進行するとは考えづらいため，1号機由来の粒子は還元雰囲気下で生成し，高温のまま大気中に放出されたことで，一部の元素が酸化したものと考えられる．1号機由来の粒子とCsボールの双方とも，SiやCr，Mn，Fe，Znといった炉の構成材料に由来する元素を多く含むことから，どちらの炉においても粒子の生成過程で燃料周辺のみならず炉自体も一部熔融していたことがわかる．また，放出までの熔融の進行状況，または1号機と2号機で使用されていた炉材の違いが，これらの元素の含有量の違いに現れていると考えられる．

特定の時間に捕集された大気エアロゾルと異なり，土壌試料の場合には時間分解能を持たないため，本来は今回の粒子がいつ福島第一原発から放出されたものであるかは判断できない．ただし今回発見された1号機由来とされる粒子について，2011年3月12～13日のベントや水素爆発などにより放出された放射性物質が原発から北側に輸送されたとする鶴田ら[15]の結果を踏まえると，これらの粒子は3月12～13日に放出された可能性が高いと推察される．この場合，11日14時46分に発生した地震からわずか1日の

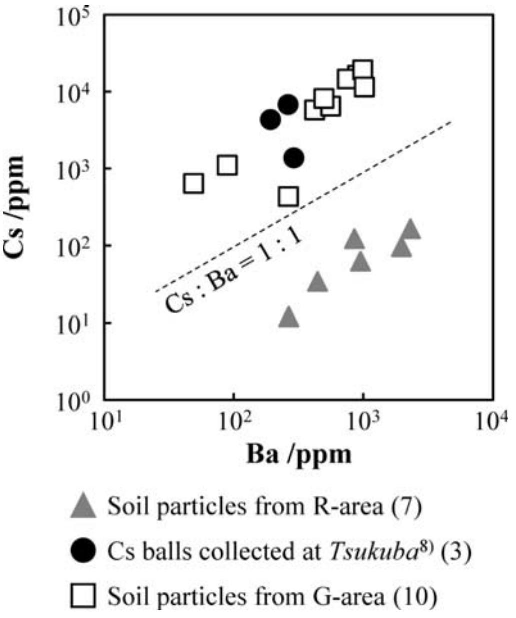

Fig. 6　Plot of semi-quantitative values of Cs and Ba in the radioactive particles separated from soil collected at R-area（$n = 7$），the Cs-balls collected at Tsukuba（$n = 3$）8) and the radioactive particles separated from soils collected at G-area（$n = 10$）．

間に，1号機炉内で核燃料と周辺炉材の熔融反応が進行したことになる．先述のように，これらの粒子の生成当時に炉内が還元雰囲気にあったとする分析結果が示されているが，12日の時点で1号機炉内には水素ガスが充満していたと考えられ，推定された炉内状況と対応している．また，これらの粒子の化学組成及び化学状態の不均一性は，事故発生から放出までの時間が短かったとする推察とも合致する．12日の水素爆発は炉心ではなく原子炉建屋で発生したものであるため，今回の放射性粒子の生成過程に水素爆発が直接的に関係しているとは判断できない．ただし，これらの粒子が比較的大きく，また歪な形状を持つ点を踏まえると，水素爆発がその主要な放出過程の一つであった可能性は高く，格納容器の破損及びベント（容器内圧力を下げるための蒸気の放出作業）に伴い2号機より放出されたCsボールとは異なる放出過程であったと考えられる．

3･5　化学組成を用いた発生源の分類

冒頭に述べた通り，福島第一原発の1号機と2～3号機では放射性物質の^{134}Cs/^{137}Cs放射能比に差が見られるが，事故後6年以上が経過したことにより，^{134}Csの検出が困難になりつつある．そこで1号機由来の放射性物質と2～3号機由来の放射性物質の新しい判別基準として，化学組成による分類を提案する．ここまで述べてきた通り，1号機由来の放射性物質と2号機由来のCsボールには化学組成に差が見られる．そこで，R-areaの1号機由来の放射性粒子7粒子と，G-areaの土壌から分離した放射性粒子10粒子，先行研究8)で分析されたCsボール3粒子を対象に，SR-µ-XRFにより検出された15元素（Table 2）について，トムソン散乱線で強度を規格化した蛍光X線強度と，標準物質より算出した感度係数を用いて，半定量値を算出した．得られた半定量値のうち，BaとCsについてプロットを作成した（Fig. 6）．この図から1号機由来の粒子とCsボールには，明確な組成の差があることが見てとれる．ここでG-areaの土壌より分離された10粒子を見てみると，Csボールと同様の組成的特徴を有していた．G-areaには2～3号機由来の放射性物質が飛来していた可能性が指摘されていることから5)，土壌の分析結果と粒子の分析結果が矛盾なく対応した．現時点でこれらの数値は半定量値であり，本法の定量精度については検証・改良の余地があるものの，ここまで明確な組成差があれば十分に分類することが可能であると言えよう．よって環境試料から分離された放射性物質に対しては，^{134}Cs/^{137}Cs放射能比に代わる新たな分類指標として化学組成が有効であることが本研究により実証された．

4　結　　論

本研究は，福島第一原発1号機より放出された放射性粒子の化学性状を非破壊の放射光X線分析により解明し，2号機由来とされるCsボールとは異なることを実証した．1号機由来の粒子はCsボールに比べて明らかに大型で歪な形状なものが多かったが，比放射能はCsボールに比べて低かった．SR-µ-XRFにより，1号機由来の粒子はCsボールに比べて含有する重金属の種類に富み，特にSrやBaといった還元雰囲気で揮発性が高くなる元素を特徴的に含むことが明らかとなった．また粒子内で元素が不均一に分布しており，Csを含む一部の元素は表面に多く存在していたのに対し，FeやU等，一部の元素が数µmの範囲に濃集している点も見られた．粒子本体はSi及びOを主成分としており，SR-µ-XANES及びSR-µ-XRDからも，この粒子がケイ酸塩ガラスであることが示された．ただしFe等の元素が濃集していた点では，X線回折データにより酸化物等の結晶性物質が存在しており，粒子内で化学状態にも不均一性が見られた．これらの粒子は2011年3月12～13日に放出されたと考えられ，あるいは12日の水素ガス爆発がその主要な放出要因であった可能性が示唆された．この結果は，1号機炉内において，きわめて早い段階で燃料と周辺の構成物の熔融が進行していたことを示すものである．さらに，放射性粒子の化学組成が放出源を推定の指標として有効であることが示された．

こうした環境中より分離された放射性粒子の化学性状の理解は，事故事象を読み解くための情報を与えるだけでなく，人体及び環境への影響の評価，さらには環境中からの

効率的な除去法の開発へもつながる重要な知見である．福島第一原発の解体作業が進行することで，本研究で扱ったような粒子と，実際に炉内に残されていた物質との直接的な比較が可能になると期待される．

謝　辞

本研究をご理解いただき，ご協力くださった福島県双葉郡浪江町自治体に厚く御礼申し上げます．

本研究の一部は，科研費新学術領域「福島原発事故により放出された放射性核種の環境動態に関する学際的研究（領域代表恩田裕一筑波大学教授）」の一環として，研究費補助金（公募研究，課題番号：25110510，15H00978/計画研究，課題番号：24110003）の支援により実施されました．並びに，「平成28年度放射性物質環境動態・環境および生物への影響に関する学際共同研究（重点共同研究A）」による支援を受けました．

本研究の放射光実験は高輝度光科学研究センター SPring-8 一般利用課題（課題番号：2014A1403，2014B1493，2015A1895，2015B1828，2016A1705）として行われました．ここに謝意を表します．

（平成27年9月9日，平成28年9月14日，日本分析化学会第64，65年会及び平成28年1月11日，第29回日本放射光学会において，一部発表）

文　献

1) MEXT : Japanese Ministry of Education, Culture, Sports, Science and Technology, <http://www.mext.go.jp/>, (accessed 2016-10-11).
2) NAIIC : The National Diet of Japan Fukushima Nuclear Accident Independent Commission, <http://warp.da.ndl.go.jp/info:ndljp/pid/3856371/naiic.go.jp/report/>, (accessed 2016-10-11).
3) TEPCO : Tokyo Electric Power Company Holdings, Inc., <http://www.tepco.co.jp/index-j.html>, (accessed 2016-10-11).
4) 小森昌史，小豆川勝見，野川　憲，松尾基之：分析化学 (*Bunseki Kagaku*), **62**, 475 (2013).
5) 佐藤志彦，末木啓介，笹　公和，松中哲也，柴山尚大，高橋　努，木下哲一：放射化学，**31**, 28 (2015).
6) N. Niimura, K. Kikuchi, N. D. Tuyen, M. Komatsuzaki, Y. Motohashi : *J. Environ. Radioactiv.*, **139**, 234 (2014).
7) K. Adachi, M. Kajino, Y. Zaizen, Y. Igarashi : *Sci. Rep.*, **3**, 2554 (2013).
8) Y Abe, Y Iizawa, Y Terada, K Adachi, Y Igarashi, I Nakai : *Anal. Chem.*, **86**, 8521 (2014).
9) N. Yamaguchi, M. Mitome, K. Akiyama-Hasegawa, M. Asano, K. Adachi, T. Kogure : *Sci. Rep.*, **6**, 20548 (2016).
10) T. Kogure, N. Yamaguchi, H. Segawa, H. Mukai, S. Motai, K. Akiyama-Hasegawa, M. Mitome, T. Hara, T. Yaita : *Microsc.*, doi:10.1093/jmicro/dfw030, (2016).
11) Y. Satou, K. Sueki, K. Sasa, K. Adachi, Y. Igarashi : *Anthr.*, **14**, 71 (2016).
12) Y. Terada, H. Yumoto, A. Takeuchi, Y. Suzuki, K. Yamauchi, T. Uruga; *Nucl. Instrum. Meth. Phys. Res. A*, **616**, 270 (2010).
13) 三輪周平，天谷政樹，田中康介，逢坂正彦，永瀬文久：JAEA-Review, 2013-034 (2013).
14) ICDD : The Powder Diffraction File, PDF. International Centre for Diffraction Data, (2006).
15) 鶴田治雄，中島映至：地球化学，**46**, 99 (2012).

Investigation of the Chemical Characteristics of Individual Radioactive Microparticles Emitted from Reactor 1 by the Fukushima Daiichi Nuclear Power Plant Accident by Using Multiple Synchrotron Radiation X-ray Analyses

Takahiro ONO[*1], Yushin IIZAWA[1], Yoshinari ABE[*1], Izumi NAKAI[1], Yasuko TERADA[2],
Yukihiko SATOU[3], Keisuke SUEKI[4], Kouji ADACHI[5] and Yasuhito IGARASHI[5]

[*] E-mail : B115651@alumni.tus.ac.jp, y.abe@rs.tus.ac.jp

[1] Department of Applied Chemistry, Faculty of Science, Tokyo University of Science, 1-3, Kagurazaka, Shinjuku-ku, Tokyo 162-8601

[2] Japan Synchrotron Radiation Research Institute (JASRI), SPring-8, 1-1-1, Kouto, Sayo-cho, Sayo-gun, Hyogo 679-5148

[3] Japan Atomic Energy Agency, 2-4, Shirakata, Tokai-mura, Naka-gun, Ibaraki 319-1195

[4] Faculty of Pure and Applied Sciences, University of Tsukuba, 1-1-1, Tennodai, Tsukuba-shi, Ibaraki 305-8577

[5] Meteorological Research Institute, 1-1, Nagamine, Tsukuba-shi, Ibaraki 305-0052

(Received October 14, 2016; Accepted February 15, 2017)

Seven radioactive particles were separated from a soil sample collected at the Northwest region of the Fukushima Daiichi Nuclear Power Plant (FDNPP). It has been pointed out that the soil is contaminated by radioactive materials emitted from reactor 1 of the FDNPP by the accident that occurred in March, 2011. The physical characteristics of these radioactive particles with –100 μm in diameter and non-uniform shape are clearly different from those of spherical microparticles, known as Cesium-balls, thought to be emitted from the FDNPP reactor 2. Three kinds of synchrotron radiation-based X-ray analyses (X-ray fluorescence analysis, X-ray absorption near edge structure analysis and X-ray diffraction analysis) were nondestructively applied to radioactive particles using a micro-focused X-ray beam at the SPring-8 to investigate their detailed chemical properties. Various elements related to fission products of nuclear fuel and components of the reactor were detected from the particles emitted from the FDNPP reactor 1 with an obvious heterogeneous elemental distribution. In particular, the chemical compositional feature of these particles was characterized by several elements (Sr, Ba *etc.*), which were easily volatilized in a reducing atmosphere. Although a main component of the particles was identified as silicate glass similar to the Cesium-balls, some crystalline materials were also found in microscopic regions containing Fe and other metallic elements. We concluded that these radioactive particles were emitted from reactor 1 to the atmosphere during 12th to 13th March, 2011. Our results suggest the fact that the nuclear fuel and the reactor vessels around the fuel were melted together at a very early stage of the accident. In addition, it was demonstrated that chemical compositional information of individual radioactive materials can be a new indicator as an alternative to the radioactive ratio to estimate the source of emissions.

***Keywords*:** Fukushima Daiichi Nuclear Accident; radioactive material; synchrotron radiation X-ray analysis; micro-XANES; radioactive microparticles.

Anthropocene 14 (2016) 71–76

Contents lists available at ScienceDirect

Anthropocene

journal homepage: www.elsevier.com/locate/ancene

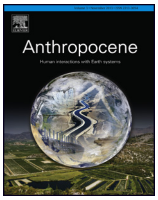

Short communication

First successful isolation of radioactive particles from soil near the Fukushima Daiichi Nuclear Power Plant

Yukihiko Satou[a,*], Keisuke Sueki[b], Kimikazu Sasa[b], Kouji Adachi[c], Yasuhito Igarashi[c]

[a] *Graduate School of Pure and Applied Sciences, University of Tsukuba, 1-1-1 Tennodai, Tsukuba, Ibaraki 305-8577, Japan*
[b] *Faculty of Pure and Applied Sciences, University of Tsukuba, 1-1-1 Tennodai, Tsukuba, Ibaraki 305-8577, Japan*
[c] *Atmospheric Environment and Applied Meteorology Research Department, Meteorological Research Institute, 1-1 Nagamine, Tsukuba, Ibaraki 305-0052, Japan*

ARTICLE INFO

Article history:
Received 25 November 2015
Received in revised form 27 April 2016
Accepted 8 May 2016
Available online 10 May 2016

Keywords:
Fukushima Dai-ichi Nuclear Power Plant accident
Silicate compounds
Radiocaesium-bearing particle

ABSTRACT

The Fukushima Daiichi Nuclear Power Plant (F1NPP) accident in 2011 released radionuclides into the atmosphere in both aerosol and gaseous form. Subsequent studies of contamination in the environment have focused on the bulk radioactivity in samples. Comparatively little is known about the relative contribution and patterns of soluble versus particulate deposition of the radionuclides.

We investigated a sample of heavily contaminated surface soil from a site 20 km northwest of the F1NPP and isolated four radioactive particles from the surrounding soil. These particles had a maximum particle area equivalent diameter of 6.4 μm and a maximum ^{137}Cs radioactivity of 67.5 ± 0.1 Bq per particle. They were larger than the particles identified in aerosol samples shortly after the accident at a location 170 km southwest of the F1NPP. Two of the particles were spherical and two were fragmental.

Silicates were a major component of the Fukushima radioactive particles. These characteristics clearly differ from the so-called hot particles observed at the Chernobyl accident in 1986. Clarifying the physical and chemical properties of the radionuclides released from the F1NPP accident is important for assessing the potential long-term impacts to humans.

1. Introduction

The Fukushima Daiichi Nuclear Power Plant (F1NPP) accident, caused by tsunami damage following the Great East Japan Earthquake on 11 March 2011, released enormous amounts of radioactive material into the atmosphere. Radiocaesium (Radioactive Cs) was one of the most abundant radionuclides released into the environment during the F1NPP accident, with an estimated radioactive Cs release on the order of 9–36 PBq (Terada et al., 2012; Stohl et al., 2012; Katata et al., 2015; Winiarek et al., 2012). Understanding the physical and chemical properties of the emitted radioactive caesium is important to accurately evaluate the possible impacts to human health and to assess the long-term distributions of these particles after deposition in residential areas, agricultural fields, mountains, and aquatic environments. In the early stages of the F1NPP accident, radioactive Cs-bearling particles 2–10 μm in diameter was dominant (Doi et al., 2013; Miyamoto et al., 2014). In addition, radioactive Cs were transported from catchment to downstream as suspended matters (Chartin et al., 2013; Lepage et al., 2016). And, it was stored in river basin as sediment (Kitamura et al., 2014). However, the chemical forms of radioactive Cs were unclear at that time.

To investigate the chemical forms of radioactive Cs, Adachi et al. (2013) isolated radioactive water-insoluble microspheres from atmospheric samples collected on 14 and 15 March in Tsukuba, which is approximately 170 km southwest of the F1NPP. The radioactive particles were isolated from the aerosol samples using a scanning electron microscope equipped with an energy dispersive X-ray spectrometer (SEM–EDS). The particles contained Cs, O, Fe, and Zn and were several micrometres in diameter; the ^{137}Cs activity of the particles was approximately 2–3 Bq per particle. These particles were collected from the plume that was released on 14 and 15 March, but they were not observed in aerosol samples from other plumes, such as one that occurred 20–21 March 2011. Abe et al. (2014) used state-of-the-art synchrotron X-ray spectroscopy to examine the chemistry of the Cs-bearing particles isolated by Adachi et al. (2013). They concluded that the particles: (1) contained elements derived from nuclear fission processes and from nuclear reactor and fuel materials; (2) were amorphous; (3) were highly oxidized; and (4) consisted of glassy

---

[*] Corresponding author.
E-mail address: yukihiko@ied.tsukuba.ac.jp (Y. Satou).

http://dx.doi.org/10.1016/j.ancene.2016.05.001
2213-3054/

spherules formed from a molten mixture of nuclear fuel and reactor material. Yamaguchi et al. (2016) recently found similar Cs-bearing particles from deposits on non-woven fabric cloth and on a needle of Japanese cedar in Fukushima and showed their internal compositions using a focused ion beam and a transmission electron microscope. In contrast, Kaneyasu et al. (2012) showed that radioactive Cs was hosted in sulfate aerosols, as determined by a particle size analysis of the radioactive material and measurements of non-radioactive aerosol chemical components in April–May 2011. Kaneyasu et al. (2012) argued that the Cs-bearing sulfate aerosols were submicron in size and soluble in water; such particles would behave differently than the Cs-bearing particles reported by Adachi et al. (2013). Therefore, it is thought that the physical and chemical forms of the radioactive Cs emitted during the F1NPP accident, as well as their release times, varied considerably. In particular, soluble radioactive Cs has been assumed to distribute rather uniformly in the dose calculation in human body. However, the presence of high concentrated insoluble radioactive Cs-bearing particle in the early F1NPP plume could result in underestimation of internal exposure in human body who had been exposed to such plume. For instance, effective dose coefficients for inhalation become the larger if radioactive Cs is the less soluble (e.g. ICRP Publication 119).

The radioactive solid particles observed at nuclear power plant accidents, nuclear tests, operations of nuclear fuel reprocessing factory, and other nuclear disasters (Salbu, 2011). For example, radioactive particles so-called hot-particles were observed around the Chernobyl Nuclear Power Plant site (Sandalls et al., 1993). Most of the radioactive particles were fine particles of uranium oxide. The Chernobyl accident happened phreatic explosion, and nuclear reaction resulting fire (Tcherkezian et al., 1994). Windscale accident in 1957 also happened core fire, which resulting in emission of radioactive particles from the stack to the atmosphere (Salbu et al., 1994). Emissions of radioactive particles were anticipated in the F1NPP accident (Salbu, 2011). However, a core fire and phreatic explosion did not occur in the F1NPP accident. The explosions of unit 1, 3, and 4 were hydrogen explosions (TEPCO, 2012). The unit 4 hydrogen explosion occurred in the reverse flow of hydrogen generated in unit 3. In addition, in the Cs-bearing particles isolated by Adachi et al. (2013) and Abe et al. (2014) only isotopes of radioactive Cs were detected by activity measurements. Other radionuclides (e.g. Co, Ru, Ag, Sn, Sb, and Am) were not detected. Thus, it is suspected that radioactive particles were released directly from the reactor, and further investigation of the Cs-bearing particles is necessary to reveal their chemical and physical features. It is also necessary to identify the differences between the Fukushima radioactive particles and those in other incidents to gain basic scientific information useful for efforts such as environmental and health impact assessment, decontamination, and decommission.

The Cs-bearing particles have not been found from aerosol samples from known plumes in Fukushima Prefecture, which is closer to the release site and the location of the most severe contamination. In contrast, studies applying autoradiography have shown high-intensity spots of autoradiographic images in samples of soil (Itoh et al., 2014; Niimura et al., 2015; Satou et al., 2015; Yanaga and Oishi, 2015), forest leaves, vegetables, and dust from inside a building 40 km south of the F1NPP (Kashimura et al., 2013; Shibata et al., 2013; Tanaka et al., 2013). These results imply the presence of radioactive particles. None of the studies, however, have confirmed the chemical and physical properties of Cs-bearing radioactive particles by isolating them.

Heavy contamination by radionuclides occurred to the area northwest of the F1NPP on the same day (Katata et al.,2015). Within 30 km-range from the F1NPP site is about the same range of much of the radioactive particles (so-called hot particles) were found in the case of the Chernobyl accident (Sandalls et al., 1993). The particles had different characteristics, depending on the sampling locations and the distance from the accident site (Salbu and Kerkling, 1998). Therefore, the radioactive particles obtained closer to the nuclear power plant would be expected to give even more information about the accident. Thus, we aim to investigate the radioactive particles' distribution in the northwest area of the F1NPP which has not been made hitherto. We addressed the following questions. First, did radioactive particles come from the F1NPP? Second, did spot type contaminations come from Cs-bearing particle?

2. Materials and methods

2.1. Sample collection

A soil sample was collected at a location approximately 20 km northwest of the F1NPP on 12 June 2013, twenty-seven months after the accident. We collected five surface samples of soil from a location at 37°33′30″N, 140°49′38″E (Fig. 1), inside the exclusion zone located northwest of the F1NPP. This zone is distinguished by high air dose rates, based on airborne monitoring by the Ministry of Education, Culture, Sports, Science and Technology (MEXT). The location was the highest air dose rate spot within our entry permission. This land, which was used as a paddy field before the accident, has been abandoned and vegetation has therefore regrown. We sampled the surface soil (0–5 cm) with a 5-cm-diameter core sampler (DIK-115B, Daiki-Rika, Saitama, Japan). The soil samples were bulked and homogenised in a plastic bag (Onda et al., 2015) and then transported to the laboratory and stored at ambient temperature.

2.2. Particle isolation and analysis

The radioactivity of the bulk soil sample was measured with a high-purity germanium (HPGe) semiconductor detector (GEM-type, Seiko EG&G, Tokyo, Japan). After the radionuclide determination, the soil sample was packed into a polyethylene bag for imaging plate (IP) autoradiography using a BAS IP MS 2025 (high-sensitivity model, GE Healthcare Japan, Tokyo, Japan) and a digital imager (BAS-1800II, Fujifilm, Tokyo, Japan). Because high concentrations of radioactive Cs were detected in the soil sample, a relatively short IP exposure time (5 min) was applied to the sample to detect only relatively strong radioactive emissions from particles; such emissions produce distinctive spots on the autoradiograph. Soil near high-strength spots detected by IP was separated from the surrounding soil for further analysis. The IP and separation procedures were repeated on increasingly smaller samples until relatively few soil particles remained. The selected soil particles were collected on sticky carbon tape and the existence of gamma emitter activity in the γ-spectrum, was demonstrated by using an HPGe detector.

We then cut the carbon tape into successively smaller pieces to isolate any radioactive particles from non-radioactive soil particles using a technique developed in previous studies (Adachi et al., 2013; Abe et al., 2014). Backscattered electron images are very useful in searching for radioactive particles containing elements with high atomic number, such as Fe, Zn, Pb, and Cs, from carbon tape (Salbu et al., 1994). Finally, we obtained small pieces of carbon tape containing radioactive particles and analysed these particles using SEM–EDS (SEM: SU 3500, Hitachi High-Technologies Co., Tokyo, Japan; EDS: X-max 50 mm, Horiba Ltd., Kyoto, Japan) to observe the particle morphology, measure the particle size, and determine the composition. In some cases, particles on carbon tape were transferred to Gecko Tape (Nitto Denko Co. Ltd., Japan), which is of high purity elemental carbon, using a microscope (BXiS series,

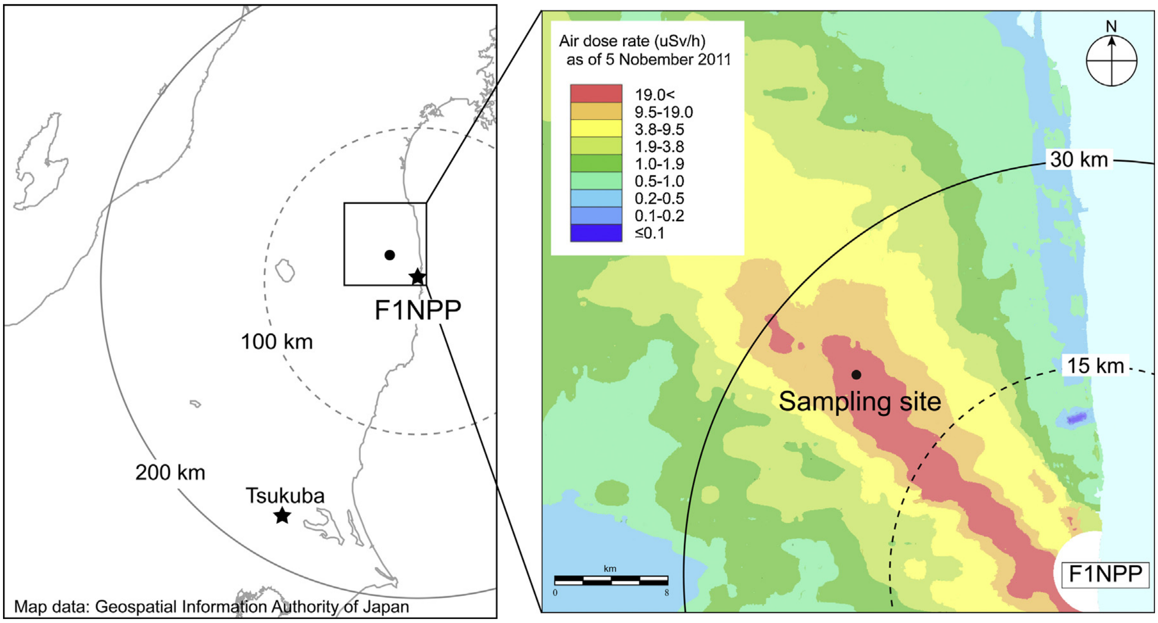

Fig. 1. Left: Map showing the location of the Fukushima Daiichi Nuclear Power Plant (F1NPP) on the east coast of Japan and the sampling site (solid dot), located ~20 km northwest of the FNDPP. Right: Map of the area northwest of the F1NPP (the location of the mapped area is indicated by the black square in the left panel), showing the air dose rate on 5 November 2011 (as determined by MEXT) and the location of the soil sampling site (black dot); the sample was collected from the most highly contaminated zone, i.e., the so-called difficult-to-return zone.

Olympus, Tokyo, Japan) and a micromanipulator (Quick Pro, Micro Support Co., Ltd., Shizuoka, Japan) equipped with tungsten needles.

3. Results

3.1. Particle figures and radioactivity

The sampling location (shown in Fig. 1) received radionuclide deposits on 15 March 2011, mainly via wet processes (Kinoshita et al., 2011; Tsuruta et al., 2014). The air dose rate at the time of sample collection was 22.3 μSv/h, measured 1 m above the ground surface. The bulk density of soil was 1.24 g/cm^3, which is within the range of the values reported for soils in Fukushima (Kato et al., 2012; Honda et al., 2015; Matsunaka et al., 2016). Radionuclides in the soil sample were measured by gamma spectrometry using a high-purity germanium semiconductor detector. On the basis of these measurements and a correction for radioactive decay, we calculated that the amount of ^{134}Cs deposited from the atmospheric plume(s) was 27.07 ± 0.06 MBq/m^2 (86,900 ± 200 Bq/kg) and that of ^{137}Cs was 27.02 ± 0.01 MBq/m^2 (86,720 ± 40 Bq/kg). The activity ratio of ^{134}Cs/^{137}Cs was 1.00 (decay corrected as of 11 March 2011) which was consistent with the results of a large-scale ground survey performed by the Japanese government (Saito et al., 2015).

IP autoradiography images of the soil sample showed that contamination by radionuclides was relatively uniform, although many spot-type contaminations were apparent (Fig. 2a). We isolated four radioactive particles from such spot-type contamination positions in the sample (Fig. 2b). Compared to the analysis of radioactive Cs adsorbed on clay minerals, the present radioactive particles were detected within ~10 min by using IP, so that the specific activity seems stronger than those found by Mukai et al. The sizes and morphologies of the particles varied: the maximum area equivalent diameter was 6.4 μm (particle B), and the particles were either spherule or fragmental in shape. The radionuclides ^{134}Cs and ^{137}Cs were detected by gamma spectroscopy in all of the particles, with particle B showing the highest concentrations (Fig. 2c); namely 69.5 ± 0.5 Bq for ^{134}Cs and 67.1 ± 0.1 Bq for ^{137}Cs (values corrected for decay). Although the particles' total radioactive Cs activity was less than 1/1000 of the total unit soil activity (Bq/kg), there were many more radioactive particles in the sample (see Fig. 2a). The activity ratio of ^{134}Cs/^{137}Cs was 1.03 ± 0.01, which is consistent with values for the bulk soil sample. However, no other gamma emitters were detected in the particles (Fig. 2c). The relationship between particle volume and ^{137}Cs concentration is proportional (Fig. 3), suggesting that these particles have the same source.

3.2. Particle compositions

The elemental constituents of the particles were measured with an EDS (Fig. 4a). All particles showed X-ray spectra of Si, O, Fe, and Zn, as well as Cs. Although X-ray peaks for Al were observed in all particles, the peaks could not be separated from those of the background sample, and we therefore could not confirm its presence in the individual particles. An element map of particle B is shown in Fig. 4b. Uniform distributions of Cs, O, Fe, Zn, and Si were observed within the particles (Fig. 4b). Approximately 80% was composed of Si and O, within each particle followed by K, Fe, and Zn.

4. Discussion

The particles, collected 27 months after the accident, were larger and more radioactive than those analysed in previous studies (Adachi et al., 2013; Abe et al., 2014; Yamaguchi et al., 2016). In particular, particle B had approximately 20 times the volume of the particles observed in aerosol samples collected in Tsukuba (Adachi et al., 2013), which is located approximately 170 km southwest of the F1NPP. Because of the high dry deposition velocity of the present particles (~10 cm/s for a 6 μm particle;

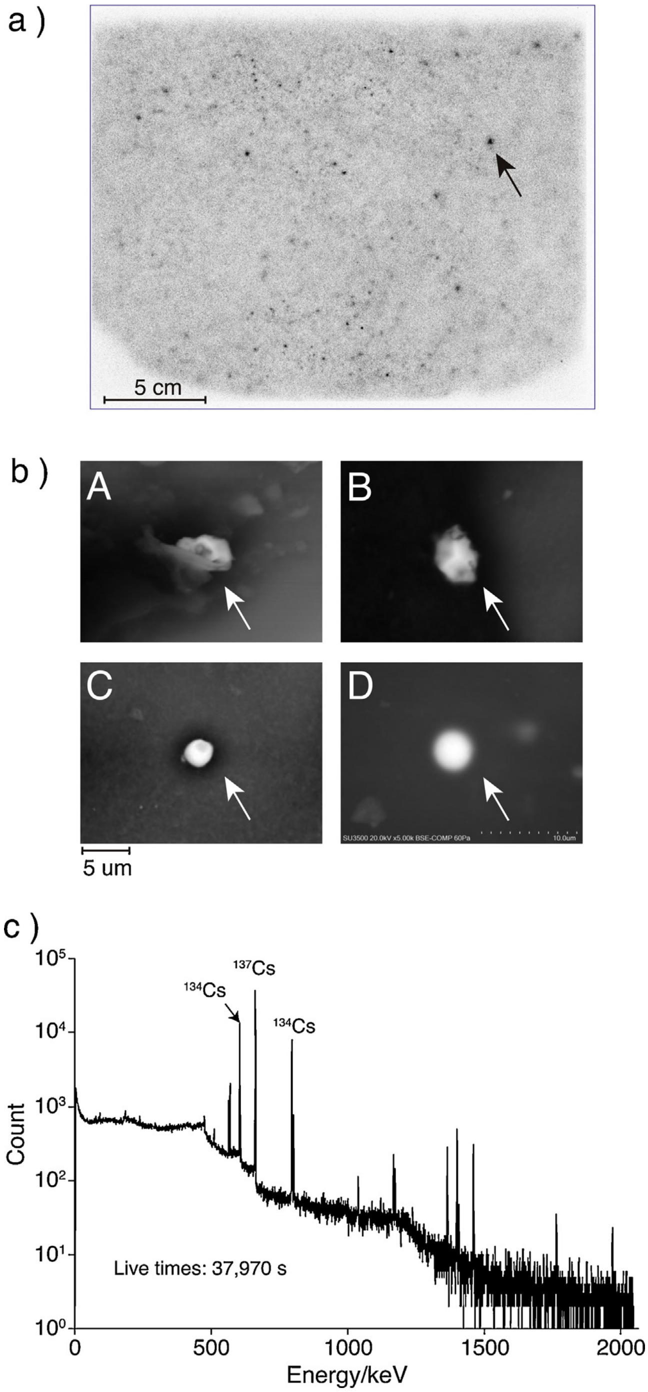

Fig. 2. Distribution of radioactive spots of different types in the soil sample and SEM images of the isolated radioactive particles. (a) Autoradiography image obtained by the imaging plate (IP) technique. The square frame represents the imaging plate and the grey colour distributed over the entire soil sample indicates that the soil was uniformly contaminated with radioactive materials. Black spots indicate aggregates of radioactive atoms, which occur throughout the soil sample. The black arrow indicates particle B. (b) SEM images of four radioactive particles (arrows) isolated from the soil sample. The particles are either spherules or fragmental in shape. Area equivalent diameters of particle A, B, C, and D are 4.5, 6.4, 4.0 and 3.0 μm, respectively. (c) Gamma ray spectrum of particle B.

Seinfeld and Pandis, 2006), it is possible that particles of the size collected in this study deposited rapidly and were therefore confined to areas near the source.

The specific radioactivity of ^{137}Cs within the present radioactive particles is consistent with those in the previous studies from the F1NPP by Adachi et al. (2013) and Abe et al. (2014) (=$2 \times 10^{16} \times$ [volume]$^{1.43}$; Fig. 3). By contrast, the specific radioactivity of hot particles observed in the Chernobyl accident (=$4 \times 10^{7} \times$ [volume]$^{0.74}$; Tcherkezian et al., 1994) is smaller than present particles from the F1NNP, indicating that the radioactive particles from the F1NNP accident have higher radioactive Cs concentration within the particle.

In addition, the diameters of the present radioactive particles range from 2 to 6.7 μm, which is consistent with the particle size distribution of aerosol containing the F1NPP ^{137}Cs (Doi et al., 2013; Miyamoto et al., 2014) and are within the range of PM_{10} and $PM_{2.5}$ (Davidson et al., 2005), which are inhalable to human body.

Particles C and D were spherules, suggesting that they formed from liquefied materials (Adachi et al., 2013). During the F1NPP accident the containment vessel pressure was observed to suddenly drop in each of the reactor units, suggesting that rapid cooling could have occurred following an adiabatic explosion during the exhaust process. Such rapid cooling offers a simple mechanism for the liquid-to-solid micro-particle conversion. In contrast, particles A and B were fragmental, suggesting that they were derived from larger fragments that had fractured in the soil during transportation or release.

The particles we collected contained Si, O, Fe, Zn, and Cs, which is consistent with the composition of previously reported particles (Adachi et al., 2013; Abe et al., 2014), although those studies could not confirm the presence of Si in the particles because Si was present in the substrate materials used in the previous analyses. We avoided this limitation by using a Gecko Tape substrate (Maeno and Nakayama, 2009). The result is consistent with the result by Yamaguchi et al. (2016) who showed the presence of Si using a transmission electron microscopy and EDS. Possible sources for the Si include silicate products that were used for the insulation in/around the reactor unit and around steam lines in the containment building of the F1NPP (Nuclear Safety Commission, Japan, 2006) as well as in the concrete of the containment vessel (Abe et al., 2014). We developed this novel point by vigorously surveying the material used for the reactor core and peripherals as well as rich in silicate.

The water solubility of these particles has important implications for human health, environmental impact, transportation, and deposition (Adachi et al., 2013). In the Chernobyl accident, highly radioactive particles were observed (Sandalls et al., 1993; Salbu et al., 1994), and they gradually collapsed and became soluble in water as time elapsed (Kashparov et al., 2004). The dissolution processes from radioactive particles contributed soluble radionuclides to the terrestrial environment. The dissolution rate depends on the soil pH (Kashparov et al., 2004). The radioactive particles in the soil sample remained stable or quasi-stable in the environment for 27 months, in a location that had experienced more than 3000 mm of precipitation during that time (Japan Meteorological Agency, 2015). Thus, the particles appear to exhibit low solubility in water and are stable in the ambient conditions of the environment where they were deposited. We could argue that, although the particles may have lost some components or been totally or partially oxidised, and although the molecular composition may have changed, these particles have remained in the ambient environment while maintaining their shape. Thus, long-term water solubility is recommended to be investigated to determine the corrosion rate of these Cs-bearing particles in the soil environment.

Decontamination of radioactive Cs from living areas are emerging issue in the area and large amount of contaminated soil and materials are being generated continuously. Volume reduction of the contaminants is pressing issue. In contrast, understanding of chemical form of radioactive Cs is important to remove radioactive Cs from contaminant. We have demonstrated

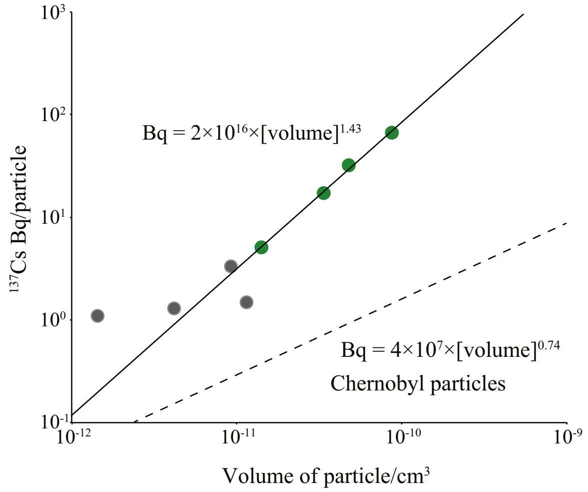

Fig. 3. Relationship between the volume of particles and the radioactivity of ^{137}Cs. The dashed line shows specific radioactivity of hot particles in the Chernobyl nuclear accident in 1986. Data were reconstructed from Tcherkezian et al. (1994).

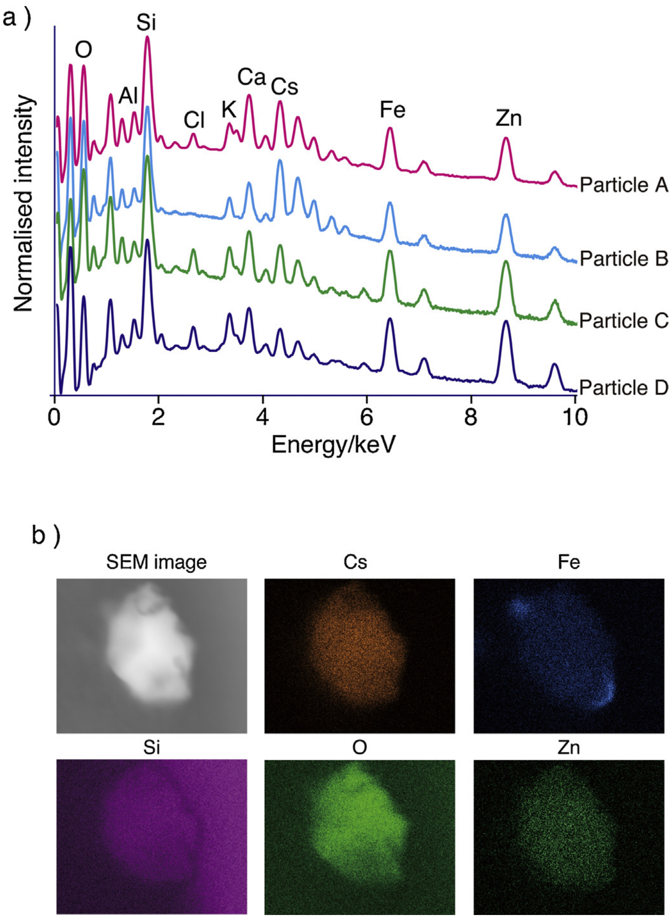

Fig. 4. EDS spectra and elemental mapping images. (a) Characteristic X-ray spectra from four radioactive particles. All particles exhibit signals characteristic of Si, O, Fe, and Zn, as well as Cs; Ca and K were also detected. (b) Elemental mapping of Cs, Si, O, Fe, and Zn in the particles. Silicone was present in the glass substrate. The Fe signal may represent material located beneath the particle.

that one of the existing forms of radioactive Cs has silicate glass state on this study and such knowledge will be helpful to the decontamination processes.

5. Conclusions

The radioactive particles we collected from the polluted soil were larger and more active than Cs-bearing particles analysed by Adachi et al. (2013), Abe et al. (2014) and Yamaguchi et al. (2016), but their constituents were similar to, those of the reported aerosol particles. In addition, the present study demonstrated that silicates are one of the major components in the radioactive particle, and that the particle characteristics were different from those of so-called hot particles observed at the Chernobyl accident in 1986. We suggest that the present radioactive particles in the soil were discharged to the atmosphere during the same F1NPP emission event on 14 and 15 March 2011 with the source of previously reported Cs-bearing solid particles. Our results provide information on the temperature of materials ejected during the accident, some of which appear to have been molten.

Our findings are useful to understand environmental dynamics studies of radioactive materials from the Fukushima accident. In addition, our findings have implications for the removal of the radioactive materials from the living areas and understanding of process of the accident. We suggest that additional investigations be conducted to analyse more particles from various distances from the F1NPP to elucidate the particle size–distance relationship, to determine the processes of synthesis of the particles in the reactor cores and peripherals, and to evaluate the effect of weathering on the particles in the environment.

Acknowledgements

The authors thank the mayor of Namie, Fukushima Prefecture, for permission to enter the exclusion zone to collect the samples. We are also indebted to Tetsuya Matsunaka, Tsutomu Takahashi, and Nao Shibayama for their help with sample collection. Takuya Yumine and his colleagues (Nitto Denko Co. Ltd.) provided the Gecko Tape. In addition, we acknowledge Anne Chin for editorial advices, and three anonymous reviewers for constructive comments and suggestions. This study was supported by MEXT/JSPS KAKENHI grants (numbers 24110003, 24110006, 15H02340, and 256895). Y.S. received a Grant-in-Aid for JSPS Fellows.

References

Abe, Y., Iizawa, Y., Terada, Y., Adachi, K., Igarashi, Y., Nakai, I., 2014. Detection of uranium and chemical state analysis of individual radioactive microparticles emitted from the Fukushima nuclear accident using multiple synchrotron radiation X-ray analyses. Anal. Chem. 86, 8521–8525.

Adachi, K., Kajino, M., Zaizen, Y., Igarashi, Y., 2013. Emission of spherical caesium-bearing particles from an early stage of the Fukushima nuclear accident. Sci. Rep. 3, 2554.

Chartin, C., Evrard, O., Onda, Y., Patin, J., Lefèvre, I., Ottlé, C., Ayrault, S., Lepage, H., Bonté, P., 2013. Tracking the early dispersion of contaminated sediment along rivers draining the Fukushima radioactive pollution plume. Anthropocene 1, 23–34.

Davidson, C.I., Phalen, R.F., Solomon, P.A., 2005. Airborne particulate matter and human health: a review. Aerosol Sci. Technol. 39, 737–749.

Doi, T., Masumoto, K., Toyoda, A., Tanaka, A., Shibata, Y., Hirose, K., 2013. Anthropogenic radionuclides in the atmosphere observed at Tsukuba: characteristics of the radionuclides derived from Fukushima. J. Environ. Radioact. 122, 55–62.

Honda, M., Matsuzaki, H., Miyake, Y., Maejima, Y., Yamagata, T., Nagai, H., 2015. Depth profile and mobility of ^{129}I and ^{137}Cs in soil originating from the Fukushima Dai-ichi Nuclear Power Plant accident. J. Environ. Radioact. 146, 35–43.

International Commission on Radiological Protection, 2012. ICRP Publication 119. Compendium of Dose Coeffcients based on ICRP Publication 60.

Itoh, S., Eguchi, T., Kato, N., Takahashi, S., 2014. Radioactive particles in soil, plant, and dust samples after the Fukushima nuclear accident. Soil Sci. Plant Nutr. 60, 540–550.

JMA: Japan Meteorological Agency, 2015. http://www.jma.go.jp/jma/menu/menureport.html, (accessed on 29.04.15).

Kaneyasu, N., Ohashi, H., Suzuki, F., Okuda, T., Ikemori, F., 2012. Sulphate aerosol as a potential transport medium of radiocaesium from the Fukushima Nuclear accident. Environ. Sci. Technol. 46, 5720–5726.

Kashimura, Y., Chida, K., Orikasa, H., Kusano, Y., Konno, K., 2013. Radioactive material discharged by the Fukushima nuclear plant accident caused black spots on digital X-ray images. Eur. Radiol. doi:http://dx.doi.org/10.1594/ecr2013/C-1844.

Kashparov, V.A., Ahamdach, N., Zvarich, S.I., Yoschenko, V.I., Maloshtan, I.M., Dewiere, L., 2004. Kinetics of dissolution of Chernobyl fuel particles in soil in natural conditions. J. Environ. Radioact. 72, 335–353.

Katata, G., Chino, M., Kobayashi, T., Terada, H., Ota, M., Nagai, H., Kajino, M., Hort, M. C., Malo, A., Torii, T., Sanada, Y., 2015. Detailed source term estimation of the atmospheric release for the Fukushima Daiichi Nuclear Power Station accident by coupling simulations of an atmospheric dispersion model with an improved deposition scheme and oceanic dispersion model. Atmos. Chem. Phys. 15, 1029–1070.

Kato, H., Onda, Y., Teramage, M., 2012. Depth distribution of ^{137}Cs, ^{134}Cs, and ^{131}I in soil profile after Fukushima Nuclear Power Plant Accident. J. Environ. Radioact. 111, 59–64.

Kinoshita, N., Sueki, K., Sasa, K., Kitagawa, J., Ikarashi, S., Nishimura, T., Wong, Y.S., Satou, Y., Handa, K., Takahashi, T., Sato, M., Yamagarata, T., 2011. Assessment of individual radionuclide distributions from the Fukushima nuclear accident covering central-east Japan. Proc. Natl. Acad. Sci. U. S. A. 108, 19526–19529.

Kitamura, A., Yamaguchi, M., Kurikami, H., Yui, M., Onishi, Y., 2014. Predicting sediment and cesium-137 discharge from catchments in eastern Fukushima. Anthropocene 5, 22–31.

Lepage, H., Laceby, J.P., Bonté, P., Joron, J.-L., Onda, Y., Lefèvre, I., Ayrault, S., Evrard, O., 2016. Investigating the source of radiocesium contaminated sediment in two Fukushima coastal catchments with sediment tracing techniques. Anthropocene doi:http://dx.doi.org/10.1016/j.ancene.2016.01.004 in press.

Maeno, Y., Nakayama, Y., 2009. Gecko like high shear strength by carbon nanotube fiber adhesives. Appl. Phys. Lett. 94, 012103.

Matsunaka, T., Sasa, K., Sueki, K., Takahashi, T., Satou, Y., Matsumura, M., Kinoshita, N., Kitagawa, J., Matsuzaki, H., 2016. Pre- and post-accident ^{129}I and ^{137}Cs levels and ^{129}I/^{137}Cs ratios in soil near the Fukushima Dai-ichi Nuclear Power Plant, Japan. J. Environ. Radioact. 151, 209–217.

Miyamoto, Y., Yasuda, K., Magara, M., 2014. Size distribution of radioactive particles collected at Tokai, Japan 6 days after the nuclear accident. J. Environ. Radioact. 132, 1–7.

NSC, 2006. Nuclear Safety Commission, 44th Regular Meeting Report (in Japanese). . (accessed on 1.05.15) http://www.nsr.go.jp/archive/nsc/anzen/shidai/genan2006/genan044/genan-si044.htm.

Niimura, N., Kikuchi, K., Tuyen, N.D., Komatsuzaki, M., Motohashi, Y., 2015. Physical properties, structure, and shape of radioactive Cs from the Fukushima Daiichi Nuclear Power Plant accident derived from soil, bamboo and shiitake mushroom measurements. J. Environ. Radioact. 139, 234–239.

Onda, Y., Kato, H., Hoshi, M., Takahashi, Y., 2015. Minh-Long, N: Soil sampling and analytical strategies for mapping fallout in nuclear emergencies based on the Fukushima Dai-ichi Nuclear Power Plant accident. J. Environ. Radioact. 139, 300–307.

Saito, K., Tanihata, I., Fujiwara, M., Saito, T., Shimoura, S., Otsuka, T., Onda, Y., Hoshi, M., Ikeuchi, Y., Takahashi, F., Kinouchi, N., Saegusa, J., Seki, A., Takemiya, H., Shibata, T., 2015. Detailed deposition density maps constructed by large-scale soil sampling for gamma-ray emitting radioactive nuclides from the Fukushima Dai-ichi Nuclear Power Plant accident. J. Environ. Radioact. 139, 308–319.

Salbu, B., Kerkling, T., 1998. Characterisation of radioactive particles in the environment. Analyst 123, 843–850.

Salbu, B., Krekling, T., Oughton, D.H., Østby, G., Kashparov, V.A., Brand, T.L., Day, J.P., 1994. Hot particles in accidental releases from Chernobyl and Windscale nuclear installations. Analyst 119, 125–130.

Salbu, B., 2011. Radionuclides released to the environment following nuclear events. Integr. Environ. Assess. Manag. 7, 362–364.

Sandalls, F.J., Segal, M.G., Victorova, N., 1993. Hot particles from Chernobyl: a review. J. Environ. Radioact. 18, 5–22.

Satou, Y., Sueki, K., Sasa, K., Kitagawa, J., Ikarashi, S., Kinoshita, N., 2015. Vertical distribution and formation analysis of the ^{131}I, ^{137}Cs, ^{129m}Te, and ^{110m}Ag from the Fukushima Dai-ichi Nuclear Power Plant in the beach soil. J. Radioanal. Nucl. Chem. 303, 1197–1200.

Seinfeld, J.H., Pandis, S.N., 2006. Atmospheric Chemistry and Physics, 2nd edition John Wiley & Sons Inc, New Jersey.

Shibata, K., Kitamura, Y., Kozaka, T., Uno, I., Shimizu, K., Masumoto, K., Hirota, M., Higaki, S., Miyoshi, H., Saze, T., Sakama, M., Yanaga, M., 2013. Decontamination of radioactivity from contaminated vegetables derived from the Fukushima nuclear accident. Radiat. Meas. 55, 26–29.

Stohl, A., Seibert, P., Wotawa, G., Arnold, D., Burkhart, J.F., Eckhardt, S., Tapia, C., Vargas, A., Yasunari, T.J., 2012. Xenon-133 and caesium-137 releases into the atmosphere from the Fukushima Dai-ichi nuclear power plant: determination of the source term atmospheric dispersion, and deposition. Atmos. Chem. Phys. 12, 2313–2343.

TEPCO, 2012. Fukushima Nuclear Accidents Investigation Report by Tokyo Electric Power Company, Web. . (accessed in 1.02.16) http://www.tepco.co.jp/en/press/corp-com/release/2012/1205638_1870.html.

Tanaka, K., Iwatani, H., Sakaguchi, A., Takahashi, Y., Onda, Y., 2013. Local distribution of radioactivity in tree leaves contaminated by fallout of the radionuclides emitted from the Fukushima Daiichi Nuclear Power Plant. J. Radioanal. Nucl. Chem. 295, 2007–2014.

Tcherkezian, V., Shkinev, V., Khitrov, L., Kolesov, G., 1994. Experimental approach to chernobyl hot particles. J. Environ. Radioact. 22, 127–139.

Terada, H., Katata, G., Chino, M., Nagai, H., 2012. Atmospheric discharge and dispersion of radionuclides during the Fukushima Dai-ichi Nuclear Power Plant accident. Part II: verification of the source term and analysis of regional-scale atmospheric dispersion. J. Environ. Radioact. 112, 141–154.

Tsuruta, H., Oura, Y., Ebihara, M., Ohara, T., Nakajima, T., 2014. First retrieval of hourly atmospheric radionuclides just after the Fukushima accident by analyzing filter-tapes of operational air pollution monitoring stations. Sci. Rep. 4, 6717.

Winiarek, V., Bocquet, M., Saunier, O., Mathieu, A., 2012. Estimation of errors in the inverse modeling of accidental release of atmospheric pollutant: Application to the reconstruction of the cesium-137 and iodine-131 source terms from the Fukushima Daiichi power plant. J. Geophys. Res. 117 doi:http://dx.doi.org/10.1029/2011jd016932D05122.

Yamaguchi, N., Mitome, M., Akiyama, H.K., Asano, M., Adachi, K., Kogure, T., 2016. Internal structure of cesium-bearing radioactive microparticles released from Fukushima nuclear power plant. Sci. Rep. 6, 20548.

Yanaga, M., Oishi, A., 2015. Decontamination of radioactive cesium in soil. J. Radioanal. Nucl. Chem. 303, 1301–1304.

SCIENTIFIC REPORTS

OPEN

Internal structure of cesium-bearing radioactive microparticles released from Fukushima nuclear power plant

Received: 03 June 2015
Accepted: 06 January 2016
Published: 03 February 2016

Noriko Yamaguchi[1,*], Masanori Mitome[2], Akiyama-Hasegawa Kotone[2], Maki Asano[1,3], Kouji Adachi[4] & Toshihiro Kogure[5,*]

Microparticles containing substantial amounts of radiocesium collected from the ground in Fukushima were investigated mainly by transmission electron microscopy (TEM) and X-ray microanalysis with scanning TEM (STEM). Particles of around 2 μm in diameter are basically silicate glass containing Fe and Zn as transition metals, Cs, Rb and K as alkali ions, and Sn as substantial elements. These elements are homogeneously distributed in the glass except Cs which has a concentration gradient, increasing from center to surface. Nano-sized crystallites such as copper- zinc- and molybdenum sulfide, and silver telluride were found inside the microparticles, which probably resulted from the segregation of the silicate and sulfide (telluride) during molten-stage. An alkali-depleted layer of ca. 0.2 μm thick exists at the outer side of the particle collected from cedar leaves 8 months after the nuclear accident, suggesting gradual leaching of radiocesium from the microparticles in the natural environment.

Although almost five years have passed since the accident of Fukushima Daiichi Nuclear Power Plant (FDNPP), radioactive contamination in the surrounding area is still a serious problem in Japan. The largest radionuclide deposition event occurred on March 15–16 and the second largest on 21–23, 2011. Wet deposition was a major source of radiocesium contamination of terrestrial environment[1], while contribution of dry deposition was larger near the FDNPP[2]. In order to understand and predict the fate of radioactive materials contaminating the terrestrial environment, it is important to clarify the physicochemical properties of the deposited materials. From previous cases of radionuclide release, it is known that the chemical species of released radiocesium is monovalent cation (Cs^+) which is soluble[3]. Deposition of radiocesium as insoluble particles has also been pointed out. Autoradiography analyses using imaging plate (IP) showed spots of particulate materials on plant tissues collected from Fukushima[4–6]. On the aerosol filter collected from March 14–15, 2011 in Tsukuba, 170 km south-southwest of FDNPP, Adachi *et al.*[7] discovered spherical particulate radiocesium of 2.0–2.6 μm in diameter, with particles insoluble in water having a glass-like structure[8]. These microparticles contain several fission products of U-235 other than radiocesium, and Fe and Zn which are also used in nuclear reactors[8]. Hence, they were considered to be released directly from nuclear reactors.

Kaneyasu *et al.*[9] suggested that vaporized radiocesium was transported with sulfate aerosol in the air, dissolved to cloud droplets and fell as rain. On the aerosol filter collected on March 20–21, 2011, rainy days in Tsukuba, the majority of radiocesium was in water-soluble form[7]. Such water-soluble radiocesium that reached the ground surface as a solute was fixed to soils, especially to clay minerals[10]. In the terrestrial environment, the majority of radiocesium is present in solid form regardless of the initial form of deposition. However, compared to clay minerals originally contaminated by soluble radiocesium in soil, the solid radiocesium, which was initially deposited as radioactive microparticles, had stronger radioactivity. Although the contribution or percentage of such radioactive microparticles in the contamination level of Fukushima has not been evaluated, its influence on human

[1]National Institute for Agro-Environmental Sciences, Kannondai, Tsukuba 305-0864, Japan. [2]National Institute for Materials Science, Namiki, Tsukuba 305-0044, Japan. [3]Graduate School of Life and Environmental Sciences, University of Tsukuba, Tennodai, Tsukuba, 305-8572, Japan. [4]Meteorological Research Institute, Nagamine, Tsukuba, 305-0052, Japan. [5]Graduate School of Sciences, The University of Tokyo, Bunkyo, Tokyo 113-0033, Japan. *These authors contributed equally to this work. Correspondence and requests for materials should be addressed to N.Y. (email: nyamag@affrc.go.jp) or T.K. (email: kogure@eps.s.u-tokyo.ac.jp)

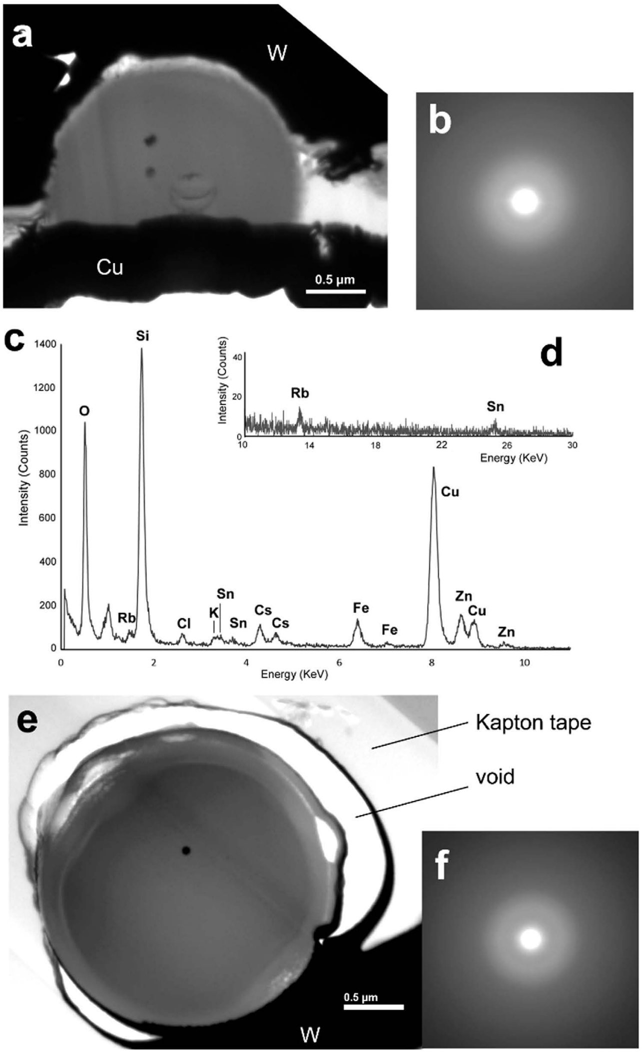

Figure 1. (**a**) Bright-field (BF) image of NWC-1. The opaque material outside the microparticle is tungsten (W) and copper (Cu) deposited in the FIB process. (**b**) Electron diffraction (ED) pattern from the particle. (**c,d**) EDS spectrum acquired from almost the whole area of the particle for the energy range of (**c**) 0–11 keV and (**d**) 10–30 keV. (**e**) BF image of CB-8. The opaque material outside the sphere is W and the thin transparent material is Kapton tape. (**f**) ED pattern from the particle.

health may be serious in terms of its intense radioactivity. Moreover, the structural detail of the microparticles may give insights into the state of the broken reactor and fuel debris.

In the present study, we investigated radioactive microparticles, similar to those reported by Adachi *et al.*[7], but collected from the ground, by observing their internal structure with transmission electron microscopic (TEM) techniques.

Results

Structure and composition of Cesium-bearing radioactive microparticles.

Cesium-bearing radioactive microparticles that had been deposited on non-woven fabric cloth (NWC-1) and on a needle of Japanese cedar (*Cryptomeria japonica*) (CB-8) were investigated. They were in the field for five and eight months, respectively, until sampling. Scanning electron microscope (SEM) images of NWC-1 of the whole microparticle before preparing thin sections for TEM analyses; and elemental composition of the whole particle determined by synchrotron radiation microbeam X-ray fluorescence (SXRF) are shown in Supplementary Figs S1 and S2 online, respectively. The activities of ^{137}Cs for the NWC-1 and CB-8 were 5.04 ± 0.472 and 3.14 ± 0.178 Bq, respectively.

Bright-field (BF) images and selected-area electron diffraction (SAED) patterns recorded in TEM from the whole area of NWC-1 and CB-8 are shown in Fig. 1, along with the energy-dispersive X-ray spectrum (EDS) acquired in TEM from NWC-1. Preparation of thin specimens from NWC-1 microparticle by focused-ion-beam (FIB) process was successful only for the upper half of the sphere. The BF contrast of NWC-1 (Fig. 1a) was almost uniform except for two dark nanoparticles inside the sphere. These nanoparticles will be described in a later subsection. The SAED pattern from the whole particle consists of only a halo (Fig. 1b) and the EDS from the whole particle (Fig. 1c,d) mainly consist of peaks of Si and O (Cu is from the supporting mesh), indicating that the particle was basically silicate glass. Additionally, Cl, K, Cs, Fe, Zn, Rb, and Sn were definitely identified. The presence of Na was not confirmed since its peak overlapped with the L-peak of Zn. These elements were previously reported[7,8] except for K. EDS Semi-quantitative analysis for almost the entire area of the TEM specimen, without considering the absorption effect estimated the glass composition (wt.%) to be SiO_2; 69.3, K_2O; 1.9, Fe_2O_3; 8.6, ZnO; 11.0, Rb_2O; 1.3, SnO_2; 1.4, Cs_2O; 3.4 with a small amount of Cl (1.4 wt.%). The valence states of cations were assumed to be in line with results in an X-ray absorption spectroscopic study[8]. Rubidium, Cs and Sn are the fission products of U-235. Tin is also used for fuel cladding[11]. Iron is used as steel for reactor pressure vessels, and Si and O are main components of concrete at the bottom of the containment vessel, where the melt-down fuel or core debris is thought to exist. Zinc had been added to the primary cooling water[12]. Potassium and Cl may originate from concrete and/or seawater, which was used to cool down the reactor.

The BF TEM image of CB-8 showed a two-layer structure having an inner core with darker contrast, an outer crust with a lighter one, and a small dark nanoparticle near the center (Fig. 1e). The thickness of the crust was around 0.2 μm. SAED pattern indicated that both are amorphous (Fig. 1f). Locally, a bubble-like structure was observed at a certain radius in the crust, or the outside part was peeled off at the radius (Fig. 1e). The chemical composition of the entire area of the specimen was SiO_2; 73.3, K_2O; 1.4, Fe_2O_3; 7.2, ZnO; 11.4, Rb_2O; 1.2, SnO_2; 1.5, Cs_2O; 3.3 and Cl; 0.7, which is similar to that of NWC-1.

Distributions of elements in microparticles. Elemental maps from NWC-1 using STEM-EDS are shown in Fig. 2a. Brighter color indicates higher concentration of the elements. All elements were almost uniformly distributed in the particle with Cs the only exception. Cesium concentration was lower near the center than the outside of the particle. The ratio of the amounts between the center and outside is around two. It is possible that vapor-phase cesium in the reactor was absorbed to the molten silicate microparticles, from their surface. The low diffusion velocity of cesium in the glass may have left the concentration gradient. On the contrary, elemental mapping for CB-8 (Fig. 2b) indicates that K, Rb and Cs were distinctively depleted in the crust but concentrated in the vicinity of the surface. Although the reason for the high concentration at the surface is not certain, it might be an artifact by diffusion of alkali cations caused by electron-beam radiation in the analysis. Chlorine was concentrated in the crust.

Crystalline nanoparticles in the glass. Two nanoparticles with dark contrast were observed in the TEM image of NWC-1 (Fig. 1a). Although EDS spectrum only from the particles cannot be obtained since they are still buried in the glass in spite of the thinning by FIB, S was distinctively identified from the particles (Fig. 3a). Elemental mapping by STEM-EDS indicated enrichment of Cu, Zn and Mo at the nanoparticles along with S, indicating that they are sulfide. The possibility of sulfate was excluded because oxygen is deficient in the nanoparticles in the oxygen map (Fig. 3a). Moreover, the locations of Cu, Zn and Mo do not overlap within the nanoparticles, suggesting that these metal elements form different sulfide phases in the nanoparticle (Fig. 3a). SAED from the left particle showed a single-crystal diffraction pattern (Fig. 3b), which can be explained by the crystallographic parameters for a high-temperature polymorph of digenite ($Cu_{2-x}S$). The origin of Cu and S may be minor elements in the concrete. On the other hand, Ag and Te were distinctively detected by EDS in TEM from the nanoparticle in CB-8 (Supplementary Fig. S3 online), indicating the particle to be silver telluride. Both elements can be fission products of U. Diffraction spots were observed in the SAED pattern from the particle, indicating that it is crystalline but the phase could not be identified. These sulfide and telluride were probably segregated and crystallized in the microparticles at the molten state.

Discussion

Our most significant finding is that the matrix of the Cs-bearing microparticles is silicate glass, based on the TEM-EDS analysis with FIB sample preparation. Previous studies suggested that Fe, Mo, Sn and Zn in the Cs-bearing microparticles had a similar X-ray absorption near-edge structure to those composed of glass[8], however the presence of Si in the microparticles has not been verified[7,8]. It is probable that the high-temperature melt-down fuel from the reactor came into contact with and melted the concrete, and then splashed microparticles of silicate melt, which were solidified by cooling to form silicate glass in the atmosphere. However, there are several questions with respect to the selection of the constituting elements in the glass from various ones in the reactor. For instance, Ca which is one of the major elements in concrete, was almost absent in the microparticles of NWC-1. Since TEM observed only a small portion of the microparticles, by making them thin using FIB, there may have been other elements in the microparticles, for instance, as a form of chalcogenide nanoparticle.

The next important finding is the alkali-depleted crust in CB-8 microparticle. This is probably the result of elution of alkali ions by contact with acidic solution in the field, commonly observed in silicate glass[13]. On the other hand, such alkali-depleted crust was not observed in NWC-1. This may be attributed to the different environments of the two microparticles after release from the nuclear plant. NWC-1 was on non-woven cloth and CB-8 on a cedar leaf before it was collected. It is well-known that silicate glass elutes alkali components from their surface by ion-exchange with proton or hydronium ions to form an alkali-leaching layer on the surface if pH of reacting solution is low, whereas the silicate framework of the glass itself is dissolved with high-pH solution[13,14]. Coniferous forest canopy induces acidic condition due to ammonia uptake, nitrification and leaching of plant-derived acid[15]. It was likely that CB-8 deposited on the cedar leaf had been in acidic conditions, which derives alkali depletion in the crust, for eight months. The finding of the alkali-depleting crust on the surface of the Cs-bearing radioactive microparticle indicates that radiocesium in the particles can be released by "weathering" of the glass in natural environments, and considering its small size, duration for the total release of the radioactive cesium from the particles is probably not long, from several years to a few decades, though it will strongly depends on the environment.

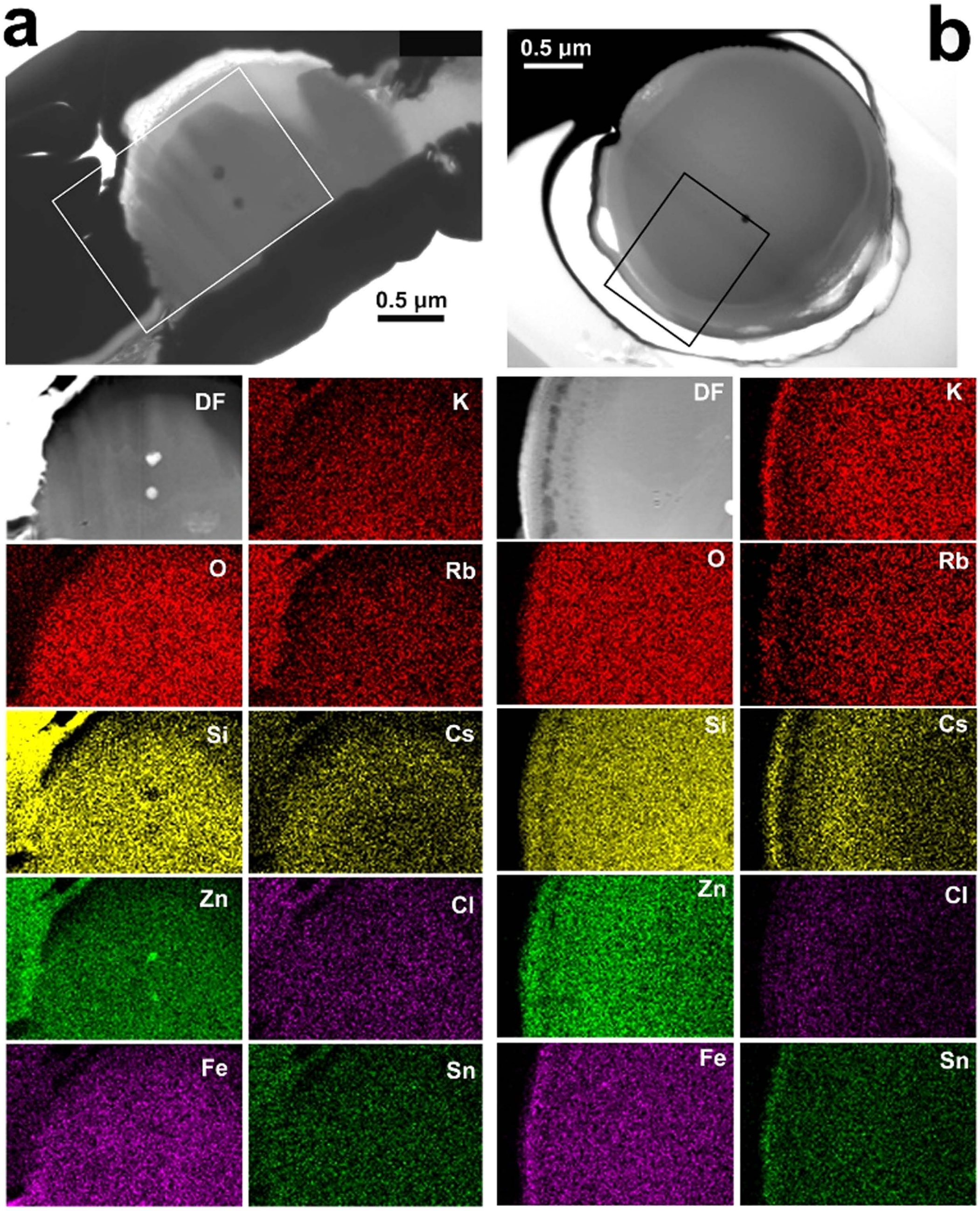

Figure 2. (**a**) Element maps of NWC-1 acquired by STEM-EDS with a STEM Dark-field (DF) image at the same area, and (top) TEM Bright-field image in which the rectangle indicates the area analyzed by STEM-EDS. The thin area around the top of the particle which was not observed in Fig. 1a was formed by a further thinning process by FIB. (**b**) Element maps and images of CB-8 with the same framing as in (**a**).

In order to investigate the dissolution rate and detailed Cs-leaching properties of the Cs-bearing radioactive microparticles, a leaching experiment should be conducted as a function of temperature and pH. However, collecting and isolating the Cs-bearing microparticles is time-consuming and it is difficult to obtain a large enough number of Cs-bearing microparticles to investigate dissolution properties. Alternatively, synthesized silicate glass with the same composition as the microparticles presented in this study may help to obtain information on the fate of Cs-bearing radioactive microparticles. However, in our preliminary experiment, we were unable to make uniform glass with the same composition at present. This is probably due to the liquid immiscibility at the composition. A solution to this problem is now being considered.

There are mainly two types of solid-phase radiocesium in the terrestrial environment affected by FDNPP accident; that fixed to clay minerals in the soil via wet deposition and that contained in the microparticles of silicate glass flown directly from the nuclear reactors. The radioactivity of the former is rather in low-density but distributed widely, therefore it is a major source of external radiation from ground. Part of the radiocesium adsorbed on

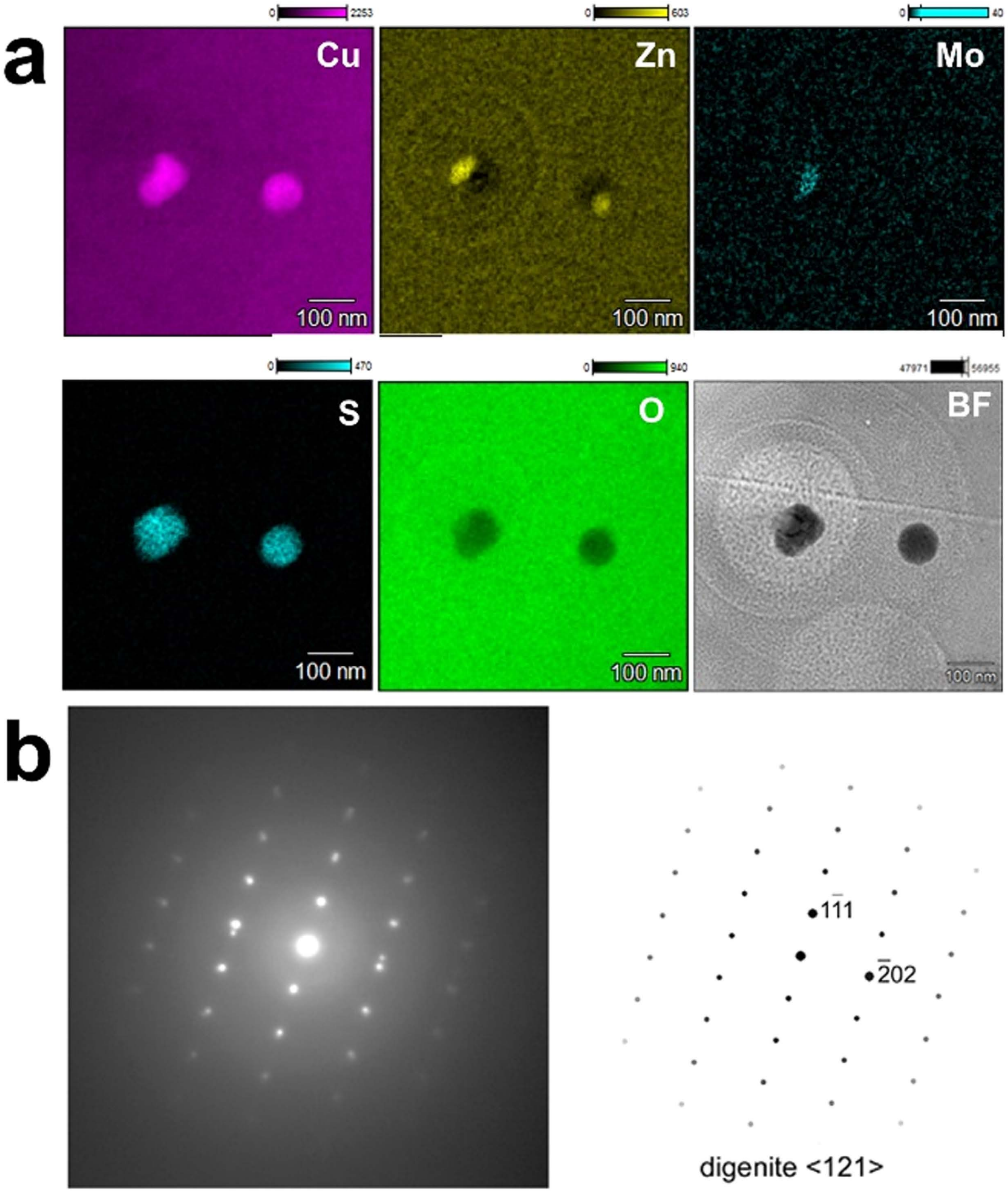

Figure 3. (**a**) Element maps and STEM bright-field (BF) image of the two nanoparticles inside NWC-1. The circular contrasts outside the nanoparticles in the BF image are radiation damage in glass formed by the electron probe for chemical analyses. (**b**) (Left) ED pattern from the left nanoparticle. (Right) Drawing of ED pattern for the high-temperature polymorph of digenite ($Cu_{2-x}S$) along <121>.

the soil clay is desorbed and transferred to crops thereby causing internal radiation. On the other hand, contribution of the microparticles to the air radiation is most likely not significant, but their radiation density is very high, which is particularly problematic for organisms including humans if the microparticles are inhaled or ingested. The plant availability of radiocesium in the microparticles should depend on its solubility. Consequently, further research on this material should be carried out as soon as possible.

Methods

Samples. Radioactive microparticles attached on non-woven fabric cloth and needles of Japanese cedar, collected from Fukushima, were identified by autoradiography followed by point-by-point analyses with scanning electron microscope (SEM; Hitachi high-Technologies SU3500) equipped with an energy dispersed X-ray spectrometer (EDS; Horiba X-max 50 mm). The identified particles were further determined by SXRF with excitation X-ray energy of 37.5 keV to ensure the detection of Cs-K line from the particle. The activities of ^{137}Cs was determined by a Ge detector (GCW2523S Canberra, USA). Detailed methods to identify the Cs-bearing microparticles are described in the supplementary information.

TEM Analyses. Cross-sectional thin TEM specimens were prepared from radioactive microparticles using a focused ion beam (FIB) instrument with micro-sampling system (Hitachi FB-2100) as described in the supplementary information. Then specimens were initially examined using a TEM (JEOL JEM-2010UHR) operated at 200 kV with an EDS analyzer system (JEOL JED-2200). Elemental mapping in the microparticles and quantitative analyses were performed using a JEOL JEM-3100FEF operated at 300 kV in the STEM mode, with an EDS analyzer system (Thermo Fisher Scientific NORAN System SIX). Finally, elemental maps for nanoparticulates inside the microparticles were acquired using a JEOL JEM-2800 operated at 200 kV with double wide-area (0.95 sr.) silicon drift detectors (SDD) for EDS analyses.

References

1. Yoshida, N. & Takahashi, Y. Land-surface contamination by radionuclides from the Fukushima Daiichi Nuclear Power Plant accident. *Elements* **8,** 201–206 (2012).
2. Katata, G., Ota, M., Terada, H., Chino, M. & Nagai, H. Atmospheric discharge and dispersion of radionuclides during the Fukushima Dai-ichi Nuclear Power Plant accident. Part I: Source term estimation and local-scale atmospheric dispersion in early phase of the accident. *J. Environ. Radioactiv*. **109,** 103–113 (2012).
3. Santschi, P. H. *et al.* Chernobyl radionuclides in the environment- tracers for the tight coupling of atmospheric, terrestrial, and aquatic geochemical processes. *Environ. Sci. Technol.* **22,** 510–516 (1988).
4. Nakanishi, T. M., Kobayashi, N. I. & Tanoi, K. Radioactive cesium deposition on rice, wheat, peach tree and soil after nuclear accident in Fukushima. *J. Radioanal. Nuclear Chem*. **296,** 985–989 (2013).
5. Nakanishi, H. *et al.* Radioactive cesium distribution in bamboo *Phyllostachys reticulata* (Rupr) K. Koch shoots after the TEPCO Fukushima Daiichi Nuclear Power Plant disaster. *Soil Sci. Plant Nutr.* **60,** 801–808 (2014).
6. Itoh, S., Eguchi, T., Kato, N. & Takahashi, S. Radioactive particles in soil, plant, and dust samples after the Fukushima nuclear accident. *Soil Sci. Plant Nutr.* **60,** 540–550 (2014).
7. Adachi, K., Kajino, M., Zaizen, Y. & Igarashi, Y. Emission of spherical cesium-bearing particles from an early stage of the Fukushima nuclear accident. *Sci. Rep*. **3,** No. 2554 (2013).
8. Abe, Y. *et al.* Detection of uranium and chemical state analysis of individual radioactive microparticles emitted from the Fukushima nuclear accident using multiple synchrotron radiation X-ray analyses. *Anal. Chem.* **86,** 8521–8525 (2014).
9. Kaneyasu, N., Ohashi, H., Suzuki, F., Okuda, T. & Ikemori, F. Sulfate aerosol as a potential transport medium of radiocesium from the Fukushima Nuclear accident. *Environ. Sci. Technol.* **46,** 5720–5726 (2012).
10. Mukai, H. *et al.* Speciation of radioactive soil particles in the Fukushima contaminated area by IP autoradiography and microanalyses. *Environ. Sci. Technol.* **48,** 13053–13059 (2014).
11. Zinkle, S. J. & Was, G. S. Materials challenges in nuclear energy. *Acta Mater.* **61,** 735–758 (2013).
12. Hori, S. & Suzuki, A. *TEPCO's challenges for occupational exposure reduction - installation of additional CF in Fukushima Daiichi NPP*., <www.nsra.or.jp/isoe/english/…/pdf/atc2009-3-1ga.pdf> (2009). (Accessed 18th May 2015).
13. Bunker, B. C. Molecular mechanisms for corrosion of silica and silicate-glasses. *J. Non-Cryst. Solids* **179,** 300–308 (1994).
14. Gin, S. *et al.* Origin and consequences of silicate glass passivation by surface layers. *Nat. Commun.* **6,** No. 6360 (2015).
15. Cronan, C. S. & Reiners, W. A. Canopy processing of acidic precipitation by coniferous and hardwood forests in New England. *Oecologia* **59,** 216–223 (1983).

Acknowledgements

Part of this work was supported by a Grant-in-Aid for science research (15H04222 and 24110003) by JSPS, Japan. This work was also supported by 2014 JAEA contract research for Fukushima environment recovery, "Study on Cs adsorption and desorption process on clay minerals" and by MAFF contract research "Development of Decontamination technologies for radioactive substances in agricultural land". The synchrotron radiation experiment was performed under approval of the SPring-8 Program Advisory Committee (Proposal Number: 2014B1282). The authors wish to thank Dr. M. Kobayashi for providing the Japanese cedar samples, Ms. E. Fujii for preparing TEM specimens, Dr. T. Hara for providing the opportunity to use the STEM instrument, Prof. Clive Langham for English edition, and Dr. Y. Igarashi for comments on the manuscript.

Author Contributions

N.Y. and T.K. designed the research and wrote the paper; N.Y. performed the IP, SEM and SXRF analyses; M.A. performed SEM and SXRF analyses; M.M. and K.A.-H. performed TEM analyses; K.A. performed SEM analyses; T.K. performed SEM and TEM analyses and supervised the study; all authors contributed to the manuscript. N.Y and T.K. contributed equally to this work.

Additional Information

Supplementary information accompanies this paper at http://www.nature.com/srep

Competing financial interests: The authors declare no competing financial interests.

How to cite this article: Yamaguchi, N. *et al.* Internal structure of cesium-bearing radioactive microparticles released from Fukushima nuclear power plant. *Sci. Rep.* **6**, 20548; doi: 10.1038/srep20548 (2016).

Atmos. Chem. Phys., 16, 13149–13172, 2016
www.atmos-chem-phys.net/16/13149/2016/
doi:10.5194/acp-16-13149-2016

Atmospheric Chemistry and Physics
Open Access

Long-term assessment of airborne radiocesium after the Fukushima nuclear accident: re-suspension from bare soil and forest ecosystems

Mizuo Kajino[1,2], Masahide Ishizuka[3], Yasuhito Igarashi[1], Kazuyuki Kita[4], Chisato Yoshikawa[5], and Masaru Inatsu[6]

[1]Meteorological Research Institute (MRI), Japan Meteorological Agency (JMA), Tsukuba, Ibaraki, Japan
[2]RIKEN Advanced Institute for Computational Science (AICS), Kobe, Hyogo, Japan
[3]Faculty of Engineering, Kagawa University, Takamatsu, Kagawa, Japan
[4]Faculty of Science, Ibaraki University, Mito, Ibaraki, Japan
[5]Japan Agency for Marine-Earth Science and Technology (JAMSTEC), Yokosuka, Kanagawa, Japan
[6]Faculty of Science, Hokkaido University, Sapporo, Hokkaido, Japan

Correspondence to: Mizuo Kajino (kajino@mri-jma.go.jp)

Received: 29 March 2016 – Published in Atmos. Chem. Phys. Discuss.: 25 April 2016
Revised: 26 July 2016 – Accepted: 19 September 2016 – Published: 27 October 2016

Abstract. The long-term effect of ^{137}Cs re-suspension from contaminated soil and forests due to the Fukushima nuclear accident has been quantitatively assessed by numerical simulation, a field experiment on dust emission flux in a contaminated area (town of Namie, Fukushima prefecture), and air concentration measurements inside (Namie) and outside (city of Tsukuba, Ibaraki prefecture) the contaminated area. In order to assess the long-term effect, the full year of 2013 was selected to study just after the start of the field experiments. The ^{137}Cs concentrations at Namie and Tsukuba were approximately 10^{-1}–1 and 10^{-2}–10^{-1} mBq m^{-3}, respectively. The observed monthly median concentration at Namie was 1 to 2 orders of magnitude larger than that at Tsukuba. This observed difference between the two sites was consistent with the simulated difference, indicating successful modeling of ^{137}Cs re-suspension and atmospheric transport. The estimated re-suspension rate was approximately 10^{-6} day^{-1}, which was significantly lower than the decreasing rate of the ambient gamma dose rate in Fukushima prefecture (10^{-4}–10^{-3} day^{-1}) as a result of radioactive decay, migration in the soil and biota, and decontamination. Consequently, re-suspension contributed negligibly in reducing ground radioactivity. The dust emission model could reproduce the air concentration of ^{137}Cs in winter, whereas the summer air concentration was underestimated by 1 to 2 orders of magnitude. Re-suspension from forests at a constant rate of 10^{-7} h^{-1}, multiplied by the green area fraction, could explain the air concentration of ^{137}Cs at Namie and its seasonal variation. The simulated contribution of dust re-suspension to the air concentration was 0.7–0.9 in the cold season and 0.2–0.4 in the warm season at both sites; the remainder of the contribution was re-suspension from forest. The re-suspension mechanisms, especially through the forest ecosystems, remain unknown. This is the first study that provides a crude estimation of the long-term assessment of radiocesium re-suspension. Additional research activities should investigate the processes/mechanisms governing the re-suspension over the long term. This could be achieved through conducting additional field experiments and numerical simulations.

1 Introduction

The Fukushima Daiichi Nuclear Power Plant (FDNPP) accidentally released nuclear fission products into the atmosphere and the ocean environment following the catastrophic earthquake and tsunami that occurred in March 2011. The accident caused serious contamination of the soil over the Tohoku region (northeastern part of Japan, including Fukushima and Miyagi prefectures) and the Kanto region (eastern part of Japan, including Ibaraki, Tochigi, Gunma, and Chiba prefectures; NRA, 2012). Since then, a number of studies have been conducted, particularly during the months that followed the accident. These assessments include primary emission estimations (Chino et al., 2011; Danielache

Published by Copernicus Publications on behalf of the European Geosciences Union.

et al., 2012; Stohl et al., 2012; Terada et al., 2012; Katata et al., 2012a, b, 2015; Winiarek et al., 2012, 2014; Hirao et al., 2013; Saunier et al., 2013; Yumimoto et al., 2016; Danielache et al., 2016), field observations (ground aerosol sampling: Masson et al., 2011, 2013; Kaneyasu et al., 2012; Adachi et al., 2013; Tsuruta et al., 2014; Igarashi et al., 2015; Oura et al., 2015; aircraft measurements: NRA, 2012; and measurements carried out on foot: Hososhima and Kaneyasu, 2015), and numerical simulations of transport and depositions (deterministic simulation: Chino et al., 2011; Morino et al., 2011; Yasunari et al., 2011; Stohl et al., 2012; Terada et al., 2012; Katata et al., 2012a, b; Winiarek et al., 2012, 2014; Hirao et al., 2013; Saunier et al., 2013; Katata et al., 2015; Yumimoto et al., 2016; Danielache et al., 2016; deterministic simulation with sensitivity runs: Morino et al., 2013; Adachi et al., 2013; Groëll et al., 2014; Saito et al., 2015; Sekiyama et al., 2015; Quérel et al., 2015; uncertainty modeling and probabilistic forecast: Girard et al., 2016; Sekiyama et al., 2016; and multi-model intercomparison and multi-model ensemble analysis: SCJ, 2014; Draxler et al., 2015; Kristiansen et al., 2016). The targeted radionuclides were species with both short and long half-lives: ^{99}Mo–^{99m}Tc (half-life 65.9–6 h), ^{129m}Te (33.6 days), ^{131}I (8.02 days), ^{132}Te–^{132}I (3.2 days–2.3 h), ^{134}Cs (2.07 years), ^{136}Cs (13.2 days), ^{137}Cs (30.1 years), ^{133}Xe (5.2 days), and ^{35}S (87.5 days).

In contrast, there have been few studies on the long-term (more than 1 year) quantitative assessment of radioactivity in the atmosphere associated with the Fukushima accident (Igarashi et al., 2015; Ishizuka et al., 2016; Kinase et al., 2016). More than 100 000 people were evacuated (METI, 2012), and most have still not been able to return to their homes and the public remains anxious about the safety of the affected areas. Radionuclides with long half-lives such as ^{134}Cs (2.07 years) and ^{137}Cs (30.1 years) are of particular concern (Evangeliou et al., 2014). Following the Chernobyl accident there were several studies on the re-suspension and long-term assessment of these radionuclides, such as Holländer and Garger (1996), Garger et al. (1998), Hatano and Hatano (2003), and Garger et al. (2012). For example, Garger et al. (2012) estimated the re-suspension "descending trend" as having a half-life of 300 days based on the surface activity concentration of ^{137}Cs. In the case of the Fukushima accident, Igarashi et al. (2015) estimated the half-reduction time by fitting multi-component exponential functions based on the ^{137}Cs concentration at the Meteorological Research Institute (Tsukuba) as 5.9 days, 16 days, and 1.1 years. These estimates were based on the trend in the observed surface air concentrations of ^{137}Cs, and thus the contributions from advection, diffusion, emission, and deposition terms were not quantified.

There are thousands of monitoring posts situated in the contaminated area in Fukushima prefecture to measure the ambient gamma dose rate. However, the data cannot be used for evaluating internal exposure: evaluation of internal exposure requires direct measurement of the surface air activity concentration. There are only a few observation sites that continuously measure the concentration of radiocesium (e.g., Igarashi et al., 2015; Ishizuka et al., 2016; Kinase et al., 2016). To assess the spatial distribution of the internal exposure hazard, 3-D numerical simulation is necessary to interpolate values for unmonitored locations. The numerical simulation requires emission flux as a boundary condition. However, the mechanism and thus the radioactivity flux associated with the re-suspension of ^{137}Cs were unknown, despite extensive efforts based on field observations (e.g., Igarashi et al., 2015; Ishizuka et al., 2016; Kinase et al., 2016).

Garger et al. (2012) summarized the re-suspension sources following the Chernobyl accident as (1) dust emission, (2) human activity in fields as well as on roads and construction sites, (3) forest fires, and (4) emissions from the power plant (i.e., opening of the Chernobyl sarcophagus). Re-suspension sources (1) (Ishizuka et al., 2016) and (4), i.e., additional emissions from the reactor buildings of FDNPP (TEPCO, 2012, 2013, 2014a, b, 2015), were considered in the present study. With respect to source (2), since the town of Namie is located in the evacuation zone, human activity has been extremely limited except for decontamination-related work. Although the decontamination-related work could be a potential source of re-suspension, it is not considered in the current simulation as the re-suspension flux has been hardly quantified. As to source (3), there is a low risk of forest fires in Japan given the high humidity, although some open biomass burning remains possible. Kinase et al. (2016) found no increase in ^{137}Cs activities when the concentration of levoglucosan, a marker of biomass burning, was increased, and thus re-suspension due to biomass burning was not considered in the present study. In addition to the four sources of ^{137}Cs from the Chernobyl accident, re-suspension from terrestrial biota was considered as suggested by Kinase et al. (2016). They found substantial amounts of bioaerosols upon scanning electron microscopy samples collected in the summer, when ^{137}Cs concentration was high.

In the present study, the long-term effect of radiocesium re-suspension from contaminated soil and terrestrial biota was quantitatively assessed using 3-D numerical simulation, a field experiment on dust emission flux in a contaminated area (Namie, Fukushima prefecture), and air concentration measurements conducted inside (Namie) and outside (city of Tsukuba, Ibaraki prefecture) the contaminated area. Even though the re-suspension mechanisms still remain unknown, by utilizing the observational data both inside and outside, together with the transport model, we aimed to provide as robust an analysis as possible of the re-suspension, transport, and re-deposition of ^{137}Cs over the Tohoku and Kanto regions of Japan.

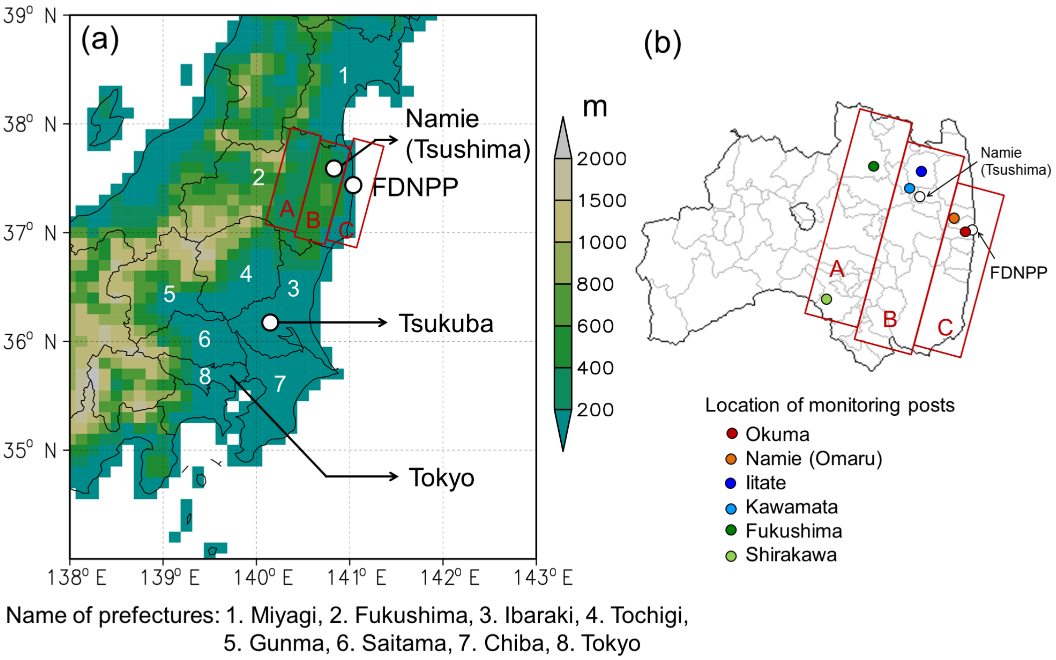

Figure 1. (a) The model domain showing the model terrestrial elevation, observation sites, and other locations described in the study. The linear distances from FDNPP to Namie (Tsushima district, town of Namie), Tsukuba and Tokyo are approximately 30, 170, and 220 km, respectively. The numbers denote prefectures: 1, Miyagi; 2, Fukushima; 3, Ibaraki; 4, Tochigi; 5, Gunma; 6, Saitama; 7, Chiba; and 8, Tokyo. **(b)** Fukushima prefecture and (colored circles) the locations (village, town, or city name) of monitoring posts used in this study (see Fig. 14). The red letters in both **(a)** and **(b)** denote the name of the area based on geographical features: A, Nakadori valley; B, Abukuma highland; and C, Hamadori coastal area.

2 Numerical simulation

A brief description of the numerical method, such as the processes considered in the model and simulation settings, is presented in this section, and detailed model formulations are described in Appendix A. Because the schemes and assumptions regarding the emissions are key to the current study, they are described in detail in the following subsections.

2.1 Lagrangian model and simulation settings

Figure 1 shows the domain of the Lagrangian model (LM) with model terrestrial elevations, covering 138–143° E and 34–39° N. The model domain covers the southern part of the Tohoku region (the northern mountainous part of the domain, including Yamagata, Miyagi, and Fukushima prefectures), and includes the FDNPP and highly polluted areas such as the habitation-restricted zone (HRZ; 20–50 $\mathrm{mSv\,yr^{-1}}$) and difficult-to-return zone (DRZ; > 50 $\mathrm{mSv\,yr^{-1}}$; METI, 2012). It also covers the Kanto region (or Kanto Plain, the largest plain in Japan, approximately 120 km × 120 km), a highly populated region that includes low to moderately polluted areas such as Tokyo, Gunma, Tochigi, Ibaraki, Saitama, and Chiba prefectures.

The LM considers horizontal and vertical diffusion and advection, gravitational settling, dry and wet depositions, and radioactive decay. It uses simple parameterizations for dry and wet deposition schemes, and it can be driven by meteorological analysis datasets so that it does not require a meteorological model to predict detailed meteorological fields and variables. The model was designed to be easily handled and computationally efficient so that non-specialists of numerical simulations can conduct long-term assessments of atmospheric diffusion problems using their desktop or laptop computers. The LM was designed for rough budget estimates, as presented in the current study, or for sensitivity analyses using a large number of parameters (e.g., Groëll et al., 2014; Quérel et al., 2015; Girard et al., 2016), rather than for process-oriented analysis (e.g., Morino et al., 2013; Katata et al., 2015) or sensitivity analyses of the physical and chemical parameters of aerosols (Adachi et al., 2013). Details of each process and parameter are described in Appendix A. Statistical error of a Lagrangian simulation is inversely proportional to the square of the number of Lagrangian particles (LPs). The statistical accuracy of the current simulation setting is discussed in Appendix B.

The Grid Point Value-Mesoscale Model (GPV-MSM) of the Japan Meteorological Agency (JMA) was used for meteorological analysis to calculate the transport of LPs. It covers 120–150° E and 23–47° N and provides 3-hourly and 16 pressure levels of 3-D meteorological variables, from 1000 to 100 hPa, with a horizontal grid resolution of approximately

Table 1. The observation sites and monitoring posts used to provide data for this study.

Name	Location	Description
Observation sites		
Namie (Tsushima)	140.7683° E, 37.5621° N	Namie High School, Tsushima Campus[1]
Tsukuba	140.1254° E, 36.0551° N	Meteorological Research Institute
Monitoring posts		
Okuma	140.9969° E, 37.4163° N	Ottozawa 3 Community Center[2]
Namie (Omaru)	140.9296° E, 37.4665° N	Omaru Multipurpose Community Center[3]
Iitate	140.7385° E, 37.6772° N	Iitate Junior High School[4]
Kawamata	140.6979° E, 37.5836° N	Yamakiya Otsu 8 Community Firehouse[5]
Fukushima	140.4765° E, 37.6870° N	Fukushima-Minami Fire Department
Shirakawa	140.1904° E, 37.1241° N	Takayama-Kita Park

[1] Original location (now moved to city of Nihonmatsu). [2] Ottozawa San-ku Chiku Shukaijo (in Japanese). [3] Omaru Tamokuteki Shukaijo (in Japanese). [4] Original location (now moved to city of Fukushima). [5] Yamakiya Otsu Hachi-ku Community Shoubou Center (in Japanese).

11 km (Δ longitude = 0.125° and Δ latitude = 0.1°) and surface variables at twice the resolution of that for the 3-D variables (Δ longitude = 0.0625° and Δ latitude = 0.05°). In the simulation, the whole model domain where LPs can travel is 138–143° E, 34–39° N and from ground surface to 500 hPa. For output of the model results, LP fields are converted to Eulerian concentration ($\mathrm{Bq\,m^{-3}}$) and deposition ($\mathrm{Bq\,m^{-2}}$) fields in the same horizontal space as the 3-D variables but are vertically allocated from the ground surface to an altitude of 1 km at 100 m intervals. The observed surface air concentration was compared with the simulated mean concentration at 0–100 m above ground level (AGL).

2.2 Re-suspension from bare soil

Ishizuka et al. (2016) developed a re-suspension scheme for radiocesium from bare soil based on measurements on the schoolyard at Namie High School, Tsushima Campus (denoted as Namie (Tsushima) in Table 1 and Fig. 1), in the DRZ.

$$F_{\mathrm{soil}} = p_{20\mu\mathrm{m}} F_{\mathrm{M}} (1 - f_{\mathrm{forest}}) B_{5\mathrm{mm}}(t), \tag{1}$$

where F_{soil} is the ^{137}Cs dust re-suspension flux from soil ($\mathrm{Bq\,m^{-2}\,s^{-1}}$), $p_{20\mu\mathrm{m}}$ is the surface area fraction of dust smaller than 20 µm in diameter against soil containing a maximum size of 2 mm particles and varies depending on soil texture (1.3×10^{-8} for sand, 0.19 for loamy sand, 0.45 for sandy loam, and 0.80 for silt loam), F_{M} is the total dust mass flux ($\mathrm{kg\,m^{-2}\,s^{-1}}$), f_{forest} is the forest area fraction, and $B_{5\,\mathrm{mm}}(t)$ is the specific radioactivity of surface soil (from the surface to a depth of 5 mm; $\mathrm{Bq\,kg^{-1}}$) as a function of time since March 2011. The formula is based on the assumption that dust particles smaller than 20 µm in diameter originating from the surface soil and to a depth of 5 mm were suspended and transported through the atmosphere. The surface area fraction was used for $p_{20\mu\mathrm{m}}$ based on the assumption that radiocesium is bound to the surface of soil particles (Evrard et al., 2015). F_{M} is formulated as being proportional to the cube of the friction velocity u_* ($\mathrm{m\,s^{-1}}$) as described by Loosmore and Hunt (2002) and was applied to the dust emission:

$$F_{\mathrm{M}} = 3.6 \times 10^{-9} u_*^3. \tag{2}$$

Since u_* is not available in GPV-MSM, u_* was estimated using a wind speed at 10 m AGL by assuming neutral stratification conditions.

$B_{5\,\mathrm{mm}}\,(t)$ was derived from the combination of B_{obs}, the observed horizontal distribution of ^{137}Cs deposition obtained from an airborne radiological survey (NRA, 2012; $\mathrm{Bq\,m^{-2}}$), and $r_{5\,\mathrm{mm}}$, the surface soil activity ratio of 0–5 mm to 0–5 cm obtained from a vertical profile measurement of ^{137}Cs in the ground soil at Namie High School (i.e., $0.57\,\mathrm{Bq\,Bq^{-1}}$), as

$$B_{5\,\mathrm{mm}}(t) = \frac{B_{\mathrm{obs}} r_{5\,\mathrm{mm}} R_{\mathrm{decay}}(t)}{5 \times 10^{-3} \rho_{\mathrm{b,\,soil}}}, \tag{3}$$

where $\rho_{\mathrm{b,\,soil}}$ is the bulk density of soil particles per unit volume in the ground space ($\mathrm{kg\,m^{-3}}$) obtained from the porosity ($0.4\,\mathrm{m^3\,m^{-3}}$) and the density of dust particles ($2650\,\mathrm{kg\,m^{-3}}$). For R_{decay}, which is the decreasing ratio of activity in the ground to its initial state ($R_{\mathrm{decay}}(t = 0) = 1$), only radioactive decay was considered for the re-suspension calculation. The decreasing rate due to other processes such as land surface processes (e.g., runoff, erosion, percolation and all the processes resulting in migration of radiocesium in the soil and biota; Evrard et al., 2015; Matsuda et al., 2015) and decontamination were not considered here. Furthermore, suppression of dust emission due to soil moisture and snow cover was not considered. Therefore, it should be noted here that F_{soil} in Eq. (1) is considered as the upper boundary of ^{137}Cs re-suspension flux from surface soil. Effects such as land surface processes, decontamination, and dust emission suppression due to snow cover are extensively discussed in Sect. 5.3

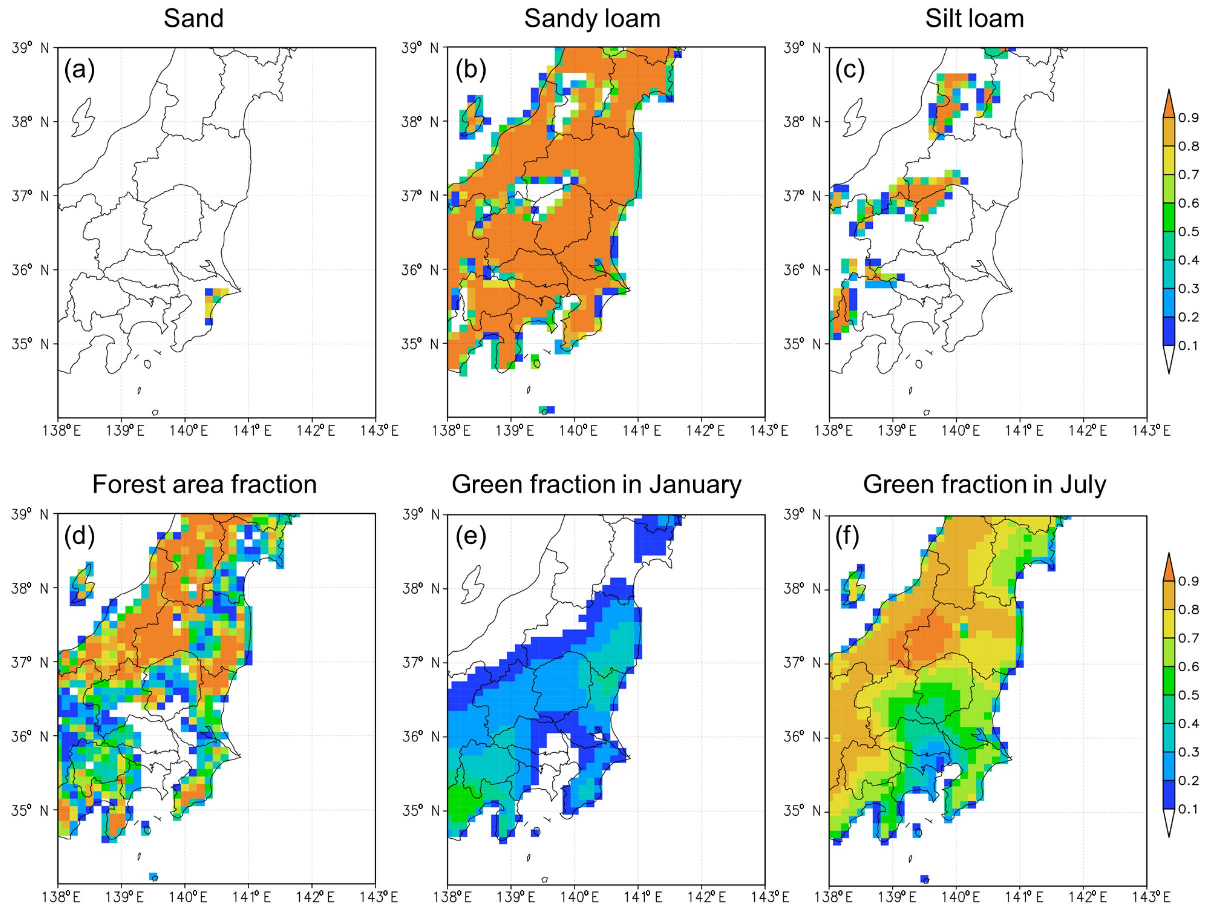

Figure 2. The areal fractions of **(a)–(c)** soil texture and **(d)–(f)** land use category used for the boundary conditions of the simulation.

using ambient gamma dose rate measurements obtained by the monitoring posts in Fukushima prefecture.

Equation (1) is a function of soil texture. The areal fraction of soil texture of the model grid was obtained from the database of the advanced research Weather Research and Forecasting model version 3 (WRFV3; Skamarock et al., 2008). Sixteen categories of soil texture (Miller and White, 1998) with a 30 arcsec resolution dataset can be obtained from the web after subscription at http://www2.mmm.ucar.edu/wrf/users/download/get_sources_wps_geog.html and were re-categorized into the above-mentioned four categories (i.e., sand, loamy sand, sandy loam, and silt loam) and interpolated to the LM resolution (∼ 11 km) as shown in Fig. 2a–c. Note that the loamy sand fraction is not presented because it is zero for the entire domain. The parameter f_{forest} (Fig. 2d) was also obtained from the database of WRFV3 and was calculated based on the 24 United States Geological Survey (USGS) land use categories, which are constant over time. The land use category dataset can also be obtained from the above website.

Ishizuka et al. (2016) validated their dust emission module by using a 1-D model and observed the surface air concentration of ^{137}Cs at Namie in the winter. After applying the module to our 3-D simulation, we found that the air concentration at Namie was underestimated by about factor of 5 for the same period. The module was formulated based on physical parameters (such as u_*) but contains parameters obtained at a single location (such as $r_{5\,\mathrm{mm}}$ and $\rho_{\mathrm{b,\,soil}}$) and under a fixed atmospheric condition (Ishizuka et al., 2016), whereas ideally parameters in Eqs. (1)–(3) should have considered variations among locations and atmospheric conditions for the 3-D simulation. We simply multiplied the dust emission flux by 5 after adjusting the simulation results against the observed concentration of ^{137}Cs at Namie in the winter. This is one of the simplest top-down approaches for adjusting the emission flux according to the air concentration. The module requires improvement in the future as more reliable parameters become available for various conditions and locations.

2.3 Re-suspension from the forest ecosystems

The re-suspension mechanism of radiocesium from land ecosystems remains unknown. Kinase et al. (2016) found substantial amounts of bioaerosols (rather than mineral dust particles) in samples collected for scanning electron microscopy in the summer, when the ^{137}Cs concentration was high. This does not prove that the bioaerosol was carrying radiocesium but that it could be a potential carrier. The behavior of Cs in the environment can be inferred by analogy with K, a congener of Cs. Potassium is a necessary and abundant element in plants and circulates between land ecosystems. The addition of potassium fertilizer to a rice field in Fukushima significantly reduced the Cs content of the rice (Ohmori et al., 2014). Substantial amounts of K-salt-rich particles, possibly emitted by active biota such as plants and fungi, and coated with secondary organic aerosols, were observed in pristine Amazonian rainforest (Pöhlker et al., 2012). The major areal fraction of the contaminated area in Fukushima is covered by biota-rich mountain forests. Despite the differences in plant species and locations, it is plausible that water-soluble radiocesium circulating in the biota and soil in the forests was somehow re-emitted into the atmosphere and contributed to the surface air concentration. The re-suspension from the forest ecosystem was simply formulated as follows:

$$F_{\mathrm{forest}} = f_{\mathrm{forest}} f_{\mathrm{green}} r_{\mathrm{const}} B_{\mathrm{obs}} R_{\mathrm{decay}}(t), \tag{4}$$

where F_{forest} is the ^{137}Cs re-suspension flux from forest ($\mathrm{Bq\,m^{-2}\,s^{-1}}$); f_{forest} is the forest area fraction; f_{green} is the monthly green area fraction; r_{const} is the constant re-suspension coefficient ($\mathrm{s^{-1}}$); and, as in Eq. (3), B_{obs} and R_{decay} are the observed ^{137}Cs deposition (NRA, 2012; $\mathrm{Bq\,m^{-2}}$) and the decreasing ratio of activity in the ground, respectively. r_{const} is a tunable parameter to adjust the simulated air concentration of ^{137}Cs to that observed. In the current study, r_{const} is set to $10^{-7}\,\mathrm{h^{-1}}$ by adjusting the simulation data using the observed ^{137}Cs concentration at Namie in the summer, when the re-suspension from soil was negligible due to the higher soil moisture content (following considerable rain) and lower wind speed. As with re-suspension from bare soil, only radioactive decay was considered for R_{decay} and the other processes were not considered. The parameter f_{green} was obtained from the database of WRFV3 and was originally derived from satellite Advanced Very High Resolution Radiometer (AVHRR) normalized difference vegetation index (NDVI) data (Gutman and Ignatov, 1998). Whereas f_{forest} remains constant, the monthly averaged f_{green} was used in order to reflect seasonal changes in the activity of the biota.

2.4 Emission from FDNPP (primary emission, additional emissions from the reactor buildings, and unexpected re-suspension associated with debris removal operations)

The Japan Atomic Energy Agency (JAEA)'s latest estimate of the primary emission from FDNPP, Katata et al. (2015), was applied for the emergency situation of March 2011 to evaluate the performance of the LM model against the horizontal distribution of ^{137}Cs deposition of the airborne radiological survey (NRA, 2012; as shown later in Fig. 4a) and surface air concentrations measured at Tsukuba (Fig. 1a). We selected this inventory because it is JAEA's most up-to-date version. Based on an integrated understanding of environmental radioactivity, atmospheric dispersion, and the nuclear reactors, the JAEA team has carefully established a series of inventories for about 5 years, starting with Chino et al. (2011), followed by Katata et al. (2012a, b) and Terada et al. (2012), and finally the current inventory (Katata et al., 2015), which is substantially improved compared to the previous versions.

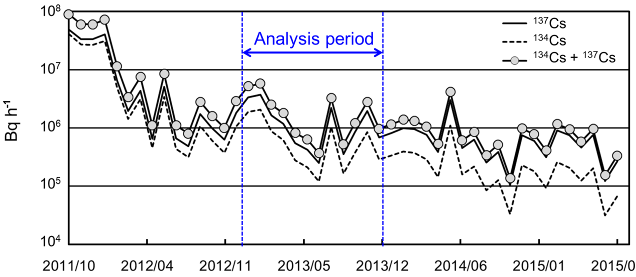

Figure 3. Monthly mean emission flux of radiocesium released from the reactor buildings of FDNPP from October 2011 to August 2015 as estimated by TEPCO (TEPCO, 2012–2015).

Ongoing emissions during the study analysis period after the emergency situation, i.e., January to December 2013, were obtained from the Tokyo Electric Power Co. Inc. (TEPCO) monthly mean emission flux from the reactor buildings (TEPCO, 2012, 2013, 2014a, b, 2015). Because only the sum of ^{134}Cs and ^{137}Cs was provided, the fractions of these two isotopes were calculated based on their half-lives and the assumption that their activities were equal in March 2011 (e.g., Katata et al., 2015), as shown in Fig. 3. The values range from 10^5 to $10^7\,\mathrm{Bq\,h^{-1}}$; however, for simplicity we set a constant value of $10^6\,\mathrm{Bq\,h^{-1}}$ in the current simulation.

In August 2013, unexpected re-suspension associated with debris removal operations was reported by TEPCO (2014c) and NRA (2014) and the gross amount was 10^{10}–10^{11} Bq of ^{137}Cs (TEPCO, 2014c; NRA, 2014; Steinhauser et al., 2015). The impact of this unexpected re-suspension is briefly discussed in Sect. 5.2 along with an additional finding, but this emission was not considered in the present LM simulation. In this study we focused on the ongoing and continuous emission, mostly from the natural environment, that is difficult to control.

3 Field observations

Details of the surface air activity concentration measurement techniques can be found in Ishizuka et al. (2016) and Kinase et al. (2016) for Namie and Igarashi et al. (2015) for

Tsukuba. At the both sites, ^{134}Cs and ^{137}Cs surface air concentrations were measured. The sampling intervals were 1–2 days at Namie and 1 week at Tsukuba for the analysis period of this study, the year 2013. The observations at Namie started on 14 December 2012, while those at Tsukuba started on 31 March 2003, before the FDNPP accident. In March 2011, the sampling interval was increased at Tsukuba to 6 h–1 day and the data for these periods were used for the validation of LM and its parameters, as presented in Sect. 4.1.

The Namie site is located on the schoolyard of Namie High School, Tsushima Campus, in the Tsushima district of Namie in Fukushima prefecture, as shown in Table 1 and Fig. 1. The town of Namie extends from the Hamadori coastal area (denoted as C in Fig. 1) to the Abukuma highland area (B in Fig. 1). There are two sites in Namie used in the study. In order to distinguish the Tsushima Campus site in the highland area from the monitoring post site located in Omaru district in Namie in the coastal area, the Tsushima site is referred to as Namie (sometimes as Namie (Tsushima)) and the Omaru site is referred to as Omaru (sometimes as Namie (Omaru)) throughout the manuscript. The Tsukuba site is located on the premises of the Meteorological Research Institute (Table 1 and Fig. 1a).

Namie (Tsushima) was located in the DRZ ($>50\,\mathrm{mSv\,yr^{-1}}$, $\sim 9.55\,\mathrm{\mu Sv\,h^{-1}}$)[1] and the observed ^{137}Cs deposition amount was $2300\,\mathrm{kBq\,m^{-2}}$ (NRA, 2012). The ambient gamma dose rate was $11.2\,\mathrm{\mu Sv\,h^{-1}}$ on 1 April 2012 at the site and had dropped to $4.8\,\mathrm{\mu Sv\,h^{-1}}$ on 16 February 2016 and at the HRZ level (20–50 $\mathrm{mSv\,yr^{-1}}$, 3.85–9.55 $\mathrm{\mu Sv\,h^{-1}}$). Tsukuba is located approximately 170 km southwest of FDNPP. The observed ^{137}Cs deposition amount was $21\,\mathrm{kBq\,m^{-2}}$ (NRA, 2012), 2 orders of magnitude lower than at Namie, and the dose rate has remained below $0.1\,\mathrm{\mu Sv\,h^{-1}}$ since 2012.

4 Results

Section 4.1 presents a validation of the LM model and the optimization of the model deposition parameters by using airborne observations (NRA, 2012) and the emission inventory of Katata et al. (2015) for the emergency situation of March 2011. Using the optimized ranges of model parameters validated in Sect. 4.1, the simulated re-suspension of ^{137}Cs from soil and forest, as well as emission from FDNPP, is presented in Sect. 4.2, and the budgets for re-suspension, transport, and re-deposition are presented in Sect. 4.3.

4.1 Model and parameter validation for the emergency situation (March 2011)

Figures 4 and 5 show the observed and simulated distribution of ^{137}Cs deposition in March 2011, and the scatterplot comparing the observational and simulation results. In the simulation shown in the figures, the "reference" sets used for dry and wet deposition parameters, namely the collection efficiency of aerosols using hydrometeors E_c (Eq. A1) and the dry deposition velocity over land v_d (Eq. A3), were 0.04 and $0.1\,\mathrm{cm\,s^{-1}}$, respectively.

Since LM uses simple parameterizations for dry and wet deposition, as described in Appendix A, sensitivity tests were conducted for model validation, together with optimization of the deposition parameters. Table 2 summarizes the ranges of the deposition parameters for the sensitivity tests and the results of the ^{137}Cs budget and statistical measurements between the observations and the simulation.

The parameter E_c was 0.05 for the JMA dispersion model (JMA, 1998) but the targeted species are different. For example, volcanic ash (particles larger than 1 µm in diameter) used for the JMA model was generally larger than the aerosols carrying ^{137}Cs (around 1 µm in diameter observed in the downwind area, Tsukuba; Kaneyasu et al., 2012; Adachi et al., 2013). Since the inertia of these smaller ^{137}Cs particles is likely to be smaller than that for volcanic ash, E_c could be smaller. The range of E_c was set as 0.02–0.06. The dry deposition velocity v_d was selected as $0.1\,\mathrm{cm\,s^{-1}}$ for ^{137}Cs in Furuno et al. (1999). The range for v_d was set as 0.05 to 0.15 in the present study.

The emission inventory of Katata et al. (2015) amounted to 14.1 PBq from 12 March to 1 April 2013. The simulated deposition over the model domain (138–143° E, 34–39° N) ranged from 3.4 to 4.7 PBq, which is approximately 24–33 % of the emission from the FDNPP. Sixty percent of the total deposition occurred over land, for a total of 2.0–2.8 PBq, which is close to the observed value of 2.68 PBq, and the observed value is within the range of the sensitivity runs. Statistical measures such as the fractional bias FB, the correlation coefficient R (linear vs. linear), and FAx (fraction of the simulated values within a factor of x) are listed in Table 2. To find better combinations of (or to optimize) the dry and wet deposition parameters, sensitivity runs were screened based on the criteria $\mathrm{FA10} > 0.9$, $\mathrm{FA5} > 0.7$, $R > 0.75$, and an absolute value of $\mathrm{FB} < 10\,\%$. Only one combination (E_c, v_d) = (0.04, $0.1\,\mathrm{cm\,s^{-1}}$) satisfied the criteria, and thus this is referred to as the "reference" parameters. To evaluate the sensitivity (or uncertainty) of the re-suspension simulation for 2013 due to the deposition parameters, the range of the combination of parameters was set as (E_c, v_d) = (0.03–0.05, 0.05–0.1 $\mathrm{cm\,s^{-1}}$) around the reference parameters (referred to as the "optimized range") by excluding the parameters with the worse performances. The ranges of the statistical measures of the optimized runs are listed in Table 2. FB, R, FA2, FA5, and FA10 after the optimization had the

---

[1] Calculated by the following equation: Annual radiation exposure = (ambient dose rate − background dose rate ($= 0.04\,\mathrm{\mu Sv\,h^{-1}}$)) × (8 h + 0.4 × 16 h) × 365 days.

Table 2. ^{137}Cs budget and statistical analysis for the comparison of observed and simulated deposition data for March 2011.

	E_c^a (–)	v_d^b ($\mathrm{cm\,s^{-1}}$)	D_{all}^c (PBq)	D_{land}^d (PBq)	FB^e (–)	R^f (–)	FA2^g (–)	FA5^h (–)
Sensitivity test								
Range	0.02–0.06	0.05–0.15	3.4–4.7	2.0–2.8	−0.25–0.00050	0.73–0.78	0.25–0.30	0.63–0.77
Optimization used for the re-suspension analysis for 2013								
Reference	0.04	0.10	4.2	2.5	−0.062	0.75	0.28	0.74
Optimized range	0.03–0.05	0.05–0.10	3.7–4.3	2.2–2.6	−0.18 to −0.036	0.74–0.77	0.26–0.30	0.68–0.74
Reference values								
Observed deposition over land D_{obs} (NRA, 2012)	2.68 PBq							
Emission amount (Katata et al., 2015)	14.1 PBq							

[a] Collection efficiency; see Eq. (A1) [b] Dry deposition velocity over land; see Eq. (A3). [c] Simulated deposited amount over the whole model domain. [d] Simulated deposited amount only over land. [e] Fractional bias between D_{land} and D_{obs}. [f] Correlation coefficient between each grid cell of the observed and simulated deposition (linear vs. linear). [g] Fraction of simulated values within a factor of 2 of the observed values. [h] Fraction of simulated values within a factor of 5 of the observed values. [f, g, h] Compared only at grids where the observed values are greater than 10 $\mathrm{kBq\,m^{-2}}$.

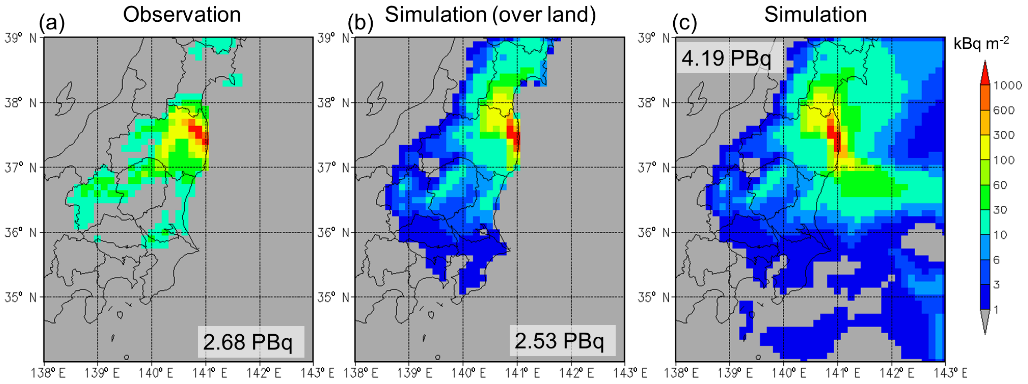

Figure 4. **(a)** Aircraft observation and **(b, c)** simulation of ^{137}Cs deposition depicted **(b)** only over land and **(c)** for the whole domain ($\mathrm{kBq\,m^{-2}}$). The observation was interpolated to the model grid (Δ longitude = 0.125° and Δ latitude = 0.1°). A decay correction for the observation was made for March–May 2012, varying depending on the region. The simulation provided a cumulative value from 12 March to 1 April 2011. The total activities are presented as numbers. The color scales are the same for **(a)–(c)** but observed values are not depicted below the detection limit, 10 $\mathrm{kBq\,m^{-2}}$. The deposition parameters of the simulation in the figure are $E_c = 0.04$ and $v_d = 0.1\,\mathrm{cm\,s^{-1}}$.

ranges −0.18 to −0.036, 0.74–0.77, 0.26–0.30, 0.68–0.74, and 0.91–0.92, respectively. These statistical measures were comparable to those reported in previous multi-model comparison studies (R: 0.27–0.85; FB: −0.84–0.56; and FA2: 0.14–0.57, in SCJ, 2014; Draxler et al., 2015). The current model is thus shown to be sufficiently credible for the budget analysis in this study, despite the simple parameterization and the low resolution in space (∼ 11 km) and time (3 h).

In agreement with many previous studies, the simulated contribution of wet deposition was larger than that of dry deposition: the ratio of the amount of dry to wet deposition ranged from 0.12 to 0.23 for the optimized parameter ranges, indicating that the results were less sensitive to the dry deposition parameter. Generally speaking, R became higher as E_c became lower, whereas FAx became higher as E_c became higher for the various ranges of the sensitivity tests. Therefore, lower E_c did not meet the criteria of FAx and higher E_c did not meet the criteria of R. Consequently, after the optimization, the maximum values of the statistical measures were lower but the minimum values became higher, indicating that the optimization was successful in excluding the parameters with the worse performances (rather than selecting

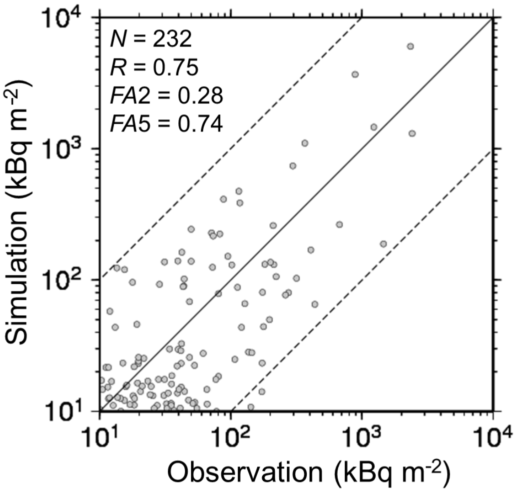

Figure 5. Scatterplot between the observational data and the simulation results for ^{137}Cs deposition (kBq m^{-2}). The deposition parameters of the simulation in the figure are $E_c = 0.04$ and $v_d = 0.1$ cm s^{-1}. N indicates the number of samples, and the statistical measures R, FA2, and FA5 are described in Table 2.

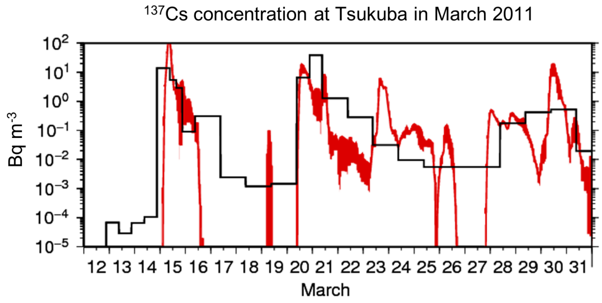

Figure 6. Time series of the surface activity concentration of (black) observed and (red) simulated ^{137}Cs concentrations at Tsukuba from 12 March to 1 April 2011 (Bq m^{-3}). The red shaded areas indicate the range of ^{137}Cs concentrations obtained when the simulations were run using the optimized parameter ranges $E_c = 0.03$–0.05 and $v_d = 0.05$–0.1 cm s^{-1}.

the best parameters). It should be noted here that the optimized deposition parameters are not necessarily physically valid but rather give simulation results consistent with the available observations. The results presented in this section indicate that the current LM simulation with these optimized parameters has the potential to reproduce consistent features of the radiocesium budget over the Tohoku and Kanto regions of Japan.

Figure 6 shows the temporal variation in simulated (red) and observed (black) ^{137}Cs concentrations at Tsukuba in March 2011. The model reproduced the three major plumes arriving at Tsukuba on 15–16, 20–21, and 28–30 March; a plume on 23 March was not observed but only appeared in the simulation. The red shaded areas indicate the range of ^{137}Cs concentrations obtained when the simulations were run using the optimized parameter ranges $E_c = 0.03$–0.05 and $v_d = 0.05$–0.1 cm s^{-1}. Due to differences in the parameters used, the surface air concentration could vary by approximately 1 order of magnitude in transported plumes that experienced wet scavenging along their pathway.

4.2 Re-suspension in 2013

Figure 7 shows the observed and daily mean simulated (with the reference parameters) surface air concentrations at Namie and Tsukuba for the year 2013. The red, green, and blue lines indicate re-suspension from soil, re-suspension from forest, and emission from the FDNPP reactor buildings, respectively. Scatterplots between the observed and the simulated total concentrations are also shown in the figure and the statistical measures between them are listed in Table 3. The correlation coefficients (linear vs. linear) are low at the both sites, but the simulated and the observed medians are close to each other and FAx shows high values at the both sites. Consequently, the current simulation is credible enough for the quantitative assessment of the annual radiocesium budget.

As discussed in Sect. 2.2, note that the re-suspension flux due to the dust emission module (Ishizuka et al., 2016) is multiplied by 5 in this study in order to adjust to the observation level at Namie in the cold season (January to March, October to December). Also note that the re-suspension coefficient r_{const} in Eq. (4) was set as 10^{-7} h^{-1} in order to adjust to the observation level at Namie in the warm season (May to September). The emission flux reported by TEPCO varied from 10^5 to 10^7 Bq h^{-1} during the study period but we set it to 10^6 Bq h^{-1} for simplicity. We did not try to precisely adjust r_{const} to the observation by, for example, using inverse modeling, and instead we simply multiplied by power-of-10 values (except for dust emission, which is five), which are constant in time and space because (1) this facilitated straightforward interpretation of the simulation results by keeping the simulated variation solely originating from the variation in boundary conditions (i.e., emission and meteorology), and therefore (2) this provided simple but useful clues for understanding the re-suspension mechanisms, which remain unknown.

Using the dust emission module (which has a physical basis), ^{137}Cs flux re-suspended from soil could account for the level of the observed surface air concentration of ^{137}Cs at Namie in the cold season. Under the influence of the northwesterly winter monsoon, the surface wind speed is high over the contaminated area compared to the summer (as shown later in Fig. 10). Note that the flux might be a maximum estimate since it does not consider land surface processes (such as soil moisture, snow cover, or migration of ^{137}Cs in the soil and biota) and decontamination, which could reduce the ^{137}Cs re-suspension flux. In contrast, in the warm season, the estimated flux significantly underestimated the observation by 1 to 2 orders of magnitude due to the weak surface wind, indicating that the dust emission

Table 3. Statistical analysis for the comparison of observed and simulated ^{137}Cs air concentration at Namie and Tsukuba for 2013.

Site	N (–)	Median, obs. (mBq m^{-3})	Median, sim. (mBq m^{-3})	R (–)	FA2 (–)	FA5 (–)	FA10 (–)
Namie	311	0.71	0.69	0.12	0.67	0.94	0.99
Tsukuba	74	0.022	0.024	0.19	0.70	0.95	1.00

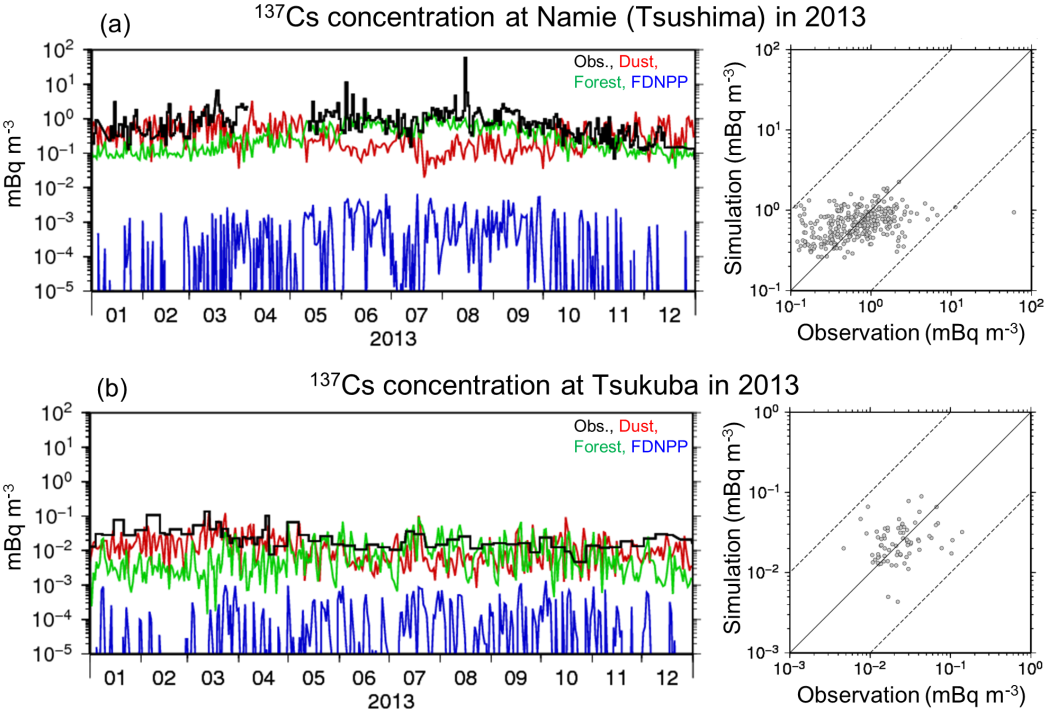

Figure 7. Time series of the surface air concentration of (black) observed ^{137}Cs and (colors) simulated daily ^{137}Cs levels on the left and scatterplots between observed and simulated total (i.e., sum of colors) ^{137}Cs at **(a)** Namie and **(b)** Tsukuba. The colored lines indicate simulated ^{137}Cs concentrations due to (red) re-suspension from soil using the scheme given in Ishizuka et al. (2016) (five times), (green) re-suspension from forest with a re-suspension rate of 10^{-7} h^{-1}, and (blue) emission from the FDNPP reactor buildings with a constant emission rate of 10^6 Bq h^{-1}. The deposition parameters of the simulation in the figure are $E_c = 0.04$ and $v_d = 0.1$ cm s^{-1}.

process may not be the sole process involved in sustaining the air concentration of ^{137}Cs during this period. Introducing the ^{137}Cs re-suspension component from forest with a resuspension coefficient of 10^{-7} h^{-1} and a monthly variation in the green area fraction (derived from NDVI) could quantitatively account for the observed air concentration together with its seasonal variation at Namie. Even though both the simulated re-suspension from soil and forests reproduced the quantity and seasonal variation in the background concentration (in other words, concentrations originating from continuously presenting emissions, such as natural emissions, and not accidental ones) at Namie, sporadic peak events, such as the daily mean ^{137}Cs concentration exceeding 10 mBq m^{-3} as observed in June and August at Namie, were not simulated. Some specific re-suspension events might occur from the highly contaminated areas such as the premises of FDNPP (e.g., debris removal operations) or very close to FDNPP on these days, as indicated later in Sect. 5.2. The simulated ^{137}Cs concentrations due to the monthly mean emission from the reactor buildings (i.e., 10^6 Bq h^{-1}) significantly underestimated the observed concentration by more than 3 orders of magnitude at Namie and by 2 orders of magnitude at Tsukuba. Even the maximum estimate of 10^7 Bq h^{-1} does not reach the observed level. The emission from FDNPP may not have been the sole process sustaining the air concentration of ^{137}Cs in 2013, supporting the discussion in Igarashi et al. (2015), which concluded that direct emission from the FDNPP played a minor role in the observed atmospheric radiocesium concentrations over Tsukuba during 2013–2014.

The observed air concentration of ^{137}Cs at Tsukuba was about 1 to 2 orders of magnitude lower than that at Namie. The simulated difference between the two sites inside and

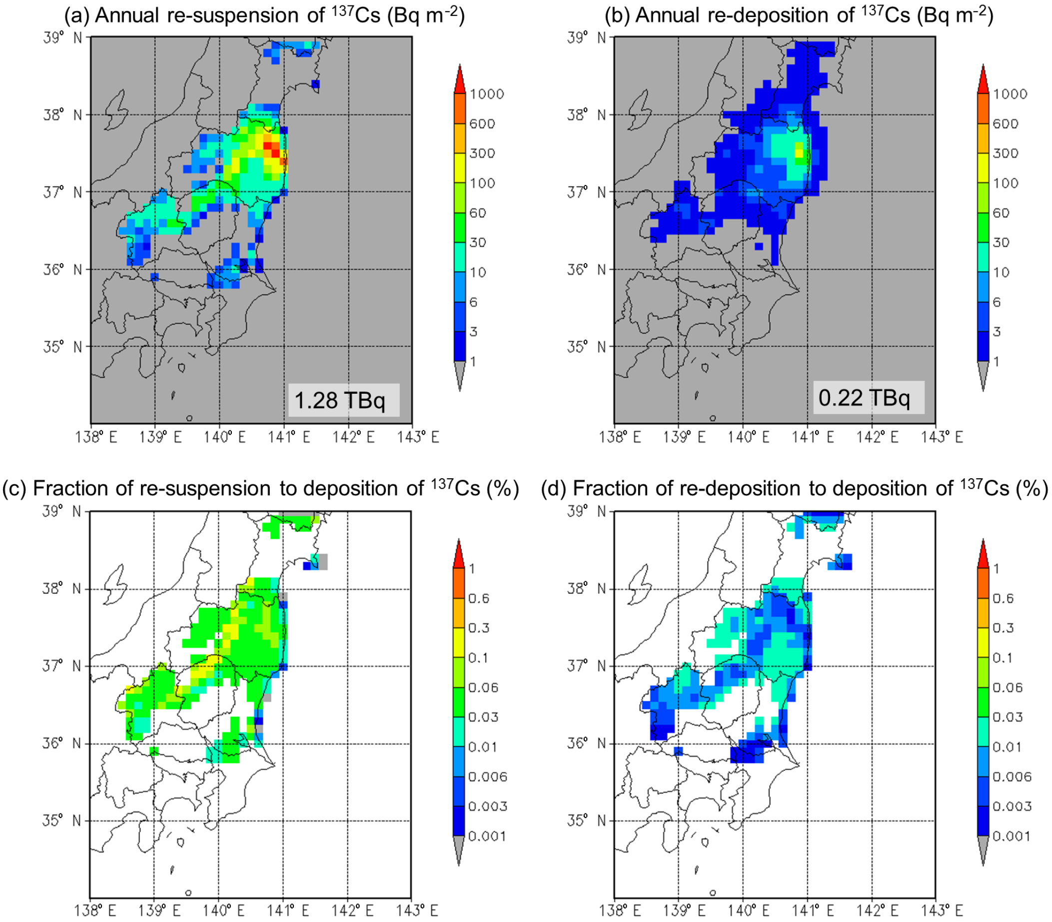

Figure 8. Annual total amounts of **(a)** the re-suspension and **(b)** the re-deposition of ^{137}Cs. The total activities are presented as numbers. Fractions of the re-suspension and the re-deposition to the observed ^{137}Cs deposited amounts are also shown in **(c)** and **(d)**, respectively. The deposition parameters of the simulation in the figure are $E_c = 0.04$ and $v_d = 0.1\,\mathrm{cm\,s^{-1}}$.

outside of the contaminated areas was consistent with the observed difference. This finding indicates that the current LM simulation provided consistent features of re-suspension, transport, and re-deposition in the Tohoku and Kanto regions of Japan of ^{137}Cs originating from Fukushima.

4.3 Budget analysis

Figure 8 illustrates the simulated (with the reference parameters) annual amounts of total re-suspension and re-deposition of ^{137}Cs, together with their ratios to the observed deposition (Fig. 4a). The simulated areal total re-suspended amount was 1.28 TBq, which was equivalent to 0.048 % of the total deposited amount, 2.68 PBq. The areal total re-deposited amount (with the reference parameters) was 0.22 TBq (0.18–0.23 TBq for the optimized range of the deposition parameters), corresponding to approximately 17.2 (14.1–18.0) % of the re-suspended amount deposited mainly in the Tohoku region, with the remainder being transported out of the model domain. Therefore, the regional mean rate in the decrease of the land surface ^{137}Cs concentration due to re-suspension was estimated to be 0.040 (0.039–0.041) % yr^{-1}[2], equivalent to 1.1 (1.06–1.12) $\times 10^{-6}$ day^{-1}. The spatial distribution of the re-suspension and re-deposition ratio to the primary deposition ranged from 0.01 to 0.3 and 0.001 to 0.03 %, respectively. The spatial distribution of the land surface ^{137}Cs deposition decay due to re-suspension ranged from 2.7×10^{-7} to 8.2×10^{-6} day^{-1}. Re-suspension therefore had a negligible effect on reducing land surface radioactive contamination.

5 Discussion

Seasonal variation in the surface activity concentration and its source contributions are extensively discussed in Sect. 5.1. A possible source of the observed sporadic peak events, which could not be reproduced by the simulation, is dis-

---

[2] The amount re-suspended, excluding re-deposition (1.28 TBq minus 0.22 (0.18–0.23) TBq) for the year 2013, divided by the total deposited amount of 2.68 PBq.

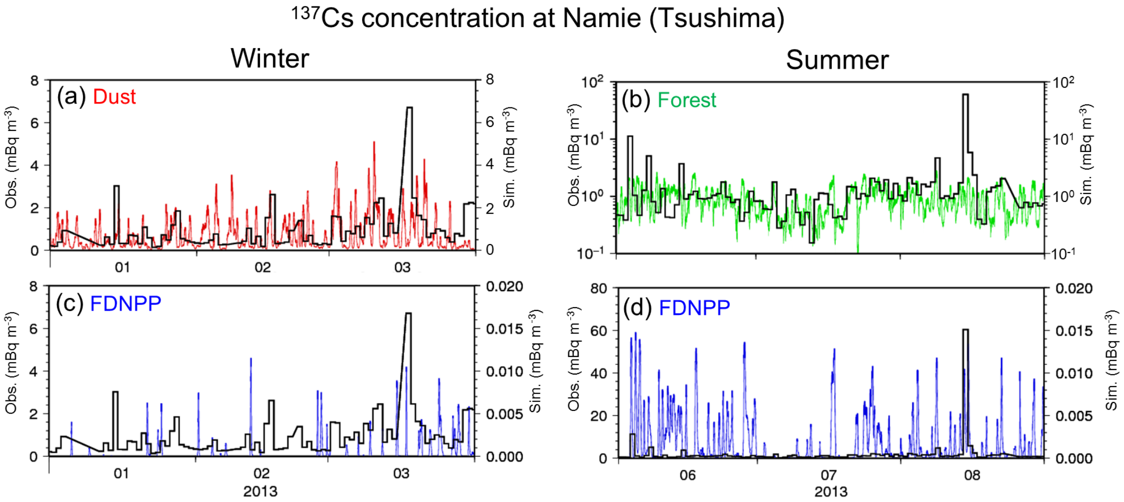

Figure 9. Time series of observed (black) and simulated (colors) ^{137}Cs surface air concentration at Namie (**a**, **c**) in winter from January to March and (**b**, **d**) in summer from June to August 2013. The colors of the lines are the same as in Fig. 7 but the time variation is hourly. The shaded areas indicate the range of ^{137}Cs concentrations obtained when the simulations were run using the optimized parameter ranges $E_\mathrm{c} = 0.03$–0.05 and $v_\mathrm{d} = 0.05$–$0.1\,\mathrm{cm\,s^{-1}}$.

cussed in Sect. 5.2. The effects of other processes that were not considered in the model, such as land surface processes and decontamination, are discussed based on the dose rate measurements from the monitoring posts in Fukushima in Sect. 5.3. Future issues are summarized in Sect. 5.4.

5.1 Seasonal variation and source contribution

The discussion in this section expands on that in Sect. 4.2. Figure 9 shows the same temporal variation as Fig. 7 but for simulated (using the optimized ranges of parameters) results for ^{137}Cs from dust and FDNPP in winter (January to March) and from forest and FDNPP in summer (June to August).

In the winter, the simulated trend for dust agreed well with the observed trend (Fig. 9a), and the surface air concentration during this period was positively correlated with the surface wind speed in both the simulation ($R = 0.88$ on an hourly basis) and the observations ($R = 0.32$ on a daily basis). There was a sporadic peak in the observational data of $6.7\,\mathrm{mBq\,m^{-3}}$ from the 17 March at 13:00 local time (LT) to 18 March at 13:00 LT that could not be reproduced by the dust module, and this peak coincided with a plume arriving from FDNPP, as shown in Fig. 9c. Therefore, the observed peak could be accounted for by specific re-suspension events on the order of $10^9\,\mathrm{Bq\,h^{-1}}$ (the left axis divided by the right axis multiplied by $10^6\,\mathrm{Bq\,h^{-1}}$ in Fig. 9c) if they occurred on the premises of FDNPP or close to the area. There are also two events exceeding $2\,\mathrm{mBq\,m^{-3}}$, one in January and another in February. It is unlikely that the two peaks originated from the direct emission from FDNPP and likely that they originated from the dust emission because the observed peaks coincided with the simulated dust peaks (Fig. 9a) and not with the simulated peaks due to the FDNPP emission (Fig. 9c).

In the summer, the simulated quantity as well as the variation in the forest data agreed well with the observed data (Fig. 9b). Because there is only monthly variation in the simulated emission, the simulated daily trend solely originated from variations in the meteorological parameters (wind field, turbulent mixing, and wet scavenging). A significant peak of $60.4\,\mathrm{mBq\,m^{-3}}$ is observed from 14 August at 13:00 LT to 15 August at 13:00 LT. This observed level was approximately 2 orders of magnitude larger than the simulated level and 1 to 2 orders of magnitude larger than the observed level for the other days in this period. Therefore, continuous emission such as re-suspension from forest is less likely to be the origin of the peak. Because the observed peak and the simulated peak of ^{137}Cs from FDNPP coincided (Fig. 9d), the observed level could be accounted for by specific re-suspension events on the order of $10^{10}\,\mathrm{Bq\,h^{-1}}$ either on the premises of FDNPP or close to the area. There have been several arguments that the observed peaks in August 2013 were associated with debris removal operations at FDNPP, and this is discussed separately in Sect. 5.2.

Figure 10 illustrates the seasonal mean surface wind vector and surface air ^{137}Cs concentration (simulated using the reference parameters) due to (a) dust re-suspension in the winter and (b) forest re-suspension in the summer. Due to the prevailing northwesterly winter monsoon, ^{137}Cs was carried southeastward in the winter. In the summer, under the influence of the Pacific high-pressure system, ^{137}Cs was carried inland. The monthly mean wind speed is high in winter and low in summer. The upper panels of Fig. 11 illustrate the observed and simulated (using the optimized ranges of parameters) total (from soil, forest, and FDNPP) ^{137}Cs concentration at Namie and Tsukuba. The time resolutions of the

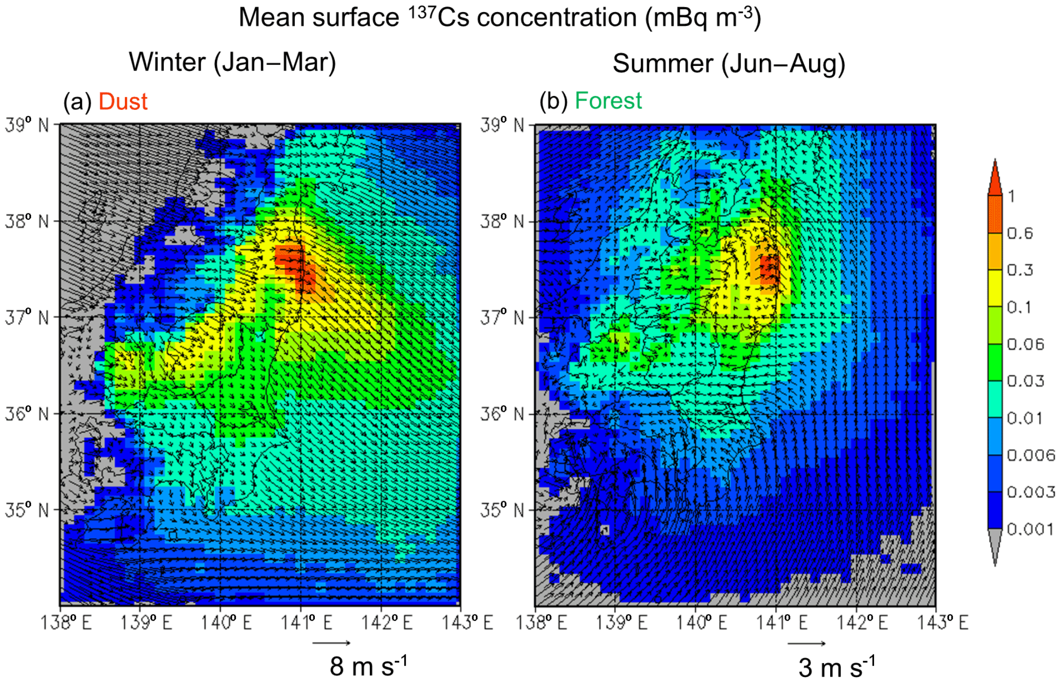

Figure 10. Seasonal mean surface (10 m above ground level) wind vector and ^{137}Cs surface concentration **(a)** due to dust re-suspension in winter from January to March and **(b)** due to forest re-suspension in summer from June to August. The deposition parameters of the simulation in the figure are $E_c = 0.04$ and $v_d = 0.1\,\mathrm{cm\,s^{-1}}$.

simulation are daily for Namie and weekly for Tsukuba to be consistent with the sampling intervals of the two respective sites. The simulation successfully reproduced the quantity and variation in the observed background concentration at Namie and Tsukuba but could not reproduce the sporadic peak events observed at Namie, as discussed above. The simulation also significantly underestimated the observations at Tsukuba from January to March, 2013. Due to the northwesterly monsoon (Fig. 10a), there was less air mass transported from FDNPP to Tsukuba in the winter and therefore this underestimation is probably due specifically to underestimation of the simulated re-suspension around Tsukuba. The lower panels of Fig. 11 show the relative contributions of ^{137}Cs from soil and forests at Namie and Tsukuba. The contribution from FDNPP was negligible throughout the year. At both sites, the contribution from dust was high (0.7–0.9) in the cold season and low (0.2–0.4) in the warm season due to higher surface wind speed in the cold season.

Figure 12a shows the observed and simulated (with the reference parameters) monthly Namie to Tsukuba ^{137}Cs concentration ratios. The mean concentration ratio exceeded 100 in June and 200 in August due to the sporadic peak events. The monthly median would be relevant for comparing the background observation with the simulation results by considering only continuous emission sources. The values of the simulated concentration ratio and its seasonal variation agreed fairly well with the observed monthly median ratio: the observed and simulated annual means were 38.9 and 31.1, respectively. Figure 12b shows the monthly mean simulated re-suspension source area contributions to the ^{137}Cs air concentration at Namie and Tsukuba. The re-suspension source area is defined as the model grid where the observed deposition amount exceeded 300 kBq m^{-2} (Fig. 4a) and includes the Namie grid (2300 kBq m^{-2}). Eighty to 90 % of the ^{137}Cs air concentration at Namie originated from the source region, and there was no clear seasonal variation in the value. In contrast, Tsukuba is characterized as a downwind region and there was clear seasonal variation in the source contribution ratio: high in summer and low in winter, due to the summer and winter monsoons, as discussed above. Nonetheless, the highest value at Tsukuba was 0.4 in July, and so more than half of the ^{137}Cs concentration at Tsukuba originated locally or from areas other than the contaminated regions throughout the year. As shown in Fig. 11a and b, the variability in the simulated concentration at Tsukuba due to uncertainty in the deposition parameters was much larger than that at Namie. The differences in the variability indicated that the Namie and Tsukuba sites can be characterized as the source area and the downwind area, respectively: as the time required for the plume to move from the emission site to the observation site increases, the variability becomes larger due to the increased chance for the plume to experience dry and wet scavenging.

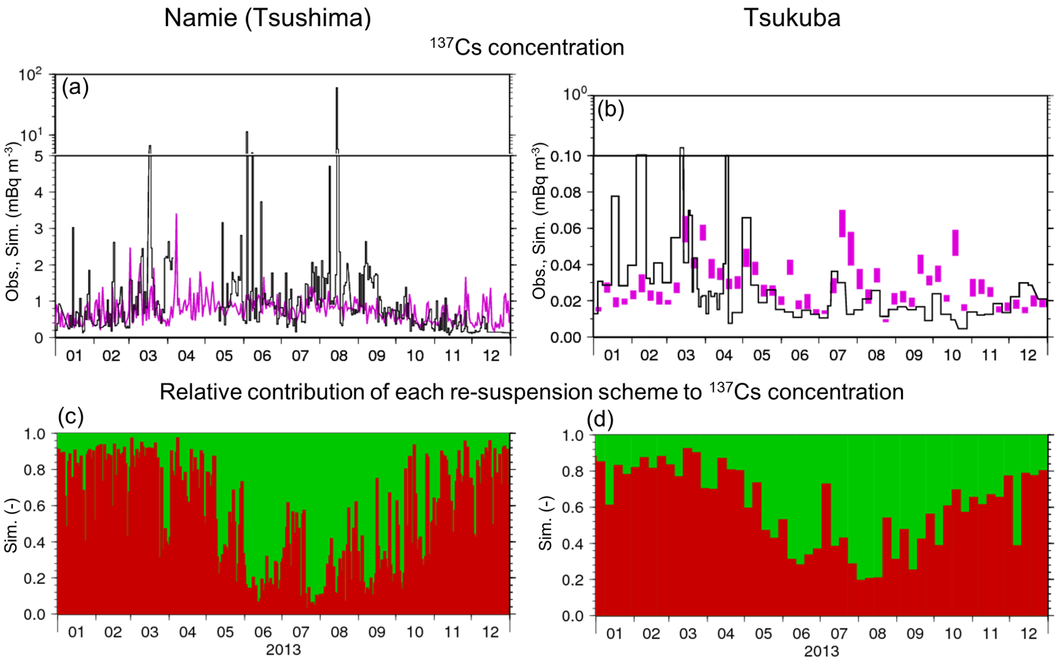

Figure 11. Time series of (**a**, **b**; black) the observed and (purple) the simulated surface ^{137}Cs concentration due to total re-suspension and (**c**, **d**) the relative contribution of (red) dust and (green) forest re-suspension to the ^{137}Cs concentration at (**a**, **c**) Namie and (**b**, **d**) Tsukuba. The shaded areas of (**a**) and (**b**) indicate the range of ^{137}Cs concentrations obtained when the simulations were run using the optimized parameter ranges $E_c = 0.03$–0.05 and $v_d = 0.05$–$0.1\,\mathrm{cm\,s^{-1}}$.

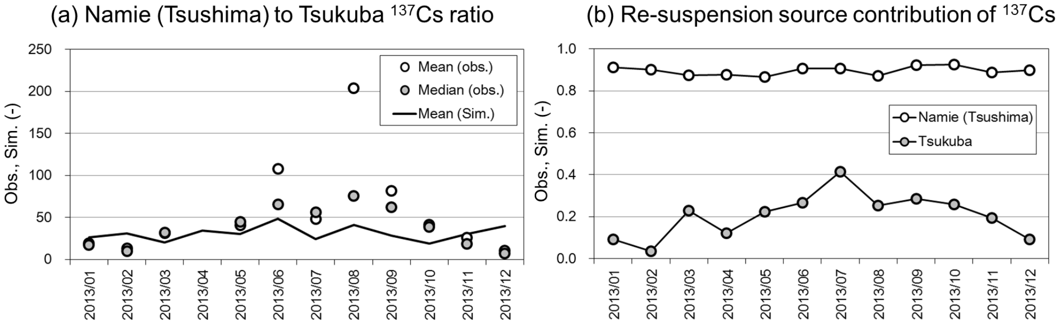

Figure 12. Monthly mean (**a**) observed mean, observed median and simulated Namie to Tsukuba ^{137}Cs concentration ratio and (**b**) simulated re-suspension source area (where the observed deposition amount $> 300\,\mathrm{kBq\,m^{-2}}$) contributions to ^{137}Cs air concentration at Namie and Tsukuba. The deposition parameters of the simulation in the figure are $E_c = 0.04$ and $v_d = 0.1\,\mathrm{cm\,s^{-1}}$.

5.2 Possible source of sporadic peak events

There have been several scientific studies and governmental reports on the unexpected re-suspension from FDNPP in August 2013. The high-dose-rate alarm was activated on August 19 within the premises of FDNPP associated with the debris removal operation. Matsunami et al. (2016) related the radiocesium contamination of brown rice in Fukushima in 2013 to this operation, whereas MAFF (2015) denied any association. The NRA estimated the ^{137}Cs emission rate during the debris removal operation as $6.7 \times 10^{10}\,\mathrm{Bq\,h^{-1}}$ and the cumulative amount as 1.1×10^{11} Bq (NRA, 2014). TEPCO (2014c) estimated the emission rate during the operation as 5.8×10^{10}–$1.2 \times 10^{11}\,\mathrm{Bq\,h^{-1}}$ and the cumulative amount as 1.3–2.6×10^{11} Bq. Steinhauser et al. (2015) estimated the gross amount as 2.8×10^{11} Bq using measurements of weekly air filter sampling and monthly deposition, and a numerical simulation. Their estimates are similar in magnitude to our estimate ($10^{10}\,\mathrm{Bq\,h^{-1}}$; see Sect. 5.1) but the dates are different: our observed peak was earlier than the reported removal operation.

Our daily sampling showed a peak concentration ($60.4\,\mathrm{mBq\,m^{-3}}$) from 14 August at 13:00 LT to 15 August at 13:00 LT before the reported operation but did not detect high

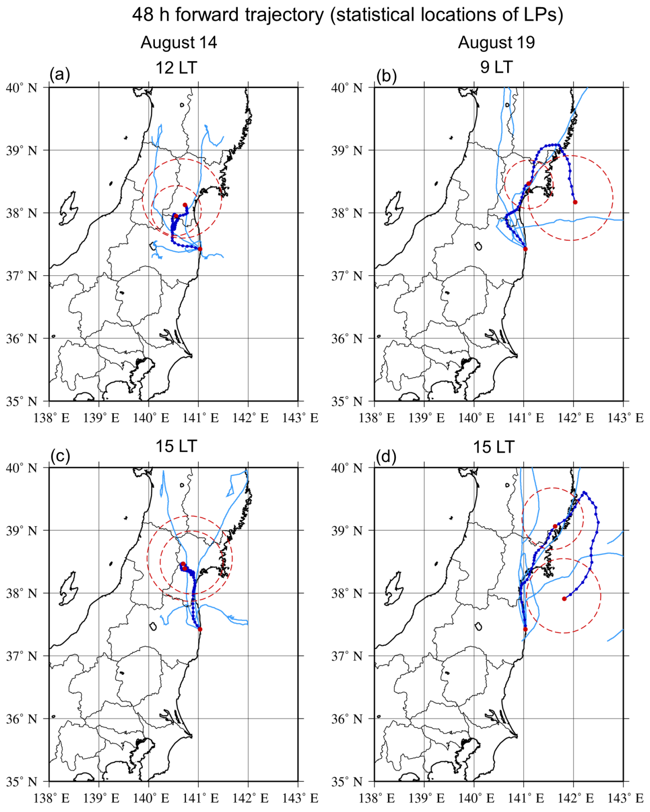

Figure 13. 48 h forward trajectory (statistical locations of LPs within 1 km AGL) predicted by the LM starting at **(a)** 12:00 LT and **(c)** 15:00 LT on 14 August and **(b)** 09:00 LT and **(d)** 15:00 LT on 19 August. Blue lines indicate median locations of LPs at 1 h and 1-day intervals as blue and red dots, respectively. Sky-blue lines indicate 17th and 83rd percentile locations of LPs and red dashed circles indicate areas containing 66 % of the LPs.

concentrations in the 19 August (0.33 mBq m^{-3} for August 18 at 13:00 LT to 19 August at 13:00 LT and 1.2 mBq m^{-3} for 19 August at 13:00 to 20 August at 13:00 LT). Figure 13 shows the forward trajectories predicted by the LM (statistical locations of LPs) starting from FDNPP on 14 August (left) and 19 August (right). The sky-blue lines and red dashed circles indicate areas containing approximately two-thirds of the LPs within 1 km AGL: the extent of the area reflects horizontal and vertical atmospheric diffusion. The highest dose rate peaks were observed from 13:50 to 14:10 LT on 19 August at 2.8–8.3 km north and north-northwest of FDNPP on the leeward side, as reported by Fukushima prefecture (https://www.pref.fukushima.lg.jp/download/1/20130827moni.pdf.pdf). The forward trajectories on 12 August indicated that plumes during the debris removal operation traveled north-northwest to north of FDNPP (Fig. 13b and d), rather than towards the west-northwest, where the Namie site is located. On 14 August, on the other hand, plumes were transported towards the west (starting at 12:00 LT, Fig. 13a), and then to the north (starting at 15:00 LT, Fig. 13c) due to fast changes in wind direction, resulting in the simulated peak concentration shown in Fig. 9d during this period. Our simulation and observations together indicated that the same order of magnitude of ^{137}Cs emission occurred on August 14–15 and on 19 August. Alarm activation was not reported on August 14–15, but debris removal operation was also conducted on August 14 and 16 (MAFF, 2015).

(a) Daily mean dose rate in a coastal area in Fukushima (Hamadori)

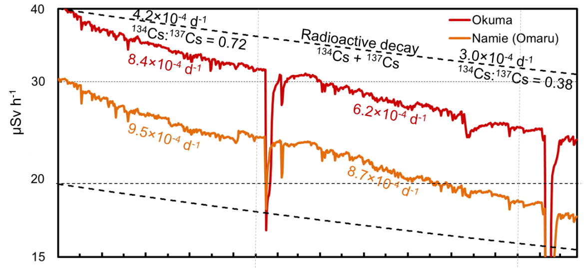

(b) Daily mean dose rate in a mountainous area in Fukushima (Abukuma)

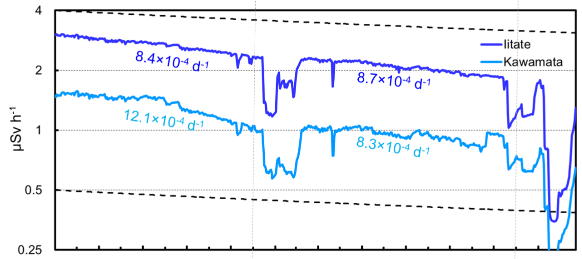

(c) Daily mean dose rate in a valley area in Fukushima (Nakadori)

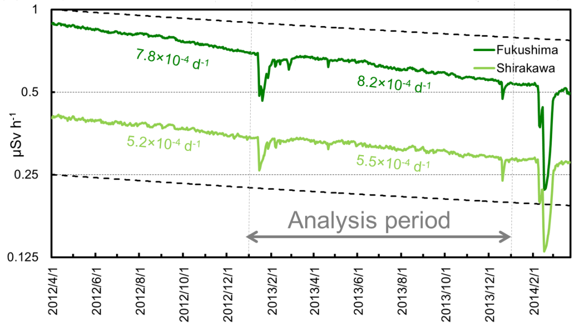

Figure 14. Daily mean gamma dose rate at the six monitoring sites: (**a**; red) Okuma and (orange) Namie (Omaru district) in the coastal area, (**b**; blue) village of Iitate and (sky blue) town of Kawamata in the Abukuma highland area, and (**c**; green) cities of Fukushima and (greenish yellow) Shirakawa in the Nakadori valley area of Fukushima prefecture as presented in Fig. 1b for two fiscal years (from April 2012 to March 2014). The first-order decreasing rates of the least-squares approximation over the period of no snow cover (May to October, 2012 and 2013) is also presented, along with the radioactive decay (^{134}Cs plus ^{137}Cs, by assuming the same amount of activity on 12 March 2011) in April 2012 and March 2013.

5.3 Land surface processes, decontamination, and dust emission suppression due to snow cover

Figure 14 presents the time series of ambient gamma dose rates measured at the monitoring posts in Fukushima prefecture indicated in Fig. 1b. The data were obtained from the Nuclear Regulation Authority (NRA), Japan, website (http://radioactivity.nsr.go.jp/map/ja/index.html). A total of six monitoring posts, two from each of the three geographical areas (Hamadori coastal area, Abukuma highland area, and Nakadori valley area), were selected. There are tens to hundreds of monitoring posts in each municipality (village, town, and city) in Fukushima prefecture. We selected a monitoring post in each municipality by applying the following conditions: a post showing the highest dose rate of all posts in the municipality at the time of downloading (around 11:00, 28 December 2015), data are available since 1 April 2012, and the instruments are situated 100 cm above the ground.

In April 2012, the government of Japan designated the evacuation-directed zones as a difficult-to-return zone (DRZ; > 50 mSv yr^{-1}; 9.55 µSv h^{-1}), a habitation-restricted zone (HRZ; 20–50 mSv yr^{-1}; 3.85–9.55 µSv h^{-1}), and a zone being prepared to have the evacuation directive lifted (< 20 mSv yr^{-1}; 3.85 µSv h^{-1}) (METI, 2012). The two sites in the Hamadori area, Okuma and Omaru, have been designated DRZ (13.6 and 11.8 µSv h^{-1} on 28 December 2015). The dose rates at the two sites in the Abukuma area, Iitate and Kawamata, dropped below the HRZ level during the analysis period in this study (1.17 and 0.521 µSv h^{-1} on 28 December 2015). The dose rates in the Nakadori area are below 1 µSv h^{-1} (0.242 and 0.201 µSv h^{-1} on 28 December 2015).

The dose rate significantly dropped when the ground was covered with snow, in January and December 2013 in Hamadori and Nakadori, and from January to early March and December 2013 in Abukuma (the elevation of Abukuma is 500–1000 m and higher than Hamadori and Nakadori). Snow cover suppresses re-suspension due to dust emission. Namie (Tsushima) is located in Abukuma and the ground was covered with snow until early March (Ishizuka et al., 2016). The observed air concentration of ^{137}Cs at Namie (Tsushima) was correlated with the wind speed in the winter from January to March, indicating that re-suspension during the period was mechanically induced. In the winter, dust re-suspension from outside Abukuma, such as from Hamadori and Nakadori, or from land surface where the snow cover was partly melted due to solar radiation, might be the dominant source contributing to the ^{137}Cs surface air concentration at Namie (Tsushima) when the ground was covered with snow.

The first-order decreasing rates fitted by the least-squares approximation for the period without snow cover, May to October 2012 and 2013, are presented in Fig. 14. The rates ranged from 5.2 to 12.1×10^{-4} day^{-1}. The monthly mean radioactive decay rates of total radiocesium (^{134}Cs + ^{137}Cs), determined by assuming that the activities of ^{134}Cs and ^{137}Cs were equivalent in March 2011, were 4.2×10^{-4} and 3.0×10^{-4} day^{-1} in April 2012 and March 2014, respectively, due to the difference in half-life of ^{134}Cs and ^{137}Cs (2.07 and 30.1 years, respectively). By assuming that the gamma dose rate primarily originated to radiation from the land surface radiocesium, the radioactive decay accounted for 35–50 % of the decreasing rate of total ground radioactivity; the exception was Shirakawa, where radioactive decay accounted for 55–80 % of the decrease. In other words, 50–65 % of the ground radioactivity decrease was likely due to land surface processes, decontamination, and re-suspension to air. As discussed in Sect. 4.3, the estimated decreasing rate due to re-suspension was 2.7×10^{-7}–8.2×10^{-6} day^{-1}, which is 2 to 3 orders of magnitude smaller than the decreasing rates due to the other processes (10^{-4}–10^{-3} day^{-1}).

It is difficult to distinguish the contributions of land surface processes and decontamination. By subtracting the radioactive decay rate (3.0–4.2×10^{-4} day^{-1}) and the decreasing rate due to re-suspension (2.7×10^{-7}–8.2×10^{-6} day^{-1}) from the gross decreasing rate (5.2–12.1×10^{-4} day^{-1}), the estimated decreasing rates due to land surface processes and decontamination ranged from 1.0 to 7.9×10^{-4} day^{-1}. Matsuda et al. (2015) summarized the depth profiles of radiocesium in soil at more than 80 locations in Fukushima, including Hamadori, Abukuma, and Nakadori. They found that the radiocesium levels have been slowly migrating downward, with rates ranging from 1.7 to 9.6 kg m^{-2} yr^{-1} (equivalent to 1.1–6.0 mm yr^{-1} for a dust particle density of 2650 kg m^{-3} and a porosity of 0.4 m^3 m^{-3}, for example). Evrard et al. (2015) summarized that significant transfer of particulate-bound radiocesium occurs during major rainfall and runoff events (e.g., typhoons and spring snowmelt). Together with the relaxation depth–dose rate relationship provided by Saito and Petoussi-Hess (2014), the decreasing rate due to land surface processes such as downward migration, runoff, and erosion could be quantified and thus the decontamination effect could be separately extracted.

5.4 Future issues

Issues that remain to be resolved in future research are summarized in this section. First of all, re-suspension from biota could be predominant in the warm season, but the re-suspension sources as well as mechanisms remain essentially unknown. Further study is needed to understand the mechanism based on field experiments and numerical simulations. The current estimation could account for the measured background concentration (0.1–1 mBq m^{-3}) but could not reproduce the observed sporadic peak concentration (1–10 mBq m^{-3}) at the Namie site. Further study is needed to identify the cause. The dust flux module has been validated at a single location. The module needs to be improved to be applicable to various land use and soil texture conditions. The decontamination may reduce resuspension afterward, whereas the resuspension may occur during decontamination-related work. This effect should be evaluated in the future. The current estimation was based on a single model simulation. Variability in multi-model simulations is rather large (SCJ, 2014; Draxler et al., 2015) and therefore multi-model assessment will be indispensable for long-term re-suspension analysis.

6 Conclusions

The long-term effect of ^{137}Cs re-suspension from contaminated soil and biota due to the Fukushima nuclear accident has been quantitatively assessed using a numerical simulation, a field experiment on dust emission in the contaminated area (Namie, Fukushima), and air concentration measurements inside (Namie) and outside (Tsukuba, Ibaraki) of the area. The re-suspension mechanism remains unknown. We therefore utilized the observational data obtained both inside and outside the contaminated area, together with a transport model, to provide a robust budget analysis of the re-suspension, transport, and re-deposition of ^{137}Cs in the eastern part (the Tohoku and Kanto regions) of Japan. Our findings are summarized as follows:

1. Optimization of the deposition parameters of the LM for simulating the emergency situation of March 2011, using aircraft observation data (NRA, 2012) and the prescribed emission inventory (Katata et al., 2015), provided 0.1 (0.05–0.1) $\mathrm{cm\,s^{-1}}$ for a dry deposition velocity over land and 0.04 (0.03–0.05) for a hydrometeor collection efficiency for aerosols. The optimized (or validated) ranges of the deposition parameters were applied to long-term re-suspension assessment for the year 2013.
2. Using the dust emission module (Ishizuka et al., 2016), which was developed based on physical parameters, simulated ^{137}Cs re-suspension from soil multiplied by 5 accounted for the observed ^{137}Cs surface air concentration measured at Namie during only the cold season; the module underestimated the ^{137}Cs concentration by 1 to 2 orders of magnitude in the warm season.
3. Introducing re-suspension from forest using a constant re-suspension coefficient of $10^{-7}\,\mathrm{h^{-1}}$ and monthly green area fraction could quantitatively account for the observed concentration together with its seasonal variation.
4. The contribution from additional emission from the reactor buildings of FDNPP ($10^6\,\mathrm{Bq\,h^{-1}}$) was negligible throughout the year and underestimated the observed air concentration by 2 to 3 orders of magnitude at both observation sites.
5. At Namie and Tsukuba, the simulated contribution of re-suspension from soil was high (0.7–0.9) in the cold season and low (0.2–0.4) in the warm season; the remaining contribution was from forest and was low in winter and high in summer. The contribution of the re-suspension from the source area (where the aircraft-observed deposition exceeded $300\,\mathrm{kBq\,m^{-2}}$) to the air concentration at Namie was 0.8–0.9 throughout the year, while that at Tsukuba varied from 0.1 to 0.4, and was high in the summer and low in the winter.
6. The simulated annual total re-suspended amount for the whole region was 1.28 TBq, equivalent to 0.048 % of the aircraft-observed total deposited amount of 2.68 PBq. The total re-deposition was 0.18–0.23 TBq, equivalent to 14.1–18.0 % of the total re-suspended amount: the rest of the ^{137}Cs was transported out of the model domain. The spatial distribution of the decreasing rate of land surface ^{137}Cs due to re-suspension ranged from 2.7×10^{-7}–$8.2 \times 10^{-6}\,\mathrm{day^{-1}}$.
7. The first-order decrease rate of the ambient gamma dose rate in Fukushima prefecture ranged from 5.2 to $12.1 \times 10^{-4}\,\mathrm{day^{-1}}$. By subtracting the radioactive decay rate of 3.0–$4.2 \times 10^{-4}\,\mathrm{day^{-1}}$, the ground radioactivity decay due to land surface processes, decontamination, and re-suspension was found to range from 1.0 to $7.9 \times 10^{-4}\,\mathrm{day^{-1}}$. The estimated re-suspension rate was 2 to 3 orders of magnitude lower than the decrease in rate due to the other processes, showing that re-suspension contributed negligibly towards reducing ground radioactivity.

7 Data availability

All data are available upon request to the authors.

Appendix A: Model description

The current study employs a Lagrangian type model for the simulation of emission (either point sources or areal sources), horizontal and vertical diffusion and advection, gravitational settling, dry and wet depositions, and radioactive decay in the air. As described in Sect. 2.1, the current Lagrangian model (LM) uses simple parameterizations for dry and wet deposition schemes for computational efficiency, so long-term assessment and parameter sweep experiments are easily feasible. The source code for the model is open with the BSD 3-Clause License and is available on the web (https://ebcrpa.jamstec.go.jp/isetr_a01-1/, in Japanese).

The coordinate system of the model is horizontal for longitude and latitude and vertical for pressure level, consistent with meteorological analysis data commonly used. The model can be driven only by fundamental meteorological parameters such as temperature, humidity, 3-D wind field, geopotential height, and surface precipitation provided by meteorological analysis data such as GPV-MSM. The model does not need to drive meteorological models to predict detailed meteorological variables such as cloud microphysics, turbulence quantities, and surface variables. Since the temporal and spatial resolution of the meteorological analysis is not very high (e.g., 3 h and ∼ 11 km, respectively, for GPV-MSM), linear interpolation is conducted in time and space. Alternatively, higher temporal and spatial resolution can be achieved by using a meteorological model. Furthermore, although currently not implemented, detailed variables predicted by a meteorological model can be used for more accurate predictions of turbulent diffusion, surface flux, and dry and wet deposition.

In the LM model, LPs are released constantly in time but the initial activity of LPs (Bq LP^{-1}) differs according to the emission flux (Bq h^{-1}). The initial positions of LPs were randomly distributed within a fixed volume (or line) of plume centered at a point emission source such as FDNPP for the primary emission case simulation, or randomly distributed within a horizontal model grid for the areal emission cases (such as re-suspension from soil and forest). LPs do not disappear unless transported across lateral and upper boundaries or if they reach the surface layer due to gravitational settling (technically, gravitational settling velocity in the surface layer is included in the dry deposition velocity). The other processes, such as dry deposition, wet deposition and radioactive decay, do not decrease the number of LPs but do decrease the radioactivity carried by LPs because LPs represent an air mass rather than an actual particle, except in the case of gravitational settling. The lowest level permitted for the position of LPs is set as 2 m AGL and LPs going down across the level due to vertical turbulent motion will rebound at the level and go up. An LP whose radioactivity is smaller than a preset value, i.e., 10^{-10} Bq, due to deposition or radioactive decay will disappear from the computation to maintain computational efficiency, since the cost of the computation is proportional to the number of LPs in the model domain. To output the model results, the LP fields are converted to Eulerian concentration (Bq m^{-3}) and deposition (Bq m^{-2}) fields on a prescribed coordinate system of grids. In Lagrangian type models, the spatial resolution of tracer emission, concentration, and deposition fields can be set independent of each other and with the spatial resolution of meteorological fields. In the current implementation of the LM, the coordinate systems of meteorological fields and radioactivity fields are horizontally in common but vertically different: meteorological fields are provided on isobaric levels, whereas radioactivity fields are calculated on height AGL.

The horizontal and vertical diffusion calculation followed JMA (2008), using the horizontal diffusion scheme of Uliasz (1990) with a constant horizontal diffusivity of 5.864×10^4 m^2 s^{-1} and using a vertical diffusivity calculated based on Louis et al. (1982; see Eqs. 8.1.8 through 8.1.15 of JMA, 2008, for details).

The wet scavenging rate Λ_{wet} (s^{-1}) is simply parameterized as a function of the surface precipitation rate P (mm s^{-1}) as

$$\Lambda_{\mathrm{wet}} = \frac{3}{4}\frac{E_{\mathrm{c}}(a_{\mathrm{m}}, r_{\mathrm{m}})}{a_{\mathrm{m}}}P, \tag{A1}$$

where E_{c} is the collection efficiency of aerosols by the hydrometeor, and a_{m} and r_{m} are the mean radii of the hydrometeor and aerosols, respectively (JMA, 2008). Empirically, a_{m} is characterized by P as

$$a_{\mathrm{m}} = 0.35P^{0.25}. \tag{A2}$$

JMA (2008) uses 0.05 for E_{c}. In the current study, instead of explicitly predicting E_{c}, its range was set for the sensitivity tests as listed in Table 2.

Conceptually, Eq. (A1) is the formulation for the washout process, i.e., the collection of aerosols by the settling hydrometeor particles such as rain and snow. a_{m} and E_{c} should differ for rain and snow, but common parameters are used in the current simulation. Also, Eq. (A1) is not applicable for the rainout process, since this process-cloud condensation nuclei or ice nuclei activation and deposition via subsequent cloud microphysical processes is totally different from the washout process. Because meteorological models were not utilized in this study and thus only relative humidity and surface precipitation rate are available and no cloud microphysical information (such as hydrometeors mixing ratio in each model grid) is available, Eq. (A1) is applied for all the LPs located above the grid with P. In order to partly account for the rainout process, Eq. (A1) is not applied to LPs in a grid, where the relative humidity is lower than the minimum value, set as 95 % in the simulation.

The dry deposition velocity v_{d} (m s^{-1}) of aerosols (or gases) is conventionally formulated, using an electrical analogy, as an inverse of the summation of resistances (s m^{-1}) representing turbulent diffusion in the surface layer, Brownian diffusion (or molecular diffusion for gases), interaction with the land surface (soil, water, and vegetation), and gravitational settling for aerosols (e.g., Wesely and Hicks, 2000). Therefore, v_d is a function of height as well as of turbulent flux and surface conditions. Nevertheless, v_d is set as constant in the simulation, but the height dependency of v_d is considered in the dry scavenging rate Λ_{dry} (s^{-1}), following Furuno et al. (1999) as

$$\Lambda_{dry} = \frac{2}{z_{srf}}\left(1 - \frac{z}{z_{srf}}\right) v_d, \tag{A3}$$

where z is the height of the LP (m AGL) and z_{srf} is the surface layer height set as 100 m AGL in the study. Instead of explicitly predicting v_d, its range was set at around 0.1 cm s^{-1}, a typical speed for a range of aerosols around 1 µm in diameter, for the sensitivity tests, as listed in Table 2. The value of v_d is applied over land, whereas v_d over the ocean is multiplied by 0.1, because v_d over a flat surface is approximately 1 and 2 orders of magnitude smaller than v_d over short vegetation such as grass and tall vegetation such as forest, respectively (e.g., Petroff and Zhang, 2010).

Appendix B: Statistical accuracy of the current simulation setting

Because the statistical error of Lagrangian simulation is inversely proportional to the square of the number of LPs, the statistical accuracy of the current simulation setting was evaluated using the following measures (relative errors of quantities of the sensitivity runs to those of the reference run):

$$E_{con}(x,y) = \frac{|C_{sens}(x,y) - C_{ref}(x,y)|}{C_{ref}(x,y)}, \tag{B1}$$

$$E_{dep}(x,y) = \frac{|D_{sens}(x,y) - D_{ref}(x,y)|}{D_{ref}(x,y)}, \tag{B2}$$

where x and y indicate grid points on the longitudinal and latitudinal axes, respectively. C_{sens} and D_{sens} indicate temporal mean surface concentrations (Bq m^{-3}) and temporal cumulative depositions (Bq m^{-2}) of the sensitivity runs, respectively. C_{ref} and D_{ref} are the same as C_{sens} and D_{sens} but for the reference run. E_{con} and E_{dep} were sampled only at grids where $C_{ref}(x, y)$ and $D_{ref}(x, y)$ are greater than their areal mean values, respectively.

B1 Point source case

The number emission rate of LPs, N_{LP}, was set as 32 000 h^{-1} (i.e., N_{LP_ref}) for a point source emission case such as the primary emission in March 2011 and additional emission from the reactor buildings in 2013. The median values together with the 25th and 75th percentile values of E_{con} and E_{dep} of the sensitivity runs (sensitivity to deposition parameters and sensitivity to N_{LP}) against the reference run are listed on the rows of the top half of Table B1. Both E_{con} and E_{dep} of $N_{LP\_ref} \times 4$ were significantly lower than those for the deposition parameters sensitivity run. This result indicates that 32 000 h^{-1} for N_{LP} was sufficient to allow a statistically significant simulation for the purpose of this study, as shown in Figs. 4 and 5: the difference in concentration and deposition due to the deposition parameters was much larger than the difference due to model uncertainty in N_{LP}. E_{con} and E_{dep} of $N_{LP\_ref} \times 0.25$ (which are also smaller than those of the deposition parameters sensitivity run) are larger than those of $N_{LP\_ref} \times 4$, indicating fairly good accuracy convergence of the LM model.

B2 Areal emission case

N_{LP_ref} was 16 h^{-1} $grid^{-1}$ for the areal emission case simulating re-suspension from soil and forests in 2013. The lower half of Table B1 is the same as the upper half except for the areal emission case (re-suspension from forest). Both E_{con} and E_{dep} of $N_{LP\_ref} \times 4$ were much lower than those for the deposition parameters sensitivity run, indicating that 16 h^{-1} $grid^{-1}$ supports a statistically significant simulation for the purpose of this study, as shown in Figs. 7–12. Usually, Lagrangian-type models are not appropriate for solving areal emission problems, because they require many more LPs for areal emission cases compared to point source cases and thus become computationally too expensive to obtain statistical accuracy (i.e., to set large number of LPs). In the case of this simulation, especially for the concentration, sensitivity to deposition parameters was much more significant than sensitivity to model uncertainty in N_{LP} using the sufficiently small number of $N_{LP\_ref} = 16$ h^{-1} $grid^{-1}$. E_{con} and E_{dep} of $N_{LP\_ref} \times 4$ are smaller than those of $N_{LP\_ref} \times 0.25$, indicating fair accuracy convergence of the LM model.

Table B1. Statistical measures of temporal mean ^{137}Cs surface concentration (E_{con}) and cumulative deposition (E_{dep}) of the sensitivity runs against the reference run for (top) the point source case and (bottom) the areal emission case.

	Number emission rate of LP, N_{LP} (h^{-1} grid^{-1})	$E_{\mathrm{c}}^{\mathrm{a}}$ (–)	$v_{\mathrm{d}}^{\mathrm{b}}$ ($\mathrm{cm\,s}^{-1}$)	Median (25th–75th percentile) of $E_{\mathrm{con}}^{\mathrm{c}}$ (%)	Median (25th–75th percentile) of $E_{\mathrm{dep}}^{\mathrm{d}}$ (%)
Point source case, March 2011					
Reference run	32 000	0.04	0.01	–	–
Sensitivity runs					
Deposition parameters	32 000	0.03–0.05	0.05–0.01	2.7 (0.37–5.0)	7.5 (3.6–13)
$N_{\mathrm{LP\_ref}} \times 4$	128 000	0.04	0.01	0.51 (0.21–0.96)	0.72 (0.32–1.5)
$N_{\mathrm{LP\_ref}} \times 0.25$	8000	0.04	0.01	0.95 (0.39–1.8)	1.6 (0.73–2.9)
Areal emission case, 2013 (re-suspension from forest)					
Reference run	16	0.04	0.10	–	–
Sensitivity runs					
Deposition parameters	16	0.03–0.05	0.05–0.01	7.3 (2.6–13)	7.7 (3.6–17)
$N_{\mathrm{LP\_ref}} \times 4$	64	0.04	0.10	0.39 (0.17–0.78)	2.0 (1.3–2.6)
$N_{\mathrm{LP\_ref}} \times 0.25$	4	0.04	0.10	0.78 (0.34–1.5)	2.3 (1.5–3.1)

[a] Collection efficiency; see Eq. (A1). [b] Dry deposition velocity over land; see Eq. (A3). [c] Relative errors of temporal mean surface concentration at each grid cell of the sensitivity run to that of the reference run; see Eq. (B1). [d] Same as E_{con} but for cumulative deposition; see Eq. (B2).

Acknowledgements. This research was mainly supported by Grants-in-Aid for Scientific Research on Innovative Areas (JP24110002 and JP20110003) from the Ministry of Education, Culture, Sports, Science and Technology (MEXT), and partly supported by the Japan Society for the Promotion of Science (JSPS), Ministère des Affaires Étrangères et du Développement International (MAEDI) under the Japan-France Integrated Action Program (SAKURA), as well as by KAKENHI grant numbers JP15K16121, JP24340115, and JP26310201 from MEXT. Partial expenses were covered by the Japanese Radioactivity Survey from the NRA, Japan. The authors are grateful for useful discussions with and comments from Yuichi Moriguchi of University of Tokyo, Hiromi Yamazawa of Nagoya University, and Haruo Tsuruta of Remote Sensing Technology Center of Japan (RESTEC). The authors are thankful to Masayuki Takigawa of JAMSTEC for the maintenance of the website of LM. The LM was developed by M. Inatsu, C. Yoshikawa, M. Takigawa, and M. Kajino.

Edited by: Y. Balkanski
Reviewed by: three anonymous referees

References

Adachi, K., Kajino, M., Zaizen, Y., and Igarashi, Y.: Emission of spherical cesium-bearing particles from an early stage of the Fukushima nuclear accident, Scientific Report, 3, 2554, doi:10.1038/srep02554, 2013.

Chino, M., Nakayama, H., Nagai, H., Terada, H., Katata, G., and Yamazawa, H.: Preliminary estimation of release amounts of ^{131}I and ^{137}Cs accidentally discharged from the Fukushima Daiichi nuclear power plant into atmosphere, J. Nucl. Sci. Technol., 48, 1129–1134, 2011.

Danielache, S. O., Yoshikawa, C., Priyadarshi, A., Takemura, T., Ueno, Y., Thiemens, M. H., and Yoshida, N.: An estimation of the radioactive ^{35}S emitted into the atmospheric from the Fukushima Daiichi Nuclear Power Plant by using a numerical simulation global transport, Geochem. J., 46, 355–339, 2012.

Danielache, S. O., Yoshikawa, C., Kajino, M., Itou, S., Kakeya, W., Yoshida, N., and Igarashi, Y.: Radioactive ^{35}S emitted from the Fukushima Nuclear Power Plan studied by a modified regional model, in preparation, Atmos. Chem. Phys., 2016.

Draxler, R., Arnold, D., Chino, M., Galmarini, S., Hort, M., Jones, A., Leadbetter, S., Malo, A., Maurer, C., Rolph, G., Saito, K., Servranckx, R., Shimbori, T., Solazzo, E., and Wotawa, G.: World Meteorological Organization's model simulations of the radionuclide dispersion and deposition from the Fukushima Daiichi nuclear power plant accident, J. Environ. Radioact., 139, 172–184, 2015.

Evangeliou, N., Balkanski, Y., Cozic, A., and Møller, A. P.: Global and local cancer risks after the Fukushima Nuclear Power Plant accident as seen from Chernobyl: A modeling study for radiocaesium (^{134}Cs & ^{137}Cs), Environ. Int., 64, 17–27, 2014.

Evrard, O., Laceby, J. P., Lepage, H., Onda, Y., Cerdan, O., and Ayrault, S.: Radiocesium transfer from hillslopes to the Pacific Ocean after the Fukushima Nuclear Power Plant accident: A review, J. Environ. Radioact., 148, 92–110, 2015.

Furuno, A., Chino, M., and Yamazawa, H.: Worldwide version of System of Prediction of Environmental Emergency Dose Information (WSPEEDI) Model Code (II) – Three-dimensional Atmospheric Dispersion Model for Synoptic Scale: GEARN, JAERI-Data/Code 99-044, Japan Atomic Energy Research Institute, Japan, 68 pp., 1999 (in Japanese).

Garger, E. K., Paretzke, H. G., and Tschiersch, J.: Measurement of resuspended aerosol in the Chernobyl area, Part III: size distribution and dry deposition velocity of radioactive particles during anthropogenic enhanced resuspension, Radiat. Environ. Bioph., 37, 201–208, 1998.

Garger, E. K., Kuzmenko, Y. I., Sickinger, S., and Tschiersch, J.: Prediction of the ^{137}Cs activity concentration in the atmospheric surface layer of the Chernobyl exclusion zone, J. Environ. Radioact., 110, 53–58, 2012.

Girard, S., Mallet, V., Korsakissok, I., and Mathieu, A.: Emulation and Sobl' sensitivity analysis of an atmospheric dispersion model applied to the Fukushima nuclear accident, J. Geophys. Res., 121, 3484–3496, doi:10.1002/2015JD023993, 2016.

Groëll J., Quélo, D., and Mathieu, A.: Sensitivity analysis of the modelled deposition of ^{137}Cs on the Japanese land following the Fukushima accident, Int. J. Environ. Pollut., 55, 67–75, 2014.

Gutman, G. and Ignatov, A.: The derivation of green vegetation fraction from NOAA/AVHRR data for use in numerical weather prediction models, Int. J. Remote Sens., 19, 1533–1543, 1998.

Hatano, Y. and Hatano N.: Formula for the resuspension factor and estimation of the date of surface contamination, Atmos. Environ., 37, 3475–3480, 2003.

Hirao, S., Yamazawa, H., and Nagae, T.: Estimation of release rate of iodine-131 and cesium-137 from the Fukushima Daiichi nuclear power plant, J. Nucl. Sci. Technol., 50, 139–147, doi:10.1080/00223131.2013.757454, 2013.

Holländer, W. and Garger, E.: Contamination of Surface by Resuspended Material, ECP–1, Final Report, Rep. EUR 16527, Office for Official Publications of the European Communities, Luxembourg, 1996.

Hososhima, M. and Kaneyasu, N.: Altitude-dependent distribution of ambient gamma dose rates in mountainous area of Japan caused by the Fukushima nuclear accident, Environ. Sci. Technol., 49, 3341–3348, 2015.

Igarashi, Y., Kajino, M., Zaizen, Y., Adachi, K., and Mikami, M.: Atmospheric radioactivity over Tsukuba, Japan: a summary of three years of observations after the FDNPP accident, Prog. Earth Planet. Sci., 2, 19 pp., doi:10.1186/s40645-015-0066-1, 2015.

Ishizuka, M, Mikami, M., Tanaka, T. Y., Igarashi, Y., Kita, K., Yamada, Y., Yoshida, N., Toyoda, S., Satou, Y., Kinase, T., Ninomiya, K., and Shinohara, A.: Use of a size-resolved 1-D resuspension scheme to evaluation resuspended radioactive material associated with mineral dust particles from the ground surface, J. Environ. Radioact., 13 pp., doi:10.1016/j.jenvrad.2015.12.023, 2016.

JMA: Japan Meteorological Agency's Non-Hydrostatic Model II, *Suuchi Yohoka Hokoku Bessatsu* (Additional Volume to Report of Numerical Prediction Division) 54, 265 pp., 2008 (in Japanese).

Kaneyasu, N., Ohashi, H., Suzuki, F., Okada, T., and Ikemori, F.: Sulfate aerosol as a potential transport medium of radiocesium from the Fukushima nuclear accident, Environ. Sci. Technol. 46, 5720–5726, 2012.

Katata, G., Terada, H., Nagai, H., and Chino, M.: Numerical reconstruction of high dose rate zones due to the Fukushima Daiichi

Nuclear Power Plant accident, J. Environ. Radioact., 111, 2–12, 2012a.

Katata, G., Ota, M., Terada, H., Chino, M., and Nagai, H.: Atmospheric discharge and dispersion of radionuclides during the Fukushima Dai-ichi Nuclear Power Plant accident, Part I: Source term estimation and local-scale atmospheric dispersion in early phase of the accident, J. Environ. Radioact., 109, 103–113, doi:10.1016/j.jenvrad.2012.02.006, 2012b.

Katata, G., Chino, M., Kobayashi, T., Terada, H., Ota, M., Nagai, H., Kajino, M., Draxler, R., Hort, M. C., Malo, A., Torii, T., and Sanada, Y.: Detailed source term estimation of the atmospheric release for the Fukushima Daiichi Nuclear Power Station accident by coupling simulations of an atmospheric dispersion model with an improved deposition scheme and oceanic dispersion model, Atmos. Chem. Phys., 15, 1029–1070, doi:10.5194/acp-15-1029-2015, 2015.

Kinase, T., Kita, K. Igarashi, Y., Adachi, K., Ninomiya, K., Shinohara, A., Okochi, H., Ogata, Y., Ishizuka, M., Toyoda, S., Yamada, K., Yoshida, N., Zaizen, Y., Mikami, M., Demizu, H., and Onda, Y.: Seasonal variation in activity concentration of atmospheric ^{134,137}Cs and their possibile resuspension host aerosol observed at Tsuahima and Yamakiya, Fukushima, Prog. Earth Planet. Sci., in review, 2016.

Kristiansen, N. I., Stohl, A., Olivié, D. J. L., Croft, B., Søvde, O. A., Klein, H., Christoudias, T., Kunkel, D., Leadbetter, S. J., Lee, Y. H., Zhang, K., Tsigaridis, K., Bergman, T., Evangeliou, N., Wang, H., Ma, P.-L., Easter, R. C., Rasch, P. J., Liu, X., Pitari, G., Di Genova, G., Zhao, S. Y., Balkanski, Y., Bauer, S. E., Faluvegi, G. S., Kokkola, H., Martin, R. V., Pierce, J. R., Schulz, M., Shindell, D., Tost, H., and Zhang, H.: Evaluation of observed and modelled aerosol lifetimes using radioactive tracers of opportunity and an ensemble of 19 global models, Atmos. Chem. Phys., 16, 3525–3561, doi:10.5194/acp-16-3525-2016, 2016.

Loosmore, G. A. and Hunt, J. R.: Dust resuspension without saltation, J. Geophys. Res., 105, 20663–20671, doi:10.1029/2000JD900271, 2002.

Louis, J. F., Tiedtke, M., and Geleyn, J. F.: A short history of the PBL parameterization at ECMWF, Workshop on planetary boundary layer parameterization, ECMWF, 59–80, 1982.

MAFF (Ministry of Agriculture, Forestry and Fisheries): Fukushima Prefecture, Tohoku Agricultural Research Center, National Institute for Agro-Environmental Sciences: Investigation of the cause for brown rice exceeding the allowable radiocesium concentration, available at: http://www.maff.go.jp/j/kanbo/joho/saigai/fukusima/pdf/150526_youin_chosa.pdf (last access: 26 July 2016), 2015 (in Japanese).

Masson, O., Baeza, A., Bieringer, J., Brudecki., Bucci, S., Cappai, M., Carvalho, F. P., Connan, O., Cosma, C., Dalheimer, A., Didier, D., Depuydt, G., De Geer, L. E., De Vismes, A., Gini, L., Groppi, F., Gudnason, K., Gurriaran, R., Hainz, D., Halldórsson, O., Hammond, D., Hanley, O., Holey, K., Homoki, Zs., Ioannidou, A., Isajenko, K., Jankovic, M., Katzlberger, C., Kettunen, M., Kierepko, R., Kontro, R., Kwakman, P. J. M., Lecomte, M., Leon Vintro, L., Leppänen, A.-P., Lind, B., Lujaniene, G., Mc Ginnity, P., Mc Mahon, C., Malá, H., Manenti, S., Manolopoulou, M., Mattila., A., Mauring., A., Mietelski, J. W., Moller, B., Nielsen, S. P., Nikolic, J., Overwater, R. M. W., Pálsson, S. E., Papastefanou, C., Penev, I., Pham, M. K., Povinec, P. P., Rameбäck, H., Reis, M. C., Ringer, W., Rodriguez, A., Rulik, P., Saey, P. R. J., Samsonov, V., Schlosser, C., Sgorbati, G., Silobritiene, B. V., Söderström, C., Sogni, R., Solier, L., Sonck, M., Steinhauser, G., Steinkopff, T., Steinmann, P., Stoulos, S., Sýkora, I., Todorovic, D., Tooloutalaie, N., Tositti, L., Tschiersch, J., Ugron, A., Vagena, E., Vargas, A., Wershofen, H., and Zhukova, O.: Tracking of Airborne Radionuclides from the Damaged Fukushima Dai-Ichi Nuclear Reactors by European Networks, Environ. Sci. Technol., 45, 7670–7677, 2011.

Masson, O., Ringer, W., Malá, H., Rulik, P., Dlugosz-Lisiecka, M., Eleftheriadis, K., Meisenberg, O., De Vismes-Ott, A., and Gensdarmes, F.: Size distribution of airborne radionuclides from the Fukushima Nuclear Accident at several places in Europe, Environ. Sci. Technol., 47, 10995–11003, 2013.

Matsunami H., Murakami, T., Fujiwara, H., and Shinano, T.: Evaluation of the cause of unexplained radiocaesium contamination of brown rice in Fukushima in 2013 using autoradiography and gamma-ray spectrometry, Sci. Rep., 6, 20386, doi:10.1038/srep20386, 2016.

METI (Ministry of Economy, Trade and Industry): Convention on Nuclear Safety National Report of Japan for the Second Extraordinary Meeting, July 2012, Government of Japan, available at: http://warp.da.ndl.go.jp/info:ndljp/pid/3512451/www.meti.go.jp/english/press/2012/pdf/0705_01b.pdf (last access: 26 July 2016), 2012.

Miller, D. A. and White, R. A.: A conterminous United States multilayer soil characteristics data set for regional climate and hydrology modeling, Earth Interact., 2, 1–26, 1998.

Matsuda, N., Mikami, S., Shimoura, S., Takahashi, J., Nakano, M., Shimada, K., Uno, K., Hagiwara, S., and Saito, K.: Depth profiles of radioactive cesium in soil using a scraper plate over a wide area surrounding the Fukushima Dai-ichi Nuclear Power Plant, Japan, J. Environ. Radioact., 139, 427–434, 2015.

Morino, Y., Ohara, T., and Nishizawa, M.: Atmospheric behavior, deposition, and budget of radioactive materials from the Fukushima Daiichi nuclear power plant in March 2011, Geophys. Res. Lett. 38, L00G11, doi:10.1029/2011GL048689, 2011.

Morino, Y., Ohara, T., Watanabe, S., Hayashi, S., and Nishizawa, M.: Episode analysis of deposition of radiocesium from the Fukushima Daiichi Nuclear Power Plant accident, Environ. Sci. Technol., 47, 2314–2322, 2013.

NRA (Nuclear Regulation Authority): Airborne Monitoring Results in each prefecture, available at: http://radioactivity.nsr.go.jp/en/list/203/list-1.html (last access: 26 July 2016), 2012.

NRA: Assessment of radionuclide emission involved in the debris removal operations for reactor 3; Handout for the 28th meeting on the supervision of a specific nuclear facility, available at: http://www.nsr.go.jp/data/000051154.pdf (last access: 26 July 2016), 2014 (in Japanese).

Ohmori, Y., Kajikawa, M., Nishida, S., Tanaka, N., Kobayashi, N. I., Tanoi, K., Furukawa, J., and Fujiwara, T.: The effect of fertilization on cesium concentration of rice grown in a paddy field in Fukushima Prefecture in 2011 and 2012, J. Plant Res., 127, 67–71, 2014.

Oura, Y., Ebihara, M., Tsuruta, H., Nakajima, T., Ohara, T., Ishimoto, M., Sawahata, H., Katsumura, Y., and Nitta, W.: A database of hourly atmospheric concentrations of radiocesium (^{134}Cs and ^{137}Cs) in suspended particulate matter collected in March 2011 at 99 air pollution monitoring stations in Eastern

Japan, Journal of Nuclear and Radiochemical Sciences, 15, 15–26, 2015.

Petroff, A. and Zhang, L.: Development and validation of a size-resolved particle dry deposition scheme for application in aerosol transport models, Geosci. Model Dev., 3, 753–769, doi:10.5194/gmd-3-753-2010, 2010.

Pöhlker C., Wiedemann, K. T., Sinha, B., Shiraiwa, M., Gunthe, S. S., Smith, M., Su, H., Artaxo, P., Chen, Q., Cheng, Y., Elbert, W., Gilles, M. K., Kilcoyne, A. L. D., Moffet, R. C., Weigand, M., Matin, S. T., Pöschl, U., and Andreae, M. O.: Biogenic potassium salt particles as seeds for secondary organic aerosol in the Amazon, Science, 337, 1075–1078, 2012.

Quérel, A., Roustan, Y., Quélo, D., and Benoit, J. -P.: Hints to discriminate the choice of wet deposition models applied to an accidental radioactive release, Int. J. Environ. Pollut., 58, 268–279, 2015.

Saito, K. and Petoussi-Henss, N.: Ambient dose equivalent conversion coefficients for radionuclides exponentially distributed in the ground, J. Nucl. Sci. Techonol., 51, 1274–1287, doi:10.1080/00223131.2014.919885, 2014.

Saito, K., Shimbori, T., and Draxler, R.: JMA's regional atmospheric transport model calculations for the WMO technical task team on meteorological analyses for Fukushima Daiichi Nuclear Power Plant accident, J. Environ. Radioact., 139, 185–199, 2015.

Saunier, O., Mathieu, A., Didier, D., Tombette, M., Quélo, D., Winiarek, V., and Bocquet, M.: An inverse modeling method to assess the source term of the Fukushima Nuclear Power Plant accident using gamma dose rate observations, Atmos. Chem. Phys., 13, 11403–11421, doi:10.5194/acp-13-11403-2013, 2013.

SCJ (Science Council of Japan): A review of the model comparison of transportation and deposition of radioactive materials released to the environment as a result of the Tokyo Electric Power Company's Fukushima Daiichi Nuclear Power Plant accident, available at: http://www.scj.go.jp/ja/info/kohyo/pdf/kohyo-22-h140902-e1.pdf (last access: 26 July 2016), 2014.

Sekiyama, T. T., Kunii, M., Kajino, M., and Shimbori, T.: Horizontal resolution dependence of atmospheric simulations of the Fukushima nuclear accident using 15 km, 3 km, and 500 m grid models, J. Meteor. Soc. Japan, 93, 49–64, 2015.

Sekiyama, T. T., Kajino, M., and Kunii, M.: Ensemble dispersion simulation of a point-source radioactive aerosol using a square root Kalman filter, J. Geophys. Res., in review, 2016.

Skamarock, W. C., Klemp, J. B., Dudhia, J., Grill, D. O., Barker, D. M., Duda, M. G., Huang, X. Y., Wang, W., and Powers, J. G.: A description of the advanced research WRF version 3, Tech. Note, NCAR/TN475+STR, 125 pp., Natl. Cent. For Atmos. Res., Boulder, Colo., 2008.

Steinhauser, G., Niisoe, T., Harada, K. H., Shozugawa, K., Schneider, S., Synal, H.-A, Walther, C., Christl, M., Nanba, K., Ishikawa, H., and Koizumi, A: Post-accident sporadic releases of airborne radionuclides from the Fukushima Daiichi Nuclear Power Plant Site, Environ. Sci. Technol., 49, 14028–14035, doi:10.1021/acs.est.5b03155, 2015.

Stohl, A., Seibert, P., Wotawa, G., Arnold, D., Burkhart, J. F., Eckhardt, S., Tapia, C., Vargas, A., and Yasunari, T. J.: Xenon-133 and caesium-137 releases into the atmosphere from the Fukushima Dai-ichi nuclear power plant: determination of the source term, atmospheric dispersion, and deposition, Atmos. Chem. Phys., 12, 2313–2343, doi:10.5194/acp-12-2313-2012, 2012.

TEPCO (Tokyo Electric Power Co., Inc.): Estimation of additional emissions from nuclear reactor buildings (30 July 2012), available at: http://www.tepco.co.jp/nu/fukushima-np/roadmap/images/m120730_05-j.pdf (last access: 26 July 2016), 2012 (in Japanese).

TEPCO: Estimation of the additional emission from nuclear reactor buildings (30 May 2013), available at: http://www.tepco.co.jp/nu/fukushima-np/roadmap/images/d130530_05-j.pdf (last access: 26 July 2016), 2013 (in Japanese).

TEPCO: Estimation of the additional emission from nuclear reactor buildings (27 March 2014), available at: http://www.tepco.co.jp/nu/fukushima-np/roadmap/images/d140327_06-j.pdf (last access: 26 July 2016), 2014a (in Japanese).

TEPCO: Estimation of the additional emission from nuclear reactor buildings (25 December 2014), available at: http://www.tepco.co.jp/nu/fukushima-np/roadmap/images/d141225_08-j.pdf (last access: 26 July 2016), 2014b (in Japanese).

TEPCO: Estimation of radioactive material released during debris removal operations at reactor unit 3 of the Fukushima Daiichi Nuclear Power Plant in August 2013, available at: http://www.nsr.go.jp/data/000051136.pdf (last access: 26 July 2016), 2014c (in Japanese).

TEPCO: Estimation of the additional emission from nuclear reactor buildings (9 October 2015), available at: http://www.tepco.co.jp/life/custom/faq/images/d151109_11-j.pdf (last access: 26 July 2016), 2015 (in Japanese).

Terada, H., Katata, G., Chino, M., and Nagai, H.: Atmospheric discharge and dispersion of radionuclides during the Fukushima Dai-ichi Nuclear Power Plant accident, Part II: Verification of the source term and analysis of regional-scale atmospheric dispersion, J. Environ. Radioact., 112, 141–154, 2012.

Tsuruta, H., Oura, Y., Ebihara, M., Ohara, T., and Nakajima, T.: First retrieval of hourly atmospheric radionuclides just after the Fukushima accident by analysing filter-tapes of operational air pollution monitoring stations, Scientific Reports, 4, 6717, doi:10.1038/srep06717, 2014.

Uliasz, M.: Development of the mesoscale dispersion modelling system using personal computers, Part I: Models and computer implementation, Z. Meteor., 40, 110–120, 1990.

Wesely, M. L. and Hicks, B. B.: A review of the current status of knowledge on dry deposition, Atmos. Environ., 34, 2261–2282, 2000.

Winiarek, V., Bocquet, M., Saunier, O., and Mathieu, A.: Estimation of errors in the inverse modeling of accidental release of atmospheric pollutant: Application to the reconstruction of the cesium-137 and iodine-131 source terms from the Fukushima Daiichi power plant, J. Geophys. Res., 117, D05122, doi:10.1029/2011JD016932, 2012.

Winiarek, V., Bocquet, M., Duhanyan, N., Roustan, Y., Saunier, O., and Mathieu, A.: Estimation of the caesium-137 source term from the Fukushima Daiichi nuclear power plant using a consistent joint assimilation of air concentration and deposition observations, Atmos. Environ., 82, 268–279, 2014.

Yasunari, T. J., Stohl A., Hayano R. S., Burkhart J. F., Eckhardt S., and Yasunari T.: Cesium-137 deposition and contamination of Japanese soils due to the Fukushima nuclear accident, P. Natl. Acad. Sci. USA, 108, 19530–19534, 2011.

Yumimoto, K., Morino, Y., Ohara, T., Oura, Y., Ebihara, M., Tsuruta, H., and Nakajima, T.: Inverse modeling of the 137Cs source term of the Fukushima Dai-ichi Nuclear Power Plant accident constrained by a deposition map monitored by aircraft, J. Environ. Radioact., 164, 1–12, 2016.

Journal of the Meteorological Society of Japan, Vol. 95, No. 6, pp. 447−454, 2017
DOI:10.2151/jmsj.2017-025

NOTES AND CORRESPONDENCE

The Impact of Surface Wind Data Assimilation on the Predictability of Near-Surface Plume Advection in the Case of the Fukushima Nuclear Accident

Tsuyoshi Thomas SEKIYAMA, Mizuo KAJINO, and Masaru KUNII

Meteorological Research Institute, Tsukuba, Japan

(Manuscript received 24 March 2017, in final form 4 August 2017)

Abstract

We investigated the predictability of plume advection in the lower troposphere and the impact of AMeDAS surface wind data assimilation by using radioactive cesium emitted by the Fukushima nuclear accident in March 2011 as an atmospheric tracer. We conducted two experiments of radioactive plume predictions over eastern Japan for March 15, 2011 with a 3-km horizontal resolution using the Japan Meteorological Agency non-hydrostatic weather forecast model and local ensemble transform Kalman filter (JMANHM-LETKF) data assimilation system. The assimilated meteorological data were obtained from the standard archives collected for the Japan Meteorological Agency operational numerical weather prediction and the AMeDAS surface wind observations. The standard archives do not contain land-surface wind observations. The modeled radioactive cesium concentrations were examined for plume arrival times at 40 observatories. The mean error of the plume arrival times for the standard experiment (assimilating only the standard archives) was 82.0 min with a 13-h lead-time on an average. In contrast, the mean error of the AMeDAS experiment (assimilating both the standard archives and AMeDAS surface wind observations) was 72.8 min, which was 9.2 min (11 %) better than that of the standard experiment. This result indicates that the plume prediction has a reasonable accuracy for the environmental emergency response and the prediction can be significantly improved by the surface wind data assimilation.

Keywords surface wind data assimilation; plume advection predictability; Fukushima nuclear accident; environmental emergency response

1. Introduction

The advection of minor constituents in the troposphere (e.g., water vapor, oxidants, and aerosols) is one of the key processes for numerical weather or environment prediction. Advection, emission, deposition, and chemical/physical changes define constituent distributions. For weather prediction, the distribution of water vapor influences the coverage and strength of precipitation. Moreover, the distributions of oxidants, aerosols, and their precursors directly impact human health and indirectly modify the weather and climate. However, it is difficult to simulate advection in the lower troposphere due to poor reproducibility of near-surface wind velocities in numerical weather simulations. Numerical weather forecast models cannot explicitly resolve fine-scale structures of real surface wind velocities due to the topographical heterogeneity and the instability (or nonlinearity) of the atmospheric boundary layer (ABL). These sub-grid scale features cause discrepancy between the measured and forecast-

---

Corresponding author: Tsuyoshi Thomas Sekiyama, Atmospheric Environment and Applied Meteorology Research Department, Meteorological Research Institute, 1-1 Nagamine, Tsukuba, Ibaraki 305-0052, Japan
E-mail: tsekiyam@mri-jma.go.jp
J-stage Advance Published Date: 28 August 2017

ed variables. Therefore, the observational datasets of surface wind velocities are usually very limited or are avoided for operational weather prediction (e.g., Japan Meteorological Agency (JMA) 2015, in Japanese) to prevent the degradation of initial conditions. To improve near-surface wind prediction, recent studies tried to assimilate surface wind observations over land (e.g., Hacker and Snyder 2005; Benjamin et al. 2010; Hacker and Rostkier-Edelstein 2007; Hacker et al. 2007; Rostkier-Edelstein and Hacker 2010; Ancell et al. 2011, 2015; Ingleby 2015; Bédard et al. 2015, 2017). In these studies, however, the surface wind observations have an influence only on extremely short-term and local forecasts (less than 6 h) even if they have a positive impact. Besides, these past studies have not particularly investigated the predictability of constituent advection.

In this context, validating constituent advection predictions and understanding the impact of surface wind data assimilation have garnered increasing attention. Especially, the predictability of near-surface plume advection is a crucial factor for the environmental emergency response (EER), in which we have to prepare for the dispersion of hazardous materials emitted from a point source on the ground to the ABL. If the plume prediction has a reasonable accuracy like weather forecast, the area in danger will have to be evacuated in advance (World Meteorological Organization 2006). As mentioned above, the surface wind data assimilation is often very limited or avoided for weather analyses and predictions, although nudging of surface wind observations has been performed for lower tropospheric advection simulations (e.g., the WRF-CMAQ ozone simulation conducted by Li et al. 2016). However, the impact of surface wind data assimilation has not been well investigated for these advection simulations, especially for predictions incorporating high-performance data assimilation.

The investigation of plume advection requires widespread tracer observations with a fine time resolution. Therefore, we used radioactive cesium emitted by the Fukushima nuclear accident in March 2011 as the atmospheric tracer. The radioactive cesium plume was dispersed from a single source (the Fukushima Daiichi Nuclear Power Plant). The surface concentration of the plume was measured at many locations at a high frequency and with high accuracy (Tsuruta et al. 2014; Oura et al. 2015). This point source plume is advantageous due to its simple tracer isolation and validation without cross-dispersion. This paper shows the accuracy of the ^{137}Cs plume advection prediction and the impact of surface wind data assimilation on the predictability of the ^{137}Cs plume advection in the following sections.

2. Methodology

In general, atmospheric advection models require a gridded point value (GPV) dataset that contains a meteorological analysis or prediction that is pre-calculated via a high-performance data assimilation system. For example, the JMA operational meso-GPV dataset was used by all regional models that participated in the multimodel intercomparison of Fukushima nuclear pollution predictions (Science Council of Japan (SCJ) 2014) except for two models. One was our model (Sekiyama et al. 2015), which used an original meteorological dataset. The other model used the European Centre for Medium-Range Weather Forecasts (ECMWF) operational global GPV dataset. All models except Sekiyama et al. (2015) utilized the GPV datasets that were prepared by others (i.e., JMA or ECMWF). However, for the purpose of our investigation, the GPV datasets have to be prepared by our own data assimilation system because we need to arrange a comparison of meteorological analyses performed in the presence or absence of surface wind data assimilation. Hence, we utilized the meteorological data assimilation system of Sekiyama et al. (2015) in this study to prepare the GPV datasets with and without land-surface wind data assimilation.

The meteorological data assimilation system of Sekiyama et al. (2015) was developed by Kunii (2014) and is composed of the JMA's non-hydrostatic regional weather prediction model (JMANHM, cf., Saito et al. 2006, 2007) and the local ensemble transform Kalman filter (LETKF, cf., Miyoshi and Aranami 2006). In this study, this system was driven by 20 ensemble members and a 3-km horizontal resolution within the model domain of eastern Japan (215 × 259 grids, cf., Fig. 2b of Sekiyama et al. 2015). The covariance localization parameters were set to 50 km in the horizontal, 0.1 natural-logarithm-pressure coordinate in the vertical, and 3 hours in the time dimension for all observations. The boundary conditions for the model domain were provided by the JMA operational global analysis and prediction. Incidentally, JMANHM has been used to produce the JMA operational meso-GPV dataset at a 5-km horizontal resolution since before March 2011 with a four-dimensional variational (4D-Var) data assimilation method. This weather forecast system is known as JNoVA (Honda et al. 2005).

Using the abovementioned JMANHM-LETKF data assimilation system, two types of meteorological initial conditions were prepared from March 11 to 31, 2011 at 3-h intervals. One was the standard analysis (STD), which was produced by assimilating only the observations archived for the JMA operational analysis of JNoVA. These observations were collected by land-surface observatories (pressure measurements only), satellites (including sea surface wind), radiosondes, pilot balloons, wind profilers, aircrafts, ships, and buoys. The satellite radiances and radar precipitation analyses were excluded from this study. This JNoVA dataset does not contain land-surface wind-velocity observations.

The other analysis was produced by assimilating the JNoVA dataset and the land-surface wind-velocity observations collected by AMeDAS. AMeDAS is the acronym of the automated meteorological data acquisition system managed by JMA, which is a land-surface observation network that comprises approximately 1,300 stations throughout Japan with an average interval of 17 km. In this study, we assimilated the land-surface wind velocities from more than 200 AMeDAS stations within the model domain (shown in Fig. 1).

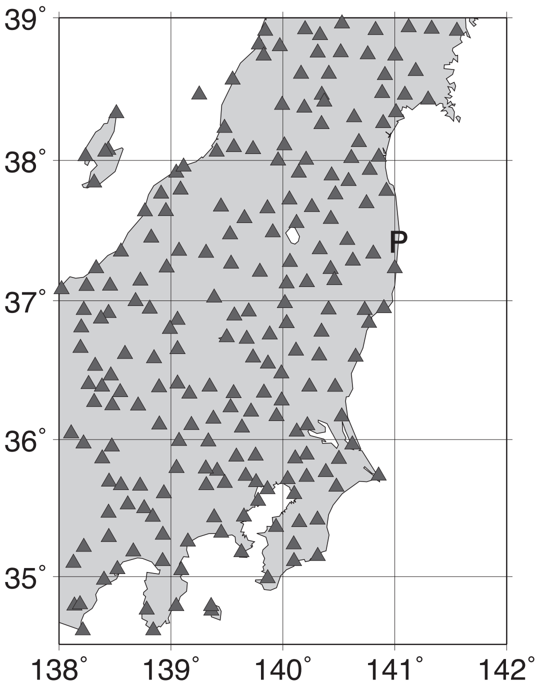

Fig. 1. Locations of the AMeDAS surface wind observing stations used for the AMeDAS experiment from 00:00 UTC on March 11 to 12:00 UTC on March 14, 2011. The letter "P" indicates the location of the Fukushima Daiichi Nuclear Power Plant.

For the surface wind data assimilation of the AMeDAS experiment, the height of the surface wind velocity was intended to be fixed at 10 m, because almost every AMeDAS anemometers are installed at a height of 10 m according to the World Meteorological Organization guideline. All observed velocities U_{obs} were transformed into U_{10} by using the following formula:

$$U_{10} = \frac{\ln\left(\frac{10}{z_0}\right)}{\ln\left(\frac{z_{obs}}{z_0}\right)} U_{obs},$$

where z_{obs} is the height of the anemometer installation and z_0 is a constant roughness length (1 m). However, the transformation was negligible in the experiment. The observation errors of the AMeDAS surface wind velocity were set to 2 m s^{-1}, which is a comparable level to the root mean square errors (RMSEs) of the STD experiment shown in Fig. 2. The RMSEs and correlation coefficients (r) in Fig. 2 were calculated by 1-h forecasts of the STD and AMeDAS experiments that were performed every 3 h from 00:00 UTC on March 11 to 12:00 UTC on March 15, 2011 at the AMeDAS stations used in this study.

Using these meteorological analyses as the initial conditions, two forecast runs (STD and AMeDAS experiments) were performed with the same JMANHM configuration for 48 h. The boundary conditions were provided by the JMA operational global prediction with the same initial time as JMANHM. The forecast initial time was set to 12:00 UTC on March 14 to reproduce the radioactive cesium plume behavior over the inland area of eastern Japan. According to Nakajima et al. (2017), the radioactive plumes moved primarily over the ocean during the Fukushima nuclear accident in March 2011. However, on March 15–16 and 20–21, the plumes moved deeper inland. However, because there was a widespread precipitation over the Tohoku and Kanto regions on March 20–21, we investigated only the case of March 15–16 in this study. When the precipitation is strong and widespread, the influence of wet deposition on the plume concentration becomes extremely large. The model simulations of precipitation strength and wet deposition are complicated and challenging. Therefore, we plan to investigate the March 20–21 event in future.

Plume advection simulations were then driven by the 48-h meteorological forecast runs by using the Eulerian regional air quality model version 2 (RAQM2). RAQM2 was developed by Kajino et al.

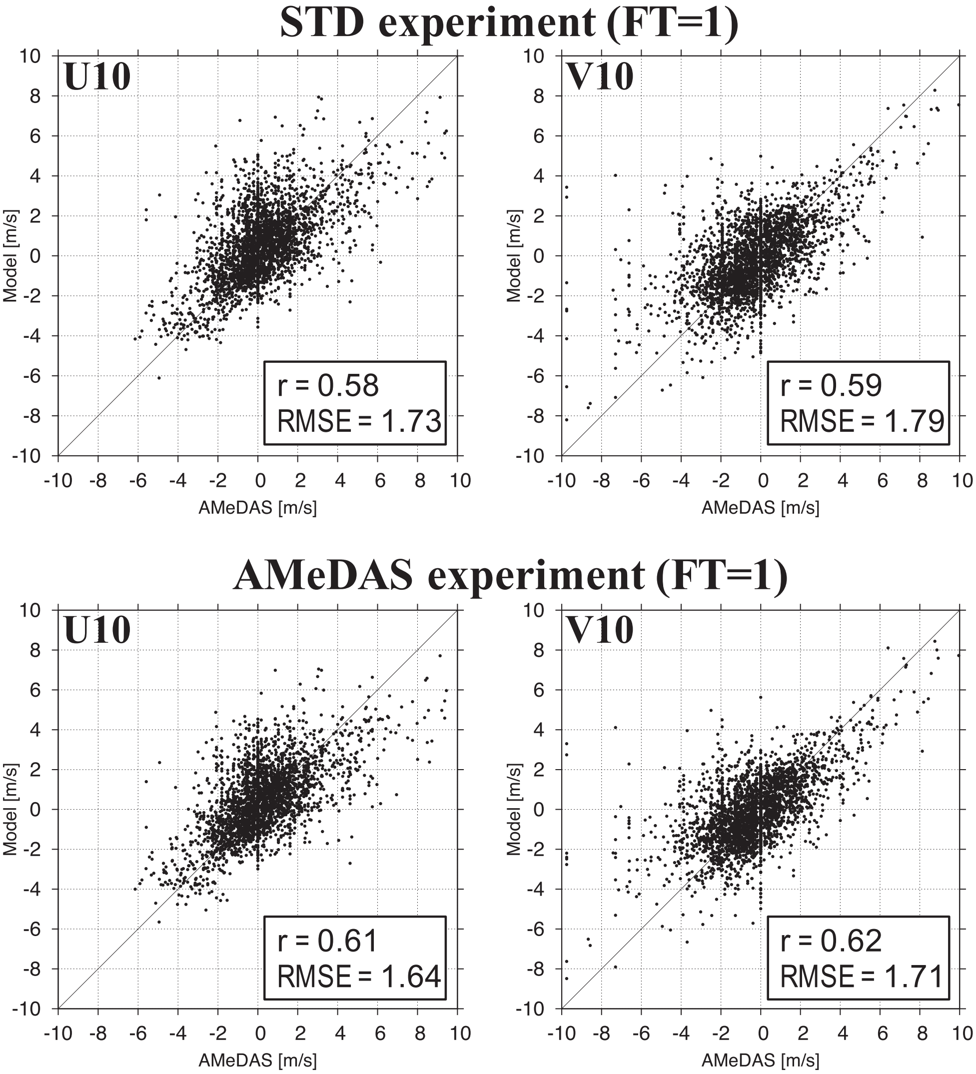

Fig. 2. Scatter diagrams with RMSEs and correlation coefficients (*r*) between the AMeDAS surface wind observations used in this study and 1-h forecasts (U_{10} and V_{10}: zonal and meridional winds at a height of 10 m) of the STD/AMeDAS experiments. The 1-h forecasts were performed every 3 h from 00:00 UTC on March 11 to 12:00 UTC on March 15, 2011.

(2012) and was used for the Fukushima nuclear accident simulation (Adachi et al. 2013; Sekiyama et al. 2015). RAQM2 and JMANHM share the same model domain (eastern Japan) and horizontal resolution (3 km), although the vertical resolution was converted from JMANHM's 60 layers (from the surface to 22 km asl) to RAQM2's 20 layers (from the surface to 10 km asl). All radioactive cesium (^{137}Cs) was expected to be contained in sulfate aerosol particles mixed with organic compounds as shown by Sekiyama et al. (2015).

The emission of radioactive cesium was fixed at a constant value (1 Bq h^{-1}), because we intended to validate only the plume arrival time at each station to rigorously examine the plume advection predictability. The Fukushima radioactive cesium plume was emitted from the point source; the background concentration was nearly zero before March 2011. The modeled concentration contrast between the background and the edge of arriving plume was larger than ten orders of magnitude. Therefore, we were easily able to identify the plume arrival time in simulations. We tried many settings of the Fukushima nuclear pollutant simulation (e.g., Adachi et al. 2013; SCJ 2014; Sekiyama et al. 2015) by using realistic emission rate datasets (e.g., Chino et al. 2011) and confirmed that we need only relative concentration values if we want to define the edge of radioactive plumes. This is because the background concentration of anthropogenic nuclear products is zero in simulation models; thus, the plume edge has a jump of values by more than ten (or sometimes twenty) orders of magnitude. Furthermore, wet deposition in the model was turned off to avoid a plume disappearance caused by the erroneous precipitation in the model.

The modeled plume arrival times were validated by comparing them with the hourly averaged radioactive cesium concentrations measured by Tsuruta et al. (2014) and Oura et al. (2015). Tsuruta et al. (2014) developed a method to retrieve the hourly averaged concentrations of radioactive cesium in the lower atmosphere using suspended particulate matter (SPM) sampling tapes with a detection limit of less than 0.6 Bq m^{-3} during the Fukushima nuclear accident. The SPM tapes were collected from the air pollution monitoring network managed by the national government and maintained by prefectural governments. Tsuruta et al. (2014) and Oura et al. (2015) reported the concentration data at 99 SPM-tape sampling stations. However, we screened these stations to clearly detect the radioactive plume arrival, which is discussed in the next section. Consequently, the data from 40 stations of the 99 stations were used in this study, as shown in Fig. 3.

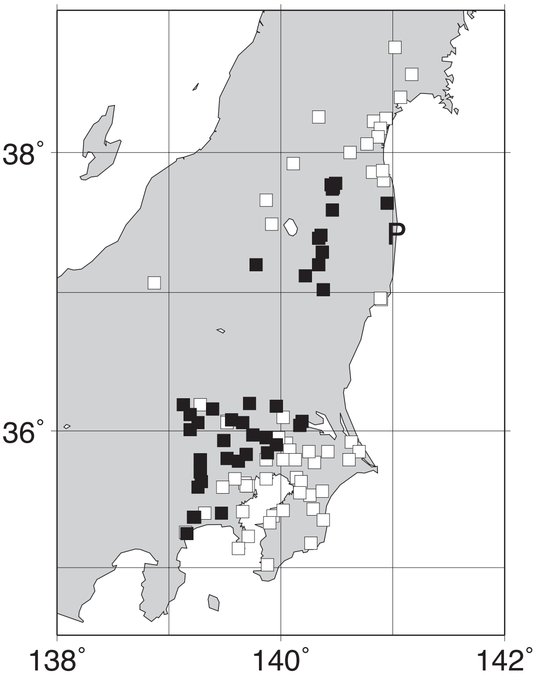

Fig. 3. Closed squares indicate the SPM-tape "radioactive cesium observing" stations of Oura et al. (2015) used in this study. Open squares indicate the SPM-tape stations shown in Oura et al. (2015) but not used in this study. The letter "P" indicates the location of the Fukushima Daiichi Nuclear Power Plant.

3. Results and discussion

The plume arrival times at the SPM-tape sampling stations were determined with a threshold of 1 Bq m^{-3} for the observations and 1×10^{-15} Bq m^{-3} for the model experiments. In general, when the plume arrived, the concentration rose sharply because the background was nearly zero (e.g., Fig. 4a). The observed concentrations changed rapidly from less than the detection limit (approximately 0.6 Bq m^{-3}) to more than 1 Bq m^{-3}. The modeled concentrations increased by more than 10 orders of magnitude. Note that the highest modeled concentrations at the SPM tape sampling stations were on the order of 10^{-13}–10^{-11} Bq m^{-3}. Hence, the threshold for the modeled plumes was set to 1×10^{-15} Bq m^{-3}. For example, the observed plume arrival time and the STD forecasted plume arrival time are shown in Fig. 4a at Station #49 in Kuki City, Saitama Prefecture, based on Oura et al. (2015).

When a concentration surge was not clearly observed, e.g., as in Fig. 4b (Station #59 in Chiba City), arrival time data were not used. In addition, more than one increase in concentration over a short period of time was also observed in a few cases, e.g., as in Fig. 4c (Station #81 in Ota Ward, Tokyo). In this case, the edge of the observed plume could not be clearly identified and compared with modeled plumes. Thus, we omitted these data from the statistical calculations. After the screening, 40 out of the 99 stations of Oura et al. (2015) remained, as shown in Fig. 3. Fortunately, most of the 40 stations were located inland; therefore, it was expected that we could distinctly observe the influence of land-surface wind observations on the plume simulation.

The STD experiment did not assimilate the land-surface wind observations; namely, it assimilated the observation dataset regularly used in the operational JNoVA system, except for the satellite radiance and radar precipitation data. We have confirmed that the difference between the STD experiment analysis and

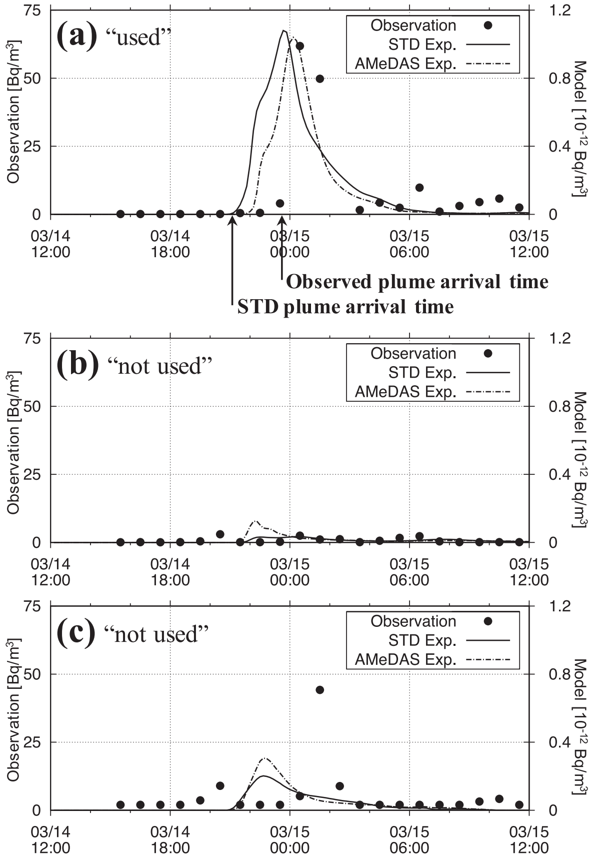

Fig. 4. Examples of time series of the radioactive cesium (^{137}Cs) concentrations derived from the SPM-tape sampling observations and two model experiments (STD and AMeDAS) from 12:00 UTC on March 14 to 12:00 UTC on March 15, 2011. The advection of the plumes was examined using the data from (a) Kuki City, Saitama Prefecture, and not using the data from (b) Chiba City, Chiba Prefecture, or (c) Ota Ward, Tokyo.

Table 1. Mean plume arrival time errors at the 40 SPM-tape sampling stations.

	STD experiment	AMeDAS experiment
mean error (min)	82.0	72.8
standard deviation (min)	83.4	79.6
significance level (p-value)		0.008

the operational JNoVA analysis is small. The influence of the satellite radiance and radar precipitation data was negligible for surface wind predictability in this study. The averaged difference (mean error) in the plume arrival times at the 40 SPM-tape sampling stations between the observational data and the STD experiment was 82.0 min (Table 1). Here, the average forecast length was 13 h. As indicated by the standard deviation (83.4 min) compared to this average, the forecasted plume arrival time was often very close to the observations. However, there were a few instances of errors exceeding 3 h. This is thought to represent the realistic ability of state-of-the-art operational weather forecast models and data assimilation systems to predict plume advection for emergency evacuations.

Conversely, the mean error of the AMeDAS experiment was 72.8 min, which was 9.2 min (11 %) smaller than that of the STD experiment, with a statistical significance level of p-value of 0.008 (Table 1). This result indicates that the land-surface wind data assimilation significantly improved the predictability of near-surface plume advection even after a half-day forecast. Although the AMeDAS surface wind observations had only a small positive impact on the surface wind reproducibility as shown in Fig. 2, the impact on the plume predictability was large with a high statistical significance. The accuracy of a half-day plume prediction depends on not only the accuracy of 12-h-forecasted wind velocities in the vicinity of the plume but also very short-term wind-velocity forecasts near the emission source. Therefore, there is possibility that the improvement of the plume arrival time predictability is caused by only the improvement of very short-term forecasts near the emission source. However, at least from the viewpoint of advection prediction, the improvement of the plume predictability was surely maintained for longer than 6 h by the AMeDAS surface wind data assimilation. Besides, the 72.8-min error will be acceptable for the EER evacuation if the prediction is available with a half-day lead time.

4. Summary

The assimilation of AMeDAS surface wind data has a positive impact on the predictability of plume advection in the lower troposphere, at least in cases of wintertime air pollution over complex terrain, e.g., the Fukushima nuclear accident. The plume arrival prediction has a 72.8-min error with a half-day lead time for Tohoku and Kanto regions for March 15, 2011 by using the AMeDAS surface wind data assimilation. If the plume arrival prediction was obtained for the EER with an accuracy of the AMeDAS experiment in this study, the information could be used for the evacuation or sheltering. Furthermore, a similar strategy for improving advection predictability would be applicable to near-surface water vapor, oxidant, and aerosol predictions by using surface wind data assimilation.

Acknowledgments

We thank Dr. Tsuruta and his colleagues for providing us with their SPM-tape radioactive cesium data. The JMA headquarters provided the weather analysis, prediction, JNoVA, and AMeDAS datasets used in this study. This work was supported by JSPS KAKENHI Grant Number JP24340115, JP16H02946, JP16H04051, JP26800247, and JP17K00533; MEXT KAKENHI Grant Number JP24110003; and the Japan-France Integrated Action Program (SAKURA) of JSPS/MAEDI.

References

Adachi, K., M. Kajino, Y. Zaizen, and Y. Igarashi, 2013: Emission of spherical cesium-bearing particles from an early stage of the Fukushima nuclear accident. *Sci. Rep.*, **3**, 2554, doi:10.1038/srep02554.

Ancell, B. C., C. F. Mass, and G. J. Hakim, 2011: Evaluation of surface analyses and forecasts with a multiscale ensemble Kalman filter in regions of complex terrain. *Mon. Wea. Rev.*, **139**, 2008–2024.

Ancell, B. C., E. Kashawlic, and J. L. Schroeder, 2015: Evaluation of wind forecasts and observation impacts from variational and ensemble data assimilation for wind energy applications. *Mon. Wea. Rev.*, **143**, 3230–3245.

Bédard, J., S. Laroche, and P. Gauthier, 2015: A geo-statistical observation operator for the assimilation of near-surface wind data. *Quart. J. Roy. Meteor. Soc.*, **141**, 2857–2868.

Bédard, J., S. Laroche, and P. Gauthier, 2017: Near-surface wind observation impact on forecasts: Temporal propagation of the analysis increment. *Mon. Wea. Rev.*, **145**, 1549–1564.

Benjamin, S. G., B. D. Jamison, W. R. Moninger, S. R. Sahm, B. E. Schwartz, and T. W. Schlatter, 2010: Relative short-range forecast impact from aircraft, profiler, radiosonde, VAD, GPS-PW, METAR, and mesonet observations via the RUC hourly assimilation cycle. *Mon. Wea. Rev.*, **138**, 1319–1343.

Chino, M., H. Nakayama, H. Nagai, H. Terada, G. Katata, and H. Yamazawa, 2011: Preliminary estimation of release amounts of ^{131}I and ^{137}Cs accidentally discharged from the Fukushima Daiichi Nuclear Power Plant into the atmosphere. *J. Nucl. Sci. Technol.*, **48**, 1129–1134.

Hacker, J. P., and C. Snyder, 2005: Ensemble Kalman filter assimilation of fixed screen-height observations in a parameterized PBL. *Mon. Wea. Rev.*, **133**, 3260–3275.

Hacker, J. P., and D. Rostkier-Edelstein, 2007: PBL state estimation with surface observations, a column model, and an ensemble filter. *Mon. Wea. Rev.*, **135**, 2958–2972.

Hacker, J. P., J. L. Anderson, and M. Pagowski, 2007: Improved vertical covariance estimates for ensemble-filter assimilation of near-surface observations. *Mon. Wea. Rev.*, **135**, 1021–1036.

Honda, Y., M. Nishijima, K. Koizumi, Y. Ohta, K. Tamiya, T. Kawabata, and T. Tsuyuki, 2005: A pre-operational variational data assimilation system for a non-hydrostatic model at the Japan Meteorological Agency: Formulation and preliminary results. *Quart. J. Roy. Meteor. Soc.*, **131**, 3465–3475.

Ingleby, B., 2015: Global assimilation of air temperature, humidity, wind and pressure from surface stations. *Quart. J. Roy. Meteor. Soc.*, **141**, 504–517.

Japan Meteorological Agency, 2015: *Kansoku data riyou no genjou to kadai, NPD report separate volume*, **61**, Japan Meteorological Agency, 98 pp (in Japanese).

Kajino, M., Y. Inomata, K. Sato, H. Ueda, Z. Han, J. An, G. Katata, M. Deushi, T. Maki, N. Oshima, J. Kurokawa, T. Ohara, A. Takami, and S. Hatakeyama, 2012: Development of the RAQM2 aerosol chemical transport model and predictions of the Northeast Asian aerosol mass, size, chemistry, and mixing type. *Atmos. Chem. Phys.*, **12**, 11833–11856.

Kunii, M., 2014: Mesoscale data assimilation for a local severe rainfall event with the NHM–LETKF system. *Wea. Forecasting*, **29**, 1093–1105.

Li, X., Y. Choi, B. Czader, A. Roy, H. Kim, B. Lefer, and S. Pan, 2016: The impact of observation nudging on simulated meteorology and ozone concentrations during DISCOVER-AQ 2013 Texas campaign. *Atmos. Chem. Phys.*, **16**, 3127–3144.

Miyoshi, T., and K. Aranami, 2006: Applying a four-dimensional local ensemble transform Kalman filter (4D-LETKF) to the JMA nonhydrostatic model (NHM). *SOLA*, **2**, 128–131.

Nakajima, T., S. Misawa, Y. Morino, H. Tsuruta, D. Goto, J. Uchida, T. Takemura, T. Ohara, Y. Oura, M. Ebihara, and M. Satoh, 2017: Model depiction of the atmospheric flows of radioactive cesium emitted from the Fukushima Daiichi Nuclear Power Station accident. *Prog. Earth Planet. Sci.*, **4**, 2, doi:10.1186/s40645-017-0117-x.

Oura, Y., M. Ebihara, H. Tsuruta, T. Nakajima, T. Ohara, M. Ishimoto, H. Sawahata, Y. Katsumura, and W. Nitta, 2015: A database of hourly atmospheric concentrations of radiocesium (^{134}Cs and ^{137}Cs) in suspended particulate matter collected in March 2011 at 99 air pollution monitoring stations in Eastern Japan. *J. Nucl. Radiochem. Sci.*, **15**, 2_1–2_12.

Rostkier-Edelstein, D., and J. P. Hacker, 2010: The roles of surface-observation ensemble assimilation and model complexity for nowcasting of PBL profiles: A factor separation analysis. *Wea. Forecasting*, **25**, 1670–1690.

Saito, K., T. Fujita, Y. Yamada, J. Ishida, Y. Kumagai, K.

Aranami, S. Ohmori, R. Nagasawa, S. Kumagai, C. Muroi, T. Kato, H. Eito, and Y. Yamazaki, 2006: The operational JMA nonhydrostatic mesoscale model. *Mon. Wea. Rev.*, **134**, 1266–1298.

Saito, K., J. Ishida, K. Aranami, T. Hara, T. Segawa, M. Narita, and Y. Honda, 2007: Nonhydrostatic atmospheric models operational development at JMA. *J. Meteor. Soc. Japan*, **85B**, 271–304.

Science Council of Japan, 2014: *A review of the model comparison of transportation and deposition of radioactive materials released to the environment as a result of the Tokyo Electric Power Company's Fukushima Daiichi Nuclear Power Plant accident*. Committee on Comprehensive Synthetic Engineering, Science Council of Japan, 103 pp. [Available at http://www.jpgu.org/scj/report/20140902scj_report_e.pdf.]

Sekiyama, T. T., M. Kunii, K. Kajino, and T. Shimbori, 2015: Horizontal resolution dependence of atmospheric simulations of the Fukushima nuclear accident using 15-km, 3-km, and 500-m Grid Models. *J. Meteor. Soc. Japan*, **93**, 49–64.

Tsuruta, H., Y. Oura, M. Ebihara, T. Ohara, and T. Nakajima, 2014: First retrieval of hourly atmospheric radionuclides just after the Fukushima accident by analyzing filter-tapes of operational air pollution monitoring stations. *Sci. Rep.*, **4**, 6717, doi:10.1038/srep06717.

World Meteorological Organization, 2006: Environmental emergency response: WMO activities. *WMO Bull.*, **55**, 37–41.

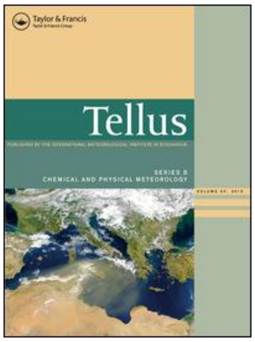

Tellus B: Chemical and Physical Meteorology

ISSN: (Print) 1600-0889 (Online) Journal homepage: http://www.tandfonline.com/loi/zelb20

Mass flux analysis of ^{137}Cs plumes emitted from the Fukushima Daiichi nuclear power plant

Tsuyoshi Thomas Sekiyama & Toshiki Iwasaki

To cite this article: Tsuyoshi Thomas Sekiyama & Toshiki Iwasaki (2018) Mass flux analysis of ^{137}Cs plumes emitted from the Fukushima Daiichi nuclear power plant, Tellus B: Chemical and Physical Meteorology, 70:1, 1-11, DOI: 10.1080/16000889.2018.1507390

To link to this article: https://doi.org/10.1080/16000889.2018.1507390

Tellus
SERIES B
CHEMICAL
AND PHYSICAL
METEOROLOGY
PUBLISHED BY THE INTERNATIONAL METEOROLOGICAL INSTITUTE IN STOCKHOLM

Mass flux analysis of ^{137}Cs plumes emitted from the Fukushima Daiichi nuclear power plant

By TSUYOSHI THOMAS SEKIYAMA[1]*, and TOSHIKI IWASAKI[2]

[1] *Meteorological Research Institute, Tsukuba, Japan;* [2] *Graduate School of Science, Tohoku University, Sendai, Japan*

(Manuscript received 6 March 2018; in final form 24 July 2018)

ABSTRACT

The flow vectors of radioactive cesium-137 (^{137}Cs) plume emitted from the Fukushima Daiichi nuclear power plant in March 2011 were quantitatively depicted by a mass flux analysis in this study. ^{137}Cs plumes were calculated by an Eulerian dispersion model with a 3-km horizontal resolution. The vertically column-integrated mass flux was consistent with the flow approximation based on ground surface ^{137}Cs observations, even though there were some discrepancies that were caused by differences in the wind direction between the ground surface and the dominant plume layer. These discrepancies were explained by combining the use of the ground surface horizontal mass flux with the column-integrated mass flux. The mass flux analysis clearly provided an illustration of ^{137}Cs dominant stream locations, directions, and depositions by reducing high-dimensional model outputs into a lower-dimensional plot. Mass flux (i.e. the product of the mass density and wind velocity) has often been used in dynamic meteorology but has not been used as frequently in atmospheric chemistry or pollutant dispersion studies. However, the concept of mass flux is a robust alternative for conventional validation approaches that only utilize a time series of pollutant concentrations. Mass flux analyses can be used further in atmospheric chemistry as a quantitative visualization tool to track the emission, advection, dispersion, and deposition of atmospheric constituents.

KEYWORDS: plume dispersion, numerical simulation, mass flux analysis, radioactive cesium-137, Fukushima nuclear accident

1. Introduction

The dispersion modeling of atmospheric constituents is essential for numerical simulation (or prediction) of precipitation, climate change, and air pollution. To improve dispersion modeling, it is crucial to quantitatively depict the modeled dispersion of pollutants and validate those results with observations. An ideal validation could be accomplished by using atmospheric constituents that are (1) chemically inert to avoid errors in the reaction rate estimation, (2) emitted from a single source to isolate plumes without cross-dispersion, and (3) observed at many locations with a high accuracy. The radioactive cesium-137 (^{137}Cs) from the Fukushima nuclear accident considerably matches these criteria. The Fukushima nuclear accident was triggered by the 2011 Tohoku earthquake and tsunami and was the largest nuclear disaster since Chernobyl, which resulted in the extensive dispersion of a large amount of radionuclides in Japan (e.g. ^{131}I, ^{133}Xe, ^{134}Cs, and ^{137}Cs). Among these radionuclides, ^{137}Cs has a relatively long half-life (~30 years) and characteristics such as chemical inertness and high detectability. It was confirmed that ^{137}Cs was emitted from a single location: the Fukushima Daiichi nuclear power plant (FDNPP). The ground surface concentration of ^{137}Cs has been retrieved at many locations at an hourly frequency with a high accuracy (e.g. Tsuruta et al. 2014; Oura et al. 2015).

After the accident, many numerical simulations were performed using atmospheric dispersion models or chemistry transport models (e.g. Science Council of Japan, 2014; Draxler et al. 2015). However, most of the simulations were validated by comparing the results with total ground surface ^{137}Cs deposition or surface dose rates. Deposition and dose rates are strongly affected by precipitation and deposition processes. However, the time variability of pollutant concentrations is rarely detectable in these types of

---

*Corresponding author. email: tsekiyam@mri-jma.go.jp

Tellus B: 2018.

Citation: Tellus B: 2018, **70**, 1507390, https://doi.org/10.1080/16000889.2018.1507390

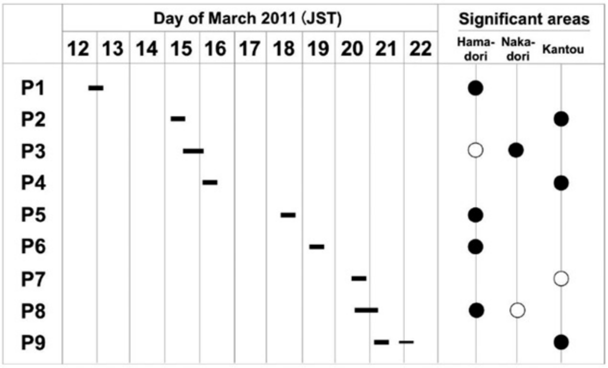

Fig. 1. Fukushima ^{137}C plumes identified by Tsuruta et al. (2014). Horizontal bars show periods with ^{137}Cs concentrations greater than 10 Bq m^{-3}. Closed (open) circles indicate areas where the highest concentrations were larger (smaller) than 100 Bq m^{-3}. This figure was reprinted from fig. 3 in Nakajima et al. (2017).

observations. Therefore, in the majority of previous model studies, deposition model errors and dispersion model errors were barely distinguished between. In contrast, Nakajima et al. (2017) isolated the individual ^{137}Cs plumes simulated by their chemistry transport models comparing with hourly concentration observations from Tsuruta et al. (2014) and Oura et al. (2015) and successfully examined the dispersion model performance separately from the deposition model performance. It should be noted that Tsuruta et al. (2014) and Nakajima et al. (2017) classified ^{137}Cs propagations over land in March 2011 into nine plumes based on their time, location, and direction, as shown in Figs. 1 and 2. These plume numbers (P1–P9) are used without any change in this study.

Nakajima et al. (2017) clearly identified these nine plumes, as shown in Fig. 2, and exhibited their model performance with hourly ^{137}Cs concentrations observed at 99 sample stations. However, we realized that several of the plume directions in Fig. 2 were inconsistent with the other forward trajectory model simulations. For example, Nakajima et al. (2017) claimed that plume P3 was transported toward the Nakadori region and crossed the Abukuma Mountains from south to north in the afternoon of 15 March 2011, Japanese Standard Time (JST); then, a part of plume P3 exhibited a northern detour from north to south in the late afternoon, as shown in Fig. 2a (geographical names are shown in Fig. 3). On the other hand, Kajino et al. (2016) calculated forward trajectories beginning at 12:00 JST, 15:00 JST, 18:00 JST, and 21:00 JST on 15 March 2011, from the FDNPP, which emitted the pollutant at 25-m height (Fig. 4). The forward trajectories described in Kajino et al. (2016) indicated that plume P3 rotated invariably clockwise and moved from south to north over the Abukuma Mountains and the Nakadori region in the late afternoon on 15 March 2011, JST. There is a discrepancy between observation-based analyses and forward trajectory analyses.

This discrepancy might be caused by dispersion model errors, meteorological analysis errors, or the vertical wind shear in the presence of the height difference between observations and the dominant stream of pollutant flows. In addition, neither the pollutant plumes in Fig. 2 nor the pollutant trajectories in Fig. 4 are quantitatively depicted regarding pollutant mass flows. We cannot determine which flow depiction is more plausible using only these simple figures. First, it is desirable that plumes of atmospheric pollutants should be identified and quantitatively determined when considering pollutant mass flows using dispersion models. This quantitative plume identification allows us to objectively validate the modeled dispersion performance and distinguish between dispersion and deposition errors.

In this study, we quantitatively depicted all of the plume streams (P1–P9) from Tsuruta et al. (2014) and Nakajima et al. (2017) using our ^{137}Cs dispersion model and attempted to determine the reasons for the above-mentioned discrepancy. In this context, we took advantage of a mass flux analysis to quantify the pollutant flows. Mass flux is often used in fluid dynamics or dynamic meteorology (e.g. Iwasaki et al. 2014; Yano 2014); however, it has not been used as much in atmospheric chemistry or dispersion modeling, except for meridional transport analyses (e.g. Stohl et al. 2003; Belikov et al. 2013) or regional pollutant outflows (e.g. Bey et al. 2001). The concept of mass flux could be a robust alternative to traditional concepts using time-variable concentrations to assess horizontal pollutant flows. We attempt to exhibit the mass flux analysis as a model visualization method or a validation metric through the depiction of Fukushima ^{137}Cs plumes. In this analysis, we defined not only the single-layer mass flux but also the column-integrated mass flux to track pollutant mass flows that are vertically distributed. Details for the mass flux equations are described in Section 2, followed by a model description in Section 3. Then, a comparison of

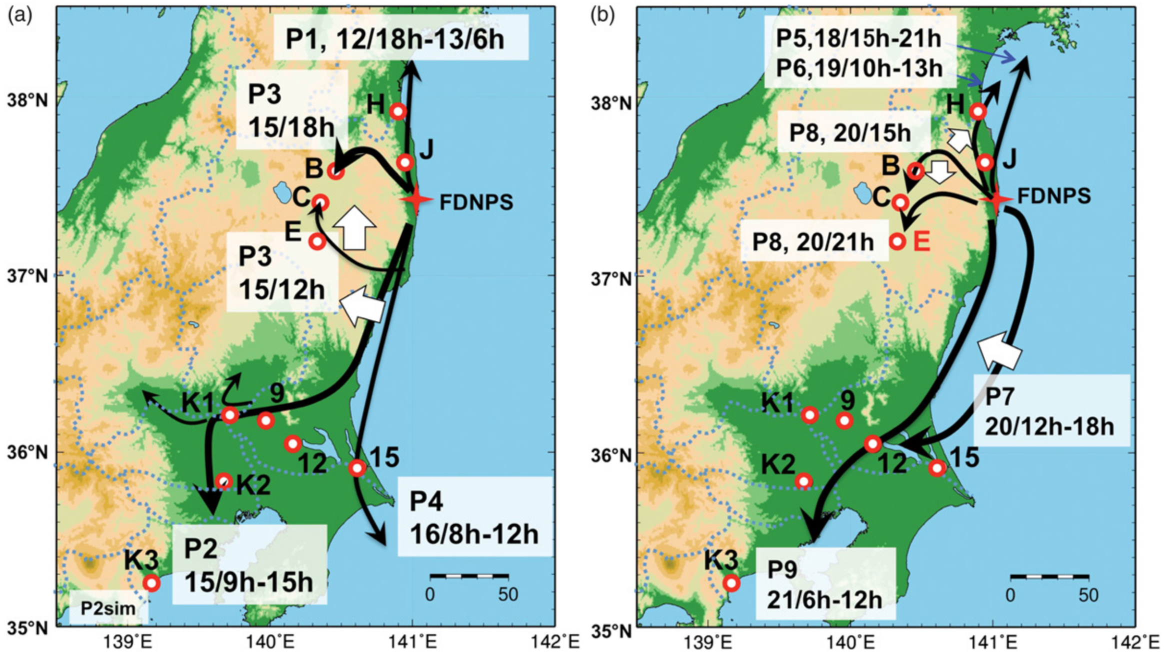

Fig. 2. Schematic diagrams of the transport routes analyzed in Nakajima et al. (2017) for plumes P1–P9 isolated in Tsuruta et al. (2014). Black arrows indicate the general movement trend for each plume. This figure is reprinted from fig. 15 in Nakajima et al. (2017). The letters, B, C, E, H, J, K1, K2, K3, 9, 12, and 15, indicate ^{137}Cs sample station locations identified in Nakajima et al. (2017) but these indications are not used in this study.

Fukushima ^{137}Cs plumes between our analysis results and those of Nakajima et al. (2017) is shown in Section 4, followed by concluding remarks in Section 5.

2. Mass flux and continuity equation

The mass flux **j** is defined by the product of the mass concentration ρ and the wind velocity $\mathbf{v} \equiv (u, v, w)$. **j** is represented as a mass per unit area per unit of time (e.g. kg m^{-2} s^{-1}) or as the rate of mass flow per unit area (e.g. [kg s^{-1}] m^{-2}), which perfectly corresponds with the momentum density or momentum per unit volume (e.g. [kg m s^{-1}] m^{-3}). The mass flux indicates the extent that a pollutant is flowing over one's head or how much a pollutant collides into one's body per unit of time. Even if the mass concentration is known, the amount of total exposure cannot be estimated without the mass flux information. Furthermore, mass flux is a vector not a scalar (e.g. concentration); therefore, we can recognize the streams and directions of pollutant transport using the mass flux distribution.

In the atmosphere, the mass concentration and mass flux are governed by the continuity equation, which conserves the total mass of a pollutant as shown below

$$\begin{aligned}\frac{\partial \rho}{\partial t} + \nabla \cdot \mathbf{j} = \frac{\partial \rho}{\partial t} + \nabla \cdot \rho \mathbf{v} = \frac{\partial \rho}{\partial t} + \frac{\partial \rho u}{\partial x} + \frac{\partial \rho v}{\partial y} + \frac{\partial \rho w}{\partial z} \\ = \frac{\partial \rho}{\partial t} + \nabla \cdot \rho \mathbf{v}_h + \frac{\partial \rho w}{\partial z} = \sigma,\end{aligned} \tag{1}$$

where t represents time, $\mathbf{v}_h \equiv (u, v)$ represents the horizontal wind, and σ represents the generation of the pollutant per unit of volume and time. When $\sigma > 0$, σ is referred to as a source term. Conversely, when $\sigma < 0$, σ is referred to as a sink term. To achieve a vertically comprehensive assessment of mass flux in the atmosphere, we integrate Eq. (1) over a column from the surface to the top of the atmosphere;

$$\begin{aligned}&\int_0^\infty \left(\frac{\partial \rho}{\partial t} + \nabla \cdot \rho \mathbf{v}_h + \frac{\partial \rho w}{\partial z} \right) \mathrm{d}z \\ &= \int_0^\infty \frac{\partial \rho}{\partial t} \mathrm{d}z + \int_0^\infty \nabla \cdot \rho \mathbf{v}_h \mathrm{d}z + \int_0^\infty \frac{\partial \rho w}{\partial z} \mathrm{d}z \\ &= \frac{\partial}{\partial t} \int_0^\infty \rho \mathrm{d}z + \nabla \cdot \int_0^\infty \rho \mathbf{v}_h \mathrm{d}z \\ &\quad + [\rho w]_{z=0}^{z=\infty} \quad (x,\ y,\ z,\ \text{and } t \text{ are mutually independent}) \\ &= \frac{\partial}{\partial t} \int_0^\infty \rho \mathrm{d}z + \nabla \cdot \mathbf{j}_{\text{column}} \quad (\because \rho(\infty) = w(0) = 0) \\ &= \int_0^\infty \sigma \mathrm{d}z = \sigma_s,\end{aligned} \tag{2}$$

where σ_s represents deposition or emission at the surface, assuming that the pollutant is inert and is added/removed

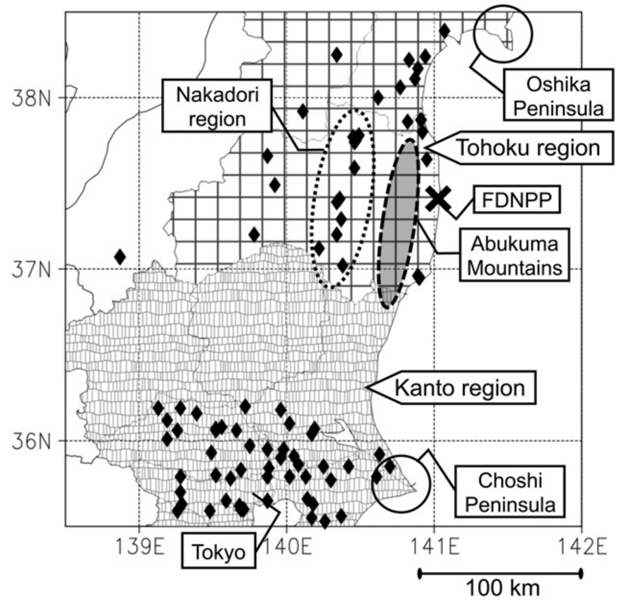

Fig. 3. Map of the area around the FDNPP. Closed diamonds indicate the ^{137}Cs sample stations in Tsuruta et al. (2014) and Oura et al. (2015).

only at the surface. Here, we introduce the column integral of the horizontal mass flux, $\int_0^\infty \rho \mathbf{v}_h \mathrm{d}z \equiv \mathbf{j}_{\text{column}}$, which indicates the total mass flow per unit width integrated vertically from the surface to the top of the atmosphere (e.g. [kg s^{-1}] m^{-1} = kg m^{-1} s^{-1}). Conveniently, the time-integral of $\mathbf{j}_{\text{column}}$ illustrates the dominant stream of the pollutant two-dimensionally. Because the column integral of the vertical mass flux $\int_0^\infty \frac{\partial \rho w}{\partial z} \mathrm{d}z = [\rho w]_{z=0}^{z=\infty} = 0$ is negligible, the dominant stream can be calculated using only horizontal wind components and neglecting the vertical wind component, which is rarely obtained with high accuracy. This illustration is helpful when tracking pollutant plumes with a vertical structure.

Next, we integrate Eq. (2) over time for a typical plume situation, where the mass concentration is zero before a plume arrives and after it leaves. In this situation,

$$\int_0^\infty \frac{\partial}{\partial t}\int_0^\infty \rho \mathrm{d}z \mathrm{d}t = \left[\int_0^\infty \rho \mathrm{d}z\right]_{t=0}^{t=\infty} = 0 \quad (\because \rho(\mathrm{t}=0) \equiv \rho(\mathrm{t}=\infty) \equiv 0);$$

therefore, the integration of Eq. (2) over time is represented as

$$\int_0^\infty \nabla \cdot \mathbf{j}_{\text{column}} \mathrm{d}t = \int_0^\infty \sigma_s \mathrm{d}t, \qquad (3)$$

which indicates that the time-integral for the divergence of the column integral in the horizontal mass flux equals the total emission or deposition per unit area (e.g. kg m^{-2}).

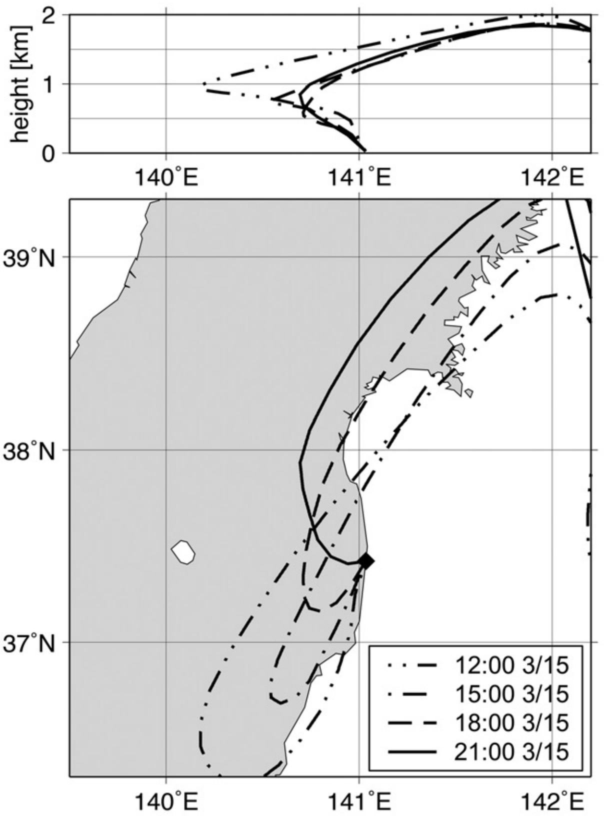

Fig. 4. Forward trajectories that began at 12:00 JST (dashed two-dot line), 15:00 JST (dashed-dotted line), 18:00 JST (dashed line), and 21:00 JST (solid line) on 15 March 2011 from the FDNPP at a height of 25 m (calculated by Kajino et al. 2016).

Actually, negative divergence (= convergence) and deposition are often very similar in ^{137}Cs plume model simulations. However, they are not exactly consistent because model simulations have numerical errors (mainly due to truncation processes) and assumption errors (e.g. non-zero background concentrations and finite limits of the model top height), as shown in Fig. 5. This figure was compiled using the ^{137}Cs dispersion model results detailed in the next section. The time-integrated period (21:00 JST on 20 March to 21:00 JST on 22 March 2011) was chosen to observe a noticeable example of wet deposition induced by widespread precipitation.

In addition, we can calculate a vertically mass-weighted mean wind, $\mathbf{v}_{\text{weighted}}$, by dividing the column integral of the horizontal mass flux by the total column mass

$$\mathbf{v}_{\text{weighted}} \equiv \frac{\mathbf{j}_{\text{column}}}{\text{Total column mass}} = \int_0^\infty \rho \mathbf{v}_h \mathrm{d}z \Big/ \int_0^\infty \rho \mathrm{d}z, \qquad (4)$$

which describes the wind velocity that forces the column-integrated mass from the ground surface to the top of the atmosphere.

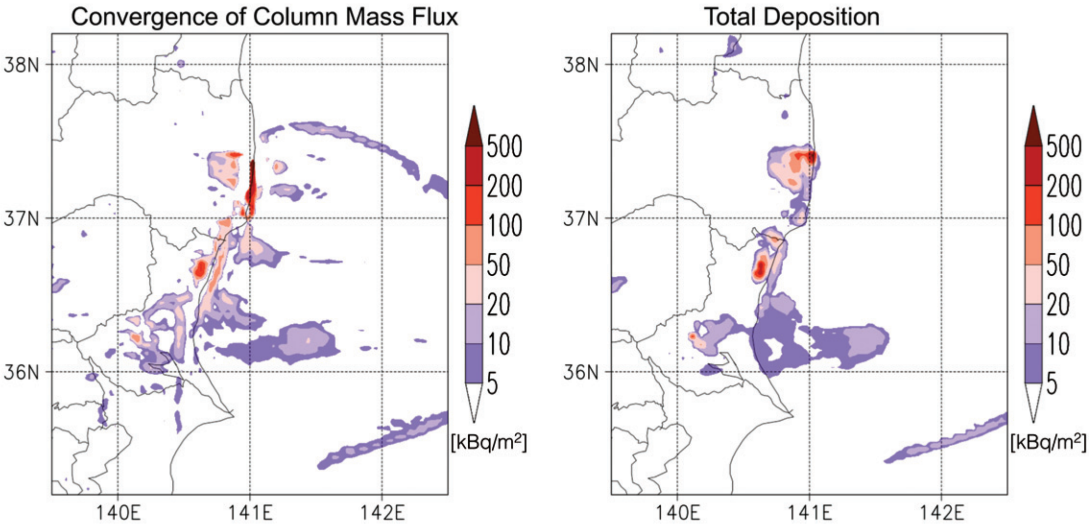

Fig. 5. Convergence (= negative divergence) of the column-integrated ^{137}Cs mass flux and the total deposition of ^{137}Cs values temporally integrated from 21:00 JST on March 20 to 21:00 JST on 22 March 2011 for the model simulation used in this study.

3. Model description

In this study, the simulation of the Fukushima ^{137}Cs plume dispersion was performed by an offline Eulerian regional air quality model, which was originally developed by Kajino et al. (2012) for non-radioactive aerosol simulations. This dispersion model has been used for Fukushima nuclear pollutant simulation by Adachi et al. (2013), the Science Council of Japan (2014), Sekiyama et al. (2015, 2017), and Kajino et al. (2016). Radioactive ^{137}Cs nuclides were assumed to be contained in sulfate aerosol particles that were mixed with organic compounds, as described in detail by Sekiyama et al. (2015). We applied the ^{137}Cs emission scenario estimated by the Japan Atomic Energy Agency (Katata et al. 2015) to this simulation. Based on the time series of this emission scenario, ^{137}Cs-containing aerosol particles were injected into a grid cell above the FDNPP. The injection height was assigned based on the emission scenario, which varied temporally from 20 to 150 m.

This offline dispersion model was driven by meteorological grid point value (GPV) data calculated by the data assimilation system in Kunii (2014) and Sekiyama et al. (2015, 2017). The data assimilation system was composed of a non-hydrostatic regional weather prediction model (referred to as NHM; cf. Saito et al. 2006, 2007) and a local ensemble transform Kalman filter (LETKF; cf. Miyoshi and Aranami 2006). The NHM has been operationally used by the Japan Meteorological Agency (JMA) for daily national weather forecasts with a four-dimensional variation method; this weather forecast system is called JNoVA (cf. Honda et al. 2005). The LETKF was driven by 20 ensemble members at a 3-km horizontal resolution within a model domain over eastern Japan (215 × 259 grids; cf. fig. 2b of Sekiyama et al. 2015) and 60 vertical layers from the surface to 22 km above the surface. Details of the LETKF settings were described in Sekiyama et al. (2015, 2017). The boundary conditions for the model domain were provided by the JMA operational global analysis. Using the NHM and LETKF system (referred to as NHM-LETKF), we simultaneously assimilated the observations archived by the JNoVA system and the land surface wind observations collected by the JMA automated meteorological data acquisition system (AMeDAS), as described in Sekiyama et al. (2017). The AMeDAS is a land surface observation network that comprises ~1300 stations throughout Japan, with an average interval of 17 km. The operational JNoVA dataset contains land surface pressure, satellite-observed sea surface winds, and observations from radiosondes, pilot balloons, wind profilers, aircrafts, ships and buoys.

The dispersion model shared the same model domain and horizontal resolution as those of the NHM-LETKF calculated meteorological GPV data, although the vertical resolution was converted from the original 60 layers (from the surface to 22 km) to 20 layers (from the surface to 10 km) to reduce the computational burden of calculations within the stratosphere. Meteorological GPV data were input into the dispersion model at 10-min intervals. In the dispersion model, the time step was set to 24 s using a linear interpolation of the meteorological GPV data. The model simulations were performed from 10 March to 31 March 2011.

4. Mass flux of Fukushima ^{137}Cs plumes

4.1. Insight into plume P3

First, we focus on Plume P3, which has a discrepancy between the observation-based analysis and the forward trajectory analysis, as mentioned in the Introduction. To track the dominant stream of the plume, the time-integral of the column-integrated mass flux ($\equiv \int_{t_1}^{t_2} \mathbf{j}_{\text{column}} \mathrm{d}t$; hereafter called the TC mass flux) of plume P3 is illustrated in Fig. 6a. The time-integration period was chosen to follow the classification of Tsuruta et al. (2014), shown in Fig. 1, and Nakajima et al. (2017), shown in Fig. 2, as much as possible. In this period (15:00 to 21:00 JST on 15 March 2011), the dominant stream (red or dark-red shading) flowed northwestward directly from the FDNPP and crossed the Abukuma Mountains toward the Nakadori region (Fig. 6a). Meanwhile, the widespread mass flux (which likely includes the residuals of plume P2 as shown in the panel P2 of Fig. 7) generally flowed northward or northeastward in the vicinity of the dominant stream of plume P3. This is consistent with the forward trajectory results of Kajino et al. (2016). The widespread and northeastward-directed TC mass flux occurred at an order of magnitude lower than that of the dominant stream directly emitted from the FDNPP. However, the arrow of plume P3 at 18:00 JST on 15 March from Nakajima et al. (2017), shown in Fig. 2 (also depicted as a large gray arrow in Fig. 6a), turns southwestward over the Nakadori region.

Here, we pay attention not only to the TC mass flux but also to the horizontal mass flux at the ground surface (20 m) for plume P3 (Fig. 6b). The horizontal mass flux at the ground surface turned southwestward over the Nakadori region. This flow direction is consistent with that of Nakajima et al. (2017). The horizontal southwestward mass flux at the surface over the Nakadori region was a non-dominant stream that was approximately two orders of magnitude lower than that in the immediate vicinity of the FDNPP. The plume P3 direction shown by Nakajima et al. (2017) was analyzed only by means of the surface observations from Tsuruta et al. (2014). Therefore, these studies derived only the southwestward stream during this time slot. The two opposite stream directions are clearly depicted by the vertical cross-section of the pollutant concentration and the meridional wind (Fig. 6c). The maximum concentration core of plume P3 was located at a height of ~900 m above the ground level (AGL), where southerly winds were occurring. In contrast, the surface wind direction was northerly beneath the plume core, although it was very weak. This indicates that a dominant stream of atmospheric pollutants cannot be determined using only ground surface observations.

4.2. Other plumes

Next, we surveyed each plume (P1–P2 and P4–P9) to analyze the TC mass flux direction and magnitude. Figure 7 shows the TC mass flux of Plumes P1–P2 and

(a) Column-integrated mass flux [GBq/m]
P3 [2011-03-15 15:00~21:00 JST]

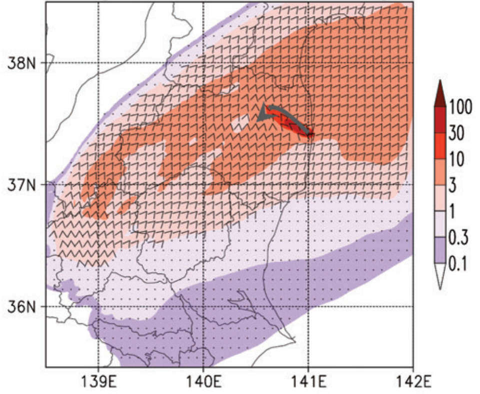

(b) Surface horizontal mass flux [MBq/m2]
P3 [2011-03-15 15:00~21:00 JST]

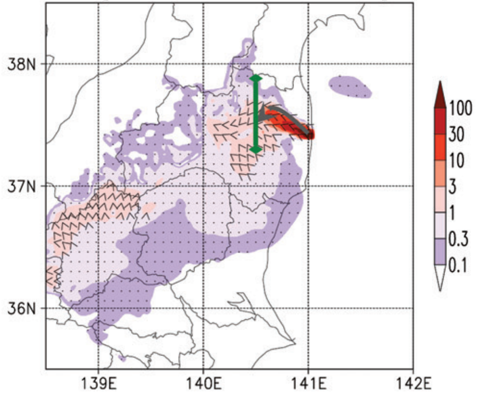

(c) 137Cs concentration [Bq/m3], meridional wind, and θ [K] at [2011-03-15 **17:00** JST 140.5ºE]

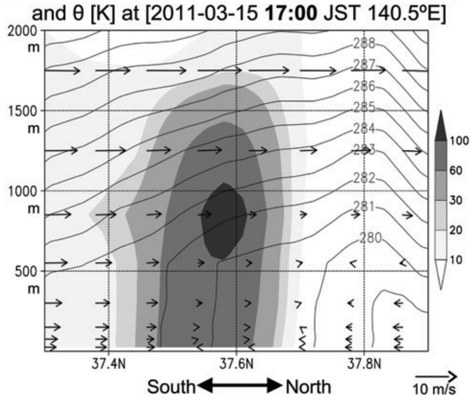

Fig. 6. Time-integrals from 15:00 to 21:00 JST on 15 March 2011 of (a) the column-integrated mass flux of plume P3 and (b) the horizontal mass flux of plume P3 at the ground surface. Color shading indicates the magnitude of the mass flux. Small arrowheads indicate the direction of the mass flux. A large gray arrow illustrates the depiction in Nakajima et al. (2017) for plume P3 at 18:00 JST on March 15, shown in Fig. 2. (c) Latitude-altitude cross-sections at 140.5°E for ^{137}Cs concentrations (gray shading), meridional winds (arrows), and potential temperature (θ; contours) at 17:00 JST on 15 March 2011. The cross-section is located at the green line in panel (b).

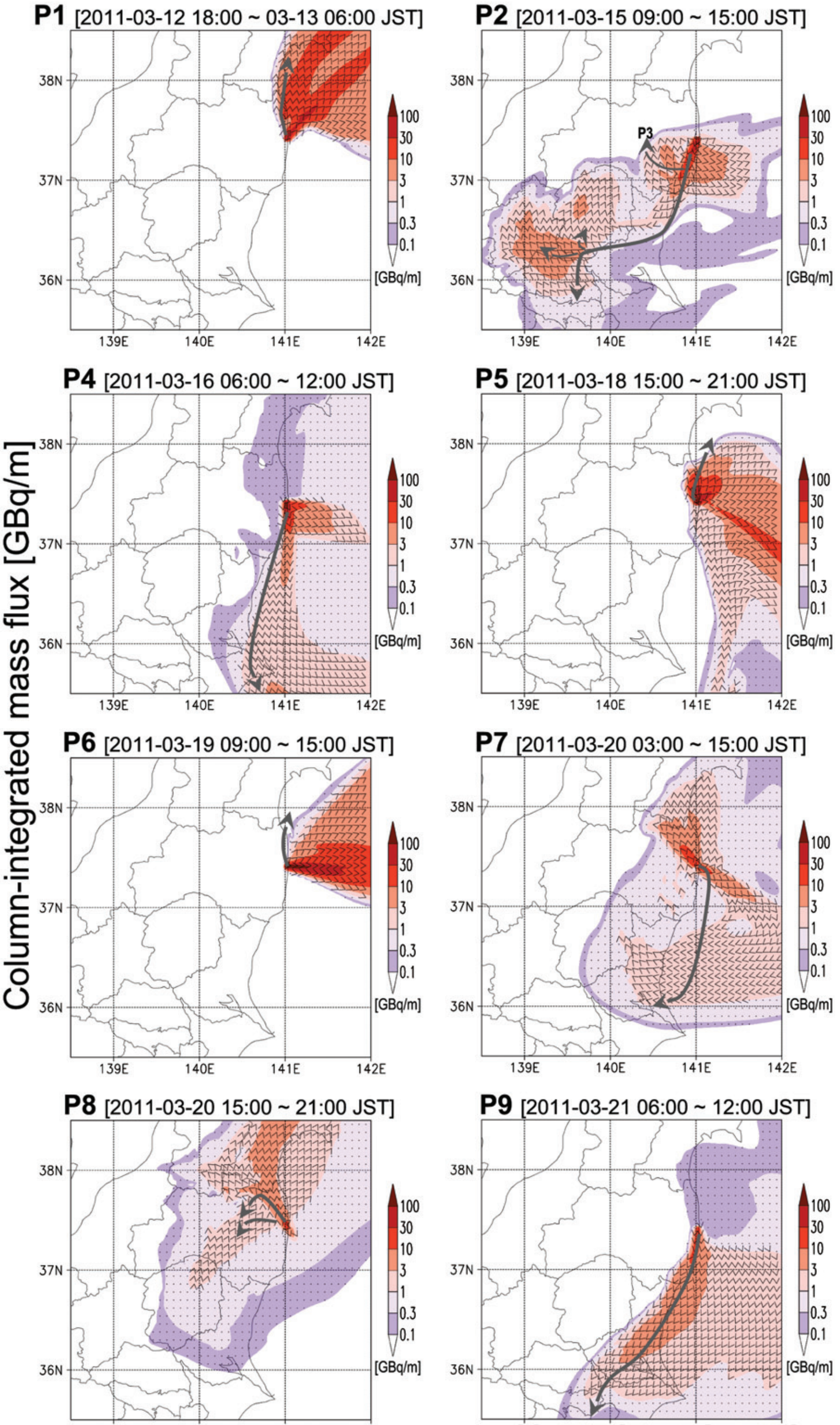

Fig. 7. Time-integrals of the column-integrated mass fluxes of plumes P1–P2 and P4–P9. Color shading indicates the magnitude of the mass flux. Small arrowheads indicate the direction of the mass flux. Gray arrows illustrate the depictions from Nakajima et al. (2017) for plumes P1–P2 and P4–P9, shown in Fig. 2. In figure P2, only part of the plume P3 arrows from Nakajima et al. (2017) in the vicinity of the FDNPP is illustrated.

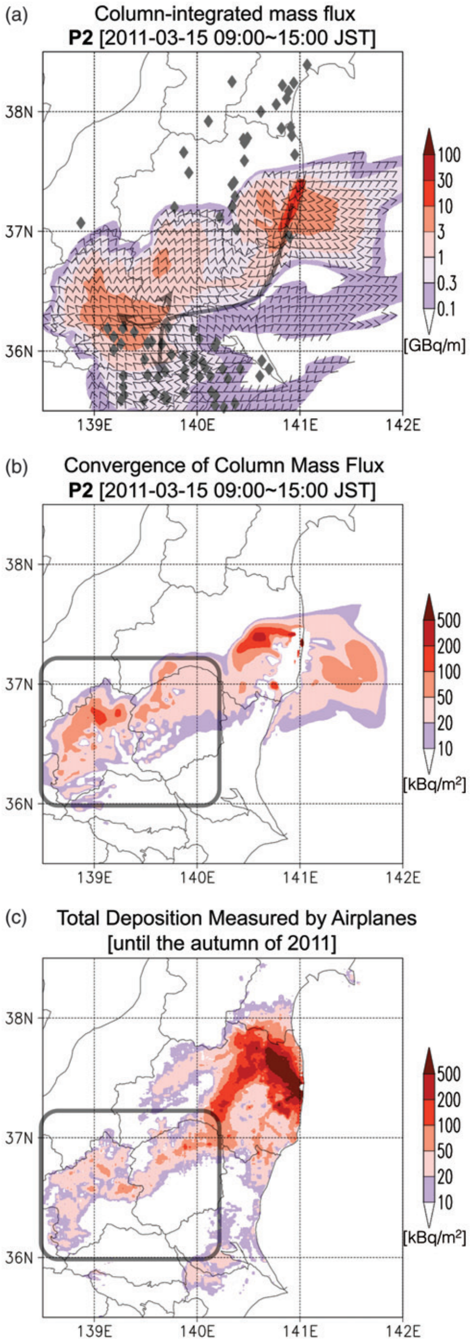

Fig. 8. (a) Same as Fig. 7 for plume 2, but the plotted arrowheads include the direction of small mass fluxes <1 GBq m^{-1}. Gray diamonds indicate the ^{137}Cs sample stations from Tsuruta et al. (2014) and Oura et al. (2015). (b) Convergence of the column-integrated ^{137}Cs mass flux time-integrated during the period of plume 2 in the model simulation. (c) Total deposition measured by airplanes, which were recorded by the Japanese government (Torii et al. 2012). Note that this deposition represents all Cs-137 emissions and plumes until autumn of 2011.

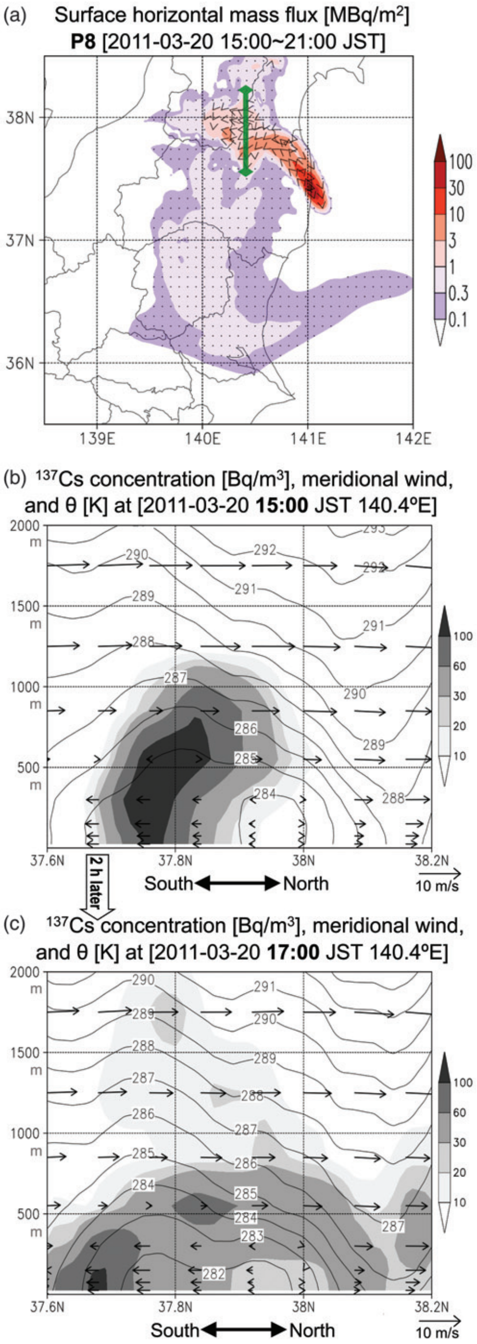

Fig. 9. (a) Time-integral of the horizontal mass flux at the ground surface for plume P8. The time-integrated period is consistent with that of plume P8 in Fig. 7. Color shading indicates the magnitude of the mass flux. Small arrowheads indicate the direction of the mass flux. Latitude-altitude cross-sections at 140.4°E for ^{137}Cs concentrations (gray shading), meridional wind (arrows), and potential temperature (θ; contours) are shown at (b) 15:00 JST on 20 March 2011 and (c) 17:00 JST on 20 March 2011. The cross-sections are located at the green line in panel (a).

P4–P9 with plume pathway arrows from Nakajima et al. (2017) that are the same as those in Fig. 6a. The corresponding time-integration periods were chosen to follow the classification of Tsuruta et al. (2014), shown in Fig. 1, and Nakajima et al. (2017), shown in Fig. 2 (hereinafter called T&N), as much as possible.

The model-calculated TC mass flux of plume P1 flowed mainly northeastward over the Pacific Ocean and partly crossed the Oshika Peninsula located 120 km north-northeast of the FDNPP. The mass flux slightly flanked a coastal area north of the FDNPP, which was consistent with the plume depiction in T&N. The mainstream of Plume P1 was detected by dose rate monitoring posts at the Onagawa nuclear power plant in the Oshika Peninsula (the Tohoku Electric Power Company, http://www.tohoku-epco.co.jp/ICSFiles/afieldfile/2011/03/14/11031401_t1.pdf, in Japanese) during the P1 time slot (18:00 JST on 12 March to 06:00 JST on 13 March 2011). The monitoring post data indicated that the dose rates at the Oshika Peninsula slowly increased after 19:00 JST on 12 March, suddenly increased at 00:00 JST on 13 March, peaked at 02:00 JST on 13 March, and plateaued after 05:00 JST on 13 March; all of these stages were occurred during the P1 time slot.

The model-calculated TC mass flux of plume P2 mainly flowed south-southwestward from the FDNPP, turned west, and spread over a large area in the Kanto region. This pathway was very consistent with those depicted in T&N. In addition, a northwestward flow was distinguished in the vicinity of the FDNPP, which was likely classified as part of plume P3 in T&N. Tsuruta et al. (2014) and Nakajima et al. (2017) proposed three terminal directions for plume P2: northeastward, northwestward, and southward over the Kanto region. The northeastward and northwestward flows were completely consistent with those illustrated by the TC mass flux. The dominant southward flows in T&N did not seem to be reproduced by the TC mass flux in Fig. 7. However, a southward (or southwestward) flow can be seen by plotting arrowheads for very small mass fluxes (Fig. 8a), although this flow was not dominant. Unfortunately, the observations in Tsuruta et al. (2014) and Oura et al. (2015) were not derived from the northern area of the Kanto region (shown in Fig. 8a). This biased distribution caused a bias in the plume analysis from T&N when the southward flow was supposed to be dominant. In practice, the northeastward/northwestward flows were presumably dominant and converged over the mountainous area of the northern Kanto region during this time period (shown by a gray rounded square in Fig. 8b). It is noted that the convergence (= deposition) was inconsistent or unnatural near the FDNPP because the time-integral length (= 6 h) was too short for the source area. The convergence area (shown by the gray rounded square) resembles the ^{137}Cs-polluted land surface over the mountainous area of the northern Kanto region in regard to shape and depth (Fig. 8c), which indicates that the convergence (= deposition) of Plume P2 is likely responsible for this land pollution. During this time period, it was drizzling (approximately <0.1 mm per 6 h) over this mountainous area in the model, which caused wet deposition.

Tsuruta et al. (2014) and Nakajima et al. (2017) inferred that plume P4 was transported by northerly winds over the ocean, which eventually reached the Choshi Peninsula. This depiction is clearly consistent with one of the two streams from the model-calculated TC mass flux during the P4 time slot. According to the TC mass flux depiction, the two streams were southward and eastward; the edge of the southward stream passed over the Choshi Peninsula, which is the easternmost area of the Kanto region.

Tsuruta et al. (2014) and Nakajima et al. (2017) reported that plumes P5 and P6 were short-duration events that occurred on 18 and 19 March, respectively, and both were observed over a limited area just north of the FDNPP. During these time slots, the plumes were mainly transported towards the Pacific Ocean, as shown by the model-calculated TC mass flux in Fig. 7. However, the peripheries of the plumes passed slightly over a coastal area north of the FDNPP. The ground surface observations in Tsuruta et al. (2014) likely detected these peripheries.

The model-calculated TC mass flux for plume P7 depicts a pathway characteristic of pollutant flows. The plume was transported over a long distance; first, it flowed southeastward with the offshore winds; second, it sharply turned clockwise toward the west over the ocean; then, it flowed onshore and landed over the Kanto region, as shown in Fig. 7. This pathway is obviously consistent with that referenced in T&N. Meanwhile, another northwestward flow was also depicted from the FDNPP, which was likely partially attributed to plume P8 because the P7 time slot overlapped with that of P8 (Fig. 1).

The depiction of plume P8 was somewhat similar to that of plume P3. The model-calculated TC mass flux indicated that a dominant stream flowed northwestward from the FDNPP and turned toward the northeast at ~38°N. However, Tsuruta et al. (2014) and Nakajima et al. (2017) reported that plume P8 was transported northwestward from the FDNPP and redirected toward the south near the Nakadori region at the northern edge of the Abukuma Mountains (shown by gray arrows in Fig. 7). In the TC mass flux and T&N depictions, the plume rotates in the opposite direction. This inconsistency is discussed in the next section in detail.

Plume P9 followed a southern route and reached the Kanto region, which had sporadic rainfall during this time slot. This rainfall caused ^{137}Cs wet deposition in a wide range of areas in the Kanto region, which dispersed the plume (cf. Science Council of Japan 2014; Tsuruta et al. 2014; Sekiyama et al. 2015; Nakajima et al. 2017). The TC mass flux depicted the plume in a tongue shape that flowed southward from the FDNPP; then, it flowed to the northern part of the Kanto region and spread over southern parts of the Kanto region, as shown in Fig. 7. This pathway is precisely consistent with that of T&N, which is based on ground surface observations.

4.3. *Inconsistency of plume P8*

In the previous section, we encountered another inconsistent depiction between the TC mass flux and the T&N illustration for plume P8. The dominant stream of plume P8 flowed with the southerly winds throughout the entire period for the model-calculated TC mass flux; however, the stream exhibited an opposite rotation at the Abukuma Mountains for the T&N illustration. The discrepancy is likely to be caused by the difference in wind direction between the ground surface and the dominant layer of the mass flux, similar to that for plume P3. The horizontal mass flux at the ground surface (20 m), shown in Fig. 9a, clearly explains the two situations. The surface mass flux turned southwestward and propagated over the Nakadori region. Here, this flow direction was completely consistent with that of T&N based on ground surface observations. As shown in Fig. 9b, the high concentration core of plume P8 was distributed from the ground surface to ~1000 m AGL at the beginning of the P8 time slot. At this time, the wind direction was northerly at <500 m AGL, and it was southerly at higher than 500 m AGL. This vertical wind shear caused an inconsistent depiction between the TC mass flux analysis and the surface observation analysis.

Then, the lower part of plume P8 was transported southward along the ground surface, while the upper part was transported northward along approximately isentropic surfaces. Consequently, the vertical cross-section shape of plume P8 arched over the ground in 2 h, as shown in Fig. 9c. Although the column-integrated mass flux is a useful tool to track atmospheric pollutants, a cross-check between the column-integrated and the ground surface mass fluxes is essential when the vertical wind shear is expected to be large.

5. Conclusions

We carried out a mass flux analysis for the Fukushima ^{137}Cs plumes by showing its usefulness and quantitative performance. The model-calculated TC mass flux was almost entirely consistent with the surface observations from Tsuruta et al. (2014) and Oura et al. (2015), although with some exceptions. However, these exceptions can be explained by the ground surface mass flux using together with the TC mass flux because the inconsistencies were only caused by the vertical wind shear between the ground surface and the dominant plume layer. The convergence of the TC mass flux was also able to explain the ^{137}Cs deposition distribution over northern Kanto region measured by airplanes.

The mass flux analysis clearly provided an overall illustration of dominant plume locations, directions, and depositions without developing movie/animation files. Unfortunately, such a useful mass flux analysis has rarely been used for dispersion simulations in atmospheric chemistry. The concept of the mass flux analysis can be further used as diagnostic or quantitative visualization tools because mass flux illustrations are a robust way for researchers to reduce high-dimensional model outputs into a lower-dimensional plot. It is inadequate to examine only a time series of concentrations at each observation point because such a conventional approach cannot validate the reproducibility of model-calculated mass flow balance. In contrast, the mass flux analysis can track the emission, advection, dispersion, and deposition of atmospheric constituents.

Acknowledgments

We thank Dr. Mizuo Kajino from the Meteorological Research Institute for providing us with his Lagrangian dispersion model. We also thank Prof. Teruyuki Nakajima from the Japan Aerospace Exploration Agency for kindly providing us with the figures in his paper.

Funding

This work was supported by JSPS KAKENHI (under Grant JP16H02946, JP16H04051 and JP17K00533) and the Environment Research and Technology Development Fund (5-1605) at the Environmental Restoration and Conservation Agency (ERCA).

ORCID

Toshiki Iwasaki http://orcid.org/0000-0003-2110-0687

References

Adachi, K., Kajino, M., Zaizen, Y. and Igarashi, Y. 2013. Emission of spherical cesium-bearing particles from an early stage of the Fukushima nuclear accident. Sci. Rep. 3, 2554. DOI:10.1038/srep02554.

Belikov, D. A., Maksyutov, S., Krol, M., Fraser, A., Rigby, M. and co-authors. 2013. Off-line algorithm for calculation of vertical tracer transport in the troposphere due to deep convection. Atmos. Chem. Phys. 13, 1093–1114. DOI:10.5194/acp-13-1093-2013.

Bey, I., Jacob, D. J., Logan, J. A. and Yantosca, R. M. 2001. Asian chemical outflow to the Pacific in spring: Origins, pathways, and budgets. J. Geophys. Res. 106, 23023–23097. DOI:10.1029/2001JD000806.

Draxler, R., Arnold, D., Chino, M., Galmarini, S., Hort, M. and co-authors. 2015. World Meteorological Organization's model simulations of the radionuclide dispersion and deposition from the Fukushima Daiichi nuclear power plant accident. J. Environ. Radioact. 139, 172–184. DOI:10.1016/j.jenvrad.2013.09.014.

Honda, Y., Nishijima, M., Koizumi, K., Ohta, Y., Tamiya, K. and co-authors. 2005. A pre-operational variational data assimilation system for a non-hydrostatic model at the Japan Meteorological Agency: Formulation and preliminary results. Q. J. R Meteorol. Soc. 131, 3465–3475. DOI:10.1256/qj.05.132.

Iwasaki, T., Shoji, T., Kanno, Y., Sawada, M., Ujiie, M. and co-author. 2014. Isentropic analysis of polar cold airmass streams in the northern hemispheric winter. J. Atmos. Sci. 71, 2230–2243. DOI:10.1175/JAS-D-13-058.1.

Kajino, M., Inomata, Y., Sato, K., Ueda, H., Han, Z. and co-authors. 2012. Development of the RAQM2 aerosol chemical transport model and predictions of the Northeast Asian aerosol mass, size, chemistry, and mixing type. Atmos. Chem. Phys. 12, 11833–11856. DOI:10.5194/acp-12-11833-2012.

Kajino, M., Ishizuka, M., Igarashi, Y., Kita, K., Yoshikawa, C. and co-authors. 2016. Long-term assessment of airborne radiocesium after the Fukushima nuclear accident: Re-suspension from bare soil and forest ecosystems. Atmos. Chem. Phys. 16, 13149–13172. DOI:10.5194/acp-16-13149-2016.

Katata, G., Chino, M., Kobayashi, T., Terada, H., Ota, M. and co-authors. 2015. Detailed source term estimation of the atmospheric release for the Fukushima Daiichi Nuclear Power Station accident by coupling simulations of an atmospheric dispersion model with an improved deposition scheme and oceanic dispersion model. Atmos. Chem. Phys. 15, 1029–1070. DOI:10.5194/acp-15-1029-2015.

Kunii, M. 2014. Mesoscale data assimilation for a local severe rainfall event with the NHM–LETKF system. Weather Forecasting 29, 1093–1105. DOI:10.1175/WAF-D-13-00032.1.

Miyoshi, T. and Aranami, K. 2006. Applying a four-dimensional local ensemble transform Kalman filter (4D-LETKF) to the JMA nonhydrostatic model (NHM). SOLA 2, 128–131. DOI:10.2151/sola.2006-033.

Nakajima, T., Misawa, S., Morino, Y., Tsuruta, H., Goto, D. and co-authors. 2017. Model depiction of the atmospheric flows of radioactive cesium emitted from the Fukushima Daiichi Nuclear Power Station accident. Prog. Earth Planet. Sci. 4, 2. DOI:10.1186/s40645-017-0117-x.

Oura, Y., Ebihara, M., Tsuruta, H., Nakajima, T., Ohara, T. and co-authors. 2015. A database of hourly atmospheric concentrations of radiocesium (134Cs and 137Cs) in suspended particulate matter collected in March 2011 at 99 Air Pollution Monitoring Stations in Eastern Japan. J. Nucl. Radiochem. Sci. 15, 2_1–26. DOI:10.14494/jnrs.15.2_1.

Saito, K., Fujita, T., Yamada, Y., Ishida, J-I., Kumagai, Y. and co-authors. 2006. The operational JMA nonhydrostatic mesoscale model. Mon. Weather Rev. 134, 1266–1298. DOI:10.1175/MWR3120.1.

Saito, K., Ishida, J-I., Aranami, K., Hara, T., Segawa, T. and co-authors. 2007. Nonhydrostatic atmospheric models operational development at JMA. J. Meterolog. Soc. Jpn. 85B, 271–304. DOI:10.2151/jmsj.85B.271.

Science Council of Japan. 2014. A review of the model comparison of transportation and deposition of radioactive materials released to the environment as a result of the Tokyo Electric Power Company's Fukushima Daiichi Nuclear Power Plant accident. *Report of Committee on Comprehensive Synthetic Engineering, Science Council of Japan*. Available online at: http://www.jpgu.org/scj/report/20140902scj_report_e.pdf.

Sekiyama, T. T., Kunii, M., Kajino, K. and Shimbori, T. 2015. Horizontal resolution dependence of atmospheric simulations of the fukushima nuclear accident using 15-km, 3-km, and 500-m grid models. J. Meteorol. Soc. Jpn. 93, 49–64. DOI:10.2151/jmsj.2015-002.

Sekiyama, T. T., Kajino, M. and Kunii, M. 2017. The impact of surface wind data assimilation on the predictability of near-surface plume advection in the case of the Fukushima nuclear accident. J. Meteorol. Soc. Jpn. 95, 447–454. DOI:10.2151/jmsj.2017-025.

Stohl, A., Wernli, H., James, P., Bourqui, M., Forster, C. and co-authors. 2003. A new perspective of stratosphere–troposphere exchange. Bull. Amer. Meteor. Soc. 84, 1565–1573. DOI:10.1175/BAMS-84-11-1565.

Torii, T., Sanada, Y., Sugita, T., Kondo, A. and Shikaze, Y. 2012. Investigation of radionuclide distribution using aircraft for surrounding environmental survey from Fukushima Daiichi Nuclear Power Plant. JAEA-Technology 2012-036, Japan Atomic Energy Agency, 182 pp (in Japanese with English abstract)..

Tsuruta, H., Oura, Y., Ebihara, M., Ohara, T. and Nakajima, T. 2014. First retrieval of hourly atmospheric radionuclides just after the Fukushima accident by analyzing filter-tapes of operational air pollution monitoring stations. Sci. Rep. 4, 6717. DOI:10.1038/srep06717..

Yano, J.-I. 2014. Formulation structure of the mass-flux convection parameterization. Dyn. Atmos. Oceans 67, 1–28. DOI:10.1016/j.dynatmoce.2014.04.002.

5. Publication list 1954-2018

論文リスト（英文誌）1954-2018

2018

1. Hirose, K., Kikawada, Y., Igarashi, Y., Fujiwara, H., Jugder, D., Matsumoto, Y., Oi, T., and Nomura, M. Plutonium, ^{137}Cs and uranium isotopes in Mongolian surface soils, Journal of Environmental Radioactivity, 166, 97-103, 2017. http://dx.doi.org/10.1016/j.jenvrad.2016.01.007
2. Igarashi, Y., Kita., K., Maki, T., Kinase, T., Hyashi, N., Hotaka, K., Adachi, K., Kajino, M., Ishizuka, M., Sekiyama, T., T., Zaizen, Y., Takenaka, C., Ninomiya, K., Okochi, H., and Sorimachi, A. Fungal spore involvement in the resuspension of radiocaesium in summer, Scientific Reports, 9:1-10, 2019. 2019. DOI:10.1038/s41598-018-37698-x
3. Iwagami, S., Tsujimura, M., Onda, Y., Nishino, M., Konuma, R., Abe, Y., Hada, M., Pun, I., Sakaguchi, , A., Kondo, H., Yamamoto, M., Miyata, Y., and Igarashi, Y. Temporal changes in dissolved ^{137}Cs concentrations in groundwater and stream water in Fukushima after the Fukushima Dai-ichi Nuclear Power Plant accident. Journal of Environmental Radioactivity, 166, 458-465, 2017. http://dx.doi.org/10.1016/j.jenvrad.2015.03.025
4. Kajino, M.., Sekiyama, T. T., Mathieu, A,. Korsakissok, I., Périllat, R., Quélo, D., Quérel, A., Saunier, O., Adachi, K., Girard, S., Maki, T., Yumimoto, K., Didier, D., Masson, O., and Igarashi, Y., Lessons learned from atmospheric modeling studies after the Fukushima nuclear accident: Ensemble simulations, data assimilation, elemental process modeling, and inverse modeling, Geochemical Journal, Vol. 52, 2018.
5. Kinase, T., Kita, K., Igarashi, I., Adachi, K., Ninomiya, K., Shinohara, A., Okochi, H., Ogata, H., Ishizuka, M., Toyoda, S., Yamada, K., Yoshida, N., Zaizen, Y., Mikami, M,. Demizu, H., and Onda, Y., The seasonal variations of atmospheric 134,137Cs activity and possible host particles for their resuspension in the contaminated areas of Tsushima and Yamakiya, Fukushima, Japan, Progress in Earth and Planetary Science, 5:12, 2018.
6. Satou, Y., Sueki, K., Sasa, K., Yoshikawa, H., Nakama, S., Minowa, H., Abe, Y., Nakai, I., Ono, T., Adachi, K., and Igarashi, Y., Analysis of two forms of radioactive particles emitted during the early stages of the Fukushima Dai-ichi Nuclear Power Station accident, Geochemical Journal, Vol. 52, 137-143, 2018. doi:10.2343/geochemj.2.0514.
7. Sekiyama, T. T. and T. Iwasaki, Mass flux analysis of ^{137}Cs plumes emitted from the Fukushima Daiichi Nuclear Power Plant, Tellus B, 70(1), 1–11, doi:10.1080/16000889.2018.1507390, 2018.

2017

1. Iwagami, S., Tsujimura, M., Onda, Y., Nishino, M., Konuma, R., Abe, Y., Hada, M., Pun, I., Sakaguchi, A., Kondo, H., Yamamoto, M., Miyata, Y., and Igarashi, Y., Temporal changes in dissolved ^{137}Cs concentrations in groundwater and stream water in Fukushima after the Fukushima Dai-ichi Nuclear Power Plant accident, Journal of Environmental Radioactivity,166, 458-465, 2017.
2. Hirose, K., Kikawada, Y., Igarashi, Y., Fujiwara, H., Jugder, D., Matsumoto, Y., Oi, T., Nomura, M., Plutonium, ^{137}Cs and uranium isotopes in Mongolian surface soils, Journal of Environmental Radioactivity, 166, 97-103, 2017.
3. Sekiyama, T. T., Kajino, M., and Kunii, K., The Impact of Surface Wind Data Assimilation on the Predictability of Near-Surface Plume Advection in the Case of the Fukushima Nuclear Accident, Journal of the Meteorological Society of Japan, Vol. 95, 447-454, 2017. doi: 10.2151/jmsj.2017-025.

2016

1. Kajino, M., Ishizuka, M., Igarashi, Y., Kita, K., Yoshikawa, C., and Inatsu, M., Long-term assessment of airborne radiocerium after the Fukushima nuclear accident: re-suspension from bare soil and forest ecosystems, Atmos. Chem. Phys, 16, 13149-13172, 2016.
2. Satou,Y., Sueki, K., Sasa, K., Adachi, K., and Igarashi, Y., First successful isolation of radioactive particles from soil near the Fukushima Daiichi Nuclear Power Plant, Anthropocene, 14, 71-76, 2016.
3. Yamaguchi, N., Mitome, M., Kotone, A-H., Asano, M., Adachi, K., and Kogure, T., Internal structure of cesium-bearing radioactive microparticles released from Fukushima nuclear power plant. Scientific Reports. 6, 20548, 2016.

2015

1. Igarashi, Y., Kajino, M., Zaizen, Y., Adachi, K., and Mikami, M., Atmospheric radioactivity over Tsukuba, Japan: a summary of three years of observations after the FDNPP accident, Progress in Earth and Planetary Science 2:44, 2015. doi: 10.1186/s40645-015-0066-1.
2. Kajino, M., G-3. NHM-Chem: Sensitivity of Cs deposition to the size and hygroscopicity of Cs-bearing aerosols, Technical Reports of the Meteorological Research Institute, 76, 132–142, 2015.
3. Sekiyama, T. T., Kunii, M., Kajino, M., and Shinbori, T., Horizontal Resolution Dependence of Atmospheric Simulations of the Fukushima Nuclear Accident Using 15-km, 3-km, and 500-m Grid Models, J. Meteorol. Soc. Jpn., 93B, 49–64, 2015.

2014

1. Abe, Y., Iizawa, Y., Terada, Y., Adachi, K., Igarashi, Y., and Nakai, I., Detection of uranium and chemical state analysis of individual radioactive microparticles emitted from the Fukushima nuclear accident using multiple synchrotron radiation X-ray analyses, Analytical Chemistry, 86, 8521-8525, 2014.

2013

1. Aoyama, M., Uematsu, M., Tsumune, D., and Hamajima, Y., Surface pathway of radioactive plume of TEPCO Fukushima NPP1 released ^{134}Cs and ^{137}Cs, Biogeosciences, 10, 3067-3078, 2013. doi: 10.5194/bg-10-3067-2013.
2. Tsumune, D., Tsubono, T., Aoyama, M., Uematsu, M., Misumi, K., Maeda, Y., Yoshida, Y., and Hayami, H., One-year, regional-scale simulation of ^{137}Cs radioactivity in the ocean following the Fukushima Daiichi Nuclear Power Plant accident, Biogeosciences, 10, 5601-5617, 2013.
3. Povinec, P.P., Aoyama, M., Biddulph, D., Breier, R., Buesseler, K., Chang, C., Golser, R., Hou, X., Ješkovský, M., and Jull, A., Cesium, iodine and tritium in NW Pacific waters-a comparison of the Fukushima impact with global fallout. Biogeosciences, 10, 5481-5496. 2013.
4. Kumamoto, Y., Murata, A., Kawano, T., and Aoyama, M., Fukushima-derived radiocesium in the northwestern Pacific Ocean in February 2012, Applied Radiation and Isotopes, 81, 335-339, 2013. doi: 10.1016/j.apradiso.2013.03.085.
5. Toyama, C., Muramatsu, Y., Igarashi, Y., and Aoyama, M., Atmospheric fallout of ^{129}I in Japan before the Fukushima accident: Regional and global contributions, 1963-2005, Environmental Science & Technology, 47(15), 8383-8390, 2013. doi: 10.1021/es401596z.
6. Adachi, K., Kajino, M., Zaizen, Y., and Igarashi, Y., Emission of spherical cesium-bearing particles from an early stage of the Fukushima nuclear accident. Scientific Reports, 3, Article number 2554, 2013. doi:10.1038/srep02554.

2012

1. Toyama, C., Muramatsu, Y., Uchida, Y., Igarashi, Y., Aoyama, M., and Matsuzaki, H., Variations of ^{129}I in the atmospheric fallout of Tokyo, Japan 1963-2003, Journal of Environmental Radioactivity, 113, 116-122, 2012. doi: 10.1016/j.jenvrad.2012.04.014.
2. Inomata, Y., Aoyama, M., Tsumune, D., Motoi, T., and Nakano, H., Optimum interpolation analysis of basin-scale ^{137}Cs transport in surface seawater in the North Pacific Ocean, Journal of Environmental Monitoring, 14, 3146-3155, 2012. doi: 10.1039/C2EM30707C.
3. Aoyama, M., Tsumune, D., Uematsu, M., Kondo, F., and Hamajima, Y., Temporal variation of ^{134}Cs and ^{137}Cs activities in surface water at stations along the coastline near the Fukushima Dai-ichi Nuclear Power Plant accident site, Japan. Geochem. J, 46, 321-325, 2012.
4. Aoyama, M., Tsumune, D., and Hamajima, Y., Distribution of ^{137}Cs and ^{134}Cs in the North Pacific Ocean: impacts of the TEPCO Fukushima-Daiichi NPP accident, Journal of Radioanalytical and Nuclear Chemistry, 1-5, 2012. doi: 10.1007/s10967-012-2033-2.
5. Honda, M. C., Aono, T., Aoyama, M., Hamajima, Y., Kawakami, H., Kitamura, M., Masumoto, Y., Miyazawa, Y., Takigawa, M., and Saino, T., Dispersion of artificial caesium-134 and-137 in the western North Pacific one month after the Fukushima accident, Geochem. J, 46, e1-e9, 2012.
6. Povinec, P. P., Hirose, K., and Aoyama, M., Radiostrontium in the Western North Pacific: characteristics, behavior, and the Fukushima impact, Environmental Science & Technology, 46, 10356-10363, 2012. doi: 10.1021/es301997c.
7. Tsumune, D., Tsubono, T., Aoyama, M., and Hirose, K., Distribution of oceanic ^{137}Cs from the Fukushima Dai-ichi Nuclear Power Plant simulated numerically by a regional ocean model, Journal of Environmental Radioactivity, 111, 100-108, 2012.

2011

1. Aoyama, M., Fukasawa, M., Hirose, K., Hamajima, Y., Kawano, T., Povinec, P.P., and Sanchez-Cabeza, J. A., Cross Equator transport of ^{137}Cs from North Pacific Ocean to South Pacific Ocean, BEAGLE2003 cruises, Progress in Oceanography, 89, 7-16, 2011. doi:10.1016/j.pocean.2010.12.003.
2. Buesseler, K., Aoyama, M., and Fukasawa, M., Impacts of the Fukushima nuclear power plants on marine radioactivity. Environmental Science & Technology, 45(23), 9931-9935, 2011. doi: 10.1021/es202816c.
3. Povinec, P. P., Aoyama, M., Fukasawa, M., Hirose, K., Komura, K., Sanchez-Cabeza, J.A., Gastaud, J., Jeskovsky, M., Levy, I., and Sykora, I., ^{137}Cs water profiles in the South Indian Ocean - an evidence for accumulation of pollutants in the subtropical gyre. Progress in Oceanography, 89 , 17-30, 2011. doi:10.1016/j.pocean.2010.12.004.
4. Gastaud, J., Povinec, P.P., Aoyama, M., Hirose, K., Sanchez-Cabeza, J.A., Levy, I., Roos, P., Eriksson, M., Bosc, E. and Rezzoug, S., Transport and scavenging of Pu in surface waters of the Southern Hemisphere Oceans, Progress in Oceanography, 89, 92-100, 2011. doi:10.1016/j.pocean.2010.12.009.
5. Hirose, K., Kim, C.S., Yim, S.A., Aoyama, M., Fukasawa, M., Komura, K., Povinec, P.P., and Sanchez-Cabeza, J.A., Vertical profiles of plutonium in the central South Pacific, Progress in Oceanography, 89, 101-107, 2011. doi:10.1016/j.pocean.2010.12.010.
6. Tsumune, D., Aoyama, M., Hirose, K., Bryan, F., Lindsay, K. and Danabasoglu, G., Transport of ^{137}Cs to the Southern Hemisphere in an Ocean General Circulation Model, Progress in Oceanography, 89, 38-48, 2011. doi:10.1016/j.pocean.2010.12.006.
7. Sanchez-Cabeza, J.A., Levy, I., Gastaud, J., Eriksson, M., Osvath, I., Aoyama, M., Povinec, P.P. and Komura, K., Transport of North Pacific ^{137}Cs labeled waters to the south-eastern Atlantic Ocean. Progress in Oceanography, 89, 31-37, 2011. doi:10.1016/j.pocean.2010.12.005.
8. Levy, I., Povinec, P.P., Aoyama, M., Hirose, K., Sanchez-Cabeza, J.A., Comanducci, J-F., Gastaud, J., Eriksson, M., Hamajima, Y., Kim, C.S., Komura, K., Osvath, I., Roos, P. and Yim, S.A., Marine anthropogenic radiotracers in the Southern Hemisphere: new sampling and analytical strategies, Progress in Oceanography, 89, 120-133, 2011. doi:10.1016/j.pocean.2010.12.012.

2010

1. Inomata,Y., Igarashi, Y., Yoshioka, K., Tanaka, T. Y., and M, Chiba., Temporal variation of ^{222}Rn at the summit of Mt. Fuji associated with the Asian continental outflow, Atmospheric Environment, 44,3856-3865, 2010.
2. Nakano, H., Motoi, T., Hirose, K., and Aoyama, M., Analysis of ^{137}Cs concentration in the Pacific using a Lagrangian approach. Journal of Geophysical Research, 115, C06015, 2010. doi:10.1029/2009JC005640.
3. Hirose, K., Igarashi, Y., Aoyama, M., and Inomata, Y., Depositional behaviors of plutonium and thorium isotopes at Tsukuba and Mt. Haruna in Japan indicate the sources of atmospheric dust. Journal of Environmental Radioactivity, 101,106-112, 2010.
4. Zhang, Y., Zeng, J., Yamada, M., Wu, F., Igarashi, Y., and Hirose, K., Characterization of Pu concentration and its isotopic composition in a reference fallout material. Science of the Total Environment, 408(5), 1139-1144, 2010.

2009

1. Aoyama, M., Hamajima, Y., Fukasawa, M., Kawano, T., and Watanabe, S., Ultra low level deep water ^{137}Cs activity in the South Pacific Ocean, Journal of Radioanalytical and Nuclear Chemistry, 2009. doi:10.1007/s10967-009-0253-x.
2. Hirose, K., Aoyama, M., and Povinec, P.P., $^{239,\,240}$Pu /^{137}Cs ratios in the water column of the North Pacific: a proxy of biogeochemical processes, Journal of Environmental Radioactivity, 100, 258-262, 2009.
3. Igarashi, Y., Inomata, Y., Aoyama, M., Hirose, K., Takahashi, H., Shinoda, Y., Sugimoto, N., Shimizu, A., and Chiba, M., Possible change in Asian dust source suggested by atmospheric anthropogenic radionuclides during the 2000s, Atmospheric Environment, 43, 2971-2980, 2009.

4. Inomata, Y., Aoyama, M., and Hirose, K., Analysis of 50-y record of surface ^{137}Cs concentrations in the global ocean using the HAM-global database, Journal of Environmental Monitoring, 11(1), 116-125, 2009. doi: 10.1039/b811421h.
5. Hirose, K., Igarashi, Y., Aoyama, M., and Inomata, Y., Depositional behaviors of plutonium and thorium isotopes at Tsukuba and Mt.Haruna in Japan indicate the sources of atmospheric dust, Journal of Environmental Radioactivity, 101(2), 106-112, 2009. doi:10.1016/j.jenvrad.2009.09.003.
6. Igarashi Y., Kikawada, Y., Oda, K., Yamauchi, R., Nomura, M., Honda, T., Oi, T., and Hirose, K., Anomalous Uranium Isotope Ratio in Atmospheric Deposits in Japan, Journal of Nuclear Science and Technology, 46(12), 1094-1098. 2009.

2008

1. Aoyama, M., Hirose, K., Nemoto, K., Takatsuki, Y., and Tsumune, D., Water masses labeled with global fallout ^{137}Cs formed by subduction in the North Pacific, Geophysical Research Letters, 35, L01604, 2008. doi:10.1029/2007GL031964.
2. Hirose, K., Igarashi, Y., and Aoyama, M., Analysis of the 50-year records of the atmospheric deposition of long-loved radionuclides in Japan, Applied Radiation and Isotopes, 66, 1675-1678, 2008.
3. Hirose, K., Aoyama, M., Igarashi, Y., and Komura, K., Improvement of ^{137}Cs analysis in small volume seawater samples using the Ogoya underground facility, Journal of Radioanalytical and Nuclear Chemistry, 276,3,795-798, 2008.
4. Aoyama, M., Hirose, K., Nemoto, K., Takatsuki, Y., and Tsumune, D., Water masses labeled with global fallout ^{137}Cs formed by subduction in the North Pacific, Geophysical Research Letters, 35, L01604, 2008. doi:10.1029/2007GL031964.

2007

1. Hirose, K., Aoyama, M., and Kim, C.S., Plutonium in Seawater of the Pacific Ocean, Journal of Radioanalytical and Nuclear Chemistry, 274 No. 3, 635-638, 2007.
2. Hirose, K., Igarashi, Y., and Aoyama, M., 50 years records of atmospheric deposition of long-lived anthropogenic radionuclides in Japan, International Conference on Environmental Radioactivity: From Measurements and Assessments to Regulation, IAEA-CN-145, 95-96, 2007.
3. Hirose, K., Igarashi, Y., and Aoyama, M., Recent trends of plutonium fallout observed in Japan: Comparison with natural lithogenic radionuclides, thorium isotopes, Journal of Radioanalytical and Nuclear Chemistry, 273 No.1, 115-118, 2007.
4. Hirose, K., Aoyama, M., Fukasawa, M., Kim, C. S., Komura, K., Povinec, P. P., and Sanchez-Cabeza, J. A., Plutonium and ^{137}Cs in surface water of the South Pacific Ocean, Science of the Total Environment, 381, 243-255, 2007.

2006

1. Yamamoto, M., Sakaguchi, A., Sasaki, K., Hirose, K., Igarashi, Y., and Kim, C.K., Seasonal and spatial variation of atmospheric ^{210}Pb and ^{7}Be deposition: features of the Japan Sea side of Japan, Journal of Environmental Radioactivity, 86, 110-131, 2006.
2. Hirose, K., Aoyama, M., Kim, C.S., Kim, C.K., and Povinec, P.P., Plutonium isotopes in seawater of the North Pacific: effects of close-in fallout, INTERNATIONAL CONFERENCE ON ISOTOPES AND ENVIRONMENTAL STUDIES. Eds. P. Povinec, J.A. Sanchez-Cabeza. Vol. 8 of Radioactivity in the Environment, Elsevier, London, 2006.
3. Aoyama, M., Hirose, K., and Igarashi, Y., Re-construction and updating our understanding on the global weapons tests ^{137}Cs fallout, Journal of Environmental Monitoring, 8, 431-438, 2006.
4. Aoyama, M., Fukasawa, M., Hirose, K., Mantoura, R.F.C., Povinec, P.P., Kim, C.S., and Komura, K., Southern Hemisphere Ocean Tracer Study (SHOTS): An overview and preliminary results, INTERNATIONAL CONFERENCE ON ISOTOPES AND ENVIRONMENTAL STUDIES. Eds. P. Povinec, J.A. Sanchez-Cabeza, Vol. 8 of Radioactivity in the Environment, Elsevier, London, 2006.

5. Inoue, H.Y., Matsueda, H., Igarashi, Y., Sawa, Y., Wada, A., Nemoto, K., Sartorius, H., and Schlosser, C., Seasonal and long-term variations in atmospheric CO_2 and ^{85}Kr in Tsukuba, Central Japan, Journal of the Meteorological Society of Japan, 84/6, 959-968, 2006.

2005

1. Hirose, K., Aoyama, M., Igarashi, Y., and Komura, K., Extremely low background measurements of ^{137}Cs in seawater samples using an underground facility (Ogoya), Journal of Radioanalytical and Nuclear Chemistry, 263, 349-353, 2005.
2. Povinec, P.P., Aarkrog, A., Buesseler, K.O., Delfanti, R., Hirose, K., Hong, G.H., Ito, T., Livingston, H.D., Nies, H., Noshkin, V.E., Shima, S., and Togawa, O., ^{90}Sr, ^{137}Cs and $^{239,\,240}$Pu concentration surface water time series in the Pacific and Indian Oceans- WOMARS results, Journal of Environmental Radioactivity, 81, 63-87, 2005.
3. Igarashi, Y., Aoyama, M., Hirose, K., Povinec, P.P., and Yabuki, S., What anthropogenic radionuclides (^{90}Sr and ^{137}Cs) in atmospheric deposition, surface soils and Aeoliandusts suggest for dust transport over JAPAN, Water, Air, and Soil Pollution: Focus, 5, 51-69, 2005.

2004

1. Hirose, K., Kim, C.K., Kim, C.S., Chang, B.W., Igarashi, Y., and Aoyama, M., Wet and dry depositions of plutonium in Daejeon, Korea, The Science of the Total Environment, 332, 243-252, 2004.
2. Povinec, P.P., Hirose, K., Honda, T., Ito, T., MarianScott, E., and Togawa, O., Spatial distribution of ^{3}H, ^{90}Sr, ^{137}Cs and $^{239,\,240}$Pu in surface waters of the Pacific and Indian Oceans - GLOMARD database, Journal of Environmental Radioactivity, 76, 113-137, 2004.
3. Aoyama, M., and Hirose, K., Artificial Radionuclides database in the Pacific Ocean: Ham database, TheScientificWorldJOURNAL, 4, 200-215, 2004.
4. Hirota, M., Nemoto, K., Wada, A., Igarashi, Y., Aoyama, M., Matsueda, H., Hirose, K., Sartorius, H., Schlosser, C., Schmid, S., Weiss, W., and Fujii, K., Spatial and Temporal Variations of Atmospheric ^{85}Kr Observed During 1995-2001 in Japan: Estimation of Atmospheric ^{85}Kr inventory in the Northern Hemisphere, Journal of Radiation Research, 45, 405-413, 2004.
5. Hirose, K., Chemical Speciation of Thorium in Marine Biogenic Particulate matter, The Scientific World JOURNAL 4, 67-76, 2004.

2003

1. Hirose, K., and Aoyama, M., Analysis of ^{137}Cs and $^{239,\,240}$Pu concentrations in surface waters of the Pacific Ocean, Deep-Sea Research II, 50, 2675-2700, 2003.
2. Hirose, K., Aoyama, and Povinec, P.P., Concentration of particulate plutonium in surface and deep-water, samples collected during the IAEA'97 expedition, Deep-Sea Research II, 50, 2639-2647, 2003.
3. Povinec, P.P., Livingston, H.D., Shima, S., Aoyama, M., Gastaud, J., Goroncy, I., Hirose, K., Huynh-Ngoc, L., Ikeuchi, Y., Ito, T., Rosa, J.L., Kwong, L.L.W., Lee, S.H., Moriya, H., Mulsow, S., Oregioni, B., Pettersson, H., and Togawa, O., IAEA'97 expedition to the NW Pacific Ocean-Results of oceanographic and radionuclide investigations of the water column, Deep-Sea Research II, 50,2607-2637, 2003.
4. Ito, T., Povinec, P.P., Togawa, O., and Hirose, K., Temporal and Spatial variation of anthropogenic radionuclides in seawater of the Japan Sea, Deep-Sea Research II, 50, 2701-2711, 2003.
5. Tsumune, D., Aoyama, M., and Hirose, K., Behavior of ^{137}Cs and concentrations in the North Pacific in an ocean general circulation model, Journal of Geophysical Research, 108, C8, 3262, 2003.
6. Hirose, K., and Aoyama, M., Present Background Levels of Surface ^{137}Cs and $^{239,\,240}$Pu Concentrations in the Pacific, Journal of Environmental Radioactivity, 69(1-2), 53-60, 2003.
7. Tsumune, D., M. Aoyama, and K. Hirose, Numerical simulation of ^{137}Cs and $^{239,\,240}$Pu concentrations by an ocean general circulation model, Journal of Environmental Radioactivity, 69(1-2), 61-84, 2003.

8. Aoyama, M., and Hirose, K., Temporal variation of ^{137}Cs water column inventory in the North Pacific since the 1960s, Journal of Environmental Radioactivity, 69(1-2),107-117, 2003.
9. Hirose, K., Igarashi, Y., Aoyama, M., Kim, C.K., Kim, C.S., Chang, B.W., Recent trends of plutonium fallout observed in Japan: plutonium as a proxy for desertification, J. Environ. Monit, 5, 302-307, 2003.
10. Igarashi, Y., Aoyama, M., Hirose, K., Miyao, T., Nemoto, K., Tomita, M., and Fujikawa, T., Resuspension: Decadal Monitoring Time Series of the Anthropogenic Radioactivity Deposition in Japan, Journal of Radiation Research, 44, 319-328, 2003.
11. Kim, C.K., Kim, C.S., Chang, B.U., Choi, S.W., Chung, C.S., Hong, G.H., Hirose, K., and Igarashi, Y., Plutonium isotopes in seas around the Korean Peninsula, The Science of the Total Environment, 318, 197-209, 2003.
12. Kim, C.K., Kim, C.S., Chang, B.U., Choi, S.W., Chung, C.S., Hong, G.H., Hirose, K., and Pettersson, H.B.L., ^{240}Pu /^{239}Pu atom ratios in the bottom sediments of the NW Pacific Ocean, Journal of Radioanalytical and Nuclear Chemistry, 258(2), 265-268, 2003.
13. Lee, H.N., Tanaka, T., Chiba, M., and Igarashi, Y., Long range transport of Asian dust from dust storms and its impact on Japan, Water, Air, and Soil Pollution, 3, 231-243, 2003
14. Hirose, K., Implication of POC/^{234}Th ratios in oceanic particulate matter: an approach to particle aggregation, Papers of Meteorology and Geophysics, 53, 4, 109-118, 2003.

2002

1. Hirose, K., Miyao, T., Aoyama, M., and Igarashi, Y., Plutonium isotopes in the Sea of Japan, Journal of Radioanalytical and Nuclear Chemistry, 252, 293-299, 2002.
2. Hirose, K., and Aoyama, M., Chemical speciation of plutonium in seawater, Analytical and Bioanalytical Chemistry, 372, 418-420, 2002.
3. Hong, G.H., Kim, Y.I., Lee, S.H., Cooper, L.W., Choe, S.M., Tkalin, A.V., Lee, T., Kim, S.H., Chung, C.S., and Hirose, K., $^{239+240}$Pu and ^{137}Cs concentrations for zooplankton and nekton in the Northwest Pacific and Antarctic Oceans 1993-1996, Marine Pollution Bulletin, 44, 660-665, 2002.

2001

1. Igarashi, Y., Aoyama, M., Nemoto, K., Hirose, K., Miyao, T., Fushimi, K., Suzuki, M., Yasui, S., Asai, Y., Aoki, I., Fujii, K., Yamamoto, S., Sartorius, H., and Weiss, W., ^{85}Kr measurement system for continuous monitoring at Meteorological Research Institute, Japan, Journal of Environmental Monitoring, 3, 688-696, 2001.
2. Igarashi, Y., Aoyama, M., Hirose, K., Miyao, T., and Yabuki, S., Is it Possible to use ^{90}Sr and ^{137}Cs as tracers for the aeolian transport?, Water. Air. And Soil Pollution, 130, 349-354, 2001
3. Hirose, K., Igarashi, Y., Aoyama, M., and Miyao, T., Long-term trends of plutonium fallout observed in Japan, In Plutonium in the Environment, 251-266, 2001.
4. Aoyama, M., Hirose, K., Miyao, T., Igarashi, Y., and Povinec, P.P., ^{137}Cs activity in surface water in the western North Pacific, J. Radioanal. Nucl. Chem., 248, 3, 789-793, 2001.
5. Aoyama, M., Hirose, K., Miyao, T., Igarashi, Y., and Povinec, P.P., Temporal variation of ^{137}Cs inventory in the western North Pacific, J Radioanal Nucl Chem, 248, 3, 785-787, 2001
6. Hirose, K., Aoyama, M., Miyao, T., and Igarashi, Y., Plutonium in seawaters on the western North Pacific, J Radioanal Nucl Chem, 248, 3, 771-776, 2001.
7. Tsumune. D., Aoyama, M., Hirose, K., Maruyama, K., and Nakashiki, N., Caluculation of Artificial Radionuclides in the Ocean by an Ocean General Circulation Model, J Radioanal Nucl Chem, 248, 3, 777-783, 2001.

2000

1. Shiraishi, K., Kimura, S., Yonehara, H., Takada, J., Ishikawa, M., Igarashi, Y., Aoyama, M., Komura, K., and Nakazima, T., Survey of external dose around the JCO facility using sugar samples and ESR method, Adv. ESR Appl, 16, 9-14, 2000.

2. Komura, K, Yamamoto, M., Muroyama, T., Murata, Y., Nakanishi, T., Hoshi, M., Takada, J., Ishikawa, M., Kitagawa, K., Suga, S., Endo, A., Tozaki, N., Mitsugashira, T., Hara, M., Hashimoto, T., Takano, M., Yanagawa, Y., Tsuboi, T., Ichimasa, M., Ichimasa, Y., Imura, H., Sasajima, E., Seki, R., Saito, Y., Kondo, M., Kojima, S., Muramatsu, Y., Yoshida, S., Shibata, S., Yonehara, H., Watanabe, Y., Kimura, S., Shiraishi, K., Bannai, T., Sahoo, S.K., Igarashi, Y., Aoyama, M., Hirose, K., Uehiro, M., Doi, T., and Matsuzawa, T., The JCO criticality accident at Tokai-mura, Japan: an overview of the sampling campaign and preliminary results, J. Environ. Radioactivity, 50, 3-14, 2000.
3. Igarashi, Y., Miyao, T., Aoyama, M., Hirose, K., Sartorius, H., and Weiss, W., Radioactive noble gases in the surface air monitored at MRI, Tsukuba, before and after the JCO accident, J. Environ. Radioactivity, 50, 107-118, 2000.
4. Miyao, T., Hirose, K., Aoyama, M., and Igarashi, Y., Trace of the recent deep water formation in the Japan Sea deduced from historical ^{137}Cs data, Geophys. Res. Lett., 27, 22, 3731-3734, 2000.
5. Aoyama, M., Hirose, K., Miyao, T., and Igarashi, Y., Low level ^{137}Cs measurements in deep seawater samples, Appl. Radiat. Isot, 53, 159-162, 2000.
6. Igarashi, Y., Sarutorius, H., Miyao, T., Weiss, W., Fushimi, K., Aoyama, M., Hirose, K., and Inoue, H.Y., ^{85}Kr and ^{133}Xe monitoring at MRI, Tsukuba and its importance, J. Environ. Radioactivity, 48, 191-202, 2000.

1999

1. Hirose, K., Amano, H., Baxter, M.S., Chaykovskaya, E., Chumichev, V.B., Hong, G.H., Isogai, K., Kim, C.K., Kim, S.H., Miyao, T., Morimoto. T, Nikitin, A., Oda, K., Pettersson, H.B.L., Povinec, P.P., Seto, Y., Tkalin, A., Togawa, O., and Veletova, N.K., Anthropogenic radionuclides in seawater in the East Sea/Japan Sea: Results of the first-stage Japanese-Korean-Russian expedition, J. Environ. Radioactivity, 43, 1-13, 1999.
2. Igarashi, Y., Aoyama, M., Miyao, T., Hirose, K., Komura, K., and Yamamoto, M., Air concentration of radiocaesium in Tsukuba, Japan following the release from the Tokai waste treatment plant: comparisons of observations with predictions, Applied Radiation and Isotopes, 50, 1063-1073, 1999.
3. Igarashi, Y., Aoyama, M., Miyao, T., Hirose, K., and Tomita, M., Anomalous ^{90}Sr deposition during the fall, 1995 at MRI, Tsukuba, Japan, J. Radioanal. Nucl. Chem, 239(3), 539-542, 1999.
4. Ikeuchi, Y., Amano, H., Aoyama, M., Berezhnov, V.I., Chaykovskaya, E., Chumichev, V.B., Chung, C.S., Gastaud, J., Hirose, K., Hong, G.H., Kim, C.K., Kim, S.H., Miyao, T., Morimoto, T., Nikitin, A., Oda, K., Pettersson, H.B.L., Povinec, P.P., Tkalin, A., Togawa, O., and Veletova, N.K., Anthropogenic radionuclides in seawater of the Far Eastern Seas, Sci. Total Environ., 237/238, 203-212, 1999.
5. Pettersson, H.B.L., Amano, H., Berezhnov, V.I., Chaykovskaya, E., Chumichev, V.B., Chung, C.S., Gastaud, J., Hirose, K., Hong, G.H., Kim, C. K., Lee, S.H., Morimoto, T., Nikitin, A., Oda, K., Povinec, P.P., Suzuki, E., Tkalin, A., Togawa, O., Veletova, N.K., Volkov, Y., and Yoshida, K., Anthropogenic radionuclides in sediments in the NW Pacific Ocean and its marginal seas:results of the 1994-1995 Japanese-Korean-Russian expeditions, Sci. Total Environ, 237/238, 213-224, 1999.

1998

1. Igarashi, Y., Hirose, K., and Otsuji-Hatori, M., Beryllium-7 Deposition and Its Relation to Sulfate Deposition, J. Atmos. Chem, 29, 217-231, 1998.
2. Miyao, T., Hirose, K., Aoyama, M., and Igarashi, Y., Temporal variation of ^{137}Cs and ^{239,240}Pu in the sea of Japan, J. Environ. Radioactivity, 40, 239-250, 1998.

1997

1. Hirose, K., Complexation-scavenging of plutonium in the ocean, Radioprotection - Colloq, 32, C2-225 - C2-230, 1997.

1996

1. Igarashi, Y., Otsuji-Hattori, M., and Hirose, K., Recent deposition of ^{90}Sr and ^{137}Cs observed in Tsukuba, J. Environ. Radioactivity, 31, 157-169, 1996.
2. Otsuji-Hatori. M., Igarashi, Y., and Hirose, K., Preparation of a Reference Fall out Material for Activity Measurements, J. Environ Radioactivity, 31, 2, 143-155, 1966.

1995

1. Aoyama, M., and Hirose, K., The temporal and spatial variation of ^{137}Cs concentration in the western North Pacific and its marginal seas during the period from 1979 to 1988, J. Environ. Radioactivity, 29, 57-74, 1995.
2. Hirose, K., Geochemical studies on the Chernobyl radioactivity in environmental samples, J. Radioanal. Nucl. Chem., Articles, 197, 315-335, 1995.

1994

1. Hirose, K., Takatani, S., and Aoyama, M., Deposition of ^{90}Sr and plutonium isotopes derived from the Chernobyl accident in Japan, J. Radioanal. Nucl. Chem., Articles, 182, 349-358, 1994.

1993

1. Hirose, K., and Sugimura, Y., Chemical speciation of particulate ^{238}U, $^{239, 240}$Pu and Th isotopes in seawater, Sci. Total Environ., 130/131, 517-524, 1993.
2. Hirose, K., Takatani, S., and Aoyama, M., Wet deposition of radionuclides derived from the Chernobyl accident, J. Atmos. Chem., 17, 61-71, 1993.
3. Shiraishi, K., Igarashi, Y., Yamamoto, M., and Nakajima, T., Concentrations of thorium and uranium in freshwater samples collected in the former USSR, J. Radioanal. Nucl. Chem., 185,157-165, 1993.

1992

1. Aoyama, M., Hirose, K., and Takatani, S., Particle size dependent dry deposition velocity of the Chernobyl radioactivity, In Precipitation Scavenging and Atmosphere - Surface Exchange.volume 3, The 22e Summers Volume: Application and Appraisals. Coordinated by S.E. Schwartz and W.G.N. Slinn. Hemisphere Publishing Corporation, Washington, 1581-1593, 1992.
2. Hirose, K., Sugimura, Y., and Aoyama, M., Plutonium and ^{137}Cs in the western North Pacific: estimation of residence time of plutonium in surface water, Appl. Radiat. Isot, 43, 349-359, 1992.

1991

1. Aoyama, M., Hirose, K., and Sugimura, Y., The temporal variation of stratospheric fallout derived from the Chernobyl accident, J. Environ. Radioactivity, 13, 103-115, 1991.
2. Hirose, K., and Sugimura, Y., Chemical speciation of particulate uranium in seawater, J. Radioanal. Nucl. Chem., Articles, 149, 83-96, 1991.

1990

1. Hirose, K., and Sugimura, Y., Plutonium isotopes in the surface air in Japan: effect of Chernobyl accident, J. Radioanal. Nucl. Chem., Articles, 138, 127-138, 1990.
2. Hirose, K., Aoyama, M., and Sugimura, Y., Plutonium and cesium isotopes in river waters in Japan, J. Radioanal. Nucl. Chem., Articles, 141, 191-202, 1990.
3. Hirose, K., Aoyama, M., and Sugimura, Y., Short and long term effects of Chernobyl radioactivity on deposition and air concentrations in Japan, IAEA-SM 306/129, 141-149, 1990.

1988

1. Aoyama, M., Evidence of stratospheric fallout of caesium isotopes from Chernobyl accident, Geophys. Res. Lett., 15, 327-330, 1988.
2. Miyake, Y., Saruhashi, K., Sugimura, Y., Kanazawa, T., and Hirose, K., Contents of ^{137}Cs, plutonium and americium isotopes in the southern ocean waters, Pap. Met. Geophys, 39, 95-113, 1988.

1987

1. Aoyama, M., Hirose, K., and Sugimura, Y., Deposition of gamma-emitting nuclides in Japan after the reactor-IV accident at Chernobyl, J. Radioanal. Nucl. Chem., Articles, 116, 291-306, 1987.
2. Hirose, K., Aoyama, M., Katsuragi, Y., and Sugimura, Y., Annual deposition of Sr-90, Cs-137 and Pu-239, 240 from the 1961-1980 nuclear explosions: a simple model, J. Meteor. Soc. Japan, 65, 259-277, 1987.

1986

1. Aoyama, M., Hirose, K., Suzuki, Y., and Sugimura, Y., High level radioactive nuclides in Japan in May, Nature, 321, 819-820, 1986.
2. Hirose, K., Sugimura, Y., and Katsuragi, Y., ^{90}Sr and $^{239+240}$Pu in the surface air in Japan: their concentrations and size distributions, Pap. Met. Geophys, 37, 255-269, 1986.
3. Katsuragi, Y., and Aoyama, M., Seasonal variation of Sr-90 fallout in Japan through the end of 1983, Pap. Met. Geophys., 37, 15-36, 1986.
4. Suzuki, Y., Inoue, H., Katsuragi, Y., and Sugimura, Y., The distribution of 85Krin the air over the North and South Pacific Ocean Mem., Natl. Inst. Polar Res., Spec. Issue, 40, 462-466, 1986.

1985

1. Hirose, K., and Sugimura, Y., A new method of plutonium speciation in seawater, J. Radioanal. Nucl. Chem, Articles, 92, 363-369, 1985.

1984

1. Hirose, K., and Sugimura, Y., Plutonium in the surface air in Japan, Health Phys., 46, 1281-1285, 1984.
2. Inoue, H., Katsuragi, Y., and Shigehara, K., Tritiated water vapor in the surface air at Tokyo, Pap. Met. Geophys, 35, 11-20, 1984.

1983

1. Katsuragi, Y., A study of ^{90}Sr fallout in Japan, Pap. Met. Geophys., 33, 277-291, 1983.
2. Katsuragi, Y., Kawamura, K., and Inoue, H., Tritium fallout in Tokyo, Pap. Met. Geophys, 34, 21-30, 1983.

1982

1. Inoue, H., and Katsuragi, Y., A study of tritium fallout in Japan, Pap. Met. Geophys, 32, 21-28, 1982.
2. Katsuragi, Y., Hirose, K., and Sugimura, Y., A study of plutonium fallout in Japan, Pap. Met. Geophys, 33, 85-93, 1982.

1981

1. Hirose, K., and Sugimura, Y., Concentration of Uranium and the activity ratio of ^{234}U /^{238}U in surface air-effect of atmospheric burn-up of cosmos-954, Pap. Met. Geophys., 32, 317-322, 1981.
2. Hirose, K., and Sugimura, Y., Plutonium content of river water in Japan, Pap. Met. Geophys, 32, 301-305, 1981.
3. Sugimura, Y., and M. Mayeda, An improved method of analysis of uranium in sea water using chelating resin, Pap. Met. Geophys, 32, 167-171, 1981.

1980

1. Sugimura, Y., The uranium content and the activity ratio ^{234}U /^{238}U in sea water in the Pacific ocean, Isotope Marine Chemistry, 211-246, 1980.

1979

1. Sugiura, Y., Saruhashi, K., and Miyake, Y., Evaluation on the disposal of radioactive wastes into the North Pacific. - the effect of steady flow and up - welling, Proc. The 3rd NEA Seminar on Marine Radioecology, 1979.

1978

1. Miyake, Y., Nuclear weapons and radioactive pollution of the earth's environment, In, Proc. Internal Symp. On the damage and after-effects of the atomic bombing of Hiroshima and Nagasaki July 21-Aug., 9, 1977, Tokyo, 164-188, 1978.

1976

1. Miyake, Y., and Saruhashi, K., A critical study on the IAEA definition of high level radioactive waste unsuitable for dumping at sea, Pap. Met. Geophys. 27, 75-80, 1976.
2. Miyake, Y., and Saruhashi, K., Disposal of radioactive waste into deep seas, J. Radiat. Res., 17, 42-43, 1976.
3. Miyake, Y., and Sugimura, Y., The plutonium content in the Pacific Ocean waters, Proc. of Symp. on Transuranium Nuclides in the Environment, San Francisco, 17-21 Nov. 1975, USERDA and IAEA, IAEA-SM-199/22, 91-105,1976.
4. Sugimura, Y., Symposium II plutonium in environment, II-1.Distribution and behavior of plutonium in the global environments, J. Radiat. Res., 17, 4-5, 1976.
5. Sugiura, Y., Saruhashi, K., and Miyake, Y., Evaluation on the disposal of radioactive wastes into the North Pacific, Pap. Met. Geophys, 27, 81-87, 1976.

1975

1. Miyake, Y., Shimada, T., Kawamura, K., Sugimura, Y., Shigehara, K., and Saruhashi, K., Distribution of tritium in the Pacific ocean, Rec. Oceanogr. Works Japan, 13, 17, 1975.
2. Miyake, Y., Katsuragi, Y., and Sugimura, Y., Plutonium fallout in Tokyo, Pap. Met. Geophys, 26, 1-8, 1975.
3. Miyake, Y., Sugimura, Y., and Hirao, Y., Uranium, thorium and potassium contents in granitic and basaltic rocks in Japan, In, The Natural Radiation Environment II, II, Proc. 2nd Intnl. Symp. On Natural Radiation Environment, Aug. 7-11, 1972, Houston, Texas, USA, ed. J. A. S. Adams, W. M. Lowder, T. F. Gesell, 535-558,1975.
4. Saruhashi, K., I-1 The global radioactive contamination due to nuclear weapon testings, J. Radiat. Res., 16, 47, 1975.
5. Saruhashi, K., Katsuragi, Y., Kanazawa, T., Sugimura, Y., and Miyake, Y., ^{90}Sr and ^{137}Cs in the Pacific waters, Rec. Oceanogr. Works Japan, 13, 1-15, 1975.

1973

1. Miyake, Y., and Saruhashi, K., The radio-carbon model of the ocean, Pap. Met. Geophys, 24, 263-271, 1973.
2. Miyake, Y., Saruhashi, K., and Sugimura, Y., The isotopic ratio ^{234}U /^{238}U in sea water and its bearings on the isotopic ratio in river waters, Oceanogr. Works Japan, 12, 23-25, 1973.
3. Miyake, Y., Sugimura, Y., and Saruhashi, K., Content of plutonium in river water in Japan, Pap. Met. Geophys, 24, 75-78, 1973.
4. Miyake, Y., Sugimura, Y., and Yasujima, T., Thorium isotope content in river water in Japan, Pap. Met. Geophys, 24, 67-73, 1973.

1972

1. Miyake, Y., Sugimura, Y., and Uchida, T., A new method of spectrophotometric determination of uranium in sea water and uranium content with ^{234}U /^{238}U ratio in the Pacific water, Rec. Oceanogr. Works Japan, 11, 53-63, 1972.

1970

1. Miyake, Y., Katsuragi, Y., and Sugimura, Y., A study on plutonium fallout, J. Geophys. Res., 75, 2329-2330, 1970.
2. Miyake, Y., Sugimura, Y., and Mayeda, M., The uranium content and the activity ratio ^{234}U /^{238}U in marine organisms and sea water in the western North Pacific, J. Oceanogr. Soc. Japan, 26, 123-129, 1970.

1969

1. Miyake, Y., Radioactive contamination of the ocean, Bull. Jpn. Soc. Fisheries Oceanogr., Nov., 1969, 1969.

1968

1. Miyake, Y., and Sugimura, Y., Plutonium content in the western North Pacific waters, Pap. Met. Geophys, 19, 481-485, 1968.
2. Miyake, Y., Katsuragi, Y., and Sugimura, Y., Deposition of plutonium in Tokyo through the end of 1966, Pap. Met. Geophys, 19, 267-276, 1968.

1967

1. Miyake, Y., and Kanazawa, T., Atmospheric ozone and radioactive fallout, Pap. Met. Geophys., 18, 311-326, 1967.
2. Miyake, Y., Radioactive contamination of the ocean, J. Radiat. Res., 8, 1, 1967.
3. Miyake, Y., Sea, radioactivity in, International Dictionary of Geophysics, 1-7, 1967.

1966

1. Miyake, Y., and Saruhashi, K., On the radio-carbon age of the ocean waters, Pap. Met. Geophys., 17, 218-223, 1966.
2. Miyake, Y., and Sugimura, Y., Ratio ^{234}U /^{238}U and the uranium concentration in seawater in the western North Pacific, J. Geophys. Res., 71, 3083-3087, 1966.

1965

1. Kuroda, P. K., Miyake, Y., and Nemoto, J., Strontium isotopes Global circulation after the Chinese nuclear explosion of 14 May 1965, Science, 150, 1289-1290, 1965.
2. Miyake, Y., Saruhashi, K., Katsuragi K., and Kanazawa, T., Radioactivity of dust and rain - the ratio of Cs-137 and Sr-90 in the radioactive fallout, Proc. Internl. Conf. On Cloud Physics,Tokyo, IAMAP, 395-399, 1965.
3. Park, K., George, M.J., Miyake, Y., Saruhashi, K., Katsuragi, Y., and Kanazawa, T., Strontium-90 and caesium-137 in Columbia river plume, July 1964, Nature, 208, 1084-1085, 1965.

1964

1. Miyake, Y., and Sugimura, Y., Uranium and radium in the western North Pacific waters, Studies on Oceanography, Prof. K. Hidaka Sixtieth Birthday Commemorative Volume, Univ. of Tokyo Press, Tokyo, 274-278, 1964.
2. Miyake, Y., and Ohtsuka, Y., Beryllium-7 in rain water, Pap. Met. Geophys, 15, 89-92, 1964.
3. Miyake, Y., A sequential procedure for the radiochemical analysis of marine material, Annex to safety series 11."Method of surveying and monitoring marine radioactivity, IAEA, Vienna, 26, 1964.
4. Miyake, Y., Atomic weapons and the pollution of the sea, The East, 3, 64-68, 1964.
5. Miyake, Y., Saruhashi, K., Katsuragi, Y., Kanazawa, T., and Sugimura, Y., Uranium, radium, thorium, Ionium, strontium 90 and cesium 137 in coastal waters of Japan, In, Recent Researches in the Fields of Hydrosphere, Atmosphere and Nuclear Geochemistry, published by Editorial Committee of Sugawara Festival Volume, Maruzen Co. Ltd., 127-141, 1964.
6. Miyake, Y., Sugimura, Y., and Tsubota, H., Content of uranium, radium, and thorium in river waters in Japan, In, The Natural Radiation Environment, ed. By J. A. S. Adams and W. M. Lowder, Univ. of Chicago Press, Chicago, Rice Univ. Semicentennial Series, 219-225, 1964.
7. Sugimura, Y., Torii, T., and Murata, S., Uranium distribution in drake passage waters, Nature, 204, 464-465, 1964.

1963

1. Folsom, T.R., and Saruhashi, K., A comparison of analytical techniques used for determination of fallout cesium in sea water for oceanographic purpose, J. Radiat. Res., 4, 39-53, 1963.
2. Miyake, Y., and Tsubota, H., Estimation of the direct contribution of meteoric water to river waters by means of fall-out radio-cesium and radiostrontium, "Radioisotopes in Hydrology" Proc. IAEA Symp., Tokyo. IAEA, Vienna, 425-431, 1963.

3. Miyake, Y., Artificial radioactivity in the Pacific ocean, IUGG Monograph, 20 Radioactive traces in oceanography, 1963.
4. Miyake, Y., Saruhashi, K., Katsuragi, K., and Kanazawa, T., Deposition of Cs-137 and Sr-90 in Tokyo through the end of July 1963, Pap. Met. Geophys, 13, 180-181, 1963.
5. Miyake, Y., Saruhashi, K., Katsuragi, Y., Kanazawa, T., and Tsunogai, S., Deposition of ^{90}Sr and ^{137}Cs in Tokyo through the end of July 1963, Pap. Met. Geophys, 14, 58-65, 1963.
6. Miyake, Y., Sugiura, Y., and Tsubota, H., II. Contents of uranium, radium, and thorium in river waters in Japan, The Natural Radiation Environment, RICE Univ. semicentennial Pub, 1963.

1962

1. Miyake, Y., Saruhashi, K., Katsuragi, Y., and Kanazawa, T., Seasonal variation of radioactive fallout, J. Geophys. Res., 67, 189-193, 1962.
2. Miyake, Y., Saruhashi, K., Katsuragi, Y., and Kanazawa, T., Penetration of ^{90}Sr and ^{137}Cs in deep layers of the Pacific and vertical diffusion rate of deep water, J. Radiat. Res., 3, 141-147, 1962.
3. Miyake, Y., Saruhashi, K., Katsuragi, Y., and Kanazawa, T., The peak in radioactive fallout in the temperate zone of the northern hemisphere, J. Radiat. Res., 3,148-152, 1962.
4. Sugimura, Y., and Sugimura, T., Uranium in recent Japanese sediments, Nature, 194, 568-569, 1962.

1961

1. Miyake, Y., Saruhashi, K., Katsuragi, Y., and Kanazawa, T., Cesium 137 and strontium 90 in sea water, J. Radiat. Res., 2 25-28, 1961.
2. Miyake, Y., Saruhashi, K., Katsuragi, Y., and Kanazawa, T., Cesium 137 and strontium 90 in sea water, Pap. Met. Geophys., 12, 85-88, 1961.

1960

1. Miyake, Y., and Saruhashi, K., Vertical and horizontal mixing rates of radioactive material in the ocean, Disposal of Radioactive wastes IAEA Vienna, 167-173, 1960.
2. Miyake, Y., and Katsuragi, Y., Strontium 90 in western North Pacific surface waters, Pap. Met. Geophys., 11, 188-190, 1960.
3. Miyake, Y., Saruhashi, K., Katsuragi, Y., and Kanazawa, T., Radioactive fallout in Japan and its bearings on meteorological conditions, Pap. Met. Geophys., 11, 151-158, 1960.

1959

1. Miyake, Y., Saruhashi, K., and Katsuragi, Y., The Sr-90 fallout and the air motion, Pap. Met. Geophys., 9, 172-176, 1959.
2. Miyake, Y., Special committee on oceanic research, Working Group on Radioactivity in the Ocean, 1959.

1958

1. Miyake, Y., and Saruhashi, K., Distribution of man-made radio-activity in the North Pacific through summer 1955, J. Mar. Res., 17, 383-389, 1958.
2. Miyake, Y., and Sugiura, Y., The method of measurement of radioactivity in sea water, Pap. Met. Geophys., 9, 48-50, 1958.
3. Miyake, Y., Hazards to human health of radioactive dust, Radio Japan, 2, 3-5, 1958.
4. Miyake, Y., The distribution of artificial radioactivity in the equatorial region in the Pacific in the summer of 1956, The Proc. 9th Pacific Science Congress, 16, 227, 1958.

1957

1. Miyake, Y., and Saruhashi, K., The world-wide strontium 90 deposition during the period from 1951 to the fall of 1955, Pap. Met. Geophys., 8, 241-243, 1957.
2. Miyake, Y., The biological effects of nuclear tests - warning by Japanese scientists, Radio Japan, 1, 3-5, 1957.

3. Miyake, Y., XI. Methods for the measurement of radioactivity in sea water, Annuals of International Geophysical Year, 5, 1957.
4. Miyake, Y., XII. Radioactivity as a tracer of air motions in the atmosphere, Symp. On radioactivity, IGY, Utrecht, 360, 1957.
5. Miyake, Y., Sugiura, Y., Saruhashi, K., and Kanazawa, T., The estimation of the amount of Sr-90 deposition and the external infinite gamma does in Japan due to man-made radioactivity, Pap. Met. Geophys., 8, 222-231, 1957.

1956

1. Miyake, Y., On the distribution of radioactivity in the North Pacific ocean in 1954-1955, Internl. Conf. For Peaceful Uses of Atomic Energy in Geneva, August 1955, 13, pp.381-384, 1956.
2. Miyake, Y., Radioactivity in rain water and air, Proc. Internl. Conf. For Peaceful Uses of Atomic Energy in Geneva, August 1955, 13, 345-349, 1956.
3. Sugiura, Y., and Kanazawa, T., On the radioactive fallout collected in Tokyo on 26th November, 1955, Pap. Met. Geophys., 7, 128-135, 1956.

1955

1. Miyake, Y., and Sugiura, Y., Radiochemical analysis of radio-nuclides in sea water collected near BIKINI atoll, Pap. Met. Geophys., 6, 90-92, 1955.
2. Miyake, Y., Effects of atomic explosions on the atmosphere and sea, The research in the effects and influences of the nuclear bomb text explosions, 1-6, 1955.
3. Miyake, Y., Kigoshi, K., and Saruhashi, K., Radiochemical analysis of fission products contained in the soil collected at Tokyo, May, 1954, Pap. Met. Geophys., 6, 1, 93-94, 1955.
4. Miyake, Y., The artificial radioactivity in rain water observed in Japan, 1954-1955, Research in the Effects and Influences of the Nuclear Bomb Test Explosions Science, 151-159, 1955.
5. Miyake, Y., The artificial radioactivity in rain water observed in Japan, from autumn 1954 to spring 1955, Pap. Met. Geophys., 6, 26-32, 1955.
6. Miyake, Y., Sugiura, Y., and Kameda, K., On the artificial radioactivity in the sea near Japan, Pap. Met. Geophys., 6, 90-92, 1955.
7. Miyake, Y., Sugiura, Y., and Kameda, K., On the distribution of radioactivity in the sea around Bikini atoll in June, 1954, Pap. Met. Geophys., 5, 253-262, 1955.
8. Miyake, Y., Sugiura, Y., and Kameda, K., Research in the effects and influence of the nuclear bomb test explosions, Soc. For Promotion of Science, 415-417, 1955.

1954

1. Miyake, Y., Kigoshi, K., Sugiura, Y., and Saruhashi, K., A study on the productivity in coastal waters by means of the radio-carbon, Pap. Met. Geophys., 5, 89-94, 1954.
2. Miyake, Y., The artificial radioactivity in rain water observed in Japan from May to August, 1954, Pap. Met. Geophys, 5, 173-177, 1954.

6. Publication list (in Japanese) 1954-2018

論文リスト（和文誌）1954-2018

2017

1. 足立光司, 福島原子力発電所事故で放出された不溶性放射性粒子の形態と組成, エアロゾル研究, 32-4,255–260, 2017.
2. 五十嵐康人, 放射性物質の大気沈着・拡散および陸域からの再浮遊について, Proceedings of the 17th Workshop Environmental Radioactivity. KEK Proceedings, 2017-6, 50-55, 2017.
3. 小野貴大, 飯澤勇信, 阿部善也, 中井 泉, 寺田康子, 佐藤志彦, 末木啓介, 足立光司, 五十嵐康人, 福島第一原子力発電所事故により1号機から放出された放射性粒子の放射光マイクロビームX線分析を用いる化学性状の解明, 分析化学66（4）, 2017.
4. 梶野瑞王, 大気エアロゾルの環境動態シミュレーション,安全工学, 57-6, 433-441, 2018
5. 木村徹, 五十嵐康人, 財前祐二, ガンマ線スペクトル解析ソフトP-SCANを用いた高精度なCs^{134}/Cs^{137}放射能比の導出, Proceedings of the 17th Workshop Environmental Radioactivity. KEK Proceedings, 2017-6, 262-266, 2017.

2016

1. 木村徹, 五十嵐康人, 財前祐二, 2016: IAEA-TEL-2015-03 Proficiency Test試料の測定, Proceedings of the 17th Workshop Environmental Radioactivity. KEK Proceedings, 2016-8, 228-231.

2015

1. 足立光司, 電子顕微鏡がとらえた放射性粒子, 地球化学, 49,185–193, 2015.
2. 木村徹, 五十嵐康人,「大気降下物試料の放射能分析の品質管理」, Proceedings of the 16th Workshop Environmental Radioactivity. KEK Proceedings 2015-4 , 23-27, 2015.

2014

1. 青山道夫, 東電福島原発事故後の海洋での放射能汚染の推移（With English Abstract）. YAKUGAKU ZASSHI, Journal of the Pharmaceutical Society of Japan. 2014.

2013

1. 青山道夫, 極低レベル放射能測定：少量表層海水および極深層海水試料への応用.放射線, 39(1), 17-20, 2013.

2012

1. 青山道夫, 福島第一原子力発電所から放出された放射性セシウム同位体の北太平洋における総量と分布, 日本原子力学会誌, 54, 780-783, 2012.
2. 青山道夫, 五十嵐康人, 1957年から始まる気象研究所における環境放射能研究の歴史, 放射線, 38(3), 123-128, 2012.
3. 青山道夫, 海洋に放出された放射性物質の長期地球規模での挙動, 検証！福島第一原発事故-放射性物質の実際と科学者たちの活動の記録（化学4月号別冊）. 4, 33-38, 2012.
4. 青山道夫, 五十嵐康人, 広瀬勝己, 月間降下物測定660ヶ月が教えること-^{90}Sr, ^{137}CsおよびPu降下量1957年4月～2012年3月-. 科学, 82(4), 0442-0457, 2012.

2011

1. 青山道夫, 福島原子力発電所事故による海洋汚染. 理大科学フォーラム, 11(通巻329号), 42-45, 2011.
2. 津旨大輔, 坪野考樹, 青山道夫, 廣瀬勝巳, 福島第一原子力発電所から漏洩した^{137}Csの海洋拡散シミュレーション(With English Abstract). 電力中央研究所報告書, V11002, PP.18, 2011.

2009

1. 五十嵐康人, 放射性同位体分析, In 岩坂泰信, 西川雅高, 山田丸, 洪天祥（編）, 黄砂, 古今書院, pp81-87, 東京, 2009.
2. Igarashi, Y., Anthropogenic Radioactivity in Aerosol -A Review Focusing on Studies during the 2000s-, 保健物理, 44(3), 2009.

3. 猪股弥生, 五十嵐康人, 千葉長, 青山道夫, 廣瀬勝己, 再現期間を用いた降水時における高ガンマ線線量率の異常値判定. Radioisotopes, 58, 37-42, 2009.

2007

1. 三浦誓也, 貝森優希, 工藤英嗣, 野呂幸男, 時枝隆之, 廣瀬勝己, 青森県における大気中クリプトン-85　濃度調査,　青森県原子力センター所報, 1, 43-44, 2007.
2. 廣瀬勝己, 青山道夫, Kim、S.A. Kim, 太平洋の海水中のプルトニウムの挙動について,　日本放射化学会誌 別冊, 8 supplement, 103, 2007.

2006

1. 青山道夫, 大気と海洋深層における核実験起源放射性降下物の超低レベル放射能測定, ADIOISOTOPES, 55, 429-438, 2006.
2. 小村和久, 青山道夫, 秋山正和, 氏平祐輔, 大田裕二, 大塚良仁, 大西勝基, 櫻井敬久, 篠原伸夫, Ge 検出器の使用状況に関するアンケート報告, RADIOISOTOPES, 55, 699-707,2006.

2004

1. 廣瀬勝己, 化学トレーサーを利用した海洋変動の研究, 測候時報第 71 巻特別号, 71,　S81-S86, 2004.
2. 五十嵐康人, 廣瀬勝己, 放射性降下物標準試料の調製を通じた ^{90}Sr, ^{137}Cs,プルトニウムなどの人工放射性核種分析の相互比較と参照値の決定,　放射化分析, No. 17, 39-42, 2004.

2002

1. 五十嵐康人, ^{90}Sr と ^{137}Cs を用いたダスト輸送過程と再飛散, エアロゾル研究, 12, 17(4), 252, 2002.

1986

1. 鈴木款, 井上久幸, 杉村行勇, 大気中の放射性クリプトンの分布, 地球化学, 20, 106-108, 1986.

1978

1. 葛城幸雄, 人工放射性物質, 天気, 25, 第 11 号, 20-23, 1978.
2. 猿橋勝子, 海洋中の放射性物質を指標とした物質の移動・拡散, 水汚染の機構と解析－環境科学持論－, 日本地球化学編, 東京, 産業図書, 271-287, 1978.
3. 三宅泰雄, 猿橋勝子, 杉村行勇, 葛城幸雄, 金沢照子, 核兵器と地球環境の放射能汚染, 被爆の実相と被爆者の実情 －1977 年 NGO 被爆問題シンポジウム報告書, ISDA－ JNPC 編集, 朝日イブニングニュース社発行, 182-212, 1978.

1976

1. 葛城幸雄, 日本における放射性降下物, 天気, 23, No. 7, 333-345, 1976.
2. 杉村行雄, 環境のなかのプルトニウム, 自然, 3 月号, 1976.

1975

1. 三宅泰雄, 島田利夫, 川村清, 重原好次, 地上大気のトリチウム含量と気象との関係, 日本地球化学会 “環境問題特別号”, 131-135, 1975.

1974

1. 三宅泰雄, 葛城幸雄, 最近の ^{90}Sr 降下物の起源, 天気, 21, 639-644, 1974.

1971

1. 葛城幸雄, 人工放射能による大気汚染, 気象研究ノート, 107, 258-282, 1971

1970

1. 三宅泰雄, 葛城幸雄, 最近の日本における放射性塵の降下, 天気, 17, 593-598, 1970.

1965

1. 葛城幸雄, 日本における Cs-137 および Sr-90 降下について(I), 天気, 12, 323-328, 1965.
2. 葛城幸雄, 日本における Cs-137 および Sr-90 降下について(II) "成層圏における人工放射性物質の滞留時間の推定", 天気, 12, 377-384, 1965.

1964

1. 三宅泰雄, 葛城幸雄, 金沢照子, 放射性降下物の現状と将来, 科学, 34, 142-148, 1964.

1963

1. 三宅泰雄, 放射性降下物の気象学の側面, 天気, 9, No. 1, 1962.

1962

1. 三宅泰雄, 放射性降下物の気象学的側面, 天気, 9, 1-6, 1962.
2. 三宅泰雄, 猿橋勝子, 放射能による水の汚染, 水利科学, 23, 1-14, 1962.

1958

1. 三宅泰雄, 猿橋勝子, 放射化学と海洋, 科学, 28, 510-513, 1958.

1956

1. 三宅泰雄, 杉浦吉雄, 葛城幸雄, 1955 年 4 月旭川地方に降った放射性の落下塵,気象集誌, 第 2 号, 34, 226-230, 1956.

1955

1. 三宅泰雄, 放射能雨の性格, 測候時報, 22, 196-202, 1955.
2. 三宅泰雄, 日本に降った人工放射性雨・雪[II]9 月～12 月, 天文と気象, 21, 1-8, 1955.
3. 三宅泰雄, 杉浦吉雄, 亀田和久, 日本近海の海水放射能について, 昭和 29 年度海洋資源開発調査報告（黒潮班）, 81-82, 1955.
4. 三宅泰雄, 放射能雨の性格, 測候時報, 22, No. 7, 196-202, 1955.

1954

1. 三宅泰雄, 日本に降った人工放射性雨(1954 年 5-7 月), 天文と気象, 20, 1-8, 1954.
2. 三宅泰雄, 杉浦吉雄,亀田和久, ビキニ海域における人工放射能の分布とその海洋学的考察" ビキニ灰とそれによる傷害 第三", 科学, 24, 601-605, 1954.
3. 三宅泰雄, 有住直介, 磯野謙治, 田島英三, ビキニの灰とそれによる傷害（つづき）日本に降った放射能雨, 科学, 24, No. 8, 405-409, 1954.

年代・雑誌名不明

1. 三宅泰雄, 放射能とその作用, 遺伝,（1975？）
2. 三宅泰雄, 第 II 編 環境の放射能汚染と化学分析,（1970？）
3. 三宅泰雄, 猿橋勝子, 杉村行勇, 海洋における放射性核種, 海洋化学講座, 第 6 巻, 海洋無機化学, 第 4 章, 109-170,（1969？）
4. 三宅泰雄, 田島英三, 日米放射能会議, 8-18,（1954？）

7. History of the studies at the Meteorological Research Institute

表：研究の歴史

研究の歴史

放射能調査研究費以前および、放射能調査研究費での研究

西暦	年度	予算項目	予算項目							
				課題名	課題名	課題名	課題名	課題名	課題名	課題名
1954	昭和29年									
1955	S30	北太平洋観測（日・米・加）								
1956	S31	北太平洋赤道海域観測（日・米・仏）								
1957	S32	国際地球観測年事業費								
1958	S33	国際地球観測年事業費	放射能調査研究費	放射化学分析(落下塵・降水・海水中の放射性物質の研究）		深海水の循環に関する研究（以下深海水）				
1959	S34		放射能調査研究費	放射化学分析		深海水				
1960	S35	国際原子力機関委託研究	放射能調査研究費	放射化学分析		深海水				
1961	S36	国際原子力機関委託研究	放射能調査研究費	放射化学分析		深海水				
1962	S37	国際インド洋観測（日・米・ソ・英・仏）	放射能調査研究費	放射化学分析		深海水				
1963	S38	国際インド洋観測（日・米・ソ・英・仏）	放射能調査研究費	放射化学分析		深海水				
1964	S39	オレゴン州立大学との共同研究	放射能調査研究費	放射化学分析		深海水				
1965	S40		放射能調査研究費	放射化学分析	海洋中の放射性廃棄物のモニタリングの測定法に関する研究（以下海洋廃棄物モニタリング）	深海水		海水中における放射廃棄物の化学的挙動の研究(以下廃棄物化学的挙動）		
1966	S41		放射能調査研究費	放射化学分析	海洋廃棄物モニタリング	深海水		廃棄物化学的挙動		
1967	S42		放射能調査研究費	放射化学分析	海洋廃棄物モニタリング	深海水		廃棄物化学的挙動		
1968	S43		放射能調査研究費	放射化学分析	海洋廃棄物モニタリング	深海水		廃棄物化学的挙動		
1969	S44		放射能調査研究費	放射化学分析		深海水		廃棄物化学的挙動		
1970	S45		放射能調査研究費	放射化学分析		深海水		廃棄物化学的挙動		
1971	S46		放射能調査研究費	放射化学分析		深海水		廃棄物化学的挙動		

放射能調査研究費以前および、放射能調査研究費での研究

西暦	年度	予算項目	予算項目							
				課題名	課題名	課題名	課題名	課題名	課題名	課題名
1972	S47		放射能調査研究費	放射化学分析				放射性固体廃棄物の海洋処分に伴う鉛直拡散に関する研究(以下廃棄物鉛直拡散）		
1973	S48		放射能調査研究費	放射化学分析				廃棄物鉛直拡散		
1974	S49		放射能調査研究費	放射化学分析				廃棄物鉛直拡散	大気中におけるKr−85およびH−3挙動と蓄積に関する調査研究(以下Kr−85／H−3）	
1975	S50		放射能調査研究費	放射化学分析				廃棄物鉛直拡散	Kr−85／H−3	
1976	S51		放射能調査研究費	放射化学分析				廃棄物鉛直拡散	Kr−85／H−3	
1977	S52		放射能調査研究費	放射化学分析				数種の放射性核種の同時測定による深海拡散の研究(以下深海拡散）	原子力施設に由来する放射性気体の広域分布に関する調査研究(以下放射性気体）	
1978	S53		放射能調査研究費	放射化学分析				深海拡散	放射性気体	環境における超ウラン元素の分布と挙動に関する研究（以下超ウラン元素）
1979	S54		放射能調査研究費	放射化学分析				深海拡散	放射性気体	超ウラン元素
1980	S55		放射能調査研究費	放射化学分析				深海拡散	放射性気体	超ウラン元素
1981	S56		放射能調査研究費	放射化学分析				深海拡散	放射性気体	超ウラン元素
1982	S57		放射能調査研究費	放射化学分析				深海拡散	放射性気体	超ウラン元素
1983	S58		放射能調査研究費	放射化学分析				深海拡散	放射性気体	超ウラン元素
1984	S59		放射能調査研究費	放射化学分析				深海拡散	放射性気体	超ウラン元素
1985	S60		放射能調査研究費	放射化学分析				深海拡散	放射性気体	超ウラン元素
1986	S61		放射能調査研究費	放射化学分析				深海拡散	放射性気体	超ウラン元素
1987	S62		放射能調査研究費	放射化学分析				深海拡散	放射性気体	超ウラン元素
1988	S63		放射能調査研究費	放射化学分析				深海拡散	放射性気体	超ウラン元素
1989	H1		放射能調査研究費	放射化学分析				深海拡散	放射性気体	超ウラン元素
1990	H2		放射能調査研究費	放射化学分析				深海拡散	放射性気体	超ウラン元素
1991	H3		放射能調査研究費	放射化学分析				深海拡散	放射性気体	超ウラン元素
1992	H4		放射能調査研究費	放射化学分析	海洋における放射性核種の挙動に関する調査研究（以下海洋放射性核種）				放射性気体	超ウラン元素
1993	H5		放射能調査研究費	放射化学分析	海洋放射性核種				放射性気体	超ウラン元素
1994	H6		放射能調査研究費	放射化学分析	海洋放射性核種				放射性気体	超ウラン元素
1995	H7		放射能調査研究費	放射化学分析	海洋放射性核種				放射性気体	超ウラン元素

放射能調査研究費以前および、放射能調査研究費での研究

西暦	年度	予算項目	予算項目							
				課題名	課題名	課題名	課題名	課題名	課題名	課題名
1996	H8		放射能調査研究費	大気圏の放射性核種の動態に関する研究（以下大気圏放射性核種）	海洋環境における放射性核種の挙動に関する研究（以下海洋環境放射性核種）					
1997	H9		放射能調査研究費	大気圏放射性核種	海洋環境放射性核種					
1998	H10		放射能調査研究費	大気圏放射性核種	海洋環境放射性核種					
1999	H11		放射能調査研究費	大気圏放射性核種	海洋環境放射性核種					
2000	H12		放射能調査研究費	大気圏放射性核種	海洋環境放射性核種					
2001	H13		放射能調査研究費	大気圏の放射性核種の長期的動態に関する研究(以下大気圏放射性核種）	海洋環境における放射性核種の長期挙動に関する研究(以下海洋環境放射性核種）				大気中の放射性気体の実態把握に関する研究　　（以下放射性気体）	
2002	H14		放射能調査研究費	大気圏放射性核種	海洋環境放射性核種				放射性気体	
2003	H15		放射能調査研究費	大気圏放射性核種	海洋環境放射性核種				放射性気体	
2004	H16		放射能調査研究費	大気圏放射性核種	海洋環境放射性核種				放射性気体	
2005	H17		放射能調査研究費	大気圏放射性核種	海洋環境放射性核種				放射性気体	
2006	H18		放射能調査研究費	放射性降下物の長期変動と再浮遊に関する研究（以下放射性降下物）	海洋環境における放射性核種の長期挙動に関する研究(以下海洋環境放射性核種）					
2007	H19		放射能調査研究費	放射性降下物	海洋環境放射性核種					
2008	H20		放射能調査研究費	放射性降下物	海洋環境放射性核種					
2009	H21		放射能調査研究費	放射性降下物	海洋環境放射性核種					
2010	H22		放射能調査研究費	放射性降下物	海洋環境放射性核種					

放射能調査研究費以前および、放射能調査研究費での研究

西暦	年度	予算項目	予算項目							
				課題名	課題名	課題名	課題名	課題名	課題名	課題名
2011	H23(8月から）		放射能調査研究費	「大気を通じた人工放射性核種の陸圏・水圏への沈着およびその後の移行過程の解明研究（以下陸圏水圏人工放射性核種）」						
2012	H24		放射能調査研究費	陸圏水圏人工放射性核種						
2013	H25		放射能調査研究費	陸圏水圏人工放射性核種						
2014	H26		放射能調査研究費	陸圏水圏人工放射性核種						
2015	H27(4月から）		放射能調査研究費	「人工放射性核種のバックグラウンド大気監視と数値解析に関する研究（以下ＢＧ放射性核種）」						
2016	H28		放射能調査研究費	ＢＧ放射性核種						
2017	H29		放射能調査研究費	ＢＧ放射性核種						
2018	H30		放射能調査研究費	ＢＧ放射性核種						

表紙の図説明

2018年 3月までの ^{90}Srおよび^{137}Cs月間降下量

福島第一原発事故後の大気の放射能汚染の実態把握を継続しています。2011年3月の事故以降に確定できた^{90}Srおよび^{137}Cs月間降下量を対数軸で誤差と併せてプロットしています。^{134}Csは事故直後には^{137}Csとほぼ等量降下していますから、放射性セシウム全体ではこのプロットのほぼ倍量となります。ただし、^{90}Sr、^{137}Csはどちらもおよそ30年の半減期で減衰しますが、^{134}Csはおよそ2年で半減します。図示した誤差は計測の統計誤差で、1シグマです。測定誤差は本来全ての測定値につき表示すべきですが、グラフが見づらくなるため、従来はあえて表示してきませんでした。また、数十年前のデータについては誤差データが伝えられていません。

福島第一原発事故以前に採取され、分析や前処理途上だった試料については、事故の汚染によって実験室環境および測定室環境、測定機器のバックグラウンドなどが大幅に上昇したため、蒸発濃縮工程においても試料の汚染（コンタミネーションと言います）の問題が発生します。そのため、観測値を求めること自体が困難になっていましたが、試料を汚染の水準の低い関西にて分析しこの問題の回避に努めました。しかし、細心の注意と努力にもかかわらず、2010年の後半および2011年初のデータは欠測となってしまいました。

徐々に実験環境の除染や測定機器の入れ替えなどを実施して事故以前のきれいな実験環境を追求し、データを求めるように努めています。また、IAEAが実施した分析相互比較に参画するなどし、その精度の維持管理に努めていますので、現状のデータの信頼性は担保できていると考えています。

8. A caption of the cover art

Monthly depositions of ^{90}Sr and ^{137}Cs before March 2018.

We have been monitoring the deposition amounts for the purpose of understanding the actual condition of radioactive pollution after the accident of Fukushima Daiichi Nuclear Power Plant (FDNPP). The monthly deposition amounts of both ^{90}Sr and ^{137}Cs, which were successfully fixed values after the accident in March 2011, are shown in logarithmic axis with error widths. Since the deposition amounts of ^{134}Cs were nearly equal to those of ^{137}Cs, the total amounts of radioactive cesium were approximately two times of the values in this figure. We would like to note that the half-lives of ^{90}Sr and ^{137}Cs are approximately 30 years, however, ^{134}Cs decays to half in about 2 years. The error widths are one sigma in statistical error of measurements. Although the error widths of all measurement values were better to be shown, error values used to be not shown on purpose to avoid busy figure in the former versions. In addition, error data before several decades are not handed down.

For the analysis of samples collected before the accident of FDNPP and not measured then, significant increase of background values were severe problem, because environments including laboratories and instruments were polluted, and it was also problem that samples could have been polluted in the operations of concentration or other preprocesses (contamination problem). We overcame the difficulty by carrying the analysis out in western Japan (Kansai area) where the pollution level was low, however, the data during the latter part of 2010 and the former part of 2011 were lacked in spite of our efforts.

We are making efforts to recover clean working environment as before the accident, by cleaning of the environments, exchanging instruments, etc. for the purpose of acquire the correct data. In addition, we maintain the precision of the data, for example, by participating inter-comparison programs performed by IAEA, so that, the credibility of the data are assured (please refer to the section: quality control of radioactive analysis of atmospheric deposition samples).